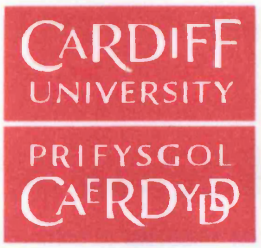

LITHOGEOCHEMISTRY AND SPINEL COMPOSITIONS IN THE ULTRAMAFIC COMPLEXES OF WESTERN ETHIOPIA: CRITERIA FOR THE IDENTIFICATION OF ALASKAN-TYPE INTRUSIONS

Matt Jackson

Submitted in fulfilment of the requirements for the degree of Ph.D.

March 2006

UMI Number: U585446

All rights reserved

INFORMATION TO ALL USERS
The quality of this reproduction is dependent upon the quality of the copy submitted.

In the unlikely event that the author did not send a complete manuscript
and there are missing pages, these will be noted. Also, if material had to be removed,
a note will indicate the deletion.

UMI U585446
Published by ProQuest LLC 2013. Copyright in the Dissertation held by the Author.
Microform Edition © ProQuest LLC.
All rights reserved. This work is protected against
unauthorized copying under Title 17, United States Code.

ProQuest LLC
789 East Eisenhower Parkway
P.O. Box 1346
Ann Arbor, MI 48106-1346

Acknowledgements

"What does not kill me, makes me stronger."

Friedrich Nietzsche, Twilight of the Idols

I would like to thank my supervisors Hazel Prichard and John Bowles. Hazel has given me a vast amount of help over the last few years, both in the field and at university. I have learnt a great deal from her and I hope we can continue to work together. Without the help of John Bowles, this project would not have continued as far as it has. His sense of duty is something which all scientists should admire. I have very much enjoyed our discussions, especially in the field. I firmly believe that there are few supervisors who could have done more to help me than Hazel and John.

There are many others who have helped with this project. Kebede Belete and I spent large amounts of time together in the field during 2001-2002. His company was fantastic and I believe he is the foremost expert on the Yubdo area. The other geologists whom I will always remember fondly are, Aberra, Tadesse and Daniel. From each of these people I have disovered much about the ways of Africa and their contribution in the field has been crucial. I will always remember our escapades, such as getting our Land Crusier stuck in mud on an unmarked road, with no communications. Dodging the lion was also fun!

Many staff of the School of Earth, Ocean and Planetary Science have contributed a great deal in time and patience in helping me, including Alun Rogers for his patience in teaching me cartography and Pete Fisher for his expertise in the use of the SEM. All of the technicians and administration staff at the school are to be thanked.

I wish to thank my parents, who have given me all the support I could ask for, even though I stay out of contact for weeks! My brother and sister, Chris and Amy, have also helped greatly and now that I have emerged from my thesis fog, I hope to spend more time with them.

My friends in Cardiff have also helped considerably. In particular, my flatmates: Justin, Jo and Penny, who have put up with me doing little washing up, cleaning and generally being difficult! Lunch breaks with Katherine have been particularly useful especially when she forced me to take them. The TA and regular staff at 104 Regt RA (V) have been responsible for keeping my feet firmly grounded, for that I am sincerely grateful. Also thanks to Dave Oldham, Richard Lilly and Kevin Jones for laughs and help during the first few years of my study.

Finally, I wish to thank Nicky, whom I love more than ever. Her mere presence is enough to calm my nerves and I wish to spend the rest of my life with her.

Abstract

This thesis covers two separate but complimentary themes. Firstly, work on the spinel composition of the ultramafic rocks of has provided evidence that they formed as Alaskan-type intrusions. This has implications both for prospectivity and for the understanding of neoproterozoic plate movements. Additionally, the study of the rock and soil geochemistry has been used to identify exploration targets and evaluate the prospectivity of the major complexes.

It is proposed here that the ultramafic complexes Tulu Dimtu, Kingy, Daleti, Ankori and Yubdo, in the Western Ethiopian Shield are Alaskan type intrusions. Alaskan-type intrusions are concentrically zoned ultramafic intrusions thought to be the feeder pipes of volcanoes. They have dunite at the core and grade outwards to clinopyroxenite and sometimes hornblendite. These intrusions typically occur in continental arc settings such as Alaska, British Colombia and the Urals. This compares with ophiolite complexes which are thought to be obducted oceanic upper mantle and crust. The two types of complex may be difficult to distinguish because if ophiolites are dismembered and deformed fragments, they may resemble Alaskan-type intrusions.

This thesis documents several features of these Ethiopian complexes that are typical of Alaskan type intrusions. Mapping of the Yubdo complex has shown a circular out crop pattern with concentric zones of clinopyroxenite at the edge to dunite at the centre. New mapping of the Tulu Dimtu area has shown a similar zoned circular body. Both the Yubdo and Tulu Dimtu complexes show concentric zones of Cr values, where the greatest values occur at the edge and the lowest in the centre.

These mafic and ultramafic intrusions are very altered by surface weathering but contain chrome-spinels which have a geochemistry which is unlike ophiolites and similar to Alaskan-type intrusions. The analysis of these spinels demonstrates how the compositions of spinel Fe^{2+}# and Cr# values may be used to distinguish between an Alaskan type or ophiolite complexes. In Alaskan-type intrusions, spinels with Fe^{2+}# values greater than 0.85 frequently have Cr# values which are lower than 0.5. Such low Cr# values in spinels with high Fe^{2+}# values are rare in ophiolite complexes.

The variations in Ni, Cu, Cr and Al contents of highly altered ultramafics and fresher ultramafics have been used to investigate the magmatic and post-magmatic ore forming processes that have influenced the Pt and Pd content of the complexes. It is expected that medium to low temperature hydrothermal activity may have had a significant impact on the geochemistry of even the fresher rocks. The discovery of high Pd values and low Pt in lithologies such as talc-schists and quartzite support the idea that Pd is more mobile than Pt in medium to low temperature conditions. Furthermore, in the Tulu Dimtu Main Intrusion, the altered rocks indicate that Pd has been removed from the magmatic sites of concentration. In a few places it is possible to see through the extensive alteration and potential magmatic processes can be considered. Within the Tulu Dimtu Main Intrusion and the Main Yubdo Intrusion, the most primitive rocks occur at the flanks. Furthermore, it is indicated that sulphide segregation may have occurred in the Tulu Dimtu Main Intrusion and Daleti Ultramafic. In the Daleti Ultramafic, regardless of the presence of sulphides, the Pt and Pd values remain low – it is therefore unlikely that the complex hosts economic grades. However, at Tulu Dimtu and Yubdo, it is recommended that any future exploration be targeted at the flanks of the complexes, where magmatic and post-magmatic processes may potentially co-incide to elevate the grade.

Much work has been published to document the nature of platinum-group minerals (PGM) in the alluvial and eluvial placers around the Yubdo area and some PGM have been discovered in the serpentinsed dunites of the main Yubdo intrusion. In this thesis further discoveries of PGM have been made in the serpentinised dunites and chromites from the Yubdo area.

In the course of this work new base maps covering the ultramafic complexes and the surrounding basement have been produced. These have revealed many smaller ultramafic bodies which are referred to here as the Lensoid Ultramafics. Both spinel and whole rock geochemistry supports the hypothesis that these are slivers of rock "sheared-off" the outside of larger complexes.

The conclusion that these complexes have an Alaskan-type origin has consequences for the understanding of plate movements in this part of the Neoproterozoic Western Ethiopian Shield. Additionally, the identification of exploration targets will help focus efforts to uncover any potential economic mineralisation.

LITHOGEOCHEMISTRY AND SPINEL COMPOSITIONS IN THE ULTRAMAFIC COMPLEXES OF WESTERN ETHIOPIA: CRITERIA FOR THE IDENTIFICATION OF ALASKAN-TYPE INTRUSIONS

Table of Contents

1	**Introduction**	**1**
1.1.	Introduction	1
1.2.	The tectonic setting of the ultramafic complexes	4
1.3.	The development of Pt and Pd	5
1.4.	The mining history of the WES	5
1.5.	The conduct of the study	7
1.6.	Aims and methods used in the thesis	7
1.7.	Layout of the thesis	8
2	**Literature Review**	**9**
2.1.	Introduction	9
2.2.	Geological Setting	9
2.3.	Previous Work on the Ultramafics of the WES	11
2.3.1.	Introduction	12
2.3.2.	Regional Studies of the Ultramafic bodies	12
2.3.3.	Tulu Dimtu and Kingy	13
2.3.4.	Daleti, Ankori, Tulu Kapi and Keley	15
2.3.5.	Yubdo, Andu and Sodu	16
2.4.	Alaskan-type intrusions versus ophiolites	17
2.4.1.	Introduction	17
2.4.2.	Scale of Alaskan-type intrusions and ophiolites	18
2.4.3.	Structure of Alaskan-type intrusions and ophiolites	19
2.4.4.	Petrology and Mineralogy	22
2.4.5.	Rare Earth Elements (REE)	24
2.4.6.	Platinum-Group Elements	25
2.4.7.	Fractionation of Nickel, Copper and Chromium	27
2.4.8.	Summary	27
3	**Petrology and Mineralogy**	**29**
3.1.	Introduction	29
3.2.	Methods	29
3.2.1.	Scanning Electron Microscopy	29
3.2.2.	Energy Dispersive X-Ray analyzer	29
3.3.	Petrology	29
3.3.1.	Introduction	30
3.3.2.	Dunite	31
3.3.3.	Clinopyroxenite	33
3.3.4.	Birbirite	33
3.3.5.	Summary	34
3.3.6.	Classification of Rock Types	34
3.4.	Oxide Minerals	36
3.4.1.	Introduction	36
3.4.2.	Tulu Dimtu	36
3.4.3.	Kingy	37
3.4.4.	Daleti, Ankori, Tulu Kapi and Keley	37
3.4.5.	Yubdo, Andu and Sodu	38
3.4.6.	Summary	38
3.4.7.	Discussion	39
3.5.	Sulphide Minerals	39
3.5.1.	Introduction	39
3.5.2.	Tulu Dimtu	40
3.5.3.	Kingy	41

3.5.4.	Daleti, Ankori, Tulu Kapi and Keley	42
3.5.5.	Yubdo, Andu and Sodu	43
3.5.6.	Summary	43
3.5.7.	Discussion	44
3.6.	Platinum Group Minerals	45
3.6.1.	Introduction	45
3.6.2.	Sample AYR-016-01	45
3.6.3.	Sample KYR-019-02	46
3.6.4.	Sample Y30	47
3.6.5.	Discussion	48
4	**Terrain Mapping**	**49**
4.1.	Introduction	49
4.2.	Aerial Photography	50
4.2.1.	Introduction	50
4.2.2.	The Aerial Photographs of the WES	50
4.2.3.	The Acquisition of Aerial Photographs	52
4.2.4.	Image Processing	55
4.3.	Terrain Analysis	56
4.3.1.	Introduction	56
4.3.2.	Stereoscopy	56
4.3.3.	Terrain Elements: Introduction	57
4.3.4.	Terrain Elements: Drainage pattern	58
4.3.5.	Terrain Elements: Erosion	60
4.3.6.	Terrain Elements: Topography	62
4.3.7.	Terrain Elements: Relative image tone and texture	63
4.3.8.	Terrain Elements: Land use	64
4.3.9.	Photomorphic Regions	64
4.3.10.	Ground Truth	65
4.4.	The Terrain in the WES	65
4.4.1.	The photomorphic regions	65
4.4.2.	Tulu Dimtu	68
4.4.3.	Kingy	69
4.4.4.	Daleti, Ankori, Tulu Kapi and Keley	70
4.4.5.	Yubdo, Sodu and Andu	71
4.4.6.	Summary	72
5	**Geological Mapping**	**73**
5.1.	Introduction	73
5.2.	Method	73
5.3.	Geological Maps of the WES	74
5.3.1.	Tulu Dimtu	74
5.3.2.	Kingy	76
5.3.3.	Daleti, Ankori, Tulu Kapi and Keley	78
5.3.4.	Yubdo, Sodu and Andu	80
5.3.5.	Summary	81
6	**Ground Magnetics**	**82**
6.1.	Introduction	82
6.2.	Methods	82
6.2.1.	Data collection	83
6.2.2.	Diurnal correction	86
6.2.3.	Data presentation	87
6.2.4.	Limitations and accuracy	88
6.3.	Results	89
6.3.1.	Sensor orientation test	89
6.3.2.	Wide spacing survey	90
6.3.3.	Tight spacing survey	96
6.4.	Discussion	97
6.5.	Conclusions	99
6.5.1.	Pull out section	101
7	**Soil Geochemical Data**	**102**
7.1.	Introduction	102

7.2.	The overburden of the WES	102
7.3.	Sampling strategy	106
7.4.	Method of Analysis	107
7.5.	Soil Forming processes and geochemical dispersion	107
7.5.1.	Ni, Cu, Cr and Al	107
7.5.2.	Pt and Pd	108
7.6.	Tulu Dimtu: Selected Major and Trace elements	109
7.6.1.	Introduction	109
7.6.2.	Summary of Analytical Results	109
7.6.3.	Nickel	114
7.6.4.	Copper	115
7.6.5.	Chromium	116
7.6.6.	Aluminium	117
7.6.7.	Summary of Ni, Cu, Cr and Al values	117
7.6.8.	Platinum and Palladium	118
7.6.9.	Discussion	120
7.6.10.	Ni, Cu, Cr, and Al distribution in soils	120
7.6.11.	Genesis of Pt and Pd in soils	121
7.6.12.	Conclusion	122
7.6.13.	Maps of the elemental distribution in the soils of the Tulu Dimtu areas	123
7.7.	Kingy: Selected Major and Trace Elements	124
7.7.1.	Introduction	124
7.7.2.	Summary of Analytical Results	125
7.7.3.	Nickel	129
7.7.4.	Copper	130
7.7.5.	Chromium	131
7.7.6.	Aluminium	132
7.7.7.	Summary of Ni, Cu, Cr and Al values	132
7.7.8.	Platinum and Palladium	133
7.7.9.	Discussion	135
7.7.10.	Trace Element distribution in soils	135
7.7.11.	Genesis of Pt and Pd in soils	135
7.7.12.	Conclusions	136
7.7.13.	Maps of the elemental distribution in the soils of the Kingy areas	138
7.8.	Daleti, Ankori, Tulu Kapi and Keley: Selected Major and Trace Elements	139
7.8.1.	Introduction	139
7.8.2.	Summary of Analytical Results	140
7.8.3.	Nickel	144
7.8.4.	Copper	145
7.8.5.	Chromium	146
7.8.6.	Aluminium	147
7.8.7.	Summary of Ni, Cu, Cr and Al values	147
7.8.8.	Platinum and Palladium	148
7.8.9.	Discussion	150
7.8.10.	Trace element distribution in soils	150
7.8.11.	Genesis of Pt and Pd in soils	150
7.8.12.	Conclusions	151
7.8.13.	Maps of the elemental distribution in the soils of the Daleti, Ankori, Tulu Kapi and Keley areas	152
7.9.	Yubdo, Andu and Sodu: Selected Major and Trace Elements	153
7.9.1.	Introduction	153
7.9.2.	Summary of Analytical Results	154
7.9.3.	Nickel	158
7.9.4.	Copper	159
7.9.5.	Chromium	160
7.9.6.	Aluminium	161
7.9.7.	Summary of Ni, Cu, Cr, Al, Pt and Pd values	161
7.9.8.	Platinum and Palladium	162
7.9.9.	Discussion	163
7.9.10.	Ni and Cr values in soils above the Main Yubdo Ultramafic	163

7.9.11.	Genesis of Pt and Pd in soils	164
7.9.12.	Conclusions	165
7.9.13.	Maps of the elemental distribution in the soils of the Yubdo, Andu and Sodu areas	166
7.10.	Discussion of the distribution of Ni, Cu, Cr, Al, Pt and Pd in the soils of the WES	167
7.11.	Summary of the Soil development in the WES	170
7.11.1.	Ni, Cu, Cr and Al	170
7.11.2.	Pt and Pd	171
8	**Rock Geochemical Data**	172
8.1.	Introduction	172
8.2.	Analytical Techniques	173
8.2.1.	Introduction	173
8.2.2.	Pb Fire Assay	174
8.2.3.	Aqua Regia Digestion	176
8.2.4.	Inductively Coupled Plasma - Optical Emmission Spectroscopy	177
8.3.	Methods	178
8.3.1.	Definition of a fresher sample	178
8.3.2.	The samples	182
8.4.	Tulu Dimtu: Selected Major and Trace Elements	183
8.4.1.	Introduction	183
8.4.2.	Data	185
8.4.3.	Nickel	187
8.4.4.	Copper	188
8.4.5.	Chromium	188
8.4.6.	Aluminium	189
8.4.7.	Summary of the Ni, Cu, Cr and Al values in the Main Intrusion and Sheared Ultramafic	189
8.4.8.	Summary of the Ni, Cu, Cr and Al values in the Lensoid Ultramafics	190
8.4.9.	Summary of the Ni, Cu, Cr and Al values in the Shear Zones	190
8.5.	Tulu Dimtu: Pt and Pd Distribution	190
8.5.1.	Rock	190
8.5.2.	Summary of Pt and Pd distribution in the Main Intrusion and Sheared Ultramafic	191
8.5.3.	Summary of Pt and Pd distribution in the Lensoid Ultramafics	194
8.5.4.	Summary of Pt and Pd distribution in the Shear Zones	194
8.5.5.	Summary of Pt and Pd distribution in the basement	194
8.5.6.	Comparison of the geochemistry of the soil versus rock samples	194
8.6.	Review of processes concentrating Pt and Pd	195
8.6.1.	Introduction	195
8.6.2.	The fractionation of Ni	195
8.6.3.	The fractionation of Cr	197
8.6.4.	Sulphide immiscibility and solubility	198
8.6.5.	Sulphide fractionation	198
8.6.6.	Filter-pressing	199
8.6.7.	Magma mixing	200
8.6.8.	Hydrothermal remobilisation	201
8.7.	Tulu Dimtu: Discussion	202
8.7.1.	Zonation of nickel and chromium in fresher rocks	202
8.7.2.	Locations of highest copper and chromium values in fresher rocks	205
8.7.3.	Trace element distribution in fresher rocks of the Lensoid Ultramafics	207
8.7.4.	Trace element distribution in Shear Zones	207
8.7.5.	Zonation of trace elements in altered rocks	208
8.7.6.	Genesis of Pt and Pd in fresher rocks	209
8.7.7.	Genesis of Pt and Pd in altered rocks	210
8.8.	Tulu Dimtu: Conclusions	211
8.9.	Maps of the elemental distribution in the Tulu Dimtu areas	213
8.10.	Kingy: Selected Major and Trace Elements	214
8.10.1.	Introduction	214
8.10.2.	Data	215
8.10.3.	Nickel	217
8.10.4.	Copper	218
8.10.5.	Chromium	218

8.10.6.	Aluminium	219
8.10.7.	Summary of Ni, Cu, Cr and Al distribution in the Kingy Ridge Ultramafic and Extra Ultramafic	219
8.10.8.	Summary of Ni, Cu, Cr and Al distribution in the Lensoid Ultramafics	220
8.10.9.	Summary of Ni, Cu, Cr and Al distribution in the Isolated Gabbro	220
8.11.	Kingy: Pt and Pd distribution	220
8.11.1.	Comparison of the geochemistry of the soil versus rock samples	223
8.12.	Kingy: Discussion	223
8.12.1.	The locations of the highest Ni and Cu values in fresher rocks	223
8.12.2.	Locations of highest Cu and Cr values in fresher rocks	223
8.12.3.	Zonation of Ni and Cr in altered rocks from the Kingy Ridge Ultramafic	224
8.12.4.	Uneven Cu and Al distribution in the altered rocks from the Kingy Ridge Ultramafic	225
8.12.5.	Trace element distribution in the altered rocks from the Lensoid Ultramafics	225
8.12.6.	Genesis of Pt and Pd in fresher rocks	226
8.12.7.	Genesis of Pt and Pd in altered rocks	226
8.13.	Kingy: Conclusions	227
8.14.	Maps of elemental distribution in the Kingy areas	229
8.15.	Daleti, Ankori, Tulu Kapi and Keley: Selected Major and Trace Elements	230
8.15.1.	Introduction	230
8.15.2.	Data	232
8.15.3.	Nickel	235
8.15.4.	Copper	235
8.15.5.	Chromium	236
8.15.6.	Aluminium	236
8.15.7.	Summary of Ni, Cu, Cr and Al values in the Daleti Ultramafic	237
8.15.8.	Summary of Ni, Cu, Cr and Al values at Ankori and the Lensoid Ultramafics	237
8.15.9.	Summary of Ni, Cu, Cr and Al values in the Shear Zones	237
8.15.10.	Summary of Ni, Cu, Cr and Al values in the southwestern Shear Zones and gabbro	238
8.16.	Daleti, Ankori, Tulu Kapi and Keley: Pt and Pd distribution	238
8.17.	Daleti, Ankori, Tulu Kapi and Keley: Discussion	241
8.17.1.	The highest Ni and Cu values in the fresher rocks from the Daleti Ultramafic	241
8.17.2.	Zonation in Cr values in the fresher rocks from the Daleti Ultramafic	242
8.17.3.	Trace element distribution in Shear Zones	242
8.17.4.	Copper values in altered rocks	242
8.17.5.	High Ni values within the ultramafic complexes	243
8.17.6.	Genesis of Pt and Pd in fresher rocks from the Daleti Ultramafic	243
8.17.7.	Genesis of Pt and Pd in altered rocks	244
8.18.	Daleti, Ankori, Tulu Kapi and Keley: Conclusions	245
8.19.	Maps of elemental distribution in the Daleti, Ankori, Tulu Kapi and Keley areas	247
8.20.	Yubdo, Sodu and Andu: Selected Major and Trace Elements	248
8.20.1.	Introduction	248
8.20.2.	Data	249
8.20.3.	Nickel	251
8.20.4.	Copper	251
8.20.5.	Chromium	252
8.20.6.	Aluminium	253
8.20.7.	Summary of the Ni, Cu, Cr and Al values from the Yubdo Main Intrusion	253
8.21.	Yubdo, Sodu and Andu: Pt and Pd distribution	254
8.22.	Yubdo, Sodu and Andu: Discussion	256
8.22.1.	The locations of the highest Ni and Cu values in the fresher rocks from the Main Yubdo Ultramafic	256
8.22.2.	Locations of highest Cu and Cr values in fresher rocks	258
8.22.3.	Zonation of Cr values the altered rocks from the Main Yubdo Ultramafic	258
8.22.4.	The locations of high Ni and Cu values in altered rocks from the Main Yubdo Ultramafic	259
8.22.5.	Genesis of Pt and Pd in fresher rocks	259
8.22.6.	Genesis of Pt and Pd in altered rocks	260
8.23.	Yubdo, Sodu and Andu: Conclusions	261
8.24.	Maps of elemental distribution in the Yubdo, Andu and Sodu areas	262

8.25.	Pt and Pd prospectivity and ore forming processes	263
8.25.1.	Magmatic ore forming processes	263
8.25.2.	Post-magmatic ore forming processes	265
8.25.3.	Prospectivity	266
9	**Results: Spinel Geochemistry**	**267**
9.1.	Introduction	267
9.2.	Methods	268
9.2.1.	Sample Preparation	268
9.2.2.	Energy Dispersive X-ray Analysis	268
9.3.	Fe-Valency Estimation	269
9.3.1.	Introduction	269
9.3.2.	Method	270
9.3.3.	The Analyses	271
9.4.	Alteration Assessment	272
9.4.1.	Introduction	272
9.4.2.	Method	274
9.4.3.	Results	275
9.4.4.	Discussion	277
9.5.	Tulu Dimtu: Spinel Geochemistry	277
9.5.1.	Introduction	277
9.5.2.	Data	278
9.5.3.	Fe2+# (Fe2+/(Mg+Fe2+))	280
9.5.4.	Cr# (Cr / (Cr+Al))	280
9.5.5.	TiO2	280
9.5.6.	Fe3+# (Fe3+ / (Fe3+ + Al2+ + Cr3+ + V3+))	281
9.5.7.	Minor Elements (Si, Co, and Zn)	281
9.5.8.	Summary of the spinel Geochemistry in the Tulu Dimtu area	281
9.6.	Discussion	282
9.6.1.	Alteration	282
9.6.2.	Magmatic effects	284
9.6.3.	Comparison with Alaskan-type intrusions and Ophiolite complexes	285
9.7.	Conclusions	287
9.7.1.	Pull-out section	289
9.8.	Kingy: Spinel Geochemistry	290
9.8.1.	Introduction	290
9.8.2.	Data	290
9.8.3.	Fe2+# (Fe2+/(Mg+Fe2+))	291
9.8.4.	Cr / (Cr+Al)	291
9.8.5.	TiO2	291
9.8.6.	Fe3+# / (Fe3+ + Al2+ + Cr3+ + V3+)	291
9.8.7.	Minor Elements (Na, Si, and Zn)	292
9.8.8.	Summary of Spinel Geochemistry in the Kingy area	292
9.9.	Discussion	292
9.9.1.	Alteration	292
9.9.2.	Magmatic Effects	293
9.9.3.	Comparison with Alaskan-type intrusions and ophiolite complexes	294
9.10.	Conclusions	294
9.11.	Pull-out section	295
9.12.	Daleti, Ankori, Tulu Kapi and Keley: Spinel Geochemistry	296
9.12.1.	Introduction	296
9.12.2.	Data	296
9.12.3.	Fe2+# (Fe2+/(Mg+Fe2+))	299
9.12.4.	Cr# (Cr / (Cr+Al))	299
9.12.5.	TiO2	299
9.12.6.	Fe3+# (Fe3+ / (Fe3+ + Al2+ + Cr3+ + V3+))	299
9.12.7.	Minor Elements (Co and Zn)	300
9.12.8.	Summary of Spinel Geochemistry in the Daleti Ultramafic	300
9.12.9.	Summary of Spinel Geochemistry in the Ankori Ultramafic	301
9.13.	Discussion	301
9.13.1.	Alteration	301

9.13.2.	Magmatic Effects	303
9.13.3.	Comparison with Alaskan-type intrusions and ophiolite complexes	304
9.14.	Conclusions	305
9.14.1.	Pull-out section	306
9.15.	Yubdo, Sodu and Andu: Spinel Geochemistry	307
9.15.1.	Introduction	307
9.15.2.	Data	307
9.15.3.	Fe2+# (Fe2+/(Mg+Fe2+))	308
9.15.4.	Cr# (Cr / (Cr+Al))	308
9.15.5.	TiO2	309
9.15.6.	Fe3+# (Fe3+ / (Fe3+ + Al2+ + Cr3+ + V3+))	309
9.15.7.	Minor Elements (SiO2, CoO and ZnO)	309
9.15.8.	Summary of Spinel Geochemistry in the Main Yubdo Intrusion	309
9.16.	Discussion	310
9.16.1.	Alteration	310
9.16.2.	Magmatic Effects	311
9.16.3.	Comparison with Alaskan-type intrusions and Ophiolites	311
9.17.	Conclusions	312
9.17.1.	Pull-out section	313
9.18.	Summary of Spinel Geochemistry in the WES	314
9.18.1.	Alteration	316
9.18.2.	Magmatic Effects	316
9.18.3.	Comparison with Alaskan-type intrusions and ophiolite complexes	317
10	**Summary**	**318**
10.1.	Introduction	318
10.2.	Tulu Dimtu	319
10.3.	Kingy	320
10.4.	Daleti, Ankori, Tulu Kapi and Keley	321
10.5.	Yubdo, Andu and Sodu	322
10.6.	Exploration Summary	324
10.7.	Comparison with published work on the tectonic setting of the complexes	325
11	**References**	**327**
12	**Appendix**	**335**
12.1.	Repeat Analyses	335
12.2.	Analysis of Standards	336

List of Figures

Figure	Caption	Page
Figure 1.1	A geological map of the WES. (Johnson et al., 2004).	2
Figure 1.2	A map of the four field areas of this thesis, showing the largest ultramafic complexes and major roads and settlements.	3
Figure 1.3	An aerial photograph of the opencast workings of the laterite in the Yubdo area (within the black lines) in 1957. The bright line is the course of the Birbir river.	6
Figure 2.1	The "ophiolite belts" of northeast Africa (modified after Berhe, 1990).	10
Figure 2.2	The average chondrite normalized Ru, Rh, Pt and Pd analyses for dunite from the Tulu Dimtu area (Sighinolfi, 1993).	15
Figure 2.3	Schematic diagrams of the mafic and ultramafic units of the Josephiene Ophiolite and Tulameen Alaskan-type intrusion showing similar zoned outcrop patterns (modified from Findlay, 1969 and Harper, 1984).	20
Figure 2.4	The typical REE geochemistry of Alaskan-type intrusions compared to Oman ophiolite (Johan, 2002; Lippard et al., 1986).	24
Figure 2.5	A comparison of the chrondrite normalized PGE abundances for Alaskan Type intrusions and the Troodos ophiolite. (After Johan, 2002 and Prichard and Lord, 1990).	26
Figure 3.1	A photograph of a dunite sample under crossed polars. The lower edge of the image is 120μm in length.	31
Figure 3.2	A photograph of a dunite sample under crossed polars. The lower edge of the image is 120μm in length.	31
Figure 3.3	A photograph of a dunite sample under crossed polars. The lower edge of the image is 120μm in length.	32
Figure 3.4	A photograph of a dunite sample under crossed polars. The lower edge of the image is 120μm in length.	32
Figure 3.5	A photograph of a dunite sample under crossed polars. The lower edge of the image is 120μm in length.	32
Figure 3.6	A photograph of a clinopyroxenite sample from Kingy area under crossed polars.	33
Figure 3.7	A photograph of a clinopyroxenite sample from the Kingy area under crossed polars.	33
Figure 3.8	A photograph of a birbirite sample from the Tulu Dimtu Main Intrusion area.	33
Figure 3.9	SEM photomicrographs of a disseminated spinel (white colour, high mean atomic number) in a clinopyroxenite sample (DTR-019-02). The spinel shows a pull apart tecture and is hosted by a gangue of fibrous amphibole.	36
Figure 3.10	SEM photomicrographs of disseminated spinels (white colour, high mean atomic number) hosted by olivine in sample DTR-057-02. Some spinels are subhedral and zoned.	37
Figure 3.11	SEM photomicrographs of disseminated spinels (white colour, high mean atomic number) hosted by partially serpentinised olvines from sample D19. Many spinels show pull-apart textures.	37
Figure 3.12	SEM photomicrographs of anhedral spinels (white colour, high mean atomic number) from sample Y28. The spinels occur in serpentine filled cracks between fresh clinopyroxenes minerals.	38
Figure 3.13	SEM photomicrographs of disseminated spinels (white colour, high mean atomic number) partially serpentinised olivines from sample Y30.	38

Figure 3.14	SEM photomicrographs of an altered bornite (white colour, high mean atomic number in the centre of image) in the altered rim of a Cr-spinel (grey colour), hosted by serpentine (black). This image has been taken from sample TDR19/01 which is located on the southern flank of the Tulu Dimtu Main Intrusion.	40
Figure 3.15	SEM photomicrographs of an anhedral glaucodot split into three parts (white colour, high mean atomic number) hosted by serpentine. The sulphide mineral on the left hosts a Ni-As-bearing magnetite inclusion. This image has been taken from sample DTR-019-02 from the Tulu Dimtu Lensoid Ultramafics.	41
Figure 3.16	SEM photomicrographs of an anhedral chalcopyrite mineral (white colour, high mean atomic number) hosted by quartz in an extremely altered olivine-clinopyroxenite sample. This image has been taken from sample KTR-049-02 from the Kingy Ridge Ultramafic.	41
Figure 3.17	SEM photomicrographs of several anhedral barite crystals (white specs, high mean atomic number) on the edge of larger partially serpentinised olivine minerals. There are many anhedral Fe-rich spinels. This image has been taken from sample DR22/01 from the Daleti Ultramafic.	42
Figure 3.18	SEM photomicrographs of a Ni-sulphide mineral (white spec, high mean atomic number) in the altered rim of a zoned spinel hosted by serpentine (black). In addition to the subhedral spinels (centre of image) there are many fine anhedral Fe-rich spinels which sometimes form schlieren. This image has been taken from sample AYR-016-01 from the northwestern flank of the Main Yubdo Intrusion.	43
Figure 3.19	An SEM back-scattered electron image photomicrographs of a subhedral Pt-Fe alloy (white colour, high mean atomic number) in a Cr-spinel hosted by serpentine. This image has been taken from sample AYR-016-01 from the northwestern edge of the Main Yubdo Intrusion.	45
Figure 3.20	An SEM back-scattered electron image photomicrographs of an anhedral Os-Ir alloy (white colour, high mean atomic number) hosted by serpentine. This image has been taken from sample KYR-019-01 located the northwestern flank of the Main Yubdo Intrusion.	46
Figure 3.21	An SEM back-scattered electron image photomicrographs of a subhedral Ir-Os alloy (white colour, high mean atomic number) within a Cr-spinel hosted by partially serpentinised olivine. This image has been taken from sample AYR-016-01 located on the far western flank of Main Yubdo Intrusion.	47
Figure 4.1	A photograph of a barren ridge above the Daleti Ultramafic. The ridge is almost devoid of vegetation when compared to the foreground. Furthermore, the houses to the right indicate the presence of fertile subsistence farmland.	49
Figure 4.2	A typical aerial photograph with the data block enlarged.	52
Figure 4.3	Principle components of a single-lens mapping camera (after Lillesand and Kiefer, 2000)	53
Figure 4.4	A section from an aerial photograph showing the boundary between a coarse dendritic (top left) and fine dendritic (bottom right) drainage patterns.	58
Figure 4.5	The six basic drainage patterns, after Lillesand and Keifer (2000)	59
Figure 4.6	Illustrations of drainage texture. A: coarse-textured and B: fine-textured, after Lillesand and Keifer (2000).	60
Figure 4.7	A section from an aerial photograph showing the boundary	60

	between areas with round-bottomed gullies (left) and v-shaped gullies (right).	
Figure 4.8	A section from an aerial photograph showing a ridge (center) and smaller hills around the outside.	62
Figure 4.9	A section from an aerial photograph showing the boundaries between bright and dark image tones. The darkest mottled texture is tree cover, however the dark tone of the soil can be observed between trees.	63
Figure 4.10	A section from an aerial photograph showing the boundary between cultivated land (bottom and top) and non-cultivated land (center). Subsistence farms in Ethiopia typically cultivate fields of no larger than 500m in width. These appear on aerial photographs as a "patchwork" texture.	64
Figure 4.11	A map of photmorphic regions for the Tulu Dimtu area. White lines indicate the course of the major rivers. Inset is a representative aerial photograph showing the main ultramafic formation.	68
Figure 4.12	A map of photmorphic regions for the Kingy area. White lines indicate the course of the major rivers. Inset is a representative aerial photograph showing the main ultramafic formation.	69
Figure 4.13	A map of photmorphic regions for the Daleti, Ankori, Tulu Kapi and Keley areas. White lines indicate the course of the major rivers. Inset is a representative aerial photograph showing the main ultramafic formation.	70
Figure 4.14	A map of photmorphic regions for the Yubdo, Andu and Sodu areas. White lines indicate the course of the major rivers. Inset is a representative aerial photograph showing the main ultramafic formation.	71
Figure 5.1	The geological map of the Tulu Dimtu area. Black lines indicate the course of the major rivers.	74
Figure 5.2	The geological map of the Kingy area. Black lines indicate the course of the major rivers.	76
Figure 5.3	The geological map of the Daleti, Ankori, Tulu Kapi and Keley areas. Black lines indicate the course of the major rivers.	78
Figure 5.4	The geological map of the Yubdo, Andu and Sodu areas. Black lines indicate the course of the major rivers.	80
Figure 6.1	The magnetometer sensor set up aligned to N and attached to a tree.	84
Figure 6.2	The survey point locations for the ground magnetic survey of the Main Yubdo Intrusion overlaid onto the geological map (see chapter 5).	85
Figure 6.3	The magnetic field strength at the base station over a 24 hour period (30^{th} to the 31^{st} of May 2002)	86
Figure 6.4	A 3D surface to illustrate the diurnally corrected magnetic field strength for the horizontal sensor orientation test.	89
Figure 6.5	A 3D surface to illustrate the diurnally corrected magnetic field strength for the vertical sensor orientation test.	90
Figure 6.6	Maps of the diurnally corrected magnetic field strength (Log10). The different colour schemes are used to highlight different aspects of the data,	92
Figure 6.7	Maps of the diurnally corrected magnetic field strength (Log10) with different orientations. The different colour schemes are used to highlight different aspects of the data.	93
Figure 6.8	The interpretation map of the magnetic field overlaid onto the geological map produced in chapter 5.	94
Figure 6.9	Maps of the diurnally corrected magnetic field strength (nT) over an area near to Yubdo School.	96
Figure 6.10	A map of the diurnally corrected magnetic field strength	101

	(Log10) displayed as a 3D surface.	
Figure 6.11	An interpretation map of the features of the magnetic field over the Main Yubdo Intrusion.	101
Figure 6.12	Schematic map of the model proposed to explain the nature of the magnetic field over the Main Yubdo Intrusion.	101
Figure 7.1	A schematic diagram of the stucture of the lateritic soils in the WES.	103
Figure 7.2	The interface between the pristine (top left) and weathered bedrock (bottom right) in the opencast workings near Yubdo. The left of the photograph shows a quartz stockwork which resists weathering to a greater degree than the surrounding serpentinite.	103
Figure 7.3	A photograph indicating the position of the saprolite layer (white arrow). Variations in the thickness of the laterite as seen in the quarry near the summit at Daleti. The light coloured rock at the base is the pristine serpentinite, the red material at the top is the laterite layer and between these is the yellow saprolite layer.	104
Figure 7.4	The extensive laterite layer in the workings at Yubdo. The laterite seen here is over 15m in thickness and the base of the horizon (the saprolite) is indicated by the arrow.	105
Figure 7.5	The distribution of soil samples in the Tulu Dimtu area.	109
Figure 7.6	Arithmetic and Log_{10} transformed histograms of Ni in the soils of the Tulu Dimtu area. The grey lines indicate the class-boundaries used in figure 7.12 .	114
Figure 7.7	Arithmetic and Log_{10} transformed histograms of Cu in the soils of the Tulu Dimtu area. The grey lines indicate the class-boundaries used in figure 7.12 .	115
Figure 7.8	Arithmetic and Log_{10} transformed histograms of Cr in the soils of the Tulu Dimtu area. The grey lines indicate the class-boundaries used in figure 7.12 .	116
Figure 7.9	Arithmetic and Log_{10} transformed histograms of Al in the soils of the Tulu Dimtu area. The grey lines indicate the class-boundaries used in figure 7.12 .	117
Figure 7.10	Arithmetic and Log_{10} transformed histograms of Pt in the soils of the Tulu Dimtu area. The grey lines indicate the class-boundaries used in figure c.	118
Figure 7.11	Arithmetic and Log_{10} transformed histograms of Pd in the soils of the Tulu Dimtu area. The grey lines indicate the class-boundaries used in figure 7.12.	119
Figure 7.12 A-F	Six geological maps of the Tulu Dimtu area with symbols representing Ni, Cu, Cr, Al, Pt and Pd values in soil samples overlaid.	123
Figure 7.13	The distribution of soil samples in the Kingy area.	124
Figure 7.14	Arithmetic and Log_{10} transformed histograms of Ni in the soils of the Kingy area. The grey lines indicate the class-boundaries used in figure 6.20.	129
Figure 7.15	Arithmetic and Log_{10} transformed histograms of Cu in the soils of the Kingy area. The grey lines indicate the class-boundaries used in figure 6.20.	130
Figure 7.16	Arithmetic and Log_{10} transformed histograms of Cr in the soils of the Kingy area. The grey lines indicate the class-boundaries used in figure 6.20.	131
Figure 7.17	Arithmetic and Log_{10} transformed histograms of Al in the soils of the Kingy area. The grey lines indicate the class-boundaries used in figure 6.20.	132
Figure 7.18	Arithmetic and Log_{10} transformed histograms of Pt in the soils of the Kingy area. The grey lines indicate the class-boundaries used in figure 6.20.	133
Figure 7.19	Arithmetic and Log_{10} transformed histograms of Pd in the	134

	soils of the Kingy area. The grey lines indicate the class-boundaries used in figure 6.20.	
Figure 7.20 A-F	Six geological maps of the Kingy area with symbols representing Ni, Cu, Cr, Al, Pt and Pd values in soil samples overlaid.	138
Figure 7.21	The distribution of soil samples in the Daleti, Ankori, Tulu Kapi and Keley areas.	139
Figure 7.22	Arithmetic and Log_{10} transformed histograms of Ni in the soils of the Daleti, Ankori, Tulu Kapi and Keley areas. The grey lines indicate the class-boundaries used in figure 6.28.	144
Figure 7.23	Arithmetic and Log_{10} transformed histograms of Cu in the soils of the Daleti, Ankori, Tulu Kapi and Keley areas. The grey lines indicate the class-boundaries used in figure 6.28.	145
Figure 7.24	Arithmetic and Log_{10} transformed histograms of Cr in the soils of the Daleti, Ankori, Tulu Kapi and Keley areas. The grey lines indicate the class-boundaries used in figure 6.28.	146
Figure 7.25	Arithmetic and Log_{10} transformed histograms of Al in the soils of the Daleti, Ankori, Tulu Kapi and Keley areas. The grey lines indicate the class-boundaries used in figure 6.28.	147
Figure 7.26	Arithmetic and Log_{10} transformed histograms of Pt in the soils of the Daleti, Ankori, Tulu Kapi and Keley areas. The grey lines indicate the class-boundaries used in figure 6.28.	148
Figure 7.27	Arithmetic and Log_{10} transformed histograms of Pd in the soils of the Daleti, Ankori, Tulu Kapi and Keley areas. The grey lines indicate the class-boundaries used in figure 6.28.	149
Figure 7.28 A-F	Six geological maps of the Daleti, Ankori, Tulu Kapi and Keley areas with symbols representing Ni, Cu, Cr, Al, Pt and Pd values in soil samples overlaid.	152
Figure 7.29	The distribution of soil samples in the Yubdo, Andu and Sodu areas.	153
Figure 7.30	Arithmetic and Log_{10} transformed histograms of Ni in the soils of the Yubdo, Andu and Sodu areas. The grey lines indicate the class-boundaries used in figure 6.34.	158
Figure 7.31	Arithmetic and Log_{10} transformed histograms of Cu in the soils of the Yubdo, Andu and Sodu areas. The grey lines indicate the class-boundaries used in figure 6.34.	159
Figure 7.32	Arithmetic and Log_{10} transformed histograms of Cr in the soils of the Yubdo, Andu and Sodu areas. The grey lines indicate the class-boundaries used in figure 6.34.	160
Figure 7.33	Arithmetic and Log_{10} transformed histograms of Al in the soils of the Yubdo, Andu and Sodu areas. The grey lines indicate the class-boundaries used in figure 6.34.	161
Figure 7.34	Arithmetic and Log_{10} transformed histograms of Pt in the soils of the Yubdo, Andu and Sodu areas. The grey lines indicate the class-boundaries used in figure 6.34.	162
Figure 7.35	Arithmetic and Log_{10} transformed histograms of Pd in the soils of the Yubdo, Andu and Sodu areas. The grey lines indicate the class-boundaries used in figure 6.34.	162
Figure 7.36 A-F	Six geological maps of the Yubdo, Andu and Sodu areas with symbols representing Ni, Cu, Cr, Al, Pt and Pd values in soil samples overlaid.	166
Figure 7.37	A graph comparing the distribution of Ni in each of the four areas studied. For histograms further illustrating the data see individual sections.	167
Figure 7.38	A graph comparing the distribution of Cu in each of the four areas studied. For histograms further illustrating the data see individual sections.	168
Figure 7.39	A graph comparing the distribution of Cr in each of the four areas studied. For histograms further illustrating the data see individual sections.	168

Figure 7.40	A graph comparing the distribution of Al in each of the four areas studied. For histograms further illustrating the data see individual sections.	169
Figure 7.41	A graph comparing the distribution of Pt in each of the four areas studied. For histograms further illustrating the data see individual sections.	169
Figure 7.42	A graph comparing the distribution of Pd in each of the four areas studied. For histograms further illustrating the data see individual sections.	169
Figure 8.1	A graph of the cumulative percent (by rank) of the Mg values of the dunite samples from the Tulu Dimtu area.	181
Figure 8.2	The distribution of rock samples within the Tulu Dimtu area.	184
Figure 8.3	Graphs of Ni, Cu, Cr and Al versus Pt and Pd in the fresher rocks of the Tulu Dimtu area. The key to symbols in the top right corner.	193
Figure 8.4 A-F	Six geological maps of the Tulu Dimtu area with symbols representing Ni, Cu, Cr, Al, Pt and Pd values in rock samples overlaid.	213
Figure 8.5	The distribution of rock samples within the Kingy area.	214
Figure 8.6	Graphs of Ni, Cu, Cr and Al versus Pt in the fresher rocks from the Kingy area. No Pd has been detected in the Kingy area.	222
Figure 8.7 A-F	Six geological maps of the Kingy area with symbols representing Ni, Cu, Cr, Al, Pt and Pd values in rock samples overlaid.	229
Figure 8.8	The distribution of rock samples within the Daleti area, with a map of the Daleti Ultramafic inset.	231
Figure 8.9	Graphs of Ni, Cu, Cr and Al versus Pt in the fresher dunites from the Daleti Ultramafic.	240
Figure 8.10 A-F	Six geological maps of the Daleti, Ankori, Tulu Kapi and Keley areas with symbols representing Ni, Cu, Cr, Al, Pt and Pd values in rock samples overlaid.	247
Figure 8.11	The distribution of rock samples within the Yubdo area.	248
Figure 8.12	Graphs of Ni, Cu, Cr and Al versus Pt in the fresher rocks from the Main Yubdo Ultramafic.	255
Figure 8.13 A-F	Six geological maps of the Yubdo, Andu and Sodu areas with symbols representing Ni, Cu, Cr, Al, Pt and Pd values in rock samples overlaid.	262
Figure 9.1	SEM backscattered electron image of a zoned spinel mineral from sample KYC-007-01.	273
Figure 9.2	The concept of an alteration rim around a 3-dimensional spinel.	274
Figure 9.3	Graphs showing the effect of alteration on the spinels from the WES.	276
Figure 9.4	The differences between magamtic trends and alteration trends on a graph of spinel Fe^{2+}# versus Cr# values.	288
Figure 9.5 A-G	Graphs and map presenting the spinel geochemistry of the Tulu Dimtu area.	289
Figure 9.6 A-G	Graphs and map presenting the spinel geochemistry of the Kingy area.	295
Figure 9.7 A-G	Graphs and map presenting the spinel geochemistry of the Daleti, Ankori, Tulu Kapi and Keley areas. A larger scale map of the Daleti Ultramafic is provided.	306
Figure 9.8 A-G	Graphs and map presenting the spinel geochemistry of the Yubdo, Andu and Sodu areas. A larger scale map of the Daleti Ultramafic is provided.	313
Figure 9.9	The Cr# and Fe^{2+}# values of the spinels of the five ultramafic complexes of the WES compared to Alaskan-type intrusions and ophiolites.	315

List of Tables

Figure	Caption	Page
Table 2.1	Pt/Pd ratios for dunites in Alaskan-type intrusions and dunite pods in ophiolite complexes.	27
Table 4.1	The details of the aerial photographs.	51
Table 4.2	Relief Displacements of Yubdo Village and Sodu Ridge.	51
Table 4.3	The mapping parameters used in the study.	56
Table 4.4	Gully cross-sections and their related textures.	61
Table 4.5	A table of the photomorphic regions of the WES.	67
Table 6.1	A table of magnetic susceptibility values in order of decreasing susceptibility (after Robinson and Coruh, 1988).	98
Table 7.1	A summary of the Pt values in the soil samples from Tulu Dimtu.	110
Table 7.2	A summary of the Pd values in the soil samples from Tulu Dimtu.	110
Table 7.3	A summary of the Au values in the soil samples from Tulu Dimtu.	111
Table 7.4	A summary of the Ni values in the soil samples from Tulu Dimtu.	111
Table 7.5	A summary of the Cu values in the soil samples from Tulu Dimtu.	112
Table 7.6	A summary of the Cr values in the soil samples from Tulu Dimtu.	112
Table 7.7	A summary of the Al values in the soil samples from Tulu Dimtu.	113
Table 7.8	A summary of the Pt values in the soil samples from Kingy.	125
Table 7.9	A summary of the Pd values in the soil samples from Kingy.	125
Table 7.10	A summary of the Au values in the soil samples from Kingy.	126
Table 7.11	A summary of the Ni values in the soil samples from Kingy.	126
Table 7.12	A summary of the Cu values in the soil samples from Kingy.	127
Table 7.13	A summary of the Cr values in the soil samples from Kingy.	127
Table 7.14	A summary of the Al values in the soil samples from Kingy.	128
Table 7.15	A summary of the Pt values in the soil samples from Daleti, Ankoiri, Tulu Kapi and Keley.	140
Table 7.16	A summary of the Pd values in the soil samples from Daleti, Ankoiri, Tulu Kapi and Keley.	140
Table 7.17	A summary of the Au values in the soil samples from Daleti, Ankoiri, Tulu Kapi and Keley.	141
Table 7.18	A summary of the Ni values in the soil samples from Daleti, Ankoiri, Tulu Kapi and Keley.	141
Table 7.19	A summary of the Cu values in the soil samples from Daleti, Ankoiri, Tulu Kapi and Keley.	142
Table 7.20	A summary of the Cr values in the soil samples from Daleti, Ankoiri, Tulu Kapi and Keley.	142
Table 7.21	A summary of the Al values in the soil samples from Daleti, Ankoiri, Tulu Kapi and Keley.	143
Table 7.22	A summary of the Pt values in the soil samples from Yubdo, Andu and Sodu.	154
Table 7.23	A summary of the Pd values in the soil samples from Yubdo, Andu and Sodu.	154
Table 7.24	A summary of the Au values in the soil samples from Yubdo, Andu and Sodu.	155
Table 7.25	A summary of the Ni values in the soil samples from Yubdo, Andu and Sodu.	155
Table 7.26	A summary of the Cu values in the soil samples from Yubdo, Andu and Sodu.	156
Table 7.27	A summary of the Cr values in the soil samples from Yubdo, Andu and Sodu.	156

Table 7.28	A summary of the Al values in the soil samples from Yubdo, Andu and Sodu.	157
Table 7.29	The maximum Pt and Pd values found in the soils above the ultramafic complexes of the WES.	171
Table 8.1	Summary statistics of 41 analyses of the standard sample SARM7b.	174
Table 8.2	The weight percent of minerals dissolved by aqua regia (Chruch et al., 1987).	176
Table 8.3	Percentages of various metals leached by aqua regia from olivine and spinel relative to total recovery calculated from an HF-HNO3-NClO4 digestion (Chruch et al., 1987).	176
Table 8.4	A table of 48 analyses of the OMAC laboratories in-house standard with a summary of the ranges of values obtained and a measurement of precision.	177
Table 8.5	Typical values of Mg for selected fresh ultramafic lithotypes.	179
Table 8.6	Table 6.2: The ranges of Mg values used to define the fresher rock samples.	180
Table 8.7	The Mg values for the dunite samples in the Tulu Dimtu area before classification into fresher and altered.	181
Table 8.8	The numbers of samples from the different ultramafic complexes of the WES.	183
Table 8.9	A summary of the numbers and types of samples used in the four geographic areas in this study.	183
Table 8.10	A summary of the rock samples from the Tulu Dimtu area.	185
Table 8.11	Mg, Ni, Cu, Cr, Al, Pt and Pd values for the fresher samples.	185
Table 8.12	Mg, Ni, Cu, Cr, Al, Pt and Pd values for the altered samples collected from the Tulu Dimtu area.	187
Table 8.13	A summary of Ni, Cu, Cr and Al values in the dunite samples of highest Pt and Pd grade of the fresher rocks.	192
Table 8.14	Partition co-efficients of Ni between olivine and melt or host rock type.	196
Table 8.15	Partition co-efficients of Cr between olivine and melt or host rock type.	197
Table 8.16	Partition co-efficients of Cr between spinel or magnetite and melt or host rock.	197
Table 8.17	The range of Ni values in analyses of olivine minerals.	203
Table 8.18	A summary of the rock samples from the Kingy area.	215
Table 8.19	Mg, Ni, Cu, Cr, Al, Pt and Pd values for the fresher samples collected from the Kingy area.	215
Table 8.20	Mg, Ni, Cu, Cr, Al, Pt and Pd values for the altered samples collected from the Kingy area.	217
Table 8.21	A summary of Ni, Cu, Cr and Al values in the dunite samples with the highest Pt and Pd grade from the fresher rocks of the Kingy area.	221
Table 8.22	A summary of the rock samples from the Daleti, Ankori, Tulu Kapi and Keley areas.	232
Table 8.23	Mg, Ni, Cu, Cr, Al, Pt and Pd values for the fresher samples collected from the Daleti, Ankori, Tulu Kapi and Keley areas.	232
Table 8.24	Mg, Ni, Cu, Cr, Al, Pt and Pd values for the altered samples collected from the Daleti, Ankori, Tulu Kapi and Keley areas.	234
Table 8.25	A summary of Ni, Cu, Cr and Al values in the dunites of highest Pt and Pd grade from the fresher rocks within the Daleti Ultramafic.	239
Table 8.26	A summary of the rock samples from the Yubdo, Andu and Sodu areas.	249
Table 8.27	Mg, Ni, Cu, Cr, Al, Pt and Pd values for the fresher samples collected from the Yubdo, Andu and Sodu areas.	249
Table 8.28	Mg, Ni, Cu, Cr, Al, Pt and Pd values for the altered samples collected from the Yubdo, Andu and Sodu areas.	251
Table 8.29	A summary of Ni, Cu, Cr and Al values in the fresher samples	254

	from the Main Yubdo Ultramafic.	
Table 8.30	Partition co-efficients of Cu between olivine and clinopyroxene and melt or host rock type.	257
Table 8.31	The maximum Pt and Pd values found in the fresher rocks of the ultramafic complexes of the WES.	262
Table 8.32	The maximum Pt and Pd values found in the altered rocks from the ultramafic complexes of the WES.	265
Table 9.1	The molecules used in the estimation of Fe valency with the minerals they represent.	270
Table 9.2	A worked example of the method used to calculate Fe^{2+} and Fe^{3+}.	271
Table 9.3	The numbers of analyses at various stages of manipulation of the data.	272
Table 9.4	The numbers of analyses in the various ultramafic formations of the WES.	272
Table 9.5	The results of analyses of the cores and the zones immediately surrounding the cores of zoned spinels in sample KYC-007-01.	275
Table 9.6	The geochemistry of the spinels analysed from the Tulu Dimtu area in wt %.	280
Table 9.7	A table of the minimum Cr# values for spinel analyses from dunite and olivine-clinopyroxenite samples.	284
Table 9.8	The geochemistry of the spinels analysed from the Kingy area in wt %.	291
Table 9.9	The geochemistry of the spinels analysed from the Daleti, Ankori, Tulu Kapi and Keley areas in wt %.	298
Table 9.10	The minimum Cr# values for spinel analyses from the samples of the Daleti Ultramafic.	303
Table 9.11	The geochemistry of the spinels analysed from the Yubdo, Sodu and Andu areas in wt %.	308
Table 9.12	A summary of the rocks which host acceptable spinel analyses for each geographic area.	314
Table 12.1	A comparison of Pb Fire Assay results from analyses performed on the same samples from OMAC and Genalysis	335
Table 12.2	A table detailing the repeat analyses performed by OMAC during the course of the sample analysis.	335
Table 12.3	A table of analysis of the standard sample SARM7b with a summary of the ranges of values obtained and a measurement of precision.	336
Table 12.4	A table of analysis of the OMAC laboratories in-house standard with a summary of the ranges of values obtained and a measurement of precision.	337

1. Introduction

1.1. Introduction

The Western Ethiopian Shield (WES) is 500 km west of the capital Addis Ababa (see figure 1.2). It is a Neoproterozoic ancient mining district (United Nations, 1971; Jelenc, 1966) and the alluvial and eluvial deposits around the Yubdo ultramafic complex have been mined for Pt-Fe alloys and Au since 1926 (Mogessie and Belete, 2000). Yubdo forms part of a line of ultramafic complexes located along a NNE-SSW trending structure. The ultramafic complexes from the WES are (from north to south) Tulu Dimtu, Kingy, Daleti, Ankori and Yubdo (see figure 1.2). None of these bodies are mined on a commercial scale but Pt-Fe alloys are known in the surrounding placers. Most of the WES is only accessible on foot. The rocks are covered by a thick laterite which is frequently over 15m in thickness and exposure is generally less than 5%.

Ethiopia is covered by extensive Quaternary and Tertiary flood basalts. In some areas, the older rocks can be observed as inliers between these sequences (Mohr, 1983). The WES is one of such inliers and has been correlated northwards to join the Arabian Nubian Shield and southwards to the Mozambique belt, all of which form part of the East African Orogen. Johnson et al. (2004) believe that the WES records a history of crustal formation and deformation of around 500Ma in duration, this may have begun with a rifting event starting at around 900Ma (Stern, 1994). The eastern and western flanks of the WES are orthogneissic and they surround a central zone of volcano-sediments and ultramafics (Johnson et al., 2004). These ultramafic bodies are the subject of this thesis (see figure 1.2).

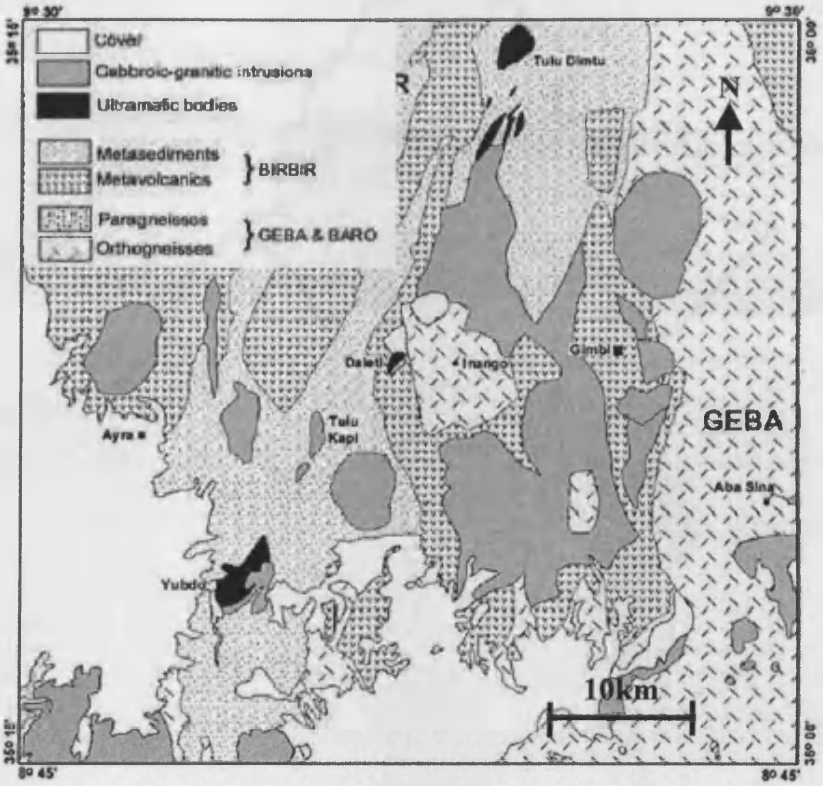

Figure 1.1: A geological map of the WES. (Johnson et al., 2004).

The southernmost ultramafic body (Yubdo) has been the subject of several publications (for a review see Mogessie et al., 1999). It is concentrically zoned with dunite at the core and clinopyroxenite on the outside (Kazmin and Demessie, 1971). The northernmost complex is also the subject of several petrological investigations (see Tadesse and Allen, 2005 and Sighinolfi et al., 1993). There are three additional, smaller, complexes which occur between Yubdo and Tulu Dimtu, these are Kingy, Daleti and Ankori which have been studied very little. All five bodies are highly altered and serpentinisation is greater than 50% in each case.

It is estimated that over 2700 kg of Pt has been mined from the laterites of the Yubdo area and an inferred resource of 20tons at a grade of $0.4g/m^2$ has been calculated (Mogessie and Belete, 2000). Although Pt-Fe nuggets are found in the rivers around the other five complexes, the origin of these grains is uncertain.

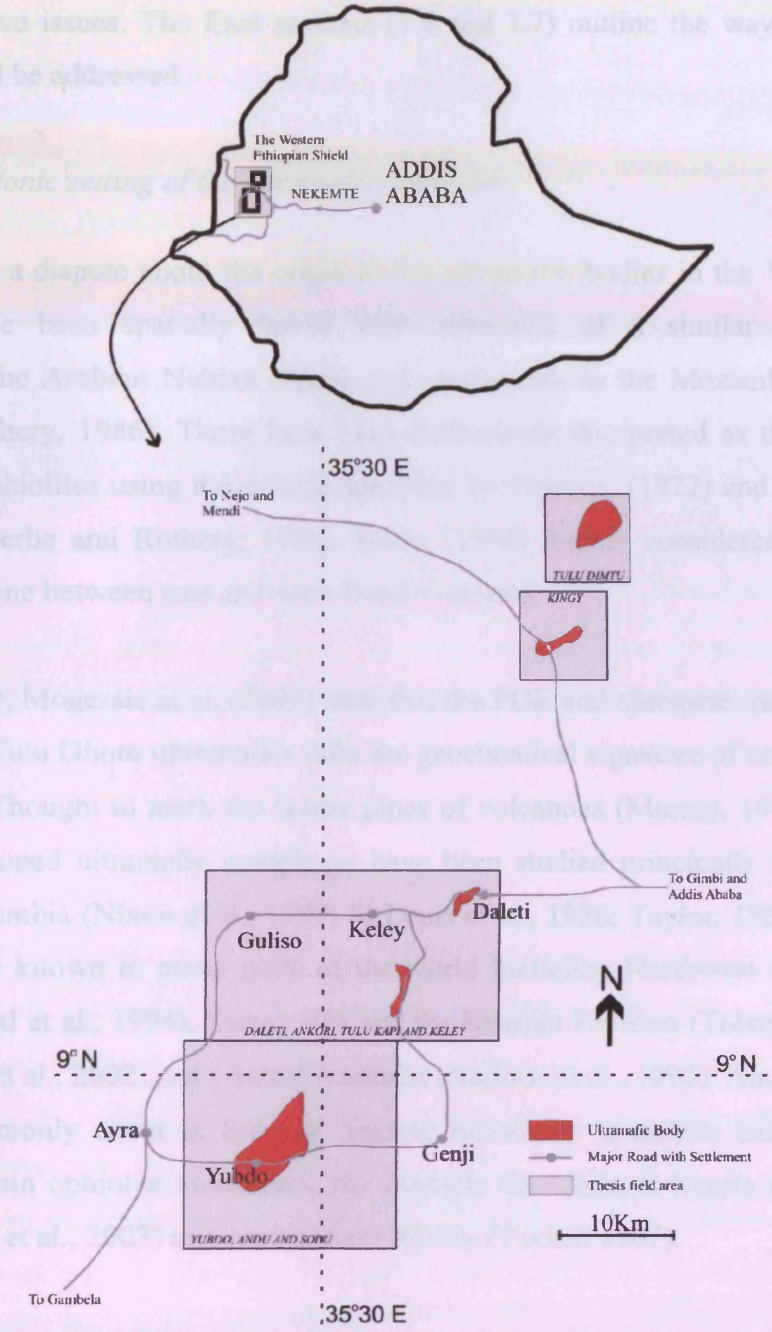

Figure 1.2: A map of the four field areas of this thesis, showing the largest ultramafic complexes and major roads and settlements. The map at the top of the figure is the outline of Ethiopia showing the location of the field area.

This thesis is intended to address two issues concerning the ultramafics in the WES. Firstly, there is a dispute over the tectonic setting of the complexes, many authors regard them to ophiolite complexes but others consider them to be Alaskan-type intrusions. Secondly, platinum group minerals (PGM) are extensively documented in the placers of the WES. However, little is known about the prospectivity of the primary mineralisation. The next two sections (1.2 and 1.3)

introduce the two issues. The final sections (1.6 and 1.7) outline the way in which these issues will be addressed.

1.2. The tectonic setting of the ultramafic complexes

There is a dispute about the origin of the ultramafic bodies in the WES. The complexes have been spatially linked with intrusions of a similar petrology northwards in the Arabian Nubian Shield and southwards in the Mozambique belt (Berhe and Rothery, 1986). These have been collectively interpreted as the mantle sequences of ophiolites using the criteria specified by Penrose, (1972) and structural observations (Berhe and Rothery, 1986). Berhe (1990) further considered these to mark a suture zone between east and west Gondwanaland.

However, Mogessie et al. (2000) state that the PGE and chromite chemistry of the Yubdo and Tulu Dimtu ultramafics infer the geochemical signature of an Alaskan-type intrusion. Thought to mark the feeder pipes of volcanoes (Murray, 1972), these concentrically zoned ultramafic complexes have been studied principally in Alaska and British Columbia (Nixon et al., 1997; St Louis et al., 1986; Taylor, 1967; Johan, 2002). They are known in many parts of the world including Northwest Columbia (Tistl, 1994, Tistl et al., 1994), Kamchatka and the Russian Far East (Tolstykh et al., 2000; Tolstykh et al., 2002) and Central Australia (Andrew et al., 1995). Alaskan-type complexes commonly occur in lines of discrete intrusions in mobile belt settings which also contain ophiolite complexes, for example the Urals, E Russia (Garuti et al., 1997; Garuti et al., 2003) and southeastern Alaska (Taylor, 1967).

Mogessie et al. (2000) suggested that an Alaskan-type intrusion origin for these bodies indicates that the Mozambique belt and Arabian Nubian Shield are not spatially linked and may only have an inter-fingering relationship.

This thesis includes an extensive study of the spinel geochemistry from the ultramafic samples throughout the WES (chapter 7). The results are compared with published spinel analyses from Alaskan-type intrusions and ophiolites worldwide.

1.3. The development of Pt and Pd

Research into Pt and Pd in the area has focused on studies of placer platinum group minerals (PGM) from the Yubdo area (see Belete et al., 2000 and Mogessie et al., 1999). Further mineralogical studies have characterized some PGM from serpentinised dunite within drill core (Mogessie et al., 1999). The only published geochemical work on the area is that of Mogessie et al. (1999) and Signolfi et al. (1993). Both studies discuss the likely effect of serpentinisation and comment only briefly on the mechanisms by which Pt and Pd may have become concentrated into the primary rocks before alteration.

An assessment of the geochemistry of altered ultramafic rocks with fresher rocks is included in this thesis (chapter 6). This may uncover some of the ore forming processes by which Pt and Pd may have been concentrated and hence develop future targets for exploration.

1.4. The mining history of the WES

Although it has been speculated that platinum grains from Yubdo were used to decorate objects in Egypt in the 7th century BC (Mogessie and Belete, 2000), the platinum deposit at Yubdo is generally regarded to have been discovered by a Russian missionary sometime in the early 20th century. In their account of the mining history of the area, Mogessie and Belete (2000) state that large scale extraction did not begin until 1926. Mining was conducted initially under a French company, which was then taken over by and Italian firm and by 1941 the mine was in the hands of the government. During the 1960's some mining and exploration was carried out by the Duval corporation. At the time of writing mining licences for the Yubdo and Sodu areas are held by Golden Prospect Mining (Ethiopia) Ltd, a wholly owned subsidiary of Golden Prospect Plc.

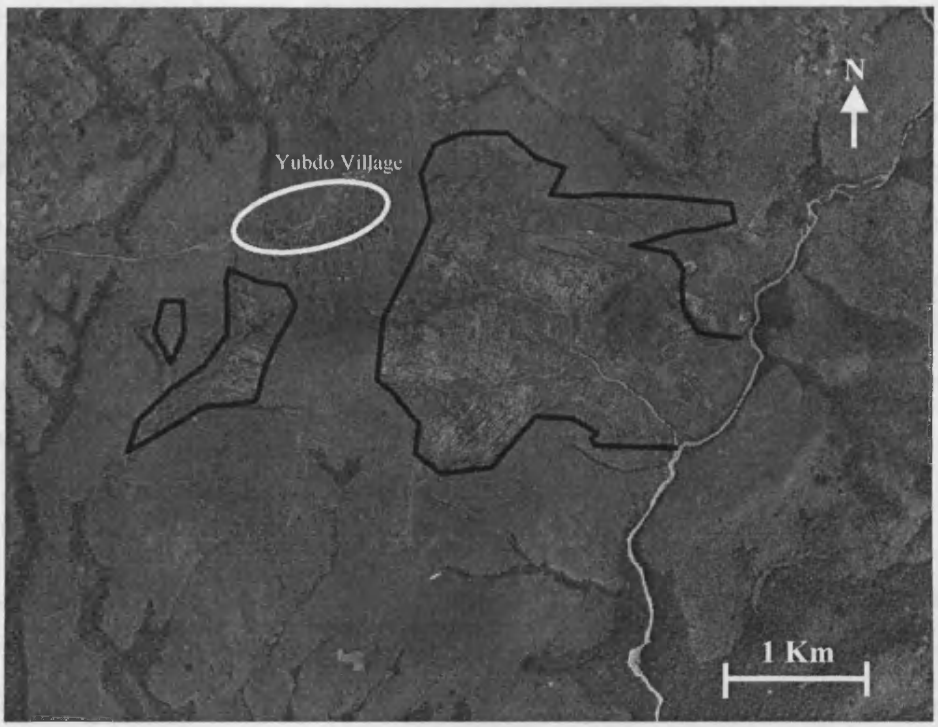

Figure 1.3: An aerial photograph of the opencast workings of the laterite in the Yubdo area (within the black lines) in 1957. The bright line is the course of the Birbir river.

The mining was conducted in two large open pits (see figure 1.3). In 2001, mining was conducted by pumping water into reservoirs high up in the soil profile. This water is then released and allowed to flow through the laterite where the soil particles are then taken into suspension. These waters then flow through a sluice system whereby selected fractions are panned to produce a concentrate. A study of the effectiveness of these systems was performed by Childs (2001). In the past these methods have been assisted by the use of monitors and also shaker tables (Mogessie and Belete, 2000).

Artisanal mining of both platinum group minerals and Au grains from stream sediments is common throughout the WES. It is not possible to determine when this practice started, the skill of panning has been past down through several generations of the local people. During the course of the fieldwork conducted for this project, Tan Range Exploration Corporation owned exploration licences for the area around Tulu Kapi and the eastern half of the Tulu Dimtu Main Intrusion.

1.5. The conduct of the study

This project was conducted in co-operation with and partially sponsored by Golden Prospect Mining Co Ltd (GPM). As a result these circumstances, there were certain constraints on the way in which the work could be performed. As detailed in chapters 7 and 8, many samples were collected and analysed for a suite of chemical elements. Although the author participated in the exploration programme which collected the samples, the geochemical analysis was conducted without his involvement.

Three bore-holes were sunk into the Yubdo Main Intrusion by the Duval corporation in 1969 (for a review see section 2.3.5). Studies of these cores were performed by Mogessie et al. (1999) and Belete et al. (2000). The rock retrieved by this method has been kept in archive by the Ethiopian Ministry of Mines and was available for study by members of the GPM team. Some geochemical analyses were performed on a few grab samples from within the core. A description of the core itself was not included within this study as this work had already been performed by other workers (see above). Furthermore, the manner in which samples had been taken from the drill-core meant that a scientific analysis of the geochemical variations was not possible.

1.6. Aims and methods used in the thesis

This thesis aims to use Ni, Cu, Cr, Al and Mg to investigate the differences in geochemistry between altered and fresher ultramafic rocks and hence suggest the mechanisms by which Pt and Pd have been concentrated. Furthermore, it aims to use spinel geochemistry investigate the tectonic origin of the ultramafic complexes of the WES with particular reference to Alaskan-type intrusions and ophiolites. The methods used for each theme are summarized as follows.

In chapter 8, the distribution of Ni, Cu, Cr, Al, Pt and Pd in the ultramafics is examined. The rocks are classified as fresher or altered (see section 8.3.1). The disitribution of these elements has lead to the development of ideas about potential magamtic and post-magmatic ore forming processes. These allow an assessment of

the prospectivity of the ultramafic bodies of the WES and the identification of possible exploration targets. To compliment this, a discussion of the possible factors affecting the distribution of Pt and Pd in the overburden of the WES is also included (see chapter 7).

To evaluate the tectonic origin of the ultramafic complexes, the geochemistry of spinels is studied (see chapter 7). The results of this analysis are compared with published spinel analyses from Alaskan-type intrusions and ophiolites. Furthermore, the relative influence of alteration and magmatic processes is evaluated using core and rim analyses and comparison with published work.

1.7. Layout of the thesis

In order to fulfill the above aims, chapter 2 describes the geological background to the area, introduces Alaskan-type intrusions and ophiolites, and discusses the key differences between them. Subsequently, chapter three describes the alteration to which the rocks have been exposed and the key minerals of interest to the thesis. Chapters 4 and 5 show the production of geological base-maps for the subsequent chapters using the analysis of terrain and geological observations. To support an understanding of the alteration processes in the Main Yubdo Intrusion, a magnetic survey was carried out, this is described in chapter 6. As a way of understanding the redistribution of the pathfinder elements in the overburden, chapter 7 describes the geochemistry of the soils. Chapter 8 describes an attempt to use rock geochemistry to ascertain the prospectivity of the complexes. Following this, the geochemistry of spinels is described in chapter 9 in order to investigate the tectonic origin of the complexes.

Each results chapter (4, 5, 6, 7, 8 and 9) considers each of the four geographic areas shown in figure 1.2 in turn. At the end of each results chapter the conclusions from all four areas is compared. Finally, in chapter 9 the conclusions for each method are summarized for each geographic area.

2. Literature Review

2.1. Introduction

Due to its position within the large Precambrian shield that extends from Egypt to Mozambique there have been several studies of the structural aspects of the WES. These are used in section 2.2 to set this thesis into context within East Africa. Studies of the ultramafic rocks in the area are less common, although there is an abundance of petrological studies which have been undertaken and these are reviewed in section 2.3. Two preliminary geochemical studies have been published and section 2.3 describes these along with a review of the research published on the famous Pt-Fe nuggets from Yubdo (see section 2.3.5)

An important theme of this thesis is the question of the tectonic origin of the ultramafic complexes. Section 2.4 introduces the structure, petrology, mineralogy and geochemistry of the Alaskan-type intrusions and ophiolite complexes and proposes several differences that may be used to distinguish the two.

2.2. Geological Setting

Most of Ethiopia is covered by Tertiary or Quaternary volcanic flood basalt sequences. The area of western Ethiopia examined in this thesis occurs within a window through this basalt plateau which allows the underlying Precambrian basement to be observed (United Nations, 1971). This 100 by 300 kilometer inlier is a N-S trending mobile belt hosting: metavolcano-sedimentary sequences, zones of gneiss and migmatite and the ultramafic complexes that are the subject of this study.

Using remote sensing, Berhe and Rothery (1986) linked the ultramafic complexes in western Ethiopia with those further north and south in East Africa and identified the position of five N-S trending sutures in this part of East Africa. In his discussion of the tectonic consequences, Berhe (1990) considers that these sutures with remnant ophiolites

represent the remnants of back arc basins, supra-subduction zones and sutures between two continental blocks. Berhe (1990) identified the Baraka – Yubdo - Sekerr suture (which includes the ultramafic complexes in this study) as being juxtaposed against a similar suture from Eastern Sudan that may continue southward into Tanzania. Satellite interpretation has shown that the structure continues northwards to Baraka in NE Sudan and Eritrea (Berhe and Rothery, 1986).

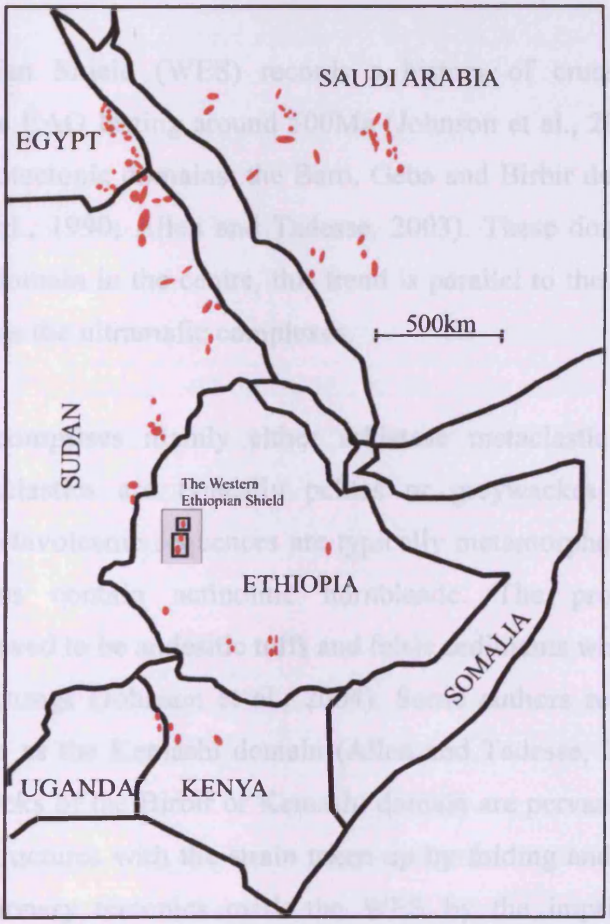

Figure 2.1: The "ophiolite belts" of northeast Africa (modified after Berhe, 1990).

The ultramafic complexes covered by this study are located within the the Western Ethiopian Shield (WES) which itself forms part of the greater East African Orogen (EAO). The deformational history of the EAO is divided into two phases: structures associated with collision and post accretionary structures (Abdelsalam and Stern, 1996). Of the collisional structures, two suture types are identified: arc-arc and arc-continental.

The Baraka – Yubdo – Sekerr suture is the result of the accretion of two arc terranes (Abdelsalam and Stern, 1996). The deformation within this suture is characterized by north trending sinistral transpression. Arc-arc sutures in the EAO typically have nappes containing ophiolitic material associated with them, and these were steepened by upright folding during the final stages of collision (Abdelsalam and Stern, 1996). Another aspect of the post accretionary deformation is the development of northwest trending strike slip faults and shear zones (Belete et al., 2000; Abelsalam and Stern, 1996).

The Western Ethiopian Shield (WES) records a history of crustal formation and deformation within the EAO lasting around 500Ma (Johnson et al., 2004). The shield is divided into three lithotectonic domains: the Baro, Geba and Birbir domains (Johnson et al., 2004; Ayalew et al., 1990; Allen and Tadesse, 2003). These domains strike NNE-SSW with the Birbir domain in the centre, this trend is parallel to the trend of the EAO. The Birbir domain hosts the ultramafic complexes.

The Birbir domain comprises mainly either schistose metaclastic or metavolcanic sequences. The metaclastics are typically pelites or greywackes with intercalated metavolcanics. The metavolcanic sequences are typically metamorphosed to greenschist facies and sometimes contain actinolitic hornblende. The protoliths for such metavolcanics are believed to be andesitic tuffs and felsic sediments which are commonly associated with arc settings (Johnson et al., 2004). Some authors refer to the domain hosting the ultramafics as the Kemashi domain (Allen and Tadesse, 2003; Tadesse and Allen, 2005). These rocks of the Birbir or Kemashi domain are pervasively deformed by NNE-SSW trending structures with the strain taken up by folding and westerly directed thrusting. Post accretionary tectonics mark the WES by the imprint of NNE-SSW transcurrent shearing and strike-slip faulting on top of the earlier N-S directed folds (Johnson et al., 2004). The shear zones related to this late stage of deformation appear to have been the conduits for hydrothermal fluids and further north in Baruda these deform the flanks of the mafic-ultramafic complexes (Braathen et al., 2001).

2.3. *Previous Work on the Ultramafics of the WES*

2.3.1. Introduction

Studies of the ultramafic rocks in the WES fall into two categories. Some authors consider the ultramafic complexes together and relate them to the other lithological and structural domains in the region. Other studies have focused on the individual bodies. In the following sections, the regional studies including the ultramafics are described and then an account of the work on individual ultramafic complexes is summarised.

2.3.2. Regional Studies of the Ultramafic bodies

The Yubdo complex is considered to be the southernmost ultramafic body in the WES. There are several more bodies north of Tulu Dimtu (these are not covered in this study). These additional bodies include: Jaja Kubsa (Alemu and Abebe 1998), Korka Meti (Alemu and Abebe, 1999; Tadesse and Allen, 2005) and Baruda (Braathen et al., 2001; Allen and Tadesse, 2003). The publications summarized in this section treat all complexes together and therefore some observations described may have originated from outside the coverage area of this study.

There is a general consensus that the ultramafic complexes studied here are elongate and occur in a zone associated with metavolcanics and metasediments (Johnson et al., 2004; Allen and Tadesse, 2003; Alemu and Abebe, 1998; Warden et al., 1982). The bodies are orientated parallel to the regional tectonic fabric (NNE-SSW). Allen and Tadesse (2003) report the presence of associated gabbros, diorites and plagiogranites. One publication states that the terrain associated with the ultramafic units is low-lying with some elevated areas where the rocks are less altered (Tadesse and Allen, 2005) but another reports that the ultramafics form prominent ridges almost devoid of vegetation (Alemu and Abebe, 1998).

Altered dunites and pyroxenites have been observed in all studies of petrology. Several publications report that the dunites are completely serpentinised, however, Alemu and

Abebe (1998) also report that fresh olivine is present at up to 20% in some samples. Furthermore, Tadesse and Allen (2005) describe metre-scale blocks of harzburgite, lherzolite and wehrlite within ultramafic schists. Warden et al. (1982) observed a relict cumulate texture in some samples from the WES. Tadesse and Allen (2005) also report only partial replacement towards the centre of the ultramafic masses. Alteration minerals such as talc and carbonate are found along thrust faults and shear-zones and also in rims around massive serpentinite blocks (Alemu and Abebe, 1998; Warden et al., 1982). Pyroxenite samples show variable alteration to chlorite, albite, epidote and sometimes actinolite (Johnson et al., 2004). Furthermore, pyroxene psedomorphs containing secondary hornblende suggests lower amphibolite facies metamorphism (Warden et al. 1982). In most publications, the strongest alteration is reported closest to fault or shear-zones. All descriptions of petrology report the presence of magnetite and chromite.

An account of the whole-rock geochemistry of the ultramafic rocks in the WES is provided by Warden et al. (1982) and is accompanied by a comprehensive study of alteration petrology. Chondrite normalized REE analyses show that the intrusive ultramafic rocks of the area have a very strong LREE enrichment and HREE depletion.

2.3.3. Tulu Dimtu and Kingy

This section covers Tulu Dimtu and Kingy together. This is because the publications summarized here do not distinguish between the two and they are jointly referred to as "Tulu Dimtu". Later in this thesis these two areas are described separately.

The Tulu Dimtu area was mapped at a scale of 1:50,000 by de Wit and Aguma (1977), they identified a large mass of partially serpentinised dunites surrounded by serpentinite schists. They also identified a zone of other more elongate bodies which extend southwards into the Kingy area. Many accounts comment on the fact that the largest ultramafic body in the area stands out as a conspicuous hill which is barren of vegetation. The rocks forming this large hill are referred to in this study as the Tulu Dimtu Main Intrusion.

The most comprehensive study of the petrology of the Tulu Dimtu area is that of de Wit and Aguma (1977), but further descriptions are given by Sighinolfi et al. (1993) and Alemu and Abebe (1998). The lithologies discovered in the Tulu Dimtu and Kingy areas include dunite, olivine-clinopyroxenite and hornblendite. Serpentinisation is never reported at less than 80% and it is often over 95% (de Wit and Aguma, 1977; Signolfi et al., 1993). The relict outlines of forsteritic olivine crystals with diameters of 0.2-0.5mm are observable and olivines can be observed now as chrysotile mesh and window structures. Fine grained magnetite occurs along silicate grain boundaries and Cr-spinel and chromite are also present. Furthermore, de Wit and Aguma (1977) describe original "magmatic" (sic, see chapter 3) galena and barite crystals within dunite. The olivine-clinopyroxenites include clinopyroxene crystals of up 0.5mm which all have tremolitic rims. There are believed to have been at least two phases of alteration which include one of serpentinisation and a separate silicification phase (de Wit and Aguma, 1977; Alemu and Abebe, 1998).

A study of the geochemistry of the rocks in the Tulu Dimtu complex was undertaken by Sighinolfi et al. (1993). The PGE analysed from serpentinised dunites were depleted with respect to chondrite, but Pt was found to be more enriched than the other elements. Furthermore, Sighinolfi et al. (1993) only found significant PGE values in serpentinised dunites and the silicified equivalents were almost barren. Although Ni is reported to increase with serpentinisation, the distribution in the altered lithotypes is similar to that of the less altered rocks suggesting that Ni remobilization is a local effect (Sighinolfi et al, 1993). A depletion in Cu values with serpentinisation led Sighinolfi et al. (1993) to suggest that serpentinisation had removed sulphides and chalcophile elements from the complex.

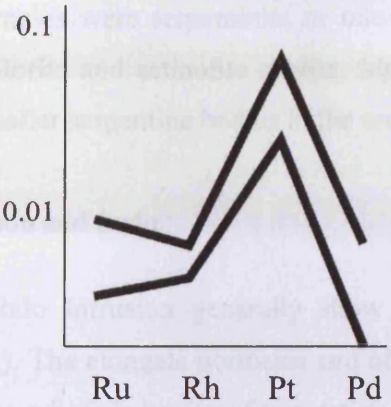

Figure 2.2: The average chondrite normalized Ru, Rh, Pt and Pd analyses for dunite from the Tulu Dimtu area (Sighinolfi, 1993).

2.3.4. Daleti, Ankori, Tulu Kapi and Keley

The ultramafics at Daleti (refered to in this study as the Daleti Ultramafic) occur in two parts, firstly a prominent ridge trending NE-SW and secondly a lower-lying area to the northeast (United Nations, 1971). The ridge is barren of vegetation. A report by the United Nations (1971) suggests that these two areas are offset by intersection faults and at least partially surrounded by diorites and gabbros. Athough the limited exposure only shows serpentinised dunite, a drill-hole has revealed an alternation of dunite and peridotite bands (Mogessie and Hoinkes, 1998). These bands are believed to be "concentric zoning" (United Nations, 1971).

The petrology of the ultramafic samples often reveals completely serpentinised rocks (United Nations, 1971; Mogessie and Hoinkes, 1998). However relict olivine grains can sometimes be observed with a mesh of chrysotile and antigorite. Fine grained magnetite and chromite is sometimes observed (Mogessie and Hoinkes, 1998). The faulted eastern contact of the intrusion is rich in hydrous alteration minerals such as talc, talc-serpentine, chlorite and chlorite-serpentine (United Nations, 1971). Birbirite can be found on the crest of the ridge (see chapter 3 for a definition of birbirite).

The United Nations report (1971) briefly mentions the Ankori Ultramafics near the road from Tulu Kapi to Genji. No fresh rocks were observed by the team of the United

Nations (1971) and most samples were serpentinite or talc-serpentine. The complex is reported to host lenses of chlorite and actinolite schists. Mogessie and Hoinkes (1998) also report the presence of smaller serpentine bodies in the area.

2.3.5. Yubdo, Andu and Sodu

The maps of the Main Yubdo Intrusion generally show a "pear" shaped intrusion (Kazmin and Demessie, 1971). The elongate northeast end of the intrusion forms a NNE-SSW trending prominent ridge which is barren of vegetation. The United Nations (1971) report that the eastern contact of the intrusion dips gently to the east and that further ultramafics to the north are caps of the same intrusion. The western contact is reported to be a steeply dipping thrust fault associated with shearing (United Nations, 1971). A system of NNE-SSW trending "en-echelon" shear-zones is said to cross-cut the centre of the complex. Furthermore, a set of WNW-ENE transcurrent faults are recorded that are frequently associated with both shearing and quartz-veins. The ultramafics are found to be zoned having dunite at the core, with peridotite then pyroxenite surrounding it (United Nations, 1971; Mogessie and Hoinkes, 1998). Some peridotites are found to be intercalated with dunite in the eastern and southern parts of the intrusion (Mogessie et al., 1999). Several cross-cutting diorite dykes are reported (United Nations, 1971). Most of the geological features recorded in the literature are also mentioned in a drilling report by the Duval Corporation (Howell, 1969). All the drill holes were sunk into the dunite zone and they only intersected dunite and peridotite layers. The drill core also intersected hairline magnetite veinlets which extend along fault zones and talc-chlorite dykelets.

There are two large studies of the petrology (United Nations, 1971 and Mogessie and Hoinkes, 1998) and these are supplemented by the work of Belete et al. (2000) and Mogessie et al. (1999). All studies report that the central dunites are serpentinised to a large degree and a relict cumulate texture can be observed (Mogessie and Hoinkes, 1998; Mogessie et al., 1999). The olivines have a forsterite content of 81-84% (Mogessie et al., 1999) and are typically rimmed by talc, carbonate and opaque minerals. Pyroxene is mainly diopside and is associated with chlorite. The United Nations report (1971)

commented that pyroxenes tend to be coarser than olivine minerals and are often found with tremolite and chlorite. Euhedral and subhedral chromites with altered rims can be observed in all the ultramafic host rocks. The United Nations (1971) report the occurrence of pyrite and arsenopyrite in the shear-zone on the northeastern contact of the intrusion.

Platinum-group minerals (PGM) have been found in both the rocks and placers around Yubdo. The two largest petrological studies report sperrylite ($PtAs_2$) in both dunite and pyroxenite (United Nations, 1971; Mogessie and Hoinkes, 1998). Furthermore, Augustithis (1965) discovered sperrylite in birbirite samples. The more systematic accounts of primary PGM in the area are of Pt-Fe nuggets in both chromite and serpentinite (Belete et al., 1999; Belete et al., 2002). These were discovered in the boreholes sunk by the Duval Corporation (Howell, 1969). The Pt-Fe alloys in the chromite appear to be rounded in shape and contain minor Ir (Mogessie et al., 1999). The Pt-Fe alloys (with minor Rh and Cu) found in the serpentinites are reported to be elongate and between 20μm and 30μm (Mogessie et al., 1999).

The placer Pt-Fe nuggets from Yubdo historically generated controversy over the formation of Pt-nuggets (Bowles, (1986); Hattori and Cabri, 1992). All nuggets reported from Yubdo are Pt-Fe (isoferroplatinum and tetraferroplatinum) in composition and Belete et al. (2000) analysed a wide variety of inclusions from these nuggets. The most abundant inclusions found were hollingworthite (RhAsS), genkinite ($(Pt,Pd)_4Pb_3$), irarsite (IrAsS), platarsite (PtAsS) and native Os.

2.4. Alaskan-type intrusions versus ophiolites

2.4.1. Introduction

Alaskan-type complexes and ophiolites represent different tectonic settings and have differing implications for mineralisation. Ophiolites are fragments of ancient oceanic lithosphere now emplaced on land at fossil subduction zones (eg Gass, 1990). The setting of Alaskan-type complexes is less well defined. There have been many attempts to

explain the characteristics of Alaskan-type intrusions (see Johan, 2002). The generally accepted model is that they originate as the feeder pipes of volcanoes in continental subduction zones (Murray, 1972).

Both comprise mafic and ultramafic sequences and considering the two genetic models, it may at first glance be hard to understand why the two may be confused. However the various modifications and complications of the models result in some overlap in structure, petrology, mineralogy and geochemistry. The ophiolite descriptions given here focus on the Troodos massif of Cyprus and the Semail nappe in eastern Arabia, as these provide the best exposed and studied complexes.

2.4.2. Scale of Alaskan-type intrusions and ophiolites

Complete ophiolite complexes typically consist of a basaltic unit predominantly composed of up to 0.5 to 1 km thickness of pillow lavas and sheeted dykes. This in turn is underlain by plutonic gabbro and ultramafic crustal units which in the Oman ophiolite make up a total of 3.6 km in thickness (Nicolas et al., 1996) and lie on top of mantle lherzolite or harzburgite which may also be several km thick. These sequences extend along strike for 450km (Lippard et al., 1986). Ophiolites are often truncated at the base by a thrust, below which is a metamorphic aureole that continues into lower grades of metamorphism away from the contact with the ophiolite (Gass, 1990).

In contrast, Alaskan-type intrusions are concentrically zoned with dunite in the centre grading outwards to clinopyroxenite and hornblendite, they are often associated with an outer gabbro zone. In many cases, one or more of these zones may be missing from the complex. The two largest Alaskan-type intrusions include Nizini Tagil ($70km^2$) and Tulameen ($80km^2$), but most range between $12km^2$ and $40km^2$ (Johan, 2002).

Both ophiolites and Alaskan-type intrusions are commonly highly fragmented. The Troodos and Oman complexes display the full lithological sequence and both are exposed over several hundreds of square kilometers. However, most ophiolites are much smaller,

are frequently highly deformed and occur in fault bounded blocks. The primary igneous textures of ophiolites are offset and juxtaposed against country rocks by thrust faulting related to their emplacement onto continental crust. Similarly, Alaskan-type complexes such as the Hickman and Polaris, British Columbia (Nixon et al., 1997) are highly disrupted by faulting and other types of deformation. There are further complications in that the proportions and sizes of primary igneous lithologies in Alaskan-type complexes may vary. The complete zonal structure of Alaskan-type intrusions is only seen in a few localities such as the Konder and Inagli intrusions of the Aldan shield, Eastern Siberia (Malitch, 1991) and Alto Condoto complex in NW Columbia (Tistl et al., 1994; Tistl, 1994). Konder and Inagli show central dunite cores comprising 60% of the total volume whereas in the Alto Condoto complex the dunite occupies around 20% of the intrusion. As with ophiolites, Alaskan-type complexes may either have one or more zones missing and/or the zonal structure could be disrupted by deformation. In some cases the central dunite core is missing, such as in the Duke Island western body (Taylor, 1967), Gnat Lakes and Menard Creek (Nixon, 1997). In others, there is no clinopyroxenite zone as in Duke Island East, Annette Island and Blashke Island (Taylor, 1967).

2.4.3. Structure of Alaskan-type intrusions and ophiolites

The large components of ophiolites (described above) cover much larger areas than those of Alaskan-type complexes. However, smaller features of fragmented ophiolites may resemble Alaskan-type intrusions (see figure 2.3). Lippard et al. (1986) and Robertson and Xenophontos (1993) describe how the ultramafic rocks of ophiolites within smaller features occur as three distinct lithological associations:

- The Mantle sequence: a residual suite of massive lherzolite or harzburgite frequently containing dunite pods.
- The Crustal layered sequence: a rhythmically layered series of dunite, wherlite and pyroxenite.
- The Late intrusive complexes: usually composed of wehrlite, peridotite or gabbro; these plutonic bodies intrude the crustal sequence.

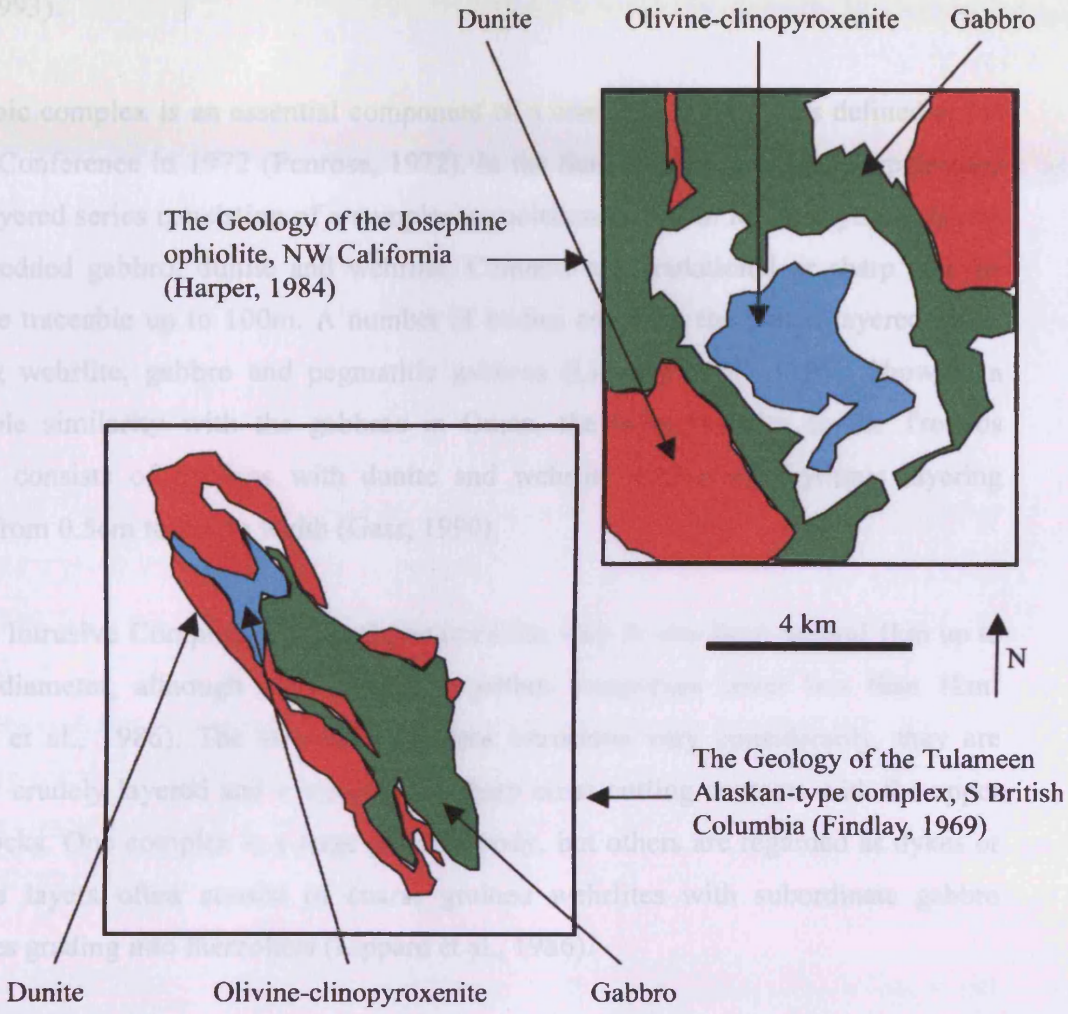

Figure 2.3: Schematic diagrams of the mafic and ultramafic units of the Josephiene Ophiolite and Tulameen Alaskan-type intrusion showing similar zoned outcrop patterns (modified from Findlay, 1969 and Harper, 1984).

Dunite bodies are common in the uppermost parts of the mantle sequence (Roberts and Neary, 1993; Gass, 1990). These bodies have relatively sharp interfingering contact relationships with the enclosing harzburgite (Gass, 1990). They are irregular with anastomosing offshoots. The more tectonised bodies, closer to the paleo Moho, are more elongate (Lippard et al., 1986). In the Oman ophiolite, dunites are generally under 100m in length but extremely tectonised and elongate bodies can be up to 14km in length Lippard et al., 1986). The dunites themselves envelop nodular, massive and schlieren

chromitite deposits, these display a gradational relationship with their host (Roberts and Neary, 1993).

A gabbroic complex is an essential component of a complete ophiolite as defined at the Penrose Conference in 1972 (Penrose, 1972). In the Semail ophiolite this is represented by the layered series consisting of a complex association of 0.5cm to 2m rhythmic layers of interbedded gabbro, dunite and wehrlite. Contacts are gradational or sharp and the layers are traceable up to 100m. A number of bodies cross-cut the Oman layered series including wehrlite, gabbro and pegmatitic gabbros (Lippard et al., 1986). Showing a remarkable similarity with the gabbros in Oman, the layered series in the Troodos ophiolite consists of gabbros with dunite and wehrlite displaying rhythmic layering ranging from 0.5cm to 2m in width (Gass, 1990).

The Late Intrusive Complexes in the Oman ophiolite vary in size from around 1km up to 5km in diameter, although some peridotite-gabbro complexes cover less than $1km^2$ (Lippard et al., 1986). The structures of these intrusions vary considerably, they are generally crudely layered and irregular with sharp cross-cutting contacts with the upper crustal rocks. One complex is a large plutonic body, but others are regarded as dykes or sills. The layers often consist of coarse grained wehrlites with subordinate gabbro sometimes grading into lherzolites (Lippard et al., 1986).

In contrast to the layering in ophiolites, Alaskan-type intrusions exhibit a pipe-like concentrically zoned structure with a dunite core (Taylor, 1967; Johan, 2002). The idealized sequence displays dunite surrounded successively by clinopyroxenite, hornblendite and monzonite-gabbro rims. The contacts at the rim of the dunite core of and Alaskan-type complex are typically gradational and it is common to find olivine-bearing clinopyroxenite rafts. However, dunite to clinopyroxenite contacts in ophiolites can be either sharp or gradational. The contact between Alaskan-type gabbro zones and the associated ultramafics is normally sharp (Johan, 2002; Taylor, 1967), however, the gabbros of ophiolites have either sharp or gradational contacts. Massive chromitite lenses and pods occur at the rims of some Alaskan-type intrusions (Nizini Tagil, Garuti et al.,

1997). In ophiolites, chromitites also form in dunite pods in the mantle sequence, however, they are more abundant towards the centre of each dunite body (Roberts and Neary, 1993).

Both ophiolites and Alaskan-type intrusions are often disrupted and deformed to the point at which they are indistinguishable on the basis of structure. Therefore, based on structure or proportions of lithotypes alone, it is difficult to distinguish between an Alaskan-type intrusion and a dismembered ophiolite.

2.4.4. Petrology and Mineralogy

The mantle sequences of the Semail and Troodos ophiolites consist of variably serpentinised peridotites (85%) with associated lherzolites and dunites (5 to 15%) (Gass, 1990; Lippard et al., 1986). The harzburgites are medium to coarse-grained and are composed of 75 to 85% olivine and 15 to 20% orthopyroxene. Within these, clinopyroxene forms an average <1% abundance and a maximum of 5% of the mode and chrome spinel forms 0.5 to 2%. Chromite is a ubiquitous and accessory phase. The dunites typically comprise >98% olivine and <2% chromite and are largely massive dunite with chromite segregations (Gass, 1990; Lippard et al., 1986).

The dominant lithology in the Layered Series is gabbro with dunites (including minor chromite) and wehrlite as the other main rock types (Gass, 1990). The primary minerals of the Semail and Troodos ophiolites are plagioclase, clinopyroxene, olivine, chrome spinel, orthopyroxene, hornblende and titanomagnetite (Lippard et al., 1986; Gass, 1990). Within each cyclic unit of the Semail Nappe the most common crystallization sequence shows that olivine and chromite form the earliest phases, followed by pyroxene and plagioclase as intercumulus phases, then titanomagnetite and hornblende as minor phases (Lippard et al., 1986). This means that the most common rock sequence is: dunite → wehrlite → olivine-gabbro → gabbro (Gass, 1990). Other ophiolites can display differing orders of crystallization including olivine → plagioclase → clinopyoxene (eg the Lizard ophiolite).

The Late Intrusive Complexes of the Semail are divided into two broad groups: gabbro-diorite-plagiogranite bodies and peridotite-gabbro complexes (Lippard et al., 1986; Browning and Smewing, 1981). The former composed mainly of layered gabbros, diorites and subordinate plagiogranite (Lippard et al. 1986). These gabbros are typically medium grained with plagioclase and interstitial clinopyroxene grading upwards into coarser diorites. The Mashin intrusion is a typical peridotite-gabbro complex in the Semail. Lippard et al. (1986) describes this as wehrlite grading upwards into coarse grained gabbros and diorites. The wehrlites are typically coarse grained poikilitically enclosed by clinopyroxenes and orthopyroxenes. Smaller peridotite-gabbro intrusions sometimes grade from wehrlite into lherzolite (Lippard et al., 1986).

Alaskan-type intrusions are composed of dunite, olivine-clinopyroxenite, clinopyroxenite, hornblendite and gabbro zones (Taylor, 1967). This compares with the more orthopyroxene-rich lherzolites and harzburgites which dominate ophiolite mantle sequences. Alaskan-type intrusions are noted for the absence of orthopyroxene. Considered on their own, the petrologies of the ophiolitic crustal sequence are similar to the zones of Alaskan-type intrusions. However, in Alaskan-type intrusions the contact between clinopyroxenites and gabbros is generally sharp whereas gabbro contacts in ophiolites may be either sharp or gradational. Additionally, plagioclase in Alaskan-type complexes is only observed in the peripheral hornblendite zone whereas it is ubiquitous in the typical ophiolite crustal sequence. Accessory chromite in Alaskan-type intrusions occurs exclusively and throughout the dunite zones (Johan, 2002). Alaskan-type intrusions show the crystalisation sequence olivine → clinopyroxene → plagioclase (Murray, 1972). The same crystallization sequence is observed in the Semail and Troodos ophiolites although some complexes show plagioclase crystalising before clinopyroxene. In both Alaskan-type intrusions and ophiolites, olivine generally crystallizes first.

2.4.5. Rare Earth Elements (REE)

Godard et al. (2000) showed that mantle sequence dunite pods from the Semail Nappe are highly depleted in REEs with respect to chondrite. The patterns show a smooth positive slope from La to Lu (Figure 2.4).

Light REEs from the Layered Series in the Semail Nappe are slightly enriched compared to chondrite (Lippard et al., 1986), however, analysis of the CY-4 drill core from the Troodos ophiolite shows considerable depletion in LREE. These wide ranging values converge for the heavier elements.

The Late Intrusive Complexes of the Semail Nappe display an enrichment of REE with respect to chondrite (figure 2.4). A slightly positive slope is observed with a pronounced negative Eu anomaly (Lippard et al., 1986).

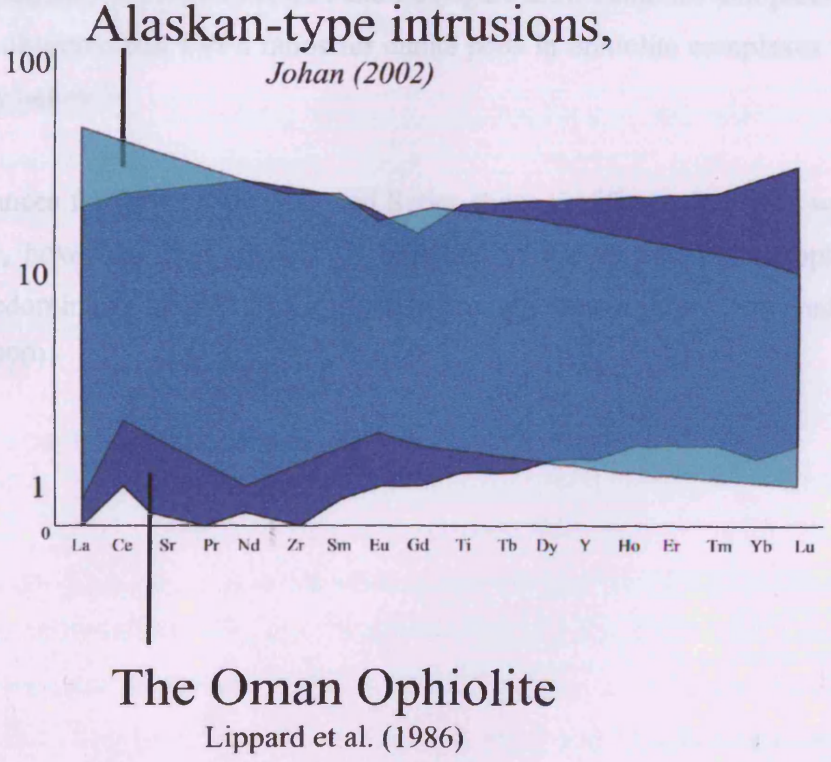

Figure 2.4: The typical REE geochemistry of Alaskan-type intrusions compared to Oman ophiolite (Johan, 2002; Lippard et al., 1986).

Alaskan-type intrusions are generally enriched in REE with respect to chondrites and the Late Intrusives complexes of the Semail Nappe are enriched to the same extent. These late Intrusive Complexes show a similar degree of enrichment, however, they have positive slopes. In general, the REE patterns from the Alaskan-type intrusions of Owendale and the Urals display gentle negative slopes with only slight Eu anomalies (Fershtater et al., 1997; Johan, 2002). This also contrasts with the mantle sequence dunites which display severe depletion and positive slopes. Commonly, the REE abundances in ophiolites show pronounced anomalies such as Ce, Eu and Gd - only broad anomalies are observed in Alaskan-type intrusions (figure 2.4).

2.4.6. Platinum-Group Elements

Platinum-group elements (PGE) in ophiolites are depleted in comparison with chondrite, they show a generally neutral slope with Os, Ir and Ru enrichment, however, some samples are slightly enriched in Rh, Pt and Pd (figure 2.5). Table 2.1 compares Pt and Pd values, it is observed that Pt/Pd ratios for dunite pods in ophiolite complexes worldwide are generally below 7.

PGE abundances for the Troodos Layered Series show significant depletion with respect to chondrite, however, they are slightly enriched in Rh, Pt and Pd. In ophiolites Pd typically predominates over Pt and a negative Ru anomaly is rarely observed (Prichard and Lord, 1990).

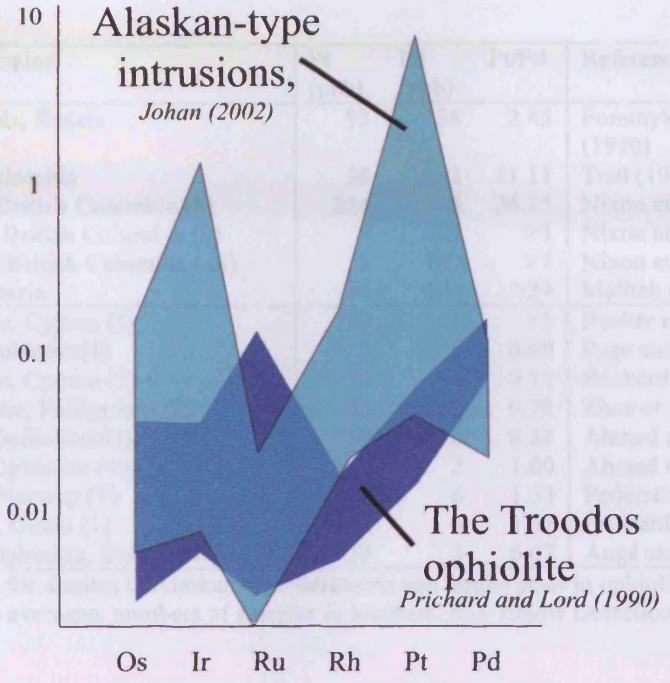

Figure 2.5: A comparison of the chrondrite normalized PGE abundances for Alaskan Type intrusions and the Troodos ophiolite. The Alaskan-type intrusions show strong negative Ru anomalies and a high Pt/Pd ratios when compared to ophiolites (After Johan, 2002 and Prichard and Lord, 1990).

Alaskan-type intrusions frequently display a negative Ru anomaly when displayed on a chrondrite normalised PGE diagram (Johan, 2002). The PGE patterns in the Troodos ophiolite rarely have negative Ru anomalies (Prichard and Lord, 1990). The elemental abundances of the mantle sequences of ophiolites are generally depleted in all the PGE whereas in Alaskan-type intrusions Ir and Pt are often enriched with respect to chondrite (Johan, 2002).

A significant difference between the dunites of ophiolites and Alaskan-type intrusions is in the Pt and Pd ratio. Table 2.1 shows Pt/Pt ratios for dunites from 7 ophiolite bodies and 6 Alaskan-type intrusions. The Pt/Pd ratios in ophiolites are normally less than Pt/Pd = 2 although the Pt/Pd ratio of the New Caledonia ophiolite is Pt/Pd = 6.67. The Pt/Pd ratio of Alaskan-type intrusions is normally significantly higher with values of Pt/Pd = 21-27 being recorded. The Pt/Pd ratio of the Nizhni Tagil and Wrede Creek Alaskan-type intrusions are, however, lower (Pt/Pd = 2.45 and >1).

	Complex and Location	Pt (ppb)	Pd (ppb)	Pt/Pd	Reference
Alaskan-type intrusions	Nizhni Tagil, Urals, Russia	93	38	2.45	Fominykh and Khvostova (1970)
	Alto Condoto, Colombia	38	2	21.11	Tistl (1994)
	Lunar Complex, British Columbia (8)	214	8	26.75	Nixon et al., 1997
	Wrede Complex, British Columbia (8)	7	BD	>1	Nixon et al., 1997
	Polaris Complex, British Columbia (18)	1	BD	>7	Nixon et al., 1997
	Chad, Eastern Siberia	24	BD	>24	Malitch (1996)
Ophiolites	Troodos Ophiolite, Cyprus (5)	BD	1	<1	Becker and Agiorgtis (1978)
	Newfoundland Ophiolite(4)	3	5	0.69	Page and Talkington (1984)
	Troodos Ophiolite, Cyprus (1)	3	4	0.71	Prichard and Lord (1990)
	Zambales Ophiolite, Philippines (2)	25	32	0.78	Zhou et al. (2000)
	Northern Oman Ophiolite(63)	14	16	0.88	Ahmed and Arai (2002)
	Northern Oman Ophiolite (40)	2	2	1.00	Ahmed and Arai (2002)
	Leka Ophioilite, Norway (7)	8	6	1.33	Pedersen et al. (1993)
	Semail Ophiolite, Oman (1)	10	6	1.67	Prichard et al. (1996)
	New Caledonia Ophiolite, South Pacific (8)	20	3	6.67	Augé and Maurizot (1995)

Table 2.1: Pt/Pd ratios for dunites in Alaskan-type intrusions and dunite pods in ophiolite complexes. Abundances are averages, numbers of samples in brackets. BD: Below Detection Limits

2.4.7. Fractionation of Nickel, Copper and Chromium

In the Layered Series in the Semail Nappe, the compatible elements Ni and Cr are most abundant in the early formed olivine- and pyroxene-rich lithologies. Their abundances decrease in the more mafic lithotypes (Lippard et al. 1986). The same is seen in ultramafics of Alaskan-type intrusions. Ni is concentrated and Cu depleted in the early dunites in the Urals. These abundances fall and rise respectively in the mafic lithotypes (Garuti et al., 1997). Similar patterns are observed in the Tulameen and Condoto complexes of British Columbia and Columbia (Findlay 1969; Tistl, 1994).

2.4.8. Summary

Alaskan-type intrusions are pipe-like concentrically zoned ultramafic-mafic intrusions (Taylor, 1967; Johan, 2002), in some cases this may be sufficient to distinguish them from the layering of ophiolites. However, due to the dynamic setting into which Alaskan-type complexes are intruded and ophiolites are obducted, both may be deformed so that the layering or zoning cannot always be observed.

In such geological situations, the following criteria are suggested to distinguish the type of mafic-ultramafic complex:

- In ophiolite sequences, gabbros can display both gradational and sharp contacts with ultramafic rocks, whereas, in Alaskan-type complexes such contacts are typically sharp.
- The mantle sequences of ophiolites are dominated by orthopyroxene-rich lithotypes. Conversely, Alaskan-type intrusions are noted for the absence of orthopyroxene.
- The ratio Pt/Pd for ophiolitic dunites is typically <7 whereas Alaskan-type dunites are generally >2 (Table 2.1)
- Alaskan-type intrusions frequently display negative Ru anomalies on chrondrite normalized PGE diagrams (see figure 2.5), whereas ophiolites rearely show negative Ru anomalies.
- Ophiolitic mafic and ultramafic rocks show neutral to positive gradients on REE abundance diagrams, whereas, similar mafic-ultramafics in Alaskan-type intrusions display negative gradients (figure 2.4)
- Ophiolite REE patterns can include pronounced positive or negative Ce, Eu and Gd anomalies. Whereas, all lithologies in Alaskan-type intrusions only display a slight rise in Sm, Eu and Gd abundances (figure 2.4).

3. Petrology and Mineralogy

3.1. Introduction

Samples of ultramafic rocks from the each of the four geographic areas of study within the WES were cut and mounted as either thin sections or polished blocks. These samples were then observed using transmitted light microscopy and scanning electron microscopy. The sulphide minerals were analysed using an energy dispersive X-ray analyzer attached to a Scanning Electron Microscope (SEM).

This chapter is divided into four sections. The first section describes the study of thin sections to define the rock-types and to document the degree of alteration present in the WES. The second section describes the texture of oxide minerals in order to support a study of their geochemistry. Another section describes typical sulphide minerals and lastly three PGM are described.

3.2. Methods

3.2.1. Scanning Electron Microscopy

Polished blocks were analysed using a Carl Zeiss SMT (Cambridge) S360 scanning electron microscope (SEM). The search for PGM and photographs of spinels and sulphides were performed using a 4-quadrant back-scattered electron detector. Photographs of PGM were taken using a Veeco FEI (Philips) XL30 environmental SEM.

3.2.2. Energy Dispersive X-Ray analyzer

Both quantitative and qualitative analyses were obtained using an Oxford Instruments INCA ENERGY (EDX) X-ray analyzer. Quantitative analyses were undertaken using an accelerating voltage of 20kV, a probe current of 1nA and a working distance of 25mm. During petrological studies, mineral identification was confirmed by qualitative analyses the SEM.

3.3. Petrology

3.3.1. Introduction

The petrology of the rocks from the WES was investigated using both transmitted light microscopy and electron microscopy. This section describes the typical petrology of the ultramafic rocks and is illustrated by photographs of thin sections taken under transmitted light. The degree of alteration is described and subsequently a definition and description of rock-types is described.

The petrology of each of the ultramafic complexes covered in this thesis has been documented by other workers (see chapter 2). Furthermore, many studies comment on the significant degree of alteration to which each complex has been subjected (eg Mogessie and Hoinkes, 1998). This section aims to describe the variation in alteration through the two key rock types: dunite and clinopyroxenite. Additionally, some rocks may be classified as olivine-clinopyroxenite, as this is composed of two minerals it is not described here because it is easier to describe the alteration of olivine and clinopyroxene separately. In order to demonstrate the degrees of alteration present, this study focuses only on the two mono-mineralic lithotypes. For both rock types, a number of thin sections are described from the least to most altered. In addition to this, a description of the little known lithotype known as birbirite is included. Birbirite is an alteration product and is widely distributed in the soils of the area. It is named after the Birbir river which flows around the Main Yubdo Intrusion.

3.3.2. Dunite

The following images illustrate the range of serpentinisation within the ultramafic rocks of the WES. The Mg values are quoted for reference with the geochemical assessment of alteration as described in chapter 8.

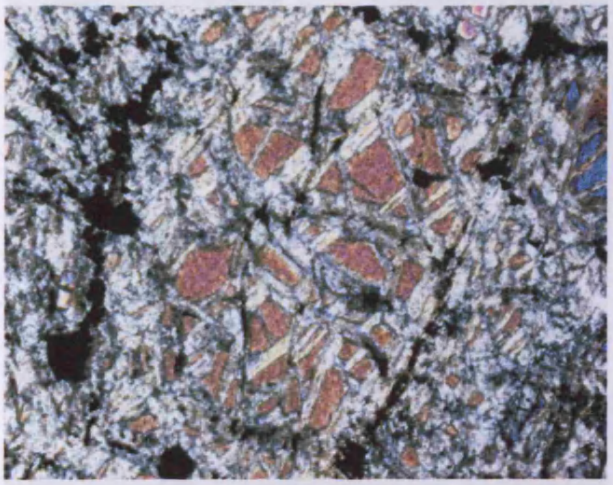

Figure 3.1: A photograph of a dunite sample under crossed polars. The lower edge of the image is 120μm in length.

This sample is composed of approximately 50% serpentine. The high birefringence marks relict olivine minerals. The olivine crystal in the centre of the image has been pulled-apart and partially replaced by serpentine. Fine anhedral Fe-rich spinels decorate the original edge of the olivine mineral.

This sample has 25.8% Mg

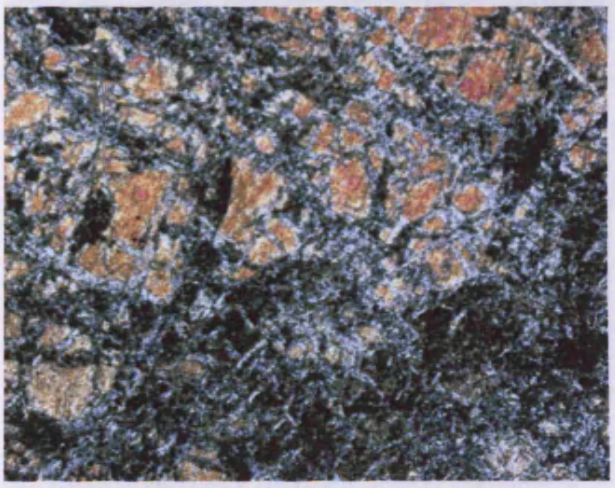

Figure 3.2: A photograph of a dunite sample under crossed polars. The lower edge of the image is 120μm in length.

This sample is composed of approximately 60% serpentine with a typical mesh texture. Some relict olivine minerals show high birefringence colours and slightly wavy extinction but are otherwise they are undeformed. The arrangement of the relict crystal edges indicates that the protolith had an adcumulate texture.

This sample has 22.0% Mg

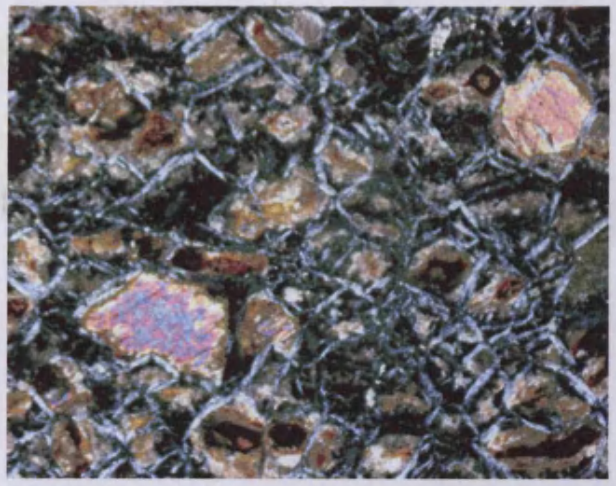

Figure 3.3: A photograph of a dunite sample under crossed polars. The lower edge of the image is 120μm in length.

This sample is composed of approximately 85% serpentine. Unaltered olivine grains have a high birefringence and they are surrounded a serpentine mesh.

This sample has 20.4 % Mg

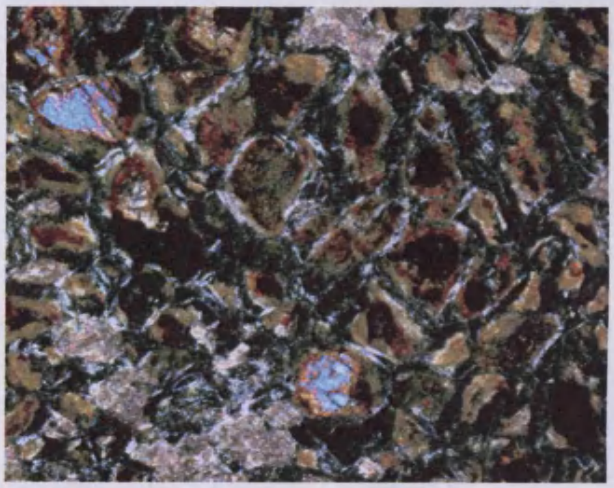

Figure 3.4: A photograph of a dunite sample under crossed polars. The lower edge of the image is 120μm in length.

This sample is composed of approximately 90% serpentine. Grains with a high birefringence indicates the presence of a few remaining fresh olivine minerals. This sample shows intense alteration along cracks and patchy alteration in places (not shown). Some minor pyroxene (<5%) is observed.

This sample has 16.4% Mg

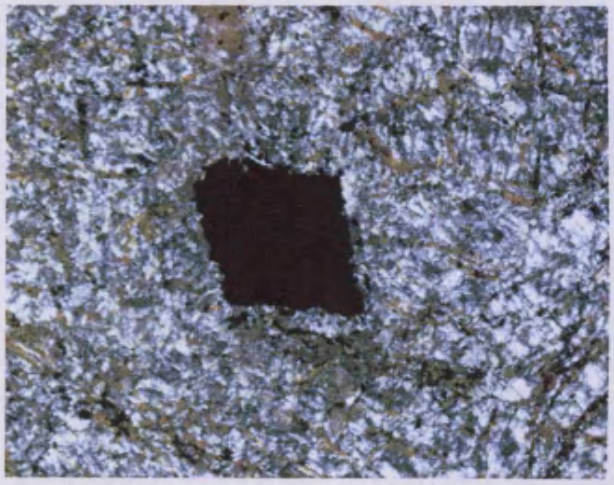

Figure 3.5: A photograph of a dunite sample under crossed polars. The lower edge of the image is 120μm in length.

This sample is completely serpentinised (not including the oxide minerals). This sample shows a relict olivine texture within the serpentine mesh which is decorated with fine anhedral spinels. Additionally, the sample contains subhedral spinels such as the one shown in the centre of the image.

This sample has 7.0% Mg

3.3.3. Clinopyroxenite

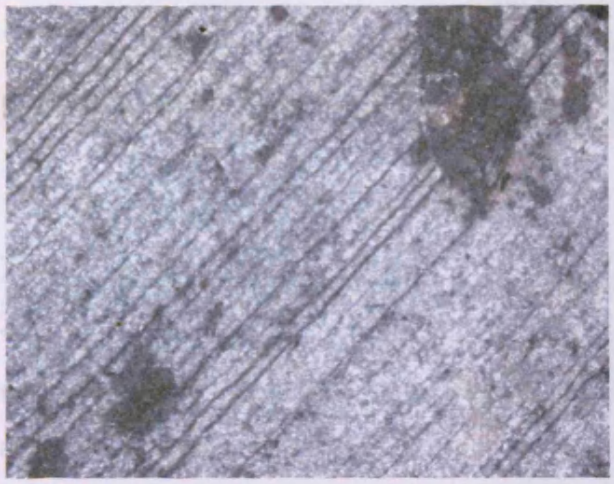

Figure 3.6: A photograph of a clinopyroxenite sample from Kingy area under crossed polars. The lower edge of the image is 120μm in length.

This sample is 100% replaced by fibrous amphibole. The clinopyroxene has a poikilitic texture enclosing minor olivine and can form up to 1cm in length.

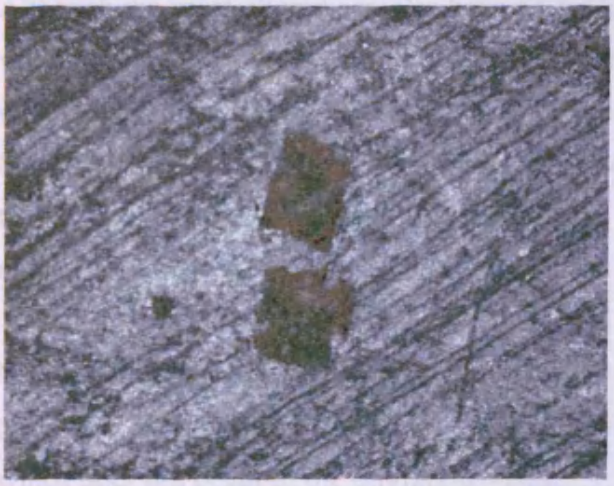

Figure 3.7: A photograph of a clinopyroxenite sample from the Kingy area under crossed polars. The lower edge of the image is 120μm in length.

This sample is 100% by fibrous amphibole minerals. The field of view is occupied by one large clinopyroxene and it is recognised by closely spaced which would be expected for orthopyroxene. The clinopyroxene minerals frequently occur in sizes over 1.5cm.

3.3.4. Birbirite

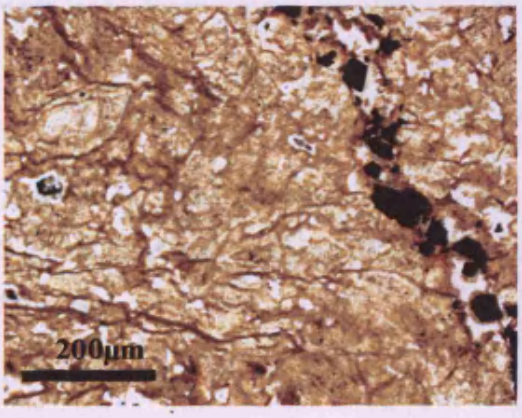

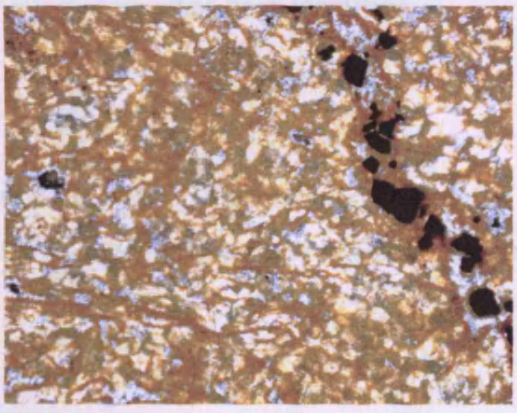

Figure 3.8: A photograph of a birbirite sample from the Tulu Dimtu Main Intrusion area. The lower edge of the image is 120μm in length. **Left: Plane polarized light. Right: Crossed polars**

This sample contains a fine silica network with highly altered spinels (hematite) sometimes disseminated and sometimes in veins (see figure 3.8).

3.3.5. Summary

The dunites show a gradual change in texture with serpentinisation (from 50% to 100%). The least altered samples (50%) show serpentine forming around fresh olivine grains and the edges of the original minerals are decorated with fine anhedral spinels. With further alteration serpentine becomes more abundant and the mesh texture more extensive. Although the most altered samples have no fresh olivine, a relict olivine texture remains visible within the serpentine mesh and fine spinels are visible. Regardless of the degree of alteration, euhedral to subhedral spinels can be observed in most samples in addition to the fine grained anhedral spinels found at the edges of the olivine grains. Furthermore throughout all samples, olivines show pull-apart textures and some show slightly wavy extinction.

No fresh clinopyroxene has been observed in this study of the WES. Some minor olivine (<10%) is observed. The clinopyroxene is recognized by a closely spaced relict cleavage which does not occur in the olivines or spinels. In one sample the clinopyroxene shows a poikilitic texture around olivine. The clinopyroxene has been replaced by fibrous amphibole and cleavage can continue as far as 1.5cm, indicating that the original crystals were large. Furthermore, no relict or fresh orthopyroxene has been identified.

3.3.6. Classification of Rock Types

This study uses the recommendations made by the IUGS subcommission on the Sytematics of Igneous Rocks (Streckeisen, 1976). The rock types used here are defined as follows:

- Dunite: greater than 90% olivine and less than 10% pyroxene
- Clinopyroxenite: greater than 90% clinopyroxene and less than 10% olivine.
- Olivine-olinopyroxenite: Greater than 60% clinopyroxene and less than 40% olivine.

Given the high degree of alteration observed in the WES (a minimum of 50%) minerals are often completely replaced. However, even in the most altered dunites (figure 3.5) and clinopyroxenites (figures 3.6 and 3.7) relict features of the key minerals can be observed. Therefore, in this study the identification of the primary magmatic minerals is made either using observations of fresh minerals (eg high birefringence for olivines) or by the identification of relict features. The following relict features have been used to identify olivine and clinopyroxene:

- Olivine: A relict olivine texture preserved within a serpentine mesh with or without fine anhedral spinels decorating the relict mineral edge.
- Clinopyroxene: A closely spaced cleavage which does not occur in spinels or olivines.

An ultramafic rock as classified here may not actually contain any of the igneous minerals specified by Streckeisen (1976). For example the term dunite as used in this thesis may refer to a rock entirely composed of serpentine, so long as pseudomorphed olivines can be recognized using a mesh texture. A further account of the degrees of alteration within each area is undertaken in chapter 6 which attempts to quantify the alteration using geochemical data.

In a situation where no relict features are observed the sample is classified as "unidentified".

3.4. Oxide Minerals

3.4.1. Introduction

Spinels often resist alteration and, therefore, a study of their morphology and geochemistry can help us understand the magmatic processes. The crustal cumulates and mantle tectonites of ophiolite complexes can host chromitite layers. Further down the crustal sequences of ophiolites, podiform chromitite bodies can form (eg Lippard et al., 1986). Disseminated spinels are common in many parts of ophiolite mantle sequences. Similarly, in Alaskan-type intrusions disseminated spinels are common but they can also form into schlieren and in some complexes podiform ore-bodies have been observed (Johan, 2002). In the WES, the only descriptions concerning spinels are those of Belete et al. (2000) who describe both magmatic and metamorphic forms.

In this section, photomicrographs of spinels and their host minerals were taken using the Cardiff S360 SEM (see section 3.2.1). This section presents an account of the typical textures of spinels from the WES in order to accompany a study of the geochemistry of the spinels described in chapter 7.

3.4.2. Tulu Dimtu

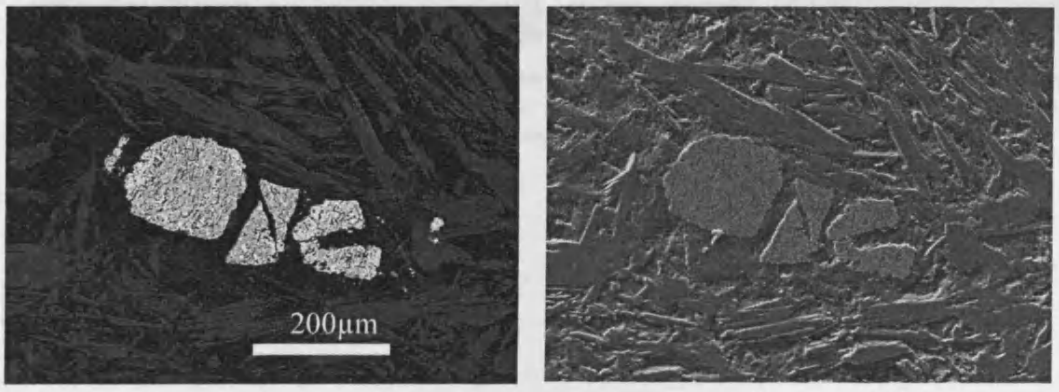

Figure 3.9: SEM photomicrographs of a disseminated spinel (white colour, high mean atomic number) in a clinopyroxenite sample (DTR-019-02). The spinel shows a pull apart tecture and is hosted by a gangue of fibrous amphibole. **Left: back-scattered electron image, Right: secondary electron image.**

3.4.3. Kingy

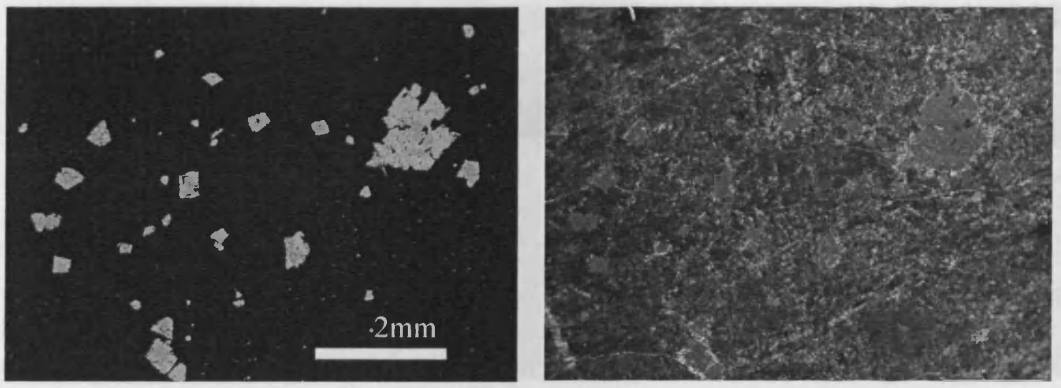

Figure 3.10: SEM photomicrographs of disseminated spinels (white colour, high mean atomic number) hosted by olivine in sample DTR-057-02. Some spinels are subhedral and zoned. **Left: back-scattered electron image, Right: secondary electron image.**

3.4.4. Daleti, Ankori, Tulu Kapi and Keley

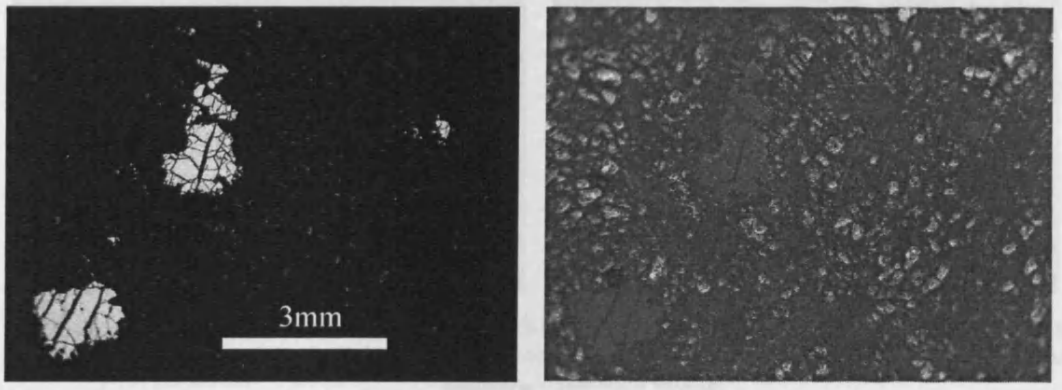

Figure 3.11: SEM photomicrographs of disseminated spinels (white colour, high mean atomic number) hosted by partially serpentinised olvines from sample D19. Many spinels show pull-apart textures. **Left: back-scattered electron image, Right: secondary electron image.**

3.4.5. Yubdo, Andu and Sodu

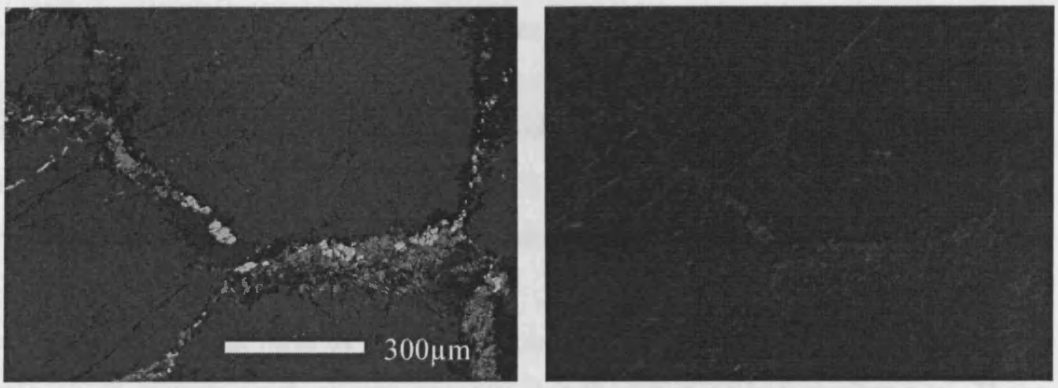

Figure 3.12: SEM photomicrographs of anhedral spinels (white colour, high mean atomic number) from sample Y28. The spinels occur in serpentine filled cracks between fresh clinopyroxenes minerals (large grey coloured minerals. **Left: back-scattered electron image, Right: secondary electron image.**

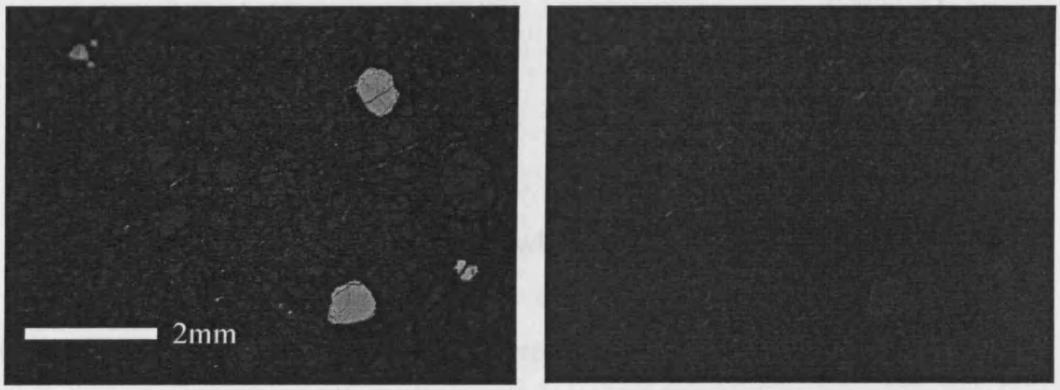

Figure 3.13: SEM photomicrographs of disseminated spinels (white colour, high mean atomic number) partially serpentinised olivines from sample Y30. **Left: back-scattered electron image, Right: secondary electron image.**

3.4.6. Summary

In all areas, two distinct groups of spinels are found, fine anhedral minerals and coarser subhedral to euhedral ones. In some samples anhedral spinels up to 100µm across occur (see figures 3.1 and 3.12). These form at the edges of silicate phases in association with serpentine. In contrast, it is common to find more regular disseminated spinels which are hosted by olivine, serpentine or fibrous amphibole. These minerals commonly show pull-apart textures and are often well over 500µm in length.

3.4.7. Discussion

The observation that there are two types of spinel textures is common in ultramafic rocks (Sack and Giorso, 1995). The serpentinisation of olivine minerals releases Fe from the crystal lattice to form Fe-oxides. The irregular shapes, formation at the edges of olivines and association with serpentine support this hypothesis. Furthermore, preliminary analysis of the geochemistry of these minerals show a high Fe content.

The euhdral to subhedral form of the second spinel group and their association with host minerals which include fresh olivine suggests that they formed before alteration. These may be cumulus spinels and therefore their geochemistry may reflect magmatic processes (see chapter 7).

3.5. Sulphide Minerals

3.5.1. Introduction

PGE are known to form a close association with sulphide minerals and many models have been developed whereby the behaviour of sulphur is used to help explain the development of PGE deposits. In magmas where sulphur is present, geochemical models suggest that PGE are likely to be taken into solution within sulphide melts (Naldrett and Duke, 1980). Furthermore, Pt and Pd are most likely to partiton into Cu-rich sulphides (Barnes et al., 1997). Such geochemical models are complimented by mineralogical studies. Prichard et al. (2004) have observed the expression of such geochemical models in sulphide blebs from a mafic dyke in Uruguay. After the crystallization of the magma, it is believed that the same hydrothermal fluids which remobilize sulphur also remobilize PGE (Wood, 2002)

This section provides a description of sulphide minerals from the WES and the subsequent discussion may provide a further insight into the processes which influence the PGE distribution.

3.5.2. Tulu Dimtu

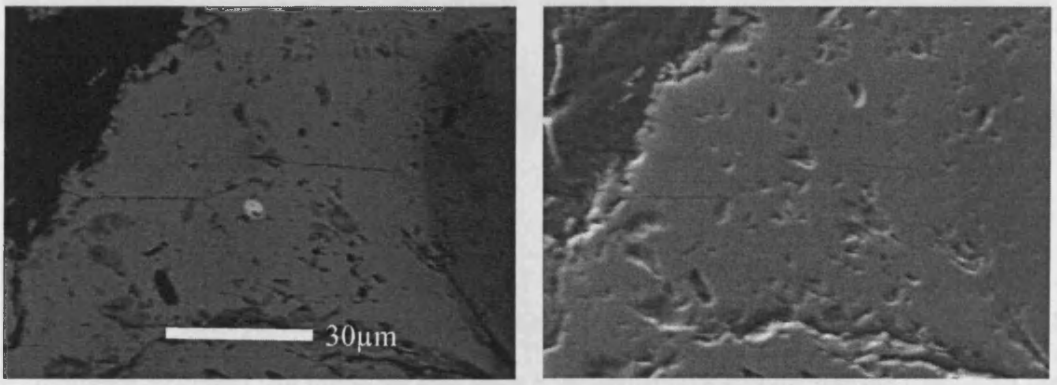

Figure 3.14: SEM photomicrographs of an altered bornite (white colour, high mean atomic number in the centre of image) in the altered rim of a Cr-spinel (grey colour), hosted by serpentine (black). This image has been taken from sample TDR19/01 which is located on the southern flank of the Tulu Dimtu Main Intrusion. **Left: back-scattered electron image, Right: secondary electron image.**

Cu	S	Fe	O	Total
59.41	24.47	12.24	2.64	98.76

This analysis can be quoted as $Cu_{4.88}Fe_{1.14}S_{3.98}$ – ignoring oxygen - which is close to bornite (Cu_5FeS_4). The oxygen indicates that the mineral has been altered. As bornite is an alteration product of chalcopyrite, this mineral infers that at least two phases of alteration have occurred.

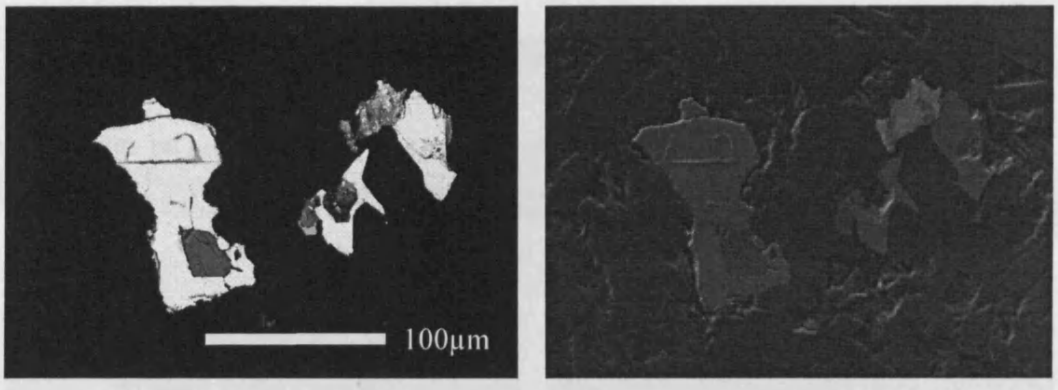

Figure 3.15: SEM photomicrographs of an anhedral glaucodot split into three parts (white colour, high mean atomic number) hosted by serpentine. The sulphide mineral on the left hosts a Ni- As-bearing magnetite inclusion. This image has been taken from sample DTR-019-02 from the Tulu Dimtu Lensoid Ultramafics. **Left: back-scattered electron image, Right: secondary electron image.**

As	S	Co	Ni	Fe	O	Total
44.88	17.77	15.77	13.74	4.44	3.7	100.3

If the oxygen is ignored then this analysis may be quoted as $(Co,Ni,Fe)_{1.01}As_{1.04}S_{0.96}$ which is close to glaucodot and is represented by the formula (Co,Fe)AsS. This assumes that the Ni has substituted for Co. The oxygen could indicate that the mineral has been altered.

3.5.3. Kingy

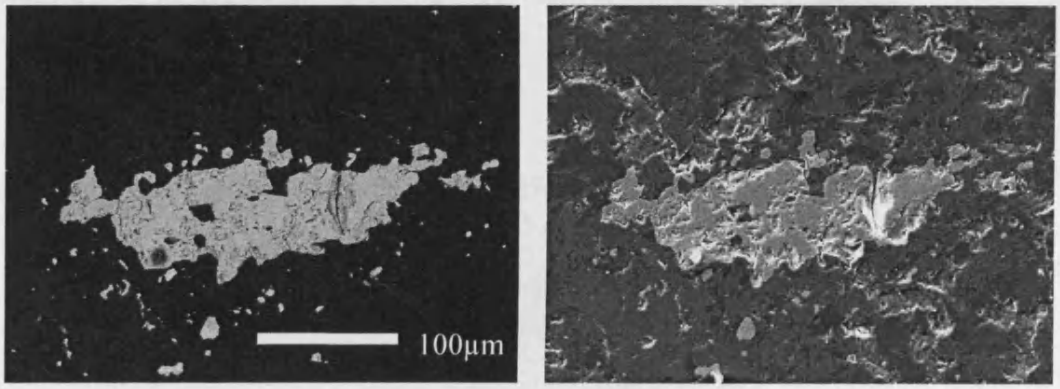

Figure 3.16: SEM photomicrographs of an anhedral chalcopyrite mineral (white colour, high mean atomic number) hosted by quartz in an extremely altered olivine-clinopyroxenite sample. This image has been taken from sample KTR-049-02 from the Kingy Ridge Ultramafic. **Left: back-scattered electron image, Right: secondary electron image.**

S	Cu	Fe	Total
34.3	32.69	29.9	96.89

This mineral can be quoted as $Cu_{0.97}Fe_{1.01}S_{2.02}$ which is close to chalcopyrite ($CuFeS_2$).

3.5.4. Daleti, Ankori, Tulu Kapi and Keley

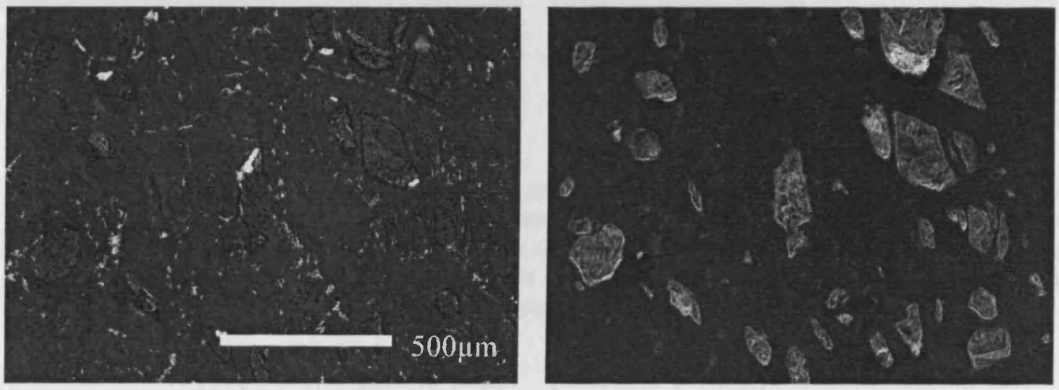

Figure 3.17: SEM photomicrographs of several anhedral barite crystals (white specs, high mean atomic number) on the edge of larger partially serpentinised olivine minerals. There are many anhedral Fe-rich spinels. This image has been taken from sample DR22/01 from the Daleti Ultramafic. **Left: back-scattered electron image, Right: secondary electron image.**

Ba	S	Fe	Si	Al	Mg	O	Total
55.16	12.19	0.66	0.29	0.25	0.18	24.21	92.94

This analysis can be quoted as $Ba_{1.03}S_{0.98}O_{3.89}$ which is close to barite ($BaSO_4$)

3.5.5. Yubdo, Andu and Sodu

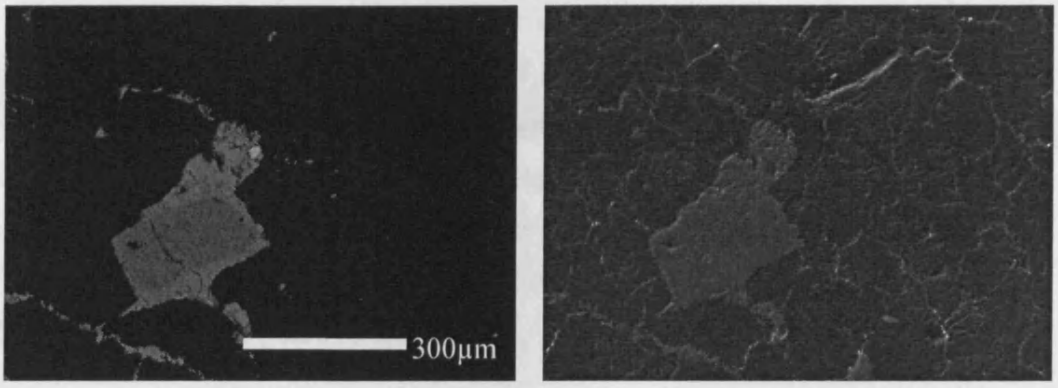

Figure 3.18: SEM photomicrographs of a Ni-sulphide mineral (white spec, high mean atomic number) in the altered rim of a zoned spinel hosted by serpentine (black). In addition to the subhedral spinels (centre of image) there are many fine anhedral Fe-rich spinels which sometimes form schlieren. This image has been taken from sample AYR-016-01 from the northwestern flank of the Main Yubdo Intrusion. **Left: back-scattered electron image, Right: secondary electron image.**

S	Ni	Fe	Co	Total
33.19	25.96	22.8	18.93	100.88

This analysis could be quoted as $Fe_{1.30}(Ni,Co)_{2.42}S_{3.28}$. The most similar mineral found is violarite ($FeNi_2S_4$), unfortunately the fit for this mineral is poor and attempts to fit the analysis to the following minerals less successful: bravoite, $(Fe,Ni,Co)S_2$; pentlandite, $(Fe,Ni)_9S_6$; siegenite, $(Co,Ni)_3S_4$.

3.5.6. Summary

Most sulphides are hosted by serpentine but some by quartz or altered spinel. Those sulphides sufficiently large to be resolved by the SEM, they appear to be anhedral in shape.

It is observed that Ni-barren, Cu-sulphides occur in both the southern flank of the Tulu Dimtu Main Intrusion and the Kingy Ridge Ultramafic. However, in the Tulu Dimtu Lensoid Ultramafics, several Ni-sulpharsenides have been discovered. In the Main Yubdo Intrusion only Cu barren, Ni-sulphide minerals are observed.

3.5.7. Discussion

Most sulphides described here are hosted by minerals such as serpentine and quartz which are often associated with the action of medium and low temperature fluids. A highly irregular shape is observed for the base-metal sulphides in most cases and this is unlike the euhedral or rounded shapes expected if these minerals crystallised from a magma. Furthermore, the presence of magnetite inclusions within the sulphides from the Tulu Dimtu Lensoid Ultramafics suggests that they formed after the magma cooled and possibly after at least one phase of alteration.

Given the affinity of these sulphides with high temperature fluids (as discussed above), the division between the Cu-bearing sulphides (Tulu Dimtu Main Intrusion and Kingy Ridge Ultramafic) and the Ni bearing-sulphides (Tulu Dimtu Lensoid Ultramafics and the Main Yubdo Intrusion) could have two interpretations. Firstly, the Cu and Ni could have formed in the same magmatic site and then been remobilized different degrees by alteration – maybe one Ni-rich phase and another Cu-rich. Alternatively, the Ni and Cu could have been driven apart at a magmatic stage (as proposed by Barnes et al., 1997 and Prichard et al., 2004).

Two sulphide minerals are observed in the altered rims of spinels, one Cu-rich and the other Ni-rich (figures 3.9 and 3.19 respectively). Although their presence in the alteration rim of a spinel suggests that alteration fluids have affected their host, there is no direct evidence for large amounts of fluid transport through the spinel itself. Furthermore, as spinels resist alteration to a greater degree than silicate phases, it is possible that little transport of fluid has been made into the mineral. Even if the sulphide phases have recrystallised in situ, these two minerals may infer the possibility that Ni and Cu formed at different sites during magmatic processes.

The low number of sulphide minerals studied here means that this study does not provide a comprehensive account of the behaviour of S, Cu and Ni in the WES. However it is one of the first accounts of sulphide minerals in these igneous complexes in the WES.

3.6. Platinum Group Minerals

3.6.1. Introduction

A search for PGM was performed in the 10 rock samples with the highest Pt and Pd values which included two samples from the Tulu Dimtu Main Intrusion (see chapter 6). Three PGM were discovered in rock samples from the Main Yubdo Intrusion and none from the Tulu Dimtu Main Intrusion. In the following section the geochemistry and association of each PGM is described.

3.6.2. Sample AYR-016-01

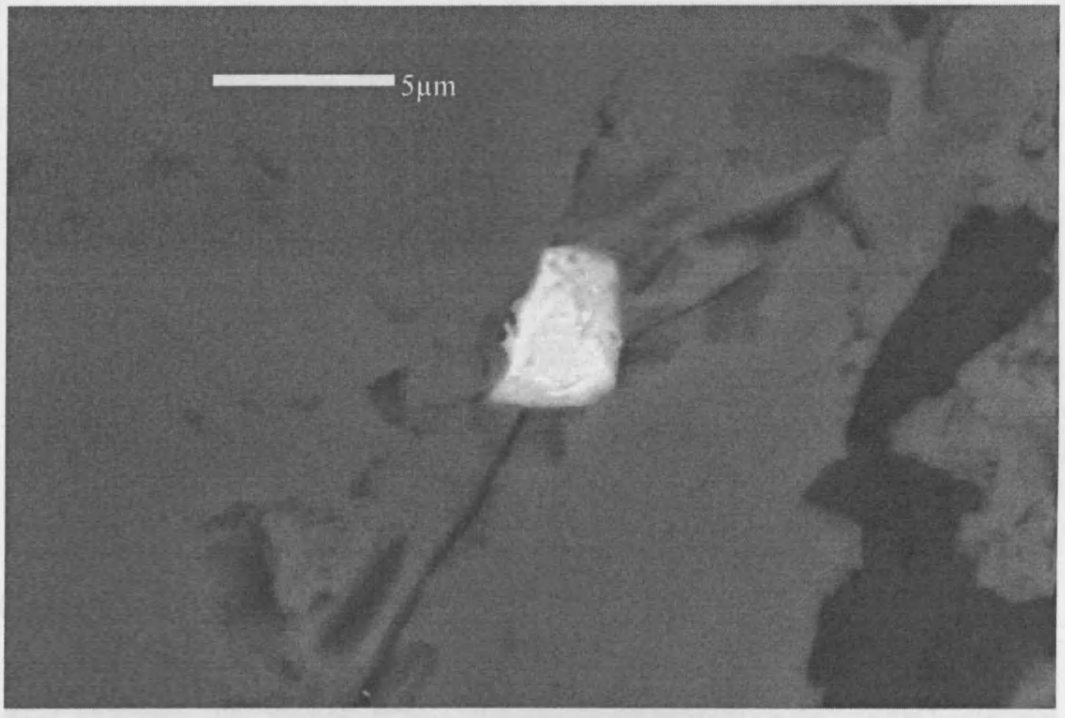

Figure 3.19: An SEM back-scattered electron image photomicrographs of a subhedral Pt-Fe alloy (white colour, high mean atomic number) in a Cr-spinel hosted by serpentine. This image has been taken from sample AYR-016-01 from the northwestern edge of the Main Yubdo Intrusion.

Pt	Fe	Cr	O	Total
92.29	11.86	1.12	2.27	107.55

It is possible that all Cr and Fe in this analysis originated from chromite and hematite as a result of fluorescence. If chromite and hematite are removed (resulting in a total of 99.87), then the analysis can be quoted as $Pt_{3.10}Fe_{0.89}$ which is close to Pt_3Fe. Although both Cr and Fe are common in the host rock, the poor total raises suspicion about the quality of original analysis.

3.6.3. Sample KYR-019-02

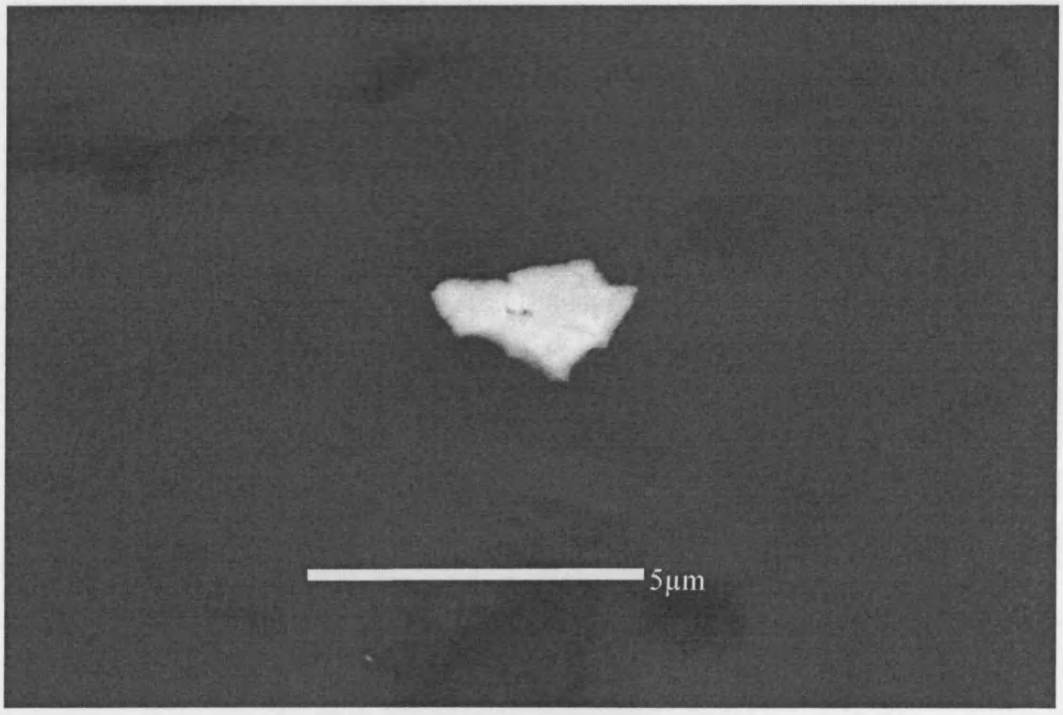

Figure 3.20: An SEM back-scattered electron image photomicrographs of an anhedral Os-Ir alloy (white colour, high mean atomic number) hosted by serpentine. This image has been taken from sample KYR-019-01 located the northwestern flank of the Main Yubdo Intrusion.

Qualitative analysis shows that this mineral contains major Os and Ir, lesser amounts of Ru, Fe and O, and traces of Si and Mg.

3.6.4. Sample Y30

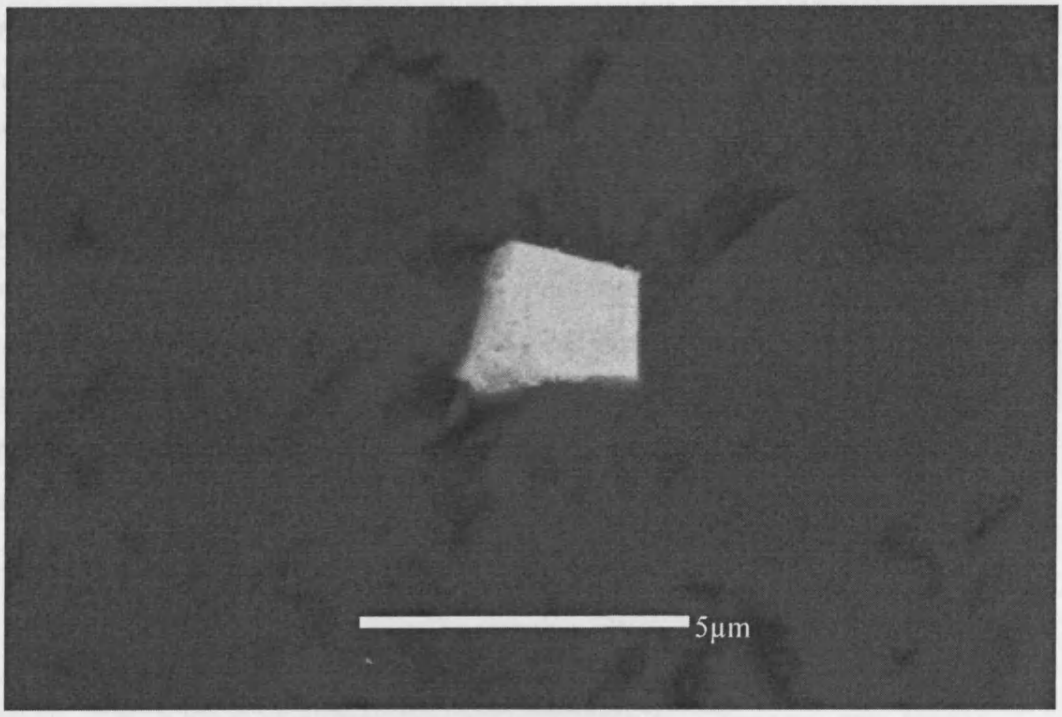

Figure 3.21: An SEM back-scattered electron image photomicrographs of a subhedral Ir-Os alloy (white colour, high mean atomic number) within a Cr-spinel hosted by partially serpentinised olivine. This image has been taken from sample AYR-016-01 located on the far western flank of Main Yubdo Intrusion.

Ir	Os	Zr	Ru	Fe	Rh	Cr	S	O	Total
79.11	9.25	6.33	2.76	2.18	2.55	1.71	0.45	1.14	105.48

It is possible that all Cr and Fe in this analysis originated from chromite and hematite as a result of fluorescence. If chromite and hematite are removed (resulting in a total of 101.50), then the analysis can be quoted as $Ir_{0.67}Os_{0.08}Ru_{0.04}Rh_{0.04}Zr_{0.11}Fe_{0.03}S_{0.02}$. Although both Cr and Fe are common in the host rock, the poor total raises suspicion about the quality of original analysis.

3.6.5. Discussion

The only other account of PGM in the rocks from the Yubdo area is a description of Pt-Fe alloys (Mogessie et al., 1999). These contain minor Ir and are hosted by either chromite or serpentine. The Zr found in the Ir-Os alloy from sample Y30 is unusual for a platinum group mineral. The Pt-Fe alloy described here (sample AYR-016-01) has a similar chemistry and shape to those found by Mogessie et al. (1999) however it is considerably smaller. The Pt-Fe alloys which are hosted by serpentine are typically 20-30μm in diameter.

There are many studies of placer PGM from the rivers and laterites around Yubdo (as reviewed in chaper 2). Most of the placer PGM described are Pt-Fe nuggets and a recent study documents 3 grains which contain Os-Ir inclusions (Belete et al., 2000). It is possible that the Os and Ir bearing PGM described here could be magmatic or postmagmatic minerals around which further PGE-bearing phases will nucleate. This preliminary study is one of the few accounts of PGM in the WES and may prompt further work to understand the genesis of placer Pt-Fe alloys.

4. Terrain Mapping

4.1. Introduction

This chapter details the use of terrain mapping from aerial photographs to identify the characteristic terrain for the larger ultramafic complexes in the WES (Yubdo and Tulu Dimtu) and to map these features elsewhere in the WES. In this area terrain mapping is more appropriate than normal geological mapping as there is little exposure (<5% in some areas), the rocks are very weathered and access is often difficult. Preliminary studies around the Yubdo and Daleti areas have indicated that the ultramafic complexes form high ridges on which vegetation is sparse and no cultivation is being undertaken. By contrast, the surrounding terrain is densely vegetated and subsistence farming is common.

Figure 4.1: A photograph of a barren ridge above the Daleti Ultramafic. The ridge is almost devoid of vegetation when compared to the foreground. Furthermore, the houses to the right indicate the presence of fertile subsistence farmland.

The lack of vegetation and agriculture may result from high Ni or low Ca values in the soil, which is characteristic of lateritic soils above ultramafic rocks. As detailed in chapter 2, the ultramafics of the WES are commonly surrounded by volcano-sedimentary sequences. These units are less resistant to weathering and therefore the harder ultramafic complexes are likely to stand out from the softer sedimentary sequences and therefore form ridges. Hence it is thought likely that the "barren-ridge" terrain will be characteristic of the ultramafic complexes.

A set of aerial photographs were procured from the Ministry of Mines (Addis Ababa). In section 4.2, the method of acquisition of these images and their compilation into map form is described. Subsequently, a description of the use of terrain elements to describe the terrain in the WES is provided (see section 4.3). The results are recorded as a set of maps containing photomorphic regions covering four geographic areas (as described in chapter 5), the boundaries of which were confirmed by field observations (see section 4.4).

4.2. Aerial Photography

4.2.1. Introduction

When aerial photographs are used for mapping, the user must consider the method by which the photograph was acquired, as the equipment used will create distortions of the scene being recorded. Before maps are created, these distortions must be corrected. This section describes the acquisition and processing of the aerial photographs from the WES. Finally an account of the specifications of the aerial photographs is provided.

4.2.2. The Aerial Photographs of the WES

The aerial photographs (from the Ministry of Mines, Addis Ababa) used in this study can be divided into two groups: those acquired during 1957/58 and those taken in 1980. The images taken in 1957/58 covered the Yubdo and Daleti areas however the 1980 set covered Tulu Dimtu and Daleti.

	1957/58	1980
Camera Type	Single Lens Frame	Single Lens Frame
Camera Focal Length	53.046mm	53.66
Film Format	230mm	233mm
Dates of acquisition	19-Dec-1957 20-Dec-1957 1-Jan-1958	15-Jan-1980 18-Jan-1980 22-Jan-1980 24-Jan-1980 31-Jan-1980
Time of acquisition	Between 9:45AM and 11:49AM	*
Lens Serial Number	XF6751	UAGII 3119
Orientation of Flight	North - South	East - West
Average Scale	1:55715	1:53063
Mean distance between Aerial photographs (m)	5,233	4,667
Average distance to Terrain (m)	9,370	*
Apparent Stereoscopic Viewing Distance (cm)	24	*
Stereoscopic Vertical Exaggeration	1.97	*
Digital resolution	10m	10m

Table 4.1: The details of the aerial photographs. *: Data obscured during development.

To demonstrate the degree of distortion present in the images, figures for the relief displacement of two prominent features have been calculated. This is done using an equation based on the distance from the feature to the centre of the image image and the altitude (see table 4.2). Sodu ridge is the highest point in the image and is close to the edge and therefore is likely to have the largest relief displacement. However, this figure is only 3mm which equates to around 150m on the ground. These figures show that relief displacements are negligible for these images.

Feature	Distance from photograph centre to top of feature (m)	Altitude of feature (m)	Relief Displacement (m)
Yubdo Village	0.02	1670	0.00059
Sodu Ridge	0.102	1668	0.00300

Table 4.2: Relief Displacements of Yubdo Village and Sodu Ridge.

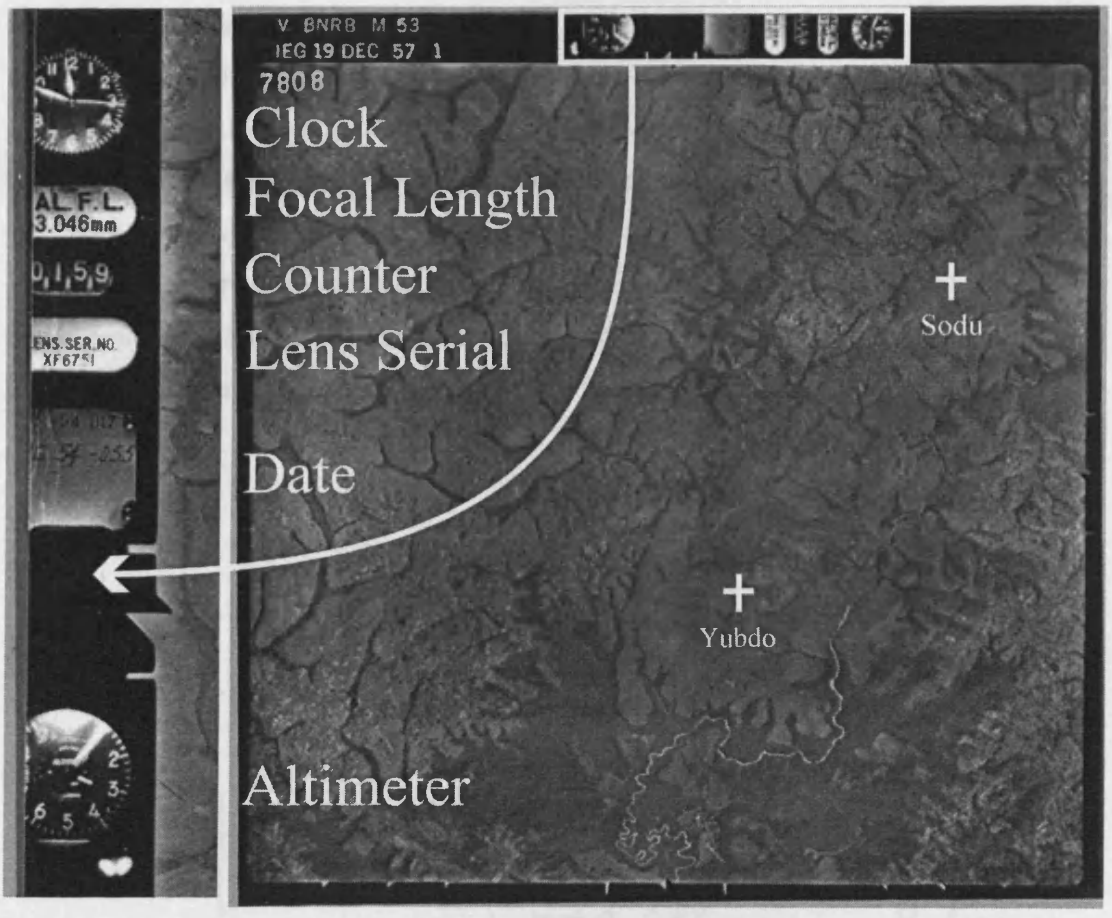

Figure 4.2: A typical aerial photograph with the data block enlarged.

4.2.3. The Acquisition of Aerial Photographs

This section covers the physics of the acquisition of aerial photography. Typical cameras used in aerial photography are described, followed by an account of the properties of photographic film. The characteristics of photographic films and cameras cause several distortions and displacements which are described at the end of this section.

There are several types of camera used on aircraft; panoramic, multilens, strip (for a review see Wolf, 1983). However in this study, airphotos were aquired using a single lens frame mapping camera. Single lens frame cameras are the simplest type of aerial camera. The setup of the camera is based around the focal length, which is selected according to the intended application for the resulting images. The focal length of a camera is of

importance as it determines the angular field of view of the photographs. As the camera is always set up with the image distance as the focal length of the lens, the shorter the focal length the wider the field of view (Wolf, 1983; Paine, 1981). Figure 4.3 shows the three main sections of the single lens frame mapping camera: magazine, body and lens cone assembly (Lillesand and Kiefer, 2000). The "data block" is shown on figures 4.3 and 4.2. In this feature several measurements are displayed so that the photograph includes a number of key readings including: altitude, time of day, focal length, exposure number, lens serial number and date.

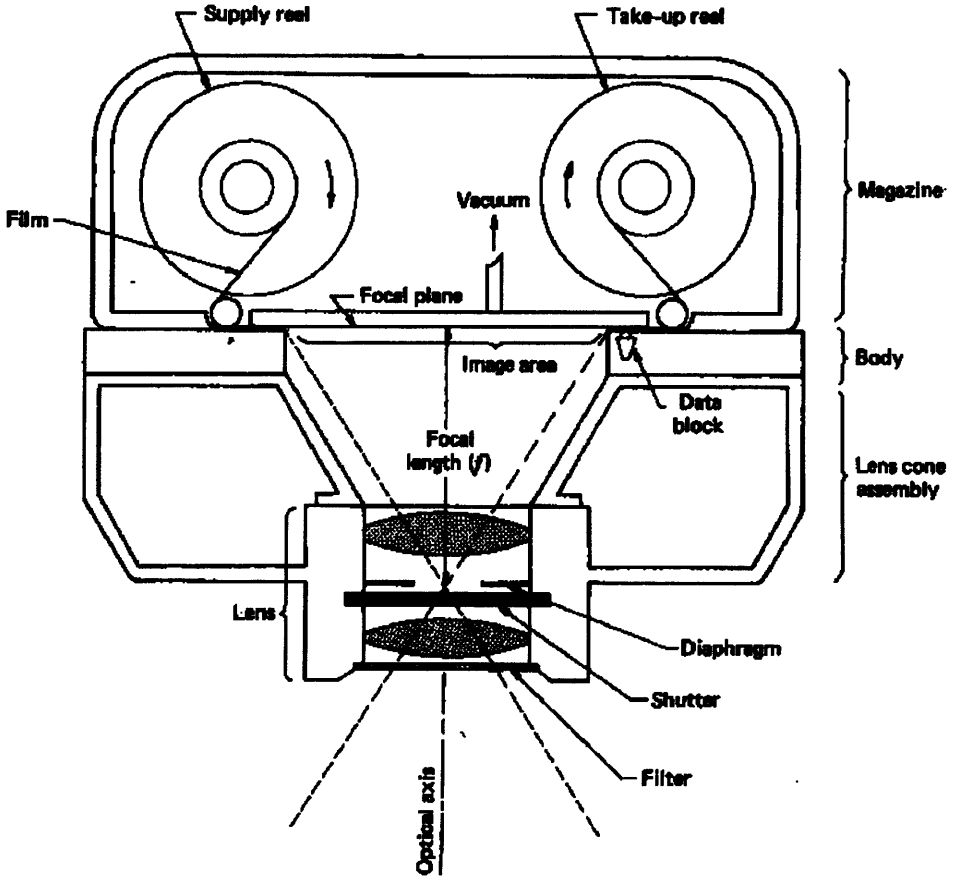

Figure 4.3: Principle components of a single-lens mapping camera (Lillesand and Kiefer, 2000)

Within the camera, light rays traveling from the scene are focused through a lens onto a film creating an invisible "latent" image. As a result the image acquired in the camera is negative (black and white exchanged) and reversed both left for right and top for bottom through the camera lens. Printing then produces a visible image on print paper and the

image is positive with axes corrected. Although many types of film are available such as colour and infra-red, the film used in this study is panchromatic. Such films are not the same as a "black and white" films. Panchromatic films produce an image based on the total light intensity, so a bright scene at any wavelength appears as white on the image (Lillesand and Kiefer, 2000).

A vertical aerial photograph is not a map. It is the product of a perspective projection and as such there are displacements and distortions which affect the image which are as follows:

- **Exposure fall-off.** The image appears brighter in the centre than at the edges of the scene. This is because the light collected from the further points has traveled further through the dust in the air and the scene is viewed from a more oblique angle. This is more obvious when using wide angle lenses.
- **Vignetting.** These are shadowing effects as a result of lens imperfections and parts of the camera.
- **Relief displacement.** This has the strongest effect in mountainous or urban scenes. The top of a vertical object is observed as being further away from the centre of the image than the bottom of the object (Wolf, 1983).
- **Tilt displacement.** An aerial photograph is never truly vertical and as such, relief displacement (see above) is exaggerated in particular directions.
- **Lens distortion.** This is the effect of imperfections in the grinding and production of the lens causing the image to be blurred or distorted mainly on the outside of the image and depends on the f-stop used in the aperture.

Some of these problems, such as exposure fall-off, vignetting and lens distortion are normally corrected through calibration. A scene of known and uniform brightness is imaged and the systematic variations in image tone recorded on the film are used to

create a filter, or recalibrate parts of the camera apparatus (Lillesand and Kiefer, 2000). However, the problems associated with relief and tilt displacement need to be addressed by image processing.

4.2.4. Image Processing

An aerial photograph does not exactly match the scene it represents due to a number of factors (see section 4.2.3). The process of orthocorrection reduces the impact of relief and tilt displacement. Furthermore the images must be associated with a map projection to allow other spatial data to be compared with it, a process known as georeferencing. The aerial photography used in this study was orthocorrected and georeferenced simultaneously, using PCI Geomatica Orthoengine (version 8.3).

Geomatica is a suite of programs used to create Geographic Information System (GIS) databases. Within this software package, Orthoengine is an image processing tool which can be used to allow aerial photographs to be used with GIS applications. In this study it is used to correct geometric distortions and to georeference the aerial photographs. The method used to correct the photographs is called polynomial correction. The aerial photograph is scanned at a resolution of 600dpi and saved in TIFF file format. The user defines 5 to 10 points on the image and these are known as Ground Control Points (GCPs). Each point is then located on a map and each GCP is assigned to a location based on the grid system used on the map. Each image has a number of defined points with a grid reference assigned, the program uses an iteration technique to determine a polynomial function (unique to each image) which describes the translation and rotation necessary to distort those image points to fit the grid defined by the grid references. It then uses this polynomial to distort the entire image to fit the grid. This process is completed for all images. These corrected images were then combined as a mosaic and saved as one image.

The cartographic system chosen for this study is the Universal Transverse Mercator which matches the Ethiopian national grid. It was chosen to allow an easy comparison between this study and other work in the area and provides a smaller degree of distortion

than latitude and longitude grids. The aerial photographs of this study were georeferenced to the following grid:

Grid	UTM Zone 36
Projection	Transverse Mercator
Spheroid	Clarke 1880 (modified)
Unit of measurement	Metre
Meridian of origin	33°E
Latitude at origin	Equator
Datum	Adindan (30th Arc)

Table 4.3: The mapping parameters used in the study.

4.3. Terrain Analysis

4.3.1. Introduction

In this study, the technique of Terrain Analysis is used to evaluate the landforms in the WES with the aim of producing a map of photomorphic regions which the reflect the underlying geology and the soil geochemistry. The term "Terrain Analysis" has been used to describe a variety of activities which evaluate landforms (for example see Wilson and Gallant, 2000 or Townshend, 1981). The method used here is the form of Terrain Analysis which is reviewed by Lillesand and Kiefer (2000). For a more detailed account of the method see Way (1973).

The aerial photographs described in section 4.2 were viewed using a mirror stereoscope (see section 4.3.2) and the landforms in each stereo-pair were analysed using five "terrain elements" which are explained in section 4.3.3. These landform properties were then used to delineate "photomorphic regions" (see section 4.3.9) and the boundaries of such regions were then tested by field work (see section 4.3.10).

4.3.2. Stereoscopy

A stereoscope was used to aid in the analysis of the landforms which have been photographed. This enables an operator to view two images simultaneously and thereby observe the landforms in 3-dimensions. The two photographs are referred to as a stereo-pair. The aerial photographs used here have an overlap at least 50% with of the

4.3.4. Terrain Elements: Drainage pattern

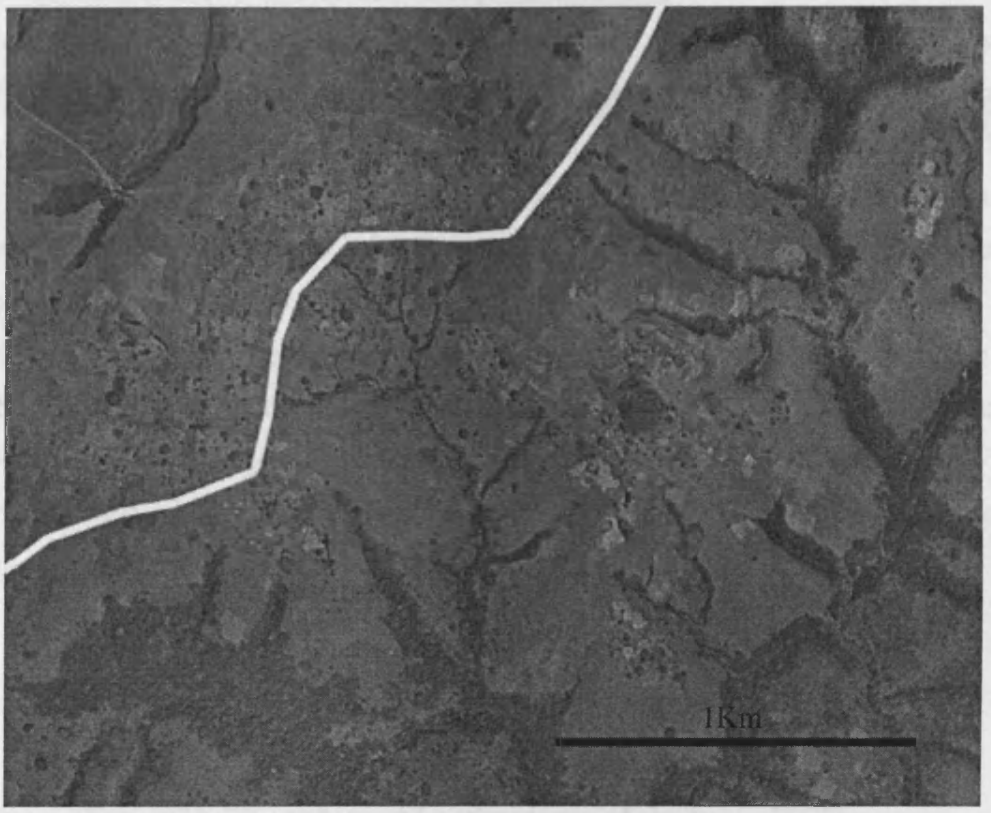

Figure 4.4: A section from an aerial photograph showing the boundary between a coarse dendritic (top left) and fine dendritic (bottom right) drainage patterns. This image is uncorrected and therefore the scale is approximate.

The drainage pattern of an area is the pattern made by the network of waterways. Drainage patterns are classified according both pattern and texture. The pattern is determined according to the direction and shape of the waterways (see figure 4.5). The texture is the density of waterways in an area, ranging from fine to coarse (see figure 4.6). In this study drainage pattern textures are classified as follows:

- **Coarse.** Less than or equal to 3 waterway intersections per km^2
- **Medium.** Between 3 and 6 waterway intersections per km^2
- **Fine.** Greater than 6 waterway intersections per km^2

There are many factors which affect the drainage pattern. Some factors are equal over areas the size of the WES, these include: rainfall, temperature and evaporation rate. However over a few kilometers, the relative proportions of overland flow to groundwater flow determine the texture of drainage pattern. In a situation where rain falls onto ground which is entirely impermeable, all runoff must be overland, and therefore due to the large flux of water over the surface, many waterways will be formed. Where most runoff passes through the groundwater, few waterways will form and the drainage texture will be coarser. Thus drainage pattern directly reflects underlying rock and soil type Furthermore, the strike of geological layering will affect the direction in which water runs off the land surface and therefore drainage pattern can reflect the underlying structure. For example trellis drainage patterns typically form over inclined sedimentary beds whereas dendritic may form over homogenous igneous bodies. For further discussion of the interpretation of drainage patterns see Way (1973).

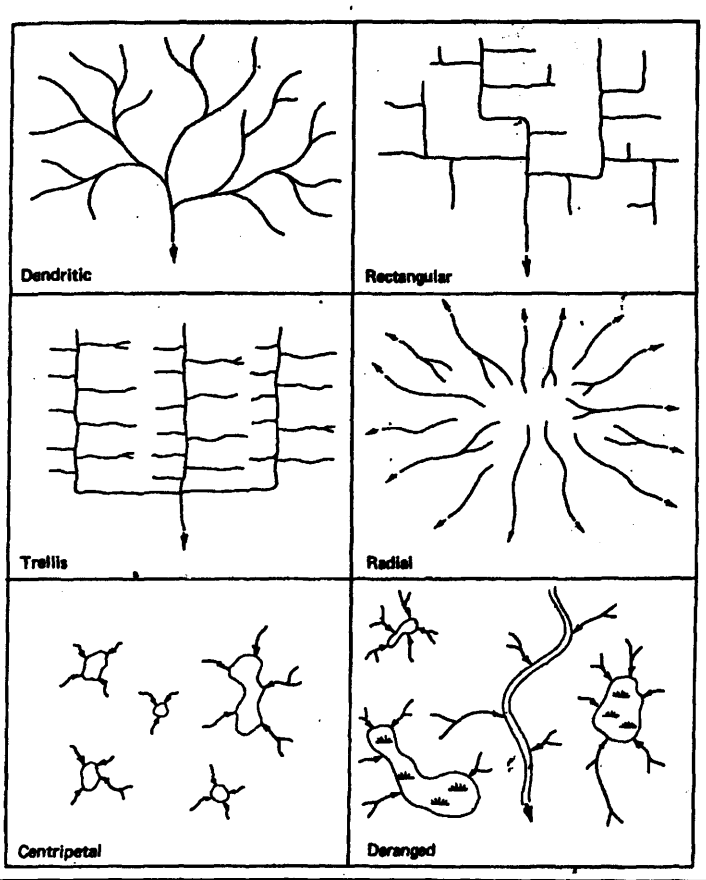

Figure 4.5: The six basic drainage patterns, after Lillesand and Keifer (2000)

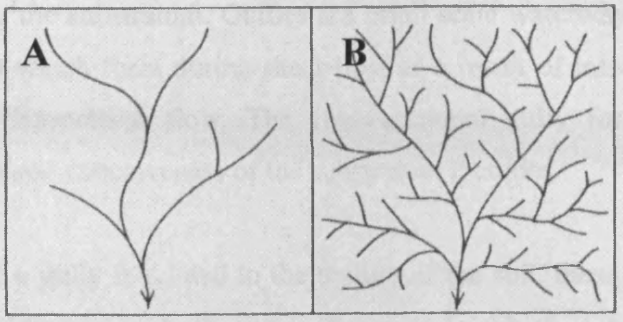

Figure 4.6: Illustrations of drainage texture. A: coarse-textured and B: fine-textured, after Lillesand and Keifer (2000).

4.3.5. Terrain Elements: Erosion

Figure 4.7: A section from an aerial photograph showing the boundary between areas with round-bottomed gullies (left) and v-shaped gullies (right). This image is uncorrected and therefore the scale is approximate.

The form of gullies in an area is assessed in order to determine the way in which erosion has been controlled by the substratum. Gullies are small scale waterways (sometimes as small as 1m in width) which form during sheet flow as a result of intense precipitation which changes into channelised flow. The cross-sectional gully form is controlled partially by the texture and cohesiveness of the substratum it erodes.

Although the shape of a gully is related to the texture of the soil, these textures may be controlled by the underlying bedrock. Since the way in which a rock weathers is controlled in part by its hardness, the underlying lithotype may exert some control over the texture of the overlying soils and thereby the gully shape. Table 4.4 shows the three cross-sectional forms and the substratum textures associated with them.

Name	Cross-section	Related textures (Way, 1973; Lillesand and Kiefer, 2000)
Round bottomed		Cohesive clays and silty clays. Usually found in lake beds, marine terraces and clay-shale areas.
Flat bottomed		Moderately cohesive silt. Often loess and alluvial silt deposits.
V-Shaped		Noncohesive granular materials. Sand and Gravel. Often terraces and outwash plains.

Table 4.4: Gully cross-sections and their related textures.

4.3.6. Terrain Elements: Topography

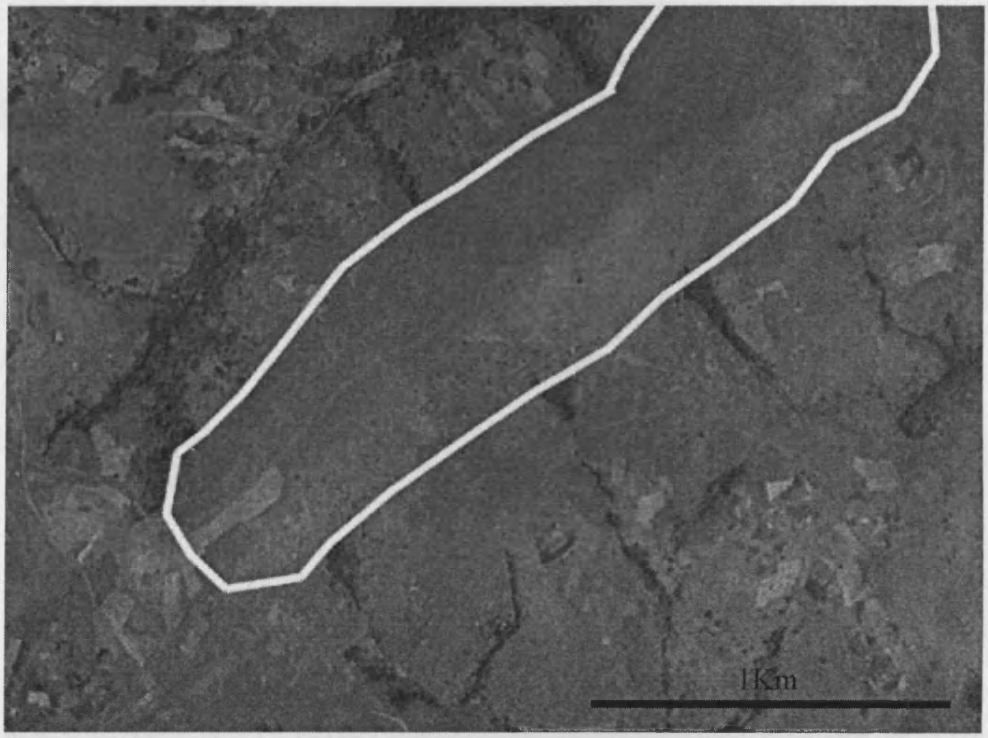

Figure 4.8: A section from an aerial photograph showing a ridge (center) and smaller hills around the outside. This image is uncorrected and therefore the scale is approximate.

There are numerous ways in which topography can be characterized (see Way, 1973) and modern landform analysis uses slope measurements from digital terrain models (Wilson and Gallant, 2000). In this study, the assessment of topography is used to record only whether or not the terrain forms a ridge (as shown in figure 4.1). Hard lithotypes are eroded less than softer rocks and hence hard formations form ridges.

4.3.7. Terrain Elements: Relative image tone and texture

Figure 4.9: A section from an aerial photograph showing the boundaries between bright and dark image tones. The darkest mottled texture is tree cover, however the dark tone of the soil can be observed between trees. This image is uncorrected and therefore the scale is approximate.

The brightness of a land-form (tone) can vary widely (see figure 4.9). Within areas of bare soil or thin vegetation, changes in image tone reflect the moisture content of that soil, this can vary according the texture of that soil and the parent rock material. Within areas of bare soil, the tone may vary and create a tonal texture. This texture can be a useful indicator of soil conditions and soil textures themselves. Within areas of apparently homogenous tone, very fine changes in tone may occur, showing the differences in moisture content.

The images used in this study are panchromatic, which means that they record the total light exposure of all colour bands (including some near-infrared). Due to the exposure fall-off (see section 4.2.3) it is only possible to determine differences in relative image tone. Absolute values for image tone cannot be determined using these images.

4.3.8. Terrain Elements: Land use

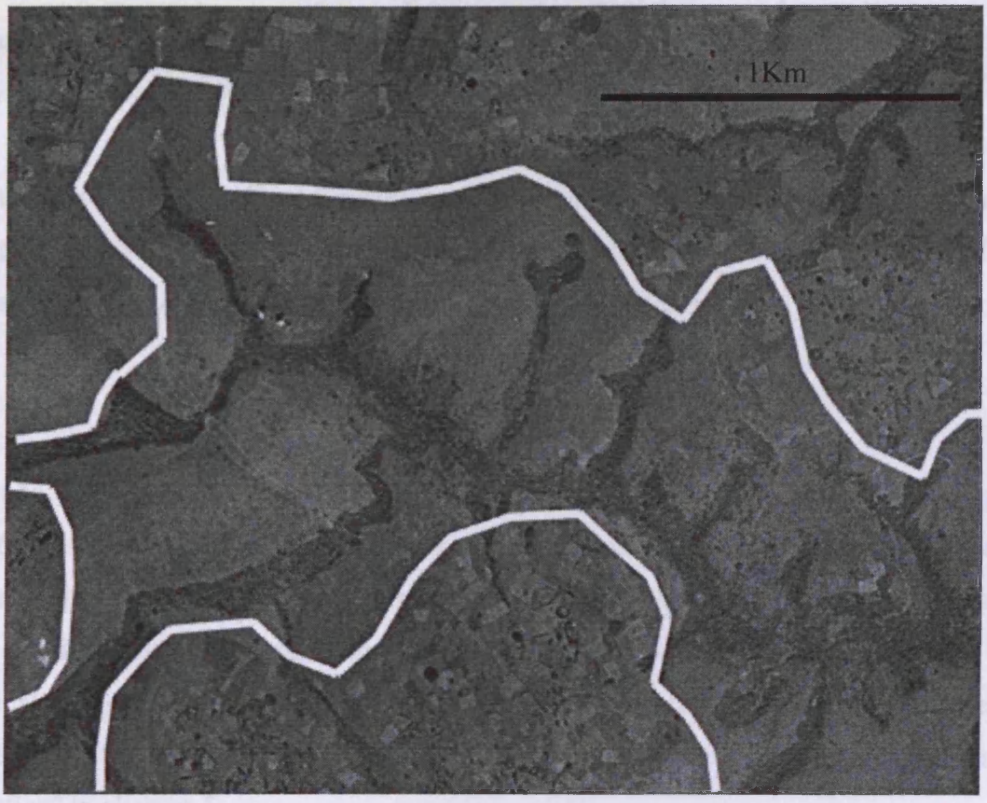

Figure 4.10: A section from an aerial photograph showing the boundary between cultivated land (bottom and top) and non-cultivated land (center). Subsistence farms in Ethiopia typically cultivate fields of no larger than 500m in width. These appear on aerial photographs as a "patchwork" texture. This image is uncorrected and therefore the scale is approximate.

This categorory is an assessment of land use either as vegetation, cultivation or neither. The type and origin of vegetation can indicate important changes in soil geochemistry which are closely related to the parent rock type. Areas of dense cultivation tend to follow water-courses and can also indicate a fertile soil and areas of dense vegetation may indicate other properties such as a high moisture content.

4.3.9. Photomorphic Regions

In order to combine and illustrate the information recorded from the analysis of the air photo stereopairs, a number of photomorphic regions are delineated. A photomorphic

region is defined as a discrete geographic unit within which at least one terrain element is uniform (Lillesand and Kiefer, 2000). In some cases more than one terrain element may be uniform within the photomorphic region. The concept of photomorphic regions is used in many remote sensing mapping applications, not only geological investigations (Lillesand and Kiefer, 2000).

Using the ArcView 3.2 software package, the photomorphic regions were overlain onto the orthocorrected and georeferenced aerial photographs (see section 4.2.4). The information has been presented as a set of four maps (see section 4.4).

4.3.10. Ground Truth

In order to validate the relationship between the land-forms and the underlying geology, each of the suspected ultramafic complexes was studied in the field and samples were collected. The petrology and geochemistry of these samples was investigated and the results are discussed in the subsequent chapters. Chapter 5 describes the full results of geological mapping in the WES. In some areas, there are landforms which have been mapped as ultramafic but no exposure has been found, these are defined as "suspected ultramafics" in chapter 5.

4.4. The Terrain in the WES

4.4.1. The photomorphic regions

A total of 25 photomorphic regions have been defined in this study but not all occur in any one of the four geographic maps. A description of the terrain for each region is contained in table 4.5. The ground truth study established that four formations can be effectively mapped by using terrain analysis, these are Basement, Graphitic Schist, Basalt and Ultramafic. In addition to this, the ground truth investigation discovered that the geological terrain information in some areas is obscured by the practice of burning savanna grass.

Photomorphic region	Drainage Pattern	Erosion	Topography	Relative Image Tone and Texture	Land use
Basalt A	coarse dendritic	flat bottomed	plateau rolling hills	bright polygonal texture.	Highly cultivated. Vegetation along roads and bottoms of valleys.
Basalt B	coarse dendritic	v-shaped	non-orientated hills and ridges	heterogenous	Sparse vegetation everywhere (individual trees) small fields everywhere.
Basalt C	medium to fine dendritic	v-shaped and flat in places	non-orientated hills and ridges	dark in most places	Dense vegetation covering most parts. Small patches of cultivation.
Basalt D	medium to fine dendritic	v-shaped	non-orientated hills and ridges	mainly heterogenous. One patch of dark tone	Cultivation in many places. Dense veg at the bottom of gullies.
Ultramafic A	very fine parallel	v-shaped	single big hill	mostly very dark some light swathes	No cultivation very little vegetation
Ultramafic B	coarse dendritic	v-shaped	large distinct hills	medium to light (dep on exp. cond.)	V. sparse veg, v. little cultivation although some.
Ultramafic C	fine dendritic	v-shaped	incline	dark tone	No cultivation, sparse vegetation in most places.
Ultramafic D	medium trellis	rounded	ridges, one elongate	light homogenous	Vegetation strictly at bottoms of valleys. No cultivation.
Basement A	fine trellis	v-shaped	steep sided, ridges NNE-SSW.	homogenous light tone on valley sides	Only ridge tops cultivated. Natural vegetation at bottom of valleys only.
Basement B	fine dendritic	v shaped	small hills and ridges	medium to dark tone. homogenous	Some vegetation out of gullies, very little cultivation.
Basement C	v fine dendritic	v-shaped	non-orientated ridges	generally dark tone	Vegetation in most areas. Very little cultivation
Basement D	medium to fine dendritic	rounded	non-orientated hills and ridges	mainly dark tone	Mostly covered by dense veg. Cultivation at the top of the ridges/hills.
Basement E	fine dendritic		non-oriented hills	dark	Dense vegetation and no cultivation.
Basement F	medium dendritic	rounded	non-orientated hills	heterogenous	Generally barren but some areas of cultivation

Basement G	medium to fine dendritic		non-orientated hills and ridges	heterogenous	Veg in bottom of gullies. Cultivation in most places
Basement H	fine dendritic	v-shaped	non-oreintated hills and ridges	heterogenous	Cultivated in most places some vegetataion out of gullies
Basement I	v fine dendritic	v-shaped	large ridge, high elevation	heterogenous	Veg in bottom of gullies. Cultivation in most places
Basement J	medium trellis	rounded	ridge	bright near the top of the ridge. Darker tone generally towards the bottoms of slopes	Cultivtaion at the top of the ridge. Spare cult in most places.
Basement K	fine parralell on the west, fine dendritic on the east	v-shaped	large ridge, high elevation	medium tone	No cultivation very little vegetation.
Basement L	N/A ?coarse?	rounded	ridge	light tone	Cultivated in most places.
Basement M	medium to fine dendritic	v-shaped	variably oriented large ridges	generally light tone	Cultivation widespread but sparse. Little dense vegetation.
Basement N	v coarse dendritic	rounded	low gradient rounded hills	homogenous medium tone	Completely uncultivated, some large patches of dense vegetation.
Basement O	medium radial	v-shaped	large hill	medium tone	No cultivation very little vegetation.
Graphitic Schist	trellis	v-shaped	small distinctive ridges	mostly dark altough some lighter	Dense vegetation no cultivation.
Burnt Grass	fine dendritic	v-shaped	variable	very dark	no cultivation or vegetation

Table 4.5: A table of the photomorphic regions of the WES.

4.4.2. Tulu Dimtu

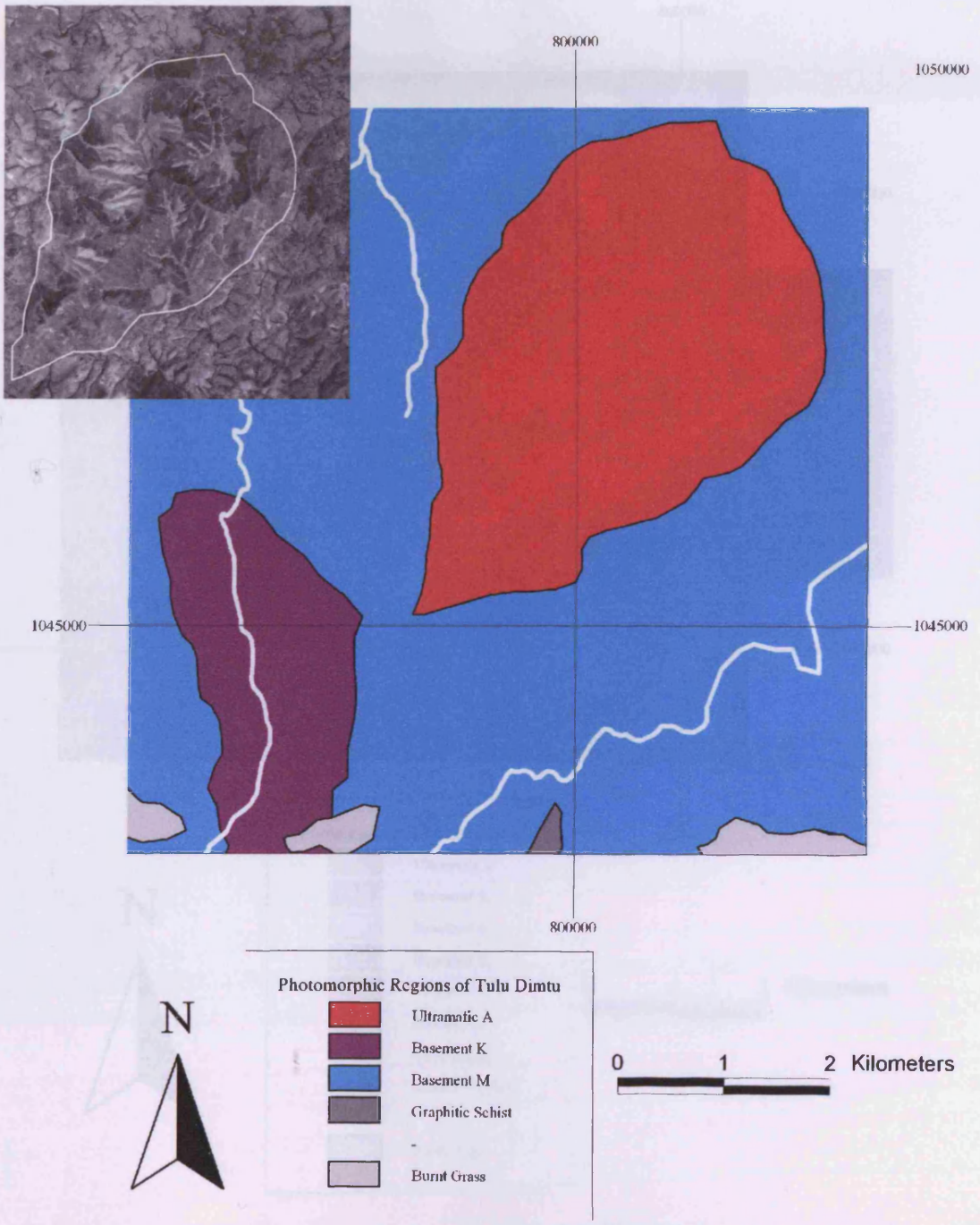

Figure 4.11: A map of photomorphic regions for the Tulu Dimtu area. White lines indicate the course of the major rivers. Inset is a representative aerial photograph showing the main ultramafic formation.

4.4.3. Kingy

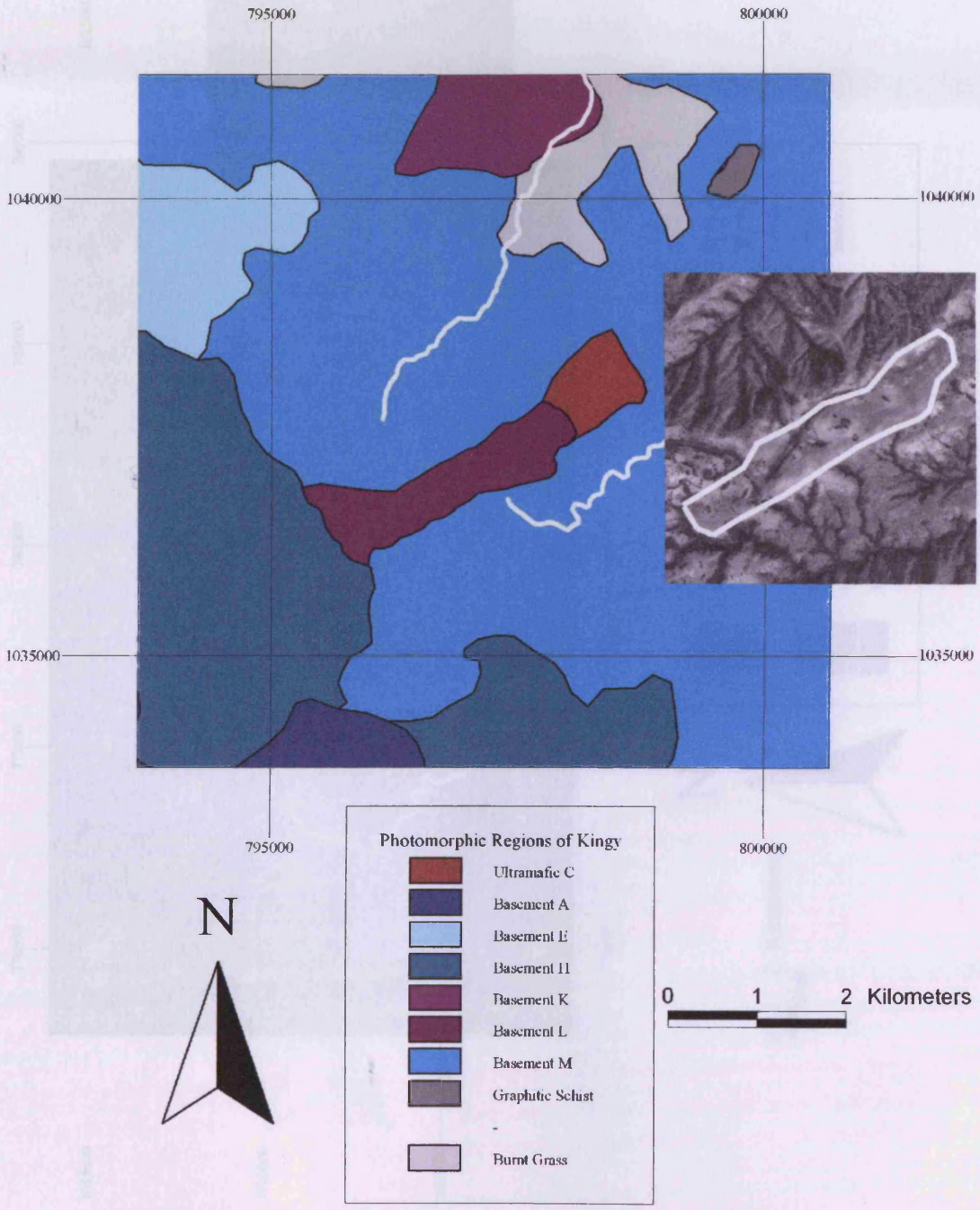

Figure 4.12: A map of photmorphic regions for the Kingy area. White lines indicate the course of the major rivers. Inset is a representative aerial photograph showing the main ultramafic formation.

4.4.4. Daleti, Ankori, Tulu Kapi and Keley

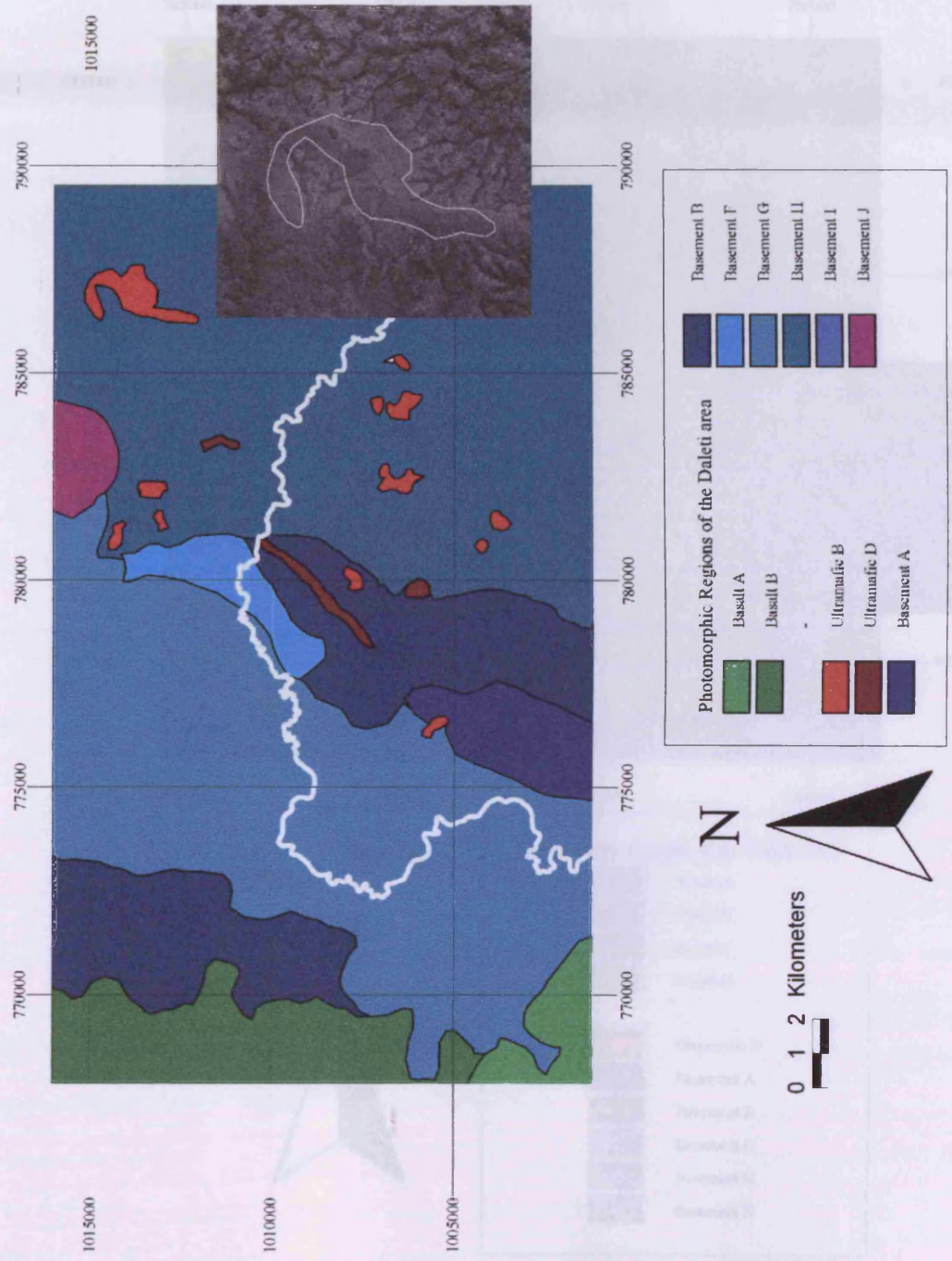

Figure 4.13: A map of photmorphic regions for the Daleti, Ankori, Tulu Kapi and Keley areas. White lines indicate the course of the Birbir river. Inset is a representative aerial photograph showing the main ultramafic formation.

4.4.5. Yubdo, Sodu and Andu

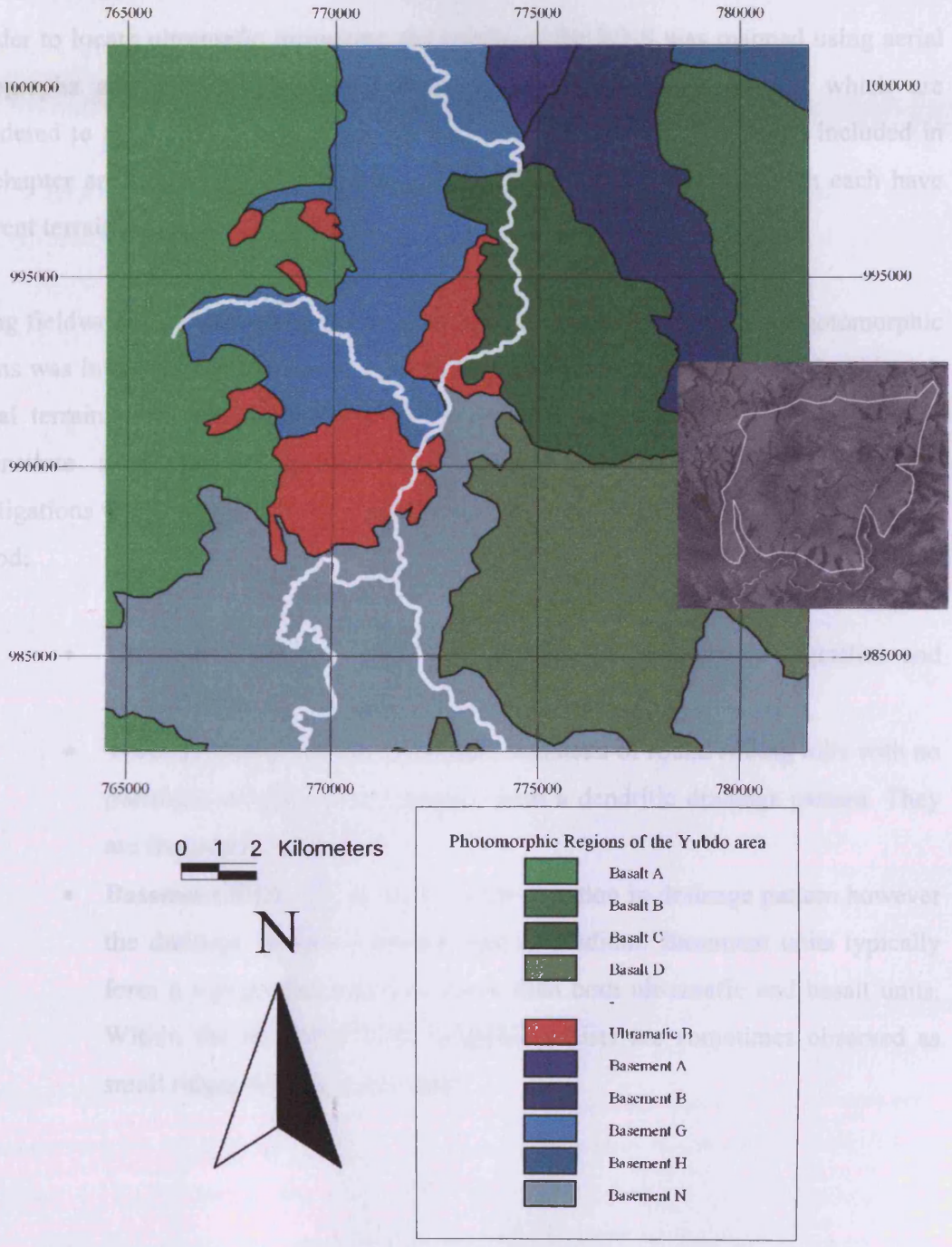

Figure 4.14: A map of photmorphic regions for the Yubdo, Andu and Sodu areas. White lines indicate the course of the major rivers. Inset is a representative aerial photograph showing the main ultramafic formation.

4.4.6. Summary

In order to locate ultramafic intrusions, the terrain of the WES was mapped using aerial photographs and the results plotted as maps of photomorphic regions which are considered to reflect the geology (see sections 4.2 and 4.3). The four maps included in this chapter are composed of a selection of 25 photomorphic regions which each have different terrain features.

During fieldwork, the changes in the geology over the boundaries between photomorphic regions was investigated. The results of such fieldwork is covered in chapter 5. Although several terrain units are identified as basement, in this study, it was not possible to demonstrate a change in geology over these boundaries. However, geological investigations have suggested that three major formations can be mapped using this method:

- **Ultramafic units.** These are identified as areas of sparse vegetation and no cultivation and almost always form ridges.
- **Tertiary Basalt units**. These form a plateau of round rolling hills with no particular orientation and always form a dendritic drainage pattern. They are frequently cultivated.
- **Basement units.** These have a wide variation in drainage pattern however the drainage texture is always fine or medium. Basement units typically form a topography which is lower than both ultramafic and basalt units. Within the basement units, graphitic schists are sometimes observed as small ridges with no cultivation.

5. Geological Mapping

5.1. Introduction

Small scale maps of the WES have been published by various authors. Additionally, large scale maps of the Main Yubdo Intrusion and the Tulu Dimtu Main Intrusion have been produced (Kazmin and Demessie, 1971; de Wit and Aguma, 1977). Of these maps, it is only those of the Main Yubdo Intrusion that provides details of the internal structure of the ultramafic complexes. It is for this reason that new maps have been produced during this study for Tulu Dimtu, Kingy and Daleti and the Kazmin and Demessie (1971) map of the Yubdo area has been modified in light of the observations made during this study.

These new maps have been created for use as a base for the presentation of geochemical data (see chapter 6) They are the result of a combination of field observations and terrain mapping. The lithologies identified here are those defined in chapter 3. Although the ultramafic formations are given names based on their fresh protoliths many of the rocks they represent may be completely replaced by metamorphic minerals (see chapters 2 and 3). Furthermore, the poor exposure and high degree of weathering makes the collection of structural measurements difficult. Although some geological structures (such as shear tension indicators) are visible in the basement, such information is not clear in the ultramafic units.

5.2. Method

The geological maps were compiled using several methods which were combined using a GIS database (ArcView 3.2). Fieldwork was carried out in four trips between September 2001 and June 2002. As a result, lithological descriptions of samples and field observations were combined with the terrain mapping information as described in chapter 4. Therefore on the maps, the basalt and basement units were mapped mainly using the terrain but verified geologically at the locations indicated on each map. The next four sections show the geological map of each of the geographic areas followed by a description of the geology.

5.3. *Geological Maps of the WES*

5.3.1. Tulu Dimtu

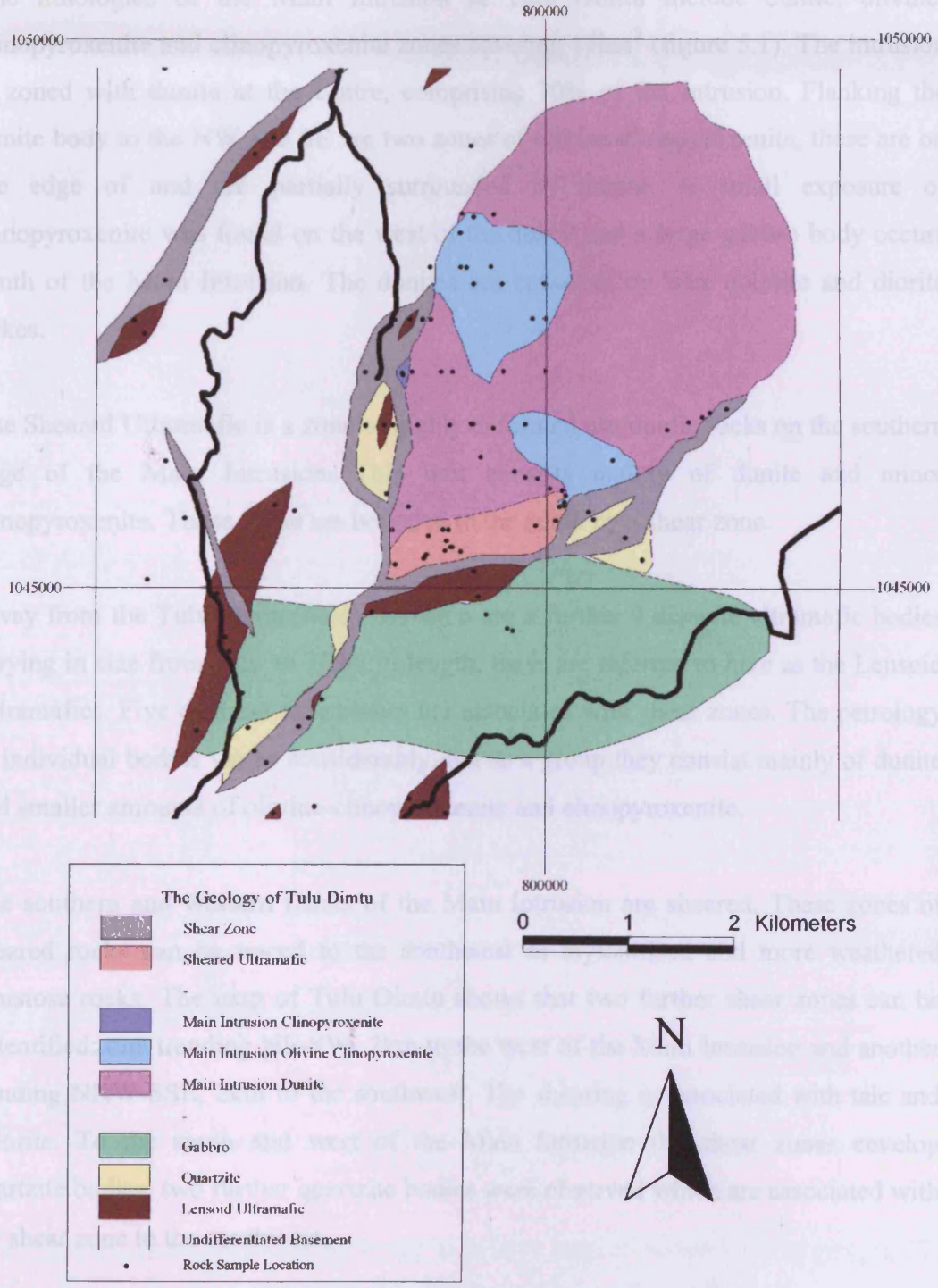

Figure 5.1: The geological map of the Tulu Dimtu area. Black lines indicate the course of the major rivers.

There are three groups of ultramafic rocks in the Tulu Dimtu area: The Main Intrusion, Sheared Ultramafic and the Lensoid Ultramafics.

The lithologies of the Main Intrusion at Tulu Dimtu include dunite, olivine-clinopyroxenite and clinopyroxenite zones covering 17km^2 (figure 5.1). The intrusion is zoned with dunite at the centre, comprising 70% of the intrusion. Flanking the dunite body to the NW and SE are two zones of olivine-clinopyroxenite, these are on the edge of and are partially surrounded by dunite. A small exposure of clinopyroxenite was found on the west of the dunite and a large gabbro body occurs south of the Main Intrusion. The dunites are cross-cut by later dolerite and diorite dykes.

The Sheared Ultramafic is a zone of highly deformed ultramafic rocks on the southern edge of the Main Intrusion. This unit consists mainly of dunite and minor clinopyroxenite. These rocks are bounded to the south by a shear zone.

Away from the Tulu Dimtu Main Intrusion are a further 9 discrete ultramafic bodies varying in size from 3km to 700m in length, these are referred to here as the Lensoid Ultramafics. Five of these nine bodies are associated with shear zones. The petrology of individual bodies varies considerably, but as a group they consist mainly of dunite and smaller amounts of olivine-clinopyroxenite and clinopyroxenite.

The southern and western flanks of the Main Intrusion are sheared. These zones of sheared rocks can be traced to the southwest as mylonitised and more weathered schistose rocks. The map of Tulu Dimtu shows that two further shear zones can be indentified: one trending NE-SW, 2km to the west of the Main Intrusion and another trending NNW-SSE, 2km to the southwest. The shearing is associated with talc and chlorite. To the south and west of the Main Intrusion the shear zones envelop quartzite bodies, two further quartzite bodies were observed which are associated with the shear zone to the southwest.

5.3.2. Kingy

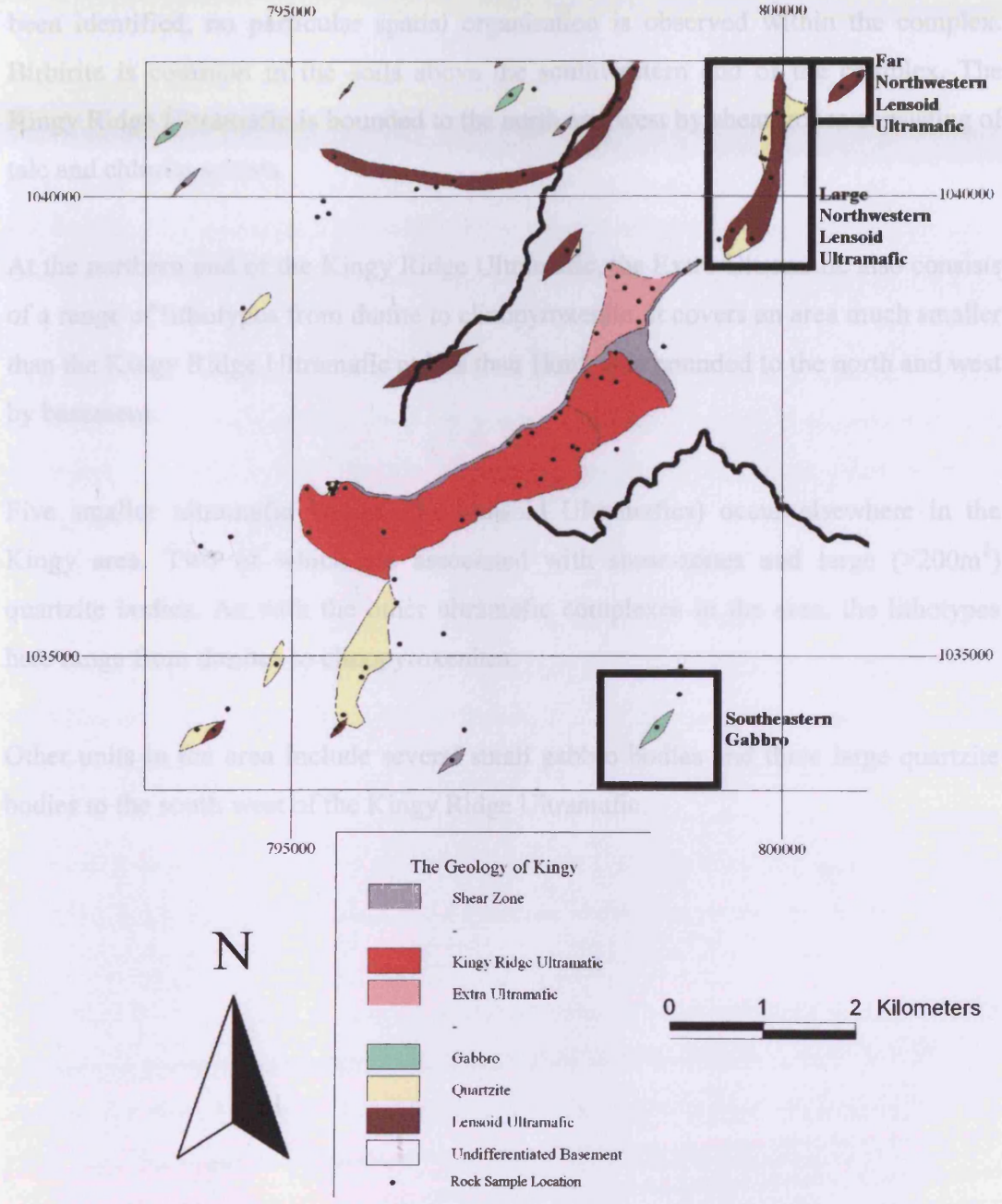

Figure 5.2: The geological map of the Kingy area. Black lines indicate the course of the major rivers.

The ultramafic complexes of the Kingy area have been allocated to three groups: The Kingy Ridge Ultramafic, the Extra Ultramafic and the Lensoid Ultramafics.

The Kingy Ridge Ultramafic is an NE-SW trending elongate body composed mainly of dunite and olivine-clinopyroxenite with a small amount of clinopyroxenite. These ultramafic lithologies cover a total area of 6km^2 and although three lithotypes have been identified, no particular spatial organisation is observed within the complex. Birbirite is common in the soils above the southwestern end of the complex. The Kingy Ridge Ultramafic is bounded to the north and west by shear-zones consisting of talc and chlorite schists.

At the northern end of the Kingy Ridge Ultramafic, the Extra Ultramafic also consists of a range of lithotypes from dunite to clinopyroxenite. It covers an area much smaller than the Kingy Ridge Ultramafic at less than 1km^2. It is bounded to the north and west by basement.

Five smaller ultramafic bodies (the Lensoid Ultramafics) occur elsewhere in the Kingy area. Two of which are associated with shear-zones and large (>200m^2) quartzite bodies. As with the other ultramafic complexes in the area, the lithotypes here range from dunites to clinopyroxenites.

Other units in the area include several small gabbro bodies and three large quartzite bodies to the south west of the Kingy Ridge Ultramafic.

of the Ankori Ultramafic have been located using terrain mapping (see chapter 4). However, no exposure could be found at these locations and therefore they are named "suspected ultramafics".

The largest complex is the Daleti Ultramafic which covers an area of around $5km^2$. The complex is a large dunite body with several pods of a mafic monomineralic rock around 6m in length and 2m in width and consisting mainly of spinel ($MgAl_2O_4$). To the northwest, the complex is bounded by a shear-zone consisting of talc-schists and a small gabbro body occurs close to the southern contact with the basement.

The Ankori Ultramafic is an elongate body of around 5km in length and up to 800m in width. It is composed mainly of dunite, but some minor clinopyroxene was observed near the northern tip. The complex is associated with some small quartzite bodies and is mostly surrounded by basement.

The five Lensoid Ultramafics occur throughout the area covered in this section. Only one locality has been found for each complex and as a result structural control on their association is very poor. Two of these bodies, in the Keley area, are closely associated with extensive shear-zones. Furthermore, a troctolite body has been located at Gudeya Guji associated with an elongate zone of talc and chlorite-schists. One Lensoid Ultramafic was located in the southern basement and a further ultramafic body was located close to a Tertiary Basalt and a quartzite in the northwest of the area.

Shear-zones are common within the basement units and they are often associated with ultramafics and quartzite bodies. The shear-zones at Gudeya Guji form in a distinctive straight NE-SW trending ridge in line with several smaller shear-zones to the southwest. Some gabbro units have been observed within the basement.

5.3.3. Daleti, Ankori, Tulu Kapi and Keley

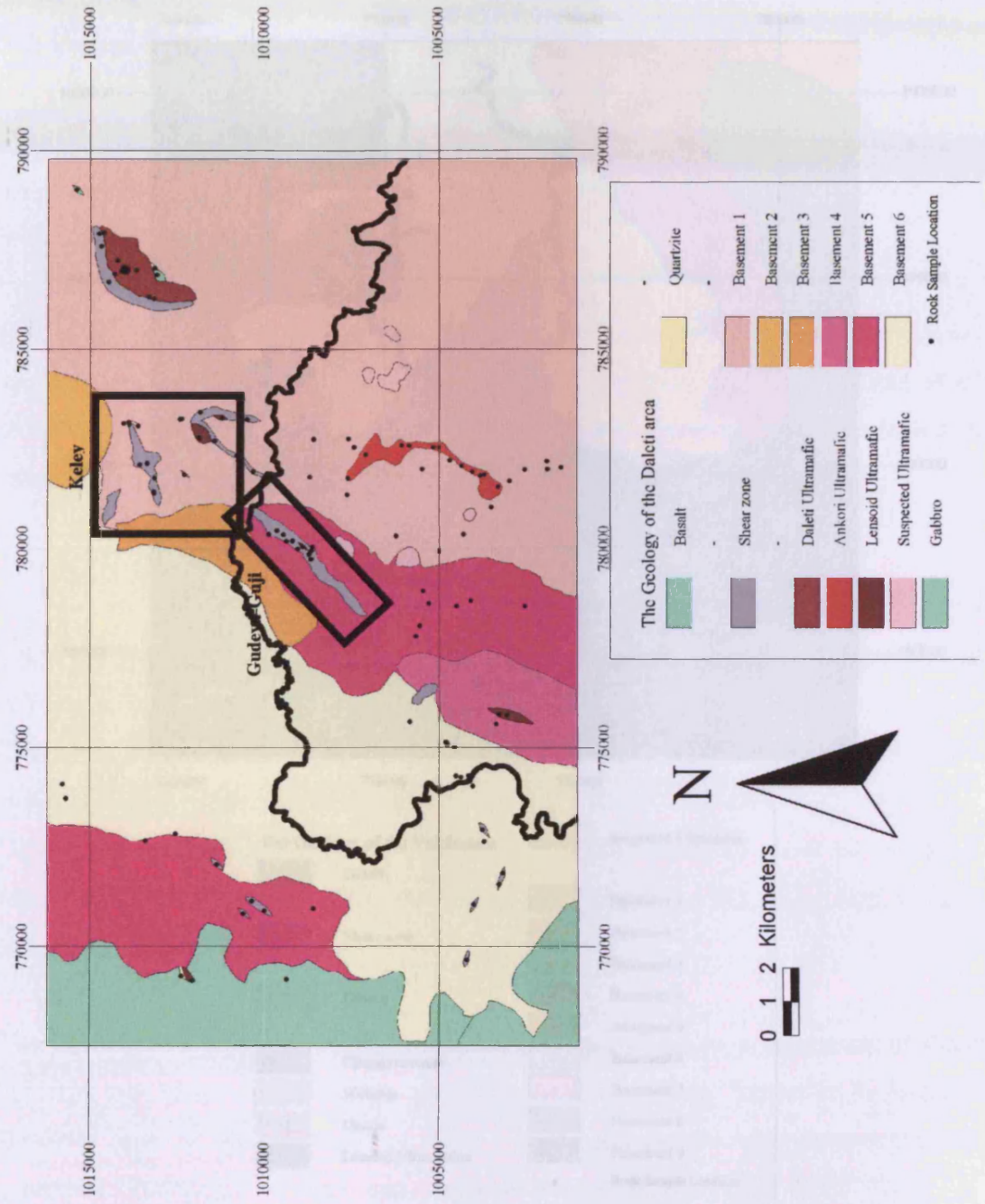

Figure 5.3: The geological map of the Daleti, Ankori, Tulu Kapi and Keley areas. Black lines indicate the course of the major rivers.

There are two large ultramafic complexes in this area, the Daleti Ultramafic and the Ankori Ultramafic. Additionally, there are five smaller complexes described here as the Lensoid Ultramafics. Several more possible ultramafic bodies to the east and west

5.3.4. Yubdo, Sodu and Andu

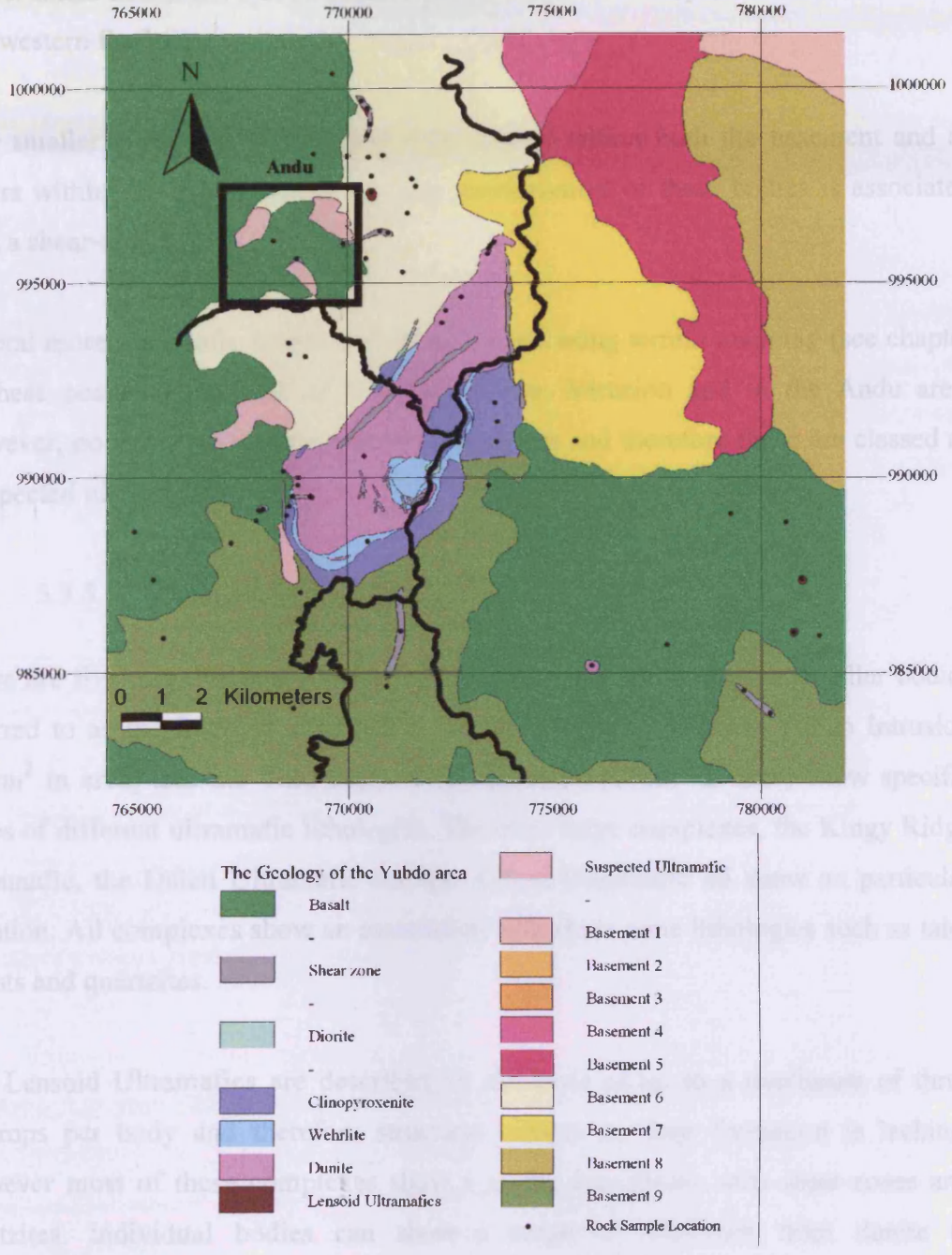

Figure 5.4: The geological map of the Yubdo, Andu and Sodu areas. Black lines indicate the course of the major rivers.

The Main Yubdo Intrusion covers an area of around 30km^2 and consists of three concentric zones with dunite in the core continuing outwards to olivine-clinopyroxenite and then clinopyroxenite. The clinopyroxenite zone is widest on the

eastern flank and only a few thin remnants are observed on the northwestern edge. Diorite dykes have been located in both the eastern and northwestern clinopyroxenite zones. Shear-zones have been observed both within the complex and on the eastern and western flanks.

Five smaller ultramafic bodies have been located within both the basement and as inliers within the Basalt formations. The northernmost of these bodies is associated with a shear-zone.

Several more ultramafic bodies have been located using terrain mapping (see chapter 4) these occur to the west of the Main Yubdo Intrusion and in the Andu area. However, no exposure was found over these bodes and therefore these are classed as "suspected ultramafics".

5.3.5. Summary

There are five large ultramafic complexes in the WES and numerous smaller bodies referred to as the Lensoid Ultramafics. The two largest, the Main Yubdo Intrusion (30km^2 in area) and the Tulu Dimtu Main Intrusion (17km^2 in area) show specific zones of different ultramafic lithologies. The other large complexes, the Kingy Ridge Ultramafic, the Daleti Ultramafic and the Ankori Ultramafic all show no particular zonation. All complexes show an association with shear-zone lithologies such as talc-schists and quartzites.

The Lensoid Ultramafics are described on the basis of up to a maximum of three outcrops per body and therefore structural control on their formation is lacking. However most of these complexes show a strong association with shear-zones and quartzites. Individual bodies can show a range of lithotypes from dunite to clinopyroxenite.

6. Ground Magnetics

6.1. Introduction

During the period from 25/5/2002 to 7/6/2002 a ground magnetic survey was conducted over the Main Yubdo Intrusion. This chapter examines the features of the magnetic field in the area and proposes a model to explain them.

The magnetic survey was conducted using two proton precession magnetometers. To allow for a high sensitivity, fluctuations in the magnetic field were eliminated by using one magnetometer as a base station. The results are displayed as 3 dimensional maps of the magnetic field in the 3rd dimension. Different colours are used to highlight high and low anomalies in the data.

In general a magnetic survey records the distribution of magnetic minerals including magnetite. Such variations may distinguish between different igneous lithologies such as pyroxenite and dunite or different degrees of alteration. In the Yubdo area there is field evidence for secondary alteration episodes such as shearing and silicification. Belete et al. (2000) suggest that hydrothermal processes are an important part of the PGE concentration mechanism. It is possible that alteration occurs either along zones of weakness related to shearing or it may be related to zoning of the igneous lithologies due to magmatic processes.

The aim of the survey described here was to understand the geometry of the alteration and therefore was carried out almost entirely within the dunitic core of the Main Yubdo Intrusion. The following sections describe the collection and description of the data and the results are displayed in several pull-out pages.

6.2. Methods

6.2.1. Data collection

Two Geometrics G856AX portable proton precession magnetometers were used, one set as the base station and one used to measure the magnetic field strength at the survey points. To allow for the greatest possible radiometric resolution, the base station was used to correct for diurnal fluctuations (see section 6.2.2). The base station was also run overnight in order to detect disturbances in the magnetic field caused by magnetic storms.

The base station magnetometer was powered using a car battery. The sensor was aligned to north and attached to a strong tree to prevent movement (figure 6.1). The strength of the magnetic field was recorded every 60 seconds and stored within a memory on the magnetometer. Each field strength reading was recorded against the day and time so that temporal fluctuations in the earth's magnetic field could be reconstructed. The sensor of the base station remained in the same place throughout the duration of the survey. The location of the base station was located at grid reference (769657,990747). The sensor was mounted 2.5m above the ground and the magnetometer was tuned to 34,400nT and the sensor coil mounted vertically. The coil orientation was decided by a test at the beginning of the survey (the results are described in section 6.3.1). Before and after the ground survey was carried out the base-station data was analysed with the aid of the Magmap program to detect the signs of any magnetic storms.

Figure 6.1: The magnetometer sensor set up aligned to N and attached to a tree.

The survey was carried out using a second G856AX magnetometer mounted on a harness. The sensor was mounted on a staff 2.5m high and oriented vertically. At each survey location, the sensor was aligned to north. For each reading stored in the magnetometer, a number of other items of data were also stored, including day, time, line number and mark number.

The two types of survey that were carried out were: wide and close grid spacing. During the wide grid spacing survey, the location of each survey point was determined using a handheld GPS receiver and stored as a waypoint. The GPS location data was combined with the magnetic field strength data using a spreadsheet. During a close grid spacing survey (<10m between survey points), the spacing between subsequent points was too small to be accurately determined using a handheld GPS, therefore the location of each point was surveyed using canvas based measuring tape. The location of the origin was determined using a GPS, the x-axis co-ordinate was recorded within the magnetometer as the line number. The Y co-ordinate was determined using pacing.

During the wide spacing survey the aim was to cover the largest possible area with 100m between each point. In open ground, a 100m spacing was achieved. However, figure 6.2 shows that large areas have no coverage at all. This is because areas of human influence should not be covered due to false readings from metal objects. Furthermore, there are two large open-cast pits which cannot be entered as they are unsafe and in places dense vegetation makes access unavailable. The location of the tight grid spacing survey is shown on figure 6.2.

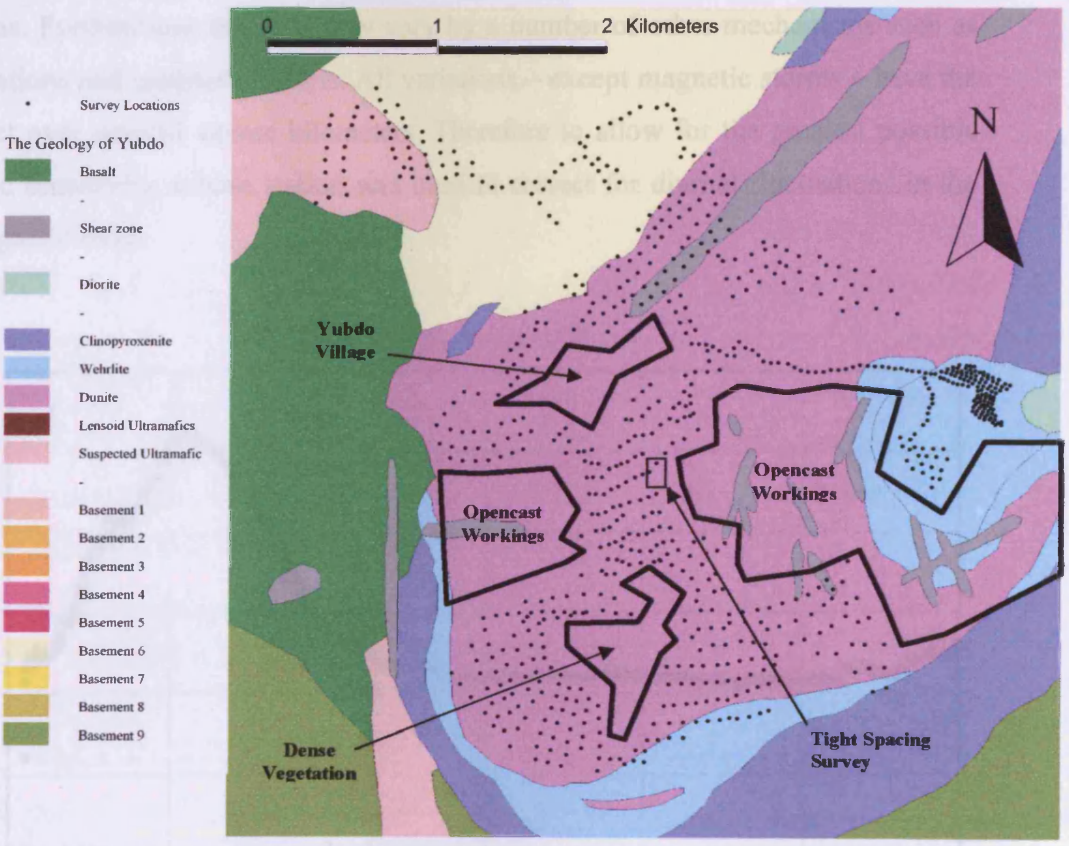

Figure 6.2: The survey point locations for the ground magnetic survey of the Main Yubdo Intrusion overlaid onto the geological map (see chapter 5).

During the coil orientation test a 4m grid spacing survey was carried out twice using two different methods: 1st with both sensors oriented vertically and 2nd with both sensor coils fixed horizontally. In both cases the origin of the grid was at grid reference (769950,990211) and the X-axis was oriented on a bearing of 196°. The aim of this test

was to assess which sensor orientation was the most radiometrically sensitive at the survey site.

6.2.2. Diurnal correction

The magnetic field at a location depends on a number of factors including the underlying geology. Diurnal variation is where the magnetic field varies with time over a 24 hour period, as illustrated in figure 6.3. At Yubdo this variation is frequently over 150gammas. Furthermore the field may vary by a number of other mechanisms such as micropulsations and magnetic storms. All variations – except magnetic storms – have the same effect over several square kilometers. Therefore to allow for the greatest possible radiometric sensitivity, a base station was used to correct for diurnal fluctuations in the Earths magnetic field.

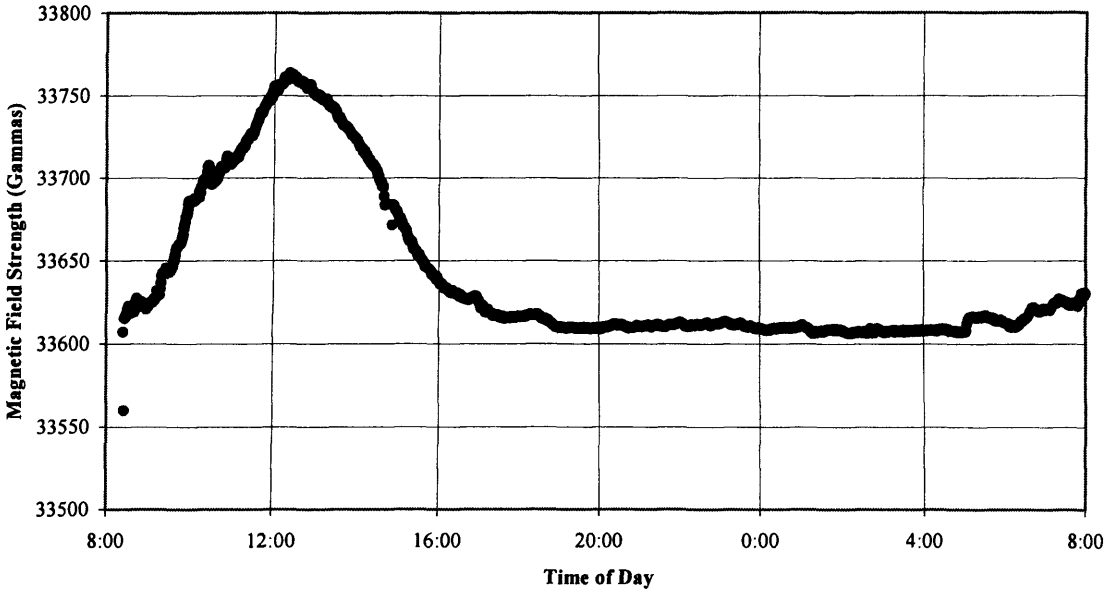

Figure 6.3: The magnetic field strength at the base station over a 24 hour period (30th to the 31st of May 2002)

Magnetic storms disrupt the magnetic field on a scale of several hundreds of metres and therefore a base station cannot cancel out this effect. No magnetic storms were detected during the period of this investigation.

As described in section 6.2.1, the base station automatically recorded the magnetic field every 60 seconds. The nearest base-station reading is subtracted from each reading taken with the portable magnetometer. Ideally, the readings at the portable magnetometer and the base station will have been taken at exactly the same time, but in reality this is unlikely to have been the case. Where no reading at the base station has been taken at the same time as the portable magnetometer, the MagMap software uses a linear time interpolation procedure to calculate an appropriate value.

6.2.3. Data presentation

The results of the survey at Yubdo are displayed as a three dimensional surface where the height of the surface is determined by the difference in the magnetic field strength at that point. The values for the locations between survey points have been interpolated using a kriging function. The magnetic field strength is diurnally corrected (see section 6.2.2) and displayed as a Log_{10} scale. Both negative and positive values for the corrected field strength occur in the dataset. These were processed separately so that the negative values remain negative on the Log_{10} scale. There are, in effect, two logarithmic scales used simultaneously: negative and positive.

The 3D maps are plotted with three different colour scales in order to emphasize key features. Figure 6.6 shows that map A uses the simplest set of colours, grading from blue at the lowest to red at the highest. Map B is the same as A except that a blue stripe is added at 0 and everything immediately lower than 0 is yellow grading to blue and everything immediately above 0 is green grading to red. Map C is the same as B except the blue stripe is just above $Log_{10} = 3$.

In order to demonstrate the variation in the field strength, Figure 6.7 shows the same area in 4 different orientations in 3D maps where the height represents the Log_{10} magnetic field strength with the same colour schemes as figure 6.6.

6.2.4. Limitations and accuracy

Two inaccuracies are involved with the method used for the collection of the data in this study and these must be considered during interpretation. One limitation is the accuracy of the handheld GPS. Although the location of each survey point is quoted to 12 figures – implying an accuracy of 1m – the location is only accurate to 10m. This does not have a direct effect on the nature of the conclusions, however any detailed work targeted by this survey should consider this inaccuracy.

The use of an interpolation function to calculate expected total field values away from survey points is necessary for the estimation of the shape of the magnetic field and the easy analysis of results. However it is possible that these estimated values are entirely incorrect. The varied results contained in this survey indicate that it is not only possible but quite likely that some estimated values are incorrect, however the use of this interpolation function is necessary for ease of analysis. The images of 3D surfaces (figures 6.6 and 6.7) show interpolated values for some areas over 1km away from the survey points. Interpolated values at large distances away from survey points are meaningless and are marked as white on figure 6.11.

The nature of the ground has meant that there were some areas where it was not possible to collect magnetic field data. As figure 6.2 shows, the size and shape of the survey means that there is barely 1km square of unbroken survey area. The areas shown in white in figure 6.11 are those areas where it is not possible to make interpretations due to lack of data. All areas delineated in figures 6.8 and 6.11 are only marked in areas where there is sufficient data to distinguish between two different patterns.

Given the use of a base station to correct for temporal changes and the use of proton precession magnetometers, the radiometric accuracy of the survey is considered to be 1 gamma which is a greater degree of accuracy than required for a geological investigation of this type.

6.3. Results

6.3.1. Sensor orientation test

The results of the sensor orientation test survey are demonstrated using the following two figures.

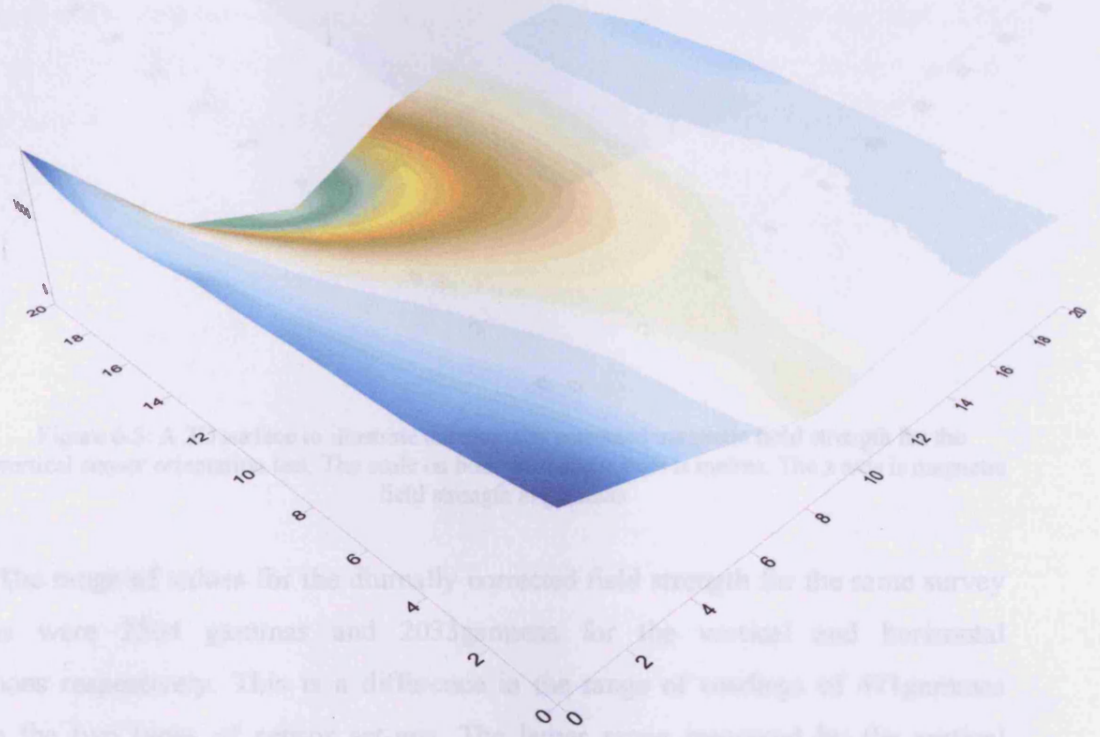

Figure 6.4: A 3D surface to illustrate the diurnally corrected magnetic field strength for the horizontal sensor orientation test. The scale on both the x and y axes is metres. The z axis is magnetic field strength in gammas

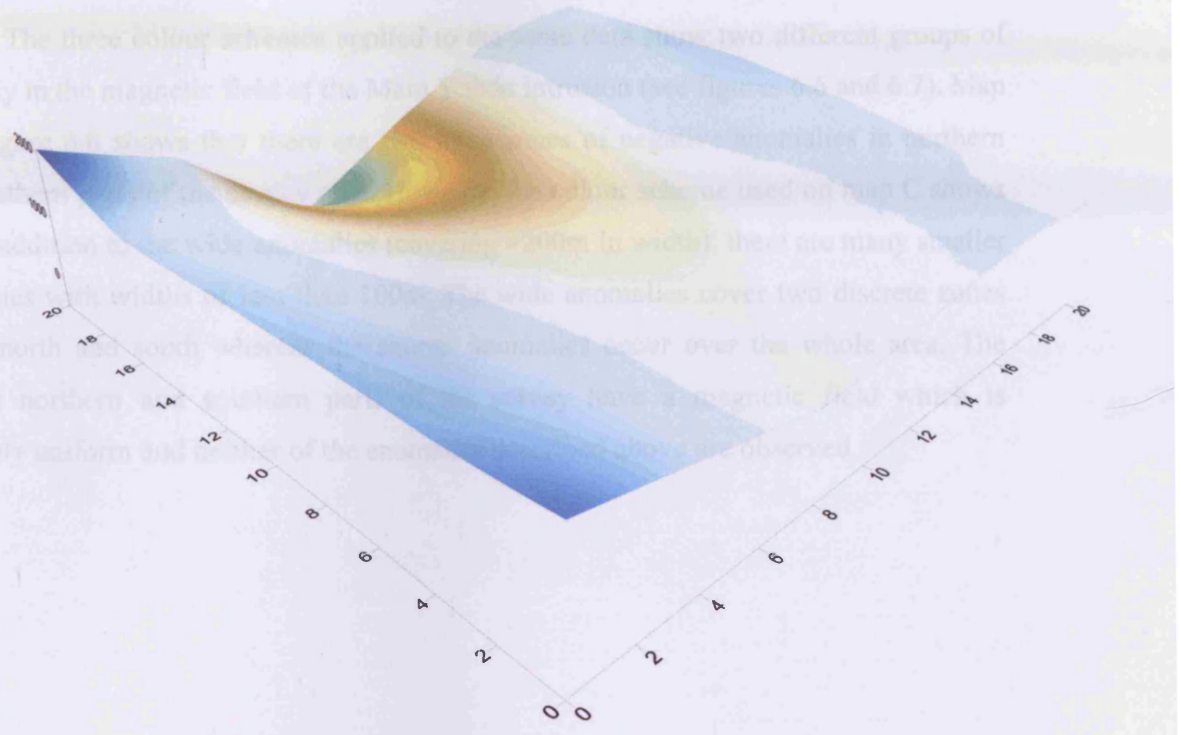

Figure 6.5: A 3D surface to illustrate the diurnally corrected magnetic field strength for the vertical sensor orientation test. The scale on both the x and y axes is metres. The z axis is magnetic field strength in gammas

The range of values for the diurnally corrected field strength for the same survey locations were 2504 gammas and 2033gammas for the vertical and horizontal orientations respectively. This is a difference in the range of readings of 471gammas between the two types of sensor set-ups. The larger range measured by the vertical method indicated a greater radiometric sensitivity and it therefore was adopted for the survey.

6.3.2. Wide spacing survey

The results of the wide spacing survey is presented in two "pull-out" pages at the back of this section. These pages include figure 6.6 which shows the maps with different colour schemes and figure 6.7 which shows 3D views of these maps. These figures are referred to throughout the following text. Additionally, figure 6.2 (see section 6.2.1) shows the location of each survey point on a base map.

The three colour schemes applied to the same data show two different groups of anomaly in the magnetic field of the Main Yubdo Intrusion (see figures 6.6 and 6.7). Map A in figure 6.6 shows that there are two large zones of negative anomalies in northern and southern parts of the survey area. However, the colour scheme used on map C shows that in addition to the wide anomalies (covering >200m in width), there are many smaller anomalies with widths of less than 100m. The wide anomalies cover two discrete zones in the north and south whereas the shorter anomalies occur over the whole area. The farthest northern and southern parts of the survey have a magnetic field which is relatively uniform and neither of the anomalies described above are observed.

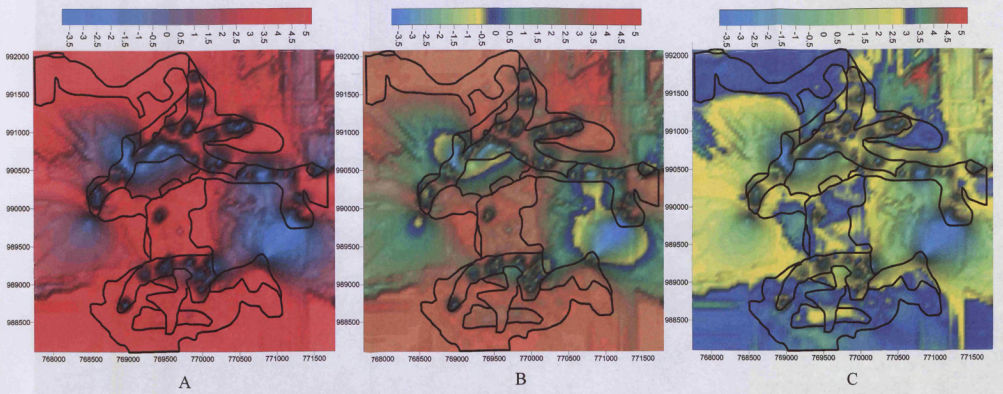

Figure 6.6: Maps of the diurnally corrected magnetic field strength (Log_{10}). The different colour schemes are used to highlight different aspects of the data, A: Illustrates the overall field values, B: Shows wide zones of low magnetic field strength and C: Short wavelength changes in areas of high field strength. The outline of the interpretation map is overlaid, for a further explanation see figure dkmagintmap.

- **Area 2 (red dots)**: Covering a total of ≈ 2.5km^2, the magnetic field strength in this area ranges from 3.2 to 3.5 Log_{10} units. It covers two large tracts in the north and south of the area shown in figure 6.8.
- **Area 3 (pink dots)**: This isolated area located at the centre of the the Main Yubdo Intrusion is characterized by an uneven magnetic field strength of around 3 Log_{10} units with small negative anomalies which can fall to 2.3 Log_{10} units.
- **Area 4 (yellow dots)**: This zone in the southern part of the survey area is entirely surrounded by area 2. The field strength is 2.5 Log_{10} units.
- **Area 5 (orange dots)**: Numerous small parts of the survey are covered by this form of non-uniform magnetic field ranging from 2.5 to 3.5 Log_{10} units.

UNIVERSITY PRIFYSGOL

6.3.3. Tight spacing survey

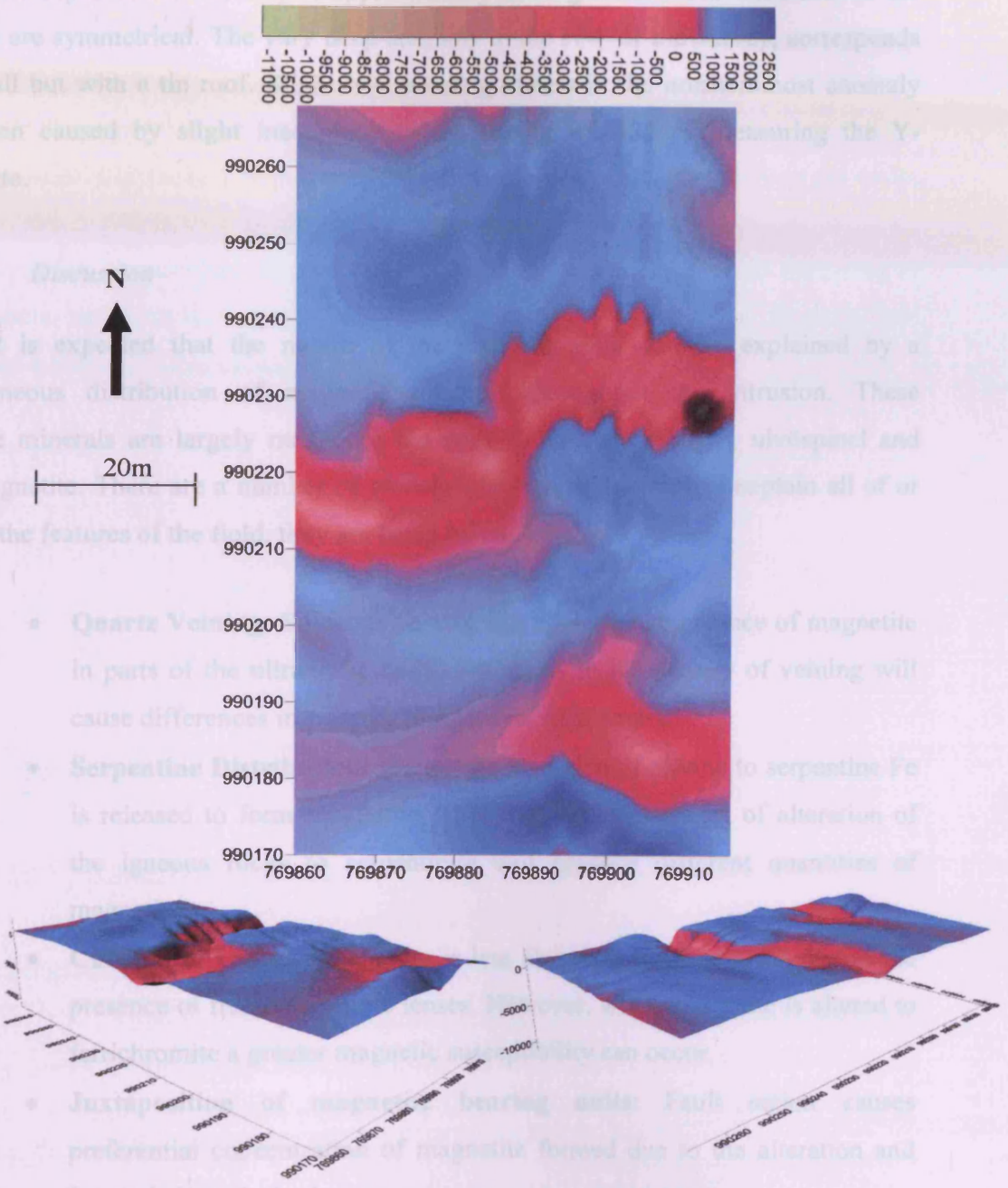

Figure 6.9: Maps of the diurnally corrected magnetic field strength (gammas) over an area near to Yubdo School. Bottom Left: facing north-east, Bottom Right: Facing south-east.

Figure 6.9 shows the results of the tight grid spacing survey at Yubdo. Two distinct negative magnetic anomalies are observed. Both anomalies have a linear sinuous shape. The depth of the anomaly is approximately 2000 gammas. The shoulders of the anomaly are symmetrical. The very deep anomaly in the NW of the survey, corresponds to a small hut with a tin roof. Slight N-S trending offsets in the northernmost anomaly have been caused by slight inaccuracy in the pacing method of measuring the Y-coordinate.

6.4. Discussion

It is expected that the nature of the magnetic field can be explained by a heterogeneous distribution of magnetic minerals throughout the intrusion. These magnetic minerals are largely magnetite but possibly also maghemite, ulvöspinel and titanomagnetite. There are a number of models which could be used to explain all of or some of the features of the field, they are listed below.

- **Quartz Veining**: Siliceous veining can dilute the abundance of magnetite in parts of the ultramafic body. Variations in the density of veining will cause differences in patterns of magnetic field strength.
- **Serpentine Distribution**: During the alteration of olivine to serpentine Fe is released to form magnetite. Therefore different stages of alteration of the igneous rocks to serpentinite will produce different quantities of magnetite.
- **Chromitite Lenses**: Magnetite is less abundant in some areas due to the presence of fresh chromitite lenses. However, where chromite is altered to ferrichromite a greater magnetic susceptibility can occur.
- **Juxtaposition of magnetite bearing units**: Fault action causes preferential concentration of magnetite formed due to the alteration and focused along fault planes.

The magnetic field surveyed above the Main Yubdo Intrusion shows generally high values with 2 zones of large negative anomalies and numerous smaller negative

anomalies. The generally high values observed here are likely to be ultramafic rocks as they have some of the highest magnetic susceptibilities known (see table 6.1). Therefore the origin of the negative anomalies could be explained by the presence of some less magnetically susceptible units. It is unlikely that the presence of magnetite or chromite could have caused such a decrease in magnetic field strength as alteration would have created a high magnetic susceptibility. As seen in table 6.1 both quartzite and serpentinite have significantly lower magnetic susceptibilities than olivine or pyroxene-bearing rocks. However, the presence of Fe-rich spinels at the rims of olivine minerals in the Main Yubdo Intrusion (see chapter 3) suggests a role for serpentinisation in the formation of ferrichromite. Hence, it is likely that this ferrichromite would increase the magnetic field strength as a result of sepentinisation.

Rock	Average Magnetic Susceptibility ($x10^6$ emu)
Andesite	13,500
Peridotite	13,000
Pyroxenite	10,500
Diorite	7,000
Basalt	6,000
Gabbro	6,000
Serpentinite*	1,000
Quartzite	350
Amphibolite	60
Sandstone	30

Table 6.1: A table of magnetic susceptibility values in order of decreasing susceptibility (after Robinson and Coruh, 1988). *: This value is for pure serpentinite with very little magnetite.

Of the possible explanations covered above, the most likely cause of the variation in magnetic field strength over the Main Yubdo Intrusion is different degrees of quartz veining through the ultramafic lithotypes. Quartz veins can frequently be observed in the rocks of the Main Yubdo Intrusion and the remnants of such veins can also be seen in the laterites exposed in the quarry faces. Furthermore, Kazmin and Demessie (1971) have mapped a shear-zone which intersects with a zone of very low magnetic field strength observed here (see figure 6.8). It is feasible that the one of the major conduits of silica-rich fluids could have been a shear-zone. Smaller siliceous fluids could well have permeated through the rest of the complex to precipitate silica and create the lower magnetic anomalies. The value quoted for the magnetitic susceptibility of serpentinite in

table 6.1 is that of pure serpentinite with very little magnetite. When olivine is serpentinised, magnetite is formed as a result and hence a serpentinised dunite (as is observed at Yubdo, see chapter 3) will have a magnetitic susceptibility comparable to peridotite.

The negative anomalies mapped in the tight grid spacing survey may also be caused by siliceous veining. In the wide spacing survey, such anomalies appear to be circular due to the kriging interpolation function. However the tight spacing survey may have uncovered the geometry of these smaller veins. E-W trending quartz-veins can be observed in a quarry cutting 300m east of the tight spacing survey.

There are two zones in the farthest north and south (classified as area 2, see figure 6.8) where the magnetic field is relatively uniform and strong negative anomalies are not seen. The northernmost of these zones is over the area mapped as basement by terrain mapping and Kazmin and Demessie (1971). A possible explanation for this is that either the ultramafics or the basalts extend further than expected from geological mapping. Alternatively, this magnetic field could have been caused by ultramafic rocks which have not been silicified.

6.5. Conclusions

The results of the wide grid spacing survey are summarized by figure magintmap. Figure magmodel is a schematic diagram to illustrate the model suggested here to explain the anomalies observed in the total field during the magnetic survey. The features of this model are as follows:

- **High Frequency Siliceous Veining**: These are thin (around 10m wide) elongate zones of silicification. There are likely to be large slivers of ultramafics surrounded by quartz veining within the zone. The frequency of veins within the zone is likely to be greater than anywhere else in the survey. This results in some very low magnetic field readings directly over

veins and some higher readings – even within the zone – over slivers of trapped ultramafic. This vein morphology could be the result of hydrothermal fluids passing through a zone of structural weakness perhaps associated with shear deformation.

- **Low Frequency Siliceous Veining**: This zone generally has a greater proportion of ultramafic than the high frequency zone described above, but the veining is thinner and distributed more pervasively throughout the host rock. The result is a generally low and variable magnetic field (see section 6.3.2).
- **Non-silicified Ultramafic rocks**: These rocks contain very little variation in composition and must be either ultramafic rock or basalt. The two zones (figure 6.11) may be different rock types but both must be generally homogenous and of a high magnetic susceptibility. This results in a high magnetic field strength which varies very little.
- **Unidentified Anomalous rock**: This small zone to the south, is completely covered by a non-silicified ultramafic rock but shows anomalously low total field readings. This may be related to silicification, but the size and restricted shape does not support this idea.

The explanation of the anomaly patterns described above is supported by the results of the of the close spaced grid survey (figure 6.9). The characteristics of the anomalies observed can be explained by the presence of a steeply dipping planar feature having a lower magnetic susceptibility than its surroundings. This fits well with the idea of a quartz vein. The location of this anomaly is in the Low frequency Siliceous Veining zone identified in the wide spaced survey.

6.5.1. Pull out section

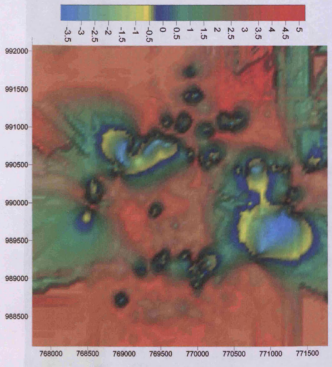

Figure 6.10: A map of the diurnally corrected magnetic field strength (Log_{10}) displayed as a 3D surface. The colour scheme is designed to highly wide zones of low magnetic field.

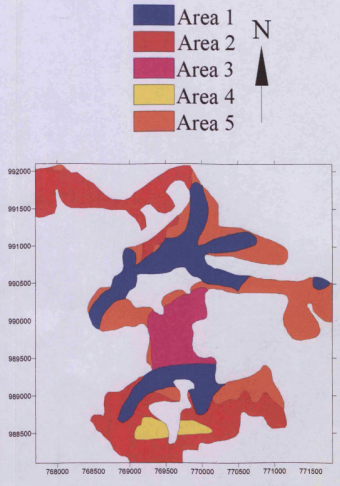

Figure 6.11: An interpretation map of the features of the magnetic field over the Main Yubdo Intrusion. For an description of each area see section 8.3.2.

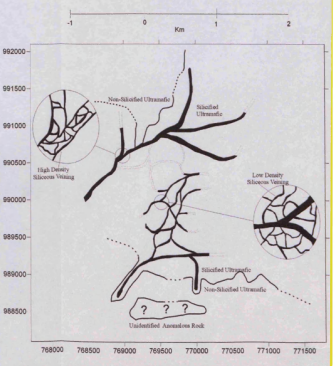

Figure 6.12: Schematic map of the model proposed to explain the nature of the magnetic field over the Main Yubdo Intrusion. Dotted lines indicate inferred or extrapolated contacts

7. Soil Geochemical Data

7.1. Introduction

The Precambrian volcano-sediments and ultramafics of the WES are overlain by a thick and extensive laterite. As part of the exploration program in the WES, a total of 930 soil samples were collected from the four areas of study in this thesis. The samples were analysed for major and trace elements by OMAC laboratories with the aim of gaining an understanding of the economic value of the prospects being studied.

This chapter contains several sections within which the soils of the WES are described and observations of several key elements are made. After the sampling strategy and methods used to analyze the samples has been considered, a number of interpretation techniques have been applied to the data. As exploration data frequently displays gaussian distributions it was considered valuable to examine the dataset by using univariate statistical methods (Sinclair, 1983; Moon, 1995). This has allowed an understanding of the populations and modes present within the dataset, which in turn can be of use in evaluating PGE prospects. To compliment the statistical methods used, maps of the elemental distribution of Ni, Cu, Cr, Al, Pt and Pd are included and these are used to evaluate the use of overburden geochemistry to exploration within the WES.

Observations are made within this chapter which indicate a control on the geochemistry of the laterites in question not only by the underlying bedrock but also by hydromorphic dispersion.

7.2. The overburden of the WES

As a result of the important PGE placer deposits they contain, accounts of the structure and morphology of the lateritic soils in the WES occur in several publications the most recent of which is an MSc thesis (Childs, 2001). Other important documents include Augustithis (1965), Molly (1959) and Jelenc (1966), who all give extensive accounts of the nature of these bodies.

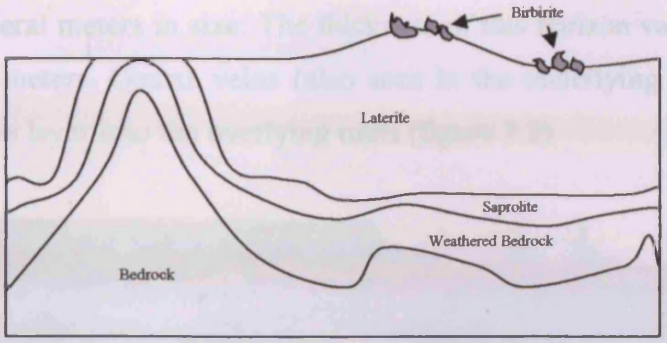

Figure 7.1: A schematic diagram of the stucture of the lateritic soils in the WES.

The laterite profile of the WES includes three principle layers (see figure 7.1), these are: weathered bedrock, saprolite and laterite. These are referred to locally as Kuha, Bondo and Chirecha respectively. Although no duricrust or hardpan layer exists at the top of the profile, in several places, patches of a silicifed rock known as the birbirite occur. Each of the four principle components of the overburden are now considered in turn from the bottom to the top.

Figure 7.2: The interface between the pristine (top left) and weathered bedrock (bottom right) in the opencast workings near Yubdo. The left of the photograph shows a quartz stockwork which resists weathering to a greater degree than the surrounding serpentinite.

The weathered bedrock layer (Kuha) consists of a green clay-rich rock containing fragments of serpentinite in various states of weathering, ranging from one centimeter to several meters in size. The thickness of this horizon varies from around 20cm to several meters. Quartz veins (also seen in the underlying bedrock) can be traced through this layer into the overlying units (figure 7.2).

Figure 7.3: A photograph indicating the position of the saprolite layer (white arrow). Variations in the thickness of the laterite as seen in the quarry near the summit at Daleti. The light coloured rock at the base is the pristine serpentinite, the red material at the top is the laterite layer and between these is the yellow saprolite layer.

Directly overlying the weathered bedrock is the saprolite layer (Bondo). In his extensive study of the soil horizons at Yubdo, Childs (2001) describes this layer as an extremely clay-rich yellow material. In comparison to the other soil horizons, the saprolite layer is thin at around 40cm in thickness.

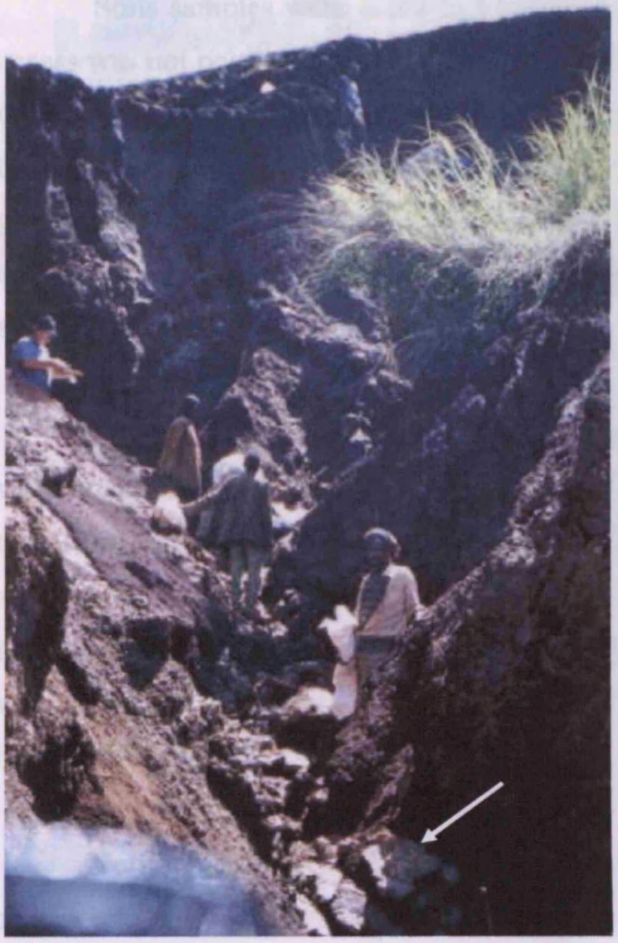

Figure 7.4: The extensive laterite layer in the workings at Yubdo. The laterite seen here is over 15m in thickness and the base of the horizon (the saprolite) is indicated by the arrow.

The soils of the WES are capped by a laterite layer which is well over 15m thickness in most places (see figure 7.4). The United Nations (1971) considered that this layer reaches at over 30m in depth in some parts of western Ethiopia. However, in a few instances this horizon may be less than 1 meter in thickness. It consists of a deep red, Fe-rich friable laterite. Resistant quartz veins are frequently found to be preserved within this horizon. The laterite is homogenous from the base to the top and no specific layers or barriers have been observed within the unit.

Large patches of birbirite can be found on the surface over the ultramafic bodies at Yubdo, Sodu, Daleti and Tulu Dimtu. These patches are generally found at the summits of these ridges. They are believed to be highly silicified and altered dunite (Jelenc, 1966; Molly, 1959; Augustithis, 1965). An account of the petrology of the birbirite (including thin sections) is given in chapter 3. Although the origin of these rocks is not well understood, they have only ever been found at the top of the laterite (chirecha) horizon and never in contact with pristine bedrock. Therefore, in this study the birbirite is considered to be part of the overburden.

7.3. Sampling strategy

Soils samples were taken in traverses across open ground and in areas where access was not possible, the samples were taken parallel to roads but away from areas of human influence. They were taken within the bounds of the licence areas stated by the Ethiopian government. Furthermore, under the terms of their agreement with the government, GPM were required to take over 900 samples covering the whole licence area. The spatial constraints on sampling areas are described at the start of each section.

For the best geological use, the soil samples collected should be as close to the weathered bedrock as possible. However, given the depth of the laterite (often greater than 15m) it was impractical to collect samples close to the bedrock. In this study, the samples were taken from a depth of 10-20cm below the surface, within the laterite horizon (see section 7.2). In the poor agricultural conditions of Western Ethiopia, this was considered to be low enough not be influenced by humic acids from plant roots or human influence.

Noting the soil profile described in section 7.2, this sampling depth was considered to be appropriate for comparison with other samples from the same dataset for a number of reasons. Studies of the soil horizons in the Yubdo area (Childs, 2001) found no significant barriers or weathered horizons within the soil profile and similarly no such horizons were found in the road cutting at Daleti or Kingy. The laterite horizon (Chirecha) is a homogenous mass of friable soils and therefore the material at the top of the layer is considered to be comparable in geochemistry to that of the bottom.

Given the arguments made above and the absence of slump and mass wasting features around the laterites in the WES (United Nations, 1971) this thesis suggests that these soil samples are likely to reflect the in-situ geochemistry and therefore are suitable for exploration activities. However given that the studies of soil profiles can only be performed in the road cuttings or open cast workings, it was always intended that anomalous values would be followed up by a pitting program. Such a system of sampling from high in the lateritic profile and validation with samples from lower in

the stratigraphy has been recommended through work in Australia (Smith et al., 2000). Furthermore, some degree of hydromorphic remobilization (as described by Smith et al., 2000) of metals is to be expected and therefore, this needs to be considered when interpreting the data. The factors affecting the geochemistry of the soils studied are described further in section 7.5).

7.4. Method of Analysis

A total of 981 soil samples were analysed by OMAC Laboratories (Co Galway, Ireland) by two different procedures: one for Pt and Pd and another for 47 additional elements. Considerably more detail about this method is given in the analytic methods section of chapter 8. For Pt and Pd analyses, each sample was ground to 100μm and split to 30g. Subsequently, the powders were analysed using a 30g lead fire assay with an inductively coupled plasma finish, resulting in detection limits of 2ppb for both Pt, Pd and Au. For other elements, the samples were also ground to 100μm but they were subjected to an Aqua Regia digestion with Inductively Coupled Plasma – Optical Emission Spectroscopy finish. It is necessary to point out that an aqua regia digestion will not be total, some of the more refractory minerals will not have been digested (see chapter 8).

7.5. Soil Forming processes and geochemical dispersion

7.5.1. Ni, Cu, Cr and Al

A high degree of Ni concentration in laterites is common over ultramafic units (Schellmann, 1989). The increase in Ni values is caused by a removal of Si and Mg which are both highly mobile in soils. The Ni concentration can be further facilitated by remobilisation to form gossans. Studies of the behaviour of Ni and Cu in the surficial environment are summarized by Smith et al. (2000). Ni and Cu (amongst other elements) are frequently used to determine the location of primary ore deposits covered by laterites in Australia by identifying dispersion haloes. Ni and Cu can be taken into solution by meteoric water, which then forms part of the aquifer system within the laterite body. The elements are then dispersed through the laterite in the direction of groundwater flow, in the same way as As groundwater contamination (Nickson et al., 2000).

When partitioned into spinel minerals, Cr is known to be highly immobile. Unlike sulphide minerals, Cr-spinels in the WES remain intact throughout severe alteration (chapter 3) and weathering. Aluminium is also known to be immobile in soils. The immobility of Al means that small amounts of it will be concentrated by volume loss during soil formation (Schellmann, 1989). It can be expected that immobile elements will become concentrated in soils compared with the underlying rocks. This is owing to the mobile components of the rock being removed and hence a soil will have originated from a rock volume larger than that of the soil.

7.5.2. Pt and Pd

The fluids involved with the remobilisation of Pt and Pd in soils could be regarded as the lower temperature equivalents (≈85°C according to Tarkian et al. 1996) of those fluids involved in the high-temperature alteration (see chapter 8). In addition to the Cl-complexes thought to occur at high temperatures, it is possible that hydroxide, thiosulphate and organic complexes may be the dominant forms of dissolved Pt and Pd. Such situations may form from natural humic and fulvic acids (Bowles et al., 1995). For example, Wood (1990) reacted with aqueous solutions of K_2PtCl_4 to discover that such acids can hold over 140ppm Pt in solution.

In addition to the Cl-rich fluid and hydrothermal fluid models, many studies have shown that PGE can be oxidised in the surficial environment (see papers in Bowles and Gize, 2005). For example, studies of the mineralogy of the Massive Sulphide Zone of the Great Dyke of Zimbabwe have shown that with progressive alteration, the PGM become oxidised with concomitant destruction of the sulphide minerals present in the fresher rock (Oberthür et al., 2003). Oberthür et al. (2003) also remark that – as in hydrothermal fluids – Pd is more mobile than Pt and is dispersed in the surficial environment. The preferential mobility of Pd over Pt is also observed by many other authors including Wood and Vlassopoulos (1990) and Bowles et al. (1994).

7.6. *Tulu Dimtu: Selected Major and Trace elements*

7.6.1. Introduction

There are 262 soil samples from the Tulu Dimtu area. Over the Tulu Dimtu Main Intrusion sample sites are located at intervals of 50 to 100m in traverses across the western flank. The eastern flank of the Tulu Dimtu Main Intrusion was not studied due to the terms of the licence agreement between Golden Prospect Mining Co Ltd and the Ethiopian government. Over the remaining areas samples were taken where access was available close footpaths and roads.

Figure 7.5: The distribution of soil samples in the Tulu Dimtu area.

7.6.2. Summary of Analytical Results

Class Upper Limit (ppm)	Frequency	Cumulative Frequency	Cumulative Frequency (%)		
58	1	261	100.0	Mean	6.5
55.1	0	260	99.6	Standard Deviation	8.3
52.2	0	260	99.6		
49.3	0	260	99.6	Minimum	0
46.4	0	260	99.6	Lower Quartile	0
43.5	0	260	99.6		
40.6	3	260	99.6	Median	4
37.7	0	257	98.5	Upper Quartile	9
34.8	1	257	98.5		
31.9	0	256	98.1	Maximum	58
29	1	256	98.1	Mode	0
26.1	6	255	97.7	Number of samples	261
23.2	9	249	95.4		
20.3	8	240	92.0		
17.4	11	232	88.9		
14.5	10	221	84.7		
11.6	19	211	80.8		
8.7	28	192	73.6		
5.8	63	164	62.8		
2.9	20	101	38.7		
0	81	81	31.0		

Table 7.1: A summary of the Pt values in the soil samples from Tulu Dimtu.

Class Upper Limit (ppm)	Frequency	Cumulative Frequency	Cumulative Frequency (%)		
31	1	261	100.0	Mean	3.0
29	0	260	99.6	Standard Deviation	3.9
28	0	260	99.6		
26	0	260	99.6	Minimum	0
25	1	260	99.6	Lower Quartile	0
23	0	259	99.2		
22	0	259	99.2	Median	2
20	0	259	99.2	Upper Quartile	4
19	0	259	99.2		
17	2	259	99.2	Maximum	31
16	2	257	98.5	Mode	0
14	4	255	97.7	Number of samples	261
12	2	251	96.2		
11	1	249	95.4		
9	2	248	95.0		
8	13	246	94.3		
6	33	233	89.3		
5	38	200	76.6		
3	53	162	62.1		
2	0	109	41.8		
0	109	109	41.8		

Table 7.2: A summary of the Pd values in the soil samples from Tulu Dimtu.

Class Upper Limitc	Frequency	Cumulative Frequency	Cumulative Frequency (%)		
4869	1	261	100.0	Mean	24
4626	0	260	99.6	Standard Deviation	301
4382	0	260	99.6		
4139	0	260	99.6	Minimum	0
3895	0	260	99.6	Lower Quartile	0
3652	0	260	99.6		
3408	0	260	99.6	Median	2
3165	0	260	99.6	Upper Quartile	5
2921	0	260	99.6		
2678	0	260	99.6	Maximum	4869
2435	0	260	99.6	Mode	0
2191	0	260	99.6	Number of samples	261
1948	0	260	99.6		
1704	0	260	99.6		
1461	0	260	99.6		
1217	0	260	99.6		
974	0	260	99.6		
730	0	260	99.6		
487	0	260	99.6		
243	164	260	99.6		
0	96	96	36.8		

Table 7.3: A summary of the Au values in the soil samples from Tulu Dimtu.

Class Upper Limit (ppm)	Frequency	Cumulative Frequency	Cumulative Frequency (%)		
10648	1	261	100.0	Mean	2406
10116	1	260	99.6	Standard Deviation	3001
9584	1	259	99.2		
9053	5	258	98.9	Minimum	12
8521	3	253	96.9	Lower Quartile	130
7989	6	250	95.8		
7457	9	244	93.5	Median	336
6925	12	235	90.0	Upper Quartile	5288
6394	18	223	85.4		
5862	9	205	78.5	Maximum	10648
5330	12	196	75.1	Mode	103
4798	6	184	70.5	Number of samples	261
4266	6	178	68.2		
3735	4	172	65.9		
3203	1	168	64.4		
2671	2	167	64.0		
2139	3	165	63.2		
1607	3	162	62.1		
1076	7	159	60.9		
544	152	152	58.2		
0	0	0	0.0		

Table 7.4: A summary of the Ni values in the soil samples from Tulu Dimtu.

Class Upper Limit (ppm)	Frequency	Cumulative Frequency	Cumulative Frequency (%)		
146	4	261	100.0	Mean	54
139	3	257	98.5	Standard Deviation	42
132	7	254	97.3		
125	4	247	94.6	Minimum	3
117	16	243	93.1	Lower Quartile	10
110	5	227	87.0		
103	16	222	85.1	Median	50
96	10	206	78.9	Upper Quartile	88
89	12	196	75.1		
82	12	184	70.5	Maximum	146
75	11	172	65.9	Mode	6
67	12	161	61.7	Number of samples	261
60	12	149	57.1		
53	18	137	52.5		
46	12	119	45.6		
39	5	107	41.0		
32	12	102	39.1		
24	9	90	34.5		
17	13	81	31.0		
10	68	68	26.1		
0	0	0	0.0		

Table 7.5: A summary of the Cu values in the soil samples from Tulu Dimtu.

Class Upper Limit (ppm)	Frequency	Cumulative Frequency	Cumulative Frequency (%)		
3098	2	261	100.0	Mean	428
2944	1	259	99.2	Standard Deviation	438
2790	0	258	98.9		
2636	0	258	98.9	Minimum	18
2482	0	258	98.9	Lower Quartile	158
2328	0	258	98.9		
2174	0	258	98.9	Median	304
2020	0	258	98.9	Upper Quartile	575
1866	3	258	98.9		
1712	3	255	97.7	Maximum	3098
1558	0	252	96.6	Mode	218
1404	2	252	96.6	Number of samples	261
1250	4	250	95.8		
1096	4	246	94.3		
942	13	242	92.7		
788	20	229	87.7		
634	28	209	80.1		
480	46	181	69.3		
326	61	135	51.7		
172	74	74	28.4		
0	0	0	0.0		

Table 7.6: A summary of the Cr values in the soil samples from Tulu Dimtu.

Class Upper Limit (%)	Frequency	Cumulative Frequency	Cumulative Frequency (%)		
7.3	1	261	100.0	Mean	3.62
7.0	7	260	99.6	Standard Deviation	1.91
6.6	8	253	96.9		
6.3	6	245	93.9	Minimum	0.4
5.9	20	239	91.6	Lower Quartile	1.4
5.6	15	219	83.9		
5.2	26	204	78.2	Median	4.0
4.9	17	178	68.2	Upper Quartile	5.1
4.5	26	161	61.7		
4.2	19	135	51.7	Maximum	7.3
3.9	7	116	44.4	Mode	1
3.5	16	109	41.8	Number of samples	261
3.2	4	93	35.6		
2.8	8	89	34.1		
2.5	6	81	31.0		
2.1	4	75	28.7		
1.8	4	71	27.2		
1.4	23	67	25.7		
1.1	30	44	16.9		
0.7	14	14	5.4		
0.0	0	0	0.0		

Table 7.7: A summary of the Al values in the soil samples from Tulu Dimtu.

The following sections describe the distribution of Ni, Cu, Cr and Al in the soils covering the Tulu Dimtu area. It is important to remember that it is unlikely that complete digestion has been acheieved during the aqua regia leach of these samples. Each section describes one element and its distribution in the soils in turn. These sections are accompanied by two fold-out pages (page 123) of maps showing the distribution of all elements which the reader should refer to as each section is read.

7.6.3. Nickel

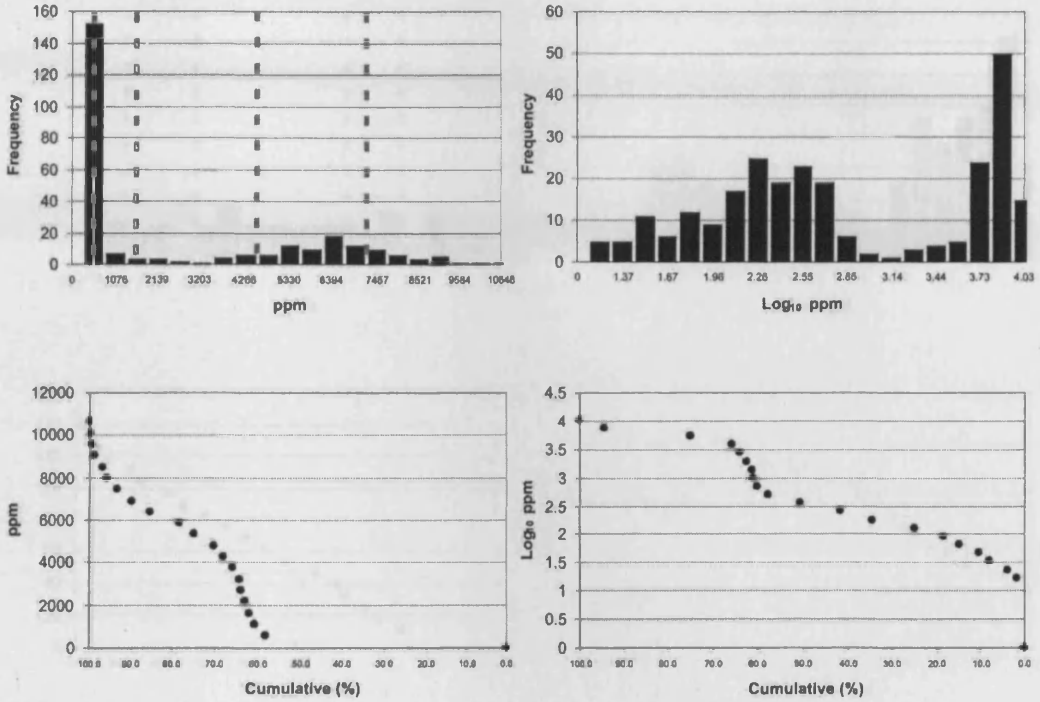

Figure 7.6: Arithmetic and Log_{10} transformed histograms of Ni in the soils of the Tulu Dimtu area. The grey lines indicate the class-boundaries used in figure 7.12A.

Nickel is enriched only over the Tulu Dimtu Main Intrusion and Sheared Ultramafic (see figure 7.12A). Two regions of high values are observed in the soils overlying the Main Intrusion. These are firstly on the flanks of the intrusion and additionally forming a N-S trending feature 1km east of the western flank; here values rise to over 8000ppm (figure 7.12A). The highest value of Ni in the Tulu Dimtu area is found in the soils above the southwestern flank of the intrusion.

There are two populations of Ni values in the Tulu Dimtu area. Figure 7.6 shows that above 3000ppm (found over the Tulu Dimtu Main Intrusion and Sheared Ultramafic), the Ni values have an approximately normal distribution. However, the samples with Ni values of lower than 3000ppm (generally found over the basement units have an approximnately log normal distribution.

7.6.4. Copper

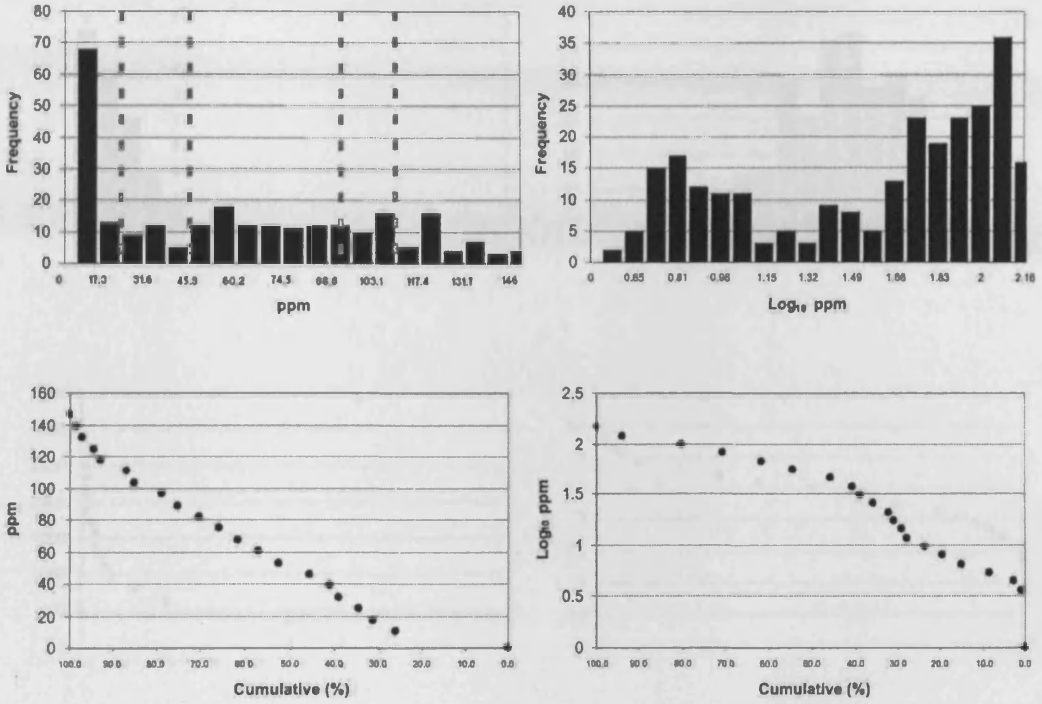

Figure 7.7: Arithmetic and Log_{10} transformed histograms of Cu the soils of the Tulu Dimtu area. The grey lines indicate the class-boundaries used in figure 7.12B.

Within the Tulu Dimtu Main Intrusion, only one soil sample – located on the western flank - contains a Cu value which is above 70ppm. All remaining samples from soils above the Tulu Dimtu Main Intrusion have Cu values below 50ppm. However, over the rest of the area, Cu rises to above 90ppm in soils overlying many different rock formations. Although some values of less than 500ppm are found in soils over the basement units.

There are two populations of Cu values in the Tulu Dimtu area. Above 25ppm there is an approximately even distribution of Cu values (not normally distributed, see figure 7.7). However, an additional population of Cu values below 25ppm show a roughly Log normal distribution.

7.6.5. Chromium

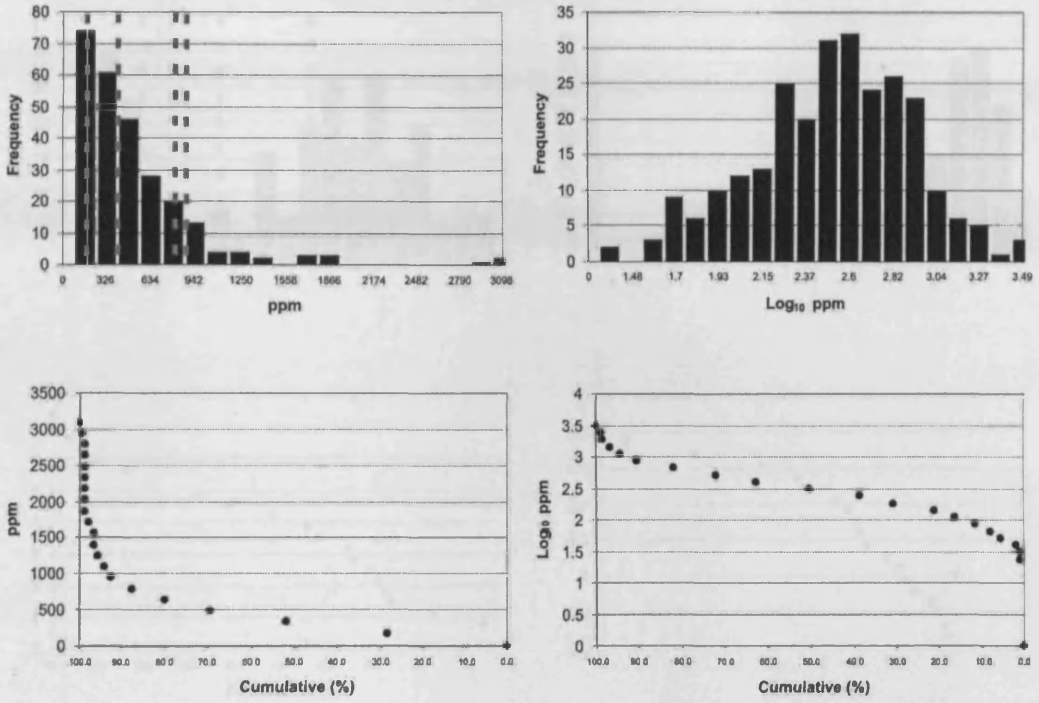

Figure 7.8: Arithmetic and Log_{10} transformed histograms of Cr the soils of the Tulu Dimtu area. The grey lines indicate the class-boundaries used in figure 7.12C.

The highest Cr values in soil (900ppm to 3098ppm) occur on the western and southeastern flank of the Main Intrusion and these zones also correspond to some high values of Cr in olivine-clinopyroxenites and clinopyroxenites (900ppm to 2728ppm, see figure 7.12C). Additionally, some high Cr values are found in the soils above the basement (several above 900ppm).

Cr values in the Tulu Dimtu area are log normally distributed and with a mode at around 216ppm (see figure 7.8 and table 7.12C).

7.6.6. Aluminium

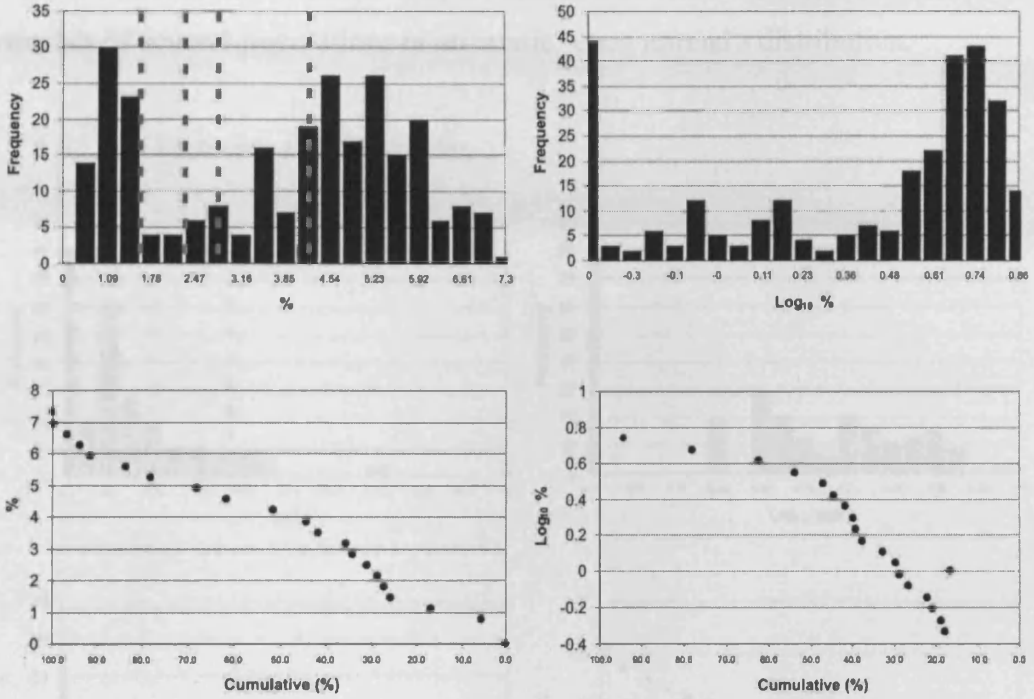

Figure 7.9: Arithmetic and Log_{10} transformed histograms of Al the soils of the Tulu Dimtu area. The grey lines indicate the class-boundaries used in figure 7.12D.

Inside the Main Intrusion, the highest values of Al in soil are above the dunites on the west and olivine-clinopyroxenites of the southeastern flank (figure 7.12D). Outside the Main Intrusion, Al shows values above 4% in almost every sample.

The distribution of Al values in the Tulu Dimtu areas is erratic. It is not possible to determine from this study whether the values represent a multi modal distribution or simply an uneven distribution.

7.6.7. Summary of Ni, Cu, Cr and Al values

High Ni values are only found in the soils above the Main Intrusion and Sheared Ultramafics and not the basement. Conversely and unlike the basement, Cu values are negligible in the soils over the Main Intrusion. However, high values of Al occur on the same flanks of the Main Intrusion and low values in the centre.

Al values in the soils of Tulu Dimtu show a unimodal distribution, whereas Ni and Cu show bimodal distributions. The distribution of Al is difficult to describe, it either consists of several populations or an erratic – non normal - distribution.

7.6.8. Platinum and Palladium

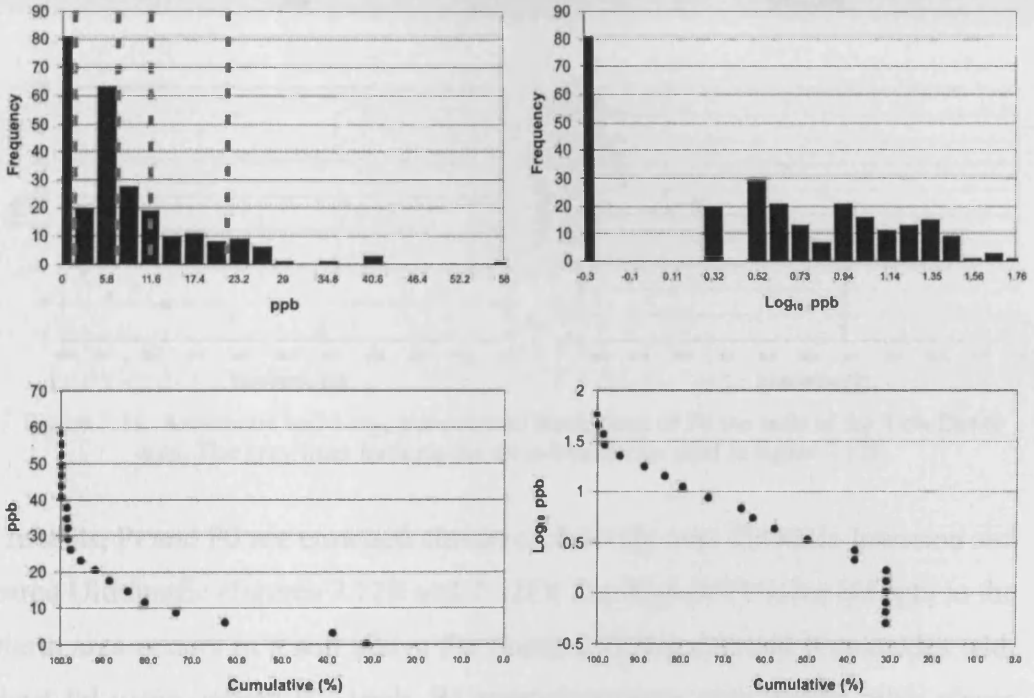

Figure 7.10: Arithmetic and Log_{10} transformed histograms of Pt the soils of the Tulu Dimtu area. The grey lines indicate the class-boundaries used in figure 7.12E.

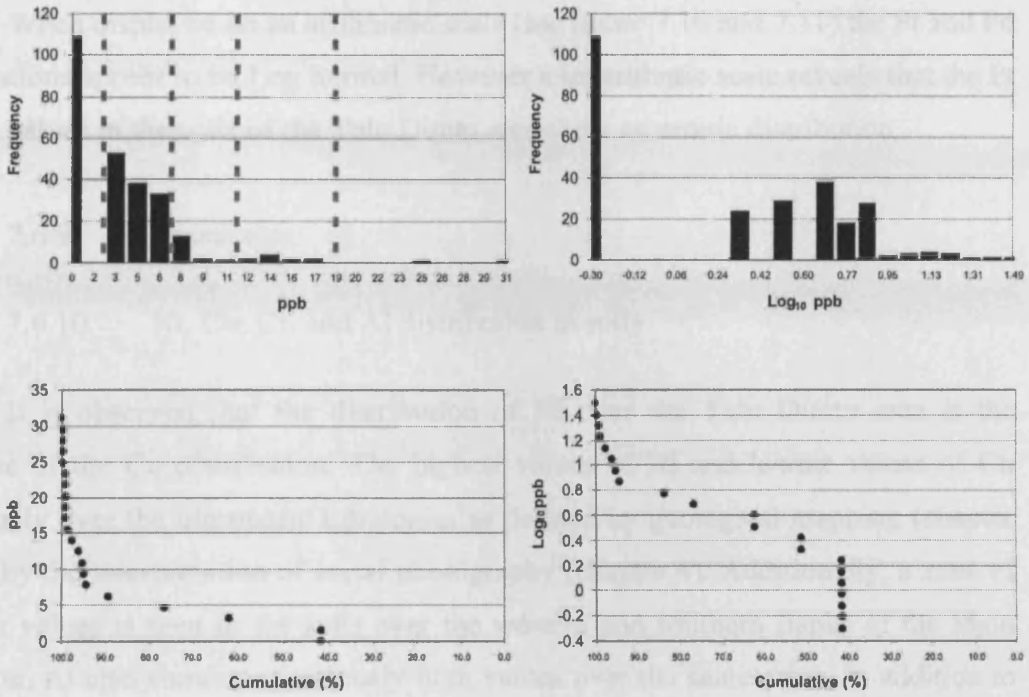

Figure 7.11: Arithmetic and Log_{10} transformed histograms of Pd the soils of the Tulu Dimtu area. The grey lines indicate the class-boundaries used in figure 7.12F.

In soils, Pt and Pd are enriched almost exclusively over the Main Intrusion and the Sheared Ultramafic (figures 7.12E and 7.12F). The highest Pt value (58ppb) in the Tulu Dimtu area occurs in a soil above the Sheared Ultramafic and it coincides with the highest Pd value, which is 31ppb. Pd anomalies occur only in two other places (13ppb and 15ppb) within the centre of the Main Intrusion, most other samples have values below detection limits. Figure 7.12E shows that the samples where Pt>20ppb form a pattern trending along the northwest flank of the Main Intrusion. These high Pt assays (>20ppb) found on the northwestern flank drop steadily towards the centre of the complex – forming a crude zonation of Pt values. None of the soil samples above the Lensoid Ultramafics are enriched in Pt or Pd. Furthermore, the soils above the Shear Zones do not contain Pt or Pd.

An area with slightly anomalous Pd values in soil occurs over the basement 4km southwest of the Main Intrusion. In this area four samples show Pt below detection limits and Pd in the range 13ppb to 16ppb.

When displayed on an arithmetic scale (see figure 7.10 and 7.11) the Pt and Pd distributions appear to be Log normal. However a logarithmic scale reveals that the Pt and Pd values in the soils of the Tulu Dimtu area show an erratic distribution.

7.6.9. Discussion

7.6.10. Ni, Cu, Cr, and Al distribution in soils

It is observed that the distribution of Ni over the Tulu Dimtu area is the opposite of the Cu distribution. The highest values of Ni and lowest values of Cu occur only over the ultramafic lithologies as defined by geological mapping (chapter 5) and by the interpretation of aerial photography (chapter 4). Additionally, a zone of high Cr values is seen in the soils over the western and southern flanks of the Main Intrusion. Al also shows anomalously high values over the same areas, in addition to the high values seen over the basement.

There are two possible explanations for the marked change in Ni and Cu values across the boundary between the Main Intrusion and the basement. Firstly, the change could be reflecting the change in rock-type below and secondly, the Cu may have been remobilized from the soils above the ultramafic rocks and redeposited at the base of the slope.

If the high increase in Cu values at the contact of the Tulu Dimtu Main Intrusion with the basement were solely due to hydromorphic dispersion then those high values would only be expected at the base of the slope. However, analysis of the aerial photographs (chapter 4) shows that high Cu values are also found in soils above the basement many of which are located at ridge summits. However, given the porous nature of the laterite and frequent rains in the area it is likely that hydromorphic dispersion will have had some effect on the Cu distribution, in combination with the effect from the relict rocks. This combined effect is discussed further in section 7.10.

The poor exposure means that the western boundary of the Tulu Dimtu Main Intrusion has been defined principally by the change in vegetation (chapter 4). The change in Ni and Cu concentrations across the same boundary supports the validity of

this method of geological mapping and suggests that some form of biogeochemical change has occurred. A high degree of Ni concentration in laterites is common over ultramafic units (Schellmann, 1989).

When partitioned into spinel minerals, Cr is known to be highly immobile. Unlike sulphide minerals, in the WES, Cr-spinels often remain intact throughout severe alteration (chapter 3) and also weathering. Therefore the locations of high Cr values in soils can be considered as being in-situ – given that soil transport is likely to have been minimal. Given that the high Cr values in soils show the same patterns and locations as those seen in altered and fresher rocks (see chapter 8), the distances by which these soils have moved are considered to be low ($\approx$<10m).

Aluminium is also known to be immobile in soils and therefore it is to be expected that Al may be present in the soils above the basement, given the high proportion of alumino-silicates in the underlying rocks. The zone of high Al at the flanks of the Main Intrusion is less easy to explain. The immobility of Al means that small amounts of it will be concentrated by volume loss during soil formation. The fresher ultramafics of Tulu Dimtu contain 1% Al at most and these values could potentially be increased to 4% if the volume loss effect of hydrothermal alteration acting at the flanks of the intrusion is also taken into account (see chapter 8).

7.6.11. Genesis of Pt and Pd in soils

In the Tulu Dimtu area, Pt is enriched over the soils of the Main Intrusion but not over the Lensoid Ultramafics. Also, a greater proportion of soil samples compared to rock samples are enriched in Pt to greater than 20ppb (see figures 7.12E and 7.12F). Theoretically, it is known that the high Eh, acid and chloride-rich conditions in lateritic soil covers can mobilise the PGE (see section 7.5.2). The predominance of Pt over Pd in the soils above the Tulu Dimtu Main Intrusion may be attributed to prefential leaching of Pd during the soil-formation. The Pt acts as a less mobile element and is retained within the soil. The increased proportion of Pt-bearing soil samples compared to rock samples over the Main Intrusion may be attributed to either the loss in volume from rock to soil or to the reconcentration of Pt within the lateritic conditions (as proposed by Bowles, 1995; see section 7.5.2). It is not possible to

assess the behaviour of Pt and Pd in the soils overlying the Lensoid Ultramafics because the rock samples are located far from the soil samples.

7.6.12. Conclusion

The distribution of Ni and Cu in the Tulu Dimtu area is likely to have been partially influenced by the geochemistry of the underlying rocks. However, it is likely that hydromorphic dispersion will have had an additional influence. Cr and Al have both acted as immobile elements and may reflect the same patterns seen in primary rocks (see chapter 8).

Redistribution of Pt and Pd is observed in the soils above the Tulu Dimtu Main Intrusion (see chapter 8). It is likely that Pt acted as a less mobile element and Pd was taken into solution. Consequently, Pd will have been leached out and some Pt may remain. The increase in Pt values from rock to soil may be accounted for by either by the volume change from rock to soil or by the reconcentration of Pt within the lateritic conditions as first suggested by Ottemann and Augustithis (1967).

7.7. *Kingy: Selected Major and Trace Elements*

7.7.1. Introduction

There are 201 soil samples from the Kingy area. Rock samples were taken where possible along roads and tracks (see figure 7.13). Due to dense vegetation, soil samples from the Kingy Ridge Ultramafic were only taken along the flanks, where the tracks occur. These samples were taken at 100 to 300m intervals parallel to roads and then only away from human influence.

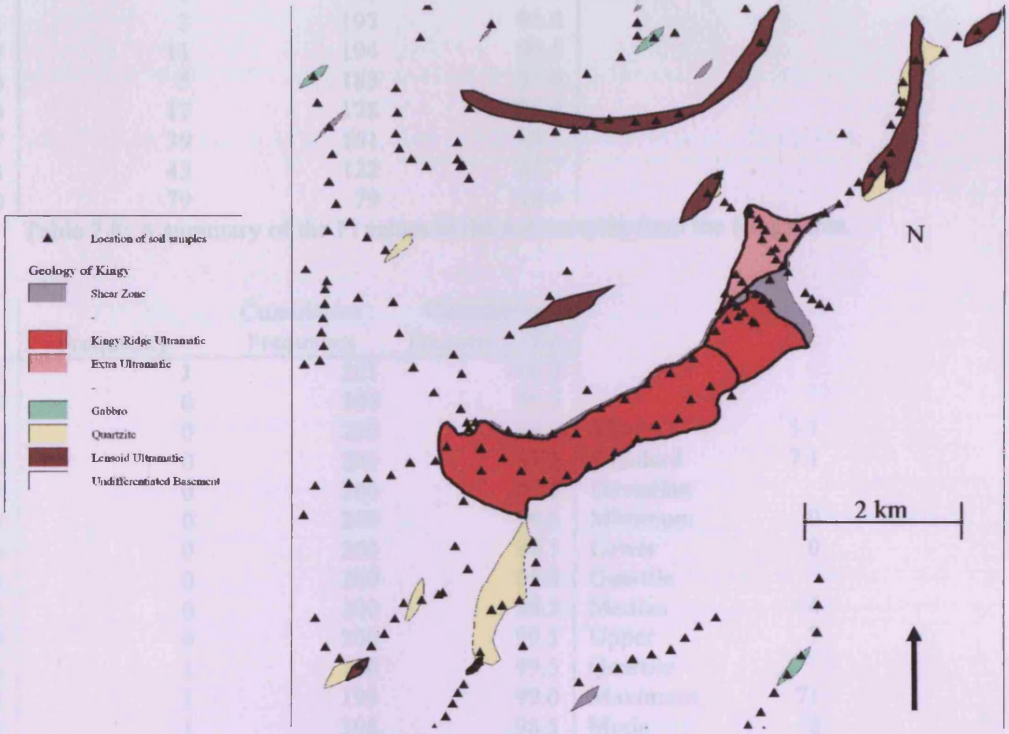

Figure 7.13: The distribution of soil samples in the Kingy area.

7.7.2. Summary of Analytical Results

Class Upper Limit (ppb)	Frequency	Cumulative Frequency	Cumulative Frequency (%)		
69	1	201	100.0		
66	0	200	99.5	Mean	4.4
62	0	200	99.5	Standard	7.1
59	0	200	99.5	Deviation	
55	0	200	99.5	Minimum	0
52	0	200	99.5	Lower	0
48	0	200	99.5	Quartile	
45	0	200	99.5	Median	3
41	0	200	99.5	Upper	5
38	0	200	99.5	Quartile	
35	1	200	99.5	Maximum	69
31	1	199	99.0	Mode	0
28	0	198	98.5	Number of	201
24	1	198	98.5	samples	
21	3	197	98.0		
17	11	194	96.5		
14	5	183	91.0		
10	17	178	88.6		
7	39	161	80.1		
3	43	122	60.7		
0	79	79	39.3		

Table 7.8: A summary of the Pt values in the soil samples from the Kingy area.

Class Upper Limit (ppb)	Frequency	Cumulative Frequency	Cumulative Frequency (%)		
71	1	201	100.0		
67	0	200	99.5		
64	0	200	99.5	Mean	5.1
60	0	200	99.5	Standard	7.1
57	0	200	99.5	Deviation	
53	0	200	99.5	Minimum	0
50	0	200	99.5	Lower	0
46	0	200	99.5	Quartile	
43	0	200	99.5	Median	4
39	0	200	99.5	Upper	7
36	1	200	99.5	Quartile	
32	1	199	99.0	Maximum	71
28	1	198	98.5	Mode	0
25	0	197	98.0	Number of	201
21	1	197	98.0	samples	
18	6	196	97.5		
14	11	190	94.5		
11	25	179	89.1		
7	59	154	76.6		
4	32	95	47.3		
0	63	63	31.3		

Table 7.9: A summary of the Pd values in the soil samples from the Kingy area.

Class Upper Limit (ppb)	Frequency	Cumulative Frequency	Cumulative Frequency (%)		
304	1	201	100.0		
289	0	200	99.5		
274	0	200	99.5	Mean	10
258	0	200	99.5	Standard	26
243	0	200	99.5	Deviation	
228	0	200	99.5	Minimum	0
213	0	200	99.5	Lower	2
198	0	200	99.5	Quartile	
182	0	200	99.5	Median	4
167	0	200	99.5	Upper	9
152	0	200	99.5	Quartile	
137	1	200	99.5	Maximum	304
122	1	199	99.0	Mode	2
106	0	198	98.5	Number of	201
91	0	198	98.5	samples	
76	2	198	98.5		
61	1	196	97.5		
46	3	195	97.0		
30	18	192	95.5		
15	148	174	86.6		
0	26	26	12.9		

Table 7.10: A summary of the Au values in the soil samples from the Kingy area.

Class Upper Limit (ppm)	Frequency	Cumulative Frequency	Cumulative Frequency (%)		
6976	1	201	100.0		
6627	1	200	99.5		
6279	0	199	99.0	Mean	460.9
5930	0	199	99.0	Standard	999.8
5581	0	199	99.0	Deviation	
5232	0	199	99.0	Minimum	1
4884	0	199	99.0	Lower	29
4535	2	199	99.0	Quartile	
4186	1	197	98.0	Median	86
3837	0	196	97.5	Upper	345
3489	2	196	97.5	Quartile	
3140	2	194	96.5	Maximum	6976
2791	3	192	95.5	Mode	29
2442	2	189	94.0	Number of	201
2094	2	187	93.0	samples	
1745	4	185	92.0		
1396	5	181	90.0		
1047	5	176	87.6		
699	20	171	85.1		
350	151	151	75.1		
0	0	0	0.0		

Table 7.11: A summary of the Ni values in the soil samples from the Kingy area.

Class Upper Limit (ppm)	Frequency	Cumulative Frequency	Cumulative Frequency (%)		
188	2	201	100.0		
179	2	199	99.0		
170	4	197	98.0	Mean	80.0
160	2	193	96.0	Standard	41.3
151	2	191	95.0	Deviation	
142	5	189	94.0	Minimum	4
133	11	184	91.5	Lower	49
124	15	173	86.1	Quartile	
114	13	158	78.6	Median	80
105	19	145	72.1	Upper	108
96	16	126	62.7	Quartile	
87	13	110	54.7	Maximum	188
78	18	97	48.3	Mode	90
68	18	79	39.3	Number of	201
59	7	61	30.3	samples	
50	17	54	26.9		
41	8	37	18.4		
32	6	29	14.4		
22	12	23	11.4		
13	11	11	5.5		
0	0	0	0.0		

Table 7.12: A summary of the Cu values in the soil samples from the Kingy area.

Class Upper Limit (ppm)	Frequency	Cumulative Frequency	Cumulative Frequency (%)		
3861	1	201	100.0		
3668	0	200	99.5		
3475	0	200	99.5	Mean	481
3282	0	200	99.5	Standard	601
3089	0	200	99.5	Deviation	
2896	0	200	99.5	Minimum	0
2703	1	200	99.5	Lower	83
2510	3	199	99.0	Quartile	
2317	2	196	97.5	Median	258
2124	1	194	96.5	Upper	635
1931	3	193	96.0	Quartile	
1737	2	190	94.5	Maximum	3861
1544	4	188	93.5	Mode	55
1351	7	184	91.5	Number of	201
1158	9	177	88.1	samples	
965	8	168	83.6		
772	13	160	79.6		
579	19	147	73.1		
386	43	128	63.7		
193	84	85	42.3		
0	1	1	0.5		

Table 7.13: A summary of the Cr values in the soil samples from the Kingy area.

Class Upper Limit (%)	Frequency	Cumulative Frequency	Cumulative Frequency (%)		
8.4	1	201	100.0		
8.0	3	200	99.5		
7.6	4	197	98.0	Mean	4.2
7.2	4	193	96.0	Standard Deviation	1.6
6.9	4	189	94.0		
6.5	11	185	92.0	Minimum	0.7
6.1	11	174	86.6	Lower Quartile	3.1
5.7	10	163	81.1		
5.3	13	153	76.1	Median	4.1
4.9	19	140	69.7	Upper Quartile	5.2
4.6	17	121	60.2		
4.2	25	104	51.7	Maximum	8.4
3.8	19	79	39.3	Mode	3.6
3.4	12	60	29.9	Number of samples	201
3.0	10	48	23.9		
2.6	12	38	18.9		
2.2	13	26	12.9		
1.9	8	13	6.5		
1.5	3	5	2.5		
1.1	2	2	1.0		
0.0	0	0	0.0		

Table 7.14: A summary of the Al values in the soil samples from the Kingy area.

The following sections cover the distribution of Ni, Cu, Cr and Al in the Kingy area. It is important to remember that it is unlikely that complete digestion has been acheieved during the aqua regia leach of these samples. Each section covers one element and describes its distribution in turn.

7.7.3. Nickel

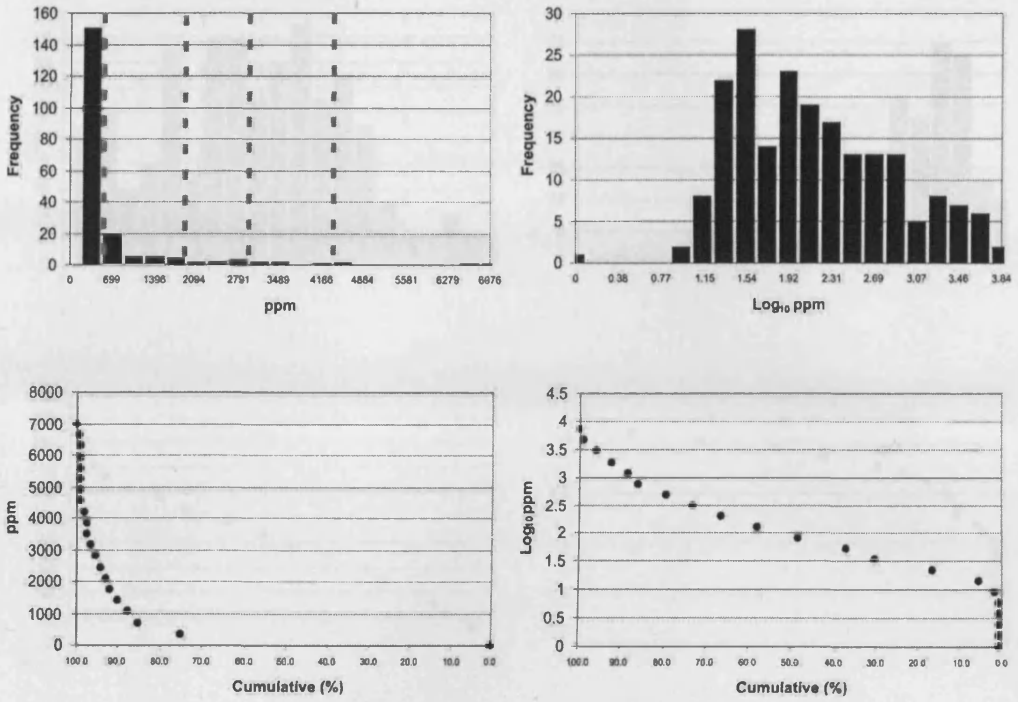

Figure 7.14: Arithmetic and Log_{10} transformed histograms of Ni the soils of the Kingy area. The grey lines indicate the class-boundaries used in figure 7.20A.

The highest Ni value in the soil samples was found over the large northeastern Lensoid Ultramafic. Another sample containing high Ni in soil (3395ppm) occurs over the shear-zone between the extra-ultramafic and Kingy Ridge Ultramafic. An isolated Ni-rich soil (4408ppm) occurs 500m west of the northeastern Lensoid Ultramafic. Any other Ni values above 100ppm are located close to or over ultramafic complexes.

The Ni values in the Kingy area show an approximately unimodal Log normal distribution with a mode at around 29ppm.

7.7.4. Copper

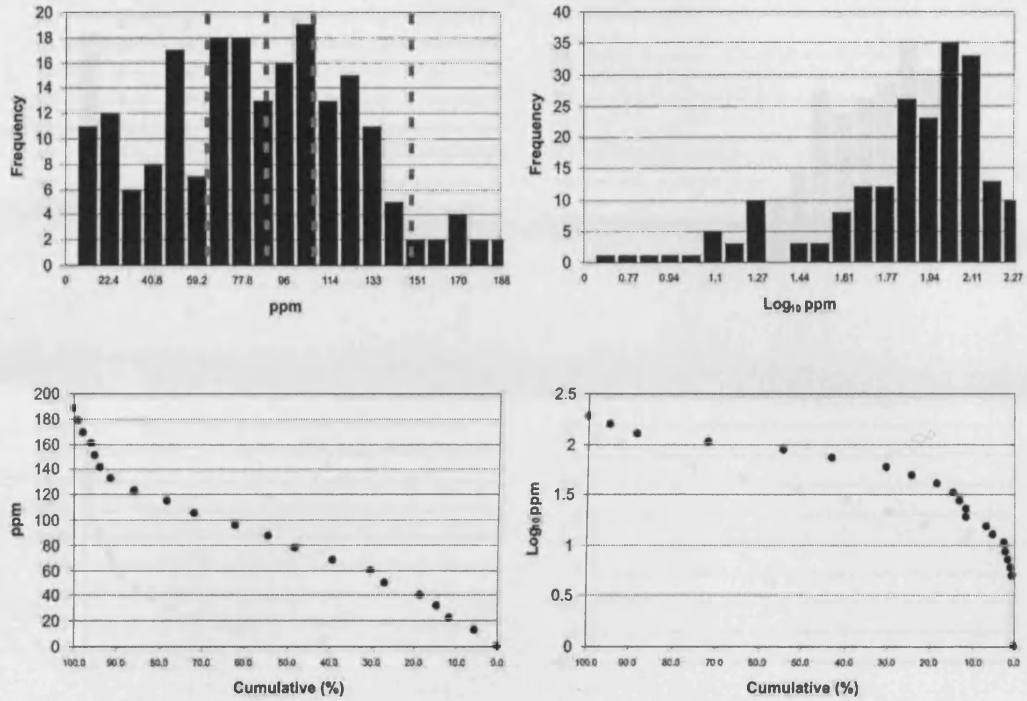

Figure 7.15: Arithmetic and Log_{10} transformed histograms of Cu the soils of the Kingy area. The grey lines indicate the class-boundaries used in figure 7.20B.

Cu values in soils are frequently over 150ppm above both the ultramafics and basement, this value may also fall to below 60ppm over all rock formations. The highest Cu value in a soil sample occurs above a shear zone near the Extra Ultramafic and may fall as low as 7ppm in soils overlying the basement.

The Cu values in the Kingy area are distributed in an erratic manner. It is not possible here to determine if this distribution is an erratic normal distribution or whether there is actually more than one population. Analysis of the logarithmic scale histogram (figure 7.15) raises the possibility that there may be two normally distributed populations. However, this is not shown on the arithmetic scaled histogram.

7.7.5. Chromium

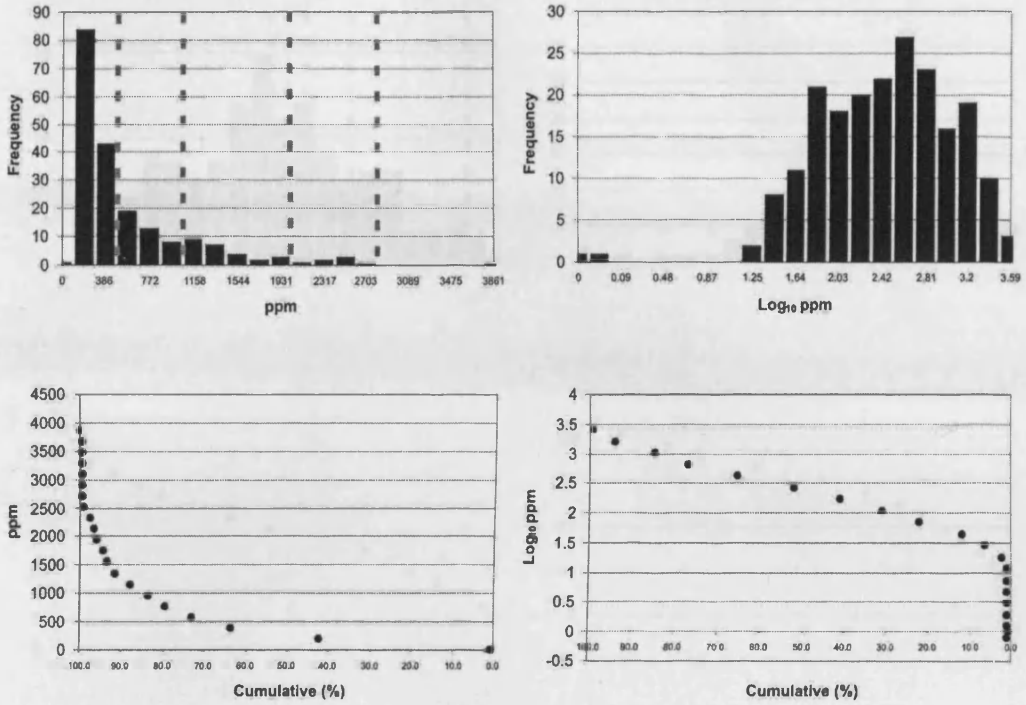

Figure 7.16: Arithmetic and Log_{10} transformed histograms of Cr the soils of the Kingy area. The grey lines indicate the class-boundaries used in figure 7.20C.

Soils with greater than 200ppm Cr only occur over the ultramafic complexes or in soils close to ultramafic complexes (see figure 7.20C). However, the highest Cr values in soil occur close to an isolated gabbro in the southeast at up to 3861ppm.

The Cr values in the Kingy area show a log normal distribution with a mode at around 400ppm with a slight negative skew.

7.7.6. Aluminium

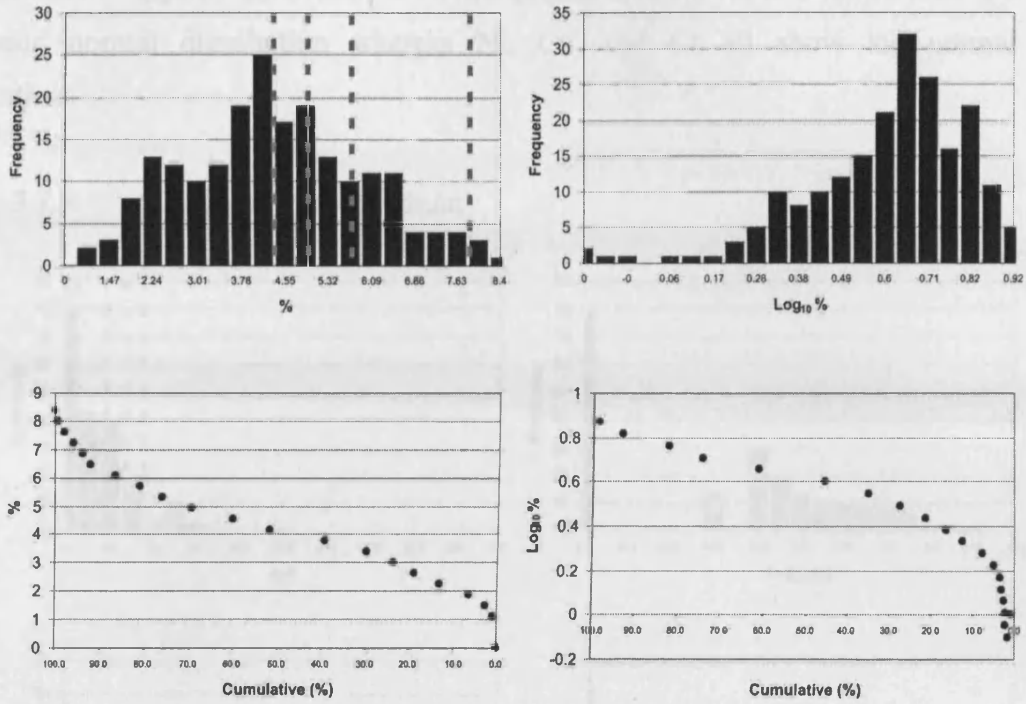

Figure 7.17: Arithmetic and Log_{10} transformed histograms of Al the soils of the Kingy area. The grey lines indicate the class-boundaries used in figure 7.20D.

The soil samples from near the quartzites to the southwest of the Kingy Ridge Ultramafics display the highest Al abundance from 4.5% up to 8.4%. However the Al abundance elsewhere is more erratically distributed and high values (>6.0%) are found over both the ultramafic units and the basement.

The Al values in the Kingy area are approximately normally distributed with a mode at around 4.0%. It is possible that an additional population exists with a mode at around 2.5%.

7.7.7. Summary of Ni, Cu, Cr and Al values

In the Kingy Ridge Ultramafic and the Extra Ultramafic – and notably not the isolated gabbro - high Cr and Ni values in soils are located solely over the ultramafic units and soils close by. Unlike Ni and Cr, Cu can rise to above 110ppm over all units, similarly Al can rise to over 6% over most formations. The soils around the isolated gabbro body are also elevated to over 3000ppm in Cr (figure 7.20C).

All four elements have distributions which are dominantly unimodal, although more detailed analysis may reveal additional populations for Ni and Al. Al shows a arithmetic normal distribution whereas Ni, Cu, and Cr all show log normal distributions.

7.7.8. Platinum and Palladium

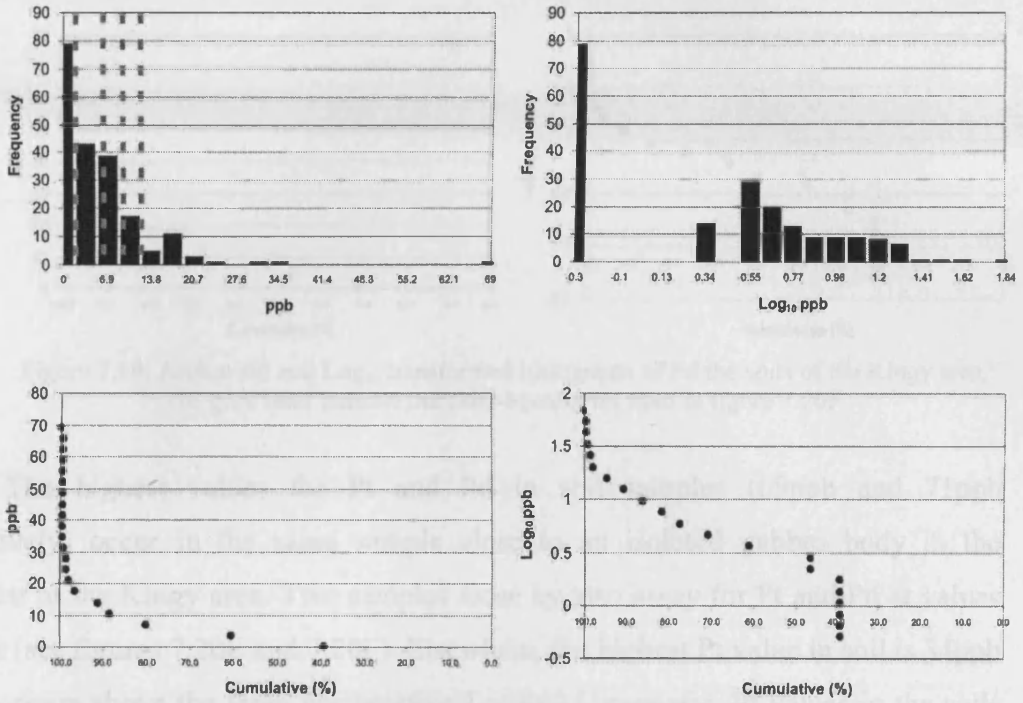

Figure 7.18: Arithmetic and Log_{10} transformed histograms of Pt the soils of the Kingy area. The grey lines indicate the class-boundaries used in figure 7.20E.

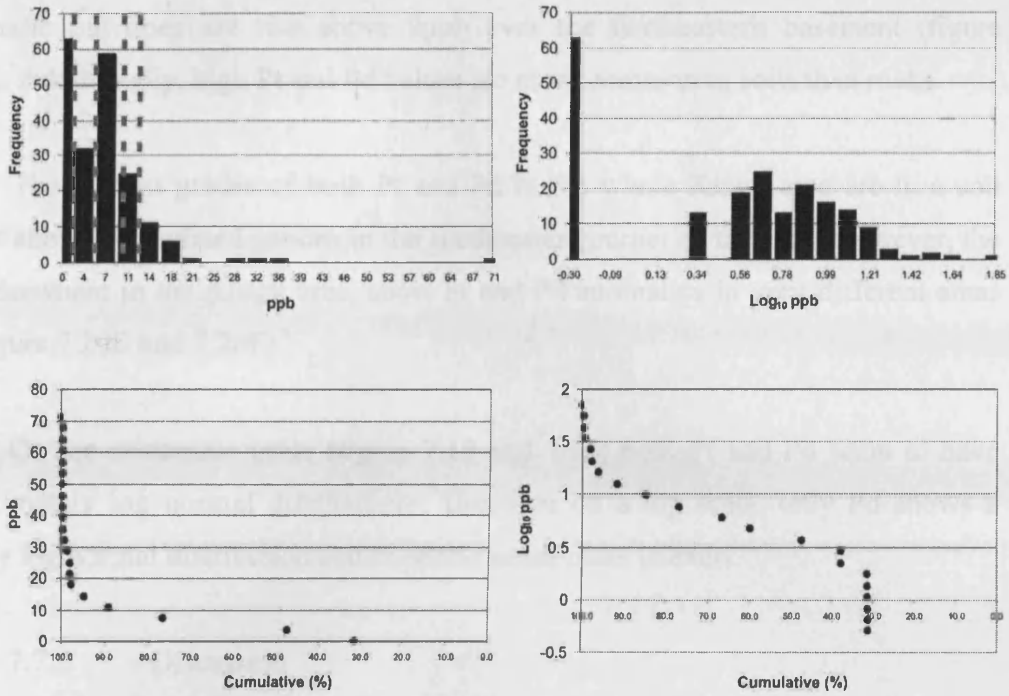

Figure 7.19: Arithmetic and Log_{10} transformed histograms of Pd the soils of the Kingy area. The grey lines indicate the class-boundaries used in figure 7.20F.

The highest values for Pt and Pd in soil samples (69ppb and 71ppb respectively) occur in the same sample close to an isolated gabbro body in the southeast of the Kingy area. Two samples close by also assay for Pt and Pd at values >12ppb (see figures 7.20E and 7.20F). Elsewhere, the highest Pt value in soil is 34ppb which occurs above the large northeastern Lensoid Ultramafic. Pt values in the soils of the Kingy Ridge Ultramafic range from 27ppb at the northeastern end to below detection limits in the southwestern end.

Figures 7.20E amd 7.20F shows a clear divide in Pt and Pd values between the soils of the northeastern and southwestern areas around Kingy. The northwestern basement is characterized by Pd values frequently over 12ppb and no samples show Pt at above 7ppb. The Extra Ultramafic and the large northeastern Lensoid Ultramafic also show Pd values frequently above 12 ppb however Pt also assays above 12ppb in many samples. However, towards the northeastern end of the ridge, the soils become richer in Pt (up to 29ppb) but still without significant Pd values (all below 10ppb).

Pt dominates soils over the Kingy Ridge Ultramafic, unlike the northwestern basement where Pd dominates. Pt rises above 12ppb 13 times over the Kingy Ridge

Ultramafic but does not rise above 9ppb over the northeastern basement (figure 7.20E). Additionally, high Pt and Pd values are more common in soils than rocks.

The highest grades of both Pt and Pd in the whole Kingy area are in a soil sample above the isolated gabbro in the southeastern corner of the area. However, the soils elsewhere in the Kingy area, show Pt and Pd anomalies in very different areas (see figure 7.20E and 7.20F).

On the arithmetic scale (figure 7.18 and 7.19) both Pt and Pd seem to have approximately log normal distributions. However on a log scale, only Pd shows a roughly log normal distribution and Pt seems much more uneven.

7.7.9. Discussion

7.7.10. Trace Element distribution in soils

Except for the isolated gabbro (see chapter 5) all high Cr and Ni values in soils of the Kingy area only occur over the ultramafic units. However, high Cu and Al values are observed over all formations. The high Cr, Cu and Ni values observed above the ultramafic units are to be expected and these reflect the geochemistry of the underlying rocks. Additionally the elevated Al content of the soils is to be expected as this immobile element will be concentrated even from the low amounts seen in the rocks from the Kingy Ridge Ultramafic.

7.7.11. Genesis of Pt and Pd in soils

The distribution of Pt and Pd values in the soils from the Kingy area show a distinct geographical split between the two elements (see figures 7.20E and 7.20F). Pd is concentrated mainly in the soils over the basement of the northwest and the Pt is concentrated over the Kingy Ridge area – although a few anomalous Pd values also occur.

As discussed in section 7.5.2, Pt and Pd are likely to be concentrated in the soils above PGE-bearing ultramafic complexes and some Pd may also be lost between the rocks and soils. It appears that Pt is more extensively mineralised in soils than in

the rocks over the Kingy Ridge Ultramafic. It is possible that due to the large volume of rock from which a thick laterite is formed (several times greater than the thickness of the laterite itself) small amounts of the immobile Pt may have become concentrated. At the same time as the immobile Pt particles are concentrated, the mobile Pd is leached out. In the soils above the Kingy Ridge Ultramafic, the relative distributions of Pt and Pd in soils versus rock support the hypothesis that Pd is more mobile than Pt in lateritic soils.

Given the mobility differences described above, it is hard to understand the origins of the Pd concentration observed over the basement in the northwest where the laterites are known to be of a similar thickness to those from the Kingy Ridge areas. If Pd is mobile in the fluids of lateritic covers from the Kingy Ridge why is it retained in the soils seen here? It is possible that there are some different aqueous conditions occurring in these laterites due to a different protolith (metavolcanic and meta sedments as opposed to ultramafic) whereby Pd becomes immobile. However, there is also a difference in vegetation type seen from aerial photography (chapter 4) between this area and the Kingy Ridge Ultramafic and it is conceivable that biochemical factors may have caused Pd to complex with humic or fulvic acid as a locked molecule.

The primary source of the Pd in the soils from the northwest of the Kingy area could be attributed to some Pd-bearing (9 or 10ppb) Shear Zones and gabbros (see figure 7.20F). However, the Pd distribution in the soils covers a wider area than the known extent of these exposures and therefore hints towards a larger system of Pd-bearing rocks not yet exposed.

The highest Pt and Pd values in soils occur above the isolated gabbro exposure in the southeast. Lack of further geological information about this area precludes precludes a definite conclusion however the presence of a high Cu value in soil hints towards either magmatic or hydrothermal origin. This area merits further investigation.

7.7.12. Conclusions

The distribution of Ni and Cr over the ultramafic complexes in the Kingy area suggests that their distribution is connected to the underlying lithotypes. However Cu and Al show no particular pattern with lithotype.

The extent of Pt mineralisation in the soils overlying the Kingy Ridge Ultramafic is wider than seen in the fresher rocks, which may be attributed to either volume loss from rock to soil or by in-situ remobilisation of Pt and Pd. The most striking feature of the Pt and Pd distribution in soils from the Kingy area is the division between northwest and southeast, the origin of this pattern cannot be ascertained here.

7.8. *Daleti, Ankori, Tulu Kapi and Keley: Selected Major and Trace Elements*

7.8.1. Introduction

There are 240 soil samples from the area in question. Over the Daleti Ultramafic samples were taken at a spacing of 300m where access was possible. Elsewhere, samples were taken along roads and tracks at 300m intervals (see figure 7.21).

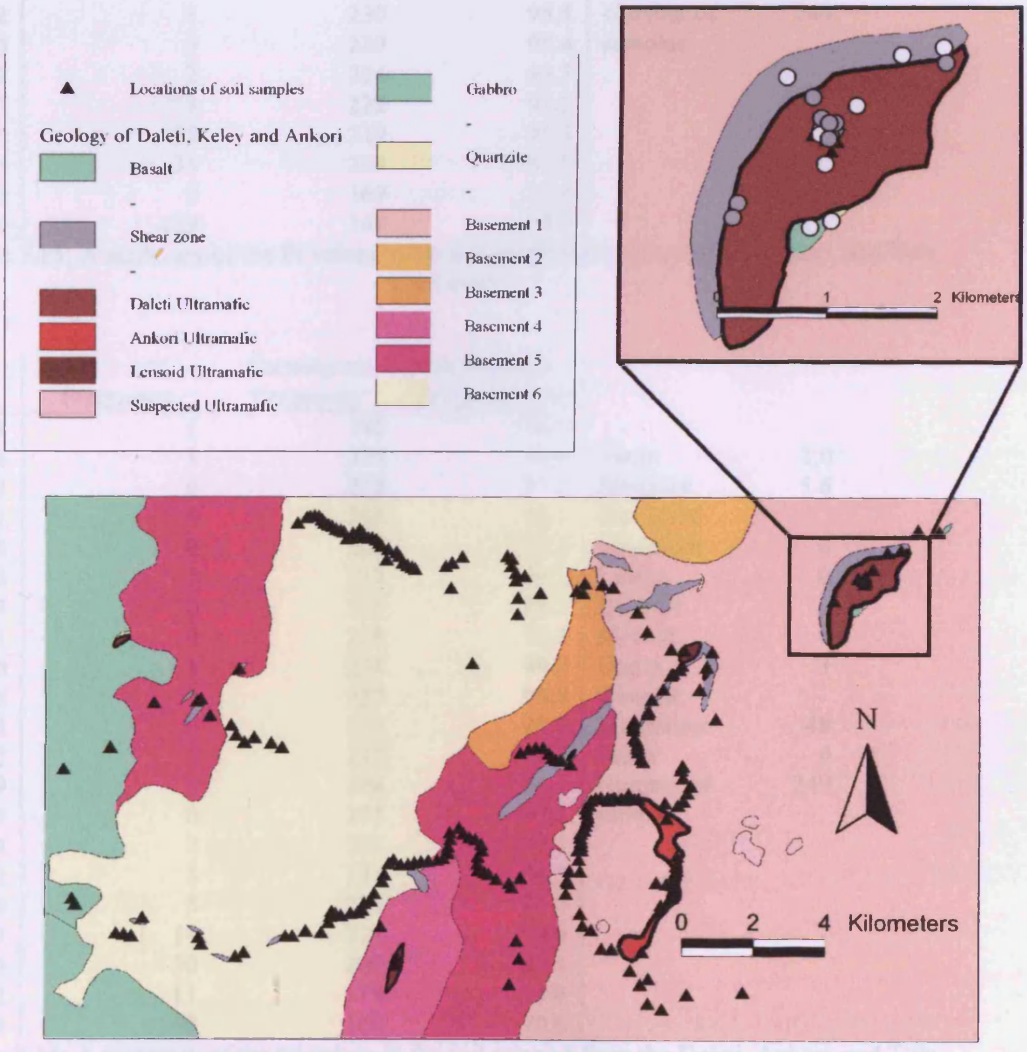

Figure 7.21: The distribution of soil samples in the Daleti, Ankori, Tulu Kapi and Keley areas.

7.8.2. Summary of Analytical Results

Class Upper Limit (ppb)	Frequency	Cumulative Frequency	Cumulative Frequency (%)		
34	2	240	100.0		
32	0	238	99.2		
31	0	238	99.2	Mean	1.8
29	0	238	99.2	Standard	4.5
27	0	238	99.2	Deviation	
26	0	238	99.2	Minimum	0
24	0	238	99.2	Lower	0
22	1	238	99.2	Quartile	
20	0	237	98.8	Median	0
19	1	237	98.8	Upper	2
17	1	236	98.3	Quartile	
15	3	235	97.9	Maximum	34
14	2	232	96.7	Mode	0
12	1	230	95.8	Number of	240
10	5	229	95.4	samples	
9	2	224	93.3		
7	3	222	92.5		
5	15	219	91.3		
3	35	204	85.0		
2	0	169	70.4		
0	169	169	70.4		

Table 7.15: A summary of the Pt values in the soil samples from the Daleti, Ankori, and Tulu Kapi areas.

Class Upper Limit (ppb)	Frequency	Cumulative Frequency	Cumulative Frequency (%)		
48	1	240	100.0		
46	1	239	99.6	Mean	2.0
43	0	238	99.2	Standard	5.6
41	0	238	99.2	Deviation	
38	0	238	99.2	Minimum	0
36	0	238	99.2	Lower	0
34	0	238	99.2	Quartile	
31	0	238	99.2	Median	0
29	1	238	99.2	Upper	3
26	0	237	98.8	Quartile	
24	0	237	98.8	Maximum	48
22	1	237	98.8	Mode	0
19	3	236	98.3	Number of	240
17	0	233	97.1	samples	
14	2	233	97.1		
12	3	231	96.3		
10	5	228	95.0		
7	14	223	92.9		
5	30	209	87.1		
2	11	179	74.6		
0	168	168	70.0		

Table 7.16: A summary of the Pd values in the soil samples from the Daleti, Ankori, and Tulu Kapi areas.

Class Upper Limit (ppb)	Frequency	Cumulative Frequency	Cumulative Frequency (%)		
17639	1	240	100.0		
16757	0	239	99.6	Mean	99
15875	0	239	99.6	Standard Deviation	1145
14993	0	239	99.6		
14111	0	239	99.6	Minimum	0
13229	0	239	99.6	Lower Quartile	2
12347	0	239	99.6		
11465	0	239	99.6	Median	4
10583	0	239	99.6	Upper Quartile	10.25
9701	0	239	99.6		
8820	0	239	99.6	Maximum	17639
7938	0	239	99.6	Mode	2
7056	0	239	99.6	Number of samples	240
6174	0	239	99.6		
5292	0	239	99.6		
4410	0	239	99.6		
3528	0	239	99.6		
2646	1	239	99.6		
1764	1	238	99.2		
882	202	237	98.8		
0	35	35	14.6		

Table 7.17: A summary of the Au values in the soil samples from the Daleti, Ankori, and Tulu Kapi areas.

Class Upper Limit (ppm)	Frequency	Cumulative Frequency	Cumulative Frequency (%)		
19266	1	240	100.0		
18303	0	239	99.6		
17340	1	239	99.6	Mean	459
16378	1	238	99.2	Standard Deviation	2161
15415	0	237	98.8		
14452	0	237	98.8	Minimum	10
13489	0	237	98.8	Lower Quartile	29
12526	0	237	98.8		
11564	0	237	98.8	Median	38
10601	0	237	98.8	Upper Quartile	57
9638	1	237	98.8		
8675	2	236	98.3	Maximum	19266
7712	0	234	97.5	Mode	41
6750	1	234	97.5	Number of samples	240
5787	0	233	97.1		
4824	0	233	97.1		
3861	1	233	97.1		
2898	0	232	96.7		
1936	6	232	96.7		
973	226	226	94.2		
0	0	0	0.0		

Table 7.18: A summary of the Ni values in the soil samples from the Daleti, Ankori, and Tulu Kapi areas.

Class Upper Limit (ppm)	Frequency	Cumulative Frequency	Cumulative Frequency (%)		
366	1	240	100.0		
348	0	239	99.6		
330	0	239	99.6	Mean	50.4
311	0	239	99.6	Standard	35.6
293	0	239	99.6	Deviation	
275	0	239	99.6	Minimum	2
257	0	239	99.6	Lower	32
239	0	239	99.6	Quartile	
220	0	239	99.6	Median	42
202	0	239	99.6	Upper	60
184	1	239	99.6	Quartile	
166	1	238	99.2	Maximum	366
148	4	237	98.8	Mode	39
129	5	233	97.1	Number of	240
111	10	228	95.0	samples	
93	17	218	90.8		
75	23	201	83.8		
57	82	178	74.2		
38	70	96	40.0		
20	26	26	10.8		
0	0	0	0.0		

Table 7.19: A summary of the Cu values in the soil samples from the Daleti, Ankori, and Tulu Kapi areas.

Class Upper Limit (ppm)	Frequency	Cumulative Frequency	Cumulative Frequency (%)		
3056	1	240	100.0		
2904	1	239	99.6		
2752	1	238	99.2	Mean	243
2599	0	237	98.8	Standard	432
2447	0	237	98.8	Deviation	
2295	1	237	98.8	Minimum	12
2143	0	236	98.3	Lower	76
1991	0	236	98.3	Quartile	
1838	1	236	98.3	Median	104
1686	1	235	97.9	Upper	154
1534	3	234	97.5	Quartile	
1382	3	231	96.3	Maximum	3056
1230	0	228	95.0	Mode	103
1077	1	228	95.0	Number of	240
925	2	227	94.6	samples	
773	8	225	93.8		
621	8	217	90.4		
469	6	209	87.1		
316	20	203	84.6		
164	183	183	76.3		
0	0	0	0.0		

Table 7.20: A summary of the Cr values in the soil samples from the Daleti, Ankori, and Tulu Kapi areas.

Class Upper Limit (%)	Frequency	Cumulative Frequency	Cumulative Frequency (%)		
7.4	1	240	100.0		
7.0	1	239	99.6		
6.7	2	238	99.2	Mean	3.82
6.3	5	236	98.3	Standard Deviation	1.24
6.0	10	231	96.3		
5.6	17	221	92.1	Minimum	0.2
5.2	15	204	85.0	Lower Quartile	3.0
4.9	21	189	78.8		
4.5	19	168	70.0	Median	3.7
4.2	27	149	62.1	Upper Quartile	4.7
3.8	32	122	50.8		
3.4	28	90	37.5	Maximum	7.4
3.1	15	62	25.8	Mode	3.6
2.7	23	47	19.6	Number of samples	240
2.4	12	24	10.0		
2.0	2	12	5.0		
1.6	3	10	4.2		
1.3	4	7	2.9		
0.9	1	3	1.3		
0.6	2	2	0.8		
0.0	0	0	0.0		

Table 7.21: A summary of the Al values in the soil samples from the Daleti, Ankori, and Tulu Kapi areas.

The following sections cover the distribution of Ni, Cu, Cr and Al in the Daleti, Ankori, Tulu Kapi and Keley areas. It is important to remember that it is unlikely that complete digestion has been acheieved during the aqua regia leach of these samples. Each section covers one element and describes its distribution in the soils.

7.8.3. Nickel

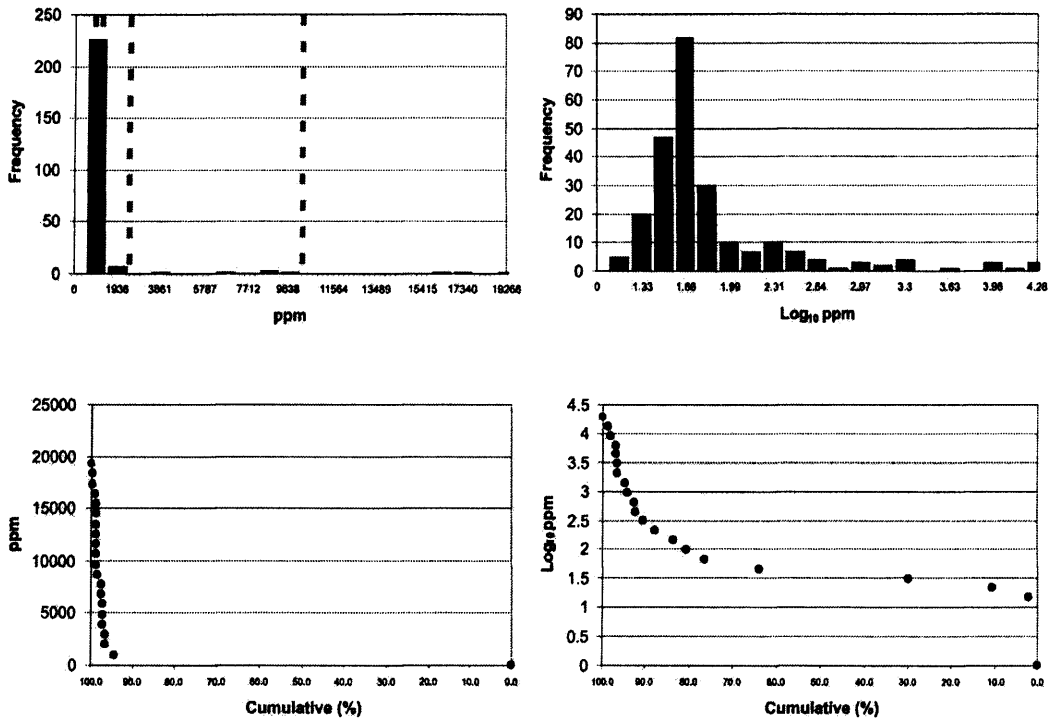

Figure 7.22: Arithmetic and Log_{10} transformed histograms of Ni the soils of the Daleti, Ankori, Tulu Kapi and Keley areas. The grey lines indicate the class-boundaries used in figure 7.28A.

High values of Ni in soil (over 1120ppm) are only seen in two areas, over the Daleti Ultramafic and the Ankori Ultramafic. The highest value of Ni in soil (19,266ppm) is seen over the Daleti Ultramafic. As with the fresher rocks, a high degree of local variation (within 250m) in Ni values is seen in soils (see figure 7.28A).

The Ni values in the soils of the Daleti, Ankori, Tulu Kapi and Keley areas show a positively skewed log normal distribution with a mode at around 41ppm.

7.8.4. Copper

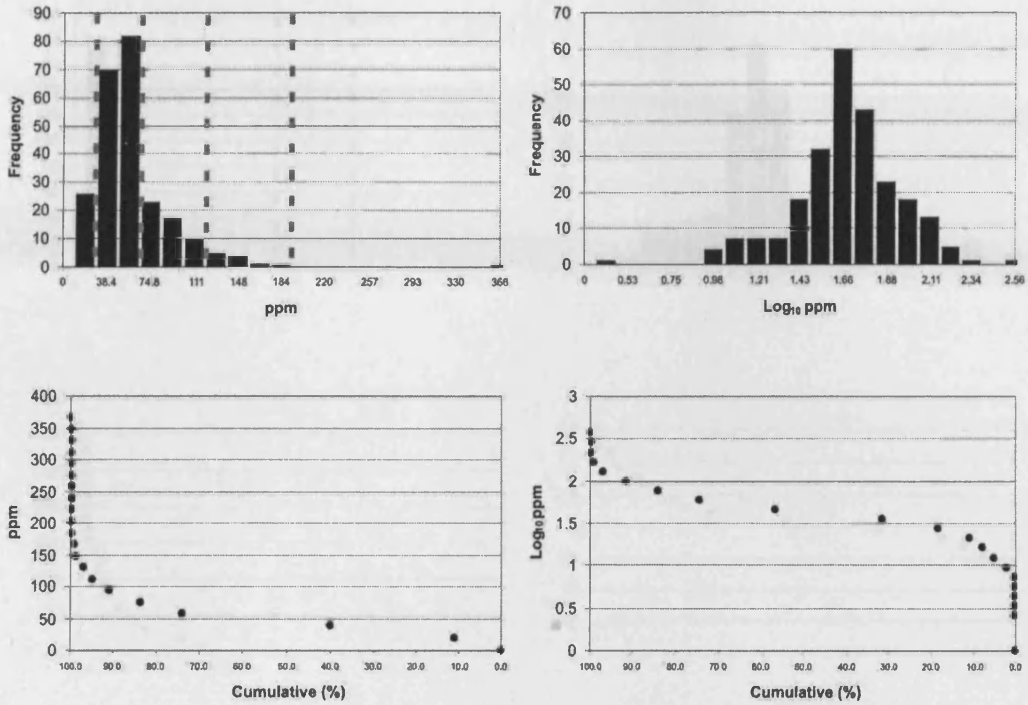

Figure 7.23: Arithmetic and Log_{10} transformed histograms of Cu the soils of the Daleti, Ankori, Tulu Kapi and Keley areas. The grey lines indicate the class-boundaries used in figure 7.28B.

Cu values in soil above the Daleti, Ankori and Keley ultramafic complexes are all below 120ppm and some Cu analyses fall below detection limits. The highest value of Cu in soil (366ppm) occurs above the Lensoid Ultramafic bearing the highest value of Cu in rock, near Keley. The two other high values of Cu in soil occur above basement rocks to the north and south of the Ankori complex (<183ppm).

The Cu values in the Daleti, Ankori, Tulu Kapi and Keley areas show a near symmetrical, log normal distribution with a mode at 1.6%.

7.8.5. Chromium

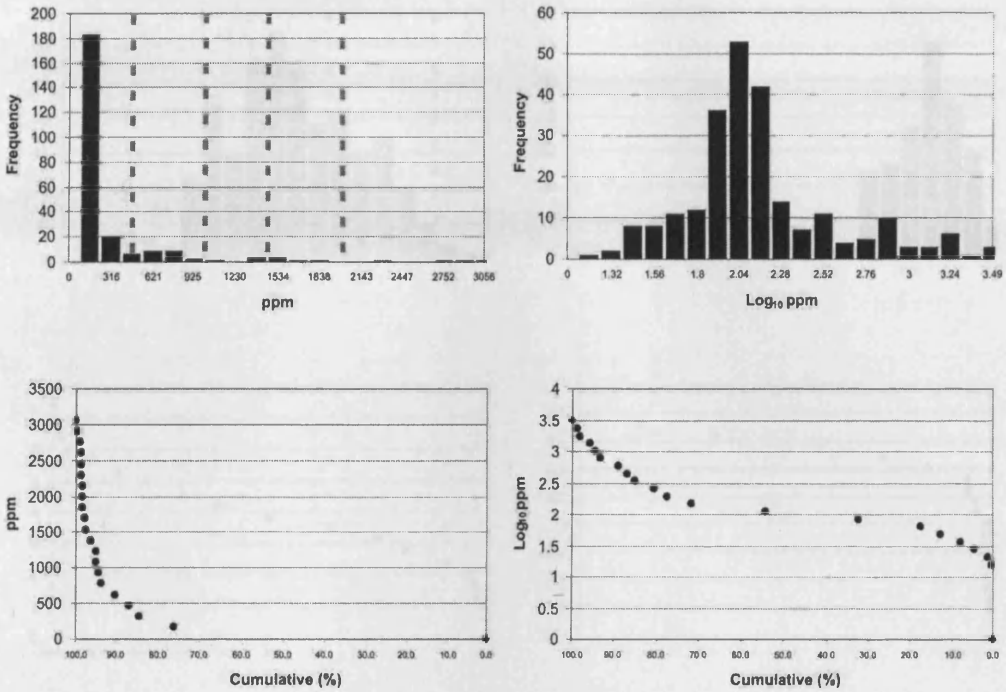

Figure 7.24: Arithmetic and Log_{10} transformed histograms of Cr the soils of the Daleti, Ankori, Tulu Kapi and Keley areas. The grey lines indicate the class-boundaries used in figure 7.28C.

All Cr values in soil of above 1000ppm are only found above the ultramafic complexes. As with the rock samples (see chapter 8), the highest Cr values in soil above the Daleti Ultramafic (3,056ppm) are found in the centre of the complex and the lowest occur over the contact with the shear zones to the north (308ppm).

The distribution of the Cr values in the Daleti, Ankori, Tulu Kapi and Keley areas is log normal and near symmetrical, the mode lies at around 100ppm.

7.8.6. Aluminium

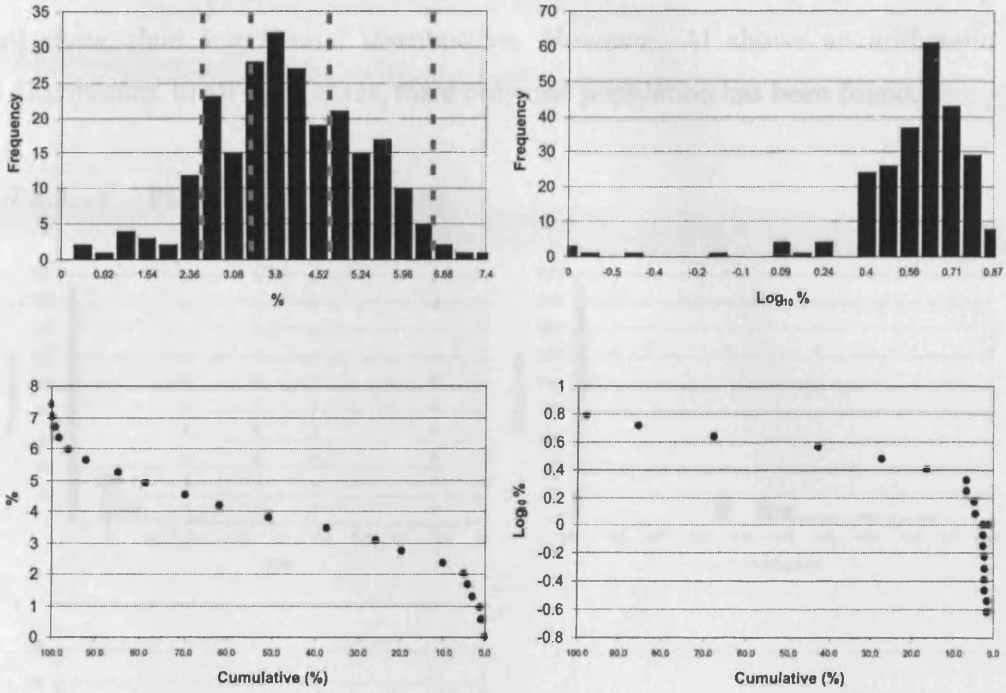

Figure 7.25: Arithmetic and Log_{10} transformed histograms of Al the soils of the Daleti, Ankori, Tulu Kapi and Keley areas. The grey lines indicate the class-boundaries used in figure 7.28D.

Al contents in soils are broadly similar over all formations of the Daleti area and Al values below detection occurr throughout the area. The highest Al values in soils above the Daleti Ultramafic (5.0%) are found in the centre of the intrusion, closely associated with some analyses which are as low as 0.2%.

There is a slightly uneven unimodal normal distribution of Al values in the soils of the Daleti, Ankori, Tulu Kapi and Keley areas. The mode lies at around 3.6%.

7.8.7. Summary of Ni, Cu, Cr and Al values

High Ni values in soil are only seen above the Daleti and Ankori complexes. Unlike Ni, Cu values in soils from the Daleti Ultramafic do not rise to the same high values which can be seen over the basement. The one exception to this is that the highest Cu value from the area (366ppm) occurs in a soil sample from above the Lensoid Ultramafic. The highest Cr values occur above the ultramafic complexes, whereas Al can occur at high values over all formations.

Ni, Cu, and Cr values in the soils of the Daleti, Ankori, Tulu Kapi and Keley areas all show clear log normal distributions. However, Al shows an arithmetic normal distribution. In all three cases, there only one population has been found.

7.8.8. Platinum and Palladium

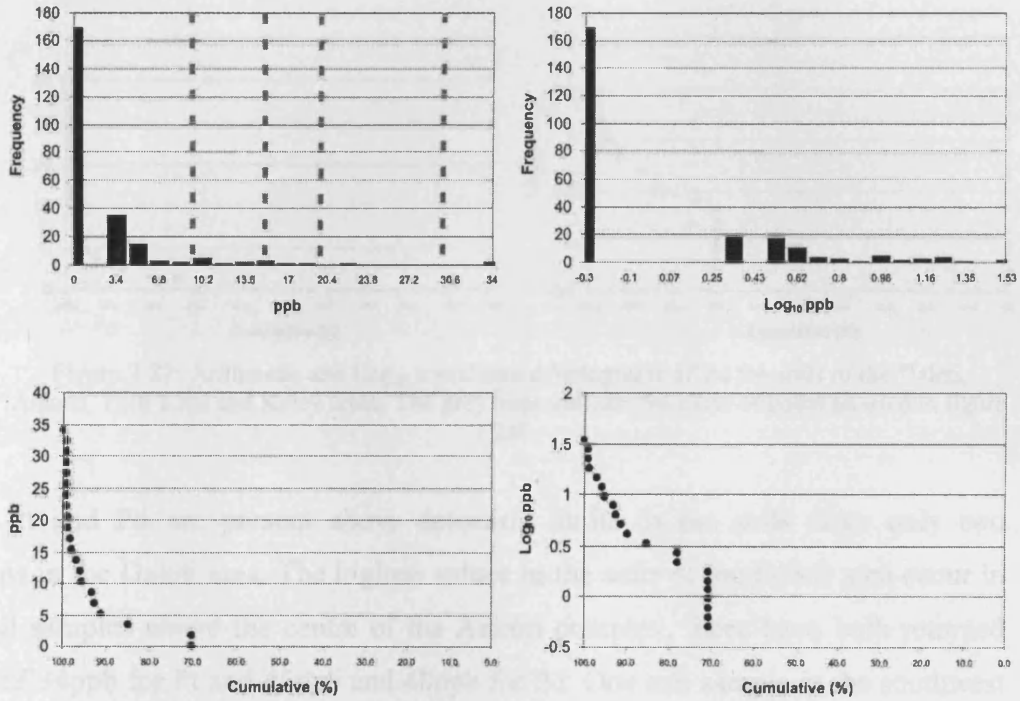

Figure 7.26: Arithmetic and Log_{10} transformed histograms of Pt the soils of the Daleti, Ankori, Tulu Kapi and Keley areas. The grey lines indicate the class-boundaries used in figure 7.28E.

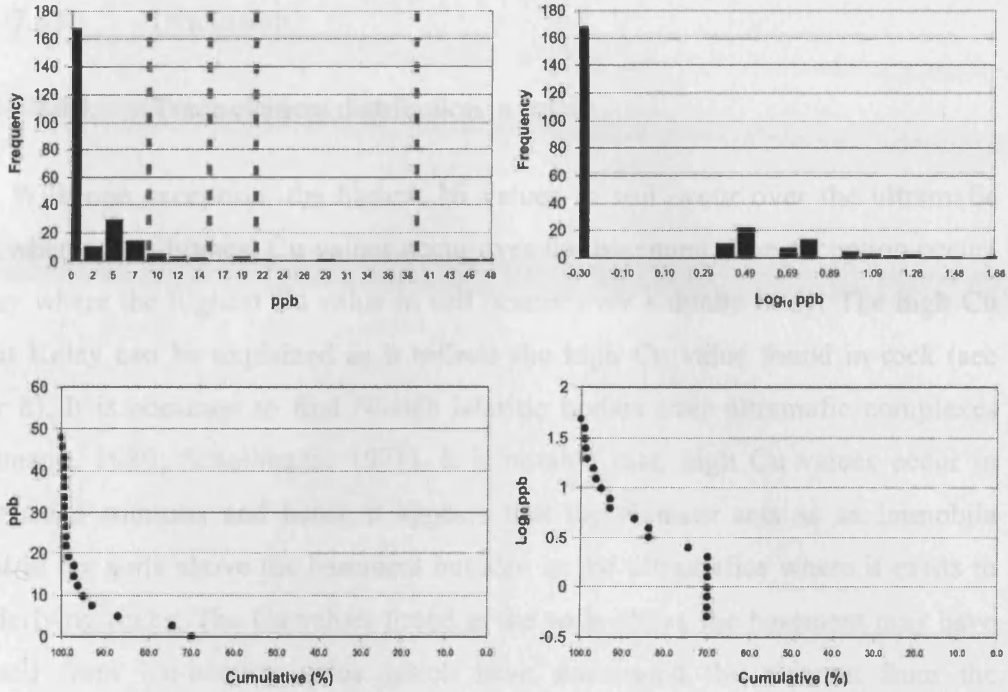

Figure 7.27: Arithmetic and Log_{10} transformed histograms of Pd the soils of the Daleti, Ankori, Tulu Kapi and Keley areas. The grey lines indicate the class-boundaries used in figure 7.28F.

Pt and Pd are present above detection limits in the soils from only two locations in the Daleti area. The highest values in the soils of the Daleti area occur in two soil samples above the centre of the Ankori complex, these have both returned assays of 34ppb for Pt and 45ppb and 48ppb for Pd. One soil sample in the southwest of the area returned values of 22ppb for Pt and 27ppb for Pd (see figures 7.28E and 7.28F). There are 9 soil samples where both Pt and Pd return assay results between 10 and 30ppb, these are all located above the Ankori complex. All soils above the Daleti Ultramafic have returned assays for Pt and Pd which are below detection limits.

Figures 7.26 and 7.27 show that the distribution of Pt an Pd values within the Daleti and Ankori areas is erratic and does not show typical normal or log normal distributions.

7.8.9. Discussion

7.8.10. Trace element distribution in soils

With one exception, the highest Ni values in soil occur over the ultramafic bodies whereas the highest Cu values occur over the basement. The exception occurs at Keley where the highest Cu value in soil occurs over a dunite body. The high Cu value at Keley can be explained as it reflects the high Cu value found in rock (see chapter 8). It is common to find Ni-rich lateritic bodies over ultramafic complexes (Schellmann, 1989; Schellmann, 1971). It is notable that, high Cu values occur in soils at ridge summits and hence it appears that the element acts as an immobile element in the soils above the basement but also in the ultramafics where it exists in the underlying rocks. The Cu values found in the soils above the basement may have originated from Cu-bearing veins which have scavenged the element from the ultramafic intrusions. The clear-boundaries between Ni and Cu distribution co-incide with the contacts mapped in this study and therefore these elements validate the mapping technique.

7.8.11. Genesis of Pt and Pd in soils

Soil samples at only two locations studied in this section contain Pt or Pd values of above 20ppb, one at the southwestern basement and one above the Ankori complex. The soils above the Daleti Ultramafic are entirely barren of both elements. As expected, both of the soil anomalies lie close to high Pt and Pd values in rock (see figures 7.28E, 8.10E, 7.28F and 8.10F). These soils probably represent the weathered equivalent of the PGE-bearing rocks.

There is an absence of PGE-bearing soils over many other Pt and Pd bearing complexes. Furthermore, the highest value PGE-bearing soils from the Ankori complex does not co-coincide with the locations of highest Pt and Pd values in rock. This difference in location of the rock and soil anomalies in the Ankori Ultramafic may be due to soil transport. However the lack of Pt and Pd over the other complexes cannot be explained here.

7.8.12. Conclusions

Both Ni and Cr show high values solely over the ultramafic intrusions whereas Al and Cu show high values over many formations, including the basement. Some notably high (>19,000ppm) Ni values occur in the laterites covering the Daleti Ultramafic. Significant Pt and Pt values are only found in two places, the Ankori complex and the soils around a system of shear zones to the southwest of Gudeya Guji (see figures 7.28E and 7.28F).

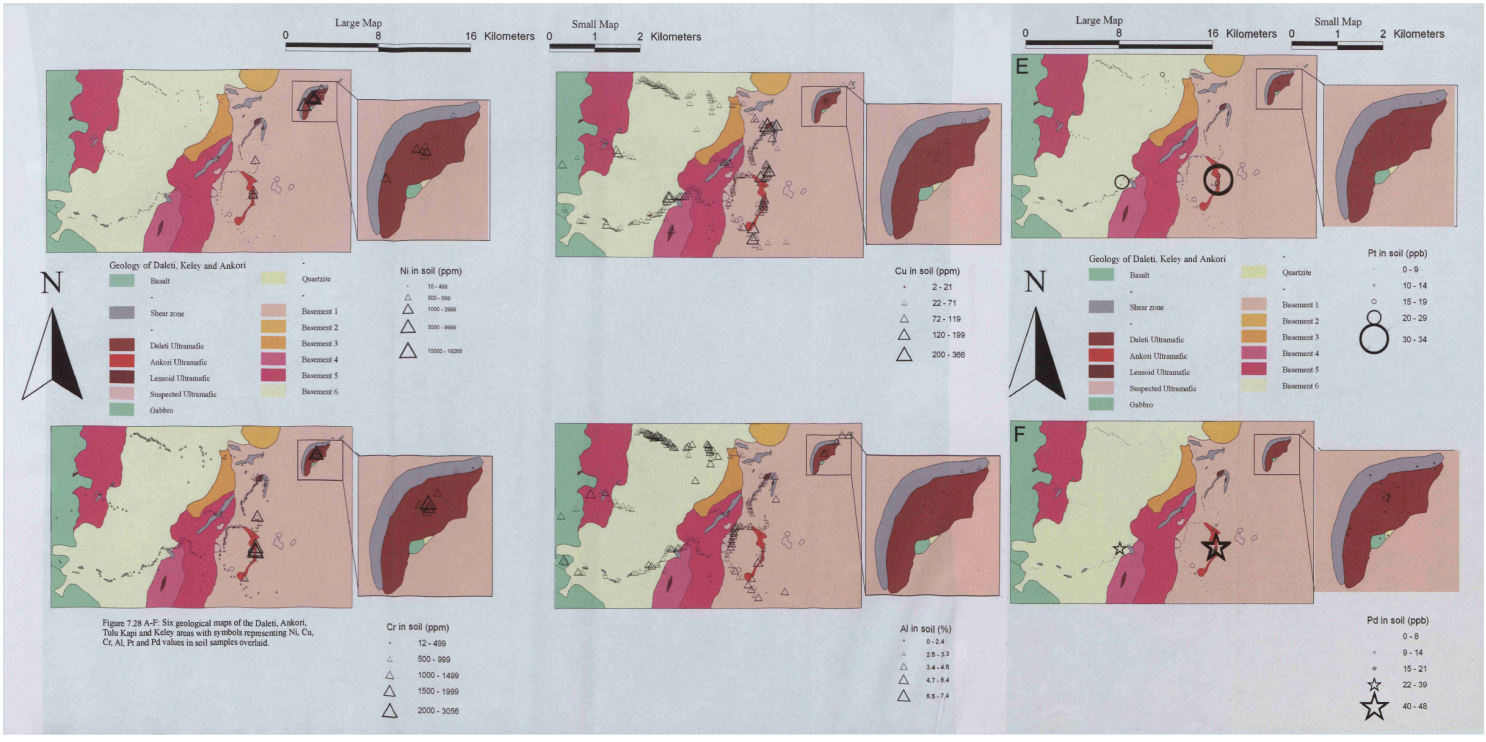

Figure 7.28 A-F: Six geological maps of the Daleti, Ankori, Tulu Kapi and Keley areas with symbols representing Ni, Cu, Cr, Al, Pt and Pd values in soil samples overlaid.

7.8.13. Maps of the elemental distribution in the soils of the Daleti, Ankori, Tulu Kapi and Keley areas

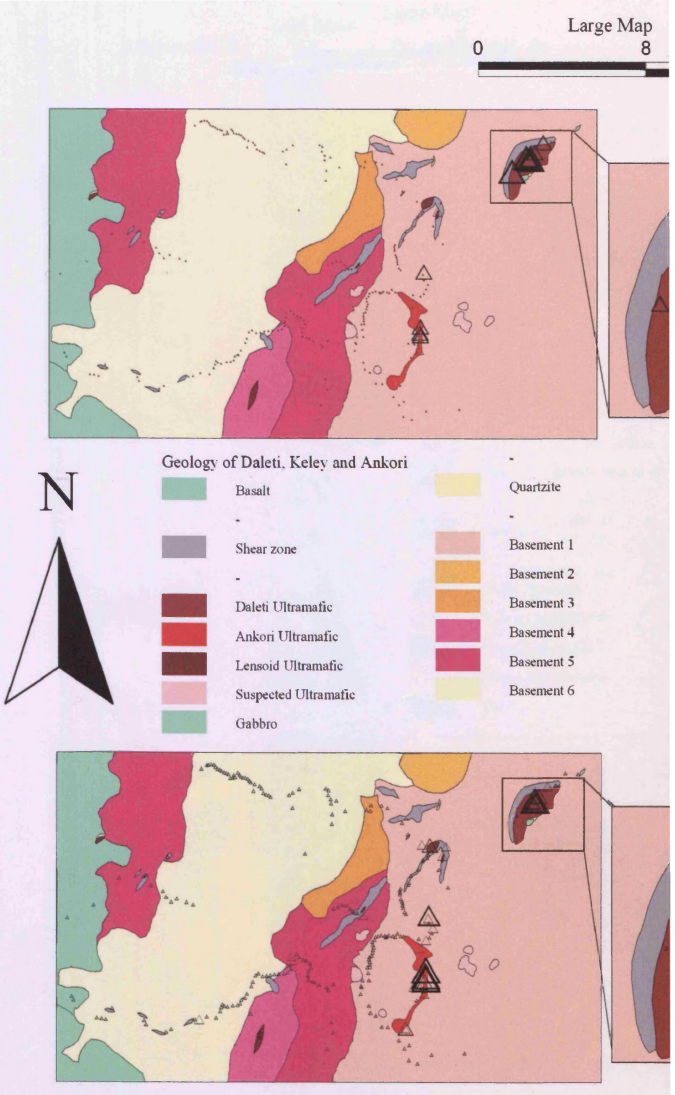

Figure 7.28 A-F: Six geological maps of the Daleti, Ankori, Tulu Kapi and Keley areas with symbols representing Ni, Cu, Cr, Al, Pt and Pd values in soil samples overlaid.

7.9. Yubdo, Andu and Sodu: Selected Major and Trace Elements

7.9.1. Introduction

A total of 227 soil samples were taken along road traverses. The samples were taken at 100 to 300m intervals parallel to roads and away from human influence (see figure 7.29). Large tracts of the Main Yubdo Ultramafic were not sampled under the exploration licence agreement with the ministry of mines.

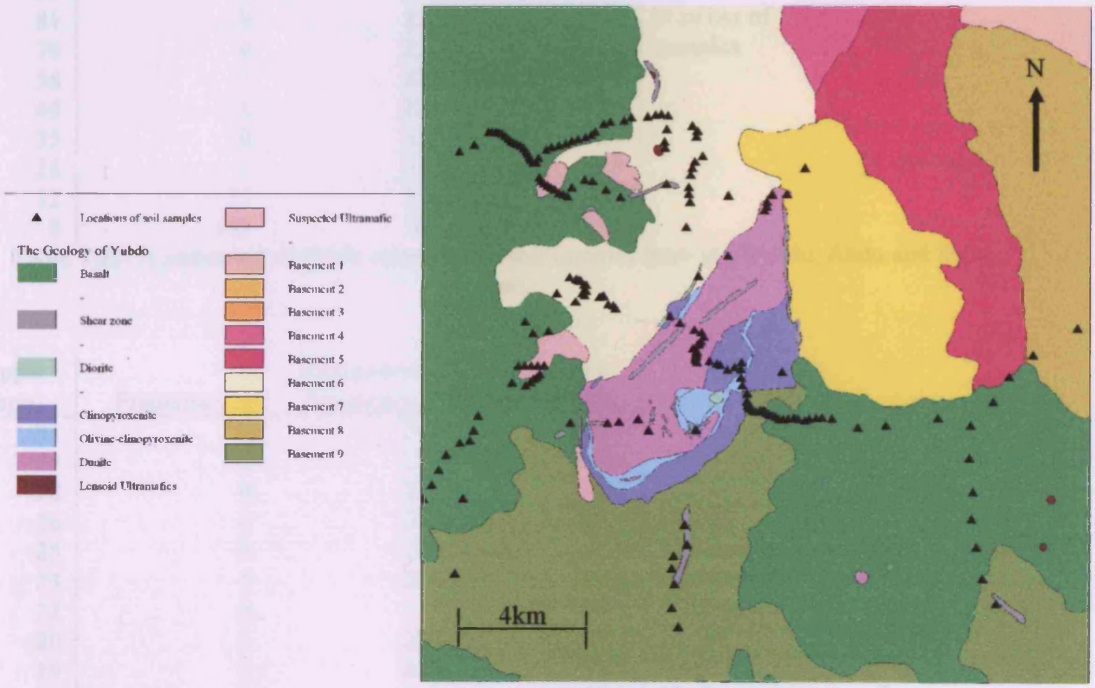

Figure 7.29: The distribution of soil samples in the Yubdo, Andu and Sodu areas.

7.9.2. Summary of Analytical Results

Class Upper Limit (ppb)	Frequency	Cumulative Frequency	Cumulative Frequency (%)		
232	1	227	100.0		
220	0	226	99.6		
209	0	226	99.6	Mean	4.7
197	1	226	99.6	Standard	25.0
186	0	225	99.1	Deviation	
174	0	225	99.1	Minimum	0
162	1	225	99.1	Lower	0
151	0	224	98.7	Quartile	
139	0	224	98.7	Median	0
128	1	224	98.7	Upper	0
116	0	223	98.2	Quartile	
104	1	223	98.2	Maximum	232
93	0	222	97.8	Mode	0
81	0	222	97.8	Number of	227
70	0	222	97.8	samples	
58	1	222	97.8		
46	1	221	97.4		
35	0	220	96.9		
23	3	220	96.9		
12	32	217	95.6		
0	185	185	81.5		

Table 7.22: A summary of the Pt values in the soil samples from the Yubdo, Andu and Sodu areas.

Class Upper Limit (ppb)	Frequency	Cumulative Frequency	Cumulative Frequency (%)		
31	1	227	100.0		
29	0	226	99.6		
28	0	226	99.6		
26	0	226	99.6	Mean	1.2
25	0	226	99.6	Standard	3.7
23	1	226	99.6	Deviation	
22	0	225	99.1	Minimum	0
20	2	225	99.1	Lower	0
19	0	223	98.2	Quartile	
17	1	223	98.2	Median	0
16	1	222	97.8	Upper	0
14	0	221	97.4	Quartile	
12	1	221	97.4	Maximum	31
11	0	220	96.9	Mode	0
9	2	220	96.9	Number of	227
8	2	218	96.0	samples	
6	3	216	95.2		
5	3	213	93.8		
3	39	210	92.5		
2	0	171	75.3		
0	171	171	75.3		

Table 7.23: A summary of the Pd values in the soil samples from the Yubdo, Andu and Sodu areas.

Class Upper Limit (ppb)	Frequency	Cumulative Frequency	Cumulative Frequency (%)		
102	1	227	100.0		
97	0	226	99.6		
92	0	226	99.6	Mean	4.2
87	0	226	99.6	Standard	11.4
82	1	226	99.6	Deviation	
77	0	225	99.1	Minimum	0
71	0	225	99.1	Lower	0
66	2	225	99.1	Quartile	
61	0	223	98.2	Median	2
56	0	223	98.2	Upper	3
51	0	223	98.2	Quartile	
46	0	223	98.2	Maximum	102
41	2	223	98.2	Mode	0
36	2	221	97.4	Number of	227
31	1	219	96.5	samples	
26	0	218	96.0		
20	3	218	96.0		
15	5	215	94.7		
10	15	210	92.5		
5	89	195	85.9		
0	106	106	46.7		

Table 7.24: A summary of the Au values in the soil samples from the Yubdo, Andu and Sodu areas.

Class Upper Limit (ppm)	Frequency	Cumulative Frequency	Cumulative Frequency (%)		
10454	1	227	100.0		
9932	0	226	99.6	Mean	504
9410	0	226	99.6	Standard	1168
8888	0	226	99.6	Deviation	
8366	0	226	99.6	Minimum	14
7844	0	226	99.6	Lower	52
7322	0	226	99.6	Quartile	
6800	0	226	99.6	Median	70
6278	1	226	99.6	Upper	416
5756	1	225	99.1	Quartile	
5234	2	224	98.7	Maximum	10,454
4712	0	222	97.8	Mode	72
4190	1	222	97.8	Number of	227
3668	2	221	97.4	samples	
3146	6	219	96.5		
2624	1	213	93.8		
2102	2	212	93.4		
1580	12	210	92.5		
1058	20	198	87.2		
536	178	178	78.4		
0	0	0	0.0		

Table 7.25: A summary of the Ni values in the soil samples from the Yubdo, Andu and Sodu areas.

Class Upper Limit (ppm)	Frequency	Cumulative Frequency	Cumulative Frequency (%)		
409	2	227	100.0		
389	0	225	99.1		
369	0	225	99.1	Mean	61
349	0	225	99.1	Standard	48
329	0	225	99.1	Deviation	
309	1	225	99.1	Minimum	8
289	0	224	98.7	Lower	40
269	0	224	98.7	Quartile	
249	1	224	98.7	Median	48
229	2	223	98.2	Upper	64
209	0	221	97.4	Quartile	
188	0	221	97.4	Maximum	409
168	2	221	97.4	Mode	40
148	3	219	96.5	Number of	227
128	6	216	95.2	samples	
108	9	210	92.5		
88	21	201	88.5		
68	66	180	79.3		
48	102	114	50.2		
28	12	12	5.3		
0	0	0	0.0		

Table 7.26: A summary of the Cu values in the soil samples from the Yubdo, Andu and Sodu areas.

Class Upper Limit (ppm)	Frequency	Cumulative Frequency	Cumulative Frequency (%)		
6504	1	227	100.0		
6180	0	226	99.6		
5855	0	226	99.6	Mean	649.7
5531	0	226	99.6	Standard	942.1
5206	0	226	99.6	Deviation	
4882	0	226	99.6	Minimum	16
4558	1	226	99.6	Lower	122.5
4233	1	225	99.1	Quartile	
3909	0	224	98.7	Median	187
3584	2	224	98.7	Upper	869
3260	4	222	97.8	Quartile	
2936	2	218	96.0	Maximum	6504
2611	3	216	95.2	Mode	238
2287	12	213	93.8	Number of	227
1962	8	201	88.5	samples	
1638	9	193	85.0		
1314	12	184	81.1		
989	6	172	75.8		
665	12	166	73.1		
340	154	154	67.8		
0	0	0	0.0		

Table 7.27: A summary of the Cr values in the soil samples from the Yubdo, Andu and Sodu areas.

Class Upper Limit (%)	Frequency	Cumulative Frequency	Cumulative Frequency (%)		
8.7	3	227	100.0		
8.3	3	224	98.7		
7.9	4	221	97.4	Mean	5.39
7.5	15	217	95.6	Standard Deviation	1.60
7.1	17	202	89.0		
6.8	35	185	81.5	Minimum	0.9
6.4	18	150	66.1	Lower Quartile	4.2
6.0	28	132	58.1		
5.6	18	104	45.8	Median	5.7
5.2	10	86	37.9	Upper Quartile	6.6
4.8	10	76	33.5		
4.4	14	66	29.1	Maximum	8.7
4.0	8	52	22.9	Mode	6.6
3.6	15	44	19.4	Number of samples	227
3.2	9	29	12.8		
2.9	12	20	8.8		
2.5	5	8	3.5		
2.1	0	3	1.3		
1.7	1	3	1.3		
1.3	2	2	0.9		
0.0	0	0	0.0		

Table 7.28: A summary of the Al values in the soil samples from the Yubdo, Andu and Sodu areas.

The spatial and statistical distribution of each element is considered in turn in the next sections. It is important to remember that it is unlikely that complete digestion has been acheieved during the aqua regia leach of these samples. The maps which accompany the section are included at the rear.

7.9.3. Nickel

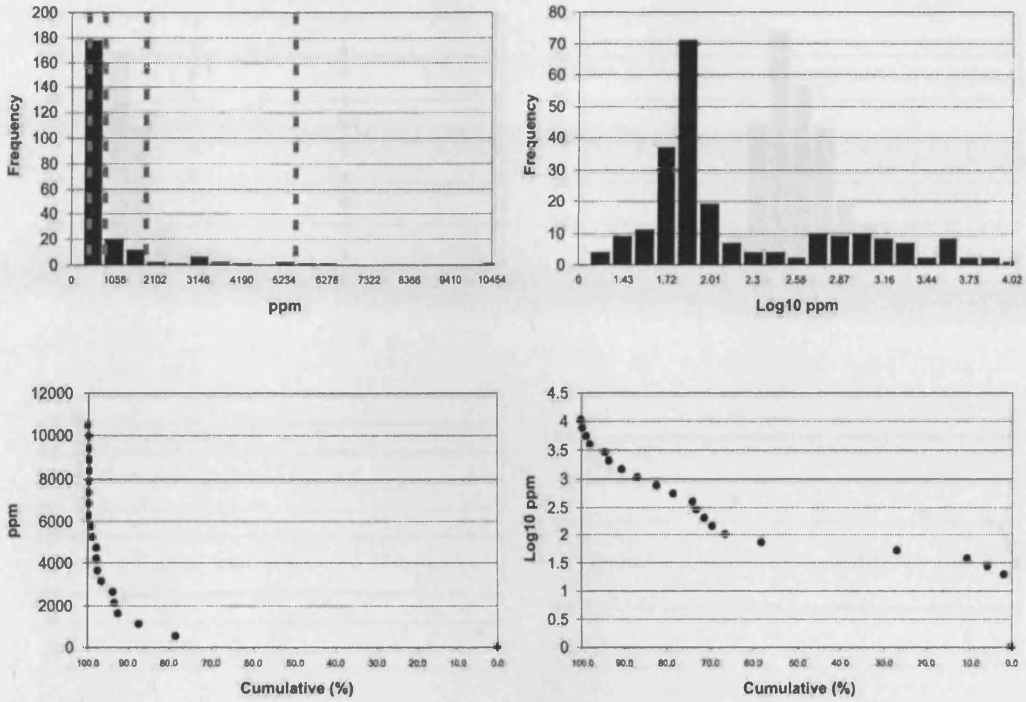

Figure 7.30: Arithmetic and Log_{10} transformed histograms of Ni the soils of the Yubdo, Andu and Sodu areas. The grey lines indicate the class-boundaries used in figure 7.36A.

All Ni concentrations of over 390ppm in soil occur over the Main Yubdo Ultramafic (figure 7.36A). As with the rocks, the highest values of Ni in soil (<10,454ppm) also occur in soils away from the edges of the intrusion, but additionally at the farthest northern tip of the Main Intrusion, close to the contact with the basement. The lowest Ni value in the soils of the Main Yubdo Ultramafic (183ppm) occur above the clinopyroxenite zone close to the northern contact with the basement.

On a logarithmic scale, the Ni values in the Yubdo, Andu and Sodu areas display two populations. One population (<160ppm) shows a distinct log normal distribution with a mode at around 70ppm. The population at higher values does not show a normal distribution (see figure 7.37).

7.9.4. Copper

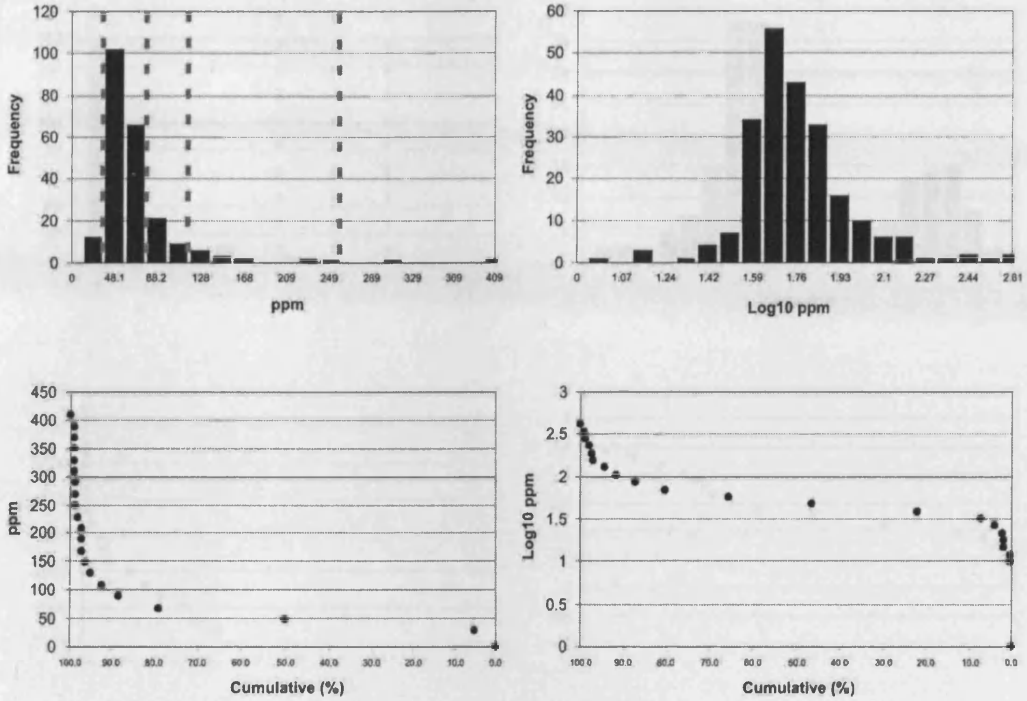

Figure 7.31: Arithmetic and Log_{10} transformed histograms of Cu the soils of the Yubdo, Andu and Sodu areas. The grey lines indicate the class-boundaries used in figure 7.36B.

The highest Cu values in soil occur outside of the Yubdo Main Intrusion. Within the Main Yubdo Ultramafic the soil samples show a slight increase in Cu values - from a minimum of 45ppm to a maximum of 86ppm - towards the eastern flank of the clinopyroxenite zone.

The Cu values in the Yubdo, Andu and Sodu areas show a slightly positively skewed log normal distribution with a mode at 40ppm.

7.9.5. Chromium

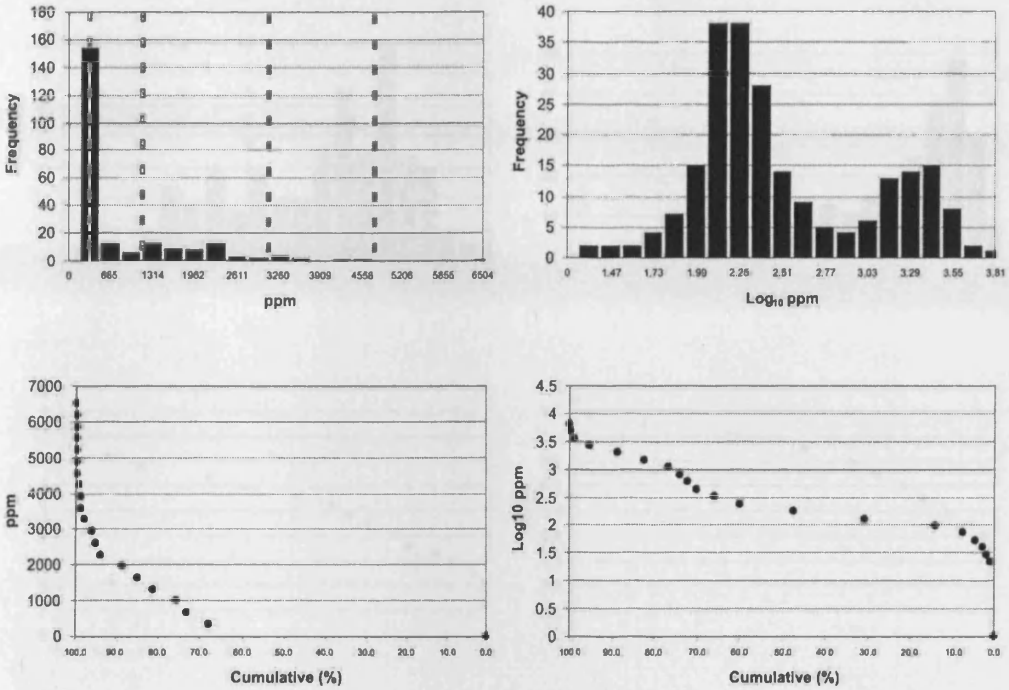

Figure 7.32: Arithmetic and Log_{10} transformed histograms of Cr the soils of the Yubdo, Andu and Sodu areas. The grey lines indicate the class-boundaries used in figure 7.36C.

High Cr contents in soils (>1000ppm) are restricted to the Yubdo Main Intrusion. Within the Yubdo Main Intrusion, elevated Cr levels (<6504ppm) are generally located away from the flanks of the intrusion. As with the altered rock samples, the lowest Cr values (108ppm) are frequently located within 100m of the highest Cr values.

There are two populations of log normal Cr values in the Yubdo, Andu and Sodu areas. These occur with modes at around 125ppm and 2511ppm.

7.9.6. Aluminium

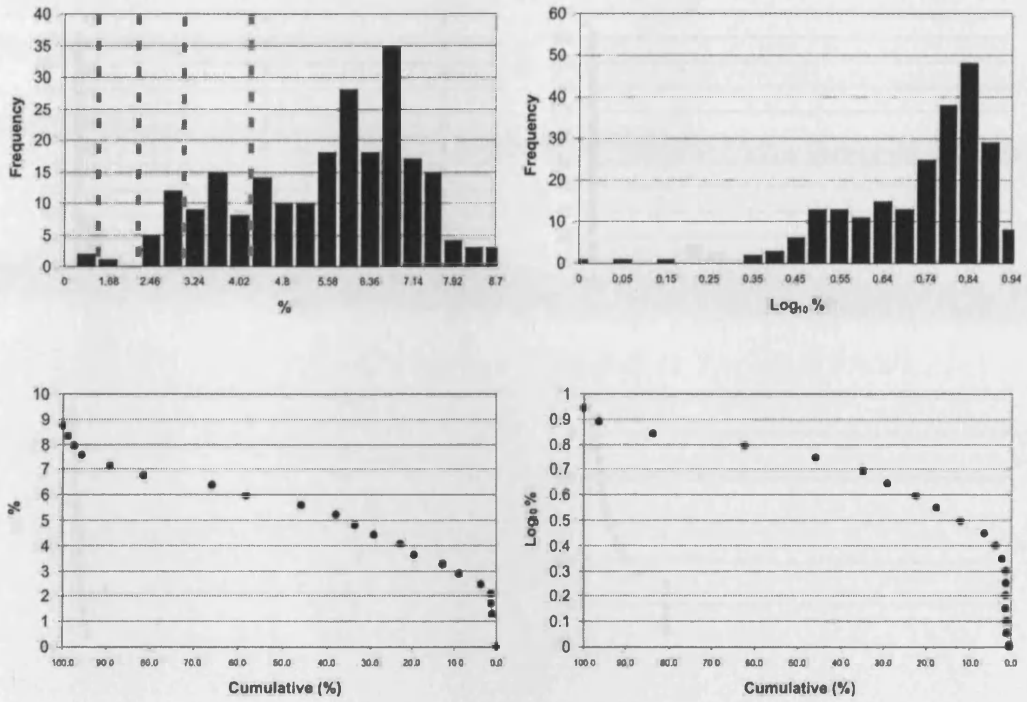

Figure 7.33: Arithmetic and Log_{10} transformed histograms of Al the soils of the Yubdo, Andu and Sodu areas. The grey lines indicate the class-boundaries used in figure 7.36D.

In soil, Al is enriched above 4% in samples covering most of the Yubdo, Andu and Sodu study areas (see figure 7.36D).

The Al distribution in the soils of this study area is erratic but may be a crude negatively skewed arithmetic normal distribution with a mode at around 6.8%.

7.9.7. Summary of Ni, Cu, Cr, Al, Pt and Pd values

The highest Ni values in soil occur over the centre or northern tip of the intrusion but the highest Cr value for the Yubdo area is found in a hard pan over the clinopyroxenite zone on the western flank of the intrusion. Additionally, the highest Cr values are found in soils over much of the intrusion, but not over the basement

Ni, Cu and Cr all show log normal distributions whereas Al shows an approximately normal distribution. Two populations of analyses are observed in Ni and Cr but Cu and Al show unimodal patterns.

7.9.8. Platinum and Palladium

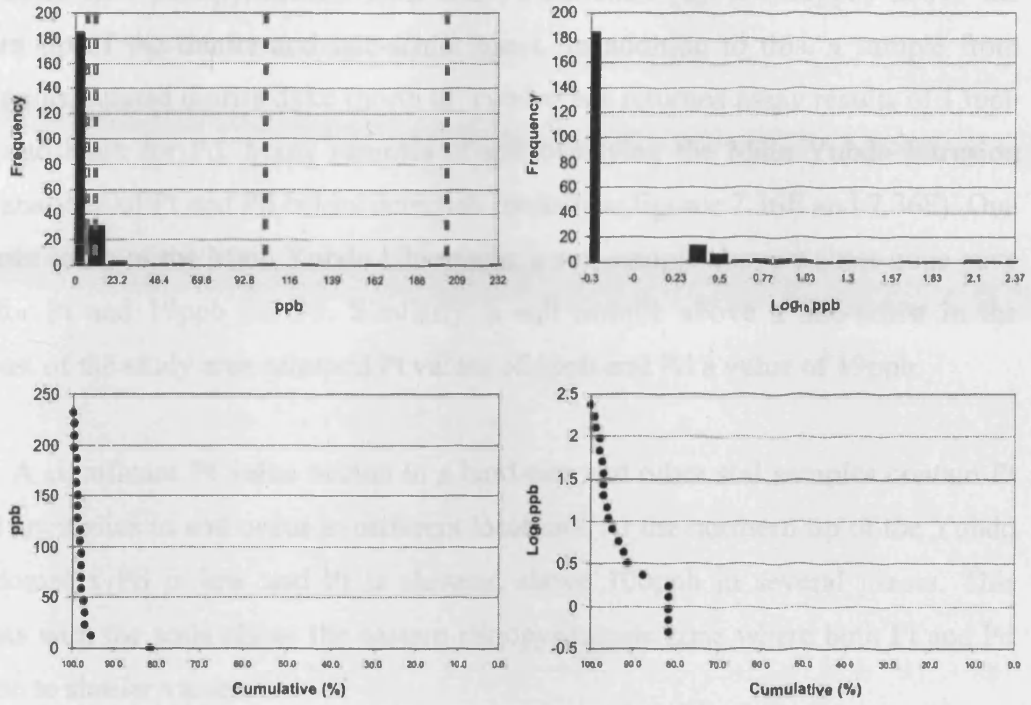

Figure 7.34: Arithmetic and Log_{10} transformed histograms of Pt the soils of the Yubdo, Andu and Sodu areas. The grey lines indicate the class-boundaries used in figure 7.36E.

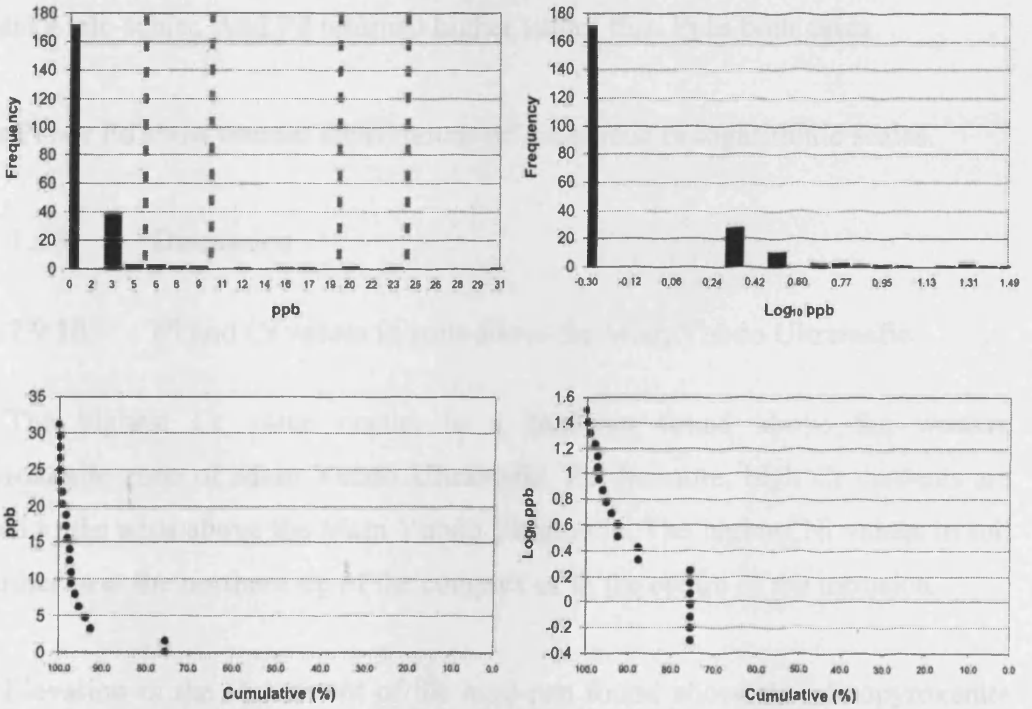

Figure 7.35: Arithmetic and Log_{10} transformed histograms of Ni the soils of the Yubdo, Andu and Sodu areas. The grey lines indicate the class-boundaries used in figure 7.36F.

Within the Main Yubdo Ultramafic, Pd is enriched (up to 31ppb) in soils over the southeastern clinopyroxenite zone and Pt enriched (up to 232ppb) above the northern tip of the dunite and talc-schist zones. In addition to this, a sample from above an associated diorite dyke (north of Yubdo) has returned assay results of 13ppb for Pt and 8ppb for Pd. Many samples of soil overlying the Main Yubdo Intrusion return analyses of Pt and Pd below detection limits (see figures 7.36E and 7.36F). One kilometre south of the Main Yubdo Ultramafic, a soil sample above a shear zone gave 5ppb for Pt and 19ppb for Pd. Similarly, a soil sample above a talc-schist in the southeast of the study area returned Pt values of 5ppb and Pd a value of 19ppb.

A significant Pt value occurs in a hard-pan and other soil samples contain Pt and Pd anomalies in soil occur in different locations. At the northern tip of the Yubdo main complex Pd is low and Pt is elevated above 100ppb in several places. This contrasts with the soils above the eastern clinopyroxenite zone where both Pt and Pd both rise to similar values.

Additionally, the soils in the southeast of the study area are enriched in Pd and Pt around a talc-schist. And Pd returned higher values than Pt in both cases

Neither Pt nor Pd show normal distributions on arithmetic or logarithmic scales.

7.9.9. Discussion

7.9.10. Ni and Cr values in soils above the Main Yubdo Ultramafic

The highest Cr value occurs in a hard-pan found above the western clinopyroxenite zone of Main Yubdo Ultramafic. Furthermore, high Cr contents are restricted to the soils above the Main Yubdo Ultramafic. The highest Ni values in soil occur either over the northern tip of the complex or in the centre of the intrusion.

Elevation in the Cr content of the hard-pan found above the clinopyroxenite zone from the Main Yubdo Ultramafic supports the evidence for high Cr-spinel concentration at the flanks of the intrusion. The high value could be attributed to the extreme volume change from rock to soil and further during the compaction into a

hard-pan lithotype. The presence of Cr in the soils overlying the flanks of the intrusion together with the known resistance of spinels to weathering indicates that the most primitive rocks occur at the flanks of the intrusion. However, surprisingly high Cr values occur in soils at the centre of the intrusion. The concentration of Cr in these samples may possibly be accounted for by a higher degree of concentration due to deeper weathering over the top of the Yubdo hill. Similarly, the variations in Ni content in the soils over the Yubdo Main Intrusion may be understood in terms of the relative degrees of weathering.

7.9.11. Genesis of Pt and Pd in soils

A hard pan of the western flank of the intrusion contains the highest Pt value in this study of the WES at 143ppb and a corresponding Pd value of 3ppb. Furthermore, the maximum Pt value in the soils collected here is over 100ppb higher than that seen in rock. Additionally, it is observed here that in the soils above the Main Yubdo Ultramafic that Pt is only enriched in soils above the northern tip and Pd is only enriched over the eastern clinopyroxenite zone.

As described in section 7.5.2 the increase in Pt grade between the rocks and soils from the Main Yubdo Ultramafic could be explained either by the element being immobile within the soil, or alternatively the element might have been reconcentrated into the soils. The hard-pan sample perhaps represents an extreme case of volume loss from rock to soil as it shows an increased Pt value from the equivalent rocks nearby (see figure 8.13E). This sample may also be the product of a longer time-period of the action of aqueous fluids in laterites. Furthermore, the hardpan may also have been cemented by circulating Si-rich fluids which could have redeposited the Pt. The difference in locations of Pt and Pd highs indicates that Pd has become immobile in the soils over the eastern clinopyroxenite zone. This may possibly be due to Pd being complexed with a different organic compound to Pt. The data presented here cannot be used to determine the aqueous conditions of these laterites and therefore we cannot determine the solution to this anomalous distribution.

7.9.12. Conclusions

Although high Ni and Cr values only occur in the soils over the Main Yubdo Ultramafic, high Cu values are only found in the basement and high Al values are found throughout the area. This indicates a relationship between the underlying lithotype and the the geochemistry of the soils. However, it is likely that both Ni and Cr will have become concentrated partially by volume loss from rock to soil.

Similarly, the immobile nature of Pt is likely to have increased the content in soils when compared to rock samples. The difference in location of the highest Pt and Pd concentrations is distinct in the soils of the Main Yubdo Intrusion, and from this study it is not possible to determine the mechanism which causes this feature.

7.9.13. Maps of the elemental distribution in the soils of the Yubdo, Andu and Sodu areas

Figure 7.36: Six geological maps of the Yubdo, Andu and Sodu areas with symbols representing Ni, Cu, Cr, Al, Pt and Pd values in soil samples overlaid.

7.10. Discussion of the distribution of Ni, Cu, Cr, Al, Pt and Pd in the soils of the WES

Some notable differences in the distribution of the elements in question can be seen between the four areas studied, as described with the following figures. For ease of comparison between the four areas studied, graphs using cumulative % are used. Histograms showing the same data can be found in the respective sections earlier in this chapter.

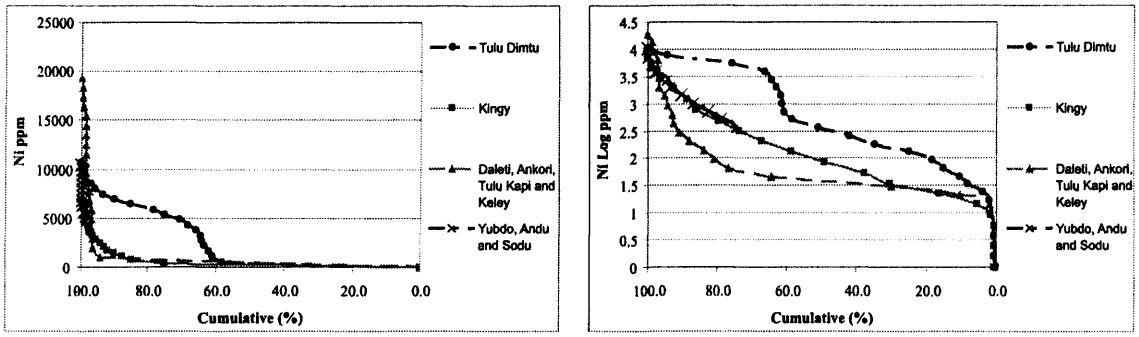

Figure 7.37: A graph comparing the distribution of Ni in each of the four areas studied. For histograms further illustrating the data see individual sections.

There are several differences in the distribution of Ni in the four areas studied in this chapter. Tulu Dimtu is the only area where an arithmetic normal distribution occurs however there is an additional population which is log normal. In the remaining three areas, all Ni disitributions are log normal. The only unimodal distribution occurs in the area containing the Daleti, Ankori, Tulu Kapi and Keley complexes.

Such distributions are difficult to understand in terms of the number of ultramafic complexes within the area, given that the only area with one population is the area with four discrete complexes (Daleti, Ankori, Tulu Kapi and Keley). It is possible that one population in each area could be created by hydromorphic dispersion in additional to the original population which reflects the bedrock values.

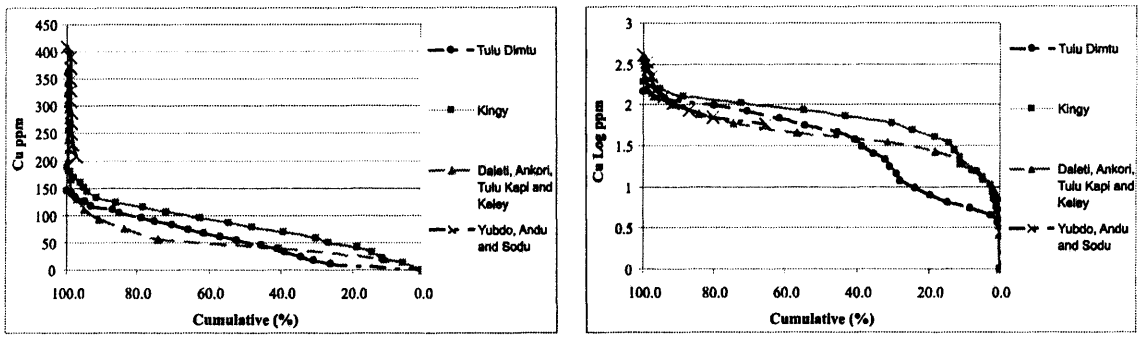

Figure 7.38: A graph comparing the distribution of Cu in each of the four areas studied. For histograms further illustrating the data see individual sections.

The Cu distribution in each area of the WES is log normal, however the distributution of the Tulu Dimtu area has two modes (see figure 7.7).

As discussed in section 7.6.4, it is possible that the Cu distribution in the Tulu Dimtu area may be influenced partially by the underlying bedrock and partially by hydromorphic dispersion. In a situation where the Cu was remobilized by groundwater, a lower value population could occur due to dilution. These lower values (<25ppm) would represent the remobilized values, and the higher population would be related to the original composition of the protolith.

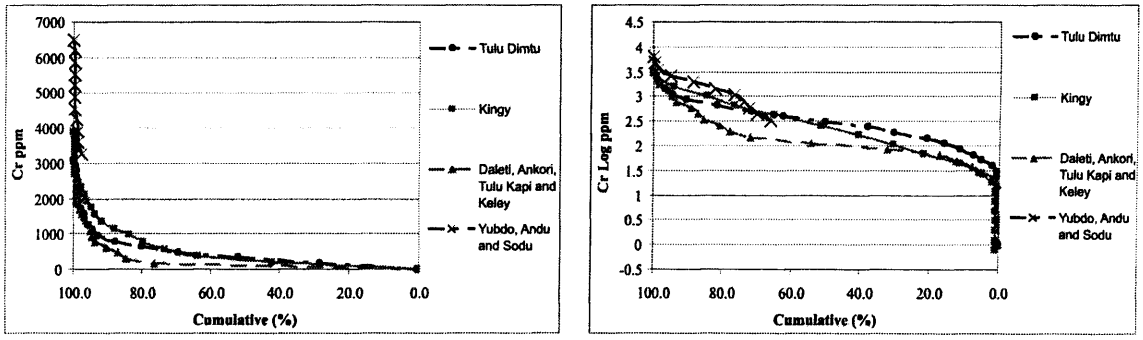

Figure 7.39: A graph comparing the distribution of Cr in each of the four areas studied. For histograms further illustrating the data see individual sections.

All Cr populations in the WES are log normal and unimodal, except the Yubdo area where two populations occur (see figure 7.32).

Unlike Ni and Cu, this additional population is difficult to explain in terms of hydromorphic dispersion as Cr typically remains intact within Cr-spinels (see chapter 3). It is possible that such an observation could be the result of two magmatic phases

of Cr-spinel precipitation. Such an interpretation would need to be supported by petrological investigation.

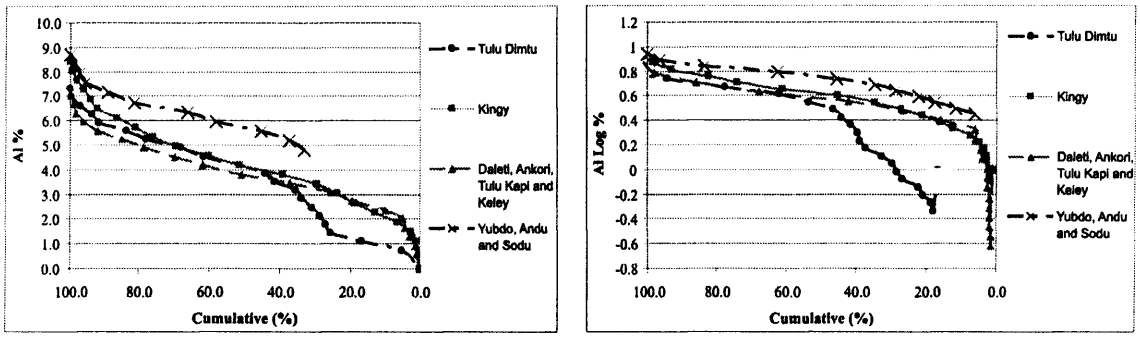

Figure 7.40: A graph comparing the distribution of Al in each of the four areas studied. For histograms further illustrating the data see individual sections.

Unlike Ni, Cu and Cr the Al values in the soils of the WES are the only ones which are normally distributed. However, in the Tulu Dimtu area, the distribution is sufficiently erratic that it cannot be regarded as being normally distributed.

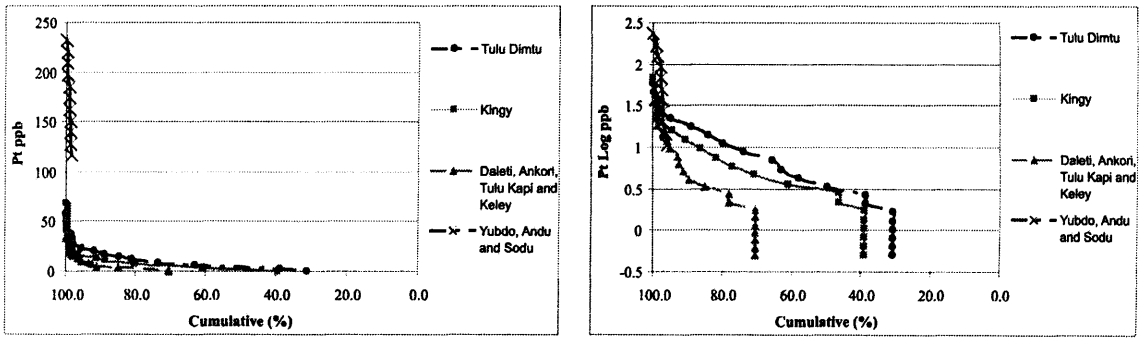

Figure 7.41: A graph comparing the distribution of Pt in each of the four areas studied. For histograms further illustrating the data see individual sections.

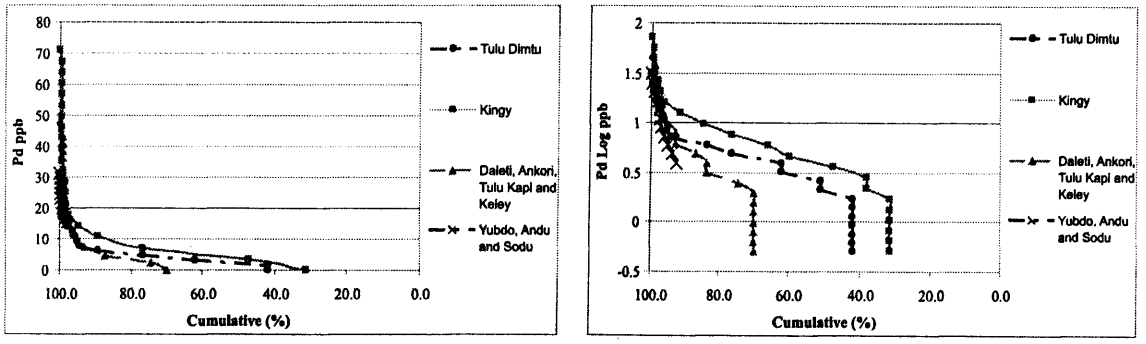

Figure 7.42: A graph comparing the distribution of Pd in each of the four areas studied. For histograms further illustrating the data see individual sections.

The distribution of both Pt and Pd in the WES is generally erratic. However, in all areas but Yubdo, this erratic nature is tends slightly towards a log normal distribution.

The erratic nature of of Pt and Pd distributions is well known given their tendency to form nuggets. However the slightly log normal patterns observed suggest that there is a more statistically uniform mechanism operating. This mechanism may be the underlying magmatic dissolution process, however given the severe degree of the alteration and weathering it is unlikely. However, the log normal patterns may reflect the dissolution of the elements the fluids within the laterite (see section 7.5.2).

7.11. Summary of the Soil development in the WES

7.11.1. Ni, Cu, Cr and Al

Distinct changes in the proportions of Ni and Cu are seen in the soils over the different lithologies of the WES. Ni is typically higher over the ultramafic units than the basement, whereas Cu tends to show higher values over the basement units, in particular the shear-zone related lithologies. Although such trends indicate a relationship between Ni and Cu distribution with lithotype, univariate statistical methods show that at Tulu Dimtu a second population exists. Such lower value populations may be the result of the hydromorphic dispersion of Ni and Cu. Although Al shows no particular relationship with the underlying lithotype, Cr is present in the highest values in soils over ultramafic units. Given the resistance of Cr-spinels to alteration and weathering (chapter 3) it is unlikely that it has undergone remobilization within the soil.

These geochemical differences are important to this study as in some places they are considered to validate the mapping technique. Large scale changes in the value of Ni (at values >1000ppm) and Cu (at values >25ppm) are likely to have been controlled by the underlying lithotype. However Ni and Cu values below those stated are likely to have been influenced strongly by hydromorphic dispersion. For example clear changes in Ni and Cu value can be seen at the contact between the Tulu Dimtu Main Intrusion and the basement (see figures 7.12A and 7.12B). This contact was

mapped using a change in vegetation seen from aerial photography (chapter 4). However, additional populations can be seen in figures 7.6 and 7.7 which are likely to have been the result of hydromorphic dispersion.

7.11.2. Pt and Pd

Area	Formation	Soil samples	
		Pt (ppb)	Pd (ppb)
Yubdo	Main Yubdo Ultramafic	232	31
Tulu Dimtu	Tulu Dimtu Main Intrusion	58	31
Daleti	Ankori	34	48
Kingy	Kingy Ridge Ultramafic	29	29
Daleti	Daleti Ultramafic	< 2	< 2
Daleti	Keley	< 2	< 2

Table 7.29: The maximum Pt and Pd values found in the soils above the ultramafic complexes of the WES.

A full understanding of the mechanisms controlling the development of Pt and Pd in the soils above the ultramafic bodies in the WES is difficult. However, this chapter gives an account of the salient features of the distribution and proposes some mechanisms which may have caused them

The distribution of the elements is nuggety, but some evidence is present for remobilization within the laterites. Figures 7.41 and 7.42 show an erratic distribution of values which may have formed through the presence of nuggets. However there is a division in the distribution of Pt and Pd in the soils above the Kingy area (figures 7.20E and 7.20F). The soils above the basement in the northwest havce greater amounts of Pd and the soils above the Kingy Ridge Ultramafic contain much more Pt. There is a similar division between Pt and Pd in the soils above the Yubdo Main Intrusion. These differences in distribution could possibly be explained by a difference in lateritic conditions as a result of the different basement lithotype. However, it is not possible to determine these conditions in this study. An alternative hypothesis is that Pd has become immobile instead of Pt in certain areas perhaps by being complexed with a different type of vegetation (see chapter 4).

8. Rock Geochemical Data

8.1. Introduction

Samples of rocks were collected from the 4 complexes: Tulu Dimtu, Kingy, Daleti and Yubdo. With the aim of assessing the prospectivity of each of the ultramafic complexes, these samples were analysed for major and trace elements including Pt, Pd and Au by the OMAC laboratories as part of an exploration program for Golden Prospect Mining Co Ltd (GPM). In order to identify targets for detailed exploration, this chapter examines this dataset describing the distribution of key elements that characterise: each rock type, fresher and altered rocks, pathfinders for PGE and the Pt and Pd distribution itself.

The dataset used in this chapter is the result of samples collected during the 2001-2002 field season by the author and several GPM geologists. The grids and traverses used are typical of those used in geological exploration, where geochemical anomalies are sought. Samples were collected in order to both characterise known ultramafics and also to discover unknown deposits.

These complexes are examined using two types of sample: fresher rocks which are used to interpret magmatic ore formation processes and altered rocks, which display magmatic features that have been overprinted by the effects of alteration.

The elements analysed include Au, Pd, Pt, Ag, Al, As, B, Ba, Be, Bi, Ca, Cd, Ce, Co, Cr, Cu, Fe, Ga, Ge, Hg, In, K, La, Li, Mg, Mn, Mo, Na, Nb, Ni, P, Pb, Rb, S, Sb, Sc, Se, Sn, Sr, Ta, Te, Th, Ti, Tl, U, V, W, Y, Zn and Zr. This chapter focuses on Ni, Cu, Cr, Al, Pt and Pd. Each of these elements - except Al - are chosen as they characterize, and are affected by, the processes which concentrate Pt and Pd. Pt and Pd are considered to be concentrated in magmas with sulphur as immiscible sulphide liquids in a silicate magma (Naldrett et al., 1979). After sulphide segregation of a magma, Pt and Pd crystallise with Ni- and Cu-rich sulphides in ultramafic or mafic complexes (Barnes et al., 1997). Sulphur

saturation in a magma is often associated with chromite crystallisation as removal of Fe and Cr from a magma will cause sulphides to segregate (Naldrett and von Gruenewaldt, 1989). Alaskan-type complexes such as those studied here, are traditionally S-poor (Nixon et al., 1997). Ophiolite complexes such as the Shetland ophiolite complex do contain small percentages (1-2%) of sulphides which are Pt and Pd enriched in the ultramafic parts of the complex (Prichard et al., 1996). Thus if base-metal sulphides are Pt and Pd collectors in these complexes in the WES then Ni, Cu and Cr should be path-finders for Pt and Pd. Hence their distribution is studied here to attempt to understand their inter-relationships during magmatic and secondary alteration processes.

The Al content of a magma should increase with fractionation, therefore if PGE content is controlled by the evolution of a magma then Al should correlate with Pt and Pd. Furthermore, the surrounding basement rocks should have a greater proportion of alumino-silicate minerals and therefore Al will help to validate the mapping technique.

Graphs of base metals and other elements against Pt and Pd show no clear trends or correlations and it was therefore decided that a different method of interpretation was required. The results were compiled to produce element concentrations on maps showing the geology. The geological sketch maps were produced using a combination of published maps (at Yubdo) and field observations made in this study (chapters 4 and 5). The GIS application ArcView 3.2 was used display these maps.

This chapter is divided into four sections covering each of the four geographic areas. At the end of each section there is a "pull-out" page which contain the maps which are referred to throughout the chapter.

8.2. Analytical Techniques

8.2.1. Introduction

A total of 481 rock samples were analysed by OMAC Laboratories (Co Galway, Ireland) by two different procedures: one for Pt, Pd, Au and another for 47 additional

elements. After crushing, each sample was ground to 100μm, split to 30g and then prepared and analysed by the two different methods. For Pt and Pd analyses, the powders were analysed using a 30g Pb fire assay with an inductively coupled plasma analysis, resulting in detection limits of 2ppb for both Pt and Pd. For other elements, the samples were subjected to an Aqua Regia digestion with Inductively Coupled Plasma – Optical Emission Spectroscopy finish.

The next sections describe the methods and validation for each stage for each of of each analytical process.

8.2.2. Pb Fire Assay

	Au (ppb)	Pd (ppb)	Pt (ppb)
min	212	1381	3624
max	986.00	1636.88	3883.36
range	774.00	255.53	259.37
Recomended Value Standard SARM-7b	310	1530	3740
Precision (range as % of recomended value)	249.68	16.70	6.94

Table 8.1: Summary statistics of 41 analyses of the standard sample SARM7b.

The standard sample SARM 7b was analysed for Pt, Pd and Au a total of 41 times through 9 batches of samples processed by OMAC laboratories. The full listing of results is included in table 12.3 in section 12.2 and a summary of the ranges of values obtained is included in table 8.1. For all three elements the range encompassed the recommended value for the standard, which can be regarded as a reasonable accuracy. Given the relative inhomogeneity of Pt, and Pd standards, both Pt and Pd varied only slightly from the recommended values (16.7% and 7.0%) in each case. The variation in measured Au values was significantly larger (see table 8.1). This indicates an acceptable degree of accuracy and precision for both Pt and Pd and a slightly lesser degree for Au analyses.

The analysis of blank samples returned values which were at or below detection limits in each case.

In order to assess the accuracy of the Pb fire assay method performed at the OMAC laboratories, four samples were analysed at a different laboratory (Genalysis). Table 12.1 (section 12.1) shows that the biggest difference in Pt values between the two laboratories was 64.7% which corresponds to a difference of 36ppb versus 102ppb. The biggest difference between the analyses of Pd was 5ppb versus below detection limts and other results are comparable. The accuracy of the analyses performed at the OMAC laboratories have been accepted for this investigation.

To test the precision of the analyses, repeat analyses were also carried by the OMAC laboratories. Within each batch, repeats were performed in every sample which produced anomalous results. If no significantly anomalous results are produced from a batch then every 10^{th} sample was repeated. In some batches, repeats were carried out at a greater frequency, in order to assure confidence in the procedure. In a some cases, two repeat analyses were performed on the same sample, this was done in situations where either the first repeat showed an unacceptable variance or where particularly unusual results were obtained at first.

Repeat analyses were performed for 48 rock samples from the WES, for three samples two repeat analyses were performed (see table 12.2 in section 12.1). For all three precious metals, there was no measurable variation in the results between each repeat for slightly less than half the samples. High repeatability was only present in analyses of low values (<5ppb). The least precise analysis is of Au, where the greatest variation between repeats is between 22ppb and below detection limits. For Pd the highest variation is between 2ppb and 33ppb (93.9% difference). The greatest degree of precision is found for Pt where the highest variance is between 7ppb and 16ppb (56.3%). Although poor repeatability occurs in some individual samples, there is an acceptable variation between analyses in most cases. It is therefore considered that this dataset is sufficiently accurate for this investigation; however, a degree of natural variation is to be expected due to nugget effect.

8.2.3. Aqua Regia Digestion

Aqua regia constitutes a 3:1 ratio of $HCl:HNO_3$. The effectiveness of this technique is due to the complexing power of the chloride ion acting in the presence of Cl_2 and NOCl as catalysts. An aqua regia leach is frequently used in exploration applications to selectively dissolve certain minerals of interest to the geologist (Snäll and Liljefors, 2000; Chao, 1984). When a sample is subjected to an aqua regia leach some minerals are taken into solution and other, more resistant minerals, remain undissolved. When interpreting the results of a partial leach, it is nessecary to consider which minerals have been taken into solution. Furthermore, when a mineral is dissolved, some elements are taken into solution easier than others (Church et al., 1987).

Mineral	Minerals dissolved (wt %) lower limit	upper limit
olivine	70	80
pyroxenes	30	40
amphiboles	20	40
quartz	10	10
plagioclaise	10	60
spinel	10	100
disulphides	50	100
monosulphides	40	100
bisulphides	40	100
arsenides	80	80

Table 8.2: The weight percent of minerals dissolved by aqua regia (Chruch et al., 1987).

Mineral	Metal	Leachability (%)
Olivine	Cr	60
	Cu	35
	Ni	98
	Al	30
	Mg	99
Spinel	Cr	2
	Cu	70
	Ni	75
	Al	20
	Mg	60

Table 8.3: Percentages of various metals leached by aqua regia from olivine and spinel relative to total recovery calculated from an HF-HNO3-NClO4 digestion (Chruch et al., 1987).

Although a quantitative dataset of the leachability of all minerals and metals by aqua regia is not available, a study of the leachability of some minerals was performed by Church et al. (1987). The most reliably dissolved minerals were sulphides, where complete digestion was possible. Additionally, table 8.2 shows that 70 to 80 wt% of the olivine minerals were dissolved. Furthermore, Church et al. (1987) (see table 8.3) showed that of the minerals tested almost all Mg and Ni could be extracted from olivine. Similarly, a large amount of Ni and Cu could leached from spinel minerals almost no Cr could be extracted.

The study by Church et al. (2000) showed that an Aqua Regia leach will attack the secondary minerals as well as the sulphides. Mafic chain silicates and the phyllosilicates (such as the serpentine minerals) are attacked and leached. With such silicates the study concluded that the method will leach many of elements attached to octahedrally coordinated lattice sites (including Mg and in some cases Al). However it will not attack the tetrahedrally coordinated sites, occupied by ions such as Si and Al (Klein and Hurlbut, 1993). Further to the studies performed by Church et al. (2000), information provided by the OMAC laboratories states that the dissolution is partial for a number of elements including Al and Cr.

8.2.4. Inductively Coupled Plasma – Optical Emmission Spectroscopy

	Mg (%)	Ni (ppm)	Cu (ppm)	Cr (ppm)	Al (%)
Min	2.80	657.83	2556.53	112.38	0.99
Max	3.01	685.98	2707.82	132.05	1.60
Range	0.21	28.15	151.29	19.67	0.62
Assigned Value	2.90	683	2650	N/A	N/A
Precision (variation as % of assigned value)	7.26	4.12	5.71	N/A	N/A

Table 8.4: A table of 48 analyses of the OMAC laboratories in-house standard with a summary of the ranges of values obtained and a measurement of precision.

An in house standard was used by the OMAC laboratories to assess accuracy and precision during elemental analysis using aqua regia, ICP-OES. A total of 48 analyses were performed throught the 9 batches processed at the laboratory. The full dataset is

included in section 12.2 (table 12.4) and a summary of the range of values is included in table 8.4. The elements Mg, Ni and Cu show a variation of around 7.26, 4.12 and 5.71% respectively. Although no assigned values are available for the analysis of Cr and Al, it is possible to see that the precision for these elements is significantly poorer. These results are as expected given that Ni and Cu will be easily leached by aqua regia and Mg can be leached from its silicate octahedral lattice sites (see section 8.2.3).

All blanks analysed showed results which were at or below detection limits.

8.3. Methods

8.3.1. Definition of a fresher sample

The rock samples from the WES lie along a spectrum of alteration from "nearly-soil" to completely fresh (see chapter 3), therefore for comparison it was necessary to divide them on that basis. This was done principally by a combination of methods including the identification of weathering and alteration minerals in hand specimen and using transmitted light microscopy.

However, the samples analysed petrologically were one half of the same sample sent for analysis. Therefore, it was necessary to make a geochemical determination of the degree of weathering and alteration on the half of the sample which was sent for analysis. As this analysis could be compared with the half analysed petrologically. This geochemical analysis was intended to support the petrological determination which is the main method for determining the degree of alteration.

The geochemical assesement of alteration was performed using the Mg value. Although Church et al. (1987) suggest that Mg ions can be leached from olivine minerals (see section 8.2.3) in practice it is known that often silicate minerals are not dissolved. As no data is available on the degree of dissolution in the samples from the WES it must be considered that the Mg values in this dataset could originate from either olivine or serpentine. Hence this method is intended simply to support petrological determination.

Ultramafic rocks are characteristically Mg-rich. Dunites and pyroxenites have a range of Mg values which are shown in table 8.6. The ranges of Mg-values for fresher ultramafic rocks can be calculated using published Mg values of fresher olivine and clinopyroxene combined with the mineral proportions of dunite, olivine-clinopyroxenite and pyroxenite as set out by Streckeisen (1976). Examples of Mg values for fresher ultramafic minerals are shown by the analyses shown in table 8.5.

Mineral	Min MgO (%)	Max MgO (%)	Min Mg (%)	Max Mg (%)	Number of samples	Reference
olivine	47.46	47.58	28.6	28.7	2	Révillon (2000)
olivine	46.46	46.46	28.0	28.0	1	Morishita (2001)
olivine	35.97	45.68	21.7	27.5	10	Neumann(2000)
olivine	38.24	44.13	23.1	26.6	12	Mattioli (2003)
olivine	30.4	41.8	18.3	25.2	2	Fodor (2001)
olivine	34.44	39.18	20.8	23.6	2	Upton (2000)
olivine	37.26	38.03	22.5	22.9	3	Renzulli (2001)
olivine	37.47	37.47	22.6	22.6	1	Leonard (2002)
olivine	36.58	37.1	22.1	22.4	2	Müller (2001)
olivine	33.41	36.49	20.1	22.0	6	Gibson (2000)
clinopyroxene	14.42	27.84	8.7	16.8	6	Spandler (2003)
clinopyroxene	14.6	17.6	8.8	10.6	4	Cole (2001)
clinopyroxene	9.27	16.96	5.6	10.2	25	Neumann (2000)
clinopyroxene	16.02	16.02	9.7	9.7	1	Leonard (2002)
clinopyroxene	15.71	15.86	9.5	9.6	2	Morishita (2001)
clinopyroxene	14.28	15.72	8.6	9.5	9	Mattioli (2003)
clinopyroxene	13.4	15.7	8.1	9.5	7	Fodor (2001)
clinopyroxene	14.54	15.53	8.8	9.4	2	Müller (2001)
clinopyroxene	13.1	13.86	7.9	8.4	2	Turner (2003)

Table 8.5: Typical values of Mg for selected fresher ultramafic lithotypes. This data was compiled using the GEOROC database (2005).

The minimum and maximum Mg values for olivine and clinopyroxene were determined from table 8.5 and combined with the proportions of minerals for each lithotype according to Streckeisen (1976). As such, the likely maximum and minimum Mg values for ideal ultramafic rocks can be calculated, as shown in table 8.6.

Rock	Min or Max	olivine value	clinopyroxene value	olivine proportion	clinopyroxene proportion	boundary
Dunite	MIN	20.1	7.9	90%	10%	18.88
Dunite	MAX	28.7	16.8	100%	0%	28.7
Olivine - Clinopyroxenite	MIN	20.1	7.9	60%	40%	15.22

Olivine - Clinopyroxenite	MAX	28.7	16.8	10%	90%	17.99
Clinopyroxenite	MIN	20.1	7.9	10%	90%	9.12
Clinopyroxenite	MAX	28.7	16.8	0%	100%	16.8

Table 8.6: The ranges of Mg values used to define the fresher rock samples. The proportions of olivine and clinopyroxene are defined by Streckeisen (1976). These values represent the range of Mg values which are likely to occur in a hypothetical fresher dunite, olivine-clinopyroxenite or clinopyroxenite.

This method of selection of fresher samples is validated by virtue of a break seen in the unclassified samples at around the boundaries calculated (see table 8.7). This break is seen in all four areas. For example, the analyses of the dunite samples from the Tulu Dimtu area show a range of Mg values from 24.8% to 1.1%. In table 8.7 these are ordered with the highest Mg values at the top and the break can be seen below 18.8% where the next value is 17.0%. This is a difference of 1.8%; the differences further up the table are all lower than 1%. A break at approximately the same level is seen in all four geographic areas (particularly at Daleti, see 8.15.2) and also with pyroxenite samples, however the lower numbers of these lithologies mean that this arguement is illustrated more effectively with dunite samples.

Sample	Mg (%)	Al (%)	Cr (ppm)	Cu (ppm)	Ni (ppm)	Petrological description
DTR-035-02	25.8	0.0	16	3	2327	Figure 3.1
TD12	24.8	0.0	102	16	1456	
ATR-051-02	24.4	0.0	19	4	3380	
DTR-005-02	23.6	0.0	40	3	2691	
TDR 20/01	23.2	0.0	97	0	2617	
DTR-009-02	22.8	0.0	13	2	2945	
ATR-053-02	22.8	0.1	131	6	2037	
ATR-057-02	22.7	0.0	55	3	2574	
KTR-035-02	22.4	0.1	61	9	2182	
DTR-026-02	22.4	0.2	72	5	2340	
DTR-001-02	22.3	0.1	18	5	2942	
TDR 12/01	22.1	0.0	46	0	2856	
TDR 24/01	22.0	0.0	42	0	2312	
TD11	22.0	0.1	366	2	1846	
DTR-007-02	22.0	0.4	33	3	2091	Figure 3.2
DTR-004-02	21.9	0.1	61	4	2686	
TD3	21.8	0.0	70	0	3575	
TD10	21.5	0.1	634	4	1909	
TDR 08/01	21.0	1.0	25	0	4543	
TDR 07/01	21.0	0.0	76	0	5860	
ATR-044-02	20.6	0.1	304	4	3880	
TDR 05/01	20.5	0.1	651	0	2155	
TTR-018A-02	20.4	0.1	119	3	2824	Figure 3.3
KTR-002B-02	20.4	0.1	379	3	3285	

TD14	20.3	0.0	64	0	3062	
TD4	19.9	0.1	292	0	1802	
TDR 19/01	19.5	0.1	436	16	2872	
ATR-056-02	19.5	0.1	196	4	2154	
DTR-034-02	19.4	0.0	27	0	3469	
TD9	18.8	0.5	2728	8	2992	
			NATURAL BREAK			
TDR 06/01	17.0	0.0	187	0	7695	
TDR 11/01	16.4	0.1	223	2	2894	Figure 3.4
TDR 22/01	16.1	0.0	91	3	1962	
TDR 09/01	16.0	0.3	383	0	2129	
DTR-050-0	9.4	0.1	139	2	2190	
TDR 25/01	7.0	0.1	48	0	586	Figure 3.5
TD17	4.6	3.7	705	22	527	
KTR-004-0	4.2	5.5	1517	95	887	
TD13	4.1	2.5	43	70	113	
TDR 10/01	3.2	3.3	88	3	1447	
TDR 27/01	2.6	3.1	1022	12	453	
DTR-029-0	1.2	2.2	64	89	75	
ATR-045-0	1.1	0.8	20	25	154	
ATR-034-0	1.1	0.9	118	180	107	
DTR-040-0	0.5	0.1	32	6	72	
DTR-039-0	0.5	2.4	21	8	87	
TDR 26/01	0.3	1.0	28	169	30	
TDR 01/01	0.0	0.0	11	3	5	
DTR-033-0	0.0	0.1	42	9	55	

Table 8.7: The Mg values for the dunite samples in the Tulu Dimtu area before classification into fresher and altered. Ordered with the highest Mg value at the top and lowest at the bottom. For validation of the method, selected samples are referred to the petrological descriptions contained in chapter 3.

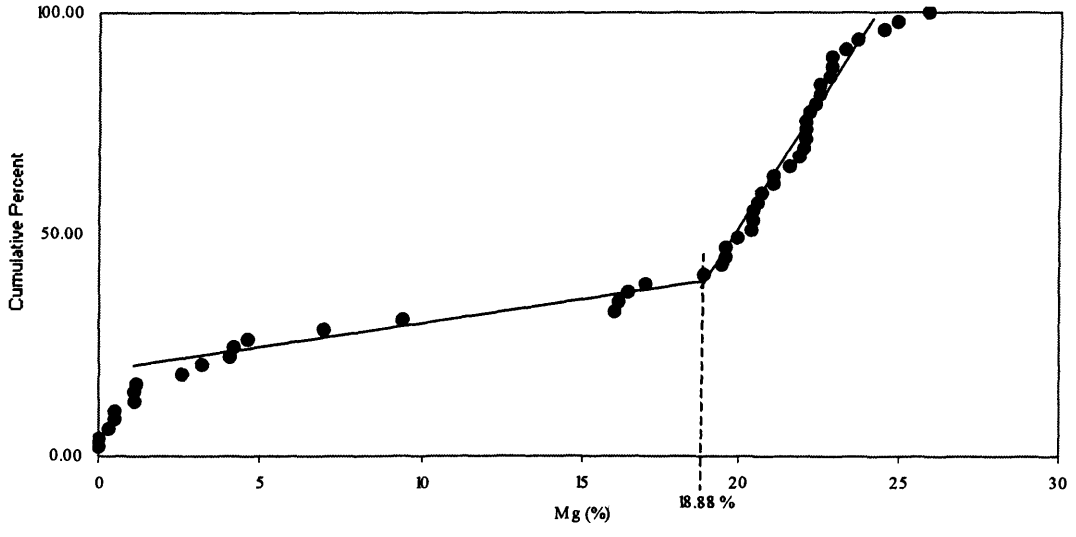

Figure 8.1: A graph of the cumulative percent (by rank) of the Mg values of the dunite samples from the Tulu Dimtu area. The value of 18.88% is marked onto the graph as it is the lowest possible Mg value for an ideal fresher dunite (see figure 8.6).

Figure 8.1 shows a clear difference between two populations of Mg values in the dunite samples from Tulu Dimtu. One population has values which are greater than 18.88% and another population has values which are less 18.88%. The two populations can be summarised with two linear lines of best fit which intercept very close to 18.88% (as calculated above). This suggests that there are two distinct groups of dunite samples from Tulu Dimtu separated at 18.88% which was calculated as the minimum Mg value for a fresh dunite.

Furthermore, figure 8.1 shows that although there is a break just below 18.8%, there are four samples which have Mg values between 16.0% and 17.0%. Below these values there is another, larger, break which may infer that the break should be below 16.0%. However, these values are still significantly lower than the ideal Mg values calculated in table 8.6. Furthermore, these values could be explained as being due to serpentinisation with very little silicification. Although alteration generally decreases the Mg content of a rock, the alteration of olivine to serpentine can retain high Mg values. For example Lecuyer et al. (1994) analysed serpentine minerals which have Mg compositions as high as 22.6%. However the action of sepentinisation also introduces some OH^- which would reduce the Mg value in some cases.

Given the fact that serpentine can contain Mg at up to 22.6% (Lecuyer et al., 1994). With the classification system described above, a 100% serpentinised dunite could be classed as "fresher". It is therefore this method using Mg is intended simply to support petrological analysis (see chapter 3). The samples classified as "fresher" in this manner are only expected simply to be more likely to retain magmatic features than the samples regarded as being altered.

8.3.2. The samples

Samples were taken from both the ultramafic complexes of the WES and also the surrounding basement. Of the ultramafic complexes, the following numbers of samples were taken:

Ultramafic Complex	Number of Samples
Tulu Dimtu Main Intrusion	59
Kingy Ridge Ultramafic (including the extra ultramafic)	30
Daleti Intrusion	21
Ankori Complex	13
Main Yubdo Intrusion	34
Lensoid Ultramafics (from all four geographic areas)	*68*

Table 8.8: The numbers of samples from the ultramafic complexes of the WES. A summary of entire dataset is provided in table 8.9.

When considering the ultramafic complexes, the greatest number of samples were taken from the Lensoid Ultramafics from over the entire study area. Of the main complexes, the greatest samples were taken from the Tulu Dimtu Main Intrusion, followed by the Main Yubdo Intrusion

After classification as fresher and altered rocks (see section 8.3.1), the following numbers of samples were used for the analysis of geochemical processes in the WES.

Area	Total	Altered ultramafic rocks	Fresher ultramafic rocks	Non-ultramafic rocks	Birbirite samples
Tulu Dimtu	116	35	31	47	3
Kingy	110	33	6	67	4
Daleti, Ankori, Keley and Tulu Kapi	155	14	13	115	13
Yubdo, Andu and Sodu	100	18	6	68	8
TOTAL	481	100	56	297	28

Table 8.9: A summary of the numbers and types of samples used in the four geographic areas in this study. A further breakdown of these is provided in each respective section.

8.4. Tulu Dimtu: Selected Major and Trace Elements

8.4.1. Introduction

There are 115 rock samples from the Tulu Dimtu area. Using the classification method shown in section 8.3.1, thirty-one are samples are fresher ultramafics, 43 are altered ultramafics and 6 are from the surrounding basement. The numbers and types of

samples from the various formations are summarized in table 8.10. The samples were taken where exposure was found. The eastern flank of the Tulu Dimtu Main Intrusion was not studied due to the terms of the licence agreement between Golden Prospect Mining Co Ltd and the Ethiopian government. Only three samples of fresher ultramafic rocks are found in the samples from the Lensoid Ultramafic formations, one of these is approximately 500m south of the Sheared Ultramafic.

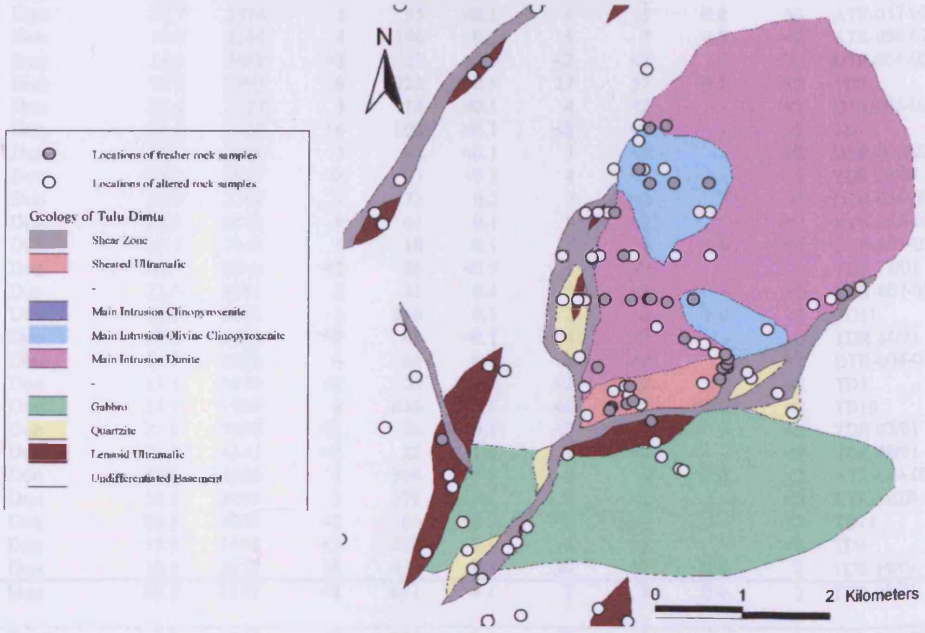

Figure 8.2: The distribution of rock samples within the Tulu Dimtu area.

Formation	#	Sub-unit	#	Altered ultramafic rocks	Fresher ultramafic rocks	Non-ultramafic rocks	Birbirite samples
Shear Zones	14			0	0	14	0
Sheared Ultramafic	10			9	1	0	0
Tulu Dimtu Main Intrusion	51	Clinopyroxenite	2	6	0	0	0
		Olivine-Clinopyroxenite	9	4	0	4	1
		Dunite	40	5	28	6	1
Gabbro	3			0	0	3	0
Quartzite	7			0	0	7	0

Lensoid Ultramafics	25	14	2	7	1
Basement	6	0	0	6	0
TOTAL	115	34	31	47	3

Table 8.10: A summary of the samples from the Tulu Dimtu area. The classification of fresher and altered rocks is covered in section 8.3.1 and the classification of ultramafic lithotypes including birbirite is covered in chapter 3.

8.4.2. Data

Formation	Description	Mg (%)	Ni (ppm)	Cu (ppm)	Cr (ppm)	Al (%)	Pt (ppb)	Pd (ppb)	Pt/Pd	Au (ppb)	Sample
Tulu Dimtu Main Intrusion	Dun	24.4	3380	4	19	<0.1	3	<2	-	3	ATR-051-02
	Dun	22.8	2037	6	131	0.1	8	3	2.7	2	ATR-053-02
	Dun	22.8	2945	2	13	<0.1	5	4	1.3	2	DTR-009-02
	Dun	22.7	2574	3	55	<0.1	4	5	0.8	35	ATR-057-02
	Dun	19.5	2154	4	196	0.1	5	7	0.7	<2	ATR-056-02
	Dun	19.4	3469	<2	27	<0.1	<2	<2	-	70	DTR-034-02
	Dun	18.8	2992	8	2728	0.5	27	37	0.7	<2	TD9
	Dun	25.8	2327	3	16	<0.1	4	<2	-	<2	DTR-035-02
	Dun	24.8	1456	16	102	<0.1	<2	<2	-	<2	TD12
	Dun	23.6	2691	3	40	<0.1	3	<2	-	<2	DTR-005-02
	Dun	23.2	2617	<2	97	<0.1	4	<2	-	2	TDR 20/01
	Dun	22.4	2340	5	72	0.2	7	<2	-	<2	DTR-026-02
	Dun	22.4	2182	9	61	0.1	9	<2	-	<2	KTR-035-02
	Dun	22.3	2942	5	18	0.1	5	5	1.0	<2	DTR-001-02
	Dun	22.1	2856	<2	46	<0.1	4	<2	-	2	TDR 12/01
	Dun	22.0	2091	3	33	0.4	5	<2	-	<2	DTR-007-02
	Dun	22.0	1846	2	366	0.1	2	2	1.0	<2	TD11
	Dun	22.0	2312	<2	42	<0.1	4	<2	-	<2	TDR 24/01
	Dun	21.9	2686	4	61	0.1	6	<2	-	<2	DTR-004-02
	Dun	21.8	3575	<2	70	<0.1	<2	<2	-	<2	TD3
	Dun	21.5	1909	4	634	0.1	40	2	20.0	<2	TD10
	Dun	21.0	5860	<2	76	<0.1	<2	<2	-	<2	TDR 07/01
	Dun	21.0	4543	<2	25	1.0	4	<2	-	<2	TDR 08/01
	Dun	20.6	3880	4	304	0.1	8	5	1.6	<2	ATR-044-02
	Dun	20.4	3285	3	379	0.1	7	<2	-	<2	KTR-002B-02
	Dun	20.3	3062	<2	64	<0.1	<2	<2	-	<2	TD14
	Dun	19.9	1802	<2	292	0.1	4	<2	-	<2	TD4
	Dun	19.5	2872	16	436	0.1	30	37	0.8	2	TDR 19/01
Sheared Ultramafic	Dun	20.5	2155	<2	651	0.1	7	8	0.9	2	TDR 05/01
Lensoid Ultramafics	Cpxite	7.3	1644	9	294	0.1	3	<2	-	4	DTR-016-02
	Dun	20.4	2824	3	119	0.1	9	<2	-	0	TTR-018A-02

Table 8.11: Mg, Ni, Cu, Cr, Al, Pt and Pd values for the fresher samples (as defined in section 8.3.1) collected from the Tulu Dimtu area. Dun: Dunite. Cpxite: Clinopyroxenite.

Formation	Description	Mg (%)	Ni (ppm)	Cu (ppm)	Cr (ppm)	Al (%)	Pt (ppb)	Pd (ppb)	Pt/Pd	Au (ppb)	Sample
Tulu Dimtu Main Intrusion	Dun	9.4	2190	2	139	0.1	6	<2	-	5	DTR-050-0
	Dun	16.1	1962	3	91	<0.1	5	<2	-	27	TDR 22/01
	Dun	7.0	586	<2	48	0.1	24	<2	-	<2	TDR 25/01
	Dun	1.1	154	25	20	0.8	<2	<2	-	2	ATR-045-0
	Dun	<0.1	55	9	42	0.1	<2	<2	-	<2	DTR-033-0
	Ol-cpxite	1.9	150	112	216	2.0	2	2	1.0	2	ATR-047-0
	Ol-cpxite	9.4	705	4	220	0.1	24	<2	-	<2	ATR-052-0
	Ol-cpxite	4.8	816	18	502	1.9	5	<2	-	<2	TD7
	Ol-cpxite	2.2	350	116	60	2.5	4	15	0.3	<2	TD8
	Cpxite	0.6	37	51	12	1.0	<2	<2	-	<2	ATR-046-0
	Cpxite	0.7	139	41	474	0.5	3	<2	-	<2	DTR-032-0
Sheared Ultramafic	Dun	4.1	113	70	43	2.5	<2	<2	-	<2	TD13
	Dun	4.6	527	22	705	3.7	4	4	1.0	<2	TD17
	Dun	17.0	7695	<2	187	<0.1	5	<2	-	4	TDR 06/01
	Dun	16.0	2129	<2	383	0.3	6	<2	-	<2	TDR 09/01

	Dun	3.2	1447	3	88	3.3	6	13	0.5	2	TDR 10/01
	Dun	16.4	2894	2	223	0.1	6	<2	-	<2	TDR 11/01
	Cpxite	1.9	232	14	17	6.3	<2	<2	-	2	KTR-034-0
	Cpxite	1.3	300	5	5	2.5	<2	<2	-	2	TD15
	Cpxite	0.8	100	4	34	3.6	<2	<2	-	<2	TD16
Lensoid Ultramafics	Dun	1.1	107	180	118	0.9	3	2	1.5	3	ATR-034-0
	Dun	4.2	887	95	1517	5.5	4	4	1.0	2	KTR-004-0
	Dun	2.6	453	12	1022	3.1	6	6	1.0	8	TDR 27/01
	Dun	<0.1	5	3	11	<0.1	<2	<2	-	3	TDR 01/01
	Dun	0.3	30	169	28	1.0	3	3	1.0	<2	TDR 26/01
	Dun	1.2	75	89	64	2.2	<2	2	0.0	4	DTR-029-0
	Dun	0.5	87	8	21	2.4	<2	<2	-	8	DTR-039-0
	Dun	0.5	72	6	32	0.1	<2	<2	-	<2	DTR-040-0
	Ol-cpxite	3.1	467	75	708	3.4	14	3	4.7	6	DTR-014-0
	Ol-cpxite	1.8	80	47	143	2.5	<2	3	0.0	3	DTR-041-0
	Ol-cpxite	1.6	31	104	33	2.0	2	10	0.2	4	KTR-006-0
	Ol-cpxite	0.7	138	4	6	2.5	<2	<2	-	<2	TTR-020-0
	Cpxite	1.6	210	34	428	1.6	21	<2	-	<2	ATR-036-0
	Cpxite	0.4	109	39	210	0.2	3	<2	-	2	DTR-015-0
Other	Basa	0.6	122	30	309	0.2	5	<2	-	<2	DTR-017-0
	Basa	1.1	215	155	2095	0.9	19	26	0.7	3	TTR-007A-
	Basa	<0.1	7	6	29	0.1	<2	<2	-	<2	TTR-010-0
	Birb	0.1	1364	12	387	0.1	3	<2	-	<2	ATR-050-0
	Birb	1.9	1437	5	280	0.2	4	<2	-	<2	KTR-002-0
	Birb	0.2	38	2	29	0.1	<2	<2	-	2	TD23
	ChSchi	0.2	16	55	17	1.8	2	3	0.7	<2	TDR 18/01
	ChSchi	19.0	6899	22	459	0.4	9	41	0.2	13	TTR-057-0
	Dior	1.2	13	60	3	1.9	<2	<2	-	3	ATR-035-0
	Dior	2.6	637	58	236	1.8	4	5	0.8	<2	TD5
	Dole	0.6	13	53	14	1.3	<2	<2	-	2	KTR-010-0
	Dole	24.7	2195	<2	26	<0.1	4	12	0.3	<2	TTR-025-0
	Fels	1.2	16	28	8	1.6	<2	6	0.0	<2	ATR-043-0
	Fels	1.3	37	110	65	1.7	<2	10	0.0	2	DTR-042-0
	Gabb	1.1	27	43	32	4.5	<2	<2	-	<2	DTR-025-0
	Gabb	0.9	29	105	23	1.5	4	4	1.0	2	TTR-050-0
	Gabb	2.5	356	41	486	2.4	8	5	1.6	<2	TTR-052-0
	GranDi	0.1	19	19	44	0.3	4	15	0.3	4	DTR-012-0
	GranDi	1.5	173	16	23	1.2	<2	<2	-	<2	DTR-038-0
	HardP	19.6	2056	6	53	<0.1	4	<2	-	8	TTR-030-0
	MetaBas	18.9	4141	4	67	<0.1	7	<2	-	<2	TTR-027-0
	MetaBas	23.2	2527	2	7	<0.1	4	<2	-	2	TTR-028-0
	Mylo	3.5	530	32	924	3.5	7	<2	-	<2	ATR-048-0
	Mylo	0.2	14	6	22	0.2	<2	<2	-	<2	DTR-030-0
	Mylo	2.0	160	148	193	2.0	7	4	1.8	<2	KTR-011-0
	Mylo	20.3	5079	5	150	0.1	25	38	0.7	<2	TTR-018-0
	Quar	0.2	36	15	22	0.1	<2	<2	-	<2	DTR-011-0
	Quar	1.5	312	12	141	0.5	<2	<2	-	<2	KTR-003-0
	Quar	0.1	25	9	22	0.2	<2	<2	-	<2	KTR-005-0
	Quar	0.2	32	3	19	0.1	<2	2	0.0	<2	TDR 13/01
	Quar	0.1	18	3	25	0.1	<2	<2	-	<2	TDR 14/01
	Quar	0.1	15	<2	17	<0.1	<2	<2	-	3	TDR 15/01
	Quar	0.1	15	41	29	0.2	31	37	0.8	3	TDR 17/01
	Schi	15.3	11044	2	842	0.1	<2	<2	-	<2	TD1
	Schi	7.8	1975	<2	1127	0.1	36	<2	-	<2	TD2
	Schi	0.2	15	3	33	1.1	<2	<2	-	<2	TDR 16/01
	Schi	0.2	29	14	43	0.3	<2	<2	-	<2	TTR-014-0
	Sed	0.1	16	36	22	0.2	<2	4	0.0	<2	DTR-031-0
	TaSchi	1.7	396	10	215	0.2	3	3	1.0	<2	DTR-010-0
	TaSchi	10.6	954	4	580	6.0	15	16	0.9	2	DTR-027-0
	TaSchi	4.4	573	71	983	4.3	7	4	1.8	19	TTR-051-0
	TCSchi	1.6	205	59	228	1.5	<2	4	0.0	8	TD18
	Unid	1.0	687	4	23	0.1	<2	<2	-	2	ATR-054-0
	Unid	0.2	29	22	19	1.5	<2	<2	-	<2	DTR-024-0
	Unid	4.9	1262	68	287	2.5	<2	<2	-	<2	TDR 21/01
	VQuar	21.1	2595	<2	169	<0.1	5	<2	-	<2	TD6
	VQuar	<0.1	3	<2	5	<0.1	7	9	0.8	<2	TDR 02/01
	VQuar	<0.1	13	<2	7	0.1	<2	<2	-	<2	TDR 03/01
	VQuar	<0.1	20	8	12	0.1	<2	<2	-	<2	TDR 04/01
	VQuar	12.1	2656	4	465	0.1	16	<2	-	<2	TDR 23/01

Table 8.12: Mg, Ni, Cu, Cr, Al, Pt and Pd values for the altered samples collected from the Tulu Dimtu area. Anor: Anorthosite. Basa: Basalt. Birb: Birbirite. ChSchi: Chlorite-Schist. ChSchi: Chlorite-Schist. Cpxite: Clinopyroxenite. Dior: Diorite. Dole: Dolerite. Dun: Dunite. Fels: Felsite. Gabb: Gabbro. GranDi: Granodiorite. HardP: Hard pan. MetaBas: Metabasalt. MetaSed: Metasediment. Mylo: Mylonite. Ol-cpxite: Olivine-clinopyroxenite. Quar: Quartzite. Schi: Schist. Sed: Sediment. TaSchi: Talc-Schist. TCSchi: Talc-Chlorite-Schist. Troc: Troctolite. Unid: Unidentified. VQuar: Vein Quartz.

The following sections describe the distribution of Ni, Cu, Cr and Al in the Tulu Dimtu area. Each section describes one element and its distribution in fresher ultramafics and then altered rocks (as defined in section 8.3.1). These sections are accompanied by a fold-out page (page 213) of maps showing the distribution of all elements which the reader should refer to as each section is read.

8.4.3. Nickel

The fresher rocks on the flanks of the Tulu Dimtu Main Intrusion are enriched in Ni to a much greater degree than those in the centre. In fresher rocks nickel rises above 3000ppm (and up to 5860ppm) only within 500m of the contact of the Main Intrusion with the surrounding basement. Figure 8.4A shows that throughout the centre of the intrusion and in two places near the flanks, Ni is below 3000ppm but not lower than 1456ppm. The two fresher samples from the Lensoid Ultramafics contain significant Ni (2824ppm and 1644ppm), the remaining samples from Lensoid Ultramafics show negligible amounts (31 to 467ppm). The highest Ni content in fresher rocks (5860ppm) is found within 150m of the southern flank of the Sheared Ultramafic.

In samples classified as altered, Ni is enriched almost exclusively in the Main Intrusion and the Sheared Ultramafic (figure 8.4A). Although most samples outside of the Main Intrusion and Sheared Ultramafic do not host significant Ni, three samples do contain significant amounts. These come from two Shear Zones (containing 11,044ppm and 6899ppm) and one Lensoid Ultramafic (5079ppm). Indeed, the highest Ni content in the samples of the Tulu Dimtu area (11044ppm) is contained in a schistose rock from a shear-zone bounding the southeast flank of the Main Intrusion.

At one location in the northwestern Lensoid Ultramafic both altered and fresher rocks show Ni enrichment. A fresher dunite has 2824ppm Ni and this value rises to 5079ppm in a mylonitised rock.

8.4.4. Copper

In fresher rocks Cu reaches a maximum of 16ppm in two samples of the Sheared Ultramafic. Everywhere else - including the Lensoid Ultramafics - Cu never rises above 5ppm in fresher rocks.

Cu values of greater than 70ppm in altered rock are almost entirely situated over the basement and units other than the Main Intrusion and Sheared Ultramafic (figure 8.4A). Within the Main Intrusion, the highest values of Cu occur close to the western and southern flanks. The highest Cu analysis within the altered samples of the Main Intrusion (116ppm) occurs close to the samples with the highest values in the fresher rocks. Analyses of Cu in samples from the Lensoid Ultramafics and Shear Zones frequently rise above 70ppm, however some samples show negligible amounts (<5ppm).

8.4.5. Chromium

The highest Cr value in the Tulu Dimtu area (2728ppm) occurs in a fresher dunite on the southern flank of the Main Intrusion, close to the Sheared Ultramafic. Of the other fresher rocks, all other Cr values above 100ppm in the Main Intrusion are found in a zone close to the western flank of the formation. None of the three fresher ultramafics of the Lensoid Ultramafics show Cr values which rise above 500ppm, however all are higher than 100ppm.

In altered rocks, the dunites and olivine-clinopyroxenites at the centre of the intrusion are depleted in Cr. As seen in the fresher rocks, some higher Cr values (<100ppm) are found towards the outside of the formation. A schistose rock in a shear-zone bounding the southeastern parts of the Main Intrusion has a Cr value of 1127ppm.

Outside the Main Intrusion high Cr values (<900ppm) can be found in Lensoid Ultramafics and Shear Zones.

8.4.6. Aluminium

In all of the fresher rocks (except two) of the Tulu Dimtu area, Al is below detection limits. Two dunites from the Sheared Ultramafic returned values of 1% for Al.

The altered dunites in the centre of the Main Intrusion are almost entirely depleted in Al. The flanks of the Main Intrusion and Sheared Ultramafic are slightly elevated in Al. A high Al value (4.5%) occurs in a gabbro on the western flank of the intrusion and a zone of slightly elevated Al values occurs on the southern flank of the formation. Several pyroxenites and dunites in the Sheared Ultramafic show Al elevated above 2%. Several high values of Al (>4%) occur in the Shear Zones and Lensoid Ultramafics.

8.4.7. Summary of the Ni, Cu, Cr and Al values in the Main Intrusion and Sheared Ultramafic

Of the fresher rocks of the Main Intrusion (including the Sheared Ultramafic) the highest Ni values in the complex are close to the edge. As such, the highest Ni (5860ppm) is found within 150m of the southern flank of the Sheared Ultramafic. Similarly, the highest Cr values are found close to the flanks. Although these high Cr values are found in five samples within the Main Intrusion, only two fresher samples contain both high Ni and high Cr. At the southern edge and near the junction between the Main Intrusion, the Sheared Ultramafic and the southern shear-zone, both Cr and Cu rise to their highest values in two separate fresher dunites. Figure 8.3 shows the relative proportions of Cu and Cr in these samples (TDR 19/01 and TD9).

As seen in the fresher rocks, the altered samples also show the largest values of Cr at the flanks of the Main Intrusion. Additionally, Cu and Al show their highest values in the same samples located near the southern flank. As with Cu, Cr and Al the altered ultramafics show the highest values of Ni close to the flanks of the Main Intrusion,

similar to those values seen in the fresher rocks. However, unlike the other elements, Ni is enriched in two samples in the centre of the intrusion (4141 and 2527ppm).

8.4.8. Summary of the Ni, Cu, Cr and Al values in the Lensoid Ultramafics

When compared to the Main Intrusion the three fresher samples of the Lensoid Ultramafics (two dunites and one pyroxenite) display elevated Cr and intermediate Ni values.

The altered ultramafics show similar patterns to those seen in the Shear Zones (see section 8.4.9). One altered dunite sample is enriched in Ni but two different dunites are enriched in Cu. Elsewhere in the Lensoid Ultramafics, one altered olivine-clinopyroxenite is enriched in both Cr and Al (700ppm and 3% respectively).

8.4.9. Summary of the Ni, Cu, Cr and Al values in the Shear Zones

Two samples within Shear Zones (a mylonite and a talc-schist) have high values of both Cr and Al. High Ni and Cu values occur in different samples, two schistose rocks show high Ni values and a mylonite shows Cu enriched above 130ppm.

8.5. Tulu Dimtu: Pt and Pd Distribution

8.5.1. Rock

The highest Pt and Pd grades of fresher rocks in the Tulu Dimtu area occur at the south of the Main Intrusion. Pt is present from below detection to 40ppb and Pd from below detection to 37ppb in the three samples. These samples are located at the junction between the Tulu Dimtu Main Intrusion, the Sheared Ultramafic and the southern shear zone. Elsewhere, neither Pt nor Pd rise above 9ppb and drop to below detection limits (<2ppb).

Within the Tulu Dimtu Main Intrusion, the three highest Pt analyses (36ppb, 24ppb and 24ppb) in the altered rocks occur at the edge of the complex and these all coincide with Pd below detection limits (<2ppb). All other altered ultramafics show Pt assays between 7ppb and 3ppb. The maximum Pd value within the altered rocks of the Main Intrusion is 15ppb found near the southern flank. A dolerite dyke cross-cutting the intrusion near the western flank has a Pt at a value of 4ppb and a Pd value of 12ppb. The two Pt- and Pd-bearing samples from the Lensoid Ultramafic units are an altered ultramafic with a Pt value of 21ppb and a Pd value below detection and a mylonitised sample with a Pt value of 25ppb and a Pd value of 38ppb. These are found in two separate ultramafic units to the northwest of the Main Intrusion (figure 8.4E and 8.4F).

Other Pt- and Pd-bearing samples include a chlorite schist in a zone cross-cutting the gabbro and this shows results of 9ppb Pt and 41ppb Pd. A talc schist occurs close to the sheared western contact of the Tulu Dimtu Main Intrusion and this has returned results of 15ppb and 16ppb for Pt and Pd respectively. A fine-grained volcanic sample close to the isolated shear zone west of the Main Intrusion has Pt and Pd concentrations of 26ppb and 19ppb respectively.

8.5.2. Summary of Pt and Pd distribution in the Main Intrusion and Sheared Ultramafic

The highest Pt and Pd grades of the Tulu Dimtu area occur in a fresher rock on the southern flank of the intrusion. This occurs with two other fresher samples which are also relatively high in both Pt and Pd (see table 8.13). These samples occur at the junction between the Main Intrusion, Sheared Ultramafic and Shear Zones.

Within the altered rocks of the Main Intrusion all Pt grades above 20ppb also occur in the flanks of the intrusion – which may suggest a zonation in Pt values. As seen with Pt, all Pd values in altered rocks are 15ppb or below and occur within 400m of the flanks of the intrusion. However - unlike the fresher rocks – Pt reaches the highest values in different altered samples from those of Pd (figure 8.4E).

The comparison between PGE and Ni, Cu, Cr and Al in the highest samples is summarised as follows:

Sample	Pt	Pd	Ni	Cu	Cr	Al
TDR 19/01	37	30	2872	16	436	0.1
TD9	37	27	2992	8	2728	0.5
TD10	2	40	1909	4	634	0.1
TD12*	< 2	< 2	1456	16	102	< 0.1

Table 8.13: A summary of Ni, Cu, Cr and Al values in the dunite samples of highest Pt and Pd grade of the fresher rocks. A graphical representation of this data is provided in figure 8.3. *: Sample TD12 is included regardless of low Pt and Pd values as it contains a high Cu value and is located close to the Pt- and Pd-bearing samples.

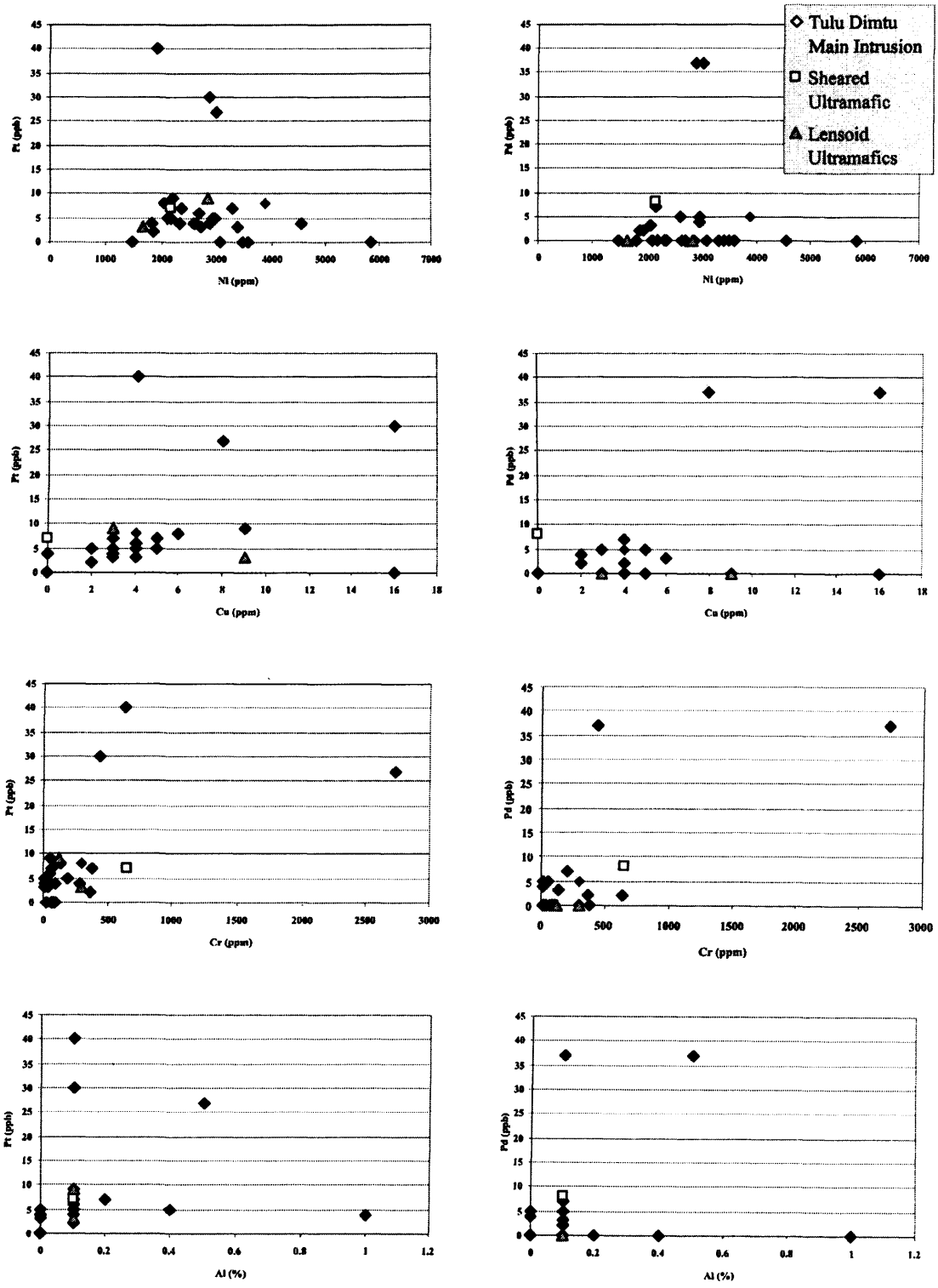

Figure 8.3: Graphs of Ni, Cu, Cr and Al versus Pt and Pd in the fresher rocks of the Tulu Dimtu area. The key to symbols in the top right corner.

8.5.3. Summary of Pt and Pd distribution in the Lensoid Ultramafics

The highest Pt and Pd values in fresher rocks are 9 and 8ppb respectively. Whereas the highest Pt and Pd values in altered Lensoid Ultramafics are 25 and 38ppb. There are three altered samples from the Lensoid Ultramafics which contain Pt or Pd. An altered pyroxenite and an olivine-clinopyroxenite sample are more enriched in Pt rather than Pd and one mylonite sample contains both Pt and Pd.

8.5.4. Summary of Pt and Pd distribution in the Shear Zones

Two samples within the Shear Zones are Pt- and Pd-bearing. These are a talc-schist close to the western contact of the Main Intrusion and a chlorite-schist in the southwestern corner of the area. In the chlorite-schist Pd predominates over Pt, but in the talc-schist Pt shows similar values to Pd.

8.5.5. Summary of Pt and Pd distribution in the basement

Two basement rocks are Pt- or Pd-bearing. These are a quartzite (with a Pt value of 31ppb and Pd value of 37ppb) and a fine-grained volcanic rock (with a Pt value of 19ppb and Pd value of 26ppb).

8.5.6. Comparison of the geochemistry of the soil versus rock samples

Ni and Cu anomalies in soil occur in different places from those of the rocks (when compared to chapter 8). As with the rock samples (see chapter 8), the highest Cr values in soil are found above the western and southern flanks of the Main Intrusion and the lowest values are in the centre of the intrusion.

There are a greater number of soil samples enriched to above 20ppb Pt compared to the number of rock samples. In fresher and altered rocks 7% of the samples (3/42) contain more than 20ppb Pt whereas in soils 33% (23/70) contain more than 20ppb. Pd anomalies (13 and 15ppb) only occur in the centre of the intrusion.

8.6. Review of processes concentrating Pt and Pd

8.6.1. Introduction

There are several mechanisms cited to explain the distribution of PGE within mafic and ultramafic complexes. Much research has been directed towards the role of sulphur in magmas but alternatively some authors advocate a role for hydrothermal fluids. Furthermore, some models have been developed whereby PGE are concentrated without sulphur or hydrothermal fluids.

The proponents of the role of sulphur argue that PGE-rich droplets of liquid sulphide segregate out of a silicate magma and then concentrate the PGE into a horizon (for a review see Naldrett, 1998). Alternatively, the study of polyphase silicate inclusions within Pt-Fe alloys from sulphur-poor complexes suggests that the magma involved in the precipitation of PGM is highly water-rich (Johan, 2002). Studies of fO_2 and fluid inclusions can also be used to support the role of high temperature fluids in concentrating PGE. Some recent work has begun to reveal an additional view on PGE concentration. Macambria and Filho (2005) cite a correlation between Al and PGE to suggest that neither sulphur nor high temperature fluids are required to create a PGE "reef".

In order to aid the subsequent discussion this section reviews the igneous processes believed to have a role in the concentration of Ni, Cu, Cr, Al and PGE. This is followed by an account of the study of PGE solubility in medium to low temperature fluids.

8.6.2. The fractionation of Ni

The partitioning behaviour of Ni can vary with magmatic conditions of formation such as fO_2 and fS_2 (Kinzler et al., 1990; Gaetani and Grove, 1997). Table 8.14 shows the range of partition co-effcient (D_{Ni}) values determined from in-situ measurements of natural examples and from experimental systems. The lowest partition cocoefficient of Ni

(D_{Ni}) seen in the literature is 1.35 with most experiments and measurements returning values of over 4. It can therefore be expected that – regardless of variations in magmatic conditions - Ni will partition into the most primitive rocks of the complex. As fractionation continues the Ni content of the melt will decrease and therefore any subsequent olivine crystals to precipitate will have proportionately less Ni. The highest known D_{Ni} values are for sulphide phases (ranging 150 to 4300, see Pedersen et al. 1979). Therefore it is reasonable to assume that if there is any sulphide present in a melt then almost all Ni will partition into those phases.

Rock Type	D_{Ni}		D_{Ni} Type	Reference
	Value	Low High		
Basalt-Andesite	58.00		Phenocrysts-Matrix	Luhr & Carmichael, 1980
Basalt-Andesite	34.00		Phenocrysts-Matrix	Villemant et al., 1981
Andesite	24.90		Phenocrysts-Matrix	Ewart & Griffin, 1994
Andesite	22.00		Phenocrysts-Matrix	Dostal et al., 1983
Andesite	15.50		Experimental	Mysen, 1978
Basalt	12.20		Phenocrysts-Matrix	Bougault & Hekinian, 1974
Basalt-Andesite		28.00 36.40	Phenocrysts-Matrix	Villemant, 1988
Andesite		15.40 20.70	Experimental	Drake & Holloway, 1981
Andesite		15.00	Experimental	Kloeck & Palme, 1988
Basalt-Andesite		10.70 12.20	Experimental	Pedersen, 1979
Andesite		9.40 24.00	Model	Nielsen, 1988
Basalt		9.30 12.80	Experimental	Nabelek, 1980
Andesite		8.63 18.54	Phenocrysts-Matrix	Dale & Henderson, 1972
Basalt-Andesite		8.25 23.50	Phenocrysts-Matrix	Leeman & Scheidegger, 1977
Andesite		7.60 11.00	Experimental	Kennedy et al., 1993
Basalt		7.60 48.00	Experimental	Duke, 1976
Basalt-Andesite		7.15 15.10	Experimental	Kinzler et al., 1990
Andesite		6.10 24.80	Experimental	Mysen, 1979
Komatiite		**4.50 7.10**	Experimental	**Gaetani & Grove, 1997**
Basalt-Andesite		4.36 5.05	Experimental	Seifert et al., 1988
Andesite		4.30 6.20	Experimental	Drake & Holloway, 1981
Basalt-Andesite		4.30 7.20	Experimental	Mysen & Virgo, 1980
Andesite		4.00 7.46	Experimental	Gaetani & Grove, 1997
Basalt		2.86 13.6	Experimental	Takahashi, 1978
Basalt		1.35 1.73	Experimental	Irvine & Kushiro, 1976
Basalt-Andesite		4.50	Phenocrysts-Matrix	Ewart & Griffin, 1994

Table 8.14: Partition co-efficients of Ni between olivine and melt or host rock type (as stated), where D_{Ni} = Olivine / Melt or Host Rock. This data was compiled using the GEOROC database (2005).

8.6.3. The fractionation of Cr

The partitioning behaviour of Cr into olivine is less certain - D_{Cr} can vary from 0 to 34 (table 8.15). Situations have been described in nature whereby Cr can partition entirely into the basaltic or andesitic host-rock or almost entirely into the olivine minerals. Although Cr partitioning into olivine is variable, Cr has a strong affinity with spinels where D_{Cr} can vary from 30 up to 340 (table 8.16).

Rock Type	D_{Cr} Value	D_{Cr} Low	D_{Cr} High	D_{Cr} Type	Reference
Basalt-Andesite	34.00			Phenocrysts-Matrix	Luhr & Carmichael, 1980
Andesite	5.00			Phenocrysts-Matrix	Mahood & Stimac, 1990
Basalt-Andesite	2.80			Phenocrysts-Matrix	Villemant et al., 1981
Basalt-Andesite	1.20			Experimental	McKay & Weill, 1976
Basalt	1.18			Experimental	Kloeck & Palme, 1988
Basalt-Andesite	1.10			Phenocrysts-Matrix	Bougault & Hekinian, 1974
Basalt-Andesite	1.08			Experimental	McKay & Weill, 1977
Basalt-Andesite	0.90			Experimental	Ringwood, 1970
Basalt	0.73			Experimental	Nikogosian & Sobolev, 1997
Basalt-Andesite	0.70			Phenocrysts-Matrix	Dostal et al., 1983
Andesite	0.00			Phenocrysts-Matrix	Michael, 1988
Andesite		5.14	5.50	Phenocrysts-Matrix	Villemant, 1988
Andesite		1.10	5.20	Experimental	Duke, 1976
Basalt-Andesite		1.06	3.06	Phenocrysts-Matrix	Leeman & Scheidegger, 1977
Andesite		1.00	1.20	Experimental	Pedersen, 1979
Andesite		0.63	1.85	Experimental	Beattie, 1994
Komatiite		**0.58**	**0.66**	**Experimental**	**Gaetani & Grove, 1997**
Basalt-Andesite		0.58	0.78	Experimental	Akella et al., 1976
Basalt-Andesite		0.45	1.30	Experimental	Kennedy et al., 1993

Table 8.15: Partition co-efficients of Cr between olivine and melt or host rock type (as stated), where D_{Cr} = Olivine / Melt or Host Rock. This data was compiled using the GEOROC database (2005).

Rock Type	Mineral	D_{Cr} Value	D_{Cr} Low	D_{Cr} High	D_{Cr} Type	Reference
Basalt	Spinel	77.00			Experimental	Ringwood, 1970
Basalt-Andesite-Dacite	Magnetite	166.00			Phenocrysts-Matrix	Sisson, 1991
Basalt-Andesite	Magnetite	153.00			Phenocrysts-Matrix	Esperança et al., 1997
Andesite-Basalt	Magnetite	30.00			Phenocrysts-Matrix	Bacon & Druitt, 1988
Andesite	Magnetite		93.00	340.00	Phenocrysts-Matrix	Beattie, 1993
Rhyolite	Magnetite		54.00	164.00	Phenocrysts-Matrix	Schwandt & McKay, 1998

Table 8.16: Partition co-efficients of Cr between spinel or magnetite and melt or host rock type (as stated), where D_{Cr} = Olivine / Melt or Host Rock. This data was compiled using the GEOROC database (2005).

8.6.4. Sulphide immiscibility and solubility

As the primitive magma rises through the Earth's crust, a small amount of precipitation of silicate or oxide minerals occurs and then sulphur may become saturated in the magma. At this point S comes out of solution in the silicate melt and a situation occurs where both silicate and sulphide melts exist together as immiscible liquids – an event called sulphide segregation. Ni, Cu, Pt and Pd are known to be concentrated into the sulphide melt within a magma by sulphide segregation (Naldrett and von Gruenewaldt, 1989) which may be triggered by several different changes in conditions.

Sulphur saturation in a magma can be achieved in a situation where sulphur becomes insoluble. The most common explanation for this is through the precipitation of silicate minerals, or a fall in temperature, or an increase in fO_2 or by a decrease in the amount of Fe^{2+} in the magma. However, there are several other factors which affect sulphide solubility (for a review see Robb, 2005) including the injection of a new magma (see section 8.6.7).

8.6.5. Sulphide fractionation

As an immiscible mixture of silicate and sulphide liquids rise through the crust crystallisation occurs in each melt. The sulphides fractionate to produce a Ni-bearing monosulphide solid solution (MSS) which is precipitated leaving a Cu-rich residual sulphide liquid (Fleet and Pan, 1994; Barnes et al., 1997). Partition coefficients confirmed by geological studies have demonstrated that during sulphide fractionation, Pt and Pd are compatible with the Cu-rich residual sulphide liquid (Barnes et al. 1997; Fleet et al., 1993). The residual sulphide liquid may then crystallise as a Pt-, Pd- and Cu-rich Intermediate Solid Solution (ISS). Alternatively, the Cu-rich liquids could be driven away from the MSS, through filter-pressing (see section 8.6.6). The products of sulphide fractionation are seen in-situ in the sulphide blebs described by Prichard et al. (2004).

It has been argued that the concentration of PGE by the action of sulphides is only valid in magmas of large bulk-S content such as the Bushveld or Sudury Intrusive complexes. Furthermore, a sulphur solubility assessment has suggested that the Bushveld complex does not contain sufficient sulphur to explain the amount of PGE present (see Cawthorn, 2005). These arguments suggest that alternative models (not involving sulphur) should also be explored. However, Peregoedova and Ohnenstetter (2002) argue that a high fS_2 can be obtained in low-S magmas through fractionation of the silicate melt and immiscibility of the sulphides. Furthermore, Tolskykh et al. (2000) have shown that in Alaskan-type intrusions – which are commonly low-S - it is common to find cooperite (PtS) rimming Pt-Fe alloys. This presence of cooperite suggests that the fS_2 of the magma must have risen high enough to allow the sulphuration of Pt (Peregoedova and Ohnenstetter, 2002).

8.6.6. Filter-pressing

After and during sulphide fractionation, the Cu-rich residual sulphide liquid can migrate away from the MSS crystals and precipitate. This is proposed by the "filter-pressing" model of Andersen et al. (1998) to explain the zonation of Au and PGE in the Skaergaard Intrusion (East Greenland). As sulphide fractionation occurs, cumulus silicate crystals precipitate, and the residual sulphide liquid will be interstitial. As further accumulation of cumulus material occurs, the volume of interstitial space will drop and the residual sulphide material will be entrained along with the other interstitial fluids and migrate towards the more evolved portions of the system. The MSS, however, will have already crystallised will therefore be trapped within the cumulate pile thereby allowing ISS to crystallise away from MSS.

In a situation where bulk sulphur content is very low, it may be hard to understand how a residual sulphide liquid can migrate. However, the validity of this model is dependant on the potential for the residual sulphide liquid to be entrained in the bulk interstitial liquids. Smaller amounts of liquid are more likely to become entrained than larger amounts and hence the model becomes more feasible with smaller amounts of

fluid. Additionally, when the residual sulphide liquid is moving away from the MSS, a "tail" will form behind the bulk of the entrained liquid. The more entrained the liquid, the larger the tail and, therefore, the less likely that ISS will be split apart from MSS. So the smaller the proportion of residual sulphide liquid, the greater the potential for filter-pressing to occur and the more likely Cu-rich sulphides (ISS) will be split apart from Ni-rich sulphides (MSS).

It may be argued that the residual sulphide liquid is unlikely to travel distances larger than 1cm. However the evolved Cu-rich liquid can behave in a number of ways. Prichard et al. (2004) describe a situation in a mafic dyke whereby both MSS and ISS crystallise together as sulphide blebs less than 1cm in diameter. In contrast, Naldrett et al. (1992) describe how the ores of the "Copper" and "Deep Copper" zones of the Strathcona mine are the end product of fractionation of the Main Zone Sulphides over 200m away. Furthermore, Andersen et al. (1998) document the effect of filter pressing in separating Au and PGE reefs over several 100s of metres in the relatively sulphur-poor Skaergaard complex. And as such, it is expected that under the appropriate conditions, the evolved residual sulphide liquid can travel up to 200m away from the location of the MSS.

8.6.7. Magma mixing

Magma mixing may result in the precipitation of large amounts of chromite which may be accompanied by sulphide immiscibility The mechanism of chromitite formation is dealt with first. Chromite saturation can be reached in a situation where a slightly evolved melt (precipitating olivine) is mixed with a primitive melt (Naldrett et al., 1990; Naldrett and von Gruenewaldt, 1989). The precipitation of chromite by the mixing of two magmas was proposed by Irvine (1977) to explain the formation of massive chromitites in the Muskox intrusion in NW Canada. His model is consistent with observations of chromitites from the Bushveld and Stillwater complexes where chromitites form at the base of well-defined cyclic units (Naldrett et al., 1990). Naldrett et al. (1990) suggest that if a magma on the olivine-chromite cotectic (point A) is mixed with a magma in the orthopyroxene field (point D) the resulting melt (AD) may fall within the chromite field

and as cooling occurs, chromite will be precipitated followed by olivine. This will then be followed by the typical fractionation sequence. This only occurs in a situation where the fresher magma intrudes the evolved melt well before plagioclase is precipitated.

Where an advanced differentiate (precipitating plagioclase) mixes with a primitive melt, sulphides may become immiscible with the silicate melt (Naldrett and von Gruenewaldt, 1989). Subsequently, suitable conditions for the crystallisation of these sulphides may then allow Ni, Cu and the PGE to become concentrated. In order for chromite to be precipitated only a slightly evolved melt is required, but for chromites to be precipitated and sulphides to become immiscible the influx of a more advanced melt is necessary. This raises the possibility within this model of the existence of sulphide-barren and sulphide-poor chromitites.

8.6.8. Hydrothermal remobilisation

When associated with primary sulphides of a small grain size, Ni and Cu are both known to be highly soluble in hydrothermal fluids. This behaviour is indicated from precipitates of hydrothermal fluids (Marshall and Gilligan, 1987; Keays, 1987; Canals et al., 1992). Furthermore, the presence of Cu in hydrothermal fluid inclusions has been noted by Vanko et al. (2001) and Baker et al., (2004) – for a synopsis of previous studies see Kesler (2005). Fluids in such systems are regarded to be of nearly neutral pH, with temperatures from 200-300°C and salinities of less than 3wt% NaCl (Kesler, 2005) all of which are obtainable in a mobile belt such as the WES. Therefore the presence of Ni and Cu in highly sheared rocks (at values much higher than in fresher rocks) may be the result of shear-zone hosted high-temperature fluids.

In comparison to sulphide-associated elements, Cr-bearing spinels are highly resistant to hydrothermal alteration. It is therefore likely that a fresher rock with high Cr will retain a high Cr value in the subsequent altered rock. Aluminium is also immobile in hydrothermal fluids and, therefore, if present it may indicate the presence of aluminosilicates in the protolith.

The evidence for the stability of Pd- and Pt-chloride complexes in fluids at equilibrium with typical alteration minerals at temperatures up to 300°C is well established (Wood, 2002; Wood 1987; Gammons et al., 1992). At higher temperatures, it is expected that the solubility of these elements in alteration fluids will increase and lower salinities and pH will be required. Solutions in equilibrium with clay minerals and/or hematite are thought to take more Pt and Pd into solution than those fluids which precipitate pyrite, pyrrhotite and other alteration minerals (Tarkian et al., 1996). The solubility of Pt- and Pd-bisulphide complexes is not well understood, but may be capable of transporting far more of the elements under less extreme conditions. Additionally, the case for preferential dissolution and transport of Pd over Pt has been made clearly by experimental studies of several conditions (see numerous references in Wood, 2002).

8.7. Tulu Dimtu: Discussion

Here the processes likely to have affected the distribution of Ni, Cu, Cr Al, Pt and Pd in the Tulu Dimtu area are discussed. The processes involved with the distribution of Ni, Cu, Cr and Al in fresher ultramafics are considered from 8.7.1 to 8.7.3, followed by those processes which affect altered rocks in 8.7.4 and 8.7.5. The mechanisms which distribute Pt and Pd are considered from section 8.7.6 to section 8.7.7.

8.7.1. Zonation of nickel and chromium in fresher rocks

The highest Ni value in the fresher rocks (5960ppm) occurs within 150m of the southern flank of the Sheared Ultramafic. Ni values then drop steadily towards the centre of the Tulu Dimtu Main Intrusion and as such, all Ni values above 3000ppm occur within 500m of the edges (figure 8.4A). Similarly, the highest Cr value (2728ppm) occurs at the edge of the Main Intrusion and all Cr values above 100ppm occur within 700m of the flanks of the complex (figure 8.4C). Although both elements show a gradual variation in values with distance away from the edge of the intrusion there are only two samples which contain both elevated Cr and elevated Ni. Additionally, the highest Cr values occur in a different location to the highest Ni values.

As Ni is compatible in olivine, the fresher rocks at the edge of the complex could be considered to be the most primitive rocks of the dunite zone and the drop in Ni values can be regarded as the product of further evolution of the melt. The geochemistry of the host-rock will affect the D_{Ni} value and all relevant studies show D_{Ni} between olivine and melt values of greater than 1.35 (table 8.14). The most relevant study – using a komatiite host rock – returned a D_{Ni} range of 4.5 to 7.1 (Gaetani and Grove, 1997).

Although fractionation could explain the trends in Ni values, the absolute figures are higher than expected for the Ni content of olivine. Typical Ni values in olivine minerals range from 1280ppm to 3293ppm (table 8.17) whereas four samples of fresher dunite contain greater than 3500ppm, it can therefore be expected that the excess Ni is contained in an additional phase or phases. It is likely that the additional phase hosting Ni is a sulphide mineral (as observed in chapter 3) and to a lesser degree oxide minerals. Although olivine will have been dissolved, sulphides are more likely to have been leached extensively by the aqua regia process.

Reference	Location	Rock Name	Method	Number of analyses	Min (ppm)	Max (ppm)
Moine et al. (2001)	Kerguelen / Ile De L^Ouest / Indian Ocean	Dunite xenolith	ICPMS (LA)	1	2695	2695
Schuth et al. (2004)	Ontong Java / Solomon Islands / Pacific Ocean	Picrite	EMP	19	2200	3293
Neumann et al. (2002)	Canary Islands / Fuerteventura / Atlantic Ocean	Harzburgite xenolith	ICPMS	9	2180	3150
Gregoire et al. (2000)	Kerguelen / Ile De L^Ouest / Indian Ocean	Harzburgite xenolith	ICPMS	12	2125	3275
Hansen and Gronvold (2000)	Iceland / Iceland / Bardarbunga / Atlantic Ocean	Basalt	ICPMS	2	1311	1405
Burton et al (2002)	Canary Islands / Gran Canaria / Basalt Series Iv / Atlantic Ocean	Picrite	EMP	4	1280	2890

Table 8.17: The range of Ni values in analyses of olivine minerals. ICPMS; Inductively Coupled Plasma Mass-Spectrometry; LA: Laser ablation; EMP: Electron microprobe. This data was compiled using the GEOROC database (2005).

As spinel minerals have been observed in these rocks (chapter 3), it is thought likely that the Cr has partitioned into these phases. In a situation where Cr has partitioned

into olivine, it would be expected that the higher Cr values would form uniform zones. However, in the Tulu Dimtu Main Intrusion (figure 8.4C) several isolated samples with high Cr values occur – an observation which is consistent with the concentration of Cr within discrete spinel minerals. In most spinel-bearing complexes, Cr-spinels precipitate with olivine early during fractional crystallization and/or relate to an increase in fO_2 (Barnes and Roeder, 2001). The refractory nature of the spinels mean that they will not go into solution easily in aqua regia. It is likely that the Cr values found in the analyses presented here represent Cr partitioned mainly into olivine and to a small degree into spinel. With this in mind, a rock with a high Cr value remains a relatively primitive rock.

It is proposed here that as a partial melt rose through the Earth's crust, olivine precipitated and took Cr and some Ni into its crystal structure. As silicates continued to crystallise from the melt a point came whereby the dissolved sulphides became immiscible (Naldrett and von Gruenewaldt, 1989). When this occurred, Ni was scavenged from the silicate melt into the immiscible sulphide liquid. Subsequently sulphur saturation of the magma occurred and Ni-bearing (and possibly Cu-bearing) sulphides crystallised. After these immiscible sulphides had precipitated, Ni continued to be partitioned to a lesser degree into the olivine and oxides in the more evolved rocks. Simultaneously as olivine crystallised, discrete spinel minerals precipitated into which Cr partitioned. It can be suggested that the rocks of the western and southern flanks of the Tulu Dimtu Main Intrusion are the most primitive and that progressive fractionation was directed towards the centre of the intrusion.

It could be argued that the action of sulphur in concentrating Ni is not relevent due to the low sulphur content. Only one fresher ultramafic rock returned S values above detection limits (0.02% found in DTR-007-02). However, Peregoedova and Ohnenstetter (2002) argue that a high fS_2 can be obtained in low-S magmas through fractionation of the silicate melt and immiscibility of the sulphides (8.6.5).

It is not possible to rule out the effects of re-mobilisation of Ni by late or post magmatic hydrothermal fluids. It is likely that hydrothermal fluids have remobilised Ni in

these rocks to some degree. However, as shown in section 8.3.1 the rocks classed as "fresher" in this study all retain Mg values which are as high as can be expected for a typical fresher dunite or clinopyroxenite. Therefore, these samples cannot have been subjected to pervasive alteration, however it is still possible that some limited action of hot fluids may have affected the Ni values (in the order of 100's of ppm) without a significant difference in Mg values. Narrow veinlets containing Ni-bearing phases may cross-cut an otherwise fresher sample and this is documented in chapter 3. However, unlike Ni, Cr is not known to be remobilised by hydrothermal fluids – even from olivine - and shows similar zoning to Ni and this therefore, supports the fractionation hypothesis.

8.7.2. Locations of highest copper and chromium values in fresher rocks

The highest values of Cu in the fresher rocks (16ppb in two samples) occur 200m from the southern flank of the intrusion. The highest Cr values occur in a different sample located close by (<100m). The highest values of Cu and Cr do not occur with the highest Ni values – which are located over 1km away.

Although crystal fractionation and the immiscibility of sulphides can explain the Ni values and some of the Cr values, this model (section 8.7.1) cannot explain why the highest Cu values are located in a different location from Ni. Furthermore, it cannot explain why the highest Cr values occur close to the highest Cu but not Ni. In a situation where sulphide minerals crystallise at the same time Cr partitions into olivine, the highest Ni and Cu values would initially occur close to the highest Cr values. Subsequently, the Cu may be moved away from the highest Ni and Cr by either filter-pressing or high temperature fluids (see below). Here, the close proximity of the highest Cu and Cr values and their dislocation from the highest Ni values suggests that a different or more complex model is required. In this section two possible explanations are discussed, firstly a combination of filter-pressing and magma-mixing and secondly the remobilisation of Cu.

During filter-pressing, the Ni-rich MSS precipitates and then the Cu-rich residual sulphide liquid migrates away from the MSS by the compaction of the cumulus olivines.

8.7.3. Trace element distribution in fresher rocks of the Lensoid Ultramafics

Ni values in the limited number of fresher samples from the Lensoid Ultramafics are above 1000ppm but lower than 3000ppm and Cr values are higher than 100ppm. These values are similar to those seen close to the edge of the Tulu Dimtu Main Intrusion. The Ni values are low enough for this element to be taken into the crystal structure of olivine without the involving other phases. The Cr values are comparable to those seen on the western flank of the Tulu Dimtu Main Intrusion. By comparison with the Tulu Dimtu Main Intrusion, it is inferred that these rocks crystallised before sulphide saturation. It is plausible that these smaller ultramafic bodies could be considered as slivers of "sheared-off" material from the flanks of a larger intrusion. Although with only three samples of fresher rocks from the Lensoid Ultramafics these interpretations are preliminary.

8.7.4. Trace element distribution in Shear Zones

The highest value of Ni in the rocks of Tulu Dimtu (11,044ppm) occurs in a sheared rock at the southeastern flank of the Tulu Dimtu Main Intrusion , this is almost twice the highest value seen in fresher rocks (5860ppm). Additionally, a mylonite sample shows Cu values of 148ppm which is much higher than the amount of Cu in fresher rocks which is 16ppm. Two samples within Shear Zones (a mylonite and a talc-schist) show high Cr and Al at over 900ppm and 4% respectively.

The necessary aqueous conditions for the remobilisation of Ni and Cu are obtainable in a mobile belt such as the WES (section 8.6.8). Therefore the presence of Ni and Cu in highly sheared rocks - at values much higher than in fresher rocks - may be the result of the redeposition by hot aqueous fluids transported along Shear Zones.

This leaves the question of how both Al and Cr are concentrated into the samples since Al is to be expected in a felsic protolith and Cr is expected in primitive ultramafics. Given that some altered rocks may more resemble soils it is possible that the Al has been

concentrated by soil-forming processes occurring above a Cr bearing ultramafic protolith or alternatively that two different protoliths have been juxtaposed in the shear-zone.

8.7.5. Zonation of trace elements in altered rocks

The altered rocks of the Tulu Dimtu Main Intrusion show a zonation in Ni and Cr similar to that seen in the zones of the fresher rocks (>3000ppm and >100ppm respectively). Patterns seen in altered rocks but not seen in the fresher samples are that Cu and Al also have high values at the edge of the intrusion (>30ppm and 0.7% respectively). Individual samples from the Lensoid Ultramafics also show elevated values for all four elements in question. Chapter 3 shows that the principle mineral in these samples is serpentine and as a phyllosilicates is likely to be affectively digested by aqua regia along with the sulphides (see section 8.2.3).

The altered samples studied here represent a magmatic signature overprinted by alteration. It has been seen (chapter 2) that the WES has been subjected to considerable deformation and the movement of hydrothermal fluids. This deformation has been observed at Tulu Dimtu by De Wit and Chewaka (1977) who described alteration in Shear Zones flanking the intrusion resulting in a talc-carbonate and serpentine-talc assemblage. It is therefore likely that the same hydrous fluids could have penetrated the flanks of the Tulu Dimtu intrusion to remobilise and precipitate both Ni and Cu. Hence the elevated Ni and Cu values could be the result of either or both hydrothermal remobilisation or magmatic concentration. Cr is unlikely to have been remobilised from its primary position and, therefore, the zonation in high Cr values at the flanks of the intrusion supports similar zones seen in fresher rocks. The values of Cr in an altered rock may be elevated slightly from the equivalent in the protolith, due to changes in volume between fresher and altered rocks (Giggenbach, 1984). Slightly elevated Al values at the flanks of the intrusion may be attributed to the concentration of the element – seen in trace amounts in fresher rocks - during soil-forming. However, the original source of the Al is unknown. For this study, an "altered" rock may be partially affected by soil-forming processes at the start of the transformation from rock to soil.

As with the Tulu Dimtu Main Intrusion, hydrothermal fluids can be invoked to explain the distribution Ni and Cu in the Lensoid Ultramafics. If the Lensoid Ultramafics are considered as deformed slivers of the Tulu Dimtu Main Intrusion (as suggested in section 8.7.3) it is to be expected that they have been subjected to similar and possibly more intense alteration systems due to the deformation required to dismember them from the Tulu Dimtu Main Intrusion. Both Ni and Cu are observed in concentrations much higher than those seen in the fresher samples of the Lensoid Ultramafics and also higher than the altered samples of the Main Intrusion. It is to be expected that the deformation required to dismember the lensoid bodies from the Main Intrusion is greater than that seen at the flanks of the Main Intrusion itself. It is possible that the subsequent alteration will have been more intense and the potential for concentration of Ni and Cu greater as a result. However, hydrothermal fluids may also act to disperse the elements which are soluble within them.

8.7.6. Genesis of Pt and Pd in fresher rocks

Three fresher dunites from the Tulu Dimtu Main Intrusion contain significant Pt and/or Pd values (TD10, TD9 and TDR 19/01). Each of these three samples contains significant amounts of either Ni, Cu and/or Cr and the variations of these elements are summarised in table 8.13 and figure 8.3. The three Pt- and Pd-bearing samples are located close to another fresher dunite (TD12) which is barren of both elements but contains the highest Cu value.

A model to explain the origin of the high Cr value found in sample TD9 by the mixing of a fresher primitive magma is outlined in section 8.7.2 and this can also explain the high Ni value as it will concentrate strongly into the early crystallised olivines. Naldrett and von Gruenewaldt (1989) have determined that magma mixing may account for sulphide segregation where an advanced differentiate (precipitating plagioclase) mixes with a primitive melt (see section 8.6.7). However plagioclase is not observed in the ultramafics from the Tulu Dimtu Main Intrusion and therefore this is seen as unlikely.

The model used to explain the dislocation of Cr and Cu anomalies from Ni (see section 8.7.2) can be used to explain the Pt and Pd distribution. In this model the Pt and Pd was filter pressed into the fresher cumulate pile along with the Cu-rich residual sulphide liquid.

As with Cu, the locations of the highest Pt and Pd values can be explained on the basis of either magmatic processes (filter-pressing) or alteration. The Pt and Pd of sample TDR 19/01 (see table 8.13) could be explained as being partitioned into a Cu-bearing residual sulphide liquid which was subsequently filter-pressed through the pile of cumulate olivines so that it is separated from the crystallised Ni-rich MSS (as described in section 8.6.6). A similar explanation may be given for the Pt- and Pd-barren sample TD12, however in this case the ISS crystals precipitated from the sulphide liquid after the precious metals had already partitioned out of this melt.

Alternatively, both Pt and Pd in each sample could have been remobilised along with Cu. The origin of high Pd in sample TD10 is hard to explain by magmatic processes as Pt should behave similarly in a magma. The absence of Pt indicates that a Pd mineral was present in this sample. The Cu value is too low to conceive the presence of residual sulphides and the Ni value is low enough to be partitioned into olivine alone. It is possible that the anomalous Pd value may have been transported in by aqueous fluids, as this is seen frequently in other deposits (section 8.6.8). The reason for the dislocation of Pt and Pd from the areas of the highest Ni can only be determined through the analysis of the morphology of the PGM.

8.7.7. Genesis of Pt and Pd in altered rocks

Pt- and Pd-bearing altered rocks occur at different locations in the Main Intrusion (figures 8.4E and 8.4F). The dislocation of Pt and Pd anomalies at the flanks of the Tulu Dimtu Main Intrusion could be explained by the preferential transport of Pd away from the sites of magmatic concentration (see section 8.6.8). The preferential remobilisation of Pd over Pt has been documented by many other authors (for example Oberthür et al.,

2003; Prichard et al., 1996). The sites of magmatic PGE concentration are likely to occur at the flanks of the intrusion which is also where hydrothermal fluids are likely to act. So the two modes of transport are likely to have been superimposed.

There are seven Pt- and Pd-bearing rocks outside of the Tulu Dimtu Main Intrusion and these are from the Shear Zones, Lensoid Ultramafics and basement units (see section 8.5.2). Five of these samples contain higher Pd values than Pt. Of particular note is a chlorite schist which returned values of 9ppb for Pt and 41ppb for Pd. This further suggests that Pd has been preferentially reconcentrated by hydrothermal fluids in the area. The higher Pd values than Pt in the Lensoid Ultramafics may indicate the redeposition of Pd in these complexes as the chlorite schist is likely to contain precipitates from the alteration fluids.

8.8. Tulu Dimtu: Conclusions

Throughout the Tulu Dimtu area, distinguishing the effects of hydrothermal alteration from magmatic processes is difficult. The geochemical analyses discussed in this chapter suggest that both hydrothermal and magmatic processes are likely influence Pt and Pd grade at the flanks of the intrusion. Consequently, it is recommended that any further exploration activities are focussed in these areas.

Some preliminary ideas have been proposed to explain the development of Pt and Pd in the fresher rocks of the Tulu Dimtu Main Intrusion. A large variation Cr values between the centre and the edges of the intrusion indicate that the most primitve rocks occur at the edge of the complex. Further variations in Cr value may indicate the presence of a second melt influx. A series of processes may then have occurred to concetrate Pt and Pd from the magma. High Ni values and significant vairaitions in Cu values indicate that sulphide immiscibility and fractionation may have occurred, in such a situation the Pt and Pd would be associated with the Cu-rich residual sulphide.

Although sulphide fractionation may explain the dislocation of Cu and Ni values, it is also possible that the Cu – along with Pt and Pd - could have become remobilised by hot aqueous fluids and then redeposited close to magmatic Cr-spinels. Analysis of PGM and sulphide mineralogy is required to test the filter-pressing and hydrothermal models. Furthermore, there is no direct evidence for the influx of a fresher batch of melt, it is nessecary for this to be validated using spinel geochemistry (see chapter 9).

A limited number of fresher ultramafic samples from the Lensoid Ultramafics have been described, these indicate that the samples formed after chromite precipitation but before sulphur saturation. These complexes may be slivers from the edges of larger intrusions, such as the Tulu Dimtu Main Intrusion.

From the presence of Ni and Cu in shear-zone related lithotypes it can be inferred that either during or after the deformation of the Lensoid Ultramafics hydrothermal fluids have been directed along Shear Zones. Furthermore, these fluids may have permeated and circulated around the flanks of the Tulu Dimtu Main Intrusion thereby remobilising and re-precipitating Ni and Cu. Both Pt and Pd are also likely to have been taken into solution, but Pd to a much greater extent. Hence, the locations of Pt and Pd anomalies have become separated (figure 8.4E and 8.4F).

8.10. Kingy: Selected Major and Trace Elements

8.10.1. Introduction

A total of 110 rock samples of the Kingy area were examined. According to the classification method set out in section 8.3.1, six of the samples are classed as fresher ultramafic rocks and 33 are classed as altered ultramafic rocks. The remaining 67 are samples of either basement rocks. There are no fresher ultramafic samples from the Kingy Ridge Ultramafic, but 2 from the Extra Ultramafic and 4 from two of the Lensoid Ultramafics. Due to dense vegetation, rock samples from the Kingy Ridge Ultramafic were only taken along the flanks, where the tracks occur.

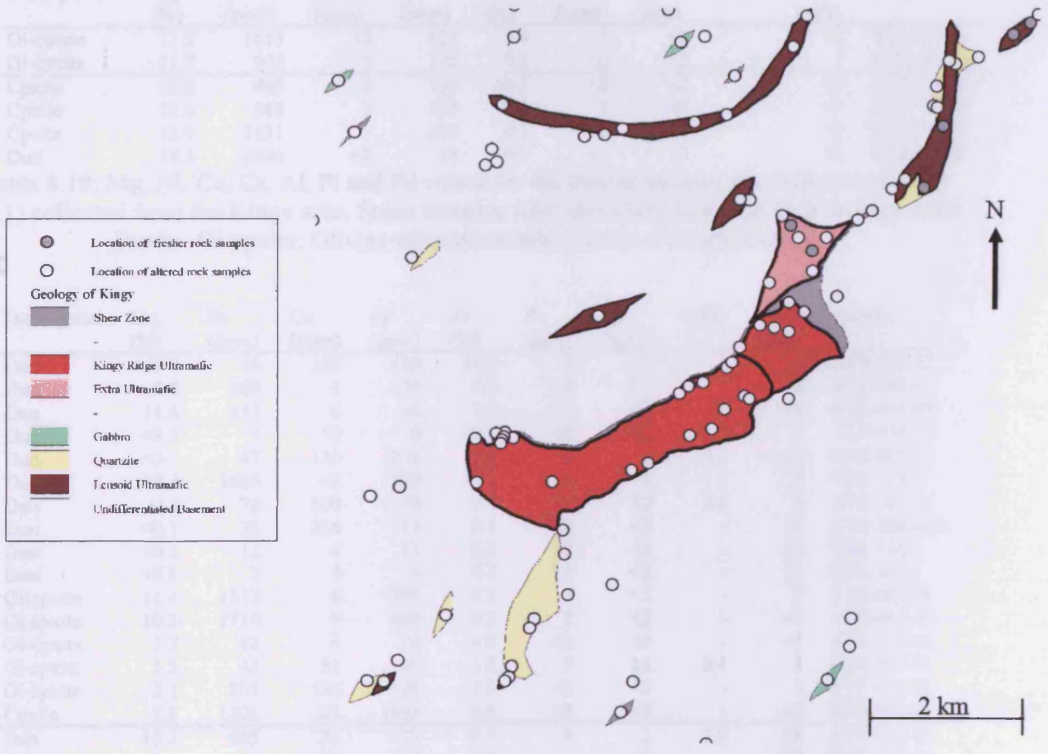

Figure 8.5: The distribution of rock samples within the Kingy area.

Formation	#	Altered ultramafic rocks	Fresher ultramafic rocks	Non-ultramafic rocks	Birbirite samples

Shear Zones	15	0	0	15	0
Kingy Ridge Ultramafic	24	16	0	4	4
Extra Ultramafic	7	5	2	0	0
Gabbro	4	0	0	4	0
Quartzite	115	0	0	15	0
Lensoid Ultramafics	21	12	4	5	0
Basement	24	0	0	24	0
TOTAL	**110**	**33**	**6**	**67**	**4**

Table 8.18: A summary of the samples from the Kingy area. The classification of fresher and altered rocks is covered in section 8.3.1 and the classification of ultramafic lithotypes is covered in chapter 3.

8.10.2. Data

Formation	Description	Mg (%)	Ni (ppm)	Cu (ppm)	Cr (ppm)	Al (%)	Pt (ppb)	Pd (ppb)	Pt/Pd	Au (ppb)	Sample
Extra Ultramafic	Ol-cpxite	11.2	1615	13	833	0.4	3	<2	-	<2	KTR-052-0
	Ol-cpxite	11.7	995	5	198	0.2	<2	<2	-	2	KTR-061-0
Lensoid Ultramafics	Cpxite	12.0	485	2	100	<0.1	<2	<2	-	<2	ATR-130-0
	Cpxite	12.6	548	2	107	0.1	3	<2	-	<2	ATR-132-0
	Cpxite	15.0	2131	5	200	0.1	<2	<2	-	<2	KTR-069-0
	Dun	18.3	4646	<2	59	<0.1	<2	<2	-	<2	KTR-072-0

Table 8.19: Mg, Ni, Cu, Cr, Al, Pt and Pd values for the fresher samples (as defined in section 8.3.1) collected from the Kingy area. Some samples were identified as fresher by petrology. Dun: Dunite. Ol-cpxite: Olivine-clinopyroxenite. Cpxite: Clinopyroxenite.

Formation	Description	Mg (%)	Ni (ppm)	Cu (ppm)	Cr (ppm)	Al (%)	Pt (ppb)	Pd (ppb)	Pt/Pd	Au (ppb)	Sample
Kingy Ridge Ultramafic	Dun	<0.1	16	168	438	14.6	7	<2	-	3	ATR-078-02
	Dun	9.8	100	4	179	8.2	<2	<2	-	<2	ATR-085-02
	Dun	11.8	147	6	45	7.7	<2	<2	-	<2	ATR-090-02
	Dun	<0.1	1	10	8	<0.1	<2	<2	-	8	ATR-094-02
	Dun	<0.1	47	139	273	0.4	2	3	0.7	<2	KTR-057-02
	Dun	10.3	1665	<2	778	0.2	7	4	1.8	2	TDR 31/01
	Dun	0.3	78	100	50	0.8	<2	10	0.0	2	ATR-081-02
	Dun	<0.1	35	216	13	0.1	<2	<2	-	16	ATR-094A-02
	Dun	<0.1	12	4	12	0.2	<2	<2	-	19	TDR 33/01
	Dun	<0.1	2	3	6	0.1	<2	<2	-	21	TDR 34/01
	Ol-cpxite	11.4	1512	8	790	0.2	5	<2	-	2	ATR-083-02
	Ol-cpxite	10.2	1718	9	692	0.2	5	<2	-	<2	ATR-084-02
	Ol-cpxite	7.7	42	4	24	4.6	<2	<2	-	<2	ATR-131-02
	Ol-cpxite	1.5	42	81	66	2.8	5	13	0.4	3	KTR-049-02
	Ol-cpxite	2.1	201	136	178	2.5	<2	<2	-	3	KTR-058-02
	Cpxite	8.8	1201	21	1993	8.8	<2	<2	-	<2	KTR-047-02
Extra Ultramafic	Dun	10.2	585	71	652	0.5	4	2	2.0	<2	ATR-089-02
	Dun	5.3	963	24	747	1.0	4	<2	-	<2	KTR-051-02
	Dun	0.2	24	77	28	0.6	<2	9	0.0	13	KTR-053-02
	Dun	1.1	171	183	50	1.7	<2	28	0.0	825	KTR-062-02
	Cpxite	9.4	697	13	449	4.7	3	<2	-	2	DTR-057-02
Lensoid Ultramafics	Dun	3.3	446	65	384	4.0	<2	<2	-	2	ATR-126-02
	Dun	0.1	8	53	13	0.3	<2	3	0.0	2	KTR-055-02
	Dun	1.5	24	27	12	2.3	<2	6	0.0	2	TTR-040-02
	Ol-Cpx	5.6	606	7	798	5.7	8	4	2.0	<2	ATR-063-02
	Ol-Cpx	3.5	304	64	702	4.5	3	6	0.5	2	ATR-064-02
	Ol-Cpx	4.0	324	32	997	3.3	6	6	1.0	<2	ATR-071-02

	Ol-Cpx	0.6	81	36	101	1.2	<2	<2	-	<2	ATR-080-02
	Ol-Cpx	0.7	13	41	22	1.8	<2	<2	-	<2	DTR-063-02
	Ol-Cpx	2.3	246	3	285	2.1	3	3	1.0	2	TTR-041-02
	Cpxite	2.2	224	26	139	2.4	<2	<2	-	2	ATR-125-02
	Cpxite	3.8	656	174	468	4.1	3	<2	-	<2	ATR-127-02
	Cpxite	11.5	465	5	11	6.9	<2	<2	-	<2	KTR-066-02
	Anor	<0.1	5	13	3	0.4	<2	<2	-	<2	ATR-067-02
	Basa	<0.1	5	15	18	0.3	5	4	1.3	4	ATR-098-02
	Basa	0.9	12	39	15	1.5	5	15	0.3	2	ATR-105-02
	Basa	2.2	82	187	30	3.2	5	8	0.6	4	TTR-031-02
	Basa	0.4	78	14	7	0.3	<2	<2	-	<2	TTR-033-02
	Birb	0.1	1178	145	329	0.3	2	<2	-	<2	ATR-087-02
	Birb	<0.1	48	152	43	1.6	4	11	0.4	32	KTR-043-02
	Birb	15.7	1999	2	1733	0.3	6	<2	-	8	TD22
	Birb	0.3	760	8	436	<0.1	<2	<2	-	2	TDR 32/01
	Dior	0.2	28	125	55	2.8	<2	<2	-	<2	DTR-062-02
	Dior	1.9	35	223	18	3.6	4	15	0.3	<2	KTR-065-02
	Dior	0.4	59	3	7	0.8	<2	<2	-	<2	KTR-074-02
	Dole	0.6	51	67	154	1.4	10	11	0.9	5	ATR-066-02
	Dole	1.3	56	14	40	1.7	6	7	0.9	<2	ATR-069-02
	Dole	0.8	80	86	77	2.4	<2	<2	-	3	ATR-087A-02
	Dole	0.9	3	23	4	1.3	<2	<2	-	2	ATR-107A-02
	Dole	0.2	8	20	75	6.0	5	10	0.5	<2	ATR-111-02
	Dole	2.2	103	78	225	2.8	<2	<2	-	3	TTR-042-02
	Fels	1.2	30	19	4	1.9	<2	<2	-	<2	ATR-062-02
	Gabb	2.4	57	43	12	3.2	<2	5	0.0	2	ATR-059-02
	Gabb	1.0	26	72	27	1.3	<2	<2	-	2	ATR-093-02
	Gabb	1.1	50	263	35	1.2	<2	<2	-	<2	ATR-109-02
	Gabb	0.7	8	66	16	1.2	2	10	0.2	3	ATR-118-02
	GranDi	1.1	13	4	16	1.6	<2	<2	-	<2	ATR-100-02
	GranDi	0.1	3	5	4	0.4	<2	<2	-	<2	ATR-112-02
	GranDi	0.2	3	3	3	1.0	<2	<2	-	<2	ATR-113-02
	GranDi	<0.1	2	29	15	0.6	<2	3	0.0	<2	ATR-114-02
	GranDi	<0.1	<2	11	5	0.5	<2	<2	-	<2	ATR-115-02
	GranDi	<0.1	21	34	14	0.1	<2	<2	-	5	KTR-039-02
	HardP	<0.1	17	112	66	1.7	<2	<2	-	2	ATR-079-02
	HardP	0.2	755	149	1099	0.8	6	<2	-	2	ATR-086-02
Other	HardP	<0.1	80	126	363	2.0	<2	<2	-	<2	ATR-104-02
	HardP	0.1	306	82	266	1.2	<2	<2	-	5	ATR-122-02
	HardP	0.4	16	22	159	0.7	<2	<2	-	<2	TTR-045-02
	MetaBas	3.0	378	30	422	2.7	2	<2	-	2	TTR-043-02
	MetaBas	1.4	37	155	31	2.0	<2	<2	-	3	TTR-044-02
	MetaSed	0.2	21	32	9	0.3	<2	2	0.0	<2	ATR-134-02
	Mylo	1.1	43	80	115	1.4	3	10	0.3	3	ATR-072-02
	Mylo	<0.1	6	111	5	0.7	2	10	0.2	<2	ATR-117-02
	Mylo	1.4	36	46	152	1.7	18	19	0.9	4	TTR-035-02
	Quar	0.1	<2	4	4	0.1	<2	<2	-	<2	ATR-103-02
	Quar	<0.1	1	4	12	0.1	<2	<2	-	13	ATR-107-02
	Quar	<0.1	7	5	6	<0.1	<2	<2	-	<2	ATR-123-02
	Quar	4.6	<2	<2	6	<0.1	<2	<2	-	<2	ATR-124-02
	Quar	0.1	37	12	39	0.1	<2	<2	-	<2	ATR-128-02
	Quar	<0.1	4	3	4	0.1	<2	<2	-	2	DTR-054-02
	Quar	0.2	21	2	27	0.2	<2	<2	-	<2	DTR-061-02
	Quar	<0.1	6	32	3	0.1	<2	<2	-	3	DTR-064-02
	Quar	0.2	20	7	12	0.1	<2	<2	-	2	KTR-037-02
	Quar	<0.1	9	7	8	0.1	<2	<2	-	19	KTR-038-02
	Quar	<0.1	5	9	8	0.1	<2	<2	-	<2	KTR-040-02
	Quar	0.3	55	52	42	<0.1	<2	<2	-	8	KTR-054-02
	Quar	<0.1	4	9	5	0.1	<2	<2	-	<2	KTR-056-02
	Quar	9.7	38	10	3	<0.1	<2	<2	-	<2	KTR-070-02
	Quar	<0.1	8	5	11	<0.1	<2	<2	-	2	TDR 29/01
	Schi	1.5	25	49	14	2.1	<2	5	0.0	<2	TD19
	Schi	0.1	6	2	<2	0.8	<2	<2	-	2	TTR-034-02
	Sed	0.2	144	83	77	2.5	3	4	0.8	6	ATR-088-02
	TaSchi	0.6	84	68	698	0.3	8	8	1.0	<2	ATR-092-02
	TaSchi	0.2	8	4	2	0.8	<2	<2	-	<2	DTR-053-02
	TaSchi	0.3	532	16	538	0.2	5	3	1.7	<2	KTR-044-02
	TaSchi	0.4	88	87	180	0.1	9	10	0.9	5	KTR-063-02
	Unid	<0.1	73	72	28	0.5	<2	<2	-	2	KTR-043B-02
	Unid	7.4	318	2	1626	0.7	6	<2	-	<2	KTR-048-02

Unid	0.1	972	11	347	0.2	4	<2	-	<2	KTR-050-02
VQuar	0.1	10	<2	8	0.1	<2	<2	-	<2	DTR-059-02
VQuar	0.1	34	8	10	0.1	<2	<2	-	2	KTR-064-02
VQuar	0.1	11	7	11	0.1	<2	<2	-	5	TD20
VQuar	<0.1	4	4	10	0.1	<2	<2	-	1262	TD21
VQuar	0.1	11	<2	28	0.1	<2	<2	-	<2	TDR 28/01
VQuar	<0.1	2	7	11	0.1	<2	<2	-	3	TDR 30/01

Table 8.20: Mg, Ni, Cu, Cr, Al, Pt and Pd values for the altered samples collected from the Kingy area. Anor: Anorthosite. Basa: Basalt. Birb: Birbirite. ChSchi: Chlorite-Schist. ChSchi: Chlorite-Schist. Cpxite: Clinopyroxenite. Dior: Diorite. Dole: Dolerite. Dun: Dunite. Fels: Felsite. Gabb: Gabbro. GranDi: Granodiorite. HardP: Hard pan. MetaBas: Metabasalt. MetaSed: Metasediment. Mylo: Mylonite. Ol-cpxite: Olivine-clinopyroxenite. Quar: Quartzite. Schi: Schist. Sed: Sediment. TaSchi: Talc-Schist. TCSchi: Talc-Chlorite-Schist. Troc: Troctolite. Unid: Unidentified. VQuar: Vein Quartz.

The following sections cover the distribution of Ni, Cu, Cr and Al in the Kingy area. Each section covers one element and describes its distribution in fresher ultramafics and altered rocks. These sections are accompanied by a fold-out page (page 229) of maps showing the distribution of all elements which the reader should refer to as each section is read.

8.10.3. Nickel

The highest Ni value in the fresher ultramafic samples is 4646ppm in a dunite located within the large Lensoid Ultramafic in north-eastern side of the Kingy area. Another sample in the same body shows Ni at 2131ppm all other Ni values are below 2000ppm but not lower than 485ppm.

The altered rocks from the Kingy Ridge Ultramafic show that the highest Ni abundances (1718ppm) occur in the centre and decrease to below detection limits towards the southwest and northeast (figure 8.7A). Elsewhere, the Ni contents in the altered ultramafics rise to a maximum of 963ppm in the Extra Ultramafic but 5 samples fall to as low as 8ppm in a Lensoid Ultramafic body. Within the basement units and quartzites, Ni remains below 100ppm and frequently falls below detection limits.

8.10.4. Copper

All Cu values in the samples of fresher ultramafics from the Kingy ridge are lower than or equal to 13ppm. The highest value of Cu (13ppm) occurs in a pyroxenite from the Extra Ultramafic all other Cu values are lower than 5ppm.

In altered rocks, the highest Cu value in the area (263ppm) occurs in an isolated gabbro body to the south-east of the study area (figure 8.7B). Of the ultramafic complexes, the highest Cu occurrences (up to 216ppm) lie in the altered dunites from the Kingy Ridge Ultramafic but some samples of the same rock formation contain Cu values below detection limits. The highest value occurs in a dunite on the farthest western point of the complex, Similarly, within the Extra Ultramafic the highest value (183ppm) occurs close to the bounding shear-zone.

8.10.5. Chromium

The highest Cr value in fresher rocks (833ppm) occurs in a pyroxenite from the Extra Ultramafic. All other Cr values in fresher rocks lie below 200ppm, the lowest of which is 59ppm in a dunite of the large northwestern Lensoid Ultramafic.

High Cr values (>200ppm) in altered rocks only occur in the ultramafic complexes and related shear-zones. The highest Cr values in altered rocks (up to 1993ppm in an olivine-clinopyroxenite occur close to the centre of the Kingy Ridge Ultramafic (figure 8.7C). The values drop to below 200ppm on the southwestern end of Kingy Ridge Ultramafic forming a crude zonation from northwest to southeast, where the lowest value is 6ppm in a dunite. Samples from the Lensoid Ultramafics contain intermediate Cr values, from 200ppm to 1000ppm.

8.10.6. Aluminium

The fresher rocks at Kingy contain up to 0.4% Al, this figure is obtained from an olivine-clinopyroxenite from the Extra Ultramafic. All other fresher ultramafics contain less than 0.2% Al.

The four largest Al values (>7%) in the altered rocks occur in samples from the Kingy Ridge Ultramafic. The highest Al value (14.6%) occurs in an altered dunite within the south western part of the Kingy Ridge Ultramafic. Al is enriched (over 5%) in some rocks from the Kingy Ridge Ultramafic and the Extra Ultramafic (figure 8.7D). Values of Al can drop below detection limits in rocks from both the Basement and the Kingy Ridge Ultramafic. The altered Lensoid Ultramafics display Al contents between 0.6% and 5% (see figure 8.7D).

8.10.7. Summary of Ni, Cu, Cr and Al distribution in the Kingy Ridge Ultramafic and Extra Ultramafic

No fresher samples are available from the Kingy Ridge Ultramafic but a sample from the Extra Ultramafic contains the highest values of Cu, Cr and Al of the fresher samples (see figure 8.6). This sample is located on the northernmost corner of the Extra Ultramafic complex.

Some spatial trends in Ni and Cr are observed in the altered dunites from the Kingy Ridge Ultramafic. The highest values of Ni and Cr occur in the central and northeastern end of the intrusion. These values drop to low values towards the southwestern end of the ridge. Unlike Ni and Cr, both Cu and Al are distributed unevenly in the Kingy Ridge Ultramafic. The four highest Al values come from samples located in the Kingy Ridge Ultramafic. A different sample contains the largest Cu value in the complex.

8.10.8. Summary of Ni, Cu, Cr and Al distribution in the Lensoid Ultramafics

The two highest Ni values in the Kingy area (4646ppm and 2131ppm) occur in the fresher rocks from the large northwestern Lensoid Ultramafic. Ni values in the altered Lensoid Ultramafics are much lower. Cu values are high, sometimes over 120ppm. Cr and Al values are intermediate compared to the Kingy Ridge Ultramafic.

8.10.9. Summary of Ni, Cu, Cr and Al distribution in the Isolated Gabbro

The highest Cu values (263ppm) occur in an altered gabbro sample in the southeastern quadrant of the Kingy area.

8.11. Kingy: Pt and Pd distribution

Aall Pt and Pd values from the fresher rocks of the Kingy area are almost below detection. Two fresher rocks resulted in assays of Pt at 3ppb each. One was an olivine-clinopyroxenite from a Lensoid Ultramafic (KTR-052-02) and the other was a pyroxenite from the small northeastern Lensoid Ultramafic (ATR-132-02). No Pd was found above detection limits in the fresher rocks from the Kingy area.

In altered rocks, assays for Pt and Pd in the samples from the Kingy area are dominated by Pd where 14 of 104 samples have >8ppb Pd and only 3 samples returned a Pt assay of >8ppb (see figures 8.7E and 8.7F). The highest Pd grade (28ppb) occurs in an altered dunite from the Extra Ultramafic and the highest Pt grade (18ppb) occurs in a clinopyroxenite from the Lensoid Ultramafics (figure 8.7E). In the Kingy Ridge Ultramafic the highest Pt value is 7ppb and occurs twice in two dunite samples. An olivine-clinopyroxenite showed the largest Pd assay of 13ppb. The three highest Pd assays occur at the periphery of the complex. The highest Pt and Pd values in the altered samples of the Lensoid Ultramafics occur in an olivine-clinopyroxenite which assays at 6ppb for Pd and 8ppb for Pt. In all ultramafic complexes of the area, both Pt and Pd can be below detection limits.

Of the lithologies associated with Shear Zones, the highest Pt and Pd values occur in the same mylonite sample showing Pt values of 18ppb and Pd values of 19ppb. The next highest Pt value is 9ppb in a talc-schist and the second highest Pd assay is 10ppb and occurs 3 times in two mylonitised samples and one talc-schist. Of the basement units, two dolerite dykes, one diorite and a basalt returned analyses of <10ppb for Pt and <15ppb for Pd and ranging to below detection for both elements. The highest Pt value in the basement (10ppb) occurs in the dolerite and highest Pd values (15ppb) occurring in the basalt and diorite samples.

A comparison between PGE and Ni, Cu, Cr and Al in the highest samples is summarised as follows:

Sample	Description	Pt (ppb)	Pd (ppb)	Ni ppm	Cu ppm	Cr ppm	Al %
KTR-052-02	Olivine-clinopyroxenite	3	< 2	1615	13	833	0.4
ATR-132-02	Pyroxenite	3	< 2	548	2	107	0.1

Table 8.21: A summary of Ni, Cu, Cr and Al values in the dunite samples with the highest Pt and Pd grade from the fresher rocks. A graphical representation of this data is provided in figure 8.6.

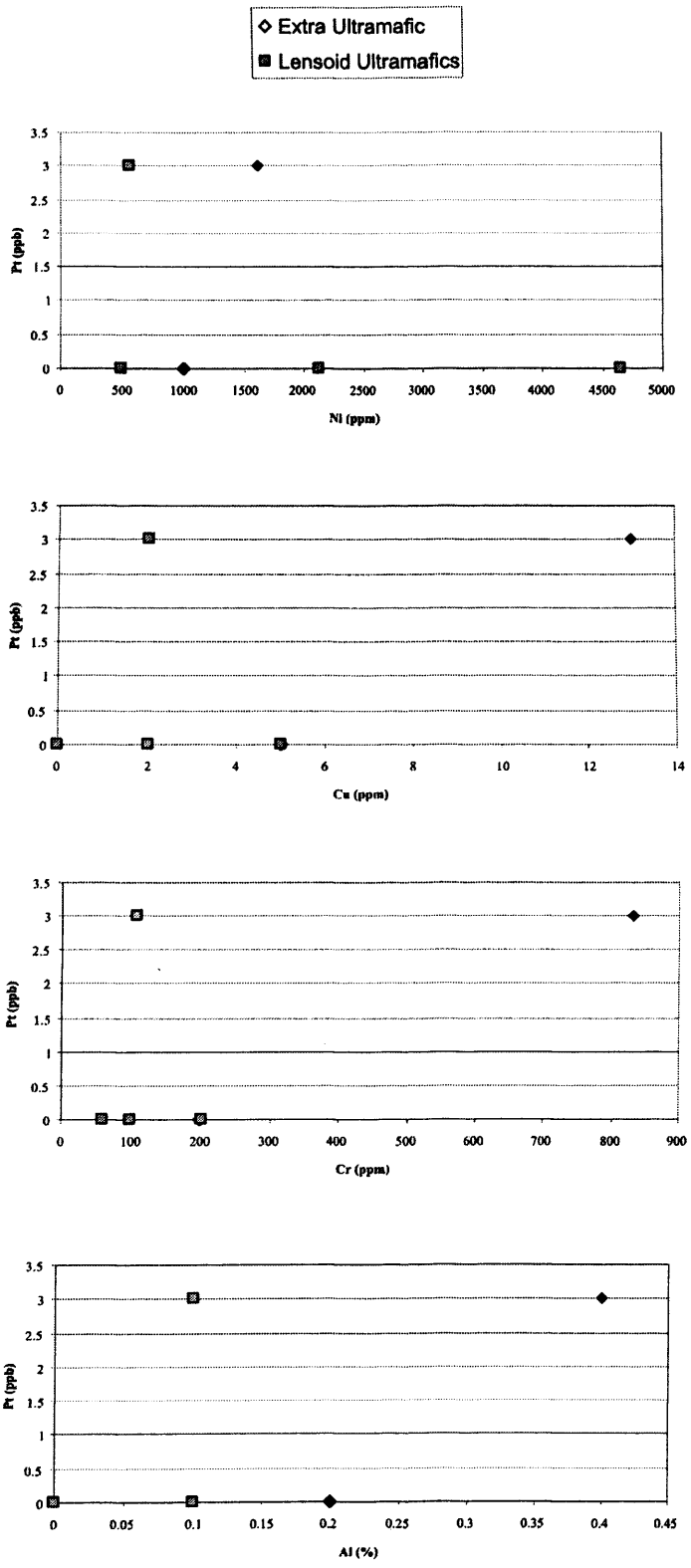

Figure 8.6: Graphs of Ni, Cu, Cr and Al versus Pt in the fresher rocks from the Kingy area. No Pd has been detected in the Kingy area.

8.11.1. Comparison of the geochemistry of the soil versus rock samples

Other than the isolated gabbro body, the largest Pd value in soil occurs above the Extra Ultramafic. Additionally, high Pt and Pd values are more common in soils than rocks. 7% (7 of 104) rock samples returned assays at >12ppb for either Pt or Pd whereas 18% (36 of 202) soil samples assayed above that figure.

8.12. Kingy: Discussion

The processes that involve the distribution of Ni, Cu, Cr and Al in fresher ultramafics are considered in 8.12.1 and 8.12.2, followed by those processes which affect altered rocks in 8.12.3 and 8.12.5. The mechanisms which distribute Pt and Pd are considered from section 8.12.6 to section 8.12.7.

8.12.1. The locations of the highest Ni and Cu values in fresher rocks

The difference in location of the highest Cu values and the highest Ni could be explained by the process of filter-pressing (see section 8.6.6). This is where an immiscible sulphide liquid fractionates then the Cu-rich liquids migrate through interstitial space to become located with more evolved rocks. Alternatively, hot aqueous fluids could have remobilised the Cu and reconcentrated it away from the site of magmatic concentration. The study of mineral morphology is required in order to understand the degree of influence of high temperature fluids on Cu mineralisation.

Although it appears that the Cu and Ni highs occur in two separate complexes, the ultramafic complexes of the Kingy area could have become dismembered from one conformable unit. Johnson et al. (2004) discuss the tectonic evolution of the WES and transcurrent movement along a NE-SW striking faults (D_3). A reconstruction of this deformation may bring the highest Ni and Cu values to within 500m of each other.

8.12.2. Locations of highest Cu and Cr values in fresher rocks

Sample KTR-052-02 from the Extra Ultramafic, contains the highest Cu and Cr values of the fresher rocks from the Kingy area (13ppb and 833ppb respectively). As discussed for a similar situation in the Tulu Dimtu Main Intrusion (see section 8.7.2), if the Cu-rich residual sulphide is filter-pressed away from the MSS then it will be forced into the more evolved cumulate pile, with less Cr. However, if a new primitive magma is mixed with a slightly evolved melt then chromite will precipitate and consequently, the residual sulphide could be filter-pressed against primitive chromite grains. Unlike the same observations made at the Tulu Dimtu Main Intrusion, the Cu analyses made here are sufficiently low that it is difficult conlude that sulphide segregation has occurred.

An alternate explanation for the location of the highest Cu values is that both Ni and Cu were located in the same location by sulphides and subsequently, later hydrothermal fluids have brought Cu into contact areas of high Cr. This assumes the preferential remobilisation of Cu over Ni. Furthermore, the small amount of Cu may have been deposited in it's position by hydrothermal fluids themselves.

8.12.3. Zonation of Ni and Cr in altered rocks from the Kingy Ridge Ultramafic

In the Kingy Ridge Ultramafic the Ni and Cr values in altered rocks drop steadily towards the southwestern end of the intrusion (see figure 8.6A and 8.6C). It is likely that the Cr has been partitioned into the spinels which have been observed in these rocks (see chapter 3). However, given the refractory nature of spinels, it is likely that the Cr analysed here was partitioned into the olivine lattice. Hence it is likely that the highest Cr values in altered rocks mark the most primitive part of the complex with apparent fractionation directed towards the south-western end of the intrusion. As Ni is compatible in olivine (see section 8.6.2) the trend seen in its concentration could also be attributed to fractionation. However due to the mobility of the element under hydrothermal conditions (see section 8.6.8), the role of alteration on the control of this distribution cannot be eliminated.

8.12.4. Uneven Cu and Al distribution in the altered rocks from the Kingy Ridge Ultramafic

The distribution of Cu and Al shows no distinct spatial pattern (see figures 8.6B and 8.6D). As Cu is known to be easily taken into solution in hydrothermal fluids of various conditions (see section 8.6.8) it is expected that the Cu has been remobilised and precipitated in association with hydrous phases throughout the complex. As Ni is soluble in similar fluids, it would be expected that it would show a similar distribution to Cu – however this is not the case. There are two possible explanations for this. Firstly, the two elements may have been remobilised by different alteration episodes under slightly different conditions or acting on different areas. Or secondly, that Ni has not been remobilised which would mean that the distribution observed (section 8.12.3) is magmatic in origin as suggested by its similarity to the Cr distribution.

Slightly elevated Al values in places throughout the intrusion may be attributed to the concentration of the element – seen in low amounts in fresher rocks - during soil forming. A study of the degree of alteration is out of the scope of this study and therefore an "altered" rock – as classified here - may be partially affected by soil forming processes.

8.12.5. Trace element distribution in the altered rocks from the Lensoid Ultramafics

Nickel values in the altered Lensoid Ultramafics are typically low and Cu values are high. Cr and Al values are intermediate when compared to the Kingy Ridge Ultramafic. The elevation of Cu values above those found in fresher rocks (<13ppm) could be attributed to alteration as hydrothermal fluids can take large amounts of Cu into solution (see section 8.6.8). The Ni values are low enough that the element could be completely contained within the olivine crystal structure, without the presence of sulphide or alteration phases although the effect of both cannot be ruled out. The low mobility of Cr-spinels means that the intermediate Cr values indicate that the fresher protoliths could have been primitive or slightly evolved – as Cr value could be increased

slightly due to volume loss from fresher rocks (see section 8.6.8). The relatively minor degree of fractionation show by the Cr values in these rocks means that they could represent slivers of rock "shaved" off from the flanks of a larger complex such as the Tulu Dimtu Main Intrusion.

8.12.6. Genesis of Pt and Pd in fresher rocks

Almost no Pt or Pd has been detected in the fresher rocks of the Kingy area. Two fresher samples are Pt-bearing (3ppb each) and no Pd has been detected in the Kingy area.

Section 8.7.2 discusses the origin of the high Cu and Cr values in sample KTR-052-02 and it is possible that sulphide segregation and fractionation has occurred - yet the Pt value is very low. If the conditions have been set for the concentration of the PGE in the magma and it remains that very little has been found then it is possible that the magma was not Pt enriched before sulphide segregation. However, the Cu value in such samples is very low and it is therefore considered difficult to demonstrate that sulphide segregaton has occurred.

An alternative hypothesis for concentration of the Cu in the Extra Ultramafic is that the magmatic Cu has been remobilised by hydrothermal fluids and redeposited near to Cr-bearing spinels (see section 8.12.2). It is, therefore, also possible that the Pt values seen are either magmatic in origin or have been redeposited by hydrothermal fluids. The determination of the origin of the Pt values seen here can only be ascertained by the analysis of PGM and associated minerals. Unfortunately, given the low values of Pt at Kingy (3ppb) it is highly unlikely that any PGM can be found.

8.12.7. Genesis of Pt and Pd in altered rocks

Pd is more common and reaches higher values than Pt in the Kingy area. Figures 8.6E and 8.6F clearly show predominance of Pd over Pt in altered rocks. This is in stark contrast to fresher rocks where Pt and Pd were barely detected. Pd is more mobile than Pt

in hydrothermal systems. The preferential mobility of Pd over Pt in chloride-rich high-temperature fluids is discussed in section 8.7.7. The increase in Pd values and the movement of Pd away from the locations of magmatic Pt concentration could be attributed to hydrothermal fluids. From the data currently available, the distribution of Pt and Pd in the altered rocks from the Kingy area can only be explained by the preferential movement of Pd by high-temperature fluids. However, it is difficult to imagine a situation where such a low and spatially restricted Pt content in the fresher rocks from a complex (3ppb) could give rise to the extent of Pd mineralisation seen in the altered lithologies. Therefore it is reasonable to believe that further and richer magmatic sources of Pt and Pd exist which have not been uncovered by this study. Further sampling around the Extra Ultramafic or investigation of the area around the isolated gabbro may give an insight into this distribution.

8.13. Kingy: Conclusions

As Pt and Pd has barely been detected in the fresher rocks of the Kingy area it is not possible to recommend a strategy to discover or evaluate a "magmatic" ore deposit. However, there is much evidence for the remobilisation of Pd along shear-zones in the area and an improved understanding of the structure and fluids involved with these features may point to a richer source material.

There is little evidence in the Kingy area to construct a magmatic model of the events. However, a fractionation trend in Cr values can be observed in altered rocks and soil samples (see chapter 7) of the Kingy Ridge Ultramafic (see figure 8.6C).

The erratic distribution of Cu-values in altered rocks indicates that the element has been remobilised. Unlike Cu, the distribution of Ni mirrors the fractionation trend seen in Cr, this suggests that Ni has been remobilised by a different alteration episode or has not been remobilised at all. The intermediate Cr values from the altered Lensoid Ultramafics raise the possibility that they may represent slivers of rock "shaved" off a

larger complex. Detailed study of the structure and geochemistry of these bodies is required to test this hypothesis.

Pd dominates Pt in the altered rocks and is distributed over a much wider extent than the Pt in fresher rocks. This suggests firstly that the PGE distribution in the altered rocks is controlled largely by hydrothermal fluids. Additionally, it is inferred that further sites of magmatic Pt and Pd exist which have not been discovered here.

8.14. Maps of elemental distribution in the Kingy areas

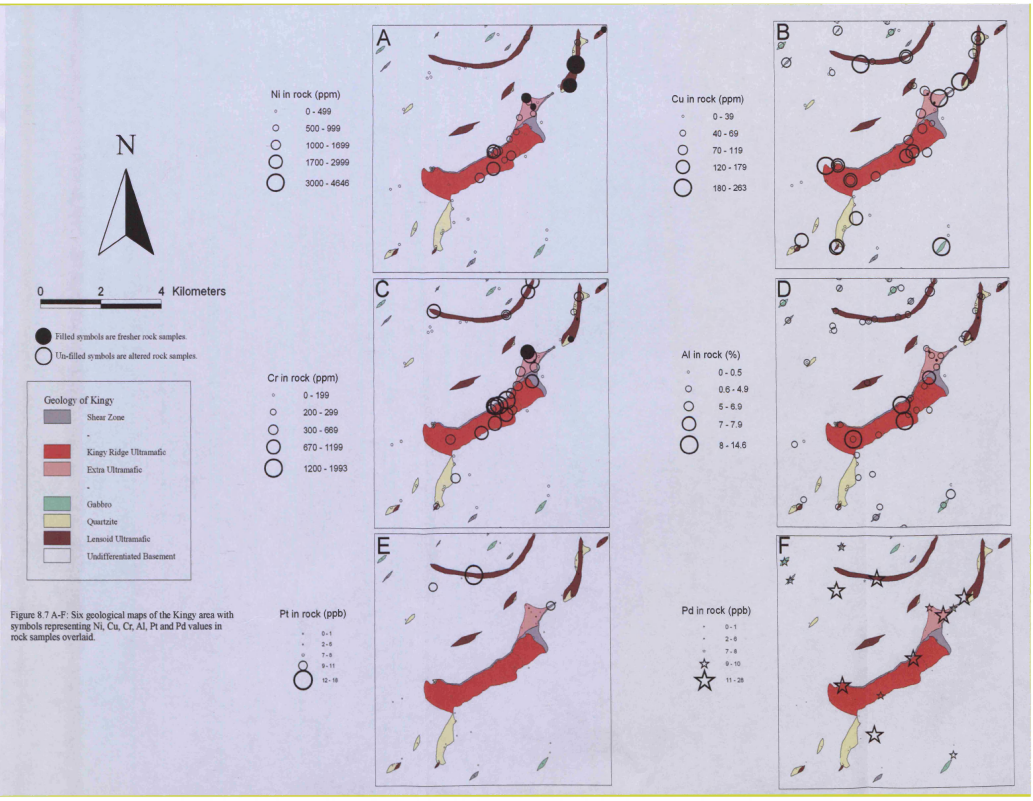

Figure 8.7 A-F: Six geological maps of the Kingy area with symbols representing Ni, Cu, Cr, Al, Pt and Pd values in rock samples overlaid.

8.15. Daleti, Ankori, Tulu Kapi and Keley: Selected Major and Trace Elements

8.15.1. Introduction

There are 155 samples from the area around Daleti, Ankori, Tulu Kapi and Keley. According to the classification method outlined in section 8.3.1 only 13 samples are considered to be fresher ultramafics and a further 14 are altered ultramafics. The remaining 128 are basement lithologies. The fresher ultramafics are all dunites from the quarry and road-cuttings at Daleti. The altered ultramafic rocks are from the Ankori Ultramafic, Daleti Ultramafic and Lensoid Ultramafics. Samples were taken along roads and tracks where exposure was found (see figure 8.8).

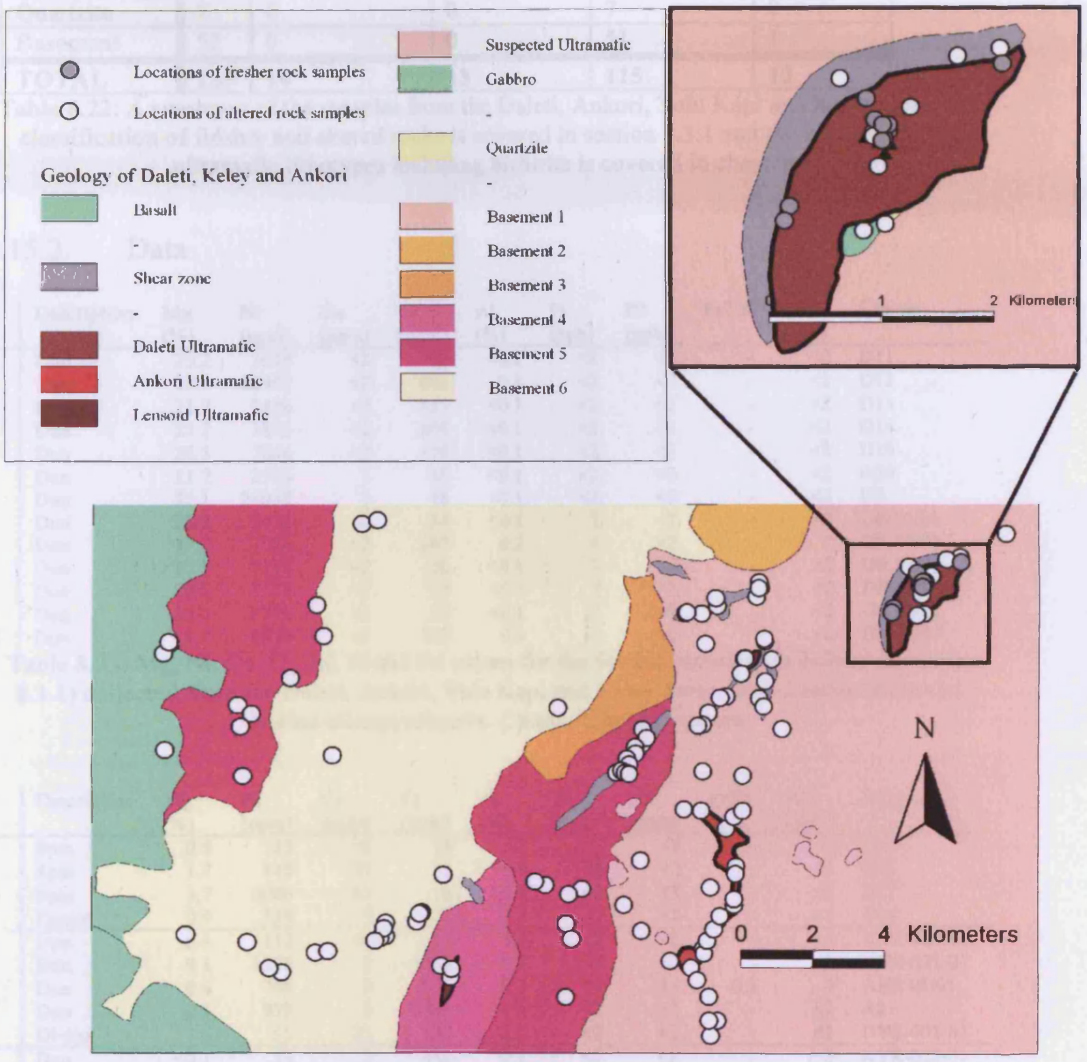

Figure 8.8: The distribution of rock samples within the Daleti area, with a map of the Daleti Ultramafic inset. The classification of fresher and altered rocks is covered in section 8.3.1.

Formation	#	Altered ultramafic rocks	Fresher ultramafic rocks	Non-ultramafic rocks	Birbirite samples
Basalt	1	0	0	1	0
Shear Zones	46	0	0	46	0
Daleti Ultramafic	21	4	13	0	4
Ankori Ultramafic	13	5	0	3	5
Lensoid Ultramafics	11	5	0	4	2

Gabbro	4	0	0	3	1
Quartzite	7	0	0	7	0
Basement	52	0	0	51	1
TOTAL	**155**	**14**	**13**	**115**	**13**

Table 8.22: A summary of the samples from the Daleti, Ankori, Tulu Kapi and Keley areas. The classification of fresher and altered rocks is covered in section 8.3.1 and the classification of ultramafic lithotypes including birbirite is covered in chapter 3.

8.15.2. Data

Formation	Description	Mg (%)	Ni (ppm)	Cu (ppm)	Cr (ppm)	Al (%)	Pt (ppb)	Pd (ppb)	Pt/Pd	Au (ppb)	Sample
Daleti Ultramafic	Dun	25.2	2629	<2	60	<0.1	<2	<2	-	<2	D11
	Dun	20.0	22952	<2	804	0.1	<2	<2	-	<2	D12
	Dun	21.7	2426	<2	455	<0.1	<2	<2	-	<2	D13
	Dun	22.2	1876	<2	604	<0.1	<2	<2	-	<2	D14
	Dun	20.3	7864	<2	174	<0.1	<2	<2	-	<2	D19
	Dun	21.7	2595	2	40	<0.1	<2	<2	-	<2	D20
	Dun	22.1	24035	3	73	<0.1	<2	<2	-	<2	D6
	Dun	23.5	2436	<2	34	<0.1	2	<2	-	<2	DR 01/01
	Dun	17.0	7726	<2	157	0.2	4	<2	-	2	DR 02/01
	Dun	17.9	7713	<2	58	<0.1	7	<2	-	<2	DR 07/01
	Dun	20.8	5173	<2	24	<0.1	7	<2	-	<2	DR 08/01
	Dun	20.0	6748	<2	27	<0.1	5	<2	-	<2	DR 09/01
	Dun	18.9	4809	<2	130	0.1	8	<2	-	<2	DR 22/01

Table 8.23: Mg, Ni, Cu, Cr, Al, Pt and Pd values for the fresher samples (as defined in section 8.3.1) collected from the Daleti, Ankori, Tulu Kapi and Keley areas. Dun: Dunite. Ol-cpxite: Olivine-clinopyroxenite. Cpxite: Clinopyroxenite.

Formation	Description	Mg (%)	Ni (ppm)	Cu (ppm)	Cr (ppm)	Al (%)	Pt (ppb)	Pd (ppb)	Pt/Pd	Au (ppb)	Sample
Daleti Ultramafic	Spin	0.8	123	<2	38	5.3	<2	<2	-	<2	D15
	Spin	1.7	142	37	22	5.8	<2	<2	-	<2	D16
	Spin	3.7	3080	65	16	3.2	<2	<2	-	<2	D17
	Cpxite	0.9	539	5	7	0.4	<2	<2	-	<2	D18
Ankori Ultramafic	Dun	6.4	113	46	45	3.9	<2	<2	-	4	KYC-007-01
	Dun	9.1	1248	3	1045	0.4	5	<2	-	2	KYR-021-01
	Dun	0.6	786	9	405	0.2	11	13	0.8	3	ANR 01/01
	Dun	0.1	979	3	1063	0.1	<2	<2	-	<2	A2
	Ol-cpx	1.6	95	25	128	2.2	<2	<2	-	<2	DYR-005-01
Lensoid Ultramafics	Dun	<0.1	33	5	322	0.1	<2	<2	-	3	KYR-032-01
	Dun	0.5	1	13	2	1.2	<2	<2	-	2	TYR-024-01
	Dun	0.3	21	60	8	0.6	3	33	0.1	12	DR 21/01
	Dun	0.7	111	298	47	1.2	<2	<2	-	<2	D3
	Troc	<0.1	138	101	26	0.2	<2	<2	-	<2	KYR-005-01
Other	Anor	<0.1	2	3	4	0.6	<2	<2	-	3	DYR-036-01
	Birb	0.1	952	2	719	0.1	<2	<2	-	<2	A1
	Birb	0.1	694	7	213	0.1	<2	<2	-	<2	ANR 02/01
	Birb	<0.1	700	42	699	0.1	<2	<2	-	<2	ANR 03/01
	Birb	0.1	1783	4	985	0.1	3	<2	-	3	ANR 05/01
	Birb	<0.1	2610	16	347	0.2	9	2	4.5	4	AYC-019-01
	Birb	<0.1	982	13	420	<0.1	<2	<2	-	5	AYR-043-01
	Birb	0.1	1325	4	799	0.1	<2	<2	-	<2	D10
	Birb	0.1	1084	12	1033	0.5	<2	<2	-	<2	D5
	Birb	0.7	2525	3	838	0.3	8	<2	-	2	DR 03/01
	Birb	0.1	654	2	425	0.1	<2	<2	-	<2	DR 05/01
	Birb	0.1	2394	7	280	<0.1	<2	<2	-	<2	DR 10/01
	Birb	0.3	1177	6	576	0.1	15	16	0.9	5	KYR-022-01
	Birb	<0.1	2	4	7	0.2	<2	<2	-	<2	TYR-004-01
	ChSchi	0.9	249	<2	164	<0.1	<2	<2	-	<2	D8
	Dole	0.1	25	39	121	10.3	<2	<2	-	2	AYC-006-01
	Dole	<0.1	124	144	1402	2.1	3	5	0.6	3	DYC-001-01
	Dole	0.2	20	35	79	1.1	<2	<2	-	<2	DYC-004-01

Dole	2.2	34	22	20	2.6	<2	<2	-	2	DYR-006-01
Dole	<0.1	17	49	21	0.1	<2	7	0.0	5	DYR-010-01
Dole	0.1	50	71	187	1.6	2	5	0.4	4	KYC-009-01
Dole	<0.1	150	88	119	0.6	<2	<2	-	3	KYR-004-01
Dole	0.9	12	89	6	1.8	3	8	0.4	4	KYR-014-01
Dole	0.7	19	39	29	0.9	<2	<2	-	2	TYR-028-01
Dole	0.4	20	24	18	1.1	4	9	0.4	<2	TYR-033-01
Dole	0.4	16	86	14	1.8	<2	<2	-	<2	TYR-034-01
Fels	0.5	16	15	25	1.1	<2	3	0.0	6	AYR-004-01
Fels	0.1	14	8	13	1.2	<2	<2	-	<2	AYR-008-01
Fels	0.2	2	4	4	1.6	<2	<2	-	<2	DYR-034-01
Fels	0.1	2	3	4	0.6	<2	<2	-	2	DYR-035-01
Fels	<0.1	<2	4	2	0.2	<2	<2	-	2	DYR-037-01
Fels	<0.1	8	16	14	0.1	<2	<2	-	<2	DYR-038-01
Fels	0.2	104	21	317	0.2	4	5	0.8	2	KYR-009-01
Gabb	0.1	187	65	335	1.1	4	3	1.3	<2	AYR-022-01
Gabb	3.9	1061	10	1650	5.3	11	13	0.8	2	AYR-023-01
Gabb	<0.1	12	68	301	23.3	2	<2	-	<2	AYR-025-01
Gabb	1.2	21	81	71	1.8	<2	<2	-	3	AYR-026-01
Gabb	1.3	17	14	29	1.9	<2	<2	-	3	AYR-037-01
Gabb	1.9	24	17	23	2.4	<2	<2	-	<2	D4
Gabb	<0.1	18	7	14	0.1	<2	<2	-	<2	DR 06/01
Gabb	0.2	19	40	30	1.1	<2	<2	-	<2	DYR-001-01
Gabb	1.2	41	19	68	1.8	<2	<2	-	8	DYR-004-01
Gabb	7.9	656	4	854	0.2	5	<2	-	<2	KYC-008-01
Gabb	0.1	2	7	9	0.4	<2	<2	-	2	KYR-011-01
Gabb	0.2	2158	66	2510	0.6	3	<2	-	4	KYR-025-01
Gabb	1.3	13	37	37	1.8	<2	<2	-	3	TYR-002-01
Gabb	3.1	104	5	279	0.4	19	3	6.3	2	TYR-006-01
Gabb	0.6	6	22	10	1.2	<2	<2	-	2	TYR-027-01
Gran	0.2	2	4	3	0.6	<2	<2	-	<2	AYR-042-01
Gran	0.5	8	8	12	1.0	<2	<2	-	<2	KYR-026-01
Gran	<0.1	5	3	5	0.3	<2	<2	-	<2	TYC-003-01
Gran	0.2	2	4	<2	0.8	<2	<2	-	<2	TYR-030-01
GranDi	0.5	24	14	22	0.9	<2	<2	-	<2	AYR-046-01
GranDi	0.4	1	7	4	1.0	<2	<2	-	<2	DYR-018-01
GranDi	0.7	11	25	12	1.7	<2	<2	-	3	DYR-040-01
GranDi	0.1	2	16	4	1.1	<2	<2	-	<2	KYR-015-01
GranDi	<0.1	2	2	2	0.3	<2	<2	-	<2	TYR-005-01
HardP	0.5	23	259	33	1.5	<2	3	0.0	5	TYR-032-01
MetaSed	0.1	12	2	14	0.2	<2	<2	-	<2	TYR-003-01
Mylo	<0.1	8	14	8	0.4	<2	<2	-	24	AYR-041-01
Mylo	<0.1	26	7	16	0.3	<2	<2	-	<2	DYC-002-01
Mylo	0.5	14	9	9	1.1	<2	<2	-	<2	DYC-005-01
Mylo	<0.1	3	24	5	0.1	<2	<2	-	214	DYR-003-01
Mylo	3.4	186	19	401	6.8	<2	<2	-	<2	DYR-030-01
Mylo	1.4	95	14	81	2.0	<2	<2	-	3	DYR-041-01
Mylo	0.1	105	70	16	0.3	<2	<2	-	3	KYR-006-01
Mylo	0.1	5	4	21	0.7	<2	<2	-	<2	TYR-029-01
Quar	<0.1	29	70	33	0.4	10	13	0.8	4	ANR 06/01
Quar	0.2	48	5	8	0.3	<2	<2	-	28	DR 04/01
Quar	0.1	759	5	273	<0.1	5	<2	-	<2	DR 14/01
Quar	<0.1	21	7	14	<0.1	<2	<2	-	2	DR 15/01
Quar	<0.1	24	143	39	0.1	2	9	0.2	12	DR 16/01
Quar	<0.1	17	101	15	0.2	2	<2	-	132	DR 17/01
Quar	0.1	26	19	16	0.1	4	33	0.1	11	DR 18/01
Quar	<0.1	5	20	18	0.2	<2	8	0.0	15	DR 20/01
Quar	<0.1	2	3	3	<0.1	<2	<2	-	3	DYR-032-01
Quar	<0.1	5	7	26	0.1	<2	<2	-	<2	KYR-010-01
Schi	<0.1	45	77	95	0.4	<2	<2	-	<2	A3
Schi	2.4	63	46	38	1.6	<2	<2	-	20	AYR-005-01
Schi	10.6	373	5	162	9.3	<2	<2	-	2	AYR-044-01
Schi	11.0	349	17	265	6.6	<2	<2	-	<2	D1
Schi	<0.1	7	<2	9	0.1	<2	<2	-	<2	DYC-003-01
Schi	<0.1	4	24	14	0.2	3	8	0.4	2	DYC-007-01
Schi	0.3	6	29	18	1.3	<2	<2	-	2	DYR-031-01
Schi	<0.1	15	88	14	0.2	2	<2	-	2	DYR-039-01
Schi	0.1	54	4	43	0.4	<2	<2	-	2	KYR-008-01
Schi	<0.1	1	<2	22	0.2	<2	<2	-	<2	TYR-001-01
Schi	0.7	15	19	27	1.9	<2	<2	-	<2	TYR-016-01

Schi	8.6	489	19	1123	6.7	<2	<2	-	45	TYR-018-01
Sed	<0.1	8	21	47	2.1	4	3	1.3	3	AYC-007-01
Sed	<0.1	15	7	19	2.1	<2	<2	-	2	AYC-008-01
Sed	<0.1	7	90	32	0.5	6	7	0.9	4	AYC-009-01
Sed	0.3	7	179	35	0.8	4	5	0.8	24	AYC-011-01
Sed	0.1	2	45	20	0.4	3	5	0.6	5	AYR-009-01
Sed	<0.1	104	140	340	1.4	<2	<2	-	3	KYR-024-01
TaSchi	0.4	64	32	531	0.1	3	<2	-	2	AYR-007-01
TaSchi	0.1	20	22	32	1.8	<2	3	0.0	2	AYR-021-01
TaSchi	3.2	422	2	987	2.8	4	6	0.7	<2	AYR-024-01
TaSchi	0.3	8	20	12	1.0	<2	<2	-	<2	AYR-038-01
TaSchi	0.6	129	19	647	0.2	<2	<2	-	<2	D2
TaSchi	9.7	159	7	49	9.3	<2	<2	-	<2	D21
TaSchi	0.3	110	<2	158	0.3	<2	<2	-	<2	D7
TaSchi	0.8	223	<2	563	0.2	<2	<2	-	<2	D9
TaSchi	0.2	238	184	205	4.8	<2	<2	-	109	DYR-002-01
TaSchi	0.1	24	10	14	0.4	<2	<2	-	<2	DYR-009-01
TaSchi	<0.1	39	9	59	0.3	<2	<2	-	2	KYR-003-01
TaSchi	0.1	21	69	21	0.9	<2	<2	-	10	TYR-017-01
TCSchi	0.7	355	8	492	0.2	5	<2	-	<2	DR 11/01
TCSchi	9.4	941	11	138	11.7	2	7	0.3	4.51	DR 19/01
Unid	<0.1	348	9	87	0.2	<2	<2	-	25	AYC-020-01
Unid	<0.1	17	159	24	0.4	6	9	0.7	13	DYC-008-01
Unid	0.9	149	35	634	0.4	<2	<2	-	4	AFYC-004-01
VQuar	<0.1	1406	3	742	0.2	<2	<2	-	<2	ANR 04/01
VQuar	<0.1	2	<2	4	0.1	<2	<2	-	<2	AYC-018-01
VQuar	8.6	47	5	17	5.7	<2	<2	-	<2	AYR-006-01
VQuar	0.2	1413	19	388	0.2	4	<2	-	2	DR 13/01
VQuar	<0.1	2	<2	8	0.1	<2	<2	-	<2	DYC-006-01
VQuar	<0.1	2	3	6	0.1	<2	<2	-	<2	DYR-007-01
VQuar	<0.1	1	2	3	0.1	2	<2	-	2	DYR-008-01
VQuar	1.2	28	15	15	1.6	<2	<2	-	2	DYR-033-01
VQuar	<0.1	13	12	10	0.1	<2	<2	-	<2	KYR-001-01
VQuar	<0.1	19	37	8	0.1	<2	<2	-	3	KYR-002-01
VQuar	<0.1	66	50	9	0.1	<2	<2	-	9	KYR-007-01
VQuar	<0.1	9	3	52	0.1	<2	<2	-	<2	KYR-012-01
VQuar	<0.1	3	<2	7	<0.1	<2	<2	-	72	KYR-013-01
VQuar	0.1	25	2	102	0.1	<2	<2	-	<2	KYR-023-01
VQuar	<0.1	3	<2	11	<0.1	<2	<2	-	<2	KYR-033-01
VQuar	<0.1	11	28	16	0.3	<2	<2	-	<2	TK1

Table 8.24: Mg, Ni, Cu, Cr, Al, Pt and Pd values for the altered samples collected from the Daleti, Ankori, Tulu Kapi and Keley areas. Anor: Anorthosite. Basa: Basalt. Birb: Birbirite. ChSchi: Chlorite-Schist. ChSchi: Chlorite-Schist. Cpxite: Clinopyroxenite. Dior: Diorite. Dole: Dolerite. Dun: Dunite. Fels: Felsite. Gabb: Gabbro. GranDi: Granodiorite. HardP: Hard pan. MetaBas: Metabasalt. MetaSed: Metasediment. Mylo: Mylonite. Ol-cpxite: Olivine-clinopyroxenite. Quar: Quartzite. Schi: Schist. Sed: Sediment. Spin: spinel-like rocks (see chapter 3) TaSchi: Talc-Schist. TCSchi: Talc-Chlorite-Schist. Troc: Troctolite. Unid: Unidentified. VQuar: Vein Quartz.

The following sections cover the distribution of Ni, Cu, Cr and Al in the Daleti, Ankori, Tulu Kapi and Keley areas. Each section covers one element and describes its distribution in fresher ultramafics and then altered rocks. These sections are accompanied by a fold-out page (on page 247) of maps showing the distribution of all elements which the reader should refer to as each section is read.

8.15.3. Nickel

The fresher dunites from the Daleti Ultramafic show the highest Ni value in the WES at 24,035ppm from the northern tip of the complex. At the centre of the Daleti Ultramafic local variations are large, of 8 samples of fresher dunite located within 250m of each other Ni content varies from 1,876ppm to above 22,952ppm.

All Ni analyses above 2,100ppm in altered rock are located in samples from the ultramafic bodies. The altered rocks from the Ankori Ultramafic and the Lensoid Ultramafics have less Ni than the samples from the Daleti Ultramafic, with maximas of 1,248ppm and 138ppm respectively (figure 8.10A). The 5 samples of ultramafic rocks from the Ankori complex show no distinct pattern in Ni content and the lowest Ni value is 95ppm in an olivine-clinopyroxenite. Ni values in the dunites of the Lensoid Ultramafics vary from 1ppm to 111ppm and no particular spatial pattern can be observed. Shear-zone related rocks show no more than 941ppm of Ni, this value occurring in a talc-chlorite-schist near Keley.

8.15.4. Copper

Only two fresher rocks returned positive results slightly above detection for Cu. These are located at the northernmost tip of the Daleti Ultramafic (3ppm) and on the western flank of the intrusion (2ppm)

Within the altered ultramafics only 2 of 31 samples contain Cu above 65ppm, these are a dunite (298ppm) and a troctolite (101ppm) from the Lensoid Ultramafics. The highest Cu value from the Daleti, Ankori, Tulu Kapi and Keley areas (298ppm) occurs in a dunite from the Lensoid Ultramafics near Keley. The maximum Cu value in the Daleti Ultramafic is 65ppm – from spinel-like rocks (see chapter 3) in the centre of the formation, some dunites have Cu values below detection limits. In the Ankori Ultramafic the maximum is 46ppm from a dunite and some values fall below detection limits. No spatial trends in Cu content can be observed within any of the ultramafic complexes. Two of 15 shear-zone related samples display high Cu values the highest of which is a talc-

schist 3km south of the Keley complex (184ppm), the next highest is a schistose-rock from Gudeya Guji (88ppm). Some shear-zone related rocks returned Cu analyses which are below detection limits.

8.15.5. Chromium

The three highest Cr values (above 500ppm) in fresher rocks occur in dunites of the centre of the Daleti Ultramafic. The maximum Cr value in the fresher rocks from Daleti is 804ppm. Most of the Cr values below 100ppm occur close to the edge of the intrusion near to the contact with the shear zones, however the lowest Cr value (24ppm) occurs in a dunite in the centre within 200m of the highest Cr value.

Chromium values above 300ppm in rock are restricted to the ultramafic complexes and related shear zones. Of all the Daleti, Ankori, Tulu Kapi and Keley areas the highest Cr value (2510ppm) occurs in a gabbro from the basement north of the Ankori complex. The lowest Cr values occur in an altered pyroxenite also in the centre of the intrusion. In the Ankori complex the highest Cr composition is 1063ppm in the southern end of the intrusion and the lowest values are 45ppm in a dunite from the centre of the intrusion. The highest Cr composition in the Lensoid Ultramafics (322ppm) is found in a dunite of the body farthest to the southwest. In addition to this the talc-schists and gabbros from the basement in the south-western part of the study area contain Cr (<1650ppm in gabbro).

8.15.6. Aluminium

Three fresher dunites from the Daleti Ultramafic contain 0.2% of Al and for 10 of 13 samples Al was not detected. All three of these rocks occur close to the centre of the complex.

With the exception of the spinel-like rocks (see chapter 3) of the Daleti Ultramafic all Al analyses above 4.1% are found in the basement or shear-zone related rocks. The highest Al content of the study area (23.3.%) is found in a gabbro from the

basement in the south-western quadrant of the study area. The three highest Al values (<5.8%) in the Daleti Ultramafic are found in the spinel-like rocks (see chapter 3) from the centre of the intrusion. Seven samples from the Daleti Ultramafic show Al which is below detection limits, they occur throughout the complex. The highest Al analysis for the Ankori area is 3.9%, found in a dunite close to the centre. Seven samples from the Ankori Ultramafic show Al values of 0.1% - the lowest amount; they occur throughout the complex. Within the Lensoid Ultramafics the largest Al value (1.2%) is also found in an altered dunite. Figure 8.10D shows that in the Daleti and Ankori complexes, the highest Al contents are found in the centre of the intrusions.

8.15.7. Summary of Ni, Cu, Cr and Al values in the Daleti Ultramafic

A dunite sample at the northern tip of the Daleti Ultramafic shows the highest Ni values from the entire Daleti, Ankori, Tulu Kapi and Keley areas. It also contains the highest Cu values of fresher rocks which is only just above the detection level. The highest Cr values occur in a different location and three fresher dunites at the centre of the formation contain high Cr values. This compares starkly to the samples at the northern edge of complex which contain much lower values.

8.15.8. Summary of Ni, Cu, Cr and Al values at Ankori and the Lensoid Ultramafics

All high Ni analyses in altered rock are located in samples from the ultramafic bodies. The highest value of Cu in the Daleti, Ankori, Tulu Kapi and Keley area (298ppm) occurs in an altered dunite near Keley. However, this is the only ultramafic sample from the area which contains high Cu, all other significant Cu are located away from the ultramafic complexes.

8.15.9. Summary of Ni, Cu, Cr and Al values in the Shear Zones

Of the talc-schists samples taken from Shear Zones, Ni and Cu rise to high values in different samples, no spatial trend can be observed. Cr values vary with proximity to the ultramafic bodies or the northwestern Shear Zones and gabbro.

8.15.10. Summary of Ni, Cu, Cr and Al values in the southwestern Shear Zones and gabbro

High Cr values are seen in a gabbro and a talc-schist in the southwestern parts of the area. Ni and Cu values are both low or intermediate

8.16. Daleti, Ankori, Tulu Kapi and Keley: Pt and Pd distribution

No Pd was detected in the fresher rocks from the Daleti Ultramafic. Six of 13 of the fresher Daleti rocks contain low values of Pt. The maximum Pt value is 8ppb found in a dunite from the south western flank of the complex. Two dunites within 400m of the edge of the intrusion contain 7ppb.

The highest Pt grade (19ppb) in the altered rocks occurs in a gabbro from the basement southwest of Gudeya Guji. The highest Pd grade (33ppb) occurs twice, firstly in a quartzite north of Keley and additionally in a dunite by the road near Keley. Within the Daleti Ultramafic the highest Pt assay of altered rocks is 8ppb in a birbirite located in the centre of the complex.

The Ankori complex has a maximum Pt assay of 15ppb in a birbirite at the northern end of the intrusion. This sample also contains the highest Pd assay, 16ppb. The second highest Pt assay (11ppb) also corresponds to the second highest Pd assay (13ppb), these analyses come from a dunite at the southern end of the intrusion. These two samples are the only ones from the Ankori complex which contain Pd above detection limits. Three further dunite samples out of 13 from the Ankori complex contain Pt above detection limits.

Within the altered samples of the Lensoid Ultramafics, the largest Pt grade found is 9ppb in a birbirite from the near Keley. Only 2 of 11 samples from the Lensoid Ultramafics contain Pt above detection limits (3ppb and 9ppb). This compares to 4 which contain Pd above detection, ranging from below detection limits to 33ppb in the dunite near Keley.

In the southwestern quadrant of the area, 6 rocks within the basement formations show anomalous Pt and Pd. These form in a line trending NE-SW. The highest Pt value from this group (19ppb in a gabbro south-west of Gudeya Guji) is also the highest Pt grade found in the whole Daleti area. Pd grades of 13ppb occur in a gabbro and a quartzite and these also correspond to Pt values of 11ppb and 10ppb respectively. Just south of Ankori, outside of the complex, a dolerite dyke returns a Pt value 4ppb and a Pd value of 9ppb. The other significant samples from this area are a metasediment which contains a Pt value of 6ppb and a Pd value 7ppb and a talc-schist containing 4ppb of Pt and 6ppb of Pd.

A comparison between PGE and Ni, Cu, Cr and Al in the highest value samples of fresher rocks within the Daleti Ultramafic is as follows:

Sample	Pt (ppb)	Pd (ppb)	Ni (ppm)	Cu (ppm)	Cr (ppm)	Al (%)
DR 22/01	8	< 2	4809	< 2	130	0.1
DR 07/01	7	< 2	7713	< 2	58	< 0.1
DR 08/01	7	< 2	5173	< 2	24	< 0.1
DR 09/01	5	< 2	6748	< 2	27	< 0.1
DR 02/01	4	< 2	7726	< 2	157	0.2
DR 01/01	2	< 2	2436	< 2	34	< 0.1
D12*	< 2	< 2	22952	< 2	804	0.1
D6*	< 2	< 2	24035	3	73	< 0.1

Table 8.25: A summary of Ni, Cu, Cr and Al values in the dunites of highest Pt and Pd grade from the fresher rocks within the Daleti Ultramafic. A graphical representation of this data is provided in figure 8.9. *: Samples D12 and D6 are included regardless of low Pt and Pd values as they contain high Ni values.

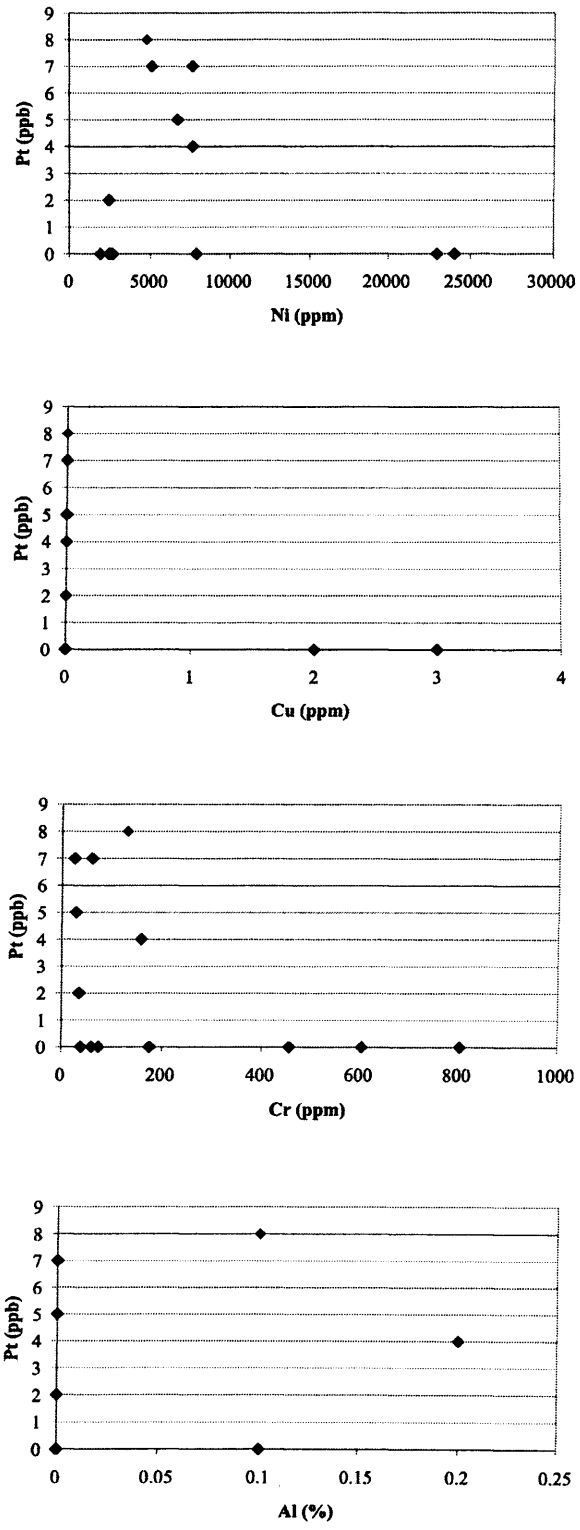

Figure 8.9: Graphs of Ni, Cu, Cr and Al versus Pt in the fresher dunites from the Daleti Ultramafic.

8.17. Daleti, Ankori, Tulu Kapi and Keley: Discussion

Here the processes likely to have affected the distribution of Ni, Cu, Cr Al, Pt and Pd in the Kingy area are discussed. The processes involved with the distribution of Ni, Cu, Cr and Al in fresher ultramafics are considered in sections 8.17.1 and 8.17.2, followed by those processes which affect altered rocks in 8.17.3 and 8.17.5. The mechanisms which distribute Pt and Pd are considered from section 8.17.6 to section 8.17.7.

8.17.1. The highest Ni and Cu values in the fresher rocks from the Daleti Ultramafic

A fresher dunite (sample D6) at the northern tip of the Daleti Ultramafic contains both the highest Ni value in the entire WES dataset and highest Cu value in fresher rocks in the complex. The Ni value seen here is over 20,000ppm too large for all the Ni to be partitioned into olivine (see section 8.6.2), it is therefore thought likely that the Ni has partitioned into sulphide minerals after sulphide segregation (see section 8.6.4). Analyses of spinel minerals have Ni values below detection (see chapter 9). Given such a large Ni content, the small Cu values are somewhat surprising. The highest Cu and Ni contents could occur in the same sample in a situation where sulphide segregation has occurred and filter-pressing or hydrothermal alteration was slight or not present (see sections 8.6.6 and 8.6.8). However, given the chalcophile behaviour of both elements, a larger Cu value than seen here would be expected. It is possible that further sampling will reveal a larger maximum Cu value, which may be in a different location from the highest Ni. However, if this is truly the largest Cu content of the complex then two interpretations can be made, firstly that any filter pressing and/or hydrothermal alteration was slight or did not occur and secondly that the Cu content of the magma itself was low. Alternatively, all Cu could have been removed from the complex.

8.17.2. Zonation in Cr values in the fresher rocks from the Daleti Ultramafic

The highest Cr values of fresher rocks (>500ppm) occurs in the centre of the Daleti Ultramafic and the samples at the northern edge of the complex contain less than 130ppm. Given that spinel minerals are unlikely to have been taken into solution during the aqua regia digestion, all Cr measured here is likely to be Cr partitioned into olivine. Firstly, in a situation where the complex formed from one pulse of magma, the most primitive rocks would be in the centre and the northwestern edge is more evolved. The alternative is that, if more than one melt had intruded the crust to form the Daleti Ultramafic then the Cr-rich rocks of the centre may indicate a phase of magma mixing (see section 8.6.7).

8.17.3. Trace element distribution in Shear Zones

Of the talc schists observed in shear zones, Ni and Cu rise to high values in different samples. Both elements are known to be taken into solution by hydrothermal fluids at conditions of nearly neutral pH, with temperatures from 200-300°C and salinities of less than 3wt% NaCl (see section 8.6.8). At higher temperatures, the solubilities of such elements are likely to rise (see section 8.6.8). The observation that Ni and Cu reach high values in the same lithotype but different samples raises several questions, as discussed for similar observations at Kingy (see section 8.12.4). It is possible that multiple alteration episodes occurred – under slightly different conditions or acting on different areas. Another alternative is that one element was not remobilised and represents a "relict" magmatic signature (as suggested for Kingy section 8.12.4).

8.17.4. Copper values in altered rocks

The highest Cu value (298ppm) occurs in a sample of altered dunite near Keley, however all other Cu values above 100ppm occur away from the ultramafic complexes. As suggested above (section 8.17.3), it is likely that Cu has been remobilised and reprecipitated in the Daleti area and therefore this elevated value could well be the result of alteration. However, the lack of Cu compared to Ni observed in the Daleti Ultramafic

(<3ppm and <24,035ppm respectively, see section 8.17.1) raises a question about the true maximum Cu value. The Cu-bearing dunite at Keley is small sliver of dunite near to a large mass of shear-zone related lithotypes around 2.5km southwest of Daleti. Given the scale of the mobile belt in which the WES exists (chapter 2) it is reasonable to expect an offset of over 2km to occur along a strike-slip fault. It is possible that the Cu-bearing dunite at Keley could represent the "missing magmatic Cu" from the Daleti Ultramafic. Although this study cannot demonstrate this relationship, further analysis of the mineral morphology of the Cu-bearing sulphides may aid understanding of this anomalous result. It is expected that structural observations are unlikely to be feasible due to the poor exposure and extensive alteration. If the high Cu value seen here was found to be formed by alteration then it may be suggested that a magmatic high Cu occurance exists nearby and this in turn could be related to the high Ni seen at Daleti.

The distribution of high Cu values (>100ppm) over formations other than the ultramafic complexes could also be explained in terms of remobilisation by high temperature fluids.

8.17.5. High Ni values within the ultramafic complexes

All Ni analyses above 2100ppm in altered rock occur in samples from the ultramafic complexes. As with Cu, Ni is considered to be mobile in hydrothermal fluids (see 8.6.8). So it is to be expected that Ni will become concentrated into these rocks by the combined processes of sulphide segregation and fractionation and subsequently be remobilised by high-temperature fluids. As seen in the Shear Zones (see section 8.17.3), there is a different geographic distribution of Ni and Cu. This suggests that either the Ni has not been remobilised and represents a "relict" magmatic signature or that the two elements were concentrated by different alteration systems (see section 8.12.4).

8.17.6. Genesis of Pt and Pd in fresher rocks from the Daleti Ultramafic

The highest Pt value found in the fresher rocks from the Daleti Ultramafic is 8ppb and no Pd has been found above detection levels. Table 8.25 shows that the samples with

highest Pt also contain Ni values which are high enough for sulphides to be present (see section 8.6.2). However the Ni values in these PGE-bearing samples are much smaller than the values seen in D12 and D6 which are barren of Pt and Pd. Additionally, none of the PGE-bearing samples contain any Cu. Although two PGE-bearing samples contain Cr values of over 100ppm, the sample with highest Cr value is barren of Pt or Pd. It appears likely that sulphides are present in the daleti area, but barely any Pt of Pd is detectable at all. Therefore, if sulphide segregation has occurred, it did so in a magma which was almost completely barren of Pt and Pd.

The low value of Cu in the Daleti Ultramafic is possibly explained by the element being leached out by hydrothermal fluids (8.17.4). In the same manner there may have been some remobilisation of Pt and Pd from its primary magmatic location and redeposited elsewhere such as Keley (see section 8.17.7).

8.17.7. Genesis of Pt and Pd in altered rocks

The highest Pt value occurs in a gabbro in the southwestern basement area – this occurs in line with a WSW trending group of Pt and Pd anomalies. Two anomalous Pd values are observed in a dunite and quartzite from the Keley area. Further significant Pt and Pd grades from the area in question occur in Ankori.

The proximity of the two highest Pd values to large shear-zone related lithotypes indicates the influence of hydrothermal fluids directed along these Shear Zones. The Pd found in quartzite further infers that silica-rich fluids have a role in the remobilisation Pd. The low Pt analysis supports the hypothesis that Pd is more mobile than Pt in the hydrothermal fluids in this area (see section 8.6.8).

Unlike the samples at Keley, the samples around the southwestern basement retain slightly elevated Pt values. As Pt is considerably less mobile than Pd in hydrothermal fluids (section 8.6.8) it is less likely that these concentrations are due to secondary remobilisation. However, the presence of a Pt anomaly in quartzite suggests

some degree of remobilisation. The gabbro samples obtained from the area and high Cr values suggest the presence of a primitive mafic-ultramafic intrusion in the area - which may represent the primary source of these Pt and Pd anomalies.

The Pt and Pd values at Ankori are co-incident with intermediate values of Ni, Cu and Cr when compared to the surrounding area. The Cr values indicate that this complex formed by the crystallization of a primitive magma. However, the severe alteration (lack of fresher samples) and poor structural control on the complex make it hard to determine the influence of magmatic processes.

8.18. Daleti, Ankori, Tulu Kapi and Keley: Conclusions

Given the low values of Pt and Pd alongside high Ni values, it is considered unlikely that the Daleti Ultramafic will host economic mineralisation. However, further investigation of the extensive Pt and Pd values found associated with shear-zones in the southwestern part of the study area may reveal a more promising prospect.

The distribution of Ni, Cu and Cr in the fresher rocks of the Daleti Ultramafic is used to discuss ideas about the magmatic genesis of the complex. The high values of Ni in the fresher rocks from the Daleti Ultramafic suggest that sulphide segregation may have occurred however the Pt and Pd values remain low.

Analyses of the talc-schists and altered ultramafic samples from the Ankori, Tulu Kapi and Keley areas show that Ni and Cu are concentrated into different samples. This may be explained by the action of two different alteration episodes under slightly different conditions or acting on different geographical areas. Alternatively, one element may not have been remobilised. The analysis of the Ni- and Cu-bearing minerals may uncover further information regarding the alteration episodes.

High Pd values are found in a quartzite and dunite sample from around the extensive Shear Zones of the Keley area. The preferential mobility of Pd over Pt in

hydrothermal fluids can explain this distribution although a primary source of Pd nearby has not been discovered.

8.19. Maps of elemental distribution in the Daleti, Ankori, Tulu Kapi and Keley areas

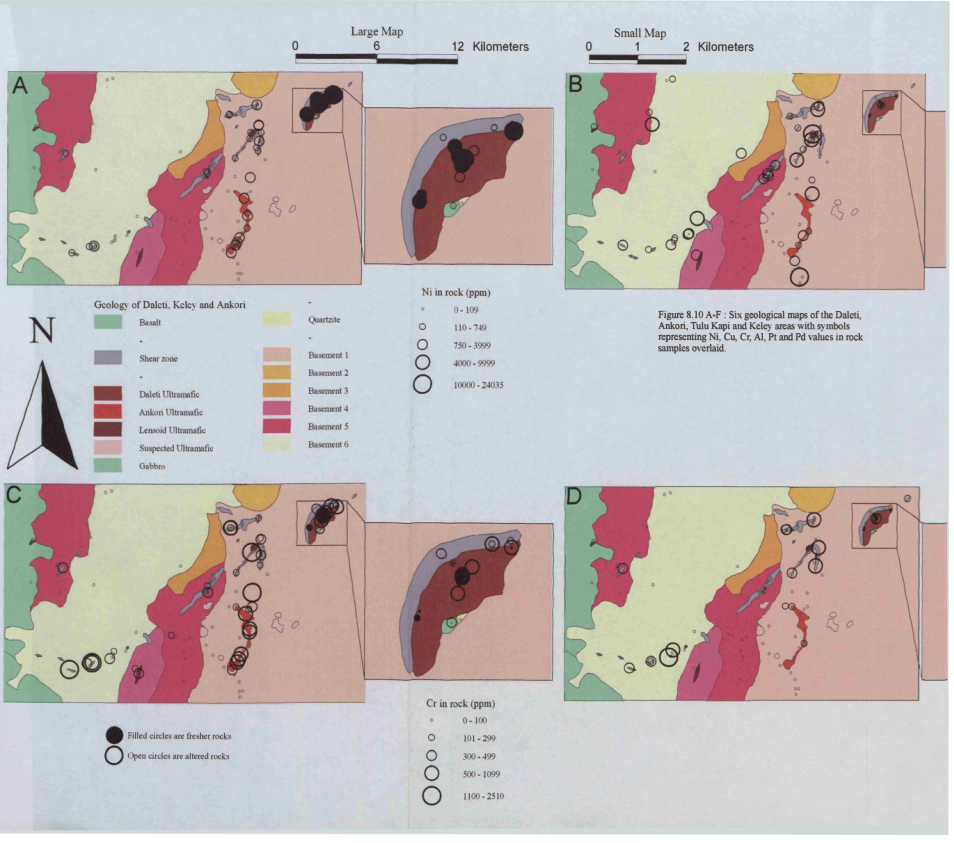

Figure 8.10 A-F : Six geological maps of the Daleti, Ankori, Tulu Kapi and Keley areas with symbols representing Ni, Cu, Cr, Al, Pt and Pd values in rock samples overlaid.

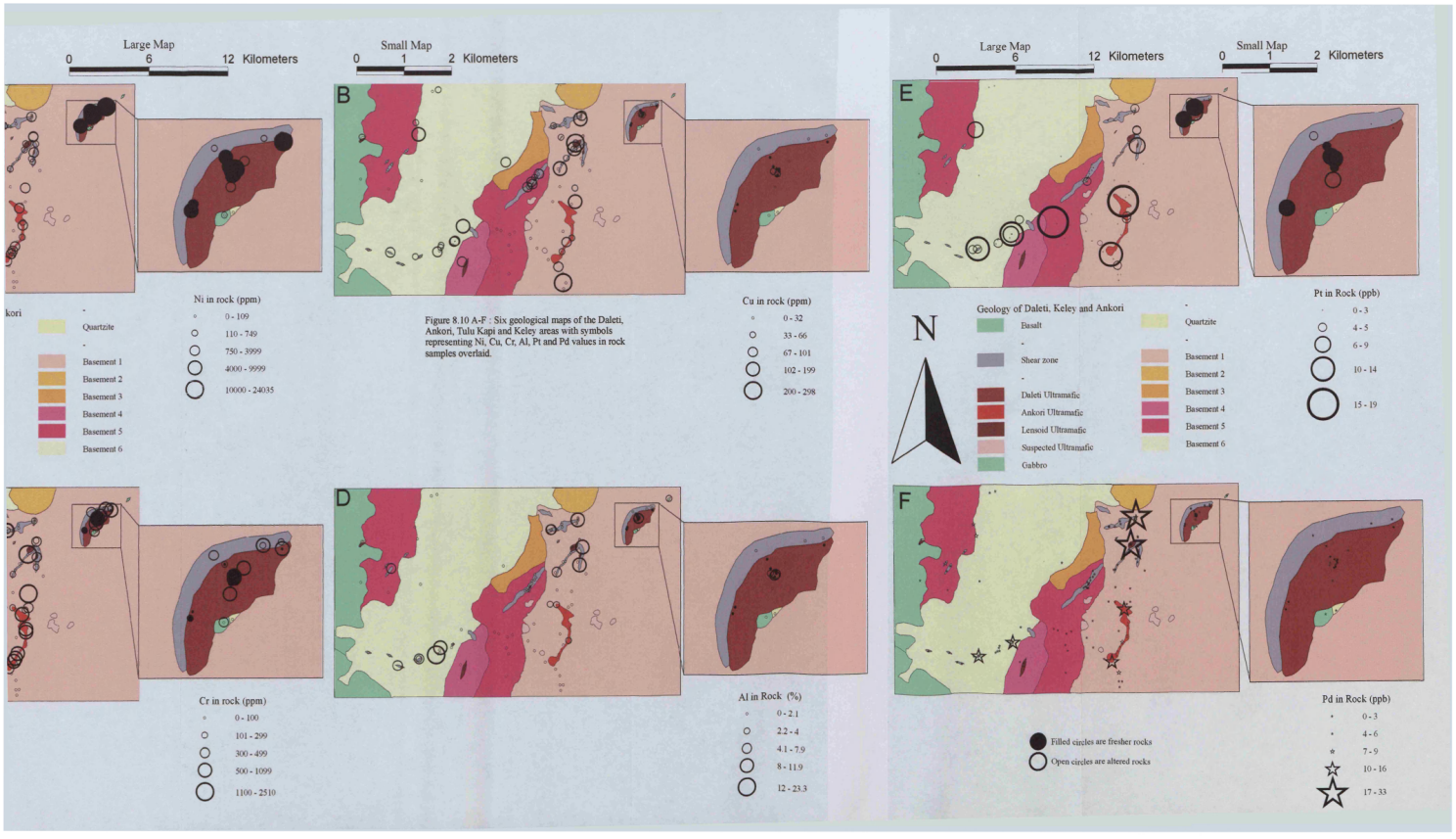

Figure 8.10 A-F : Six geological maps of the Daleti, Ankori, Tulu Kapi and Keley areas with symbols representing Ni, Cu, Cr, Al, Pt and Pd values in rock samples overlaid.

8.20. Yubdo, Sodu and Andu: Selected Major and Trace Elements

8.20.1. Introduction

100 samples were examined from the Yubdo area. According to the classification set out in section 8.3.1, sixteen of the samples are altered ultramafics and 6 are fresher ultramafics. There are a further 76 samples of basement lithologies and birbirites. All fresher ultramafic rock samples are located within the Main Yubdo Ultramafic.

The areas Yubdo, Andu and Sodu are distinguished from each other in chapter 5.

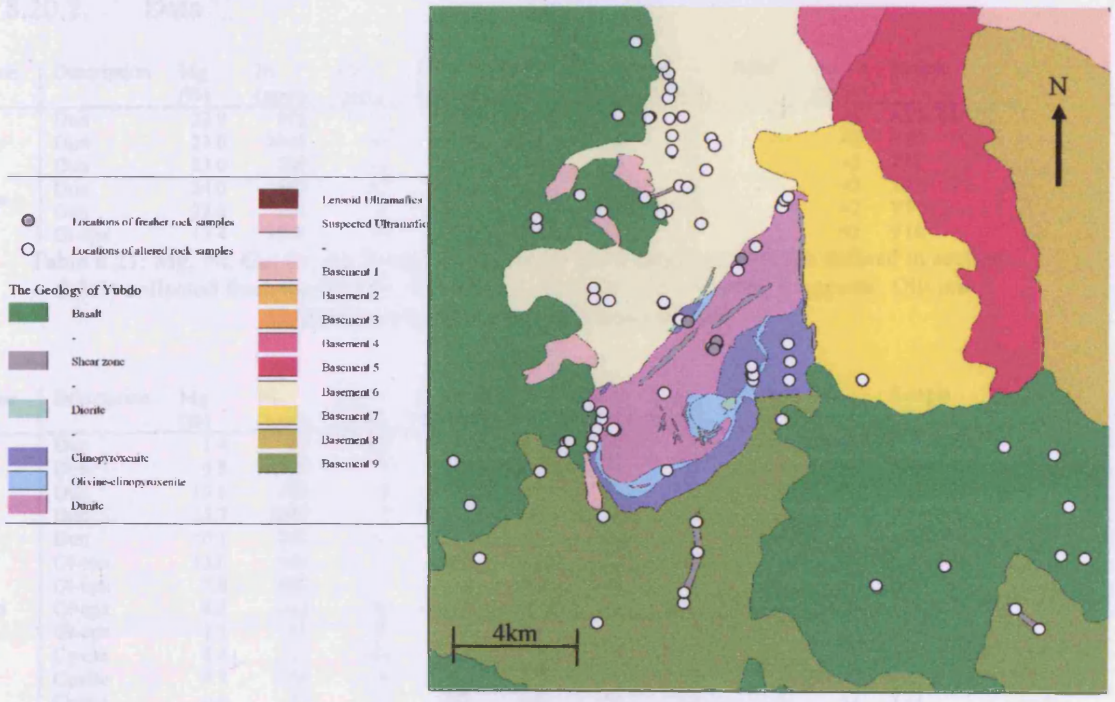

Figure 8.11: The distribution of samples within the Yubdo area.

Formation	#	Sub-unit		Altered ultramafic rocks	Fresher ultramafic rocks	Non-ultramafic rocks	Birbirite samples
Basalt	15			0	0	15	0
Shear Zones	23			0	0	21	2
Diorite	1			0	0	1	0
Yubdo Ultramafic	30	Clinopyroxenite	11	4	0	7	0
		Olivine-clinopyroxenite	5	4	1	0	0
		Dunite	14	5	5	0	4
Lensoid Ultramafics	5			5	0	0	0
Basement	26			0	0	24	2
TOTAL	**100**			**18**	**6**	**68**	**8**

Table 8.26: A summary of the samples from the Yubdo, Andu and Sodu areas. The classification of fresher and altered rocks is covered in section 8.3.1 and the classification of ultramafic lithotypes including birbirite is covered in chapter 3.

8.20.2. Data

Formation	Description	Mg (%)	Ni (ppm)	Cu (ppm)	Cr (ppm)	Al (%)	Pt (ppb)	Pd (ppb)	Pt/Pd	Au (ppb)	Sample
Main Yubdo Intrusion	Dun	22.9	912	<2	177	<0.1	121	<2	-	<2	AYR-016-01
	Dun	23.0	1043	<2	225	<0.1	<2	<2	-	<2	Y10
	Dun	23.0	784	<2	245	<0.1	<2	<2	-	<2	Y12
	Dun	24.0	583	<2	170	<0.1	<2	<2	-	<2	Y13
	Dun	22.8	711	2	301	<0.1	<2	<2	-	<2	Y7
	Ol-cpx	13.4	1016	10	905	0.1	<2	<2	-	<2	Y16

Table 8.27: Mg, Ni, Cu, Cr, Al, Pt and Pd values for the fresher samples (as defined in section 8.3.1) collected from the Yubdo, Andu and Sodu areas. Dun: Dunite. Ol-cpxite: Olivine-clinopyroxenite. Cpxite: Clinopyroxenite.

Formation	Description	Mg (%)	Ni (ppm)	Cu (ppm)	Cr (ppm)	Al (%)	Pt (ppb)	Pd (ppb)	Pt/Pd	Au (ppb)	Sample
Main Yubdo Intrusion	Dun	1.4	55	100	67	2.1	6	4	1.5	2	DYR-026-01
	Dun	9.5	774	3	784	0.2	109	<2	-	<2	KYR-019-01
	Dun	10.6	553	38	783	1.5	65	<2	-	<2	TYR-009-01
	Dun	25.7	1847	5	54	<0.1	<2	<2	-	<2	Y30
	Dun	<0.1	269	22	1835	3.8	28	2	14.0	4	YR 08/01
	Ol-cpx	13.0	949	5	536	0.8	57	<2	-	<2	DYR-023-01
	Ol-cpx	7.8	682	7	786	0.2	30	<2	-	<2	KYR-018-01
	Ol-cpx	6.2	232	7	645	0.4	23	<2	-	<2	TYR-008-01
	Ol-cpx	1.2	118	8	528	0.4	7	6	1.2	4	YR 06/01
	Cpxite	4.4	202	15	753	0.7	19	<2	-	2	AYR-002-01
	Cpxite	4.7	256	4	753	4.8	<2	<2	-	<2	Y17
	Cpxite	1.1	77	7	722	0.6	<2	<2	-	<2	Y23
	Cpxite	0.9	33	<2	179	0.4	<2	<2	-	<2	Y24
Lensoid Ultramafic	Dun	<0.1	7	24	55	0.2	<2	<2	-	55	DYR-029-01
	Dun	<0.1	24	52	92	2.3	<2	<2	-	<2	KYR-017-01
	Dun	2.8	24	30	20	2.8	<2	<2	-	2	TYR-013-01
	Ol-cpx	2.0	45	87	55	2.6	<2	<2	-	<2	AYR-032-01
	Ol-cpx	3.0	191	63	410	2.8	2	<2	-	3	AYR-036-01
Other	Basa	2.6	48	37	58	4.2	<2	<2	-	<2	AYR-018-01
	Birb	<0.1	928	8	1588	0.1	22	<2	-	<2	DYR-022-01
	Birb	<0.1	46	93	64	2.6	<2	<2	-	<2	TYC-010-01
	Birb	0.1	1599	5	1245	0.3	<2	<2	-	<2	Y29
	Birb	0.1	18	77	185	3.2	<2	<2	-	<2	YR 01/01
	Birb	<0.1	56	13	592	1.9	31	<2	-	3	YR 02/01
	Birb	<0.1	27	14	1189	4.6	21	<2	-	<2	YR 03/01

Birb	<0.1	71	25	65	1.8	<2	<2	-	<2	YR 04/01
Birb	<0.1	401	7	626	0.1	50	<2	-	2	YR 07/01
ChSchi	0.6	5	7	9	1.6	35	<2	-	<2	YR 05/01
Dior	0.5	<2	5	<2	1.1	<2	<2	-	<2	TYR-021-01
Dole	2.5	68	93	69	1.4	<2	<2	-	2	AYR-014-01
Dole	1.8	50	94	62	1.9	<2	<2	-	2	AYR-017-01
Dole	1.3	23	74	73	1.7	<2	<2	-	41	AYR-028-01
Dole	2.0	46	97	59	1.7	<2	<2	-	<2	AYR-030-01
Dole	2.5	33	26	26	1.9	<2	<2	-	<2	AYR-031-01
Dole	<0.1	152	77	237	1.9	<2	<2	-	<2	DYR-013-01
Dole	2.7	58	90	83	1.5	<2	<2	-	<2	DYR-028-01
Gabb	1.7	9	17	6	2.4	<2	<2	-	<2	AYR-013-01
Gabb	0.7	4	4	5	1.3	<2	<2	-	8	AYR-029-01
Gabb	0.4	24	5	81	0.2	17	<2	-	<2	TYR-007-01
Gabb	0.8	15	37	16	1.5	<2	<2	-	<2	TYR-026-01
Gabb	4.0	136	3	361	0.3	<2	<2	-	<2	Y3
Gabb	5.7	191	5	439	1.1	<2	<2	-	<2	Y4
HardP	<0.1	45	60	686	4.0	3	<2	-	3	AYC-012-01
HardP	<0.1	15	40	216	3.6	<2	<2	-	<2	AYC-013-01
HardP	<0.1	24	86	115	3.7	3	<2	-	<2	AYC-014-01
HardP	<0.1	8	35	281	2.5	2	<2	-	2	DYR-011-01
HardP	<0.1	7	29	512	1.7	<2	<2	-	7	DYR-015-01
HardP	0.1	632	40	8487	2.1	143	3	47.7	3	DYR-025-01
HardP	<0.1	21	62	126	1.7	<2	<2	-	<2	KYC-001-01
HardP	<0.1	66	248	408	2.8	<2	<2	-	3	KYC-002-01
HardP	<0.1	31	239	333	0.9	<2	<2	-	<2	KYC-003-01
MetaSed	1.9	125	46	183	3.2	3	5	0.6	4	AYR-015-01
MetaSed	0.8	16	198	13	1.4	<2	<2	-	4	AYR-035-01
MetaSed	0.1	346	282	52	1.2	5	9	0.6	7	TYR-010-01
Mylo	0.8	20	33	177	1.1	3	3	1.0	<2	AYR-012-01
Quar	<0.1	2	2	5	0.1	<2	5	0.0	<2	DYR-012-01
Schi	1.8	52	19	37	2.9	<2	<2	-	<2	AYR-020-01
Schi	0.6	93	95	68	1.7	<2	6	0.0	9	DYC-009-01
Schi	0.4	31	25	40	0.8	<2	<2	-	<2	DYR-014-01
Schi	1.8	45	75	221	5.1	4	<2	-	5	KYC-006-01
Schi	0.6	125	50	64	1.5	<2	<2	-	<2	TYR-011-01
Schi	0.3	861	4	716	0.1	<2	<2	-	<2	Y31
Schi	21.2	1218	<2	234	<0.1	<2	<2	-	<2	Y6
Sed	0.1	8	48	19	1.0	<2	<2	-	35	AYC-015-01
Sed	<0.1	106	61	1700	2.8	13	2	6.5	22	DYR-027-01
Sed	<0.1	22	85	260	0.6	<2	<2	-	<2	TYC-007-01
Sed	<0.1	99	86	341	1.5	5	3	1.7	3	TYC-011-01
TaSchi	0.3	51	4	1585	0.3	39	47	0.8	<2	AYR-011-01
TaSchi	0.3	124	10	225	0.1	5	<2	-	<2	DYR-019-01
TaSchi	0.5	78	3	345	0.1	19	<2	-	2	DYR-024-01
TaSchi	0.9	387	57	1846	3.9	5	3	1.7	<2	KYC-004-01
TaSchi	0.3	289	4	2089	1.0	21	<2	-	<2	KYC-005-01
TaSchi	10.6	858	8	1907	4.2	42	<2	-	2	KYR-020-01
TaSchi	<0.1	24	50	74	0.4	<2	<2	-	<2	TYC-009-01
TaSchi	0.9	20	3	15	1.4	<2	<2	-	<2	TYR-012-01
TaSchi	0.6	52	60	79	1.1	<2	9	0.0	<2	TYR-014-01
TaSchi	0.6	53	2	39	0.9	<2	<2	-	<2	TYR-015-01
TaSchi	0.4	53	14	75	2.6	4	3	1.3	4	TYR-019-01
TaSchi	<0.1	2	<2	2	1.7	<2	<2	-	<2	TYR-022-01
Unid	1.9	39	57	48	4.6	<2	<2	-	4	AYC-017-01
Unid	<0.1	4	4	19	0.1	<2	<2	-	16	DYC-010-01
Unid	0.2	12	37	36	0.5	<2	<2	-	<2	Y18
Unid	0.1	1028	6	972	0.1	<2	<2	-	<2	Y1
Unid	1.2	63	59	387	1.8	<2	<2	-	<2	Y20
Unid	3.7	26	30	47	4.0	<2	<2	-	<2	Y21
Unid	3.8	10	8	7	3.6	<2	<2	-	<2	Y22
Unid	0.2	9	2	19	0.1	<2	<2	-	<2	Y5
VQuar	<0.1	2	3	11	0.1	<2	<2	-	<2	DYR-016-01
VQuar	<0.1	3	<2	6	<0.1	<2	<2	-	<2	DYR-017-01
VQuar	<0.1	2	3	7	<0.1	3	<2	-	3	DYR-020-01
VQuar	<0.1	<2	2	3	<0.1	<2	<2	-	<2	DYR-021-01
VQuar	<0.1	2	<2	5	<0.1	<2	<2	-	<2	TYC-008-01
VQuar	8.0	324	11	923	0.6	<2	<2	-	<2	Y25
VQuar	2.2	123	11	671	0.5	<2	<2	-	<2	Y26

Table 8.28: Mg, Ni, Cu, Cr, Al, Pt and Pd values for the altered samples collected from the Yubdo, Andu and Sodu areas. Anor: Anorthosite. Basa: Basalt. Birb: Birbirite. ChSchi: Chlorite-Schist. ChSchi: Chlorite-Schist. Cpxite: Clinopyroxenite. Dior: Diorite. Dole: Dolerite. Dun: Dunite. Fels: Felsite. Gabb: Gabbro. GranDi: Granodiorite. HardP: Hard pan. MetaBas: Metabasalt. MetaSed: Metasediment. Mylo: Mylonite. Ol-cpxite: Olivine-clinopyroxenite. Quar: Quartzite. Schi: Schist. Sed: Sediment. TaSchi: Talc-Schist. TCSchi: Talc-Chlorite-Schist. Troc: Troctolite. Unid: Unidentified. VQuar: Vein Quartz.

The following sections cover the distribution of Ni, Cu, Cr and Al in the Yubdo area. Each section covers one element and describes its distribution in fresher ultramafics and altered rocks. These sections are accompanied by a fold-out page (on page 262) of maps showing the distribution of all elements which the reader should refer to as each section is read.

8.20.3. Nickel

Of the fresher ultramafics within the Main Yubdo Ultramafic the highest Ni analysis (1046ppm) was returned for a dunite close to the centre of the intrusion. It is noted that an olivine-clinopyroxenite close to the northern contact with the basement was analysed at a similar figure (1016ppm). The other samples from the area returned Ni values between 583ppm and 912ppm – no zonation can be observed.

In the Yubdo area, all Ni concentrations of over 390ppm in rock occur over the main ultramafic (figure 8.13A). Figure 8.13A shows that the samples of highest Ni in rock (>1000ppm) are all within 300m of a shear zones. The largest concentration of Ni in the rocks from the Main Yubdo Ultramafic occurs in a dunite (1847ppm). The lowest Ni value (24ppm) occurs in the eastern clinopyroxenite zone. In the Lensoid Ultramafics the olivine-clinopyroxenites contain Ni of up to 191ppm and the two dunites both contain 24ppm.

8.20.4. Copper

Two of the 6 fresher ultramafics from Yubdo contain Cu. The highest Cu value (10ppm) occurs in the olivine-clinopyroxenite in close to the northwestern flank. The other value above detection (2ppm) occurs towards the centre of the intrusion.

Copper is elevated to above 70ppm in only 6% (2 of 32) of altered samples of the Main Yubdo Ultramafic whereas in other formations 26% (18 of 69) of samples rise above this level. The highest Cu value in the Main Intrusion (100ppm) occurs in an altered dunite close to the olivine-clinopyroxenite zone of the western contact with the basement. Figure 8.13B shows that most other Cu analyses in the Main Yubdo Ultramafic fall below 15ppm and can fall as low as 3ppm (in an olivine-clinopyroxenite on the western contact with the basement). This compares with the Lensoid Ultramafics where Cu analyses of two dunite samples return values were 30ppm and 52ppm and two analyses of olivine-clinopyroxenite samples were 63ppm and 87ppm.

8.20.5. Chromium

The highest Cr values in fresher rocks (905ppm) occurs in the olivine-clinopyroxenite sample near the northwestern flank of the complex. All other Cr analyses fall below 300ppm and can be as low as 54ppm in a dunite close to the eastern contact with the basement.

In the Yubdo area, Cr is enriched dominantly in the rocks from two areas, the Main Yubdo Ultramafic and around a talc-schist near the northern Lensoid Ultramafics. In addition to this, an olivine-clinopyroxenite and a talc-schist in the southeastern corner of the area also contain significant values of Cr (410 and 1585ppm respectively). The highest Cr value for the Yubdo Main Intrusion is 8487ppm in a hard pan found above the clinopyroxenite zone on the western flank of the Main Yubdo Ultramafic. Two talc-schists in the northern tip of the complex contain high Cr values (1907ppm and 2089ppm). The highest Cr value in the altered ultramafic samples (1835ppm) occurs in a dunite of the Main Yubdo Ultramafic, this occurs at the farthest western extension of the complex. The lowest Cr value of the Main Yubdo Ultramafic is 54ppm in a dunite on the western flank but still 1km away from the sample with the highest Cr value. Within the Yubdo Main Intrusion the samples bearing high Cr contents (>1000ppm) are often located close (within 200m) to samples without such elevated contents.

8.20.6. Aluminium

One fresher sample – the only fresher olivine-clinopyroxenite on the northwestern flank - contains Al above detection limits (0.1%).

The altered rocks of the Main Yubdo Ultramafic have lower background levels of Al than the basement units in the area. Some dunites in the Yubdo Main Intrusion have Al levels below detection whereas in the basement rocks values do not drop below 0.5% (figure 8.13D). The highest value for Al content (5.1%) occurs in a schistose basement rock related to a shear zone north of Yubdo. Within the Main Yubdo Ultramafic, the highest Al value (4.8%) occurs in the pyroxenite body from the northwestern flank. In the Main Yubdo Ultramafic, the four highest Al analyses come from samples aligned along the northwestern flank. The Al contents of the Lensoid Ultramafics are higher than many parts of the Main Yubdo Ultramafic showing a minimum of 2.3% and a maximum of 2.8%.

8.20.7. Summary of the Ni, Cu, Cr and Al values from the Yubdo Main Intrusion

The highest Ni and Cu values in fresher rocks do not co-incide. The highest Cu value of the fresher ultramafic samples occurs in an olivine-clinopyroxenite at the northwestern flank, this sample also contains a high Ni value. However, the highest Ni value occurs in a dunite close to the centre of the intrusion. The highest Cr value also occurs in the same olivine-clinopyroxenite sample which has the highest Cu.

The highest Cr values in altered rocks occur at the edge of the intrusion. Similarly, the highest Cu values of the altered rocks occur close to the western edge of the intrusion. All samples with high Ni are also located at the edges, but also close to Shear Zones which pass through the centre of the complex.

8.21. Yubdo, Sodu and Andu: Pt and Pd distribution

Pt was detected in one sample of fresher rocks from the Yubdo Main Intrusion at a value of 121ppb. Pd was not detected in any fresher rocks of the Yubdo, Andu and Sodu areas.

The highest Pt assay in the rocks of the Yubdo area (143ppb) was from a hard-pan sample overlying the western pyroxenite zone of the Main Yubdo Ultramafic. Of the altered rocks, the highest Pt value (109ppb) occurs in a dunite located within at the northern tip of the Main Yubdo Ultramafic. The highest Pd value in the area (47ppb) was found in a sample of a talc-schist in the southeastern flank of the intrusion. In the Main Yubdo Ultramafic, the highest Pd value is 6ppb found in an olivine-clinopyroxenite. Only 3% (2 of 63) of samples returned Pd values above detection limits. For Pt 71% (45 of 63) of assays returned values above detection limits. For the Lensoid Ultramafics, only one sample is Pt bearing (2ppb) and all Pd assays were below detection limits. Two further assays of 9ppb Pd each were obtained from a meta-sediment and a talc-schist in the basement area north of Yubdo. Additionally, a talc-schist in the southeastern part of the study area was assayed at 39ppb and 47ppb for Pt and Pd respectively.

The comparison between PGE and Ni, Cu, Cr and Al in the highest samples is summarised as follows:

Sample	Description	Pt (ppb)	Pd (ppb)	Ni (ppm)	Cu (ppm)	Cr (ppm)	Al (%)
AYR-016-01	Dun	121	< 2	912	< 2	177	< 0.1
Y10	Dun	< 2	< 2	1043	< 2	225	< 0.1
Y16	Olivine-clinopyroxenite	< 2	< 2	1016	10	905	0.1
Y12	Dun	< 2	< 2	784	< 2	245	< 0.1
Y7	Dun	< 2	< 2	711	2	301	< 0.1
Y13	Dun	< 2	< 2	583	< 2	170	< 0.1

Table 8.29: A summary of Ni, Cu, Cr and Al values in the fresher samples from the Main Yubdo Ultramafic. A graphical representation of this data is provided in figure 8.12.

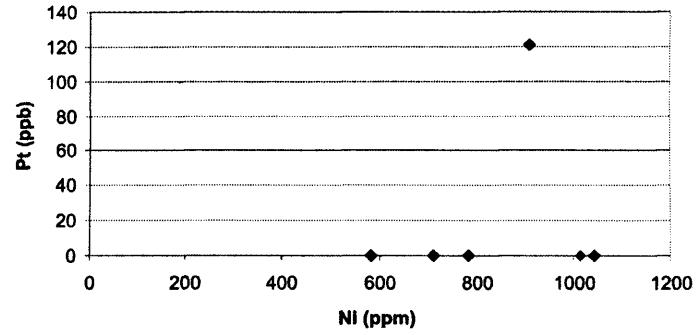

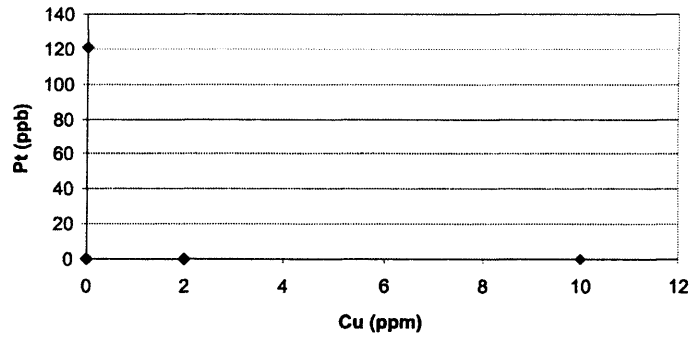

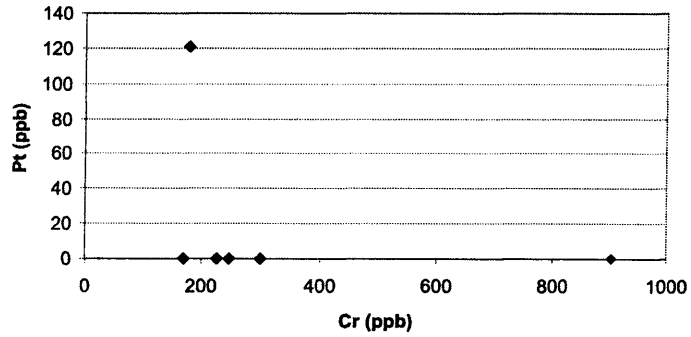

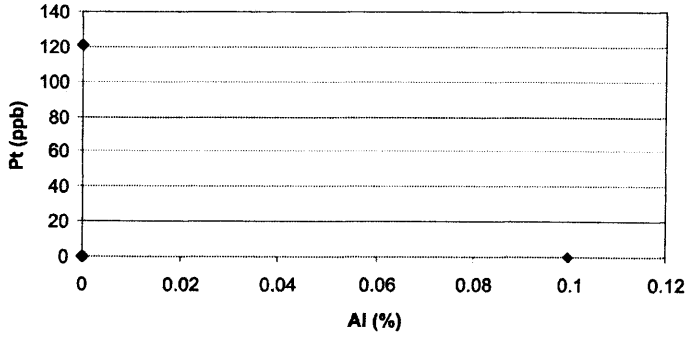

Figure 8.12: Graphs of Ni, Cu, Cr and Al versus Pt in the fresher rocks from the Main Yubdo Ultramafic.

8.22. Yubdo, Sodu and Andu: Discussion

Here the processes likely to have affected the distribution of Ni, Cu, Cr Al, Pt and Pd in the Yubdo, Andu and Sodu areas are discussed. The processes involved with the distribution of Ni, Cu, Cr and Al in fresher ultramafics are considered in sections 8.22.1 and 8.22.2, followed by those processes which affect altered rocks in 8.22.3 and 8.22.4. The mechanisms which distribute Pt and Pd are considered from section 8.22.5 and section 8.22.6.

8.22.1. The locations of the highest Ni and Cu values in the fresher rocks from the Main Yubdo Ultramafic

The highest Ni value in the fresher rocks from the Main Yubdo Ultramafic occurs in an olivine-clinopyroxenite sample close to the centre of the intrusion. Another large Ni value (1016ppm) occurs with the highest Cu value (10ppm) in an olivine-clinopyroxenite near the northwestern flank. As discussed in section 8.6.2, because all Ni values within the fresher rocks from the Yubdo dataset are lower than 3293ppm, the element could potentially be partitioned entirely into the olivine minerals without the presence of sulphides (see section 8.6.2). The partition co-efficient for Ni clearly makes the case that the element will preferentially partition into sulphide but can also partition into the olivine crystal structure. Cu on the other hand is likely to partition into sulphide but is unlikely to partition into olivine (see table 8.30). For sample Y16 (see table 8.29) it is expected that the Cu exists in ISS. In a situation where sulphide co-precipitated with olivine, the Ni would also partition into the sulphide. But as the residual sulphide liquid which forms ISS may have been filter pressed into its current position (see 8.7.2) it is not possible to determine the phase which contains Ni. The Ni-rich but Cu-barren samples may represent either Ni partitioned into olivine or into MSS. It is, therefore, suggested that sulphides are present in sample Y16, but it is not possible to ascertain whether Ni has partitioned into sulphide or olivine. Analysis of the sulphide mineral geochemistry is required to confirm the presence of sulphides and understand the behaviour of Ni in this case.

Rock Type	Mineral	Value	Low	High	D_{Cu} Type	Reference
MSS	Olivine	730			Experimental	Pedersen 1979
Basalt-Andesite	Olivine	0.55			Experimental	Kloeck & Palme 1988
Andesite	Olivine	0.11			Phenocrysts-Matrix	Bougault & Hekinian 1974
Basalt-Andesite	Olivine	0.055			Phenocrysts-Matrix	Ewart & Griffin 1994
Basalt-Andesite-Dacite	Olivine	0.05			Phenocrysts-Matrix	Dostal et al. 1983
Basalt-Andesite	Olivine	0.023			Experimental	Paster et al. 1974
Basalt-Andesite	Olivine		0.075	0.19	Experimental	Gaetani & Grove 1997
Basalt-Andesite	Olivine		0.4	0.5	Experimental	Pedersen 1979
Andesite	Olivine			2.2	Phenocrysts-Matrix	Ewart & Griffin 1994
Per-Alkaline Rhyolite	Olivine			2.7	Phenocrysts-Matrix	Ewart & Griffin 1994
Andesite	Clinopyroxene	0.66			Phenocrysts-Matrix	Ewart & Griffin 1994
Basalt	Clinopyroxene	0.36			Experimental	Hart & Dunn 1993
Basalt	Clinopyroxene	0.18			Phenocrysts-Matrix	Bougault & Hekinian 1974
Basalt	Clinopyroxene	0.071			Experimental	Paster et al. 1974
Leucosome	Clinopyroxene	0.02			Phenocrysts-Matrix	Ewart & Griffin 1994
Basalt-Andesite	Clinopyroxene		0.05	0.08	Phenocrysts-Matrix	Dostal et al. 1983
Basalt-Andesite	Clinopyroxene		0.09	1.1	Model	Ewart et al. 1973
Basalt-Andesite	Clinopyroxene		0.12	0.69	Phenocrysts-Matrix	Ewart et al. 1973
Dacite	Clinopyroxene		0.44	3.1	Model	Ewart et al. 1973
Dacite	Clinopyroxene		0.51	0.87	Phenocrysts-Matrix	Ewart et al. 1973
Low Silica Rhyolite	Clinopyroxene		0.8	2.2	Phenocrysts-Matrix	Ewart & Griffin 1994
Per-Alkaline Rhyolite	Clinopyroxene			1.1	Phenocrysts-Matrix	Ewart & Griffin 1994

Table 8.30: Partition co-efficients of Cu between olivine and clinopyroxene and melt or host rock type (as stated), where D_{Cu} = Olivine / Melt or Host Rock. This data was compiled using the GEOROC database (2005).

The "fresher" rocks as classified here contain Mg values which are high enough to expect most features to reflect magmatic processes, however some degree of alteration is present in many samples (chapter 3). It is therefore conceivable that the Cu value has been redeposited into this location from a site of magmatic concentration elsewhere. The

presence of the high Ni value in a dunite close to a shear-zone may further infer that this value could have originated from high temperature fluids.

8.22.2. Locations of highest Cu and Cr values in fresher rocks

The highest Cu value occurs in an olivine-clinopyroxenite (Y16) near the northwestern flank – this sample also has the largest Cr value of the intrusion. The Cr is most likely to have been partitioned into spinel minerals (see section 8.6.3). However, in this study it is unlikely that these spinels will have been dissolved and therefore the Cr analysed will have been the Cr partitioned into olivine. It has been suggested (section 8.22.1) that the Cu observed in this sample may occur in a sulphide phase, however it is not possible to determine whether this sulphide was precipitated in-situ or has been filter pressed into place. Furthermore the Cu values could have become transported into location by hydrothermal fluids. Similarly, the co-incidence of the highest Cu and Cr values being seen in the same sample could be explained by two models. Either a residual sulphide liquid has been filter-pressed into contact with a spinel rich cumulate layer or by sulphide segregation occurring simultaneously to Cr-spinel precipitation. Furthermore, it is possible that some Cu concentration may have originated from hydrothermal redeposition. From this data, it is not possible to determine which hypothesis could have caused the geochemical patterns seen, however a study of the sulphide mineral morphology may elucidate the origin.

8.22.3. Zonation of Cr values the altered rocks from the Main Yubdo Ultramafic

The highest Cr values from the Main Yubdo Ultramafic occur within 600m of the edge of the intrusion. As discussed in section 8.6.8, when Cr partitions into spinels it becomes highly immobile in hydrothermal fluids and weathering. Although in this case, the Cr measured is likely to be parititioned into olivine, the high Cr values are likely to reflect the same pattern which would have existed in their respective protoliths. Furthermore, the highest Cr value occurs in a rock at the edge of the Main Yubdo Ultramafic. As spinels precipitate early during fractionation - with olivine - it is

suggested that the most primitive rocks of the intrusion are those at the flanks of the intrusion.

8.22.4. The locations of high Ni and Cu values in altered rocks from the Main Yubdo Ultramafic

All Ni values of higher than 1000ppm in the altered rocks from the Main Yubdo Ultramafic occur within 300m of Shear Zones whereas high Cu values only occur close to the flanks of the intrusion. As applied to the Kingy Ridge Ultramafic (see section 8.12.4) there are two possible reasons for this difference in distribution. One possibility is that although both elements have the potential to be remobilised by high-temperature fluids under similar conditions (see section 8.6.8), - two alteration episodes have acted either on different geographic areas or under different aqueous conditions. The second possibility is that one element has not been remobilised. The proximity of samples containing high Ni close to Shear Zones indicates a possible relationship between Ni and shearing however this deformation may simply have acted over sites of magmatic concentration. Without a detailed study of mineral morphology, it is not possible to determine which of these is the case.

8.22.5. Genesis of Pt and Pd in fresher rocks

Only one sample has returned a value for Pt which is above the detection limit (121ppb) and no Pd has been detected in the fresher rocks of the Main Yubdo Ultramafic. This sample is a dunite located close to the northwestern flank of the Main Yubdo Ultramafic and contains intermediate values of Ni and Cr and is barren of Cu (see table 8.29).

In a situation where the entire complex formed from one sulphur-bearing primitive melt which had undergone sulphide saturation and fractionation, the Pt and Pd is likely to be concentrated into the Cu-rich ISS – but this is not seen at Yubdo. Furthermore, if sulphide segregation had occurred but sulphide fractionation had not then the Pt and Pd should be concentrated into samples with highest Ni value – but this is also

not seen at Yubdo. In a situation where immiscible sulphides were not present, the Pt and Pd would be distributed throughout the mass of rock but could not become concentrated to the level seen here (121ppb). Here the only Pt-bearing sample contains no Cu at all and only intermediate values of Ni.

Given that some alteration is possible in "fresher" samples (chapter 3). It is possible that high temperature aqueous fluids could have remobilised both Pt and Pd alongside Ni and Cu. This may result in either a rise or fall in values for all 4 elements with respect to a 100% fresher rock. As such, any Cu present in the in the Pt-bearing sample may have been removed or alternatively, the Pt could have been redeposited here from a different site of magmatic concentration. It is likely that a study of the mineralogy of the sample could help understand the relative effects of magmatic and hydrothermal processes.

8.22.6. Genesis of Pt and Pd in altered rocks

Within the Main Yubdo Ultramafic, an altered dunite at the northern tip of the complex contains a Pt value of 109ppb and Pd was not found above detection limits. Six additional altered samples contain Pt above detection limits, all of which occur around the flanks of the intrusion and none contain any Pd (see figure 8.13E). Furthermore, slightly elevated Pd contents (9ppb) are found in a talc-schist and a metasediment in the basement north of Yubdo. Another Pt- and Pd-bearing talc-schist sample has been found in the southeast of the study area which contains 39ppb and 47ppb respectively.

The altered rocks of the Yubdo area may potentially show processes of either magmatic concentration or hydrothermal remobilisation – and possibly both. Either process could explain the distribution of Pt in the altered rocks from the Main Yubdo Ultramafic. An argument could be made for the preferential remobilisation of Pd (see section 8.6.8). The Pd could have been remobilised by hydrothermal fluids and reprecipitated in the basement talc-schists, whereas the Pt would not be taken into solution as easily and therefore left in place. However, the only PGE-bearing fresher

sample from the dataset shows no Pd at all – which infers that there was no Pd to be remobilised. In addition to this, it would be unlikely for hydrothermal fluids to remove all the Pd from the rocks, if there was some there at first, a remnant should remain. And hence, the alternative hypothesis is that the hydrothermal fluids have not remobilised Pd, as there was none there in the first instance. It is feasible that some limited remobilisation of Pt has occurred, although it would not be possible to distinguish such a process from this data.

8.23. Yubdo, Sodu and Andu: Conclusions

It is difficult to assess the prospectivity of the Main Yubdo Intrusion with the dataset presented here due to a lack of fresher rock samples. It appears that the edges of the complex may be the most primitive but an additional zone of primitive ultramafics may exist within the complex. Furthermore, it is not possible to conclude whether sulphide segregation has or has not occurred. It is likely that fluids passing along shear zones at the flanks and through the centre of complex may have a role in the remobilisation of Pt and Pd. Future exploration should concentrate on assessing potential mineralisation around shear zones and at the flanks of the intrusion.

Pd values in talc-schists north of the Yubdo Main Intrusion suggest that the element may have been remobilised by hot fluids in the Yubdo area. As there is no Pd in the fresher rocks and Pt is largely immobile it is not possible to comment on the effects of hydrothermal fluids on PGE distribution in the Main Yubdo Ultramafic.

8.25. Pt and Pd prospectivity and ore forming processes

Here, a summary of the potential magmatic and post-magmatic ore forming processes is given and these are summarised finally by a description of the Pt and Pd prospectivity of the WES.

8.25.1. Magmatic ore forming processes

Area	Formation	Fresher Rock samples	
		Pt (ppb)	Pd (ppb)
Yubdo	Main Yubdo Ultramafic	121	< 2
Tulu Dimtu	Tulu Dimtu Main Intrusion	37	40
Daleti	Daleti Ultramafic	8	< 2
Kingy	Kingy Ridge Ultramafic	3	< 2

Table 8.31: The maximum Pt and Pd values found in the fresher rocks of the ultramafic complexes of the WES.

Throughout this chapter the Ni, Cu and Cr values of the major ultramafic complexes from the WES are discussed in relation to potential Pt and Pd ore forming processes. Here, the major processes involved are compared, these are: fractionation, sulphide segregation and PGE concentration. These models are presented on the assumption of a minimal influence of post-magmatic hydrothermal fluids on the Ni and Cu values of the fresher samples. Studies of PGM and sulphide mineral morphology are required throughout the study area in order to understand the relative influence of magmatic processes and hydrothermal fluids. Furthermore, in all four areas the analysis of spinel or olivine mineral geochemistry is required to test the possibility of the influx of multiple melts.

In both the Main Yubdo Intrusion and the Tulu Dimtu Main Intrusion Cr-values indicate that the most primitive rocks occur at the edges of the complexes. Fractionation trends can be observed in the Daleti and Kingy ridge complexes although it is harder to understand the structural relationships involved with these intrusions. Due to their refractory nature, it is unlikely that Cr-spinels will have been digested by aqua regia. Furthermore, analysis of standards (see section 8.2.4) has shown that the Cr analyses

presented here are relatively imprecise. However, many analyses return positive results with systematic spatial trends (see figure 8.4C). It is expected that in the case of these samples, the Cr analysed will have been partitioned into olivine, which can be digested in some cases (Church et al., 1987). As Cr is relatively compatible in olivine, it is considered to concentrate into primitive rocks.

Relatively reliable Ni and Cu analyses make an assessment of the presence of sulphides possible in some areas. Sulphide segregation is suggested to have occurred in the Tulu Dimtu Main Intrusion and the Daleti Ultramafic. In the Tulu Dimtu Main Intrusion sulphide segregation is thought to have occurred at the edges of the intrusion at around the same time as limited Cr-spinel precipitation. Large Ni values in the Daleti Ultramafic suggest that sulphides have been present. However, lack of samples makes it is difficult to make reliable conclusions for the Main Yubdo Intrusion. Similarly, insignificant Cu and Ni values in the Kingy area makes an assessment of sulphides difficuly.

The only fresher rocks which contain Pd above detection limits are from the Tulu Dimtu Main Intrusion. When sulphide segregation occurs - if present - both Pt and Pd should be scavenged from the melt. As sulphide segregation is believed to have occurred, it is possible that the magma from which the Daleti complex formed was largely barren of Pt and Pd.

A number of smaller ultramafic complexes (<1km^2 area) occur in the Kingy, Tulu Dimtu and Keley areas – these are referred to as the Lensoid Ultramafics. A limited number of fresher samples have been analysed from the Tulu Dimtu area. These show elevated Cr values and intermediate Ni values, such as those found at the flanks of the Tulu Dimtu Main Intrusion. These observations suggest that these small ultramafics could be slivers of rock "shaved-off" larger complexes during deformation. Detailed study of the structure and geochemistry of these bodies is required to understand their genesis.

8.25.2. Post-magmatic ore forming processes

Area	Formation	Altered Rock samples	
		Pt (ppb)	Pd (ppb)
Yubdo	Main Yubdo Ultramafic	109	47
Daleti	Keley ultramafic	33	3
Tulu Dimtu	Tulu Dimtu Main Intrusion	24	15
Kingy	Kingy Ridge Ultramafic	18	28
Daleti	Ankori	15	16
Daleti	Daleti Ultramafic	8	<2

Table 8.32: The maximum Pt and Pd values found in the altered rocks from the ultramafic complexes of the WES

In all four areas the distribution of Ni and Cu in lithologies such as talc-schists and quartzites indicate that both elements may have been remobilised by hot fluids using Shear Zones as conduits. Furthermore, the elevation of Ni and Cu values in ultramafic samples located away from known sites of concentration in fresher rocks indicates that these hot fluids may have passed through and precipitated minerals within the flanks of the ultramafic intrusions.

At Yubdo, Kingy and Daleti the highest Ni concentrations are observed in different altered samples from the highest Cu concentrations. This is seen particularly in the Daleti area where numerous talc-schist samples are elevated either in Ni or in Cu, but rarely both. This indicates a different mode of genesis for the two elements in altered rocks. These may be either different alteration episodes (under different conditions or acting on different geographical areas) or it may be that one element has not been remobilised. At Kingy, the distribution of Ni in altered rocks is very similar to the fractionation trend observed for Cr. As Cr is considered to be immobile, it is possible that Ni still retains a "relict" magmatic signature and has not been remobilised. However, at Yubdo high Ni values are obtained in samples located close to Shear Zones suggesting that it has been remobilised.

As with Ni and Cu, high values of Pd are found in certain shear-zone related lithotypes. In particular, a quartzite sample from the Keley area and a talc-schist near Yubdo. These occurrences – and a known affinity of Pd in hydrothermal fluids - strongly suggest that Pd has been taken into solution by high-temperature fluids. It is feasible that

these fluids could be similar to those which have remobilised Ni and Cu. The dislocation of Pt and Pd values (in fresher compared to altered rocks) in the flanks of the Tulu Dimtu Main Intrusion also support this argument.

With the exception of the Tulu Dimtu Main Intrusion, Pd is found in the altered rocks but not in the fresher rocks, particularly in the Kingy Ridge Ultramafic. This feature is difficult to explain but two suggestions can be offered. Either, hydrothermal fluids have reconcentrated the element from very small values in fresher rocks into larger values in the altered rocks. Or the Pd has been transported into the area from a site of magmatic Pd which has not been discovered in this study. The close proximity of high Pd values to Shear Zones flanking the Kingy intrusions indicates the latter (see figure 8.7F).

8.25.3. Prospectivity

Given the extensive weathering and alteration to which the WES has been subjected, any evaluation of magmatic ore forming processes is likely to be prone to difficulty. However, there is better evidence for the effects of post-magmatic hydrothermal processes.

In the Tulu Dimtu Main Intrusion and the Main Yubdo Intrusion the most primitive rocks are inferred to occur at the flanks of the intrusion. Therefore it is recommended that any future exploration is targeted in these areas. However, it is unknown whether or not sulphide segregation has occurred in the Main Yubdo Intrusion and hence if a PGE rich horizon can be discovered in this area. Further sampling is required.

Considerable evidence for the hydrothermal remobilisation of Pt and Pd is found in each of the four areas. The more notable occurrences are, the extensive Pd mineralisation at Kingy and shear zones in the Daleti and Yubdo areas. The presence of Pd, Cu and Ni in these lithotypes related to hydrothermal fluids indicate that a richer source of precious metals may be found in the vicinity.

9. Results: Spinel Geochemistry

9.1. Introduction

The geochemistry of spinels from the ultramafic rocks from four geographic areas was studied with the aim of understanding the magmatic conditions under which the spinels formed. Spinels were chosen over the other minerals present in the rocks for a number of reasons. Within the severe alteration conditions of the WES, spinels minerals are the most likely to retain magamatic geochemistries. Minerals such as olivine and pyroxene are often highly altered (see chapter 3). Furthermore, there has been considerable previous work on the use of Cr-spinels for tectonic discrimination (Sack and Giorso, 1991).

The major element geochemistry of the spinels was determined using an energy dispersive X-ray analyzer attached to a scanning electron microscope (SEM). Such a system can only measure the total Fe within a specimen and the estimation of the relative proportions of Fe^{2+} or Fe^{3+} was performed using the mineralogical method described in section 9.3. In an attempt to separate alteration from magmatic effects an assessment of the geochemical difference between the cores and rims of zoned spinels is described in section 9.4. Subsequently the spinel geochemistry of each of the four geographic area is considered in sections 9.5 to 9.17

This chapter examines the geochemistry of the spinels using TiO_2 analysis and the following ratios:

$Fe^{2+}\# = Fe^{2+} / (Fe^{2+} + Mg)$
$Fe^{3+}\# = Fe^{3+} / (Fe^{3+} + Al + Cr + V)$
$Cr\# = Cr / (Cr + Al)$

These parameters were chosen because they can be used to discriminate between Alaskan-type intrusions and ophiolite complexes. Published spinel analyses have been used by Barnes and Roeder (2001) to create "90^{th} percentile" fields for several plutonic

settings including Alaskan-type intrusions and ophiolite complexes. These fields use TiO_2 and the ratios above to charaterise the typical composition of spinels from each type of complex. In particular, a plot of Fe^{2+}# versus Cr# shows a clear difference in geochemistry between Alaskan-type intrusions and ophiolites. Many other authors (Evan and Frost, 1975; Stowe, 1994; Jan et al., 1985) have used the same ratios to illustrate the relative effects of hydrothermal alteration and magmatic processes. Such processes are likely to have influenced the geochemistry of the spinels studied here and the effects of these processes are considered for the dataset from these four areas.

This chapter is divided into four sections covering each of the four geographic areas. At the end of each results section there is a "pull-out" page which includes a map showing sample locations and the graphs showing the chromite geochemistry which are referred to throughout the section.

9.2. Methods

9.2.1. Sample Preparation

The samples used in this study were selected because spinels were observed in hand specimen. The samples selected were cut and mounted in a 30mm mould using a polyester resin. They were then ground on a coarse grained diamond wheel to expose the specimen. Due to the friable nature of some samples, the exposed surface was then impregnated with resin and then ground again. The mounted samples were then hand-lapped using a 600grit and then a 1000grit, both made of made of silicon carbide. The samples were polished with a Logitech PM5 using a Kemet PSU/M polishing cloth and 6μm, 3μm and 1μm diamond pastes successively. The final polish was then performed with a DAP/2 polishing machine and a 0.3μm Al_2O_3 slurry with water.

9.2.2. Energy Dispersive X-ray Analysis

The polished blocks were analysed using a Carl Zeiss SMT (Cambridge) S360 Scanning Electron Microscope fitted with an Oxford instruments INCA ENERGY X-ray analyser. Typical analytical conditions were an accelerating voltage of 20kV, a probe current of

1nA and a working distance of 25mm. Analyses were taken from the centers of euhedral or subhedral chromite grains (as discussed in section 9.4).

9.3. Fe-Valency Estimation

9.3.1. Introduction

To compare spinel analyses with others in different datasets it was necessary to determine the proportions of Fe^{2+} and Fe^{3+}. However, the X-ray analyzer used here can only measure the amount of total Fe (Fe^T) present in each specimen, it cannot measure Fe^{2+} and Fe^{3+}. Direct measurements of the proportions of Fe^{2+} and Fe^{3+} can only be made using either Mössbauer spectroscopy or by "wet" chemistry techniques. A Mössbauer spectrometer requires samples to be either in powder or film form and to determine Fe valency by wet chemistry methods it is also necessary to liberate the spinel from the matrix. It is impractical to use such techniques for the analysis of spinels which are in-situ and frequently less than 50μm in diameter and the information on the mineral association is then lost.

It was necessary therefore to make a mathematical estimation of how much of the Fe^T is divalent and how much is trivalent. Several methods have been proposed for performing this calculation and Bowles (1977) showed that the method by which the Fe-valency is estimated can have a significant impact on the interpretations made from the data. All methods group together divalent ions as RaO and trivalent ions together as Rb_2O_3 (see review by Bowles, 1977). The next stage – for all methods – is to create molecules using up RaO and Rb_2O_3. In this process Fe^T is allocated to either Fe^{2+} or Fe^{3+} in order to create appropriate molecules. The differences between each method occur in the type of molecules used and in the order in which they are allocated. Most methods only use major elements to construct the molecules, however the method of D. R Wones (as described by Buddington and Lindsley, 1964) allows the use of minor elements in addition to major elements. This is considered to provide a more reasonable result in natural samples where the proportion of minor elements is significant.

Spinels from different tectonic settings can host a wide variation in minor elements, in some cases it is these elements which are used to distinguish their origin (such as TiO_2 in ophiolitic and Alaskan-type chromitites). As it takes account of the effect of minor elements, the method selected for this study is based on that of D. R Wones as described by Buddington and Lindsley (1964) and used the modification suggested by Anderson (1968). Since the minor elements present in spinel minerals vary with tectonic setting and locality, the minerals which they form may also vary. Therefore the method for investigating the Fe-valency which is developed for one dataset may not be valid for another.

9.3.2. Method

An ideal spinel has a formula $A^{2+}B_2^{3+}O_4$. Within the spinel mineral group Mg or Fe^{2+} commonly occupy the "A" site and Al^{3+}, Cr^{3+} or Fe^{3+} occupy the "B" site. The formula AB_2O_4 can be usefully divided into $AO.B_2O_3$ so that AO is typically either MgO or FeO and Al_2O_3, Cr_2O_3 or Fe_2O_3 are represented by B_2O_3. In natural minerals Zn and Mn are commonly found in mineral analyses and it is appropriate to include them with Mg and Fe^{2+} in the A site. Similarly other elements (including V) may join Fe^{3+}, Al^{3+}, Cr^{3+} in the B site. Ulvöspinel (Fe_2TiO_4) also has the spinel structure and the quadrivalent Ti is accommodated by the extra Fe^{2+} ($2Fe^{2+}O.Ti^{4+}O_2$ means that there is FeO to correspond to AO and $Fe^{2+}Ti^{4+}O_3$ to correspond to B_2O_3 – the equal Fe^{2+} and Ti^{4+} being equivalent to a trivalent element). Si^{4+} is presumed to enter the structure in the same way at Ti^{4+}. To calculate the allocation of Fe^T to Fe^{3+} and Fe^{2+} the method needs to allocate the elements to likely spinel molecules shown in table 9.1 where Ra = Σ Mg, Mn, Zn and Rb= Σ Al, Cr, V. The molecules used this dataset are shown below in table 9.1.

Molecule
$2RaO.SiO_2$
$2FeO.SiO_2$
$2RaO.TiO_2$
$RaO.Rb2O_3$
$RaO.Fe_2O_3$
$FeO.Rb_2O_3$,

Table 9.1: The molecules used in the estimation of Fe valency with the minerals they represent. The molecules are listed according to order in which they are used in the calculation.

For each analysis the sums of the molecular proportions of the divalent ions (Mn^{2+}, Co^{2+}, Zn^{2+} and Mg^{2+}) and the trivalent ions (Al^{3+}, Cr^{3+} and V^{3+}) are calculated and referred to as RaO and Rb_2O_3 respectively. Subsequently, RaO, Rb_2O_3 and Fe^T are allocated into each molecule listed in table 9.1.

	RaO	Rb2O3	MgO	Al2O3	SiO2	TiO2	V2O3	Cr2O3	MnO	Total Fe	FeO*	Fe2O3*	CoO	ZnO	Total*
Original data (assuming all Fe to be FeO)			3.25	3.68				59.86	0.70	31.07				0.66	99.22
Convert measured FeO to Fe										24.15					
Molecular weight of the oxide			40.31	101.96	60.08	79.90	149.88	151.99	70.94	55.85	71.85	159.69	74.93	81.37	
Divide wt% by molecular wt			0.08	0.04	0.00	0.00	0.00	0.39	0.01	0.43			0.00	0.01	
Make RaO from MnO+CoO+ZnO+MgO and Make Rb2O3 from Al, Cr, V	0.10	0.43													
Make 2RaO.SiO2	0.00				0.00										
Remainders:	0.10				0.00										
Make 2FeO.SiO2					0.00						0.00				
Remainders: (SiO2 should equal zero)					0.00					0.43					
Make 2RaO.TiO2	0.00					0.00									
Remainders (TiO2 should = 0)	0.10					0.00									
Make RaO.Rb2O3	0.10	0.10													
Remainders:	0.00	0.33													
Make RaO.Fe2O3	0.00											0.00			
Remainders: (RaO should =0)	0.00									0.43					
Make FeO.Rb2O3		0.33									0.33				
Remainders: (Rb2O3 should = 0)		0.00								0.10					
Split remaining total Fe between FeO and Fe2O3											0.05	0.05			
Wt%			3.25	3.68	0.00	0.00	0.00	59.86	0.70		27.44	4.04	0.00	0.66	99.63

Figure 9.2: A worked example of the method used to calculate Fe^{2+} and Fe^{3+}.

In some analyses, the Fe-valency calculation shows that the analysis may not correctly represent a spinel formula. In such a situation, there will be an excess of RaO, Rb_2O_3, TiO_2 or SiO_2 remaining at the end. These analyses were considered to represent other mineral and were removed from the dataset. Furthermore, analyses with totals which fall outside of the range 98.5% to 101.5% were also removed from the dataset as this is the range within which the analyses are considered to be of good quality.

9.3.3. The Analyses

The following tables summarize the number of analyses taken from specimens, those accepted after the Fe-valency estimation (table 9.3) and the number of analyses in the various formations of the WES (table 9.4). During the analysis the computer program

controlling the energy dispersive X-ray analyzer calculates all Fe^T as FeO and therefore a sample with a high Fe_2O_3 may display a total lower than 98.5% before the Fe allocation is carried out. However this total may rise to higher than 98.5% after some Fe^T has been allocated to Fe_2O_3. Table 9.3 shows that the number of analyses in the range 98.5% to 101.5% is larger after Fe-valency is carried out.

	Number of Analyses
Raw analyses	497
Before Fe-allocation. Analyses with totals between 98.5% and 101.5%	258
Analyses rejected as outside the range 98.5% and 101.5% even after Fe-allocation	146
Analyses rejected as appearing not to conform to the spinel formula. (See section 9.3.2)	12
Final accepted analyses	339

Table 9.3: The numbers of analyses at various stages of manipulation of the data.

Formation	Lithology	Number of analyses	Total number of analyses in each area
Tulu Dimtu Main Intrusion	dunite	14	93
	olivine-clinopyroxenite	31	
Tulu Dimtu Sheared Ultramafic	dunite	28	
Tulu Dimtu Lensoid Ultramafics	clinopyroxenite	20	
Kingy Extra Ultramafic	clinopyroxenite	19	40
Kingy Lensoid Ultramafics	clinopyroxenite	21	
Daleti Ultramafic	dunite	110	139
Ankori Ultramafic	dunite	29	
Main Yubdo Intrusion	dunite	67	67
Total		339	

Table 9.4: The numbers of analyses in the various ultramafic formations of the WES

9.4. Alteration Assessment

9.4.1. Introduction

Spinels from ultramafic complexes worldwide are known to re-equilibrate with both the surrounding silicate minerals and migrating fluids during metamorphism (Stowe, 1994). This results in the alteration of the outer surface of the mineral to form a "rim" of a different composition from the core. These rims can be observed in a section and appear

as zoned minerals (see figure 9.1). The composition of the rims is commonly that of ferrichromite, magnetite and sometimes contains inclusions of chlorite (Stowe, 1994; Barnes and Roeder, 2001).

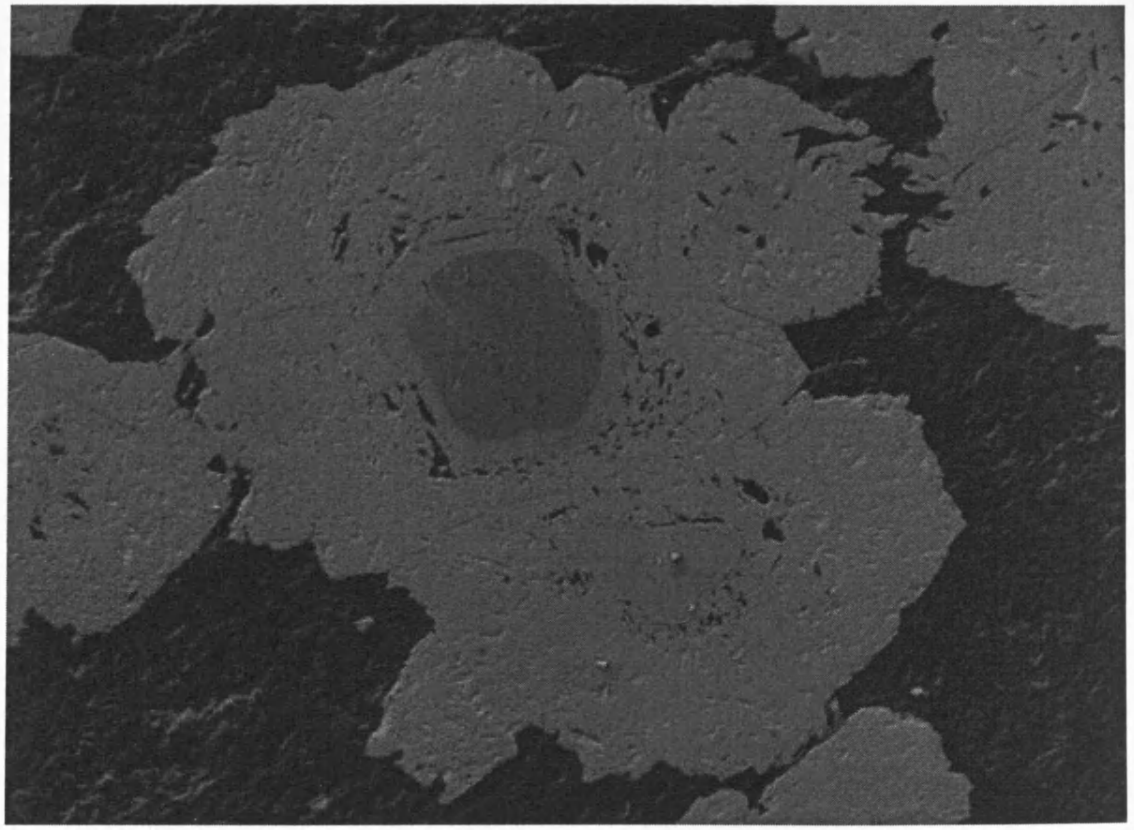

Figure 9.1: SEM backscattered electron image of a zoned spinel mineral from sample KYC-007-01. The fresh core is observed as slightly lower mean atomic number (darker) than the altered rim. The rim is separated from the core by an alteration front. Alteration can be identified through a greater degree of "pitting" and a higher mean atomic number when compared to the fresh core.

In the WES, zoned spinels were observed in samples KYC-007-01, A2, and DTR-057-02, however altered spinels where no fresh centre is visible are common also. This is to be expected as an individual spinels can be considered to be a 3-dimensional "sphere" with a more "magmatic" composition in the centre and an altered shell surrounding it (figure 9.2). It is for this reason that analyses were always located at the centre of all the spinels to obtain the best estimate of the core composition. Altered rims can be identified visually, through a greater degree of pitting and a higher mean atomic number when compared to fresher core (see figure 9.1). And hence analyses are not knowingly taken

from minerals showing these characteristics. However, visual identification is prone to "user-error" and it is possible that some altered analyses have been included as part of the dataset. It is therefore necessary to take account of the geochemical effect of alteration. In this section the geochemical differences between the core and rim of spinels is investigated in order to understand this geochemical effect.

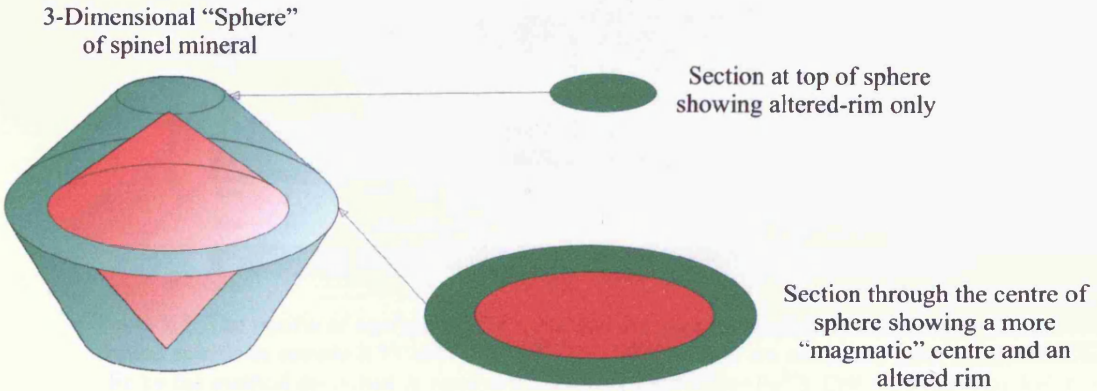

Figure 9.2: The concept of an alteration rim around a 3-dimensional spinel. The centre (red) represents the fresher mineral which should retain the more "magmatic" composition.

9.4.2. Method

The geochemistry of the cores and rims of spinels from 3 samples were analysed. In this section the geochemistry of the cores and rims of four zoned spinels from only sample KYC-007-01 are described. Only one sample was shown here in order to eliminate the effect of magmatic processes on the variation in geochemistry. The two other samples show the same effects. The proportion of Fe^{2+} and Fe^{3+} was estimated using the method outlined in 9.3 and some analyses were rejected as part of this process. Furthermore some analyses were rejected as their totals fell outside of the range 98.5 to 101.5%. As can be seen in figure 9.2, there are three zones in each spinel as defined by the textures and analyses were taken from all three zones. Analyses from the outermost (pitted) zone were all rejected as they had totals which fell outside of the above range. Furthermore, all analyses from one mineral (spinel A) were rejected.

9.4.3. Results

Several analyses were taken from the centre and outwards towards the edge in 3 zoned spinels from the WES. The results are contained in table 9.5 and shown in the graphs in figure 9.3.

Spinel Mineral	Core or Rim	Analysis	MgO	Al_2O_3	TiO_2	V_2O_3	Cr_2O_3	MnO	FeO*	Fe_2O_3*	ZnO	Total	Fe^{2+}#	Cr#	Fe^{3+}#
B	Core	2	3.85	22.32	nd	nd	39.95	1.30	28.00	3.68	2.21	101.31	0.803	0.546	0.046
	Core	7	3.14	22.37	nd	0.27	37.96	1.44	28.55	3.87	2.30	99.90	0.836	0.532	0.032
	Rim	3	0.46	3.13	0.31	nd	34.98	1.20	37.04	22.56	0.68	100.36	0.978	0.882	0.351
	Rim	6	0.51	1.65	0.28	0.29	33.45	1.26	36.79	24.35	0.73	99.31	0.976	0.932	0.225
C	Core	5	3.73	23.09	0.21	nd	38.18	1.37	28.66	3.35	1.43	100.02	0.812	0.526	0.042
	Core	1	3.72	22.83	0.24	nd	38.92	1.29	29.26	3.43	1.09	100.79	0.815	0.534	0.043
	Rim	3	0.50	2.41	0.29	nd	34.14	1.13	36.95	23.49	0.71	99.62	0.976	0.905	0.372
	Rim	4	0.48	3.12	0.29	nd	33.89	1.22	36.66	22.71	0.60	98.97	0.977	0.879	0.359
D	Core	1	3.71	22.49	nd	nd	39.70	1.23	29.02	3.56	1.35	101.06	0.814	0.542	0.044
	Rim	2	0.57	3.41	0.38	nd	35.26	1.34	36.67	22.05	0.80	100.48	0.973	0.874	0.342

Table 9.5: The results of analyses of the cores and the zones immediately surrounding the cores of zoned spinels in sample KYC-007-01. *: Fe^{2+} and Fe^{3+} values are estimated from measured total Fe by the method described in section 9.3. Fe^{2+}# = Fe2+/(Mg+Fe^{2+}). Cr# = Cr/(Cr+Al). Fe^{3+}# = Fe^{3+}/(Fe^{3+}+Al+Cr+V).

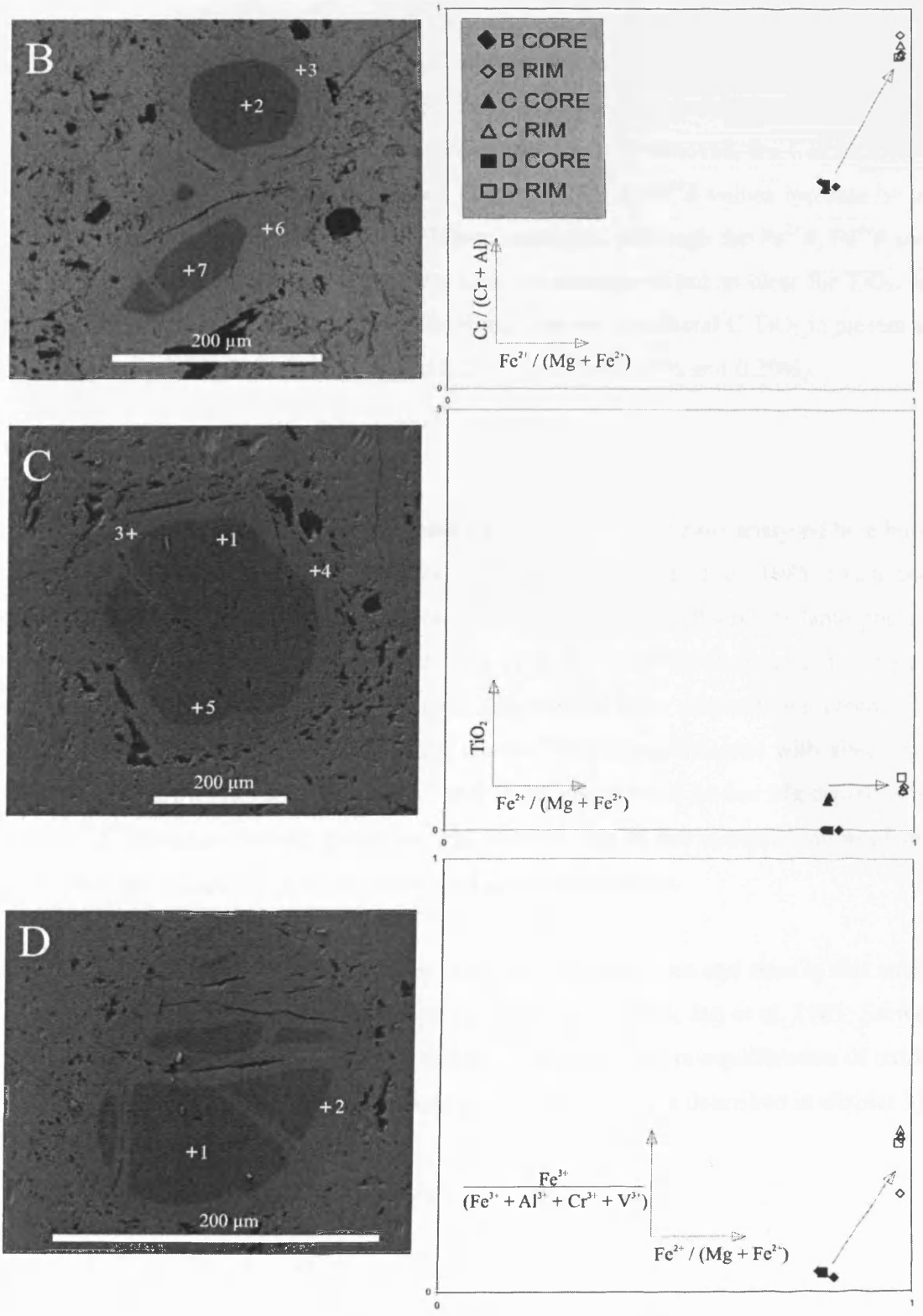

Figure 9.3: Graphs showing the effect of alteration on the spinels from the WES. Arrows indicate the effect of alteration, see 9.4.4 for an explanation.

In each mineral there is an increase in Fe^{2+} and a decrease in Mg values from the core to the rim and this results in an increase in the Fe^{2+}# of at least 0.142. Both Cr_2O_3 and Al_2O_3 decrease from the core to the rim and, as nearly all Al_2O_3 is removed, the Cr# increases by more than 0.332 in all three examples. Furthermore, the Fe^{3+}# values increase by at least 0.193 from the core to the rim in all three examples. Although the Fe^{2+}#, Fe^{3+}# and Cr# increase from the core to rim in every case the situation is not so clear for TiO_2. In examples B and D, TiO_2 only occurs in the rims, however in mineral C TiO_2 is present at similar levels in both the core (0.21% and 0.24%) and rim (0.29% and 0.29%).

9.4.4. Discussion

The difference in spinel geochemistry between the cores and the rims analysed here have been observed also by other workers (Evans and Frost, 1975; Jan et al. 1985; Evans and Frost, 1975). Evans and Frost (1975) compared spinels from different metamorphosed ultramafic complexes and also the cores and rims of zoned minerals and discovered several systematic changes. They observed that spinels from serpentinites commonly contain very low Al_2O_3 values (<5%) and that Fe^{2+}/Mg ratios increase with alteration. Furthermore, Stowe (1994) described Fe^{3+} and Ti enrichment and Al and Mg depletion in the rims of serpentine hosted chromites. He ascribed this to the re-equilibration of the spinels with the adjacent silicate minerals during serpentinisation.

Thus the changes in Fe^{2+}#, Fe^{3+}# and Cr# observed between cores and rims in this study agree with previous studies of alteration (Evans and Frost, 1975; Jan et al. 1985; Stowe, 1994). It is possible that such changes could be attributed to the re-equilibration of oxide minerals with the surrounding silicates during serpentinisation (as described in chapter 3).

9.5. Tulu Dimtu: Spinel Geochemistry

9.5.1. Introduction

A total of 8 samples from the Tulu Dimtu area contain acceptable spinel analyses (as defined in 9.3) and there are 93 analyses in total. From the Tulu Dimtu Main Intrusion spinel analyses were obtained from a dunite sample, two olivine-clinopyroxenite samples and a birbirite sample. Additionally, the spinels from two dunite samples from the Sheared Ultramafic and two clinpyroxenite samples from the Lensoid Ultramafics have been analysed. Table 9.4 summarizes the number of analyses from each each lithotype and each ultramafic formation within the Tulu Dimtu. In the pull-out section on page 289, figure 9.5A shows that the samples from the Tulu Dimtu Main Intrusion are located on the western side of the complex. The eastern side of the complex was not sampled due to restrictions imposed under the licence agreement with the Ethiopian government.

9.5.2. Data

The results of the analysis of the spinels from the Tulu Dimtu area are as follows.

Formation	Sample	Analysis	Host Rock	Na_2O	MgO	Al_2O_3	SiO_2	TiO_2	V_2O_3	Cr_2O_3	MnO	FeO*	Fe_2O_3*	CoO	ZnO	Total	Fe^{2+}#	Cr#	Fe^{3+}#
Tulu Dimtu Main Intrusion Dunite	DTR-001-02	1	Dun	nd	7.92	5.22	nd	nd	nd	65.56	nd	21.24	0.76	nd	nd	100.70	0.601	0.885	0.010
		10		nd	3.53	4.63	nd	nd	nd	61.65	0.76	27.17	2.03	nd	nd	99.77	0.812	0.875	0.027
		12		nd	4.25	4.92	nd	nd	nd	61.40	nd	27.04	2.36	nd	nd	99.97	0.781	0.865	0.032
		14		nd	4.03	4.64	nd	nd	nd	64.16	nd	27.36	1.05	nd	nd	101.24	0.792	0.890	0.014
		18		nd	5.66	5.15	nd	nd	nd	64.48	nd	24.54	0.57	nd	nd	100.40	0.709	0.887	nd8
		19		nd	6.99	5.18	nd	nd	nd	65.30	nd	22.76	0.78	nd	nd	101.01	0.646	0.885	0.010
		2		nd	6.20	5.04	nd	nd	nd	64.76	nd	23.66	0.61	nd	nd	100.27	0.682	0.889	nd8
		20		nd	7.68	5.06	nd	nd	nd	65.41	nd	21.51	0.80	nd	nd	100.46	0.611	0.887	0.010
		3		nd	6.66	4.89	nd	nd	nd	64.67	nd	23.05	1.00	nd	nd	100.27	0.660	0.887	0.013
		4		nd	6.74	5.07	nd	nd	nd	64.07	nd	23.02	1.30	nd	nd	100.20	0.657	0.879	0.017
		5		nd	5.58	5.00	nd	nd	nd	63.44	0.83	24.27	1.72	nd	nd	100.85	0.709	0.875	0.023
		6		nd	6.62	5.29	nd	nd	nd	64.23	0.65	22.78	1.27	nd	nd	100.84	0.659	0.876	0.017
		7		nd	3.85	4.88	nd	nd	nd	62.53	0.76	27.08	1.90	nd	nd	101.00	0.798	0.873	0.025
		9		nd	4.66	5.49	nd	nd	nd	63.98	nd	26.28	0.53	nd	nd	100.95	0.760	0.880	nd7
Tulu Dimtu Main Intrusion Olivine-clinopyroxenite	ATR-051-02	1	Ol-cpxite	nd	5.65	6.25	nd	nd	nd	62.97	0.57	24.27	0.83	nd	nd	100.54	0.707	0.862	0.011
		10		nd	4.38	5.22	nd	nd	nd	61.99	0.57	25.86	1.50	nd	0.50	100.01	0.768	0.871	0.020
		11		nd	3.25	3.68	nd	nd	nd	59.86	0.70	27.67	3.78	nd	0.66	99.60	0.827	0.868	0.052
		2		nd	5.30	6.01	nd	nd	nd	62.62	nd	25.39	1.11	nd	nd	100.43	0.729	0.862	0.015
		3		nd	4.70	5.40	nd	nd	nd	62.45	nd	26.44	1.66	nd	nd	100.65	0.759	0.866	0.022
		4		nd	5.58	6.35	nd	nd	nd	61.31	0.57	24.15	1.46	nd	0.56	99.98	0.708	0.850	0.019
		6		nd	4.13	4.94	nd	nd	nd	59.64	0.61	26.33	3.04	nd	0.57	99.26	0.782	0.853	0.041
		7		nd	5.71	5.63	nd	nd	nd	62.36	0.84	23.82	1.56	nd	nd	99.92	0.701	0.863	0.021
		8		nd	5.87	6.00	nd	nd	nd	61.98	0.80	23.81	1.73	nd	nd	100.20	0.695	0.854	0.023
		9		nd	4.88	4.77	nd	nd	nd	61.51	0.80	25.45	2.80	nd	nd	100.21	0.745	0.863	0.037
	ATR-057-02	1	Ol-cpxite	nd	5.20	5.02	nd	nd	nd	63.35	nd	25.41	1.33	nd	nd	100.31	0.733	0.879	0.018
		10		nd	3.25	3.63	nd	nd	nd	59.19	0.75	28.24	4.73	nd	nd	99.80	0.830	0.857	0.065
		11		nd	4.92	5.33	nd	nd	nd	62.30	nd	25.54	1.23	nd	nd	99.33	0.744	0.872	0.016
		12		nd	4.85	5.46	nd	nd	nd	61.51	nd	25.44	1.29	nd	nd	98.54	0.746	0.868	0.017
		13		nd	5.85	5.43	nd	nd	nd	64.64	nd	24.26	0.45	nd	0.59	101.23	0.699	0.883	nd6
		14		nd	4.65	4.72	nd	nd	nd	62.94	0.74	25.68	1.82	nd	nd	100.56	0.756	0.878	0.024
		15		nd	4.50	5.16	nd	nd	nd	62.46	0.95	26.13	2.17	nd	nd	101.37	0.765	0.865	0.029
		16		nd	3.74	4.13	nd	nd	nd	62.65	0.78	26.54	1.76	nd	0.63	100.23	0.799	0.889	0.024

Formation	Sample	Analysis	Host Rock	Na_2O	MgO	Al_2O_3	SiO_2	TiO_2	V_2O_3	Cr_2O_3	MnO	FeO*	Fe_2O_3*	CoO	ZnO	Total	Fe^{2+}#	Cr#	Fe^{3+}#
Sheared Ultramafic	ATR-050-02	17	Birb	nd	4.19	4.92	nd	nd	nd	63.30	nd	26.78	1.07	nd	0.61	100.87	0.782	0.883	0.014
		18		nd	4.33	4.90	nd	nd	nd	62.93	0.72	26.00	1.38	nd	nd	100.26	0.771	0.880	0.018
		2		nd	4.61	5.20	nd	nd	nd	62.76	0.90	25.19	1.10	nd	nd	99.76	0.754	0.877	0.015
		3		nd	5.57	5.23	nd	nd	nd	62.87	0.79	23.96	1.43	nd	nd	99.85	0.707	0.873	0.019
		4		nd	5.70	5.18	nd	nd	nd	63.55	nd	24.12	0.65	nd	nd	99.20	0.704	0.884	nd9
		5		nd	5.30	5.21	nd	nd	nd	63.52	nd	25.23	1.08	nd	nd	100.34	0.728	0.878	0.014
		7		nd	4.62	4.98	nd	nd	nd	61.95	0.69	25.54	1.87	nd	nd	99.65	0.756	0.871	0.025
		8		nd	4.33	4.98	nd	nd	nd	61.85	nd	26.21	1.31	nd	nd	98.68	0.773	0.877	0.018
		9		nd	4.91	5.23	nd	nd	nd	62.02	0.97	24.62	1.61	nd	0.57	99.92	0.738	0.869	0.021
		3		nd	6.42	15.65	nd	nd	0.36	52.67	0.55	24.86	0.84	nd	nd	101.35	0.685	0.683	0.010
		6		nd	7.49	14.21	nd	nd	nd	55.91	nd	23.38	0.32	nd	nd	101.30	0.637	0.722	nd4
		7		nd	8.29	13.89	nd	nd	0.52	55.70	nd	22.01	0.57	nd	0.50	101.48	0.598	0.719	nd7
		8		nd	6.10	13.98	nd	nd	nd	54.30	0.64	24.46	0.62	nd	0.54	100.63	0.692	0.717	nd8
	KTR-035-02	1/2	Dun	nd	6.07	8.44	nd	nd	nd	60.24	nd	24.52	1.02	nd	nd	100.30	0.694	0.816	0.013
		1/9		nd	5.07	7.92	nd	nd	0.38	59.47	0.76	25.35	1.48	nd	0.52	100.95	0.737	0.814	0.019
		10/		nd	5.58	7.77	nd	nd	nd	60.42	nd	25.00	1.01	nd	nd	99.77	0.715	0.828	0.013
		11/		nd	3.46	6.32	nd	nd	nd	58.80	nd	28.23	2.39	nd	nd	99.20	0.821	0.834	0.032
		2/2		nd	5.56	8.88	nd	nd	nd	60.47	nd	25.39	0.51	nd	nd	100.81	0.719	0.815	nd7
		2/9		nd	3.57	6.64	nd	nd	0.43	57.72	0.56	27.80	2.98	0.52	0.69	100.91	0.814	0.814	0.040
		3/2		nd	3.65	6.37	nd	nd	nd	57.88	nd	27.90	2.84	nd	nd	98.65	0.811	0.826	0.039
		3/9		nd	3.26	5.52	nd	nd	0.56	57.27	nd	29.05	4.15	0.36	0.60	100.77	0.833	0.818	0.056
		4/2		nd	3.19	5.46	nd	nd	0.76	56.72	nd	28.96	4.03	nd	nd	99.12	0.836	0.817	0.055
		4/9		nd	2.91	4.70	nd	nd	0.74	55.36	0.66	28.65	5.25	nd	0.53	98.80	0.847	0.813	0.073
		5/2		nd	3.15	5.21	nd	nd	0.82	57.46	nd	29.27	4.06	nd	nd	99.97	0.839	0.822	0.055
		5/9		nd	2.74	4.12	nd	nd	0.95	55.99	0.61	29.02	5.33	0.32	0.60	99.68	0.856	0.821	0.074
		6/2		nd	3.31	5.14	nd	nd	0.83	55.90	nd	29.30	5.28	nd	nd	99.76	0.832	0.805	0.072
	TD14	1	Dun	nd	4.49	3.59	nd	nd	nd	65.09	nd	26.16	0.96	nd	nd	100.29	0.766	0.912	0.013
		10		nd	5.68	4.33	nd	nd	nd	65.30	nd	24.38	0.65	nd	nd	100.35	0.707	0.902	nd9
		11		nd	4.39	4.01	nd	nd	nd	64.24	nd	26.48	1.23	nd	nd	100.35	0.772	0.900	0.016
		12		nd	3.92	3.99	nd	nd	nd	64.43	0.97	26.24	1.05	nd	nd	100.60	0.790	0.903	0.014
		13		nd	4.93	3.61	nd	nd	nd	63.81	nd	25.35	1.59	nd	nd	99.29	0.743	0.902	0.021
		14		nd	5.21	4.14	nd	nd	nd	65.59	nd	25.22	0.65	nd	nd	100.81	0.731	0.906	nd9
		15		nd	5.91	4.35	nd	nd	nd	65.35	0.90	23.40	0.99	nd	nd	100.90	0.690	0.898	0.013
		16		nd	5.42	4.17	nd	nd	nd	64.87	1.19	24.06	1.47	nd	nd	101.18	0.714	0.895	0.019
		17		nd	5.12	4.29	nd	nd	nd	63.76	nd	25.18	1.26	nd	nd	99.61	0.734	0.894	0.017
		18		nd	4.51	4.05	nd	nd	nd	64.01	nd	26.13	1.17	nd	nd	99.87	0.765	0.899	0.016
		19		nd	4.06	3.99	nd	nd	nd	63.55	0.92	26.12	1.60	nd	nd	100.24	0.783	0.895	0.021
		2		nd	4.78	3.96	nd	nd	nd	65.22	nd	26.21	1.23	nd	nd	101.40	0.755	0.902	0.016
		5		nd	4.70	4.07	nd	nd	nd	64.54	nd	25.82	0.91	nd	nd	100.04	0.755	0.903	0.012
		6		nd	4.92	4.50	nd	nd	nd	65.36	nd	25.57	0.30	nd	nd	100.65	0.745	0.903	nd4
		9		nd	5.00	4.01	nd	nd	nd	65.45	nd	25.82	1.07	nd	nd	101.35	0.743	0.903	0.014
Tulu Dimtu Lensoid Ultramafics	DTR-015-02	1/2	Cpxite	nd	nd	4.73	0.69	nd	nd	52.95	1.73	33.18	5.63	nd	1.33	100.24	1.000	0.810	0.082
		1/9		0.48	nd	4.48	nd	nd	nd	54.05	1.59	32.37	6.04	nd	1.35	100.36	1.000	0.813	0.086
		2/2		nd	0.99	16.40	nd	nd	nd	38.68	1.18	33.60	7.59	nd	0.94	99.37	0.950	0.550	0.103
		2/9		nd	nd	3.59	nd	nd	nd	55.62	1.24	32.01	5.11	nd	1.35	98.93	1.000	0.845	0.074
		3/9		nd	nd	5.82	nd	nd	nd	53.36	1.44	32.52	5.33	nd	1.24	99.71	1.000	0.795	0.076
		4/9		0.40	nd	7.78	nd	nd	nd	50.20	1.48	33.06	6.13	nd	1.44	100.49	1.000	0.742	0.086
		5/9		nd	nd	4.58	nd	nd	nd	56.12	1.56	31.69	4.07	nd	1.36	99.38	1.000	0.840	0.058
		6/9		nd	nd	3.36	nd	nd	nd	54.08	1.72	32.83	7.56	nd	1.48	101.03	1.000	0.816	0.109
		8/9		0.43	nd	5.21	nd	nd	nd	54.35	1.45	32.70	5.52	nd	1.43	101.09	1.000	0.807	0.078
	DTR-019-02	10	Cpxite	nd	nd	6.01	nd	nd	nd	54.50	1.46	32.72	4.82	nd	1.21	100.72	1.000	0.801	0.067
		11		nd	nd	9.55	nd	nd	nd	48.74	1.64	33.05	5.63	nd	1.11	99.72	1.000	0.713	0.078
		12		nd	nd	7.54	nd	nd	nd	49.81	1.66	33.21	6.85	nd	1.10	100.17	1.000	0.737	0.096
		13		nd	nd	6.55	nd	nd	nd	50.12	1.32	33.42	7.17	nd	nd	98.58	1.000	0.751	0.102
		14		nd	nd	5.71	nd	nd	nd	52.23	1.57	32.94	6.47	nd	nd	98.92	1.000	0.781	0.092
		18		nd	0.83	20.40	nd	nd	nd	41.54	1.54	32.67	2.15	nd	2.22	101.35	0.957	0.561	0.028
		19		nd	0.71	11.33	nd	nd	nd	45.74	1.44	33.10	7.05	nd	1.10	100.47	0.963	0.660	0.097
		2		nd	2.42	6.34	3.52	nd	nd	45.49	1.41	33.97	5.91	nd	nd	99.06	0.887	0.751	0.093
		20		nd	2.16	6.47	2.99	nd	nd	47.23	1.64	33.94	6.02	nd	nd	100.46	0.898	0.754	0.092
		4		nd	nd	7.72	nd	0.68	nd	42.92	1.53	35.15	10.83	nd	nd	98.83	1.000	0.663	0.159

Formation	Sample	Analysis	Host Rock	Na_2O	MgO	Al_2O_3	SiO_2	TiO_2	V_2O_3	Cr_2O_3	MnO	FeO*	Fe_2O_3*	CoO	ZnO	Total	Fe^{2+}#	Cr#	Fe^{3+}#
		9		nd	0.60	5.80	nd	nd	nd	51.38	1.65	32.19	7.44	nd	1.31	100.37	0.968	0.766	0.106

Table 9.6: The geochemistry of the spinels analysed from the Tulu Dimtu area in wt %. Analyses from a birbirite sample are included here, however these are not plotted on any graphs as there is considerable uncertainty over their mode of formation (see chapter 3). Nd: not detected. *: Fe^{2+} and Fe^{3+} values are estimated from measured total Fe by the method described in section 9.3. Fe^{2+}# = Fe2+/(Mg+Fe^{2+}). Cr# = Cr/(Cr+Al). Fe^{3+}# = Fe^{3+}/(Fe^{3+}+Al+Cr+V).

9.5.3. Fe^{2+}# (Fe^{2+}/(Mg+Fe^{2+}))

In the Tulu Dimtu area there are two populations of spinel Fe^{2+}# values. These are analyses from the clinopyroxenite hosted spinels and those from the dunite and olivine-clinopyroxenite hosted spinels. The spinels from the two clinopyroxenite samples (from the Lensoid Ultramafics) show Fe^{2+}# values from 0.887 to 1.000, whereas the analyses from the dunites and clinopyroxenites are lower than these values ranging from 0.601 to 0.830. The spinels hosted by birbirite contain even lower Fe^{2+}# values than other samples and range from 0.598 to 0.692.

9.5.4. Cr# (Cr / (Cr+Al))

The spinel analyses from the Tulu Dimtu area show two populations of Cr# values. Both populations show similar upper values but have very different lower values. The clinopyroxenite hosted spinels from the Lensoid Ultramafics range from 0.550 to 0.845. However, the dunite and olivine-clinopyroxenite samples from the Tulu Dimtu Main Intrusion range from 0.805 to 0.910. Twelve of the 20 analyses of spinels from the clinopyroxenite samples have Cr# values lower than those from the dunite or olivine-clinopyroxenite hosted spinels. The Cr# values from the birbirite hosted spinels are within the range of clinopyroxenite samples but lower than the other samples (from 0.683 to 0.722).

9.5.5. TiO_2

Only one analysis from the Tulu Dimtu area has returned TiO_2 values above detection limits (0.63%). This occurs in an analysis from a clinopyroxenite sample from a Lensoid Ultramafic unit in the northern part of the area.

9.5.6. $Fe^{3+}\#$ ($Fe^{3+} / (Fe^{3+} + Al^{2+} + Cr^{3+} + V^{3+})$)

All $Fe^{3+}\#$ values obtained from the Tulu Dimtu area occur within a similar range. However, some analyses from the two clinopyroxenite samples have slightly elevated values. The $Fe^{3+}\#$ values for the clinopyroxenite samples (from the Lensoid Ultramafics) range from 0.028 to 0.159. Whereas $Fe^{3+}\#$ values for spinels hosted by dunite and olivine-clinopyroxenite (from the Tulu Dimtu Main Intrusion and the Sheared Ultramafic) range from 0.006 to 0.074. Seventeen of the 20 analyses from the clinopyroxenite hosted spinels have $Fe^{3+}\#$ values which are higher than the dunite or olivine-clinopyroxite hosted samples. The birbirite samples show $Fe^{3+}\#$ ratios which are lower than most other analyses, ranging from 0.004 to 0.010.

9.5.7. Minor Elements (Si, Co, and Zn)

Two analyses from spinels in the northernmost Lensoid Ultramafic (hosted by clinopyroxenite) display SiO_2 values above detection limits (3.52% and 2.99%). V_2O_3 is detected in the spinels from the birbirite sample and a dunite sample from the Sheared Ultramafic with values of up to 0.95%. CoO was detected in three spinels from a dunite sample in the Sheared Ultramafic (0.52%, 0.36% and 0.32%). Additionally, ZnO was detected in 26 analyses from 6 different samples including olivine-clinopyroxenites and a birbirite from the Tulu Dimtu Main Intrusion. ZnO values were also returned from a dunite in the Sheared Ultramafic. However the highest ZnO values occur in the clinopyroxenites from the Lensoid Ultramafics at up to 2.22. No Na_2O has been detected at Tulu Dimtu.

9.5.8. Summary of the spinel Geochemistry in the Tulu Dimtu area

There are two main groups of analyses from the Tulu Dimtu area. These are firstly pyroxenite hosted spinels from the Lensoid Ultramafics and secondly those hosted by dunite and olivine-clinopyroxenites from the Tulu Dimtu Main Intrusion. They each have distinctly different $Fe^{2+}\#$ values and slightly different Cr#, TiO_2 and $Fe^{3+}\#$ values. All the

analyses from the clinopyroxenites have much higher Fe^{2+}# values than those derived from the dunites and olivine-clinopyroxenites. Most of the clinopyroxenite hosted spinels also show much lower Cr# ratios and higher Fe^{3+}# ratios than the dunites and olivine-clinopyroxenites (figure 9.5B and 9.5F). Furthermore, one of the clinopyroxenite hosted spinels contains TiO_2 above detection limits.

In addition to the ranges described above, within each dunite or olivine-clinopyroxenite sample the range of spinel Cr# values is narrower than the range of Fe^{2+}# values whereas the opposite is true for the clinopyroxenites.

Trends in Cr# and Fe^{3+}# when compared to Fe^{2+}# values can be seen in figures 9.5B and 9.5G. In each dunite and olivine-clinopyroxenite sample the spinel Cr# increases with Fe^{2+}#. The gradient within each sample differs and the trends appear to converge towards one point where Fe^{2+}# $\approx$ 0.840 and Cr# $\approx$ 0.850. The clinopyroxenite hosted spinels show different trends – including a wide Cr# range and narrow Fe^{2+} range and do not converge towards the same point.

The birbirite hosted spinels have compositions which fall outside of the ranges of other spinels studied. They have lower Fe^{2+}# and Fe^{3+}# values than all other groups however, the Cr# values are equivalent to those from the clinopyroxenite samples.

9.6. Discussion

9.6.1. Alteration

In the Tulu Dimtu area, spinels which are hosted by olivine clinopyroxenite and dunite show a trend whereby Cr# increases slightly with Fe^{2+}#. These trends are similar to the trend in geochemistry observed within zoned spinels in the WES and in other ultramafic complexes (see section 9.4). Although the possibility that these trends are controlled by magmatic processes cannot be eliminated, it is highly likely that the spinels have undergone some alteration. The presence of serpentine (see chapter 3) and zoned spinels suggests that these minerals have undergone some degree of alteration and as such will

display a geochemical expression of this alteration. Furthermore, it is common to find alteration trends such as these in spinel datasets from areas such as Western Pakistan and the Swiss Alps (Jan et al., 1985; Stowe, 1995). It is therefore likely that the trend of increasing Cr# and Fe^{2+}# is the result of alteration. There are two possible explanations for these trends, either different spinels in the sample have been exposed to slightly more or less severe alteration conditions or the polishing process has revealed different levels within equally altered zoned spinels (see section 9.4.1).

The analyses from the clinopyroxenite hosted spinels have a very steep gradient, higher Fe^{2+}# values and some very low Cr# values when compared to the other samples (see figure 9.5B). These trends are much steeper than the dunite and olivine-clinopyroxenite hosted spinels and also steeper than the trends seen in zoned spinels (section 9.4). These occur because there is a large Al_2O_3 content in some spinels. This phenomenon cannot easily be explained by magmatic processes as the range of Al_2O_3 within one sample is too large. Although most authors only describe a decrease in Al_2O_3 values from the cores to rims of zoned spinels (Stowe, 1994; Jan et al., 1985), a systematic comparison of spinel composition with the metamorphic facies of the host rocks has revealed a more complex situation. Evans and Frost (1975) describe the spinel compositions from greenschist through amphibolite to granulite facies. Although the compositions of the altered spinels from greenschist facies rocks show a similar trend to those observed in the dunite and olivine-clinopyroxenite rocks from this study, the spinels from amphibolite facies rocks are enriched in Al_2O_3. The "alteration trend" observed by Evans and Frost (1975) is one whereby the Cr# and Fe^{2+}# values first increase and then with further alteration Cr# drops. It is therefore possible that the spinels from the Lensoid Ultramafics (hosted by clinopyroxenites) have been altered to a greater degree than those from the Tulu Dimtu Main Intrusion. It is conceivable that the Lensoid Ultramfics could have been exposed to more intense alteration conditions than those of the Tulu Dimtu Main Intrusion if they are dismembered bodies as inferred from rock geochemistry (chapter 8). However, the metamorphic facies cannot be determined only from spinel analyses and requires a petrological study (chapter 3).

Although the Al_2O_3 enrichment in some spinels could be explained by comparison with spinels from amphibolite facies rocks, the effect of the clinopyroxene host minerals has to be considered. It is possible that some of the Al^{3+} enrichment may occur by re-equilibration of the rims with the Al-bearing clinopyroxene minerals regardless of the degree of metamorphism. However, no data has been found for the partitioning of Al^{3+} between clinopyroxene and spinel.

In addition to the changes in Cr# values, some spinels from the dunites and olivine-clinopyroxenites show a gradual increase in Fe^{3+}# with Fe^{2+}#. Furthermore, several analyses from the clinopyroxenites show elevated Fe^{3+} values. This is in general agreement with variation in these ratios from the core to rims of zoned spinels (see section 9.4). The slight increase in TiO_2 may be due to alteration – however - no systematic change in TiO_2 was observed from the core to rim in this study. Neverthless, other workers have described similar elevated values in the altered rims (Stowe, 1994; Jan et al., 1985).

9.6.2. Magmatic effects

Although the dominant trend in the Cr# and Fe^{2+}# values of the dunite and olivine-clinopyroxenite hosted spinels is likely to be due to alteration (see section 9.6.1) each of these 5 samples shows slightly different minimum Cr# values (see figure 9.5B). These differences are due to changes in both Cr_2O_3 and Al_2O_3. Within each sample the analysis with the lowest Cr# value also has the lowest Mg# value and is likely to be the least altered of each sample. Therefore within each sample the analysis with the lowest Cr# value is the most likely to retain the magmatic composition.

Sample	Host Rock	Min Cr#	Fe^{2+}#	Fe^{3+}#	TiO_2
TD14	Dunite	0.894	0.690	0.004	nd
DTR-001-02	Dunite	0.865	0.601	0.007	nd
ATR-057-02	Olivine-clinopyroxenite	0.857	0.699	0.006	nd
ATR-051-02	Olivine-clinopyroxenite	0.850	0.695	0.011	nd
KTR-035-02	Dunite	0.805	0.694	0.007	nd

Table 9.7: A table of the minimum Cr# values for spinel analyses from dunite and olivine-clinopyroxenite samples. In order with the highest at the top. Nd: not detected.

In a situation where the Tulu Dimtu Main Intrusion formed by the differentiation of one magma it would be expected that the first formed spinels would have the highest Cr^{3+}values and lowest Al^{3+} values. In this case it is suggested that the samples at the top of table 9.7 should be the most primitive and have formed first. However, figure 9.5A shows that the most primitive sample (TD14) is located close to the most evolved sample (KTR-035-02). If the complex has crystallized from one magma it would be expected that the most primitive samples would be found far from the most evolved with the intermediate samples between. This apparent lack of a systematic trend in fractionation could be explained by the intrusion of multiple melts, however such a model could only be demonstrated using analysis of geochemistry through a continuous section of the complex. As spinels do not occur in every sample, such an analysis could not be performed using the method detailed here. Methods such as olivine mineral geochemistry could be of use in determining the number of melt influxes.

Table 9.7 shows that there is a crude negative correlation in Cr# and Fe^{2+}# in the analyses of lowest Cr# of each sample. This infers that crystal fractionation may increase Fe^{2+}# alongside a decrease in Cr# as illustrated in figure 9.4. Such fractionation trends are not apparent in Fe^{3+}# as all the data falls within a very similar range. Furthermore, TiO_2 was only detected in one analysis.

9.6.3. Comparison with Alaskan-type intrusions and Ophiolite complexes

Figures 9.5B to 9.5G can be used to compare the data of this study with the published data from the ophiolite and Alaskan-type intrusion 90th percentile fields from the Global Spinel Database (Barnes and Roeder, 2001) . Almost all spinels from the Tulu Dimtu area lie within the Alaskan-type field for Cr# and Fe^{2+}# and not the Ophiolite field.

A feature of the Fe^{2+}# vs Cr# Alaskan-type intrusion field (Barnes and Roeder, 2001) - which is not shared by the ophiolite spinels - is a limb whereby spinels with high Fe^{2+}# also contain extremely low Cr#. The spinels hosted by clinopyroxenite from the Lensoid Ultramafic fit within this limb. As described in section 9.6.1, even though the analyses

were from the cores of the spinels, the cause of the low Cr# values could be alteration by amphibolite facies metamorphism (Evans and Frost, 1975) or due to the requilibration of the minerals with Al-bearing clinopyroxene. Both explanations for this unique feature of Alaskan-type intrusions could be described as forms of alteration.

Some of the spinel compositions from the Tulameen complex in British Columbia – a classic Alaskan-type intrusion - also have low Cr# values with high Fe^{2+}# values (Nixon et al., 1990). As at Tulu Dimtu, it is the clinopyroxenite hosted spinels which show the lowest Cr# values and therefore occupy the "Alaskan-type" intrusion limb. Although in both complexes (Tulu Dimtu and Tulameen) it is the clinopyoxenite hosted spinels which plot within this limb, this does not necessarily suggest that requilibration with clinopyroxene is the only cause for the high Al_2O_3 values. Alaskan-type intrusions typically form with clinopyroxenite or hornblendite zones at the edge of the complex (chapter 2). As ultramafic complexes typically behave as competent bodies, it is likely that the outermost (clinopyroxenite) zones will be the most heavily deformed and altered. Therefore it is thought likely that the origin of the "Alaskan-type limb" (low Cr# at high Fe^{2+}#) is intense alteration of clinopyroxenite hosted spinels at the flanks of the intrusion. The innermost dunites and olivine-clinopyroxenites are less altered as a result of being located further away from alteration fluids.

If the Alaskan-type limb is a result of alteration and it is possible that ophiolite complexes could be exposed to the same alteration, it is possible to ask why the ophiolite fields do not show the same trend. The fields only include 90% of the data in the Global Spinel Database (Barnes and Roeder, 2001) and therefore a few outliers do not fall within the field. Some outlying ophiolite analyses from the Barnes and Roeder (2001) dataset do show high Fe^{2+}# values with low Cr# values as at Tulu Dimtu and Tulameen. These outliers could be explained as being anomalously altered spinels whereas most other ophiolite analyses are originated from much fresher areas. Samples collected for geochemical analysis to investigate primary fractionation trends would be the freshest lithologies possible. Given that Alaskan-type intrusions are nearly always intruded into

mobile belts it is much more likely that their clinopyroxenite zones will become altered. Whereas in ophiolite complexes the clinopyroxenites are more likely to be fresh.

The alteration trend suggested in section 9.6.1 is distinctly different from the magmatic trend of minimum Cr# values seen for spinels hosted by dunites and olivine-clinopyroxenites proposed in section 9.6.2 (see also figure 9.4).

Although the Fe^{2+}#, Cr# and TiO_2 values are similar to those of Alaskan-type intrusions from the Barnes and Roeder (2001) database, the situation is more complicated when Fe^{3+}# is plotted against Fe^{2+}#. Figure 9.5G shows that although the Fe^{2+}# values have a similar range to those of other Alaskan-type intrusions the corresponding Fe^{3+}# values are too low. Irrespective of this, the Fe^{2+}# values are still considerably higher than for the ophiolite field.

9.7. Conclusions

This study presents a comparison of the geochemistry of spinels from the ultramafic rocks from the Tulu Dimtu area with published spinel analyses from ophiolite complexes and Alaskan-type intrusions. The Fe^{2+}# and Cr# geochemistry of the spinels from Tulu Dimtu is typical of Alaskan-type intrusions (Barnes and Roeder, 2001). However, Fe^{3+}# values are lower than typical Alaskan-type intrusions. Furthermore, the spinels hosted by clinopyroxenites from the Lensoid Ultramafics show low Cr# values and high Fe^{2+}# values, an observation which is also made in the spinels from the Tulameen complex – a classic Alaskan-type intrusion (Nixon et al., 1990).

Although the spinels from Tulu Dimtu are typical of Alaskan-type intrusions, the work of Evans and Frost (1975) can be used to suggest that the differences in spinel geochemistry could be explained by alteration. Due to their tectonic setting, Alaskan-type intrusions are potentially altered to a greater degree than ophiolites and as a result, some spinels can be altered to amphibolite facies and show very low Cr# values at high Fe^{2+}# values.

Although the dominant trend within samples from the Tulu Dimtu area could be attributed to alteration there are features of this data that cannot be explained by such a process. These include differences between samples in the minimum Cr# values. It is possible that such differences could be accounted for by each sample forming at different stages during crystal fractionation. In such a situation, it is unlikely that the Tulu Dimtu Main Intrusion formed by the differentiation of a single melt influx.

The trends proposed here for alteration and magmatic processes are different when plotted on a graph of Cr# versus Fe^{2+}# Figure 9.4 illustrates these differences.

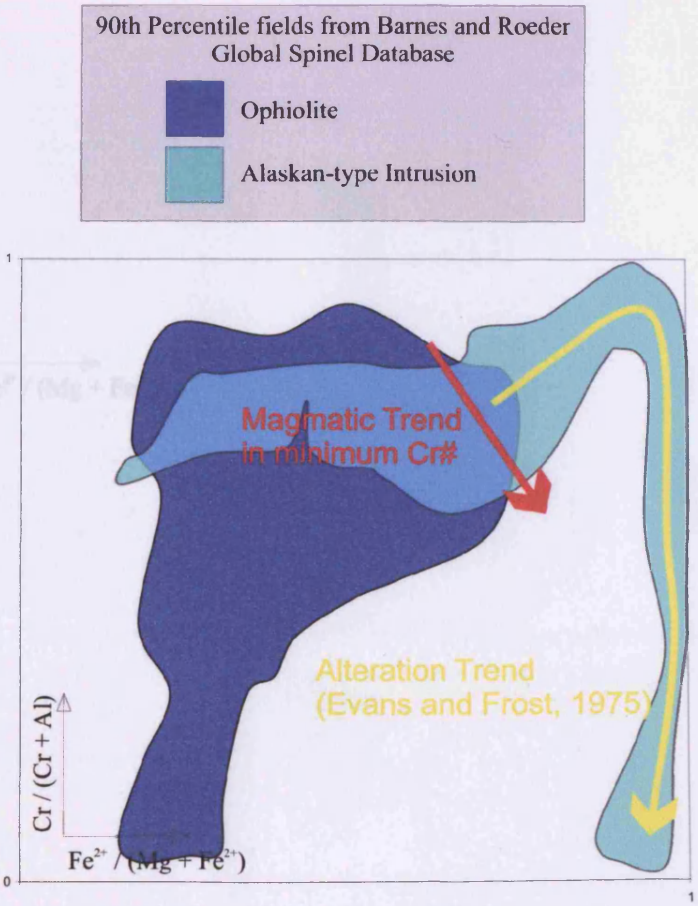

Figure 9.4: The differences between magamtic trends and alteration trends on a graph of spinel Fe^{2+}# versus Cr# values. For a discussion of the magmatic trend see section 9.6.2 and for the alteration trend see 9.6.1.

9.8. Kingy: Spinel Geochemistry

9.8.1. Introduction

Three samples from the Kingy area contain acceptable spinel analyses (as defined in section 9.3) and there are 40 analyses in total. The samples which host acceptable analyses from the Kingy area are clinopyroxenites. There is one sample from the Extra Ultramafic and two samples from two different Lensoid Ultramafic complexes. Spinels from several samples within the Kingy Ridge Ultramafic were analysed but the results were not considered to be acceptable under the conditions set down in section 9.3. Table 9.4 summarizes the number of analyses from each formation. In the pull-out section on page 295, figure 9.6A shows the locations of each sample.

9.8.2. Data

The results for the analysis of the spinels from the Kingy area are as follows.

Formation	Sample	Analysis	Host Rock	Na_2O	MgO	Al_2O_3	SiO_2	TiO_2	V_2O_3	Cr_2O_3	MnO	FeO*	Fe_2O_3*	CoO	ZnO	Total	Fe^{2+}#	Cr#	Fe^{3+}#
Kingy Extra Ultramafic	DTR-057-02	1/3	Cpxite	nd	0.85	10.93	nd	0.41	nd	47.92	2.36	31.10	4.73	nd	1.58	99.88	0.954	0.697	0.066
		1/4		nd	0.67	8.61	nd	0.27	nd	52.30	2.53	31.72	4.67	nd	nd	100.77	0.964	0.752	0.064
		13		nd	0.83	8.28	nd	0.25	nd	52.96	2.10	31.75	4.49	nd	nd	100.66	0.955	0.761	0.061
		16		nd	1.00	9.51	nd	nd	nd	50.22	2.42	31.50	5.88	nd	nd	100.53	0.946	0.717	0.080
		18		nd	0.81	10.19	nd	0.37	nd	49.68	2.27	32.16	5.08	nd	nd	100.56	0.957	0.713	0.069
		19		nd	0.95	11.95	nd	0.50	nd	46.10	2.15	32.74	6.11	nd	nd	100.51	0.951	0.661	0.083
		2/		nd	0.64	9.52	nd	0.28	nd	49.58	2.17	31.21	4.61	nd	1.26	99.28	0.965	0.727	0.064
		2/		nd	0.74	10.83	nd	0.51	nd	45.69	2.07	32.68	7.07	nd	1.65	101.24	0.961	0.666	0.098
		21		nd	0.76	8.83	nd	nd	nd	51.27	2.56	31.64	5.70	nd	nd	100.75	0.959	0.734	0.078
		22		nd	0.79	10.58	nd	nd	nd	47.30	2.41	32.38	7.13	nd	nd	100.59	0.958	0.677	0.097
		24		nd	1.09	6.74	nd	nd	nd	56.91	2.18	30.77	3.63	nd	nd	101.32	0.941	0.808	0.049
		25		nd	0.78	11.60	nd	nd	nd	46.71	2.25	32.49	6.57	nd	nd	100.40	0.959	0.665	0.089
		27		nd	0.71	6.82	nd	nd	nd	57.18	2.14	31.24	3.16	nd	nd	101.25	0.961	0.813	0.043
		28		nd	0.90	11.03	nd	0.55	nd	48.57	2.10	32.54	5.06	nd	nd	100.75	0.953	0.696	0.069
		29		nd	0.68	9.42	nd	0.54	nd	49.39	2.40	32.54	5.81	nd	nd	100.79	0.964	0.716	0.080
		3/4		nd	0.68	10.68	nd	0.36	nd	47.20	2.07	32.23	5.95	nd	1.43	100.60	0.964	0.686	0.082
		4/3		nd	0.61	10.09	nd	0.47	nd	47.57	2.33	31.79	5.78	nd	1.69	100.33	0.967	0.698	0.081
		4/4		nd	0.91	9.13	nd	0.35	nd	52.35	2.08	31.75	4.08	nd	nd	100.65	0.951	0.750	0.056
		6/4		nd	0.72	6.72	nd	nd	nd	56.25	2.33	31.10	3.80	nd	nd	100.92	0.960	0.805	0.052
Kingy Lensoid Ultramafic	ATR-132-02	12	Cpxite	nd	8.91	8.19	nd	nd	nd	62.02	0.79	19.75	1.49	nd	nd	101.15	0.554	0.820	0.019
		17		nd	2.77	7.46	nd	nd	nd	59.63	0.57	28.75	0.91	nd	nd	100.09	0.853	0.833	0.012
		18		nd	0.72	4.17	0.35	nd	nd	40.30	nd	36.49	16.84	nd	1.28	100.15	0.966	0.644	0.256
		19		nd	3.60	7.63	nd	nd	nd	60.20	1.01	27.46	1.19	nd	nd	101.09	0.811	0.828	0.016
		2		nd	7.65	8.18	nd	nd	nd	60.92	0.87	21.13	1.20	nd	nd	99.95	0.608	0.820	0.015
		3		0.44	5.80	7.62	nd	nd	nd	60.49	0.91	23.78	1.19	nd	nd	100.23	0.697	0.829	0.016
		4		nd	8.38	8.45	nd	nd	nd	61.23	0.74	20.31	1.22	nd	nd	100.33	0.576	0.817	0.016
		5		nd	7.11	8.11	nd	nd	nd	60.71	1.00	21.76	1.14	nd	nd	99.83	0.632	0.822	0.015
		7		nd	1.26	6.83	nd	nd	nd	58.50	nd	30.80	0.93	nd	1.58	99.90	0.932	0.841	0.013

Formation	Sample	Analysis	Host Rock	Na_2O	MgO	Al_2O_3	SiO_2	TiO_2	V_2O_3	Cr_2O_3	MnO	FeO*	Fe_2O_3*	CoO	ZnO	Total	Fe^{2+}#	Cr#	Fe^{3+}#
		8		nd	3.82	7.64	nd	nd	nd	58.45	0.71	26.68	1.46	nd	0.77	99.53	0.797	0.821	0.020
		9		nd	4.52	8.11	nd	nd	nd	59.33	0.75	25.98	1.25	nd	0.52	100.46	0.763	0.817	0.016
		10		nd	9.36	7.65	nd	nd	nd	63.91	0.81	18.69	0.65	nd	nd	101.07	0.528	0.842	nd8
		11		nd	9.16	7.46	nd	nd	nd	63.77	0.84	18.72	0.55	nd	nd	100.51	0.534	0.846	nd7
		13		nd	9.35	7.59	nd	nd	nd	63.93	0.62	19.04	0.85	nd	nd	101.38	0.533	0.841	0.011
		2		nd	8.75	7.61	nd	nd	nd	63.57	0.73	19.73	0.72	nd	nd	101.11	0.559	0.841	nd9
	KTR-069-02	3	Cpxite	nd	7.81	8.30	nd	nd	nd	62.20	0.72	20.93	0.37	nd	nd	100.33	0.601	0.830	nd5
		4		nd	8.52	7.95	0.37	nd	nd	62.02	0.81	20.40	0.73	nd	0.55	101.36	0.573	0.832	nd9
		5		nd	8.02	7.92	nd	nd	nd	62.51	0.72	20.75	0.72	nd	nd	100.64	0.592	0.833	nd9
		6		nd	8.33	7.84	0.30	nd	nd	61.86	0.89	20.79	1.17	nd	nd	101.18	0.583	0.829	0.015
		7		nd	3.85	6.19	nd	nd	nd	50.63	1.19	28.10	8.87	nd	1.11	99.94	0.804	0.741	0.124
		9		nd	8.29	7.77	nd	nd	0.40	62.13	1.03	20.11	1.06	nd	0.56	101.35	0.576	0.827	0.013

Table 9.8: The geochemistry of the spinels analysed from the Kingy area in wt %. Analyses from a birbirite sample are included here, however these are not plotted on any graphs as there is considerable uncertainty over their mode of formation (see chapter 3). Nd: not detected. *: Fe^{2+} and Fe^{3+} values are estimated from measured total Fe by the method described in section 9.3. $Fe^{2+}\# = Fe^{2+}/(Mg+Fe^{2+})$. $Cr\# = Cr/(Cr+Al)$. $Fe^{3+}\# = Fe^{3+}/(Fe^{3+}+Al+Cr+V)$.

9.8.3. $Fe^{2+}\#$ ($Fe^{2+}/(Mg+Fe^{2+})$)

All analyses from the Kingy area are from spinels hosted by clinopyroxenites. The samples from the Lensoid Ultramafics in the Kingy area contain spinels with a high range of $Fe^{2+}\#$ values (0.554 to 0.966), whereas the sample from the Extra Ultramafic contains spinels with a narrower range of $Fe^{2+}\#$ values from 0.941 to 0.967.

9.8.4. Cr / (Cr+Al)

The samples from the Lensoid Ultramafics of the Kingy area contain spinels with a narrow range of Cr# values (0.817 to 0.820), whereas the sample from the Extra Ultramafic contains spinels with a wide range of $Fe^{2+}\#$ values from 0.661 to 0.813.

9.8.5. TiO_2

TiO_2 is only detected in the sample from the Extra Ultramafic but 12 analyses out of 19 contain TiO_2 up to a maximum of 0.55%.

9.8.6. $Fe^{3+}\# / (Fe^{3+} + Al^{2+} + Cr^{3+} + V^{3+})$

All analyses, with two exceptions, of the spinels from the Lensoid Ultramafics show a narrow range and a low range of $Fe^{3+}\#$ numbers from 0.005 to 0.20. The exceptions are

where two analyses, one from each sample, show that Fe^{3+}# rises to 0.124 and 0.256. The spinels from the Extra Ultramafic have a wider range of Fe^{3+}# values and many analyses rise to higher values than most of the spinels from the Lensoid Ultramafics

9.8.7. Minor Elements (Na, Si, and Zn)

Na_2O has been detected in one analysis from the northernmost Lensoid Ultramafic. (0.44%). Two analyses, one from each of the Lensoid Ultramafics, contain SiO_2 at abundances of 0.35% and 0.37%. ZnO is present in abundances up to 1.69% in all samples from the Kingy area. No V_2O_3 or CoO has been detected in spinels from the Kingy area.

9.8.8. Summary of Spinel Geochemistry in the Kingy area

Spinels have been analysed from three clinopyroxenite samples from the Kingy area. The geochemistry of the spinels from the Lensoid Ultramafics is markedly different from those from the Extra Ultramafic. All analyses from the two samples from the Lensoid Ultramafics (except one) contain spinels with a wide range of Fe^{2+}# ratios and a narrow Cr# range. Conversely, the spinels analysed from the Extra Ultramafic show a narrow Fe^{2+}# and a wide Cr# range. Furthermore, TiO_2 has been detected in the spinels from the Extra Ultramafic but not in those from the Lensoid Ultramafics. There are further differences observed in the Fe^{3+}# content, namely the values are low in most spinels from the Lensoid Ultramafics and higher in those from the Extra Ultramafic. However two analyses from the Lensoid Ultramafics are higher than those from the Extra Ultramafic.

9.9. Discussion

9.9.1. Alteration

In general, the two analyses from the Lensoid Utramafics have a very narrow Cr# range and an extensive Fe^{2+}# range. One analysis, from the far northwestern Lensoid Ultramafic has a much lower Cr# analysis accompanied by a higher Fe^{2+}# a geochemistry

which is similar from the spinels of the Extra Ultramafic. This trend in the spinel geochemistry from the Extra Ultramafic fits the amphibolite facies alteration trends suggested by Evans and Frost (1975) which were discussed further in section 9.6.1. Furthermore, the low Cr# from one analysis from the Lensoid Ultramafics suggests that this analysis maybe from an extremely altered version of the other analyses. However, the lack of correlation between Cr# and Fe^{2+}# in the Lensoid Ultramafics does not fit the model of spinel alteration suggested from other studies or the analyses of core and rims (see section 9.4).

Although the lack of correlation between Cr# and Fe^{2+}# in the Lensoid Ultramafics is unlike a classic "alteration trend" there is one analysis from sample KTR-069-01 which shows a high Fe^{3+}# with high Fe^{2+}# value. Furthermore an analysis from another sample from the Lensoid Ultramafics contains elevated Fe^{3+}# and Fe^{2+}# along along with a lower Cr# value. These outliers could both be interpreted as more altered versions of the other analyses within each sample. However, the lack of correlation between Fe^{2+}# and Cr# may not be attributed to alteration and the possible control by magmatic processes is discussed in the next section.

9.9.2. Magmatic Effects

In order to understand the effect which magmatic processes have on the geochemistry of spinels it is necessary to take account of the alteration which overprints them. As discussed in section 9.9.1, although the spinels from the Extra Ultramafic and some individual analyses appear to show alteration effects, the trends in the Lensoid Ultramafics remain unexplained. Therefore it is not possible to discuss the effects of magmatism using this dataset. The analysis of spinels hosted by dunite or olivine-clinopyroxenite may help to eluidate magmatic processes.

It may be argued that if a trend in spinel composition cannot be attributed to alteration then it must be the result of magmatic proceses. However the origin of such a wide

variation in Fe^{2+}# within one sample is hard to explain by magmatic processes without some variation in Cr# accompanying it.

9.9.3. Comparison with Alaskan-type intrusions and ophiolite complexes

The analyses of spinels from the Kingy area can be compared with the Global Spinel Database (Barnes and Roeder, 2001) using figures 9.6B to 9.6G. Unlike the ophiolite complexes summarized by the fields of Barnes and Roeder (2001) the analyses from the Kingy Extra Ultramafic have both high Fe^{2+}# values and low Cr#. This geochemistry is typical of Alaskan-type intrusions (see section 9.6.3). Furthermore, most analyses from the Kingy area plot within the Alaskan-type intrusion fields and not within the ophiolite fields.

Although the geochemistry of the spinels at Kingy is more typical of those of Alaskan-type intrusions rather than ophiolites this is due to the fact that the analyses with the highest Fe^{2+}# also have low Cr#. It is believed that this geochemistry may occur in an any spinel which has been subjected to sufficient alteration (Evans and Frost, 1975). Therefore, these spinels could originate from either a typical Alaskan-type intrusion or an extremely altered ophiolite.

9.10. Conclusions

The $Fe^{2+\#}$ and Cr# geochemistry of the spinels from the Kingy area is generally typical of Alaskan-type intrusions as characterized by the Global Spinel Database (Barnes and Roeder, 2001) . However, the Fe^{3+}# values are lower than typical Alaskan-type intrusions. The spinels form two clear populations based on Fe^{2+}#, those from the Extra Ultramafic and those from the Lensoid Ultramafics. The spinels of the Extra Ultramafic show a trend similar to the amphibolite facies alteration trend observed by Evans and Frost (1975). However, the spinels from the Lensoid Ultramafics do not show the change in Cr# values which would not be expected from alteration. The poor understanding of alteration effects in the Kingy area makes the interpretation of magmatic effects not possible.

9.12. Daleti, Ankori, Tulu Kapi and Keley: Spinel Geochemistry

9.12.1. Introduction

Seven samples from the Daleti Ultramafic and two samples from the Ankori Ultramafic contain acceptable spinel analyses (as defined in section 9.3). This section describes a total of 139 analyses, 110 of which are located within the Daleti Ultramafic and the remaining 28 occur in the Ankori Ultramafic. All the spinels in question are hosted by dunites. Table 9.4 summarizes the number of analyses from each formation. The pull-out section on page 306 figure 9.7A shows the location of each sample. Furthermore, figure 9.7A shows that the four samples are located in a traverse from the centre of the Daleti Ultramafic towards the northern contact with a shear-zone.

9.12.2. Data

The results for the analysis of the spinels from the Daleti, Ankori, Tulu Kapi and Keley areas are as follows.

Formation	Sample	Analysis	Host Rock	Na_2O	MgO	Al_2O_3	SiO_2	TiO_2	V_2O_3	Cr_2O_3	MnO	FeO*	Fe_2O_3*	CoO	ZnO	Total	Fe^{2+}#	Cr#	Fe^{3+}#
Daleti Ultramafic	D20	1	Dun	nd	4.84	4.63	nd	nd	nd	60.51	0.62	26.41	4.22	nd	nd	101.23	0.754	0.847	0.056
		10		nd	4.62	4.60	nd	nd	nd	59.02	0.71	26.12	4.48	nd	0.63	100.18	0.760	0.841	0.061
		11		nd	4.82	5.56	nd	nd	nd	57.52	nd	26.40	4.32	nd	nd	98.62	0.754	0.823	0.059
		12		nd	4.72	4.65	nd	nd	nd	60.63	nd	27.10	3.97	nd	nd	101.07	0.763	0.850	0.053
		13		nd	5.06	7.07	nd	nd	nd	52.15	0.67	27.55	8.46	nd	nd	100.95	0.753	0.737	0.114
		14		nd	5.34	7.84	nd	nd	nd	54.71	0.67	26.59	6.00	nd	nd	101.14	0.736	0.759	0.079
		15		nd	4.69	5.05	nd	nd	nd	58.96	0.94	25.94	4.25	nd	nd	99.83	0.756	0.836	0.057
		16		nd	4.59	5.03	nd	nd	nd	59.54	0.68	26.95	4.59	nd	nd	101.37	0.767	0.834	0.061
		17		nd	4.59	5.28	nd	nd	nd	57.40	0.65	26.83	5.48	nd	0.75	100.98	0.766	0.814	0.074
		18		nd	4.65	4.98	nd	nd	nd	57.58	nd	27.18	5.37	nd	0.63	100.39	0.766	0.821	0.073
		19		nd	4.62	4.88	nd	nd	nd	59.90	0.65	26.55	4.10	nd	nd	100.70	0.763	0.843	0.055
		20		nd	4.53	4.96	nd	nd	nd	60.21	nd	26.69	3.12	nd	nd	99.51	0.768	0.853	0.042
		21		nd	4.69	4.85	nd	nd	nd	59.30	nd	26.56	3.97	nd	0.70	100.06	0.761	0.843	0.054
		22		nd	4.71	4.81	nd	nd	nd	59.49	0.64	26.12	4.05	nd	nd	99.82	0.757	0.844	0.055
		24		nd	4.68	4.83	nd	nd	nd	60.79	0.70	26.52	3.81	nd	nd	101.34	0.761	0.849	0.051
		25		nd	5.07	4.95	nd	nd	nd	61.13	nd	26.38	3.36	nd	nd	100.89	0.745	0.852	0.045
		26		nd	4.80	4.96	nd	nd	nd	59.23	0.84	26.42	4.81	nd	nd	101.06	0.755	0.832	0.064
		28		nd	5.01	4.85	nd	nd	nd	60.38	nd	26.34	3.68	nd	nd	100.26	0.747	0.849	0.049
		3		nd	4.84	4.77	nd	nd	nd	61.09	nd	26.44	3.15	nd	nd	100.29	0.754	0.858	0.042
		4		nd	4.77	4.71	nd	nd	nd	59.95	0.81	26.05	4.13	nd	nd	100.43	0.754	0.846	0.055
		5		nd	4.30	5.09	nd	nd	nd	57.08	nd	28.36	6.07	nd	nd	100.90	0.787	0.810	0.082
		6		nd	4.63	4.80	nd	nd	nd	60.28	0.78	26.66	4.26	nd	nd	101.41	0.764	0.843	0.057
		7		nd	4.80	4.89	nd	nd	nd	60.57	0.73	26.17	3.77	nd	nd	100.93	0.754	0.848	0.050
		8		nd	5.02	4.76	nd	nd	nd	60.99	nd	26.21	3.30	nd	nd	100.27	0.745	0.856	0.044
		9		nd	4.85	4.88	nd	nd	nd	60.52	nd	26.42	3.36	nd	nd	100.03	0.754	0.853	0.045
	D11	11	Dun	nd	5.45	2.49	nd	nd	nd	63.28	0.61	24.69	3.85	nd	0.72	101.09	0.718	0.896	0.052

Formation	Sample	Analysis	Host Rock	Na_2O	MgO	Al_2O_3	SiO_2	TiO_2	V_2O_3	Cr_2O_3	MnO	FeO*	Fe_2O_3*	CoO	ZnO	Total	Fe^{2+}#	Cr#	Fe^{3+}#
		12		nd	5.41	3.49	nd	nd	nd	59.23	0.64	25.00	5.37	nd	nd	99.14	0.722	0.852	0.073
		1/9		nd	5.31	2.86	nd	nd	nd	63.21	nd	25.18	3.06	nd	nd	99.62	0.727	0.898	0.041
		2/9		nd	5.83	3.91	nd	nd	nd	61.17	0.75	24.52	4.51	0.37	nd	101.05	0.702	0.858	0.060
		3/9		nd	5.14	4.10	nd	nd	nd	58.01	nd	26.45	5.95	0.38	nd	100.03	0.743	0.831	0.081
		4/9		nd	5.15	2.46	nd	nd	nd	62.81	0.69	25.02	3.86	nd	nd	99.99	0.732	0.895	0.052
		5/9		nd	5.33	5.73	nd	nd	nd	50.33	0.63	26.70	10.14	nd	0.73	99.59	0.738	0.735	0.141
		6/9		nd	5.14	3.88	nd	nd	nd	57.60	nd	26.30	6.23	nd	0.66	99.81	0.742	0.831	0.086
		7/9		nd	5.19	2.74	nd	nd	nd	62.48	0.70	24.83	3.88	0.41	0.66	100.88	0.729	0.889	0.053
		9/9		nd	4.95	2.28	nd	nd	nd	63.53	0.67	25.53	3.77	nd	nd	100.73	0.743	0.901	0.051
		1		nd	5.14	2.84	nd	nd	nd	62.43	0.88	25.45	4.44	nd	nd	101.18	0.735	0.881	0.060
		10		nd	5.30	5.15	nd	nd	nd	51.20	0.67	27.02	10.44	nd	0.63	100.41	0.741	0.744	0.144
		11		nd	5.25	2.20	nd	nd	nd	62.26	0.90	24.57	4.28	nd	nd	99.46	0.724	0.894	0.059
		12		nd	5.04	2.86	nd	nd	nd	60.64	nd	25.45	4.29	nd	0.79	99.07	0.739	0.879	0.059
		14		nd	5.42	4.22	nd	nd	nd	56.63	0.80	26.27	7.77	nd	nd	101.11	0.731	0.805	0.105
		15		nd	5.16	2.46	nd	nd	nd	62.96	1.07	25.11	4.33	nd	nd	101.10	0.732	0.890	0.058
		2		nd	5.27	3.47	nd	nd	nd	58.56	0.64	25.96	6.65	nd	0.78	101.33	0.734	0.836	0.090
		21		nd	5.27	2.81	nd	nd	nd	62.16	nd	26.21	4.71	nd	nd	101.17	0.736	0.878	0.063
		22		nd	5.23	5.39	nd	nd	0.41	49.59	0.80	27.78	11.64	nd	nd	100.84	0.749	0.717	0.160
	DR 01/01	23		nd	5.02	5.34	nd	nd	nd	50.66	0.86	27.74	10.95	nd	nd	100.57	0.756	0.734	0.151
		24	Dun	nd	4.88	3.03	nd	nd	nd	50.54	0.94	27.95	12.86	nd	nd	100.19	0.763	0.751	0.182
		25		nd	4.94	4.22	nd	nd	nd	50.45	nd	28.62	11.78	nd	nd	100.00	0.765	0.742	0.165
		26		nd	4.98	5.57	nd	nd	nd	49.56	nd	28.38	11.14	nd	0.89	100.52	0.762	0.724	0.155
		3		nd	5.34	4.18	nd	nd	nd	55.58	0.82	25.80	7.80	nd	0.60	100.13	0.731	0.803	0.107
		4		nd	5.15	4.84	nd	nd	nd	53.34	0.87	26.80	9.16	nd	nd	100.16	0.745	0.770	0.126
		5		nd	5.24	4.54	nd	nd	nd	56.52	0.63	26.44	7.22	nd	nd	100.59	0.739	0.806	0.098
		6		nd	4.95	4.19	nd	nd	nd	55.81	0.60	26.49	7.32	nd	nd	99.37	0.750	0.809	0.101
		7		nd	4.80	2.55	nd	nd	nd	62.29	0.63	25.65	4.00	nd	nd	99.92	0.750	0.891	0.055
		8		nd	4.87	3.18	nd	nd	nd	59.33	nd	26.33	5.25	nd	nd	98.96	0.752	0.859	0.072
		9		nd	5.11	3.68	nd	nd	nd	57.57	0.79	25.73	6.48	nd	nd	99.36	0.739	0.832	0.089
		1/6		nd	4.34	5.99	nd	nd	nd	47.34	0.83	29.52	12.78	nd	nd	100.79	0.792	0.692	0.178
		1/7		nd	4.31	5.41	nd	nd	nd	49.45	0.71	29.21	11.58	nd	nd	100.67	0.792	0.721	0.161
		10		nd	4.17	5.23	nd	nd	nd	49.51	0.93	29.51	12.00	nd	nd	101.36	0.799	0.720	0.166
		10		nd	4.00	5.74	nd	nd	nd	48.43	nd	30.42	11.79	nd	nd	100.38	0.810	0.710	0.164
		11		nd	4.01	5.69	nd	nd	0.39	47.90	0.90	29.86	12.31	nd	nd	101.06	0.807	0.699	0.171
		11		nd	3.96	5.42	nd	nd	0.48	48.64	0.73	30.05	12.01	nd	nd	101.30	0.810	0.709	0.167
		12		nd	3.01	5.67	nd	nd	nd	50.84	nd	30.72	9.06	nd	0.67	99.97	0.851	0.749	0.127
		13		nd	4.20	5.32	nd	nd	nd	51.10	0.96	29.09	10.71	nd	nd	101.38	0.795	0.738	0.147
		2/6		nd	4.02	5.50	nd	nd	nd	48.59	0.69	29.45	11.63	nd	nd	99.88	0.804	0.716	0.163
	DR 07/01	3/6	Dun	nd	4.27	5.80	nd	nd	nd	47.99	0.73	29.71	12.55	nd	nd	101.05	0.796	0.700	0.174
		4/6		nd	4.65	5.48	nd	nd	nd	49.82	0.81	28.59	11.43	nd	nd	100.78	0.775	0.723	0.158
		5/6		nd	4.05	5.99	nd	nd	nd	48.47	1.04	29.47	11.79	nd	nd	100.82	0.803	0.706	0.164
		5/7		nd	4.39	5.08	nd	nd	nd	52.16	0.65	28.93	10.20	nd	nd	101.42	0.787	0.751	0.140
		6/6		nd	4.08	5.76	nd	nd	nd	48.03	0.93	29.64	12.32	nd	nd	100.76	0.803	0.703	0.172
		6/7		nd	4.29	5.07	nd	nd	nd	51.17	0.88	28.92	10.78	nd	nd	101.11	0.791	0.742	0.149
		7/7		nd	4.11	5.46	nd	nd	nd	51.11	nd	29.62	9.94	nd	nd	100.24	0.802	0.744	0.138
		8/6		nd	4.21	5.29	nd	nd	nd	49.62	0.62	29.52	11.63	nd	nd	100.89	0.797	0.724	0.161
		8/7		nd	4.34	4.49	nd	nd	nd	54.08	nd	28.86	8.75	nd	nd	100.52	0.789	0.783	0.120
		9/7		nd	4.28	4.32	nd	nd	nd	55.33	0.82	28.09	8.16	nd	nd	101.00	0.786	0.796	0.112
		1		nd	4.74	5.07	nd	nd	nd	59.38	0.68	26.41	4.39	nd	0.36	101.02	0.758	0.835	0.059
		10		nd	5.11	4.03	nd	nd	nd	62.46	0.89	25.01	3.00	nd	0.38	100.88	0.733	0.876	0.040
		11		nd	4.94	4.48	nd	nd	nd	61.90	0.59	25.49	2.75	nd	nd	100.16	0.743	0.869	0.037
		13		nd	2.69	2.55	nd	nd	0.64	48.88	0.81	31.02	12.78	nd	0.59	99.97	0.866	0.746	0.186
		14		nd	3.88	4.88	nd	nd	0.39	51.95	0.77	28.73	9.16	nd	nd	99.76	0.806	0.760	0.128
		15		nd	3.39	3.53	nd	nd	0.60	47.42	0.67	30.61	13.57	nd	0.58	100.37	0.835	0.716	0.195
	DR 08/01	16		nd	4.29	4.84	nd	nd	nd	55.84	0.58	28.17	7.38	nd	0.38	101.48	0.787	0.797	0.100
		17	Dun	nd	4.72	4.46	nd	nd	nd	60.16	0.58	26.18	4.08	nd	0.60	100.78	0.757	0.851	0.055
		18		nd	4.75	4.60	nd	nd	nd	60.84	0.81	26.06	3.72	nd	nd	100.79	0.755	0.854	0.050
		4		nd	4.83	4.95	nd	nd	nd	59.18	0.84	26.34	4.82	nd	nd	100.97	0.754	0.832	0.065
		5		nd	4.63	6.51	nd	nd	0.40	51.89	nd	28.54	8.32	nd	nd	100.29	0.776	0.742	0.113
		6		nd	4.52	5.35	nd	nd	nd	56.37	0.68	27.37	6.34	nd	nd	100.63	0.773	0.801	0.086
		8		nd	5.08	4.36	nd	nd	nd	62.42	0.73	25.35	2.86	nd	nd	100.80	0.737	0.871	0.038
		9		nd	5.17	4.76	nd	nd	nd	61.42	0.71	25.31	3.26	nd	0.56	101.19	0.733	0.858	0.043
	DR	c1	Dun	nd	4.99	5.10	nd	nd	nd	43.25	0.65	30.08	17.33	nd	nd	101.40	0.772	0.642	0.245

Formation	Sample	Analysis	Host Rock	Na_2O	MgO	Al_2O_3	SiO_2	TiO_2	V_2O_3	Cr_2O_3	MnO	FeO*	Fe_2O_3*	CoO	ZnO	Total	Fe^{2+}#	Cr#	Fe^{3+}#
Ankori Ultramafic	DR 22/01	10	Dun	nd	5.00	4.72	nd	nd	nd	47.88	0.71	28.86	13.93	nd	nd	101.10	0.764	0.702	0.194
		11		nd	4.68	4.74	nd	nd	nd	43.41	0.71	30.06	17.03	nd	0.54	101.17	0.783	0.651	0.243
		12		nd	4.65	4.70	nd	nd	nd	41.65	0.73	30.31	18.15	nd	nd	100.19	0.785	0.632	0.262
		15		nd	4.69	4.98	nd	nd	nd	42.79	0.87	29.54	16.72	nd	nd	99.59	0.779	0.647	0.241
		16		nd	4.75	5.06	nd	nd	nd	42.22	0.63	29.98	17.29	nd	nd	99.93	0.780	0.638	0.249
		19		nd	3.47	2.26	nd	nd	nd	40.62	0.63	32.98	21.13	nd	nd	101.09	0.842	0.634	0.314
		2		nd	3.90	5.53	nd	nd	nd	44.33	0.65	30.07	14.26	nd	nd	98.74	0.812	0.670	0.205
		3		nd	4.88	5.06	nd	nd	nd	44.55	nd	29.48	15.06	nd	nd	99.02	0.772	0.671	0.216
		4		nd	5.37	4.63	nd	nd	nd	50.65	0.81	27.18	11.52	nd	nd	100.17	0.740	0.739	0.160
		5		nd	5.34	3.20	nd	nd	nd	59.22	0.63	25.75	6.28	nd	nd	100.42	0.730	0.846	0.085
		6		nd	5.27	5.25	nd	nd	nd	43.55	0.79	29.03	16.60	nd	nd	100.49	0.756	0.648	0.235
		8		nd	5.56	5.00	nd	nd	nd	50.30	0.59	27.62	12.04	nd	nd	101.11	0.736	0.727	0.166
		9		nd	4.34	3.61	nd	nd	nd	43.40	0.59	30.84	17.90	nd	nd	100.68	0.799	0.659	0.259
		10		nd	3.54	2.81	nd	nd	0.45	42.61	0.70	31.27	17.72	nd	nd	99.10	0.832	0.664	0.263
		12		nd	4.17	5.10	nd	nd	0.38	43.59	0.67	31.10	16.48	nd	nd	101.49	0.807	0.648	0.233
		13		nd	4.60	6.16	nd	nd	0.44	42.84	0.64	30.52	16.18	nd	nd	101.38	0.788	0.631	0.227
		14		nd	4.03	4.13	nd	nd	0.42	42.65	0.73	31.15	17.56	nd	nd	100.66	0.813	0.647	0.253
		15		nd	3.99	3.29	nd	nd	0.34	44.11	0.81	31.02	17.36	nd	nd	100.92	0.814	0.670	0.251
		2		nd	4.54	6.96	nd	nd	0.53	39.39	0.58	31.01	17.77	nd	0.62	101.41	0.793	0.586	0.252
		8		nd	3.84	3.33	nd	nd	0.41	42.79	nd	31.42	17.22	nd	nd	99.01	0.821	0.663	0.254
		9		nd	4.95	6.81	nd	nd	nd	43.14	nd	30.40	15.59	nd	nd	100.89	0.775	0.633	0.218
	KYC-007-01	1/9	Dun	nd	3.70	21.74	nd	nd	nd	38.79	1.13	29.17	3.78	0.48	0.91	99.70	0.816	0.519	0.048
		10		nd	3.79	22.32	nd	0.29	nd	38.62	1.09	28.91	3.00	nd	2.22	100.24	0.811	0.517	0.038
		11		nd	3.64	22.13	nd	nd	nd	38.45	1.07	28.78	3.11	nd	2.20	99.37	0.816	0.517	0.040
		12		nd	3.75	22.11	nd	0.31	nd	39.66	1.11	29.39	2.96	nd	1.81	101.10	0.815	0.526	0.037
		13		nd	3.84	22.13	nd	nd	nd	39.52	1.12	28.89	3.13	0.34	1.90	100.88	0.808	0.524	0.040
		14		nd	3.57	22.04	nd	nd	nd	39.02	1.33	29.21	3.46	nd	1.60	100.23	0.821	0.519	0.044
		15		nd	3.64	21.70	nd	nd	nd	39.36	1.08	28.74	2.93	nd	2.18	99.63	0.816	0.528	0.037
		16		nd	3.68	21.58	nd	nd	nd	39.71	1.33	28.73	3.23	0.36	2.07	100.69	0.814	0.530	0.041
		17		nd	3.49	21.50	nd	nd	nd	39.52	1.29	28.83	3.07	0.37	2.06	100.13	0.823	0.531	0.039
		18		nd	3.94	22.07	nd	nd	nd	39.22	1.27	28.33	3.10	0.31	2.15	100.39	0.801	0.522	0.039
		19		nd	4.01	22.04	nd	nd	nd	39.30	1.26	28.19	3.01	nd	2.03	99.85	0.798	0.524	0.038
		2/9		nd	3.94	22.53	nd	nd	nd	38.50	1.52	28.82	3.81	nd	1.25	100.37	0.804	0.509	0.048
		20		nd	3.55	22.12	nd	nd	nd	39.58	1.19	29.31	2.98	nd	1.37	100.10	0.822	0.525	0.038
		21		nd	3.40	21.48	nd	nd	nd	39.34	1.28	29.24	3.43	nd	2.24	100.42	0.828	0.527	0.044
		22		nd	3.29	22.24	nd	nd	nd	39.08	1.59	29.29	3.17	nd	2.32	100.98	0.833	0.519	0.040
		23		nd	3.32	21.85	nd	nd	nd	39.04	1.25	29.14	3.06	0.41	2.35	100.42	0.831	0.524	0.039
		24		nd	2.99	21.94	nd	nd	nd	38.74	1.34	29.57	3.07	0.40	2.42	100.47	0.847	0.521	0.039
		25		nd	2.94	21.31	nd	nd	nd	38.85	1.25	29.42	3.08	nd	2.30	99.15	0.849	0.528	0.040
		3/9		nd	4.08	21.50	nd	nd	nd	39.14	1.36	28.45	3.99	nd	1.35	99.87	0.796	0.522	0.051
		4/9		nd	4.29	21.65	nd	0.28	nd	39.05	1.26	27.93	3.17	nd	1.14	98.76	0.785	0.525	0.041
		5/9		nd	3.27	21.62	nd	nd	nd	38.66	1.15	28.97	2.97	nd	2.12	98.76	0.833	0.524	0.038
		6/9		nd	3.21	21.52	nd	0.36	nd	39.47	1.25	29.76	2.97	nd	1.95	100.49	0.839	0.531	0.038
		7/9		nd	3.51	21.95	nd	nd	nd	38.73	1.35	28.65	3.06	0.37	2.13	99.75	0.821	0.521	0.039
		8/9		nd	3.75	22.41	nd	nd	nd	39.02	1.24	28.67	2.86	nd	2.05	100.00	0.811	0.519	0.036
		9/9		nd	3.84	22.29	nd	nd	nd	38.59	1.17	28.62	3.24	nd	2.13	99.88	0.807	0.515	0.041
	A2	19		nd	11.03	10.97	nd	nd	nd	57.74	0.99	16.52	2.48	nd	0.43	100.16	0.457	0.755	0.031
		20		nd	10.82	10.73	nd	nd	nd	58.37	0.98	16.52	1.83	nd	nd	99.26	0.461	0.767	0.023
		21	Dun	nd	10.75	10.89	nd	nd	nd	58.52	1.14	16.07	1.16	nd	nd	98.53	0.456	0.771	0.015
		22		nd	11.47	11.16	nd	nd	nd	59.17	1.15	15.56	1.57	nd	0.47	100.55	0.432	0.765	0.019

Table 9.9: The geochemistry of the spinels analysed from the Daleti, Ankori, Tulu Kapi and Keley areas in wt %. Analyses from a birbirite sample are included here, however these are not plotted on any graphs as there is considerable uncertainty over their mode of formation (see chapter 3). Nd: not detected. *: Fe^{2+} and Fe^{3+} values are estimated from measured total Fe by the method described in section 9.3. Fe^{2+}# = Fe2+/(Mg+Fe^{2+}). Cr# = Cr/(Cr+Al). Fe^{3+}# = Fe^{3+}/(Fe^{3+}+Al+Cr+V).

9.12.3. Fe^{2+}# (Fe2+/(Mg+Fe^{2+}))

All spinels analysed from the Daleti Ultramafic and the Ankori Ultramafic are hosted by dunite. Most spinels from the Daleti area – including one sample from the Ankori Ultramafic – have Fe^{2+}# values which fall into the range 0.702 to 0.866. Within this range, there are no notable differences in Fe^{2+}# values between samples. However sample A2 from the Ankori complex contains Fe^{2+}# which are much lower than all other samples and range from 0.432 to 0.461.

9.12.4. Cr# (Cr / (Cr+Al))

The spinels from the Daleti area have Cr# values ranging from 0.509 to 0.898. The lowest spinel Cr# values (0.509 to 0.531) are those hosted by sample KYC-007-02 from the Ankori Ultramafic. The second lowest Cr# ratios occur in sample DR 22/01 with a range of 0.586 to 0.670. All other samples occupy the range 0.632 to 0.898. Although one sample from the Ankori complex (KYC-007-02) has spinel Cr# values which are below those of the Daleti Ultramafic the spinels from the other sample from the Ankori Ultramafic (A2) have higher values (see figure 9.7C).

9.12.5. TiO_2

TiO_2 was detected in only four analyses from the Ankori Ultramafic (sample KYC-007-02) and range from 0.28 to 0.36%

9.12.6. Fe^{3+}# (Fe^{3+} / (Fe^{3+} + Al^{2+} + Cr^{3+} + V^{3+}))

All analyses of spinels from the Daleti Ultramafic and Ankori Ultramafic have Fe^{3+}# ratios which range from 0.015 to 0.314. The lowest Fe^{3+}# values are found in the spinels from sample A2 from the Ankori Ultramafic which range from 0.015 to 0.031. The spinels from the other sample from the Ankori Ultramafic have slightly higher Fe^{3+}# values, ranging from 0.036 to 0.051. The highest Fe^{3+}# value (0.314) occurs in a spinel from sample DR 09/01 however some other spinels from this sample host some of the

lowest values (>0.085) seen in this area. The analyses from sample DR 22/01 are noteworthy for their uniformly high Fe^{3+}# values (0.218 to 0.263).

9.12.7. Minor Elements (Co and Zn)

CoO is detected in two samples from the Daleti Ultramafic, these are three analyses from sample D11 from the Daleti Ultramafic with values ranging from 0.37 to 0.41%. Eight analyses from sample KYC-007-01 returned positive analyses for CoO with values ranging from 0.31 to 048%. ZnO was detected (<0.89%) in 22 analyses from the Daleti Ultramafic and it has been detected in at least one analysis from each sample. Unlike the other samples, in one sample from the Ankori Ultramafic (KYC-007-02) every analysis returned ZnO values above detection limts, ranging from 0.91 to 2.42%. No Na_2O, SiO_2, S, NiO, ZnO or AsO has been detected in the the Daleti or Ankori Ultramafics.

9.12.8. Summary of Spinel Geochemistry in the Daleti Ultramafic

The spinels from the Daleti Ultramafic all cover a similar range of Fe^{2+}#, Fe^{3+}# and Cr# values and TiO_2 has not been detected. Each sample shows similar upper limits of Cr# and similar lower limits of Fe^{3+}#. Most samples cover similar ranges of Cr# and Fe^{3+}# however samples DR 09/01 and DR 22/01 have slightly lower Cr# and higher Fe^{3+}# values. These two samples are both situated at the northwestern edge of the intrusion. Another sample (D20) is located close to DR 22/01 but it does not share the same restricted Cr# and elevated Fe^{3+}# values.

For each sample, the range of Fe^{2+}# ratios is more restricted than the ranges of Cr# and Fe^{3+}#. As such, all spinels in the Daleti Ultramafic tend to show a broad negative trend between Fe^{2+}# and Cr#. Furthermore within each sample there is a negative correlation between Cr# and Fe^{3+}#.

9.12.9. Summary of Spinel Geochemistry in the Ankori Ultramafic

The two samples from the Ankori Ultramafic which contain spinels (A2 and KYC-007-01) are both dunites. The analyses from each sample display similar Fe^{3+}# values yet very different Fe^{2+}# and Cr# values. The spinels from sample A2 have lower Fe^{2+}# and higher Cr# values than sample KYC-007-01. The difference in Fe^{3+}# values is 0.005 which is much smaller than the difference in Fe^{2+}# values (0.324) and the difference in Cr# (0.224). Furthermore, TiO_2 is detected in KYC-007-04 but not detected in A2.

The ranges of both Cr# and Fe^{3+}# values for the analyses of spinels hosted by sample KYC-007-01 are narrower than the range of Fe^{2+}# values. Due to the low number of analyses of spinels from sample A2 an assessment of the relative ranges would not be reliable.

When compared to the Daleti Ultramafic the two samples both show similar Fe^{3+}# values, however in the other ratios considered here the samples are different. Sample A2 has much lower Fe^{2+}# values than the Daleti Ultramafic but similar Cr# and TiO_2 values. Whereas sample KYC-007-01 has lower Cr# values and higher TiO_2 but similar Fe^{2+}# values.

9.13. Discussion

9.13.1. Alteration

Although the trend of analyses from most samples shows a restricted range of Fe^{2+}# and a wide range of Cr#, many samples include at least one analysis which contains a larger Fe^{2+}# than the others. Analyses of the cores and rims of zoned spinels and from several complexes worldwide (see section 9.4) have suggested that post magmatic alteration increases both Cr# and Fe^{2+}#. Although it is not possible to demonstrate the geochemistry of a truly "fresh" spinel from this dataset, there are some outliers which have higher Fe^{2+}# than most of the other analyses within each sample. These outliers could be considered to be altered equivalents of the analyses that from the main trend.

Some samples show no outliers and others show a continuous trend where Fe^{2+}# increases with Cr#. This is to be expected if the Fe^{2+}# and Cr# increases with alteration. As all analyses were taken from the cores of spinels, if a truly "fresh" core was exposed then the analysis would reflect this. However some samples will have been pervasively altered and therefore the only trend which could be represented would be the alteration trend. There may also be some samples where the alteration was very slight and these would show a dominantly magmatic trend with few outliers. Therefore the extent of alteration (as opposed to severity of the conditions eg, amphibolite versus granulite facies) could be expressed by the degree of fit between alteration and magmatic trends - such as those suggested in section 9.7.

If the extent of alteration could be estimated by the degree of fit to the alteration trend - as suggested above - then the samples which are the most extensively altered from Daleti Ultramafic would be DR22/01 and DR 09/01 (see figure 9.7C). Both of these samples are located near the shear-zone/ultramafic contact northwestern flank of the intrusion. This is consistent with the hypothesis that the alteration fluids used shear-zones as conduits and as such the most altered rocks should occur near such features and at the edges of the ultramafic intrusions. Trends in Fe^{2+}# versus Cr# could be used to estimate the degrees of alteration only if magmatic fractionation is understood (which are discussed in section 9.13.2)

Figure 9.7G shows the correlation between Fe^{2+}# and Fe^{3+}# within samples. It is considered that such trends may also be used to help understand alteration. However the effects of magmatic processes on the Fe^{3+}# ratio needs to be understood before such interpretations can be made. Furthermore, the strong negative correlation between Cr# and Fe^{3+}# infers that fractionation may have the same effect as alteration in figure 9.7G. Therefore it may not be possible to separate their relative influences using diagrams such as figure 9.7G.

9.13.2. Magmatic Effects

Several samples from the Daleti Ultramafic show a narrow Fe^{2+}# range and a wide Cr# range (with a few outliers which are discussed in section 9.13.1). This creates a trend which is different from the alteration trend suggested in section 9.13.1. The variation in Cr# is due to a variation in Cr_2O_3 values within each sample and this variation could be explained in terms of crystal fractionation where the highest Cr^{3+} values occur in the most primitive minerals.

As alteration should increase the Cr# values, the lowest Cr# values for each sample should be the least altered of each sample (see section 9.6.2). However fractionation will act to decrease the amount of Cr# values (irrespective of Fe^{2+}#). Therefore the analysis with the lowest Cr# from each sample will represent the least altered, but possibly the most evolved, spinel in the sample.

Sample	Min Cr#	Fe^{2+}#	Fe^{3+}#
D20	0.737	0.736	0.042
D11	0.735	0.702	0.051
DR 01/01	0.717	0.724	0.055
DR 08/01	0.716	0.733	0.037
DR 07/01	0.692	0.775	0.112
DR 09/01	0.632	0.730	0.085
DR 22/01	0.586	0.775	0.218

Table 9.10: The minimum Cr# values for spinel analyses from the sample of the Daleti Ultramafic. All spinels are hosted by dunite and analyses are listed with the highest minumum Cr# at the top. Nd: not detected.

In a situation where all the samples formed by the differentiation of a single magma, the spinels which formed first should have the highest Cr^{3+} values (and lowest Al^{3+} values. Furthermore, the most primitive samples should form near to each other and the more evolved samples located further away. However, the situation in the Daleti intrusion does not show this. Figure 9.7A shows that of the 7 samples from the Daleti intrusion, the two with highest minimum Cr# (D20) and lowest minimum Cr# (DR 22/01) occur next to each other. Furthermore, the samples with the intermediate minimum Cr# occur over 1km away. The lack of systematic variation in minimum Cr# could be explained by the intrusion of multiple melts. However this would need to be confirmed by studying

geochemical variations through a continuous section of the complex. As many samples from the Daleti intrusion do not contain spinels, this would need to be performed using a more common mineral such as olivine.

There is a crude negative correlation between the Cr# and Fe^{2+}# in the analyses of lowest Cr#. This infers that fractionation may have had an effect on the Fe^{2+} or Mg^{2+} values.

9.13.3. Comparison with Alaskan-type intrusions and ophiolite complexes

Figures 9.7B to 9.7G can be used to compare the geochemistry of spinels from the Daleti area with the 90th percentile fields of disseminated spinels and chromitites from the Global Spinel Database (Barnes and Roeder, 2001). A clear difference in the geochemistry of Alaskan-type intrusions and ophiolites can be demonstrated by comparing Fe^{2+}# values with Cr# values (see figure 9.7F). When studying the Fe^{2+}# and Cr# values of the Daleti Ultramafic very few from the analyses fall into the ophiolite field and those which are similar to ophiolites also fall into the Alaskan-type field. Most other analyses either fall into the Alaskan-type field, or contain Cr# values lower than typical Alaskan-type intrusions. These slightly lower Cr# values may indicate that these samples are slightly more evolved than typical Alaskan-type intrusions. Figure 9.7G shows that although the analyses plot into Fe^{2+}# and Fe^{3+}# ranges which are different from both ophiolite and Alaskan-type intrusion fields, the Fe^{3+}# range is larger than most ophiolite complexes. TiO_2 has not been detected in the Daleti Ultramafic.

Although the ranges Fe^{3+} and TiO_2 values in the Daleti Ultramafic do not show similarity to either type of complex, figure 9.7C shows that the geochemistry of most spinels is similar to most Alaskan-type intrusions. Furthermore, very few spinels show geochemistries similar to ophiolite complexes. However – as discussed in section 9.6.3 – the difference in spinel geochemistry between Alaskan-type intrusions and ophiolites could be attributed to a greater degree of alteration. Therefore, although the compositions described here are more typical of Alaskan-type intrusions, they could have originated from a highly altered ophiolite complex.

The two samples from the Ankori Ultramafic show starkly different compositions. The low minimum Cr# in sample KYC-007-01 may represent a highly evolved Alaskan-type intrusion or may originate from another type of complex altogether. The low Fe^{2+}# values of the spinels from sample A2 when compared to the Daleti Ultramafic cannot be explained here. However figure 9.7C shows that it has Cr# values similar to both Alaskan-type intrusions and ophiolites. As is the case with the spinels from the Daleti Ultramafic, figures 9.7E and 9.7G show that the Ankori spinels have different TiO_2 and Fe^{3+}# values to both ophiolites and Alaskan-type intrusions.

9.14. Conclusions

The geochemistry of spinels from the Daleti Ultramafic are unlike typical analyses of ophiolitic spinels. Furthermore, many of the analyses plot within the Alaskan-type intrusion on a plot of Fe^{2+}# versus Cr# (see figure 9.7C). Of the two samples from the Ankori Ultramafic, one shows a geochemistry unlike both types of complex and the other plots within both fields.

The samples from the Daleti Ultramafic show a variety of trends which could be interpreted as being controlled either by alteration, magmatic processes or a combination of the two. Within the Daleti intrusion the two samples which show the strongest alteration trend lie close to the contact with a shear-zone.

A study of the minimum Cr# values in each sample suggests the least evolved and most evolved samples from the Daleti Ultramafic occur within 200m of each other. This raises the possibility that the Daleti Ultramafic may have formed through the differentiation of more than one melt influx.

9.15. Yubdo, Sodu and Andu: Spinel Geochemistry

9.15.1. Introduction

Three samples from the Main Yubdo Intrusion contain acceptable spinel analyses (as defined in 9.3). There are 67 analyses in total, however only 6 acceptable analyses were obtained from sample Y30 . All the samples which host the spinels covered here are dunites. In the pull-out section , figure 9.8A shows that the three samples are located in the centre of the intrusion.

9.15.2. Data

The results for the analysis of the spinels from the Yubdo, Sodu and Andu areas are as follows.

Formation	Sample	Analysis	Host Rock	Na_2O	MgO	Al_2O_3	SiO_2	TiO_2	V_2O_3	Cr_2O_3	MnO	FeO*	Fe_2O_3*	CoO	ZnO	Total	Fe^{2+}#	Cr#	Fe^{3+}#
Main Yubdo Intrusion	Y1	1/8	Dun	nd	5.56	9.77	nd	0.49	nd	48.03	0.66	27.25	8.18	nd	nd	99.93	0.733	0.682	0.111
		1/9		nd	4.59	9.77	nd	0.39	nd	44.01	0.72	29.59	11.24	nd	nd	100.31	0.783	0.635	0.154
		10		nd	3.21	10.17	nd	0.43	nd	42.87	0.66	31.49	10.75	nd	nd	99.58	0.846	0.628	0.150
		11		nd	4.17	10.34	nd	0.49	nd	45.92	0.56	30.43	9.51	nd	nd	101.42	0.804	0 652	0.129
		12		nd	4.47	9.99	nd	0.45	nd	43.72	0.81	29.35	10.69	nd	nd	99.48	0.786	0.636	0.148
		13		nd	5.50	9.46	nd	0.36	nd	47.72	nd	27.84	8.63	nd	nd	99.51	0.740	0.681	0.117
		14		nd	3.96	9.80	nd	0.34	nd	46.11	0.51	30.71	9.97	nd	nd	101.39	0.813	0.657	0.135
		15		nd	3.50	8.93	nd	0.33	nd	44.31	0.89	30.52	10.92	nd	nd	99.40	0.830	0.651	0.153
		15		nd	6.52	8.90	nd	0.35	nd	48.40	nd	27.11	9.94	nd	nd	101.22	0.700	0.680	0.133
		16		nd	5.69	9.43	nd	0.39	nd	47.97	0.55	27.43	9.01	nd	nd	100.48	0.730	0.679	0.121
		17		nd	5.69	9.72	nd	nd	nd	48.01	0.72	27.33	9.62	nd	nd	101.10	0.729	0.670	0.128
		18		nd	4.99	9.33	nd	0.57	nd	46.36	nd	29.26	9.60	nd	nd	100.12	0.767	0.668	0.132
		18		nd	5.38	9.06	nd	0.34	nd	5nd	0.51	27.62	7.97	0.34	nd	101.22	0.742	0.703	0.107
		19		nd	4.51	9.57	nd	0.45	nd	45.41	0.69	29.75	10.53	nd	nd	100.91	0.787	0.652	0.144
		2/		nd	6.04	10.09	nd	0.43	nd	47.91	0.60	27.23	8.97	nd	nd	101.26	0.717	0.670	0.119
		2/		nd	2.91	8.69	nd	0.29	nd	43.08	0.82	31.65	11.93	0.38	nd	99.75	0.859	0.639	0.168
		20		nd	4.51	9.16	nd	0.37	nd	44.17	0.86	29.16	11.19	nd	nd	99.42	0.784	0.645	0.156
		20		nd	5.30	8.95	nd	0.36	nd	48.22	nd	28.71	9.34	nd	nd	100.88	0.752	0.684	0.126
		21		nd	3.09	11.89	nd	0.51	nd	35.89	0.62	33.60	14.97	nd	nd	100.56	0.859	0.529	0.210
		21		nd	5.64	9.13	nd	0.39	nd	49.57	0.53	27.36	8.20	nd	nd	100.83	0.731	0.698	0.110
		22		nd	1.65	4.67	nd	0.86	nd	30.41	0.67	37.47	24.31	nd	nd	100.04	0.927	0.503	0.382
		22		nd	2.94	8.61	nd	0.45	nd	46.29	0.76	31.96	10.23	nd	nd	101.24	0.859	0.672	0.141
		23		nd	0.98	0.38	nd	0.95	nd	16.86	nd	42.37	37.97	nd	nd	99.51	0.960	0.315	0.675
		23		nd	4.77	8.92	nd	0.39	nd	49.28	0.73	28.75	8.57	nd	nd	101.41	0.772	0.697	0.115
		25		nd	3.27	9.06	nd	nd	nd	45.96	1.03	30.97	10.82	nd	nd	101.11	0.842	0.659	0.148
		25		nd	3.84	8.99	nd	0.33	nd	45.72	0.72	29.87	9.89	nd	nd	99.37	0.814	0.667	0.137
		26		nd	3.84	9.99	nd	0.45	nd	41.91	1.08	31.28	12.84	nd	nd	101.39	0.820	0.607	0.177
		27		nd	5.30	9.07	nd	0.40	nd	45.81	0.69	27.70	10.09	nd	nd	99.05	0.746	0.665	0.139
		29		nd	2.43	8.92	nd	0.41	nd	39.45	nd	34.13	14.21	nd	nd	99.55	0.887	0.595	0.204
		3/9		nd	3.66	8.79	nd	0.37	nd	45.68	0.67	30.45	10.35	0.50	nd	100.47	0.824	0.666	0.143
		4/8		nd	4.01	9.64	nd	0.50	nd	47.69	0.87	29.96	8.61	nd	nd	101.28	0.807	0.679	0.117
		4/9		nd	3.65	8.72	nd	0.45	nd	43.05	0.55	31.36	12.36	nd	nd	100.14	0.828	0.635	0.173

Formation	Sample	Analysis	Host Rock	Na_2O	MgO	Al_2O_3	SiO_2	TiO_2	V_2O_3	Cr_2O_3	MnO	FeO*	Fe_2O_3*	CoO	ZnO	Total	Fe^{2+}#	Cr#	Fe^{3+}#
		5/8		nd	4.53	9.69	nd	0.42	nd	48.66	0.75	28.80	7.84	nd	nd	100.69	0.781	0.690	0.106
		5/9		nd	2.94	8.91	nd	0.50	nd	47.82	0.72	30.83	7.90	0.39	nd	100.01	0.855	0.697	0.110
		6/8		nd	4.17	9.78	nd	0.44	nd	47.68	0.60	29.61	8.25	nd	nd	100.53	0.799	0.680	0.112
		6/9		nd	3.08	8.98	nd	0.38	nd	47.87	nd	30.87	7.46	nd	nd	98.64	0.849	0.700	0.104
		7/8		nd	2.93	9.79	nd	0.40	nd	44.90	0.78	31.65	9.80	nd	nd	100.25	0.858	0.652	0.136
		7/9		nd	5.62	9.12	nd	0.42	nd	48.41	0.62	27.18	8.62	nd	nd	99.99	0.731	0.690	0.117
		8/8		nd	2.86	9.77	nd	0.35	nd	43.22	0.53	32.23	11.02	nd	nd	99.98	0.863	0.633	0.154
		8/9		nd	3.31	9.32	nd	0.47	nd	45.34	0.86	30.95	9.87	nd	nd	100.12	0.840	0.661	0.137
		9/8		nd	2.81	9.89	nd	0.36	nd	40.66	0.80	32.09	12.30	nd	nd	98.91	0.865	0.606	0.174
		9/9		nd	5.40	9.22	nd	0.33	nd	47.47	0.62	27.40	9.03	nd	nd	99.47	0.740	0.680	0.123
		10		nd	5.76	9.26	nd	nd	nd	44.87	1.01	27.06	11.80	nd	nd	99.76	0.725	0.642	0.161
		11		nd	5.18	9.51	nd	0.41	nd	40.86	1.37	27.85	13.30	nd	1.15	99.64	0.751	0.604	0.187
		14		nd	6.33	10.45	nd	0.39	nd	44.67	1.02	26.78	11.15	0.56	nd	101.35	0.704	0.630	0.150
		15		nd	6.13	10.42	nd	0.45	nd	46.02	1.12	26.56	9.80	0.44	nd	100.94	0.709	0.649	0.132
		16		nd	7.42	10.81	nd	0.47	nd	46.83	0.68	25.32	9.60	nd	nd	101.14	0.657	0.650	0.127
		17		nd	3.89	6.86	nd	0.39	nd	42.60	1.64	28.71	13.22	nd	1.26	98.57	0.805	0.651	0.192
		18		nd	4.41	8.05	nd	nd	nd	38.77	1.37	30.48	17.55	nd	0.67	101.30	0.795	0.575	0.248
		2		nd	7.74	9.68	nd	0.41	nd	45.25	0.86	25.30	12.25	nd	nd	101.49	0.647	0.634	0.163
		21		nd	7.46	10.33	nd	0.51	nd	46.46	0.66	25.41	10.25	nd	nd	101.08	0.657	0.649	0.136
	Y12	22	Dun	nd	5.52	9.90	nd	0.44	nd	44.75	1.54	27.51	11.10	nd	nd	100.76	0.737	0.639	0.151
		24		nd	4.84	9.24	nd	nd	nd	43.22	1.57	28.59	13.26	nd	0.64	101.36	0.768	0.621	0.181
		25		nd	2.49	2.58	0.45	nd	nd	24.54	1.01	37.75	31.91	nd	nd	100.73	0.895	0.418	0.517
		26		nd	5.80	10.37	nd	0.50	nd	44.45	1.21	26.99	10.54	nd	0.63	100.49	0.723	0.636	0.143
		4		nd	7.14	10.29	nd	0.32	nd	44.65	0.94	25.91	11.84	nd	nd	101.09	0.671	0.627	0.158
		5		nd	5.43	10.16	nd	0.42	nd	44.15	1.23	27.85	11.10	nd	nd	100.35	0.742	0.632	0.151
		6		nd	5.39	8.97	nd	0.34	nd	43.09	1.15	28.67	13.49	nd	nd	101.10	0.749	0.622	0.185
		7		nd	7.19	9.52	nd	0.43	nd	45.73	0.74	25.96	11.59	nd	nd	101.15	0.670	0.645	0.155
		8		nd	6.37	10.08	nd	0.51	nd	46.13	1.03	26.65	10.25	nd	nd	101.02	0.701	0.651	0.138
		9		nd	7.60	10.56	nd	0.39	nd	46.38	0.75	25.03	10.30	nd	nd	101.01	0.649	0.645	0.136
		10		nd	8.50	11.16	nd	0.52	nd	42.95	nd	25.49	12.82	nd	nd	101.44	0.627	0.598	0.170
		3		nd	1.95	1.21	nd	1.40	nd	45.88	0.73	34.21	14.85	nd	nd	100.23	0.908	0.742	0.229
		4		nd	1.76	1.24	nd	2.51	nd	30.78	0.59	38.38	24.65	nd	nd	99.91	0.924	0.549	0.418
	Y30	5	Dun	nd	4.82	11.32	nd	0.40	nd	37.69	0.62	30.83	15.04	nd	nd	100.72	0.782	0.547	0.208
		7		nd	2.08	0.75	nd	2.35	nd	39.73	0.80	35.84	18.69	nd	nd	100.24	0.906	0.678	0.303
		8		nd	1.70	0.46	nd	2.69	nd	28.12	nd	39.57	26.83	nd	nd	99.38	0.929	0.517	0.470

Table 9.11: The geochemistry of the spinels analysed from the Yubdo, Sodu and Andu areas in wt %. Analyses from a birbirite sample are included here, however these are not plotted on any graphs as there is considerable uncertainty over their mode of formation (see chapter 3). Nd: not detected. *: Fe^{2+} and Fe^{3+} values are estimated from measured total Fe by the method described in section 9.3. Fe^{2+}# = Fe2+/(Mg+Fe^{2+}). Cr# = Cr/(Cr+Al). Fe^{3+}# = Fe^{3+}/(Fe^{3+}+Al+Cr+V).

9.15.3. Fe^{2+}# (Fe^{2+}/(Mg+Fe^{2+}))

The spinels from each of the samples from the Main Yubdo Intrusion cover similar Fe^{2+}# ranges - from 0.627 to 0.960. However, most of the analyses fall within the range 0.629 to 0.860. There are 10 outliers which have Fe^{2+}# ratios which are larger than 0.860.

9.15.4. Cr# (Cr / (Cr+Al))

The full range of Cr# values in the MainYubdo Ultramafic is 0.315 to 0.742. There are four outliers with Cr# values lower than 0.500. However the upper limits of sample Y1

(0.703) are higher than those of sample Y12 (0.651). The highest Cr# values occur in sample Y30 (<0.742).

9.15.5. TiO_2

TiO_2 is below detection limits in only 6 of the 67 analyses of spinels from the Main Yubdo Intrusion. The four highest TiO_2 values occur in spinels from sample Y30 (<2.690%) and two anomalously high values occur in sample Y1. Most analyses fall between the ranges 0.29% to 0.52% and no distinction can be made between samples Y1 and Y12.

9.15.6. Fe^{3+}# (Fe^{3+} / (Fe^{3+} + Al^{2+} + Cr^{3+} + V^{3+}))

The Fe^{3+} values of the spinels from the Main Yubdo Intrusion fall between 0.104 and 0.675. Both the highest and lowest values were obtained from the spinels from sample Y1. The Fe^{3+}# values from sample Y30 lie above most of the analyses of samples Y1 and Y12.

9.15.7. Minor Elements (SiO_2, CoO and ZnO)

One analysis from sample Y12 has returned a positive SiO_2 value (0.45%). Five analyses from samples Y1 and Y12 contain CoO above detection limits at abundances of up to 0.56. ZnO has been detected in five analyses from sample Y12 up to a maximum of 1.26%

9.15.8. Summary of Spinel Geochemistry in the Main Yubdo Intrusion

The three samples from the Main Yubdo Intrusion share similar spinel Cr#, TiO_2, Fe^{3+} and Fe^{2+} values, however there are outliers in each sample. In sample Y1 there are two outliers with slightly elevated Fe^{2+}# values, and these analyses also share much lower Cr# but elevated TiO_2 and Fe^{3+}#. Sample Y12 has one outlier also with elevated Fe^{2+}# and Fe^{3+}# and lower Cr#, however unlike sample Y1 this outlier is not enriched in TiO_2.

There are 6 analyses from sample Y30 and 2 of these have similar values to the other two samples. As with samples Y1 and Y12 the outliers in sample Y30 have elevated Fe^{2+}# and Fe^{3+}# but also show elevated TiO_2.

If the outliers are not considered, then the range Fe^{2+}# values is wider than those of Cr#, TiO_2 and Fe^{3+}#.

9.16. Discussion

9.16.1. Alteration

Figure 9.8C shows a broad negative correlation between Fe^{2+}# and Cr# in samples Y1 and Y12. The alteration trend proposed in section 9.4 is positive and therefore it is thought unlikely that these trends could have been caused by alteration (see figure 9.4). The evidence presented in section 9.4 suggests that, at low Fe^{2+}# values it is likely that alteration may have increased the Cr# from the true "magmatic" value. Hence alteration could be partially responsible for the "broadness" of the trend seen in figure 9.8C.

In samples Y1 and Y12 there are several outliers from the trend described above, these have very low Cr# and high Fe^{2+}#. These may be explained either by extreme alteration (into amphibolite facies) or by the continuation of the main trend, however it is not possible to distinguish between the two models with this dataset.

Of the six analyses from sample Y30 four appear to follow the same main trend as samples Y1 and Y12 and two outliers have much higher Cr# values. The two outliers with high Cr# values are likely to represent spinels which have been altered to a greater degree than the main trend. However, it is not possible to determine whether the two analyses with the highest Fe^{2+}# are a continuation of the main trend or are extremely altered spinels. Analysis of further spinels from this sample may help to reveal more distinctive alteration trends.

The outliers from samples Y30 and Y1 also show elevated TiO_2 and Fe^{3+}# values. Although Stowe (1994) suggested that TiO_2 was enriched into ferrit-chromite rims, the comparison between cores and rims in this study (section 9.4) shows that some cores are also enriched in TiO_2. Furthermore a close negative correlation (see section 9.12.8) between Fe^{3+}# and Cr# suggests that Fe^{3+}# values may also increase with magmatic processes. Therefore it is unlikely that alteration and magmatic effects could be separated using a plot of Fe^{2+}# versus Fe^{3+}#.

9.16.2. Magmatic Effects

It is not possible to distinguish between alteration and magmatic effects for the outliers in this dataset (see section 9.16.1) however, most spinels of the Main Yubdo Intrusion show a negative trend where Cr# decreases with Fe^{2+}#. This negative trend is unlike the trend which would be expected from alteration (see figure 9.4). During crystal fractionation it would be expected that Cr# would decrease and the most primitive spinels would contain the largest Cr^{3+} values. In the Main Yubdo Intrusion, the decrease in Cr# values is accompanied by a decrease in Fe^{2+}# values. A negative trend of Fe^{2+}# with Cr# is also found in the spinels hosted by the Daleti Ultramafic (see section 9.13.2). As the Cr# changes could be explained in terms of crystal fractionation it is possible that Fe^{2+}# may also increase.

9.16.3. Comparison with Alaskan-type intrusions and Ophiolites

Figures 9.8B to 9.8G can be used to compare the spinels from the Main Yubdo intrusion with those from Alaskan-type intrusions and ophiolite complexes contained in the Global Spinel Database (Barnes and Roeder, 2001) . The samples with the highest Cr# values plot within both the ophiolite and Alaskan-type intrusion fields. Most other spinels plot along a trend whereby Cr# decreases with Fe^{2+}#. As discussed in section 9.16.2, this trend may be the result of some form of magmatic process such as crystal fractionation whereby the spinels with the highest Cr# are the most primitive. Therefore these spinels may be evolved from Alaskan-type intrusions or ophiolite complexes.

The TiO_2 and Fe^{3+}# values are highest at the highest Fe^{2+}# values. These features are typical of Alaskan-type intrusions and the great Fe^{3+}# range is not common in ophiolite complexes (see figures 9.8E and 9.8G). However it is not possible to determine whether these features originate from alteration or magmatic processes. Therefore it is only possible to conclude that although the geochemistry is similar to Alaskan-type intrusions, it may also have formed through the alteration of ophiolite complex lithologies.

9.17. Conclusions

A comparison of the spinel geochemistry from the Main Yubdo Intrusion with the Barnes and Roeder (2001) Global Spinel Databse shows that the Fe^{2+}#, Fe^{3+}# and TiO_2 ranges are similar to Alaskan-type intrusions. The Cr# values are lower than typical Alaskan-type intrusions.

There are several outliers from the main trends within the three samples. It is not possible to determine whether these spinels are more altered or more evolved than their counterparts. It is likely that alteration has caused a degree of scatter in the dataset, however no distinct alteration trend can be observed.

The decrease in Cr# with Fe^{2+}# is the reverse of the trend expected for alteration and could be explained by a decrease in Cr# with crystal fractionation. This indicates that Fe^{2+}# increases with fractionation.

9.18. Summary of Spinel Geochemistry in the WES

The spinel geochemistry presented here attempts address the relative influence of alteration versus and processes such as crystal fractionation. Although several ratios and TiO_2 values are described in this study it is concluded that a plot of Fe^{2+}# versus Cr# is of most use. The following sections summarize the use of this plot to assess alteration, magmatism and tectonic setting.

	Tulu Dimtu	Kingy	Daleti, Ankori and Keley	Yubdo, Andu and Sodu
Dunite and olivine-clinopyroxenite	YES		YES	YES
Clinopyroxenite	YES	YES		

Table 9.12: A summary of the rocks which host acceptable spinel analyses (as set down in section 9.3) from this study. It shows that at Tulu Dimtu, spinel analyses are described from both dunite and clinopyroxenite whereas in the three other areas, there are only analyses from either dunite or clinopyroxenite hosted spinels. This means that each area can be compared with Tulu Dimtu but not each other.

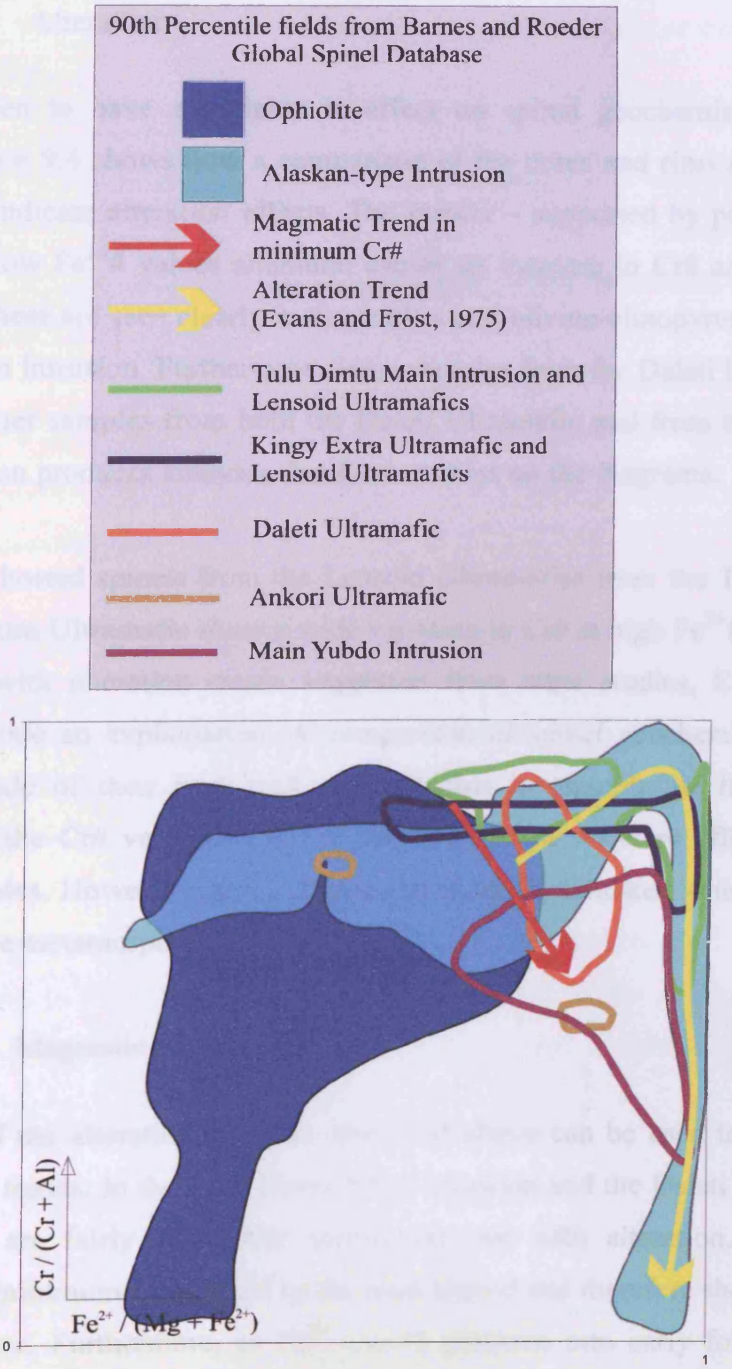

Figure 9.9: The Cr# and Fe^{2+}# values of the spinels of the five ultramafic complexes of the WES compared to Alaskan-type intrusions and ophiolites.

9.18.1. Alteration

Alteration is seen to have a variable in effect on spinel geochemistry through the intrusions. Section 9.4 shows how a comparison of the cores and rims of zoned spinels can be used to indicate alteration effects. The results – supported by published work – show that with low Fe^{2+}# values alteration causes an increase in Cr# and Fe^{2+}# values. Trends such as these are seen clearly in the dunites and olivine-clinopyroxenites from the Tulu Dimtu Main Intrusion. Furthermore, some samples from the Daleti Ultramafic show this effect. In other samples from both the Daleti Ultramafic and from the Main Yubdo Intrusion alteration produces analyses that form outliers on the diagrams.

Clinopyroxenite hosted spinels from the Lensoid Ultramafics from the Tulu Dimtu area and the Kingy Extra Ultramafic show a wide variation in Cr# at high Fe^{2+}#. Although this does not agree with alteration trends suggested from other studies, Evans and Frost (1975) may provide an explaination. A comparison of spinel geochemistries with the metamorphic grade of their host rock suggests that in amphibolite facies alteration actually reduces the Cr# value and hence alteration has a different effect at different metamorphic grades. However, such a hypothesis must be validated with a petrological study to determine metamorphic grade.

9.18.2. Magmatic Effects

An assessment of the alteration effect as described above can be used to help uncover hidden magmatic trends. In the Tulu Dimtu Main Intrusion and the Daleti Ultramafic the alteration trends are fairly clear. Cr# should increase with alteration, therefore the analysis with the minimum Cr# should be the least altered and therefore show the clearest magmatic signature. Furthermore, as Cr^{3+} should partition into early formed minerals during fractionation, the analysis with the least Cr# may also represent the most evolved. A comparison of the minimum Cr# in a sample with its location within the complex shows that – in both the Daleti Ultramafic and the Tulu Dimtu Main Intrusion – the most evolved sample lies close to least evolved. The intermediate samples lie elsewhere. This

lack of systematic variation indicates that each complex may have formed from more than one melt influx.

At both Tulu Dimtu and Daleti there is trend of increasing Fe^{2+}# with the minimum Cr#. This infers that the same process which causes a decrease in Cr# (possibly fractionation) also causes an increase in Fe^{2+}#. This "magmatic" trend is clearly different to the alteration trend (see figure 9.4 in section 9.7)

In the Kingy area and the Yubdo Main Intrusion the alteration effects are not well understood and it is therefore inappropriate to make interpretations about magmatic effects. Further sampling in these areas may help to uncover the effect of alteration.

9.18.3. Comparison with Alaskan-type intrusions and ophiolite complexes

A clear difference in the spinel geochemistry of Alaskan-type intrusions and ophiolite complexes can be observed in a plot of Fe^{2+}# versus Cr# (Barnes and Roeder, 2001). In the Tulu Dimtu Main Intrusion, the Kingy area and the Daleti Ultramafic most spinels plot within the Alaskan-type intrusion field. It is suggested here that the difference in spinel geochemistry between Alaskan-type intrusions and ophiolites can be accounted for by differing degrees of metamorphism (see section 9.6.3 for further discussion). As such, although the spinels from the two types of complexe are more similar to typical Alaskan-type intrusions, they could also be highly altered ophiolites.

The Ankori Ultramafic and Main Yubdo Intrusion are more complex. The two samples from the Ankori Ultramafic plot in very different places and further sampling is required here. Most spinels from the Main Yubdo Intrusion plot outside of both the Alaskan-type Intrusion and Ophiolite field, however elevated TiO_2 and Fe^{3+}# values at high Fe^{2+}# are similar to Alaskan-type intrusions.

In all the ultramafic complexes studied in here, the spinel geochemistry is typical of Alaskan-type intrusions.

10.Summary

10.1. Introduction

This thesis was designed to address two issues concerning the ultramafic bodies of the WES. Firstly, to assess the prospectivity of the ultramafic complexes in relation to the Pt and Pd distribution. Secondly, the thesis examined the tectonic origin of the ultramafic bodies with particular reference to the question of whether these complexes are Alaskan-type intrusions or ophiolites. The answer to this question is likely to affect the perceived prospectivity of the WES in the eyes of the scientific community.

Chapter 3 shows that the degree of alteration of the ultramafic lithotypes of the WES varies from 50% to 100%. Dunite samples are generally serpentinised and some clinopyroxenite samples are metamorphosed into the amphibolite facies. Given that some ultramafic samples are completely altered, section 3.3.6 establishes a classification of local rock-types based partly on the observation of relict mineral features. Also, in order to support other chapters in the thesis, chapter 3 provides an account of preliminary work on the mineralogy of spinels (see section 3.4), sulphides (see section 3.5) and platinum-group minerals (see section 3.6).

Using the rock-type classification set out in section 3.3.6 and to provide a framework for successive chapters, geological maps of the ultramafic bodies of the WES are produced. Chapter 4 details the analysis of terrain from aerial photography to establish the locations of the ultramafic bodies and in some cases the extent of these bodies (eg. the Tulu Dimtu Main Intrusion). In chapter 5 the terrain maps are validated using geological observations and the results are used to create geological maps which cover each of the four geographic areas.

In chapter 9, it was suggested that a graph of $Fe^{2+}\#$ $(Fe^{2+}/(Fe^{2+} + Mg^{2+}))$ versus Cr# (Cr / (Cr + Al)) is of most use in distinguishing Alaskan-type intrusions from ophiolites, furthermore the same graph is also of use in distinguishing magmatic processes from alteration. Additionally, it is proposed that within the spinel analyses

from each sample, the analysis with the lowest Cr# is the least altered and, therefore, it is the most likely to approach a magmatic composition.

In the following sections, the principle findings of chapters 6, 7, 8 and 9 are summarized. Each of the four geographic areas are considered in turn. Finally, a summary of the prospectivity and exploration recommendations is given (section 10.6)

10.2. Tulu Dimtu

In the Tulu Dimtu area, geological mapping (chapter 5) has identified several small ultramafic bodies, these are referred to here as the Lensoid Ultramafics. They are described along with a larger ultramafic body refered to as the Tulu Dimtu Main Intrusion (first mapped by DeWit and Aguma, 1977). As with the edges of the Tulu Dimtu Main Intrusion, the Lensoid Ultramafics are associated with talc- and chlorite-rich shear-zones.

The geochemistry of the soils in the Tulu Dimtu area shows the influence not only of the underlying lithotype but also hydromorphic dispersion within the thick laterite (see chapter 7). Although Cr and Al appear to have acted as immobile elements, Ni and Cu both show the effects of redistribution in solution with water (see figures 7.37 and 7.38). It is likely that Pt and Pd have been remobilized within the overburden in the WES, furthermore there is some evidence to suggest that Pt has increased in grade from the rocks into the soils.

In chapter 8, the differences in Ni, Cu and Cr values between fresher and altered samples has led to some ideas being developed for the concentration of the Pt and Pd within the Tulu Dimtu Main Intrusion. The distribution of Cr in the Tulu Dimtu Main Intrusion indicates that the most primitive rocks occur at the edge of the complex and that fractionation is directed inwards. In order to explain the locations of Ni, Cu and Cr in fresher rocks, the discussion includes an evaluation of the possible magmatic and alteration mechanisms. The Cu may have been driven away from Ni by sulphide fractionation and filter-pressing, however, hydrothermal remobilization may have a similar effect. In the fresher rocks, the Pt and Pd may be associated with Cu-

rich sulphide liquid, however subsequent remobilization is likely to have redistributed Pd and to a lesser degree Pt. This chapter has indicated that the ore forming processes involved in both magmatic and post-magmatic situations will act at the flanks of the intrusion. It is therefore recommended that any further exploration work is targeted in sheared contacts between the ultramafics and the basement.

To compliment the geochemistry, section 3.5.2 describes altered bornite (Cu_5FeS_4) and glaucodot ((Co,Fe)AsS) from the Tulu Dimtu Main Intrusion, both minerals indicate that sulphur has been remobilized and bornite indicates that chalcopyrite was present. No PGM were found in the Tulu Dimtu area.

Chapter 9 indicates that the Fe^{2+}# and Cr# values of the spinels from the Tulu Dimtu area are typical of those of Alaskan-type intrusions. The spinels hosted by dunite and olivine-clinopyroxenite have a different geochemistry to those hosted by clinopyroxenite. This could be explained by the fact that the clinopyroxenite hosted spinels (which typically form at the edge of Alaskan-type intrusions) have been metamorphosed to amphibolite facies, unlike those of the dunites and olivine-clinopyroxenites. The analysis of spinel minimum Cr# values for the dunite samples suggests that the Tulu Dimtu Main Intrusion may have formed through more than one melt influx. This partially supports the model proposed to explain the geochemical differences between fresher and altered rocks where a second melt influx is proposed.

10.3. Kingy

Chapter 5 shows that the largest ultramafic body in the Kingy area is the Kingy Ridge Ultramafic and another complex, the extra ultramafic, is located on the northwest flank of this. Five additional, smaller bodies are found in the area, these are associated with shear-zones and quartzite bodies and are referred to as the Lensoid Ultramafics.

Cr appears to have acted as an immobile element in the soils over the Kingy Ridge Ultramafic (chapter 7). The Ni values in the same soils also reflect the composition in the underlying rocks, suggesting that in this setting, it has acted as an immobile element. The most striking feature of the soil geochemistry in the Kingy

area is the high Pd values in soils over the basement in the northwest compared to those over the Kingy Ridge Ultramafic.

The low number of fresher ultramafic samples from the Kingy area makes an assessment of possible magmatic processes difficult (see chapter 8). However, the systematic variation in Cr values in altered rocks and soil samples from the Kingy Ridge Ultramafic indicates that the more primitive rocks may occur at the northwestern end of the complex. The distribution of Ni in the altered rocks of the Kingy Ridge Ultramafic mirrors that of Cr, however the Cu distribution is more irregular which infers the remobilization of Cu to a greater degree than Ni. The Pt and Pd values in fresher rocks are almost below detection, however Pd dominates Pt in the altered rock which suggests that the action of hydrothermal fluids was extensive (see chapter 8). Such severe alteration may obscure magmatic features, however the Pd values found in shear zone conduits are likely to have originated in a primary source in the vicinity. An investigation of the geometry and geochemistry of the shear zones may help to uncover this source.

The spinel geochemistry of the Kingy area is described in chapter 9 and it is found that the Fe^{2+}# and Cr# values are generally typical of Alaskan-type intrusions as opposed to ophiolites. However, spinels were found in only three samples and as such it is not possible to separate magmatic from alteration effects.

10.4. Daleti, Ankori, Tulu Kapi and Keley

There are two large ultramafic complexes found in this area along with five smaller bodies described here as the Lensoid Ultramafics (see section 5.3.3). The larger complexes, the Daleti Ultramafic and the Ankori Ultramafic are aligned in NE-SW and N-S directions respectively. The Lensoid Ultramafics are associated with extensive shear-zones and large quartzite bodies (see Chapter 5).

Significant Ni and Cr values are only found above the ultramafic complexes in area areas around Daleti, Ankori, Tulu Kapi and Keley. Furthermore, Pt and Pd is only found in the soils above the Ankori complex and above a set of shear-zones in the southwest of the area.

Fresher rocks (as defined in section 8.2.2) are only found in the Daleti Ultramafic and in combination with the altered rocks are used to develop an understanding of the potential ore-forming processes which may have occurred (see section 8.17). It is possible that two melt influxes may have occurred and it is likely that some sulphides were present, although they are not associated with significant Pt and Pd values. Any magmatic processes have been overprinted by the effects of hydrothermal processes. In support of this, the analysis of talc-schists and altered ultramafic samples from the whole area shows that Ni and Cu are concentrated into different samples. Anomalous Pd values (33ppb) found in a quartzite and a dunite near to an extensive shear-zone are consistent with the view that Pd is more mobile than Pt. The high Ni values alongside very low Pt and Pd values indicates that the magma from which the Daleti Ultrmafic cyrstallised was barren. Hence further exploration in the Daleti Ultramafic may not be worthwhile.

Chapter 9 shows that the spinels of the Daleti Ultramafic have a geochemistry which is unlike ophiolite complexes and many of these analyses have Fe^{2+}# and Cr# compositions which are similar to Alaskan-type intrusions. Comparison with published work and core-rim analyses (see section 9.4) shows that alteration and magmatic effects can be separated in the Daleti Ultramafic. The two most altered samples (based on spinel geochemisty alone) occur close to a shear-zone which supports the proposal that alteration fluids use these features as conduits. The minimum Cr# values for each sample indicate that the Daleti Ultramafic may have formed through more than one melt influx. This is similar to the model proposed in chapter 8 which requires two melt influxes to explain the Ni, Cu, Cr, Pt and Pd values in the complex.

10.5. Yubdo, Andu and Sodu

The largest ultramafic body of the WES is the Main Yubdo Intrusion which covers 30km^2. There are five smaller complexes, referred to here as the Lensoid Ultramafics. Shear-zones are located in both the basement and within the Main Yubdo Intrusion.

The model proposed to explain the magnetic survey described in chapter 6 uses a variation in the frequency of siliceous veining. It is suggested that the most intense veining occurs in two elongate zones through the north and south of the Main Yubdo Intrusion. The northernmost zone appears to be the continuation of a shear-zone mapped by Kazmin and Demessie (1971).

In the overburden of the Yubdo area, high Ni and Cr values are only found in the laterites above the Main Yubdo Intrusion whereas high Cu values occur above the basement. A significant difference between the locations of the highest Pt and Pd values is observed.

Chapter 8 details efforts to describe possible ore-forming processes which may have occurred within the Main Yubdo Intrusion. A lack of fresher samples hampered attempts to uncover magmatic processes. However, both fresher and altered rocks show that the highest Cr values occur at the edge of the complex, suggesting that the most primitive rocks formed at the flanks. Observations of Ni and Cu in the altered rocks of the Main Yubdo Intrusion suggest that they may have been affected by different alteration episodes, or that only one element has been remobilized. Pd has been detected in the talc-schists north of the Main Yubdo Intrusion. It is suggested here that any future attempts to uncover economic mineralisation at Yubdo be focused either at the flanks of the intrusion or around the shear-zones which pass through the centre.

Three PGM from the Main Yubdo Intrusion have been described in chapter 3. These include a Pt-Fe alloy, an Os-Ir alloy and an Ir-Os alloy. They were all discovered in samples from the northwestern flank of the complex.

In Chapter 9, observations of the spinel geochemistry show that the Fe^{2+}#, Fe^{3+}# and TiO_2 values are similar to those of Alaskan-type intrusions although the Cr# values are lower than would be expected. No distinct alteration trend can be distinguished in the Main Yubdo Intrusion although a decrease in Cr# with an increase in Fe^{2+}# is the reverse of the trend expected for alteration and therefore could be attributed to magmatic processes such as fractionation.

10.6. Exploration Summary

This thesis covers the ultramafic rocks from 4 adjacent areas of the Western Ethiopian Shield (WES). Five large complexes are described in addition to numerous smaller complexes referred to here as the Lensoid Ultramafics. The investigation is restricted to the use of Ni, Cu, Cr, Al, Pt and Pd from an aqua regia digestion followed by an ICP-OES analysis and to major elements from spinel geochemical analysis. To compliment the geochemical chapters, some preliminary observations have been made of sulphides and platinum-group minerals (PGM). The conclusions from the four geographic areas are as follows.

The principle findings from the Tulu Dimtu area concern the Tulu Dimtu Main Intrusion. A comparison of the rock geochemistry of fresher and more altered samples (as defined in section 6.2.2) has allowed the assessment of some potential ore-forming processses. The effects of alteration and magmatism on spinel geochemistry have been distinguished using a graph of Fe^{2+}# versus Cr#. Both the rock and the spinel geochemistry of the Lensoid Ultramafics is consistent with the idea these bodies may be "sheared-off" slivers from larger complexes such as the Tulu Dimtu Main Intrusion. Comparison with published work suggests that the spinel geochemistry of the Tulu Dimtu Main Intrusion and Lensoid Ultramafics is typical of Alaskan-type intrusions.

The lack of fresher samples from the Kingy area has made the understanding of magmatic processes in this area difficult. However, a systematic variation in Cr values in altered rocks and soils of the Kingy Ridge Ultramafic has indicated that the most primitive rocks occur at the northeastern end of the complex. The spinel geochemistry of the ultramafics from the Kingy area is typical of published analyses from Alaskan-type intrusions.

The high Ni values but extremely low Pt and Pd analyses suggest that, if the complex has undergone sulphide segregation then the original magma is likely to have been barren of the precious metals. Hence is it considered unlikely that further exploration in the area will uncover higher grades. The high Cr and significant Pt and Pd values found in both soils and rocks from the south west of the area are worthy of

further investigation. Investigation of these shear-zones may reveal a further – previously unknown – primary deposit. Furthermore, it is suggested here that the spinel geochemistry of the Daleti and Ankori complexes are similar to that of Alaskan-type intrusions.

The magmatic processes which have occurred in the Main Yubdo Intrusion remain uncertain and the geochemistry is strongly influenced by the action of hydrothermal fluids. Attempts to compare the fresher and more altered rocks have been largely unsuccessful, however it is suggested that the most primitive rocks are at the edge of the complex. Therefore the best locations for future exploration would be either the flanks of the intrusion or close to the shear-zones within the complex. Spinel analyses show a similarity to the published spinel geochemistry from Alaskan-type intrusions. A magnetic survey of the complex has been interpreted on the basis of variations in the frequency of siliceous veining.

10.7. Comparison with published work on the tectonic setting of the complexes

This thesis finds that the spinel geochemistry of the ultramafic rocks of the WES are unlike those of ophiolites and are similar to those of Alaskan-type intrusions. This conclusion supports the suggestion made by Mogessie et al. (2000). Furthermore, chapter 2 reviews the key differences between the two types of complex and shows that Alaskan-type intrusions generally have negative Ru and positive Pt anomalies without high Pd values on chondrite normalized diagrams - a feature which is rarely seen in ophiolites (Prichard and Lord, 1993). The PGE analyses from the Tulu Dimtu published by Sighinolfi et al. (1993) show a low Ru value and a positive Pt anomaly, both of which further support the Alaskan-type intrusion hypothesis.

The proponents of the ophiolite hypothesis (Berhe and Rothery, 1986; Tadesse and Allen, 2005; Warden et al., 1982) do not address the possibility that these complexes may be Alaskan-type intrusions. Indeed, the comparison described in section 2.4 shows that much of the data published by these authors may also fit the Alaskan-type intrusion hypothesis. For example, Berhe and Rothery (1986) classified the rocks as ophiolitic because they displayed the Penrose (1972) ophiolitic

assemblage. It is common to find features such as basalt flows, metasediments, gabbro bodies juxtaposed together in a mobile belt the size of the WES.

Warden et al. (1982) commented that although the petrological criteria and major, minor and trace elements showed an ophiolitic signature the evidence from REE was inconclusive. The ultramafics and "lower intrusive members" are enriched in LREE and depleted in HREE - this could not be explained by an ophiolitic origin or by subsequent alteration (Warden et al., 1982). Comparison with figure 2.4 shows that such enrichment in LREE and depletion in HREE is common in Alaskan-type intrusions.

ABDELSALAM, M. G. & STERN, R. J. (1996) Sutures and shear zones in the Arabian Nubian Shield. Journal of African Earth Sciences, 23, 289-310.

AHMED, A. H. & ARAI, S. (2002) Unexpectedly high-PGE chromitite from the deeper mantle sectionof the northern Oman ophiolite and its tectonic implications. Contributions to Mineralogy and Petrology, 143, 263-178.

AKELLA, J., WILLIAMS, R. J. & MULLINS, O. (1976) Solubility of Cr, Ti, and Al in co-existing olivine, spinel, and liquid at 1 atm. IN MERRILL, R. B., MORRIS, R.V., RHODES, J.M. AND USSELMAN, T.M. (Ed.) Proceedings of the 7th lunar science conference: petrogenetic studies of mare and highland rocks. New York, Pergamon Press.

ALEMU, T. & ABEBE, T. (1999) Geologic Evolution of the Tulu Dimtu Belt. Addis Ababa, Ethiopian Institute of Geological Surveys.

ALLEN, A. & TADESSE, G. (2003) Geological setting and Tectonic subdivision of the Neoproterozoic orogenic belt of Tulu Dimtu, western Ethiopia. Journal of African Earth Sciences, 36, 329-343.

ANDERSEN, A. T. (1968) Spinel stiochiometry calculation. Journal of Geology, 76, 528-547.

ANDERSEN, J. C. O., RASMUSSEN, H., NIELSEN, T. F. D. & RONSBO, J. G. (1998) The triple group and the Platinova gold and palladium reefs in the Skaergaard intrusion: Stratigraphic and Petrographic relations. Economic Geology, 93, 488-509.

ANDREW, A. S., HENSEN, B. J., DUNLOP, A. C. & AGNEW, P. D. (1995) Oxygen and Hydrogen Isotope Evidence for the Origin of Platinum-Group element mineralisation in Alaskan-type intrusions at Fifield, Australia. Economic Geology, 90, 1831-1840.

AUGE, T. & MAURIZOT, P. (1995) Stratiform and alluvial platinum mineralisation in the New Caledonia ophiolite complex. Canadian Mineralogist, 33, 1023-1045.

AUGUSTITHIS, S. S. (1965) Mineralogical and geochemical studies of the platiniferous dunite-birbirite-pyroxenite complex of Yubdo/Birbir, Western Ethiopia. Chemie der Erde, 24, 159196.

AYALEW, T., BELL, K., MOORE, J. M. & PARRISH, R. R. (1990) U-Pb and Rb-Sr ggeochronology of the Western Ethiopian Shield. Geological Society of America Bulletin, 102, 1309-1316.

BACON, C. R. & DRUITT, T. H. (1988) Compositional Evolution of the Zoned Calcalkaline Magma Chamber of Mount-Mazama, Crater Lake, Oregon. Contributions to Mineralogy and Petrology, 98, 224-256.

BAKER, T., ACHTERBERG, E. V., RYAN, C. G. & LANG, J. R. (2004) Composition and evolution of ore fluids in a magmatic-hydrothermal skarn deposit. Geology, 32, 117-120.

BARNES, S. J. & ROEDER, P. L. (2001) The range of spinel compositions in terrestrial mafic and ultramafic rocks. Journal of Petrology, 42, 2279-2302.

BARNES, S.-J., MAKOVICKY, E., MAKOVIKY, M., ROSE-HANSEN, J. & KARUP-MOLLER, S. (1997) Patition Coefficients for Ni, Cu, Pd, Pt, Rh and Ir between monosulfhide solid solution and sulphide liquid and the formation of compositionally zoned Ni-Cu sulfide bodies by fractional crystalisation of sulfide liquid. Canadian Journal of Earth Science, 34, 366-374.

BEATTIE, P. (1993) The effect of partial melting of spinel peridotite on uranium series disequilibria: constraints from partitioning studies. Earth and Planetary Science Letters, 177, 379-391.

BECKER, R. & AGIORTIS, G. (1978) Iridium osmium and palladium distribution in rocks of the Troodos complex, Cyprus. Chem. Erde., 37, 302-306.

BELETE, K. H., MOGESSIE, A. & HOINKES, G. (2000) Platinum and gold deposit of Yubdo mafic ultramafics, western Ethiopia: a late stage hydrothermal mineralisation. IN CLUER, J. K., PRICE, J. G., STRHSACKER, E. M., HARDYMAN, R. F. & MORRIS, C. L. (Eds.) Geology and Ore Deposits 2000: The Great Basin and Beyond: Geological Society of Nevada Symposium Proceedings.

BELETE, K. H., MOGESSIE, A. & BOWLES, J. F. W. (2002) Platinum-Group Minerals in the Alaskan Type Mafic-Ultramafic Intrusions of the Yubdo Area, Western Ethiopia. IN BOUDREAU, A. (Ed.) 9th International Platinum Symposium. Billings, Montana, USA.

BERHE, S. M. (1990) Ophiolites in Notheast and East Africa: implications for protereozoic crustal growth. Journal of the Geological Society of London, 147, 41-57.

BERHE, S. M. & ROTHERY, D. A. (1986) Ineractive processing of satillite images for structural and lithological mapping in northeast Africa. Geological Magazine, 123, 393-403.

BOUGAULT, H. & HEKINIAN, R. (1974) Rift Valley in Atlantic Ocean near 36 Degrees 50' N - Petrology and Geochemistry of Basaltic Rocks. Earth and Planetary Science Letters, 24, 249-261.

BOUGAULT, H. & HEKINIAN, R. (1974) Rift valley in the Atlantic Ocean near 36 degrees 50'N; petrology and geochemistry of basalt rocks. Earth and Planetary Science Letters, 24, 249-261.

BOWLES, J. F. W. (1977) Estimation of Probable Errors of Method of Tracing Cooling History of Complex Magnetite-Ilmenite Grains and a Discussion of Results Produced by Using Different Methods of Treatment of Minor Elements Contained in These Minerals When Using Buddington and Lindsley (1964) Geothermometer. Mineralogical Magazine, 41, M16-M18.

BOWLES, J. F. W. (1986) The development of platinum group minerals in laterites. Economic Geology, 81, 1278-1285.

BOWLES, J. F. W. (1995) The development of platinum group minerals (PGM) in laterites: mineral morphology. Chronique de la Recherche Miniere, 520, 55-63.

BOWLES, J. F. W., GIZE, A. P. & COWDEN, A. (1994) THe mobility of the platinum-group elements in the soils of the Freetown Penninsula, Sierra Leone. Canadian Mineralogist, 32, 957-967.

BOWLES, J. F. W., GIZE, A. P., VAUGHAN, D. J. & NORRIS, S. J. (1994) Development of Platinum-Group Minerals in Laterites - Initial Comparison of Organic and Inorganic Controls. Transactions of the Institution of Mining and Metallurgy Section B-Applied Earth Science, 103, B53-B56.

BRAATHEN, A., GRENNE, T., SELASSIE, M. G. & WORKU, T. (2001) Juxtaposition of Neoproterozoic units along the Baruda-Tulu Dimtu shear-belt of in the East Affrican Orogen of Western Ethiopia. Precambrian Research, 107, 215-234.

BROWNING, P. & SMEWING, J. D. (1981) Processes in Magma Chambers beneath Spreading Axes - Evidence from Magmatic Associations in the Oman Ophiolite. Journal of the Geological Society, 138, 279-280.

BUDDINGTON, A. F. & LINDSLEY, D. H. (1964) Fe valency in spinels. Journal of Petrolology, 5, 310-357.

CANALS, A., CARDELLACH, E., RYE, D. M. & AYORA, C. (1992) Origin of the Atrevida Vein (Catalonian Coastal Ranges, Spain) - Mineralogic, Fluid Inclusion, and Stable Isotope Study. 87, 142-153.

CAWTHORN, R. G. (2005) Contrasting sulphide contents of the Bushveld and Sudbury igneous complexes. Mineralium Deposita, 40, 1-12.

CHAO, T. T. (1984) Use of Partial Dissolution Techniques in Geochemical-Exploration. Journal of Geochemical Exploration, 20, 101-135.

CHILDS, I. (2001) Styles of PGE mineralistion in the Yubdo Ultramafic complex, Western Ethiopia. School of Earth, Ocean and Planetary Science. Cardiff, Cardiff University.

CHURCH, S. E., MOSIER, E. L. & MOTOOKA, J. M. (1987) Mineralogical Basis for the Interpretation of Multielement (ICP-AES), Oxalic-Acid, and Aqua Regia Partial Digestions of Stream Sediments for Reconnaissance Exploration Geochemistry. Journal of Geochemical Exploration, 29, 207-233.

COLE, J. W., GAMBLE, J. A., BURTON, D. M., CARROLL, L. D. & SHELLEY, D. (2001) Mixing And mingling In the evolution of andesite-dacite magmas: evidence from co-magmatic plutonic enclaves, taupo volcanic zone, new zealand. Lithos, 59, 25-46.

DOSTAL, J., DUPUY, C., CARRON, J. P., DEKERNEIZON, M. L. & MAURY, R. C. (1983) Partition-Coefficients of Trace-Elements - Application to Volcanic-Rocks of St-Vincent, West-Indies. Geochimica et Cosmochimica Acta, 47, 525-533.

DRAKE, M. J. & HOLLOWAY, J. R. (1981) Partitioning of Ni between Olivine and Silicate Melt - the Henrys Law Problem Reexamined. Geochimica Et Cosmochimica Acta, 45, 431-437.

DUKE, J. M. (1976) Distribution of the period four transition elements among olivine, calcic clinopyroxene and mafic silicate liquid; experimental results. Journal of Petrology, 17, 499-521.

ESPERANÇA, S., CARLSON, R. W., SHIREY, S. B. & SMITH, D. (1997) Dating crust-mantle separation: Re-OS isotopic study of mafic xenoliths from central Arizona. Geology, 25, 651-654.

EVANS, B. W. & FROST, B. R. (1975) Chrome-Spinel in Progressive Metamorphism - Preliminary Analysis. Geochimica Et Cosmochimica Acta, 39, 959-972.

EWART, A., BRYAN, W. B. & GILL, J. B. (1973) Mineralogy and Geochemistry of Younger Volcanic Islands of Tonga, Sw Pacific. Journal of Petrology, 14, 429-&.

EWART, A. & GRIFFIN, W. L. (1994) Application of Proton-Microprobe Data to Trace-Element Partitioning in Volcanic-Rocks. Chemical Geology, 117, 251-284.

FERSHTATER, G. B., MONTERO, P., BORODINA, N. S., PUSHKAREV, E. V., SMIRNOV, V. N. & BEA, F. (1997) Uralian Magmatism: An overview. Tectonopysics, 276, 87-102.

FINDLAY, D. C. (1969) Origin of th eTulameen ultramafic-gabbro complex, southern British Columbia. Canadian Journal of Earth Sciences, 6, 399-425.

FLEET, M. E., CHRYSSOULIS, S. L., STONE, W. E. & WEISENER, C. G. (1993) Partitioning of platinum-group elements and Au in the Fe-Ni-Cu-S system: Expleriments on the fractional crystallization of sulphide melt. Contributions to Mineralolgy and Petrolology, 115, 36-44.

FLEET, M. E. & PAN, Y. M. (1994) Fractional Crystallization of Anhydrous Sulfide Liquid in the System Fe-Ni-Cu-S, with Application to Magmatic Sulfide Deposits. Geochimica Et Cosmochimica Acta, 58, 3369-3377.

FODOR, R. V. (2001) The Role Of Tonalite And Diorite In Mauna Kea Volcano, Hawaii, Magmatism: petrology of summit-region leucocratic xenoliths. Journal of Petrolrology, 42, 1685-1704.

FOMINYKH, V. G. & KHOSTOVA, V. P. (1970) Platinum content of the Ural dunite. Dokaldy Akademii Nauk SSSR, 200, 443-445.

GAETANI, G. A. & GROVE, T. L. (1997) Partitioning of moderately siderophile elements among olivine, silicate melt, and sulfide melt: Constraints on core formation in the Earth and Mars. 61, 1829-1846.

GAMMONS, C. H., BLOOM, M. S. & YU, Y. (1992) Experimental investigation of the hydrothermal geochemistry of platinum and palladium: I. Solubility of platinum and palladium sulphide minerals in NaCl/H2S04 solutions at 300oC. Geochemica and Cosmochemica Acta, 56, 3881-3894.

GARUTI, G., FERSHTATER, G., BEA, F., MONTERO, P., PUSHKAREV, E. V. & ZACCARINI, F. (1997) Platinum-group elements as petrological indicators in mafic-ultramafic complexes of the central and southern Urals: preliminary results. Tectonophysics, 276, 181-194.

GARUTI, G., PUSHKAREV, E. V., ZACCARINI, F., CABELLA, R. & ANIKINA, E. (2003) Chromite composition and platinum-group mineral assemblage in the Uktus Uralian-Alaskan-type complex (Central Urals, Russia). Mieralium Deposita, 38, 312-326.

GASS, I. G. (1990) Ophiolites and Oceanic Lithosphere. IN MALPAS, J., MOORES, E. M., PANAYIOTOU, A. & XENOPHONTOS, C. (Eds.) Troodos 1987, Ophiolites Oceanic Crustal Analogues. Nicosia, Geological Survey Department, Republic of Cyprus.

GIBSON, R. A., THOMPSON, R. & DICKIN, A. P. (2000) Ferropicrites: Geochemical Evidence For Fe-Rich Streaks In Upwelling Mantle Plumes. Earth and Planetary Science Letters, 174, 355-374.

GIGGENBACH, W. F. (1984) Mass-Transfer in Hydrothermal Alteration Systems - a Conceptual-Approach. Geochimica Et Cosmochimica Acta, 48, 2693-2711.

GODARD, M., JOUSSELIN, D. & BODINIER, J.-L. (2000) Relationships between geochemistry and structure beneath a paleo-spreading centre: a study of the mantle section in the Oman ophiolite. 180, 133-148.

GRÉGOIRE, M., MOINE, B. N., O'REILLY, S. Y., COTTIN, J.-Y. & GIRET, A. (2000) Trace element residence and partitioning in mantle xenoliths metasomatized by highly alkaline, silicate- and carbonate-rich melts (kerguelen islands, indian ocean). Journal of Petrology, 41, 477-509.

HANSEN, N. & GRÖNVOLD, K. (2000) Plagioclase ultraphyric Basalts In Iceland: The Mush Of The Rift. Journal of Volcanology and Geothermal Research, 98, 1-32.

HARPER, G. D. (1984) The Josephine ophiolite, northwestern California. Geological Society of America Bulletin, 95, 1009-1026.

HART, S. R. & DUNN, T. (1993) Experimental cpx/melt partitioning of 24 trace elements. Contributions to Mineralogy and Petrology, 113, 1-8.

HATTORI, K. & CABRI, L. J. (1992) Origin of Platinum-Group-Mineral nuggets inferred from an Osmium-Isotope Study. Canadian Mineralogist, 30, 289-301.

HOWELL, F. H. (1969) Monthly Report, April 1969. Tucson, Arizona, Duval Corporation.

IRVINE, T. N. (1977) Origin of chromite layers in the muskox inrtusion and other stratiform intrusions; a new interpretation. Geology, 5, 273-277.

JAN, M. Q., WINDLEY, B. F. & KHAN, A. (1985) The Waziristan Ophiolite, Pakistan - General Geology and Chemistry of Chromite and Associated Phases. Economic Geology, 80, 294-306.

JELENC, D. A. (1966) Mineral Occurances of Ethoipia, Addis Ababa, Ministry of Mines.

JOHAN, Z. (2002) Alaskan-type Complexes and their Platinum-Group Element Mineralisation. IN CABRI, L. J. (Ed.) The Geology, Geochemistry, Mineralogy and Mineral Beneficiation of Platinum-Group Elements, Special Volume 54. Montreal, Quebec, Canadian Institute of Mining, Metallurgy and Petroleum.

JOHNSON, T. E., AYALEW, T., MOGESSIE, A., KRUGER, F. J. & POUJOL, M. (2004) Constraints on the geotectonic evolution of the Western Ethiopian Shield. Precambrian Research, 133, 305-327.

KAZMIN, V. & DEMESSIE, S. (1971) Geological map of the Yubdo ultrabasic complex. IN UNITED & NATIONS (Eds.) Report on the mineral survey in two selected areas of Ethiopia. Addis Ababa, UNDP.

KEAYS, R. R. (1987) Principles of mobilisation (dissolution) of metals in mafic and ultramafic rocks - the role of immiscible magmatic sulphides in the generation of hydrothermal gold and volcanogenic massive sulphide deposits. Ore Geology Reviews, 2, 47-63.

KENNEDY, A. K., LOFGREN, G. E. & WASSERBURG, G. J. (1993) An experimentalstudy of trace element partitioning between olivine, orthopyroxene and melt in chondrules: equilibrium values andf kinetic effects. Earth and Planetary Science Letters, 115, 177-195.

KESLER, S. E. (2005) Ore-forming fluids. Elements, 1, 13-18.

KINZLER, R. J., GROVE, T. L. & RECCA, S. I. (1990) An Experimental-Study on the Effect of Temperature and Melt Composition on the Partitioning of Nickel between Olivine and Silicate Melt. 54, 1255-1265.

KLEIN, C. & HURLBUT, C. S. (1993) Manual of Mineralogy, John Wiley and Sons Inc.

KLOECK, W. & PALME, H. (1988) Partitioning of siderophile and chalcophile elements between sulfide, olivine, and glass in a naturally reduced basalt from Disko Island, Greenland. IN RYDER, G. (Ed.) Proceedings of the Lunar and Planetary Science Conference. New York, Pergamon.

LECUYER, C., GRUAU, G., ANHEUSSER, C. & FOURCADE, S. (1994) The origin of fluids and the effects of metamorphism on the primary chemical compositions or Baberton komatiites; new evidence from geochemical (REE) and isotopic (ND, O, H) data;. Geochemica and Cosmochemica Acta, 58, 969-984.

LEEMAN, W. P. & SCHEIDEGGER, K. F. (1977) Olivine/liquid distribution coefficients and a test for crystal-liquid equilibrium. Earth and Planetary Science Letters, 35, 247-257.

LEONARD, G. S., COLE, J. W., NAIRN, I. A. & SELF, S. (2002) Basalt Triggering Of The C. Ad 1305 Kaharoa Rhyolite Eruption, Tarawera Volcanic Complex, New Zealand. J. Volcanol. Geotherm. Res, 115, 461-486.

LILLESAND, T. M. & KIEFER, R. W. (2000) Remote Sensing and image interpretation, New York, John Whiley & Sons, Inc.

LIPPARD, S. J., SHELTON, A. W. & GASS, I. G. (1986) The Ophiolite of Northern Oman, Oxford London Edinburgh Boston PaloAlto Melbourne, The Geological Society by Blackwell Scientific Publications.

LUHR, J. F. & CARMICHAEL, I. S. E. (1980) The Colima volcanic complex, Mexico. I: post-caldera andesites from Volcan Colima. Contributions to Mineralogy and Petrology, 71, 343-372.

MACAMBRIA, E. M. B. & FILHO, C. F. F. (2005) Exploration and origin of stratiform PGE mineralisation in the Serra Da Onça layered complex, Carajás mineral province. IN TÖRMÄNEN, T. O. & ALAPIETI, T. T. (Eds.) The 10th international platinum symposium. Oulu, Finland.

MALITCH, K. N. (1991) About the genetis affilliation of platinum-bearing circular and zoned ultramafic complexes ofthe Siberian platform. Doklady Akademii Nauk SSSR, 318, 1452-1457.

MALITCH, K. N. (1996) Assesment of the platinum potential of clinopyroxene-dunite massifs. Dokaldy Akademii Nauk, 347, 653-657.

MARSHALL, B. & GILLIGAN, L. B. (1987) An introduction to remobilisation: information from ore-body geometry and experimental considerations. Ore Geology Reviews, 2, 87-131.

MATTIOLI, M., SERRI, G., SALVIOLI-MARIANI, E., RENZULLI, A., HOLM, P. M., SANTI, P. & VENTURELLI, G. (2003) Sub-Volcanic Infiltration And Syn-Eruptive Quenching Of Liquids In Cumulate Wall-Rocks: The Example Of The Gabbroic Nodules Of Stromboli (Aeolian Islands, Italy). Mineralogy and Petrology, 78, 201-230.

MCKAY, G. A. & WEILL, D. F. (1976) Petrogenesis of KREEP. IN MERRILL, R. B., MORRIS, R. V., RHODES, J. M. & USSELMAN, T. M. (Eds.) Proceedings of the 7th lunar science conference: petrogenetic studies of mare and highland rocks. New York, Pergamon Press.

MICHAEL, P. J. (1988) Partition coefficients for rare Earth elements in mafic minerals of high silica rhyolites: The importance of accessory mineral inclusions. Geochimica et Cosmochimica Acta, 52, 275-282.

MOGESSIE, A., BELETE, K., HOINKES, G. & ETTINGER, K. (1999) Platinum mineralisation in the Yubdo ultramafic rocks, western Ethiopia. IN AL., S. E. (Ed.) Mineral Deposits: Processes to Processing. Rotterdam, Balkema.

MOGESSIE, A. & BELETE, K. H. (2000) Platinum and gold mineralisation in the Yubdo mafic-ultramafic rocks, Western Ethiopia: Historical perspective and some new results. Chronique de la Recherche Miniere, 53-62.

MOGESSIE, A., BELETE, K. H. & HOINKES, G. (2000) Yubdo-Tulu Dimtu mafic-ultramfic belt, Alaskan-type intrusions in western Ethiopia: its implication to the Arabian-Nubian Shield and tectonics of the Mozambique Belt. Abstracts: 18th Colloquium of African Geology. Graz, Elsevier Ltd.

MOGESSIE, A. & HOINKES, G. (1998) The Petrology and mineralisation of the Yubdo - Daleti - Tulu Dimtu Mafic-Ultramafic rocks and the surrounding basement in Western Ethiopia. Graz, Univerisity of Graz.

MOHR, P. (1983) Ethipian flood basalt province. Nature, 303, 557-583.

MOINE, B. N., GRÉGOIRE, M., O'REILLY, S. Y., SHEPPARD, S. M. F. & COTTIN, J.-Y. (2001) High Field Strength Element Fractionation In The Upper Mantle: Evidence From Amphibole-Rich Composite Mantle Xenoliths From The Kerguelen Islands (Indian Ocean). Journal of Petrology, 42, 2145-2167.

MOLLY, E. W. (1959) Platinum deposits of Ethiopia. Economic Geology, 54, 467-477.

MOON, C. J. (1995) Exploration Geolchemistry. IN EVANS, A. M. (Ed.) Introduction to Mineral Exploration. Oxford, Blackwell Science Ltd.

MORISHITA, T. & ARAI, S. (2001) Petrogenesis of corundum-bearing mafic rock in the horoman peridotite complex, Japan. J. Petrol., 42, 1279-1299.

MÜLLER, D., FRANZ, L., HERZIG, P. M. & HUNT, S. (2001) potassic igneous rocks from the vicinity of epithermal gold mineralization, lihir island, papua new guinea. Lithos, 57, 163-186.

MURRAY, C. G. (1972) Zoned Ultramafic complexes of the Alaskan type: Feeder pipes of andesitic volcanoes. The Geological Society of America Memoir, 132, 313-335.

MYSEN, B. O. (1978) Experimental-Determination of Nickel Partition-Coefficients between Liquid, Pargasite, and Garnet Peridotite Minerals and Concentration Limits of Behavior According to Henrys Law at High-Pressure and Temperature. American Journal of Science, 278, 217-243.

MYSEN, B. O. (1979) Trace-Element Partitioning between Garnet Peridotite Minerals and Water-Rich Vapor - Experimental-Data from 5-Kbar to 30-Kbar. American Mineralogist, 64, 274-287.

MYSEN, B. O. & VIRGO, D. (1980) Solubility Mechanisms of Water in Basalt Melt at High-Pressures and Temperatures - Nacaalsi2o7-H2o as a Model. American Mineralogist, 65, 1176-1184.

NABELEK, P. I. (1980) Nickel Partitioning between olivine and liquid in natural basalts: Henrys Law behaviour. Earth and Planetary Science Letters, 48, 293-302.

NALDRETT, A. J. (1999) World-class Ni-Cu-PGE deposits: key factors in their genesis. Mineralium Deposita, 34, 227-240.

NALDRETT, A. J., BRUGMANN, G. E. & WILSON, A. H. (1990) Models for the concentration of PGE in layered intrusions. Canadian Mineralogist, 28, 389-408.

NALDRETT, A. J., COATS, C. J. A. & JOHANNSSEN, P. (1992) Platinum, palladium, gold and copper-rich stringers at the Strathcona mine, Sudbury: their enrichment by fractionation of a sulphide liquid. Economic Geology, 87, 1584-1598.

NALDRETT, A. J. & DUKE, J. M. (1980) Platinum Metals in Magmatic Sulfide Ores. Science, 208, 1417-1424.

NALDRETT, A. J., HOFFMAN, E. L., GREEN, A. H., CHOU, L., NALDRETT, S. R. & ALCOCK, R. A. (1979) Composition of Ni-sulphide ores - constraints on ore genesis. Canadian Mineralogist, 17, 403.

NALDRETT, A. J. & VON-GRUNEWALDT, G. (1989) Association of platinum-group elements with chromitite in layered intrusions and ophiolite complexes. Economic Geology, 84, 180-187.

NEUMANN, E. R., WULFF-PEDERSEN, E., PEARSON, N. J. & SPENCER, E. A. (2002) Mantle xenoliths from tenerife (canary islands): evidence for reactions between mantle peridotites and silicic carbonatite melts including ca metasomatism. Journal of Petrology, 43, 825-857.

NEUMANN, E.-R., SOERENSEN, V. B., SIMONSEN, S. L. & JOHNSEN, K. (2000) Gabbroic xenoliths from la palma, tenerife and lanzarote, canary islands: evidence for reactions between mafic alkaline canary island melts and old oceanic crust. Journal of Volcanology and Geothermal Research, 103, 313-342.

NICKSON, R. T., MCARTHUR, J. M., RAVENSCROFT, P., BURGESS, W. G. & AHMED, K. M. (2000) Mechanism of arsenic release to groundwater, Bangladesh and West Bengal. Applied Geochemistry, 15, 403-413.

NICOLAS, A., BOUDIER, F. & ILDEFONSE, B. (1996) Variable crustal thickness in the Oman Ophiolite: Implication for oceanic crust. Journal of Geophysical Research, 101, 17,941-17,950.

NIELSEN, T. F. D. & BROOKS, C. K. (1995) Precious metals in magmas of East Greenland: Factors important to the mineralisation in the Skaergaard intrusion. Economic Geology, 90, 1911-1917.

NIKOGOSIAN, I. K. & SOBOLEV, A. V. (1997) Ion-microprobe analysis of melt Inclusions in olivine: experience in estimating the olivine-melt partition coefficients of trace elements. Geochemistry International, 35, 119-126.

NIXON, G. T., CABRI, L. J. & LAFLAMME, J. H. G. (1990) Platinum-Group-Element Mineralization in Lode and Placer Deposits Associated with the Tulameen Alaskan-Type Complex, British-Columbia. Canadian Mineralogist, 28, 503-535.

NIXON, G. T., HAMMACK, J. L., ASH, C. H., CABRI, L. J., CASE, G., CONNELLY, J. N., HEAMAN, L. M., LAFLAMME, J. H. G., NUTTALL, C., PATERSON, W. P. E. & WONG, R. H. (1997) Geology and platinum group element mineralisation of Alaskan type ultramafic-mafic complexes in British Columbia. Victoria, British Columbia, British Columbia Geological Survey.

OBERTHUR, T., WEISER, T. W. & GAST, L. (2003) Geochemistry and mineralogy of platinum-group elements at Hartley Platinum Mine, Zimbabwe. Mineralium Deposita, 38, 344-355.

OTTEMAN, J. & AUGUSTITHIS, S. S. (1967) Geochemistry and Origin of "Platinum-nuggets" in lateritic covers from ultrabasic rocks and birbirites of Western Ethiopia. Mineralium Deposita, 1, 269-277.

PAGE, N. J. & TALKINGTON, R. W. (1984) Palladium, platinum, rhodium, ruthenium and iridium in peridotites and chromitites from ophiolite complexes in Newfoundland. Canadian Mineralogist, 22, 137-149.

PAINE, D. (1981) Aerial Photography and Image Interpretation for Resource Management, John Wiley and Sons, USA.

PASTER, T. P., SCHAUWEC.DS & HASKIN, L. A. (1974) Behavior of Some Trace-Elements During Solidification of Skaergaard Layered Series. Geochimica Et Cosmochimica Acta, 38, 1549-1577.

PEDERSEN, A. K. (1979) Basaltic Glass with High-Temperature Equilibrated Immiscible Sulfide Bodies with Native Iron from Disko, Central West Greenland. Contributions to Mineralogy and Petrology, 69, 397-407.

PEDSERSEN, R.-B., JOHANNESEN, G. M. & BOYD, R. (1993) Stratiform platinum-group element mineralisation in the ultramafic cumulates, Central Norway. Economic Geology, 88.

PENROSE, CONFERENCE & PARTICIPANTS (1972) Penrose Feild Conference on Ophiolites. Geotimes, 17.

PEREGODOVA, A. & OHENSTETTER, M. (2002) Collectors of Pt, Pd and Rh in a S-poor Fe-Ni-Cu sulphide system at 760oC: Experimental data and application to ore deposits. Canadian Mineralogist, 40, 527-561.

PRICHARD, H. M., HUTCHINSON, D. & FISHER, P. C. (2004) Petrology and crystallization history of multiphase sulfide droplets in a Mafic Dike from Uruguay: Implications for the origin of Cu-Ni-PGE sulfide deposits. Economic Geology and the Bulletin of the Society of Economic Geologists, 99, 365-376.

PRICHARD, H. M. & LORD, R. A. (1990) Platinum and Palladium in the Troodos Ophiolite complex, Cyprus. Canadian Mineralogist, 28, 607-617.

PRICHARD, H. M. & LORD, R. A. (1993) An overview of the PGE concentrations in the Shetland ophiolite complex. IN PRICHARD, H. M., ALABASTER, T., HARRIS, N. B. W. & NEARY, C. R. (Eds.) Magmatic processes and plate tectonics.

PRICHARD, H. M. & LORD, R. A. (1996) A model to explain the occurrence of platinum- and palladium- rich ophiolite complexes. Journal of the Geological Society, 153, 323-328.

RENZULLI, A., SERRI, G., SANTI, P., MATTIOLI, M. & HOLM, P. M. (2001) Origin of high-silica liquids of stromboli volcano (aeolian islands, italy) inferred from crustal xenoliths. Bulletin of Volcanology, 62, 400-419.

RÉVILLON, S., ARNDT, N. T., CHAUVEL, C. & HALLOT, E. (2000) Geochemical study of ultramafic volcanic and plutonic rocks from gorgona island, colombia: the plumbing system of an oceanic plateau. Journal of Petrolology, 41, 1127-1153.

RINGWOOD, A. E. (1970) Petrogenesis of Apollo 11 basalts and implications for lunar origin. Journal of Geophysical Research, 75, 6453-6479.

ROBB, L. (2005) Copper bottomed - understanding the Central African Copperbelt. Materials World, 13, 24-26.

ROBERTSON, A. & XENOPHONTOS, C. (1993) Development of concepts concerning the Troodos ophiolite and adjacent units in Cyprus. IN PRICHARD, H. M., ALABASTER, T., HARRIS,

N. B. W. & NEARY, C. R. (Eds.) Magmatic Processes and Plate Tectonics. London, The Geological Society.

ROBINSON, E. S. & CORUH, C. (1988) Basic exploration geophysics, New York, John Wiley and sons.

SACK, R. O. & GHIORSO, M. S. (1991) Chromite as a petrogenetic indicator. IN LINDSLEY, D. H. (Ed.) Oxide Minerals: Petrologic and magnetic significance. Chelsea, Michigan, US, Mineralogical Society of America.

SCHELLMANN, W. (1971) Uber Bexiehungen lateritischer Eisen-, Nickel-, Aluminium- und Manganerze zu ihren Augangsgesteinen. Mineralium Deposita, 6, 275-291.

SCHELLMANN, W. (1989) Allochthonous surface alteration of Ni-laterites. Chemical Geology, 74, 351-364.

SCHUTH, S., ROHRBACH, A., MÜNKER, C., BALLHAUS, C., GARBE-SCHÖNBERG, C. D. & QOPOTO, C. (2004) Geochemical constraints on the petrogenesis of arc picrites and basalts, new georgia group, solomon islands. Contributions to Mineralolgy and Petrolology, 148, 288-304.

SCHWANDT, C. S. & MCKAY, G. A. (1998) Rare earth element partition coefficients from enstatite/melt synthesis experiments. Geochimica et Cosmochimica Acta, 62, 2845-2848.

SEIFERT, S., ONEILL, H. S. & BREY, G. (1988) The Partitioning of Fe, Ni and Co between Olivine, Metal, and Basaltic Liquid - an Experimental and Thermodynamic Investigation, with Application to the Composition of the Lunar Core. Geochimica Et Cosmochimica Acta, 52, 603-616.

SIGHINOLFI, G. P., ABERRA, G., GORGONI, C. & VALERA, R. (1993) Distribution of precious metals in the Tulu Dimtu ultramafic body (Welega, Ethiopia). Geology and mineral resources of Somalia and surrounding regions. Oltremare, 1st Agron.

SINCLAIR, A. J. (1983) Univariate Analysis. IN GOVETT, G. J. S. (Ed.) Statistics and Data Analysis in Geochemical Prospecting. Amsterdam, Elsevier Science Publishers.

SISSON, T. W. (1991) Pyroxene-High Silica Rhyolite Trace-Element Partition-Coefficients Measured by Ion Microprobe. Geochimica et Cosmochimica Acta, 55, 1575-1585.

SMITH, R. E., ANAND, R. R. & ALLEY, N. F. (2000) Use and implications of paleoweathering surfaces in mineral exploration in Australia. Ore Geology Reviews, 16, 185-204.

SNALL, S. & LILJEFORS, T. (2000) Leachability of major elements from minerals in strong acids. Journal of Geochemical Exploration, 71, 1-12.

SPANDLER, C. J., ARCULUS, R. J., EGGINS, S. M., MAVROGENES, J. A., PRICE, R. C. & REAY, A. (2003) Petrogenesis of the greenhills complex, southland, new zealand: magmatic differentiation and cumulate formation at the roots of a permian island-arc volcano. Contributions to Mineralolgy and Petrology, 144, 703-721.

ST.-LOUIS, R. M., NESBIT, R. D. & MORTON, R. D. (1986) Geo-chemistry of platinum-group elements in the Tulameen ultramafic complex, southern British Columbia. Economic Geology, 81, 961-973.

STERN, R. J. (1994) Arc assembly and continental collision in the neoproterozoic east African orogen. Annual Reviews of Earth and Planetary Science, 22, 319-351.

STOWE, C. W. (1994) Compositions and Tectonic Settings of Chromite Deposits through Time. Economic Geology and the Bulletin of the Society of Economic Geologists, 89, 528-546.

STRECKEISEN, A. (1976) To each plutonic rock its proper name. Earth-Science Reviews, 12, 1-33.

TADESSE, G. & ALLEN, A. (2005) Geology and geochemistry of the Neoproterozoic Tuludimtu Ophiolite suite, western Ethiopia. Journal of African Earth Sciences, 41, 192-211.

TARKIAN, M., EVSTIGNEEVA, T. & GORSHKOV, A. (1996) Synthesis of Pt- and Pd-sulphides in low temperature (85 degrees C) solutions buffered by clay minerals and graphite: Preliminary results. Mineralogy and Petrology, 58, 71-78.

TAYLOR, H. P. (1967) The zoned ultramafic complexes of southeastern Alaska. IN WYLLIE, P. J. (Ed.) Ultramafic and related rocks. New York London Sydney, John Wiley and sons Inc.

TISTL, M. (1994) Geochemistry of Platinum-Group Elements of the Zoned Ultramafic Alto Condoto Complex, Northwest Columbia. Economic Geology, 89, 158-167.

TISTL, M., BURGATH, K. P., HOHNDORF, A., KREUZER, H., MUNOZ, R. & SALINAS, R. (1994) Origin and emplacement of Tertiary ultramafic complexes in northwest Colombia: Evidence from geochemistry and K-Ar, Sm-Nd, Rb-Sr isotopes. Earth and Planetary Science Letters, 126, 41-59.

TOLSTYKH, SIDOROV, LAAJOKI, KRIVENKO & PODLIPSKIY (2000) The association of Platinum-group minerals in placers of the Pustaya River, Kamchatka, Russia. The Canadian Mineralogist, 38, 1251-1264.

TOLSTYKH, N., KRIVENKO, A., SIDOROV, E., LAAJOKI, K. & PODLIPSKY, M. (2002) Ore mineralogy of PGM placers in Siberia and the Russian Far East. Ore Geology Reviews, 20, 1-25.

TOWNSHEND, J. R. G. (1981) Terrain Analysis and Remote Sensing, London, George Allen and Unwin Ltd.

TURNER, S. P., FODEN, J. D., GEORGE, R. M., EVANS, P., VARNE, R., ELBURG, M. A. & JENNER, G. A. (2003) Rates and processes of potassic magma evolution beneath sangeang api volcano, East Sunda Arc, Indonesia. Journal of Petrology, 44, 491-515.

UNITED NATIONS (1971) Report on the mineral survey in two selected areas of Ethiopia. United Nations Development Program.

UPTON, B. G. J., SEMET, M. P. & JORON, J.-L. (2000) cumulate clasts in the bellecombe ash member, piton de la fournaise, reunion island, and their bearing on cumulative processes in the petrogenesis of the reunion lavas. Journal of Volcanology and Geothermal Research, 104, 297-318.

VANKO, D. A., BONNIN-MOSBAH, M., PHILIPPOT, P., ROEDDER, E. & SUTTON, S. R. (2001) Fluid inclusions in quartz from oceanic hydrothermal specimens and the Bingham, Utah porphyry-Cu deposit: a study with PIXE and SXRF. Chemical Geology, 173, 227-238.

VILLEMANT, B., JAFFREZIC, H., JORON, J. L. & TREUIL, M. (1981) Distribution Coefficients of Major and Trace-Elements - Fractional Crystallization in the Alkali Basalt Series of Chaine-Des-Puys (Massif Central, France). Geochimica et Cosmochimica Acta, 45, 1997-2016.

WARDEN, A. J., KAZMIN, V., KIESEL, W. & POHHL, W. (1982) Some Geochemical Data of the Mafic Ultramafic complex at Tulu Dimitri, Ethiopia, and their Genetic Significance. Sitzungsber. Osterr. Akad. Math.-Naturwiss, 191, 111-131.

WAY, D. S. (1973) Terrain Analysis: A guide to site selection using Aerial Photographic Interpretation, Hutchinson and Ross Inc.

WILSON, J. P. & GALLANT, J. C. (2000) Terrain Analysis: Principles and Applications, New York, John Wiley and Sons, Inc.

De WIT, M. & AGUMA, A. (1977) Geology of the Ultramafic and Associated rocks of Tulu Dimtu, Welega. Addis Ababa, Ministry of Mines, Energy and Water Resources, Ethiopian Institute of Geological Sciences.

WOLF, P. R. (1983) Elements of Photogrammetry, United States of America, McGraw-Hill.

WOOD, S. A. (1987) Thermodynamic calculations of the volatility of the platinum-group elements (PGE): The PGE content of fluids at magmatic temperatures. Geochemica and Cosmochemica Acta, 51, 3041-3050.

WOOD, S. A. (1990) The interaction of dissolved platinum with fulvic acid and simple organic acid analogues in aqueous solutions. Canadian Mineralogist, 28, 665-673.

WOOD, S. A. (2002) The aqueous goechemistry of the platinum-group elements with applications to ore deposits. IN CABRI, L. J. (Ed.) The geology, geochemistry and mineral beneficiation of platinum-group elements. Canadian Insitute of Mineralogy.

WOOD, S. A. & VLASSOPOULOS, D. (1990) The dispersion of Pt , Pd and Au in surficial media about two PGE-Cu-Ni prospects in Quesbec. Canadian Mineralogist, 28.

ZHOU, M.-F., YUMUL, G. P., MALPAS, J. & SUN, M. (2000) Comparitive study of platinum-group elements in the Coto and Acoje blocks of the Zambales Complex, Phillipines. The Island Arc, 9, 556-564.

12.Appendix

12.1. Repeat Analyses

	Sample Name	Au (ppb)	Pd (ppb)	Pt (ppb)	Difference (% of the highest value) Au	Pd	Pt
OMAC	TD2	<2	<2	36	0.0	100.0	64.7
Genalysis		<5	5	102			
OMAC	TD8	<2	15	4	0.0	16.7	55.6
Genalysis		<5	18	9			
OMAC	TD9	<2	37	27	0.0	15.9	43.8
Genalysis		<5	44	48			
OMAC	TD10	<2	2	40	0.0	50.0	5.0
Genalysis		<5	4	38			

Table 12.1: A comparison of Pb Fire Assay results from analyses performed on the same samples from OMAC and Genalysis.

		Elemental Analyses (ppb)									Difference (% of the highest value)		
Number of Repeats	Sample Name	Au 1	Au 2	Au 3	Pd 1	Pd 2	Pd 3	Pt 1	Pt 2	Pt 3	Au	Pd	Pt
2	KYR-018-01	0	0	0	0	0	0	28	30	28	0.0	0.0	6.7
2	TYR-008-01	0	0	0	0	0	0	21	21	23	0.0	0.0	8.7
2	TYR-006-01	0	2	0	3	3	3	10	19	10	100.0	0.0	47.4
1	TYR-009-01	0	0	0	0	0	0	60	65	0	0.0	0.0	7.7
1	DYR-023-01	0	0	0	0	0	0	57	52	0	0.0	0.0	8.8
1	YR 07/01	2	0	0	0	0	0	50	49	0	100.0	0.0	2.0
1	DYR-022-01	0	0	0	0	0	0	21	22	0	0.0	0.0	4.5
1	KYC-005-01	0	0	0	0	0	0	21	13	0	0.0	0.0	38.1
1	TYR-007-01	0	0	0	0	0	0	17	17	0	0.0	0.0	0.0
1	DYR-024-01	2	0	0	0	0	0	15	19	0	100.0	0.0	21.1
1	DYR-027-01	22	0	0	2	0	0	13	13	0	100.0	100.0	0.0
1	KTR-035-02	0	0	0	0	0	0	9	7	0	0.0	0.0	22.2
1	TDR 23/01	0	0	0	0	0	0	7	16	0	0.0	0.0	56.3
1	ATR-117-02	0	0	0	10	9	0	2	0	0	0.0	10.0	100.0
1	ATR-081-02	2	0	0	10	9	0	0	0	0	100.0	10.0	0.0
1	AYC-015-01	34	35	0	0	0	0	0	0	0	2.9	0.0	0.0
1	DTR-034-02	70	68	0	0	0	0	0	0	0	2.9	0.0	0.0
1	DTR-044-02	2	0	0	14	14	0	0	0	0	100.0	0.0	0.0
1	DYR-003-01	177	214	0	0	0	0	0	0	0	17.3	0.0	0.0
1	TYR-018-01	45	42	0	0	0	0	0	0	0	6.7	0.0	0.0
1	AYR-011-01	0	0	0	47	45	0	39	38	0	0.0	4.3	2.6
1	TTR-018-02	0	0	0	34	38	0	25	22	0	0.0	10.5	12.0
1	TD9	0	0	0	34	37	0	23	27	0	0.0	8.1	14.8
1	AYR-002-01	2	2	0	0	0	0	17	19	0	0.0	0.0	10.5
1	ATR-057-02	32	35	0	5	0	0	4	3	0	8.6	100.0	25.0
1	AYR-022-01	0	0	0	3	3	0	4	4	0	0.0	0.0	0.0
1	KTR-043-02	32	12	0	5	11	0	4	0	0	62.5	54.5	100.0
1	KTR-053-02	11	13	0	9	9	0	0	0	0	15.4	0.0	0.0
1	KTR-062-02	817	825	0	28	24	0	0	0	0	1.0	14.3	0.0
1	TTR-007-02	3	3	0	22	26	0	18	19	0	0.0	15.4	5.3
1	TTR-035-02	4	4	0	19	17	0	18	12	0	0.0	10.5	33.3
1	DTR-027-02	2	2	0	13	16	0	15	15	0	0.0	18.8	0.0
1	KYR-022-01	5	4	0	15	16	0	15	15	0	20.0	6.3	0.0
1	KTR-063-02	5	4	0	10	8	0	9	8	0	20.0	20.0	11.1
1	TTR-057-02	12	13	0	37	41	0	9	7	0	7.7	9.8	22.2
1	TTR-051-02	19	19	0	4	4	0	7	7	0	0.0	0.0	0.0
1	DYC-008-01	12	13	0	9	9	0	6	6	0	7.7	0.0	0.0
1	TTR-031-02	4	4	0	7	8	0	5	4	0	0.0	12.5	20.0
1	AYC-011-01	23	24	0	5	5	0	4	4	0	4.2	0.0	0.0
1	KTR-049-02	0	3	0	13	13	0	4	5	0	100.0	0.0	20.0
1	ATR-072-02	0	3	0	10	10	0	3	3	0	100.0	0.0	0.0
1	DR 16/01	12	11	0	0	9	0	0	2	0	8.3	100.0	100.0
1	DR 18/01	11	9	0	2	33	0	0	4	0	18.2	93.9	100.0

Table 12.2: A table detailing the repeat analyses performed by OMAC during the course of the sample analysis.

12.2. Analysis of Standards

Au (ppb)	Pd (ppb)	Pt (ppb)
264	1637	3883
326	1486	3743
282	1573	3664
270	1633	3653
238	1530	3692
244	1577	3624
986	1512	3739
246	1495	3726
264	1381	3771
226	1582	3783
354	1468	3729
284	1525	3747
236	1517	3708
264	1564	3802
212	1547	3777
292	1608	3778
304	1518	3706
256	1570	3698
238	1553	3768
298	1551	3737
268	1564	3735
230	1504	3658
242	1546	3774
242	1515	3641
248	1498	3719
266	1516	3792
244	1547	3780
254	1528	3649
238	1498	3664
386	1502	3632
264	1503	3717
300	1433	3662
246	1593	3703
278	1531	3776
232	1480	3718
296	1581	3760
224	1553	3736
256	1544	3809
224	1532	3786
290	1540	3734
274	1499	3657
212	1381	3624
986.00	1636.88	3883.36
774.00	255.53	259.37
310	1530	3740
249.68	16.70	6.94

min
max
range
Reccomended Value
Standard SARM-7b
Precision (variation as % of reccomended value)

Table 12.3: A table of analysis of the standard sample SARM7b with a summary of the ranges of values obtained and a measurement of precision.

Mg (%)	Ni (ppm)	Cu (ppm)	Cr (ppm)	Al (%)
2.87	684	2638	132	1.46
2.80	677	2672	115	0.99
3.00	679	2679	128	1.51
2.93	679	2633	122	1.32
2.93	669	2654	131	1.38
2.98	667	2690	126	1.25
3.01	672	2690	129	1.37
2.97	675	2697	124	1.44
2.98	677	2684	125	1.46
2.91	680	2639	122	1.32
2.93	679	2680	121	1.35
2.84	677	2586	114	1.19
2.90	663	2682	120	1.30
2.94	669	2682	123	1.37
2.94	673	2625	128	1.35
2.97	681	2687	121	1.16
2.97	682	2663	116	1.03
2.92	680	2708	118	1.06
2.87	673	2557	114	1.00
2.90	679	2701	117	1.04
2.91	679	2664	114	1.24
2.94	679	2671	116	1.29
3.01	685	2673	123	1.28
2.94	685	2609	125	1.33
2.85	667	2607	113	1.13
2.90	676	2656	123	1.22
2.92	678	2651	126	1.39
2.93	686	2616	112	1.11
2.89	681	2624	114	1.17
2.88	672	2679	116	1.22
2.88	682	2658	118	1.27
2.94	686	2664	124	1.49
2.94	685	2658	120	1.31
2.92	679	2585	125	1.48
2.93	681	2686	119	1.34
2.88	673	2632	121	1.36
2.86	669	2657	123	1.47
2.85	671	2651	118	1.33
2.88	681	2613	116	1.27
2.93	686	2685	120	1.36
2.91	674	2689	116	1.23
2.88	658	2662	115	1.29
2.91	671	2695	115	1.23
2.90	670	2655	113	1.19
2.80	678	2635	123	1.60
2.90	685	2627	119	1.44
2.92	684	2641	124	1.59
2.80	657.83	2556.53	112.38	0.99
3.01	685.98	2707.82	132.05	1.60
0.21	28.15	151.29	19.67	0.62
2.90	683	2650	N/A	N/A
7.26	4.12	5.71	N/A	N/A

Min
Max
Range
Assigned Value
Precision (variation as % of assigned value)

Table 12.4: A table of analysis of the OMAC laboratories in-house standard with a summary of the ranges of values obtained and a measurement of precision.

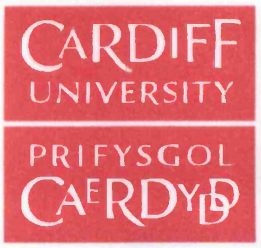

LITHOGEOCHEMISTRY AND SPINEL COMPOSITIONS IN THE ULTRAMAFIC COMPLEXES OF WESTERN ETHIOPIA: CRITERIA FOR THE IDENTIFICATION OF ALASKAN-TYPE INTRUSIONS

Matt Jackson

Submitted in fulfilment of the requirements for the degree of Ph.D.

March 2006

DECLARATION

This work has not previously been accepted in substance for any degree and is not being concurrently submitted in candidature for any degree.

Signed ..... (candidate)

Date 15 MARCH 2006

STATEMENT 1

This thesis is the result of my own investigations, except where otherwise state.

Other sources are acknowledged by footnotes and giving explicit references. A bibliography is appended.

Signed ..... (candidate)

Date 15 MARCH 2006

STATEMENT 2

I hereby give my consent for my thesis, if accepted, to be available for photocopying and for inter-library loan, **after expiry of a bar on access approved by the Univeristy of Wales on the special recommendation of the Consituent Institution/University college concerned.**

Signed ..... (candidate)

Date 15 MARCH 2006

Acknowledgements

"What does not kill me, makes me stronger."

Friedrich Nietzsche, Twilight of the Idols

I would like to thank my supervisors Hazel Prichard and John Bowles. Hazel has given me a vast amount of help over the last few years, both in the field and at university. I have learnt a great deal from her and I hope we can continue to work together. Without the help of John Bowles, this project would not have continued as far as it has. His sense of duty is something which all scientists should admire. I have very much enjoyed our discussions, especially in the field. I firmly believe that there are few supervisors who could have done more to help me than Hazel and John.

There are many others who have helped with this project. Kebede Belete and I spent large amounts of time together in the field during 2001-2002. His company was fantastic and I believe he is the foremost expert on the Yubdo area. The other geologists whom I will always remember fondly are, Aberra, Tadesse and Daniel. From each of these people I have disovered much about the ways of Africa and their contribution in the field has been crucial. I will always remember our escapades, such as getting our Land Crusier stuck in mud on an unmarked road, with no communications. Dodging the lion was also fun!

Many staff of the School of Earth, Ocean and Planetary Science have contributed a great deal in time and patience in helping me, including Alun Rogers for his patience in teaching me cartography and Pete Fisher for his expertise in the use of the SEM. All of the technicians and administration staff at the school are to be thanked.

I wish to thank my parents, who have given me all the support I could ask for, even though I stay out of contact for weeks! My brother and sister, Chris and Amy, have also helped greatly and now that I have emerged from my thesis fog, I hope to spend more time with them.

My friends in Cardiff have also helped considerably. In particular, my flatmates: Justin, Jo and Penny, who have put up with me doing little washing up, cleaning and generally being difficult! Lunch breaks with Katherine have been particularly useful especially when she forced me to take them. The TA and regular staff at 104 Regt RA (V) have been responsible for keeping my feet firmly grounded, for that I am sincerely grateful. Also thanks to Dave Oldham, Richard Lilly and Kevin Jones for laughs and help during the first few years of my study.

Finally, I wish to thank Nicky, whom I love more than ever. Her mere presence is enough to calm my nerves and I wish to spend the rest of my life with her.

Abstract

This thesis covers two separate but complimentary themes. Firstly, work on the spinel composition of the ultramafic rocks of has provided evidence that they formed as Alaskan-type intrusions. This has implications both for prospectivity and for the understanding of neoproterozoic plate movements. Additionally, the study of the rock and soil geochemistry has been used to identify exploration targets and evaluate the prospectivity of the major complexes.

It is proposed here that the ultramafic complexes Tulu Dimtu, Kingy, Daleti, Ankori and Yubdo, in the Western Ethiopian Shield are Alaskan type intrusions. Alaskan-type intrusions are concentrically zoned ultramafic intrusions thought to be the feeder pipes of volcanoes. They have dunite at the core and grade outwards to clinopyroxenite and sometimes hornblendite. These intrusions typically occur in continental arc settings such as Alaska, British Colombia and the Urals. This compares with ophiolite complexes which are thought to be obducted oceanic upper mantle and crust. The two types of complex may be difficult to distinguish because if ophiolites are dismembered and deformed fragments, they may resemble Alaskan-type intrusions.

This thesis documents several features of these Ethiopian complexes that are typical of Alaskan type intrusions. Mapping of the Yubdo complex has shown a circular out crop pattern with concentric zones of clinopyroxenite at the edge to dunite at the centre. New mapping of the Tulu Dimtu area has shown a similar zoned circular body. Both the Yubdo and Tulu Dimtu complexes show concentric zones of Cr values, where the greatest values occur at the edge and the lowest in the centre.

These mafic and ultramafic intrusions are very altered by surface weathering but contain chrome-spinels which have a geochemistry which is unlike ophiolites and similar to Alaskan-type intrusions. The analysis of these spinels demonstrates how the compositions of spinel Fe^{2+}# and Cr# values may be used to distinguish between an Alaskan type or ophiolite complexes. In Alaskan-type intrusions, spinels with Fe^{2+}# values greater than 0.85 frequently have Cr# values which are lower than 0.5. Such low Cr# values in spinels with high Fe^{2+}# values are rare in ophiolite complexes.

The variations in Ni, Cu, Cr and Al contents of highly altered ultramafics and fresher ultramafics have been used to investigate the magmatic and post-magmatic ore forming processes that have influenced the Pt and Pd content of the complexes. It is expected that medium to low temperature hydrothermal activity may have had a significant impact on the geochemistry of even the fresher rocks. The discovery of high Pd values and low Pt in lithologies such as talc-schists and quartzite support the idea that Pd is more mobile than Pt in medium to low temperature conditions. Furthermore, in the Tulu Dimtu Main Intrusion, the altered rocks indicate that Pd has been removed from the magmatic sites of concentration. In a few places it is possible to see through the extensive alteration and potential magmatic processes can be considered. Within the Tulu Dimtu Main Intrusion and the Main Yubdo Intrusion, the most primitive rocks occur at the flanks. Furthermore, it is indicated that sulphide segregation may have occurred in the Tulu Dimtu Main Intrusion and Daleti Ultramafic. In the Daleti Ultramafic, regardless of the presence of sulphides, the Pt and Pd values remain low – it is therefore unlikely that the complex hosts economic grades. However, at Tulu Dimtu and Yubdo, it is recommended that any future exploration be targeted at the flanks of the complexes, where magmatic and post-magmatic processes may potentially co-incide to elevate the grade.

Much work has been published to document the nature of platinum-group minerals (PGM) in the alluvial and eluvial placers around the Yubdo area and some PGM have been discovered in the serpentinsed dunites of the main Yubdo intrusion. In this thesis further discoveries of PGM have been made in the serpentinised dunites and chromites from the Yubdo area.

In the course of this work new base maps covering the ultramafic complexes and the surrounding basement have been produced. These have revealed many smaller ultramafic bodies which are referred to here as the Lensoid Ultramafics. Both spinel and whole rock geochemistry supports the hypothesis that these are slivers of rock "sheared-off" the outside of larger complexes.

The conclusion that these complexes have an Alaskan-type origin has consequences for the understanding of plate movements in this part of the Neoproterozoic Western Ethiopian Shield. Additionally, the identification of exploration targets will help focus efforts to uncover any potential economic mineralisation.

LITHOGEOCHEMISTRY AND SPINEL COMPOSITIONS IN THE ULTRAMAFIC COMPLEXES OF WESTERN ETHIOPIA: CRITERIA FOR THE IDENTIFICATION OF ALASKAN-TYPE INTRUSIONS

Table of Contents

1	**Introduction**	**1**
1.1.	Introduction	1
1.2.	The tectonic setting of the ultramafic complexes	4
1.3.	The development of Pt and Pd	5
1.4.	The mining history of the WES	5
1.5.	The conduct of the study	7
1.6.	Aims and methods used in the thesis	7
1.7.	Layout of the thesis	8
2	**Literature Review**	**9**
2.1.	Introduction	9
2.2.	Geological Setting	9
2.3.	Previous Work on the Ultramafics of the WES	11
2.3.1.	Introduction	12
2.3.2.	Regional Studies of the Ultramafic bodies	12
2.3.3.	Tulu Dimtu and Kingy	13
2.3.4.	Daleti, Ankori, Tulu Kapi and Keley	15
2.3.5.	Yubdo, Andu and Sodu	16
2.4.	Alaskan-type intrusions versus ophiolites	17
2.4.1.	Introduction	17
2.4.2.	Scale of Alaskan-type intrusions and ophiolites	18
2.4.3.	Structure of Alaskan-type intrusions and ophiolites	19
2.4.4.	Petrology and Mineralogy	22
2.4.5.	Rare Earth Elements (REE)	24
2.4.6.	Platinum-Group Elements	25
2.4.7.	Fractionation of Nickel, Copper and Chromium	27
2.4.8.	Summary	27
3	**Petrology and Mineralogy**	**29**
3.1.	Introduction	29
3.2.	Methods	29
3.2.1.	Scanning Electron Microscopy	29
3.2.2.	Energy Dispersive X-Ray analyzer	29
3.3.	Petrology	29
3.3.1.	Introduction	30
3.3.2.	Dunite	31
3.3.3.	Clinopyroxenite	33
3.3.4.	Birbirite	33
3.3.5.	Summary	34
3.3.6.	Classification of Rock Types	34
3.4.	Oxide Minerals	36
3.4.1.	Introduction	36
3.4.2.	Tulu Dimtu	36
3.4.3.	Kingy	37
3.4.4.	Daleti, Ankori, Tulu Kapi and Keley	37
3.4.5.	Yubdo, Andu and Sodu	38
3.4.6.	Summary	38
3.4.7.	Discussion	39
3.5.	Sulphide Minerals	39
3.5.1.	Introduction	39
3.5.2.	Tulu Dimtu	40
3.5.3.	Kingy	41

3.5.4.	Daleti, Ankori, Tulu Kapi and Keley	42
3.5.5.	Yubdo, Andu and Sodu	43
3.5.6.	Summary	43
3.5.7.	Discussion	44
3.6.	Platinum Group Minerals	45
3.6.1.	Introduction	45
3.6.2.	Sample AYR-016-01	45
3.6.3.	Sample KYR-019-02	46
3.6.4.	Sample Y30	47
3.6.5.	Discussion	48
4	**Terrain Mapping**	**49**
4.1.	Introduction	49
4.2.	Aerial Photography	50
4.2.1.	Introduction	50
4.2.2.	The Aerial Photographs of the WES	50
4.2.3.	The Acquisition of Aerial Photographs	52
4.2.4.	Image Processing	55
4.3.	Terrain Analysis	56
4.3.1.	Introduction	56
4.3.2.	Stereoscopy	56
4.3.3.	Terrain Elements: Introduction	57
4.3.4.	Terrain Elements: Drainage pattern	58
4.3.5.	Terrain Elements: Erosion	60
4.3.6.	Terrain Elements: Topography	62
4.3.7.	Terrain Elements: Relative image tone and texture	63
4.3.8.	Terrain Elements: Land use	64
4.3.9.	Photomorphic Regions	64
4.3.10.	Ground Truth	65
4.4.	The Terrain in the WES	65
4.4.1.	The photomorphic regions	65
4.4.2.	Tulu Dimtu	68
4.4.3.	Kingy	69
4.4.4.	Daleti, Ankori, Tulu Kapi and Keley	70
4.4.5.	Yubdo, Sodu and Andu	71
4.4.6.	Summary	72
5	**Geological Mapping**	**73**
5.1.	Introduction	73
5.2.	Method	73
5.3.	Geological Maps of the WES	74
5.3.1.	Tulu Dimtu	74
5.3.2.	Kingy	76
5.3.3.	Daleti, Ankori, Tulu Kapi and Keley	78
5.3.4.	Yubdo, Sodu and Andu	80
5.3.5.	Summary	81
6	**Ground Magnetics**	**82**
6.1.	Introduction	82
6.2.	Methods	82
6.2.1.	Data collection	83
6.2.2.	Diurnal correction	86
6.2.3.	Data presentation	87
6.2.4.	Limitations and accuracy	88
6.3.	Results	89
6.3.1.	Sensor orientation test	89
6.3.2.	Wide spacing survey	90
6.3.3.	Tight spacing survey	96
6.4.	Discussion	97
6.5.	Conclusions	99
6.5.1.	Pull out section	101
7	**Soil Geochemical Data**	**102**
7.1.	Introduction	102

7.2.	The overburden of the WES	102
7.3.	Sampling strategy	106
7.4.	Method of Analysis	107
7.5.	Soil Forming processes and geochemical dispersion	107
7.5.1.	Ni, Cu, Cr and Al	107
7.5.2.	Pt and Pd	108
7.6.	Tulu Dimtu: Selected Major and Trace elements	109
7.6.1.	Introduction	109
7.6.2.	Summary of Analytical Results	109
7.6.3.	Nickel	114
7.6.4.	Copper	115
7.6.5.	Chromium	116
7.6.6.	Aluminium	117
7.6.7.	Summary of Ni, Cu, Cr and Al values	117
7.6.8.	Platinum and Palladium	118
7.6.9.	Discussion	120
7.6.10.	Ni, Cu, Cr, and Al distribution in soils	120
7.6.11.	Genesis of Pt and Pd in soils	121
7.6.12.	Conclusion	122
7.6.13.	Maps of the elemental distribution in the soils of the Tulu Dimtu areas	123
7.7.	Kingy: Selected Major and Trace Elements	124
7.7.1.	Introduction	124
7.7.2.	Summary of Analytical Results	125
7.7.3.	Nickel	129
7.7.4.	Copper	130
7.7.5.	Chromium	131
7.7.6.	Aluminium	132
7.7.7.	Summary of Ni, Cu, Cr and Al values	132
7.7.8.	Platinum and Palladium	133
7.7.9.	Discussion	135
7.7.10.	Trace Element distribution in soils	135
7.7.11.	Genesis of Pt and Pd in soils	135
7.7.12.	Conclusions	136
7.7.13.	Maps of the elemental distribution in the soils of the Kingy areas	138
7.8.	Daleti, Ankori, Tulu Kapi and Keley: Selected Major and Trace Elements	139
7.8.1.	Introduction	139
7.8.2.	Summary of Analytical Results	140
7.8.3.	Nickel	144
7.8.4.	Copper	145
7.8.5.	Chromium	146
7.8.6.	Aluminium	147
7.8.7.	Summary of Ni, Cu, Cr and Al values	147
7.8.8.	Platinum and Palladium	148
7.8.9.	Discussion	150
7.8.10.	Trace element distribution in soils	150
7.8.11.	Genesis of Pt and Pd in soils	150
7.8.12.	Conclusions	151
7.8.13.	Maps of the elemental distribution in the soils of the Daleti, Ankori, Tulu Kapi and Keley areas	152
7.9.	Yubdo, Andu and Sodu: Selected Major and Trace Elements	153
7.9.1.	Introduction	153
7.9.2.	Summary of Analytical Results	154
7.9.3.	Nickel	158
7.9.4.	Copper	159
7.9.5.	Chromium	160
7.9.6.	Aluminium	161
7.9.7.	Summary of Ni, Cu, Cr, Al, Pt and Pd values	161
7.9.8.	Platinum and Palladium	162
7.9.9.	Discussion	163
7.9.10.	Ni and Cr values in soils above the Main Yubdo Ultramafic	163

7.9.11.	Genesis of Pt and Pd in soils	164
7.9.12.	Conclusions	165
7.9.13.	Maps of the elemental distribution in the soils of the Yubdo, Andu and Sodu areas	166
7.10.	Discussion of the distribution of Ni, Cu, Cr, Al, Pt and Pd in the soils of the WES	167
7.11.	Summary of the Soil development in the WES	170
7.11.1.	Ni, Cu, Cr and Al	170
7.11.2.	Pt and Pd	171
8	**Rock Geochemical Data**	172
8.1.	Introduction	172
8.2.	Analytical Techniques	173
8.2.1.	Introduction	173
8.2.2.	Pb Fire Assay	174
8.2.3.	Aqua Regia Digestion	176
8.2.4.	Inductively Coupled Plasma - Optical Emmission Spectroscopy	177
8.3.	Methods	178
8.3.1.	Definition of a fresher sample	178
8.3.2.	The samples	182
8.4.	Tulu Dimtu: Selected Major and Trace Elements	183
8.4.1.	Introduction	183
8.4.2.	Data	185
8.4.3.	Nickel	187
8.4.4.	Copper	188
8.4.5.	Chromium	188
8.4.6.	Aluminium	189
8.4.7.	Summary of the Ni, Cu, Cr and Al values in the Main Intrusion and Sheared Ultramafic	189
8.4.8.	Summary of the Ni, Cu, Cr and Al values in the Lensoid Ultramafics	190
8.4.9.	Summary of the Ni, Cu, Cr and Al values in the Shear Zones	190
8.5.	Tulu Dimtu: Pt and Pd Distribution	190
8.5.1.	Rock	190
8.5.2.	Summary of Pt and Pd distribution in the Main Intrusion and Sheared Ultramafic	191
8.5.3.	Summary of Pt and Pd distribution in the Lensoid Ultramafics	194
8.5.4.	Summary of Pt and Pd distribution in the Shear Zones	194
8.5.5.	Summary of Pt and Pd distribution in the basement	194
8.5.6.	Comparison of the geochemistry of the soil versus rock samples	194
8.6.	Review of processes concentrating Pt and Pd	195
8.6.1.	Introduction	195
8.6.2.	The fractionation of Ni	195
8.6.3.	The fractionation of Cr	197
8.6.4.	Sulphide immiscibility and solubility	198
8.6.5.	Sulphide fractionation	198
8.6.6.	Filter-pressing	199
8.6.7.	Magma mixing	200
8.6.8.	Hydrothermal remobilisation	201
8.7.	Tulu Dimtu: Discussion	202
8.7.1.	Zonation of nickel and chromium in fresher rocks	202
8.7.2.	Locations of highest copper and chromium values in fresher rocks	205
8.7.3.	Trace element distribution in fresher rocks of the Lensoid Ultramafics	207
8.7.4.	Trace element distribution in Shear Zones	207
8.7.5.	Zonation of trace elements in altered rocks	208
8.7.6.	Genesis of Pt and Pd in fresher rocks	209
8.7.7.	Genesis of Pt and Pd in altered rocks	210
8.8.	Tulu Dimtu: Conclusions	211
8.9.	Maps of the elemental distribution in the Tulu Dimtu areas	213
8.10.	Kingy: Selected Major and Trace Elements	214
8.10.1.	Introduction	214
8.10.2.	Data	215
8.10.3.	Nickel	217
8.10.4.	Copper	218
8.10.5.	Chromium	218

8.10.6.	Aluminium	219
8.10.7.	Summary of Ni, Cu, Cr and Al distribution in the Kingy Ridge Ultramafic and Extra Ultramafic	219
8.10.8.	Summary of Ni, Cu, Cr and Al distribution in the Lensoid Ultramafics	220
8.10.9.	Summary of Ni, Cu, Cr and Al distribution in the Isolated Gabbro	220
8.11.	Kingy: Pt and Pd distribution	220
8.11.1.	Comparison of the geochemistry of the soil versus rock samples	223
8.12.	Kingy: Discussion	223
8.12.1.	The locations of the highest Ni and Cu values in fresher rocks	223
8.12.2.	Locations of highest Cu and Cr values in fresher rocks	223
8.12.3.	Zonation of Ni and Cr in altered rocks from the Kingy Ridge Ultramafic	224
8.12.4.	Uneven Cu and Al distribution in the altered rocks from the Kingy Ridge Ultramafic	225
8.12.5.	Trace element distribution in the altered rocks from the Lensoid Ultramafics	225
8.12.6.	Genesis of Pt and Pd in fresher rocks	226
8.12.7.	Genesis of Pt and Pd in altered rocks	226
8.13.	Kingy: Conclusions	227
8.14.	Maps of elemental distribution in the Kingy areas	229
8.15.	Daleti, Ankori, Tulu Kapi and Keley: Selected Major and Trace Elements	230
8.15.1.	Introduction	230
8.15.2.	Data	232
8.15.3.	Nickel	235
8.15.4.	Copper	235
8.15.5.	Chromium	236
8.15.6.	Aluminium	236
8.15.7.	Summary of Ni, Cu, Cr and Al values in the Daleti Ultramafic	237
8.15.8.	Summary of Ni, Cu, Cr and Al values at Ankori and the Lensoid Ultramafics	237
8.15.9.	Summary of Ni, Cu, Cr and Al values in the Shear Zones	237
8.15.10.	Summary of Ni, Cu, Cr and Al values in the southwestern Shear Zones and gabbro	238
8.16.	Daleti, Ankori, Tulu Kapi and Keley: Pt and Pd distribution	238
8.17.	Daleti, Ankori, Tulu Kapi and Keley: Discussion	241
8.17.1.	The highest Ni and Cu values in the fresher rocks from the Daleti Ultramafic	241
8.17.2.	Zonation in Cr values in the fresher rocks from the Daleti Ultramafic	242
8.17.3.	Trace element distribution in Shear Zones	242
8.17.4.	Copper values in altered rocks	242
8.17.5.	High Ni values within the ultramafic complexes	243
8.17.6.	Genesis of Pt and Pd in fresher rocks from the Daleti Ultramafic	243
8.17.7.	Genesis of Pt and Pd in altered rocks	244
8.18.	Daleti, Ankori, Tulu Kapi and Keley: Conclusions	245
8.19.	Maps of elemental distribution in the Daleti, Ankori, Tulu Kapi and Keley areas	247
8.20.	Yubdo, Sodu and Andu: Selected Major and Trace Elements	248
8.20.1.	Introduction	248
8.20.2.	Data	249
8.20.3.	Nickel	251
8.20.4.	Copper	251
8.20.5.	Chromium	252
8.20.6.	Aluminium	253
8.20.7.	Summary of the Ni, Cu, Cr and Al values from the Yubdo Main Intrusion	253
8.21.	Yubdo, Sodu and Andu: Pt and Pd distribution	254
8.22.	Yubdo, Sodu and Andu: Discussion	256
8.22.1.	The locations of the highest Ni and Cu values in the fresher rocks from the Main Yubdo Ultramafic	256
8.22.2.	Locations of highest Cu and Cr values in fresher rocks	258
8.22.3.	Zonation of Cr values the altered rocks from the Main Yubdo Ultramafic	258
8.22.4.	The locations of high Ni and Cu values in altered rocks from the Main Yubdo Ultramafic	259
8.22.5.	Genesis of Pt and Pd in fresher rocks	259
8.22.6.	Genesis of Pt and Pd in altered rocks	260
8.23.	Yubdo, Sodu and Andu: Conclusions	261
8.24.	Maps of elemental distribution in the Yubdo, Andu and Sodu areas	262

8.25.	Pt and Pd prospectivity and ore forming processes	263
8.25.1.	Magmatic ore forming processes	263
8.25.2.	Post-magmatic ore forming processes	265
8.25.3.	Prospectivity	266
9	**Results: Spinel Geochemistry**	**267**
9.1.	Introduction	267
9.2.	Methods	268
9.2.1.	Sample Preparation	268
9.2.2.	Energy Dispersive X-ray Analysis	268
9.3.	Fe-Valency Estimation	269
9.3.1.	Introduction	269
9.3.2.	Method	270
9.3.3.	The Analyses	271
9.4.	Alteration Assessment	272
9.4.1.	Introduction	272
9.4.2.	Method	274
9.4.3.	Results	275
9.4.4.	Discussion	277
9.5.	Tulu Dimtu: Spinel Geochemistry	277
9.5.1.	Introduction	277
9.5.2.	Data	278
9.5.3.	Fe2+# (Fe2+/(Mg+Fe2+))	280
9.5.4.	Cr# (Cr / (Cr+Al))	280
9.5.5.	TiO2	280
9.5.6.	Fe3+# (Fe3+ / (Fe3+ + Al2+ + Cr3+ + V3+))	281
9.5.7.	Minor Elements (Si, Co, and Zn)	281
9.5.8.	Summary of the spinel Geochemistry in the Tulu Dimtu area	281
9.6.	Discussion	282
9.6.1.	Alteration	282
9.6.2.	Magmatic effects	284
9.6.3.	Comparison with Alaskan-type intrusions and Ophiolite complexes	285
9.7.	Conclusions	287
9.7.1.	Pull-out section	289
9.8.	Kingy: Spinel Geochemistry	290
9.8.1.	Introduction	290
9.8.2.	Data	290
9.8.3.	Fe2+# (Fe2+/(Mg+Fe2+))	291
9.8.4.	Cr / (Cr+Al)	291
9.8.5.	TiO2	291
9.8.6.	Fe3+# / (Fe3+ + Al2+ + Cr3+ + V3+)	291
9.8.7.	Minor Elements (Na, Si, and Zn)	292
9.8.8.	Summary of Spinel Geochemistry in the Kingy area	292
9.9.	Discussion	292
9.9.1.	Alteration	292
9.9.2.	Magmatic Effects	293
9.9.3.	Comparison with Alaskan-type intrusions and ophiolite complexes	294
9.10.	Conclusions	294
9.11.	Pull-out section	295
9.12.	Daleti, Ankori, Tulu Kapi and Keley: Spinel Geochemistry	296
9.12.1.	Introduction	296
9.12.2.	Data	296
9.12.3.	Fe2+# (Fe2+/(Mg+Fe2+))	299
9.12.4.	Cr# (Cr / (Cr+Al))	299
9.12.5.	TiO2	299
9.12.6.	Fe3+# (Fe3+ / (Fe3+ + Al2+ + Cr3+ + V3+))	299
9.12.7.	Minor Elements (Co and Zn)	300
9.12.8.	Summary of Spinel Geochemistry in the Daleti Ultramafic	300
9.12.9.	Summary of Spinel Geochemistry in the Ankori Ultramafic	301
9.13.	Discussion	301
9.13.1.	Alteration	301

9.13.2.	Magmatic Effects	303
9.13.3.	Comparison with Alaskan-type intrusions and ophiolite complexes	304
9.14.	Conclusions	305
9.14.1.	Pull-out section	306
9.15.	Yubdo, Sodu and Andu: Spinel Geochemistry	307
9.15.1.	Introduction	307
9.15.2.	Data	307
9.15.3.	Fe2+# (Fe2+/(Mg+Fe2+))	308
9.15.4.	Cr# (Cr / (Cr+Al))	308
9.15.5.	TiO2	309
9.15.6.	Fe3+# (Fe3+ / (Fe3+ + Al2+ + Cr3+ + V3+))	309
9.15.7.	Minor Elements (SiO2, CoO and ZnO)	309
9.15.8.	Summary of Spinel Geochemistry in the Main Yubdo Intrusion	309
9.16.	Discussion	310
9.16.1.	Alteration	310
9.16.2.	Magmatic Effects	311
9.16.3.	Comparison with Alaskan-type intrusions and Ophiolites	311
9.17.	Conclusions	312
9.17.1.	Pull-out section	313
9.18.	Summary of Spinel Geochemistry in the WES	314
9.18.1.	Alteration	316
9.18.2.	Magmatic Effects	316
9.18.3.	Comparison with Alaskan-type intrusions and ophiolite complexes	317
10	**Summary**	**318**
10.1.	Introduction	318
10.2.	Tulu Dimtu	319
10.3.	Kingy	320
10.4.	Daleti, Ankori, Tulu Kapi and Keley	321
10.5.	Yubdo, Andu and Sodu	322
10.6.	Exploration Summary	324
10.7.	Comparison with published work on the tectonic setting of the complexes	325
11	**References**	**327**
12	**Appendix**	**335**
12.1.	Repeat Analyses	335
12.2.	Analysis of Standards	336

List of Figures

Figure	Caption	Page
Figure 1.1	A geological map of the WES. (Johnson et al., 2004).	2
Figure 1.2	A map of the four field areas of this thesis, showing the largest ultramafic complexes and major roads and settlements.	3
Figure 1.3	An aerial photograph of the opencast workings of the laterite in the Yubdo area (within the black lines) in 1957. The bright line is the course of the Birbir river.	6
Figure 2.1	The "ophiolite belts" of northeast Africa (modified after Berhe, 1990).	10
Figure 2.2	The average chondrite normalized Ru, Rh, Pt and Pd analyses for dunite from the Tulu Dimtu area (Sighinolfi, 1993).	15
Figure 2.3	Schematic diagrams of the mafic and ultramafic units of the Josephiene Ophiolite and Tulameen Alaskan-type intrusion showing similar zoned outcrop patterns (modified from Findlay, 1969 and Harper, 1984).	20
Figure 2.4	The typical REE geochemistry of Alaskan-type intrusions compared to Oman ophiolite (Johan, 2002; Lippard et al., 1986).	24
Figure 2.5	A comparison of the chrondrite normalized PGE abundances for Alaskan Type intrusions and the Troodos ophiolite. (After Johan, 2002 and Prichard and Lord, 1990).	26
Figure 3.1	A photograph of a dunite sample under crossed polars. The lower edge of the image is 120μm in length.	31
Figure 3.2	A photograph of a dunite sample under crossed polars. The lower edge of the image is 120μm in length.	31
Figure 3.3	A photograph of a dunite sample under crossed polars. The lower edge of the image is 120μm in length.	32
Figure 3.4	A photograph of a dunite sample under crossed polars. The lower edge of the image is 120μm in length.	32
Figure 3.5	A photograph of a dunite sample under crossed polars. The lower edge of the image is 120μm in length.	32
Figure 3.6	A photograph of a clinopyroxenite sample from Kingy area under crossed polars.	33
Figure 3.7	A photograph of a clinopyroxenite sample from the Kingy area under crossed polars.	33
Figure 3.8	A photograph of a birbirite sample from the Tulu Dimtu Main Intrusion area.	33
Figure 3.9	SEM photomicrographs of a disseminated spinel (white colour, high mean atomic number) in a clinopyroxenite sample (DTR-019-02). The spinel shows a pull apart tecture and is hosted by a gangue of fibrous amphibole.	36
Figure 3.10	SEM photomicrographs of disseminated spinels (white colour, high mean atomic number) hosted by olivine in sample DTR-057-02. Some spinels are subhedral and zoned.	37
Figure 3.11	SEM photomicrographs of disseminated spinels (white colour, high mean atomic number) hosted by partially serpentinised olvines from sample D19. Many spinels show pull-apart textures.	37
Figure 3.12	SEM photomicrographs of anhedral spinels (white colour, high mean atomic number) from sample Y28. The spinels occur in serpentine filled cracks between fresh clinopyroxenes minerals.	38
Figure 3.13	SEM photomicrographs of disseminated spinels (white colour, high mean atomic number) partially serpentinised olivines from sample Y30.	38

Figure 3.14	SEM photomicrographs of an altered bornite (white colour, high mean atomic number in the centre of image) in the altered rim of a Cr-spinel (grey colour), hosted by serpentine (black). This image has been taken from sample TDR19/01 which is located on the southern flank of the Tulu Dimtu Main Intrusion.	40
Figure 3.15	SEM photomicrographs of an anhedral glaucodot split into three parts (white colour, high mean atomic number) hosted by serpentine. The sulphide mineral on the left hosts a Ni-As-bearing magnetite inclusion. This image has been taken from sample DTR-019-02 from the Tulu Dimtu Lensoid Ultramafics.	41
Figure 3.16	SEM photomicrographs of an anhedral chalcopyrite mineral (white colour, high mean atomic number) hosted by quartz in an extremely altered olivine-clinopyroxenite sample. This image has been taken from sample KTR-049-02 from the Kingy Ridge Ultramafic.	41
Figure 3.17	SEM photomicrographs of several anhedral barite crystals (white specs, high mean atomic number) on the edge of larger partially serpentinised olivine minerals. There are many anhedral Fe-rich spinels. This image has been taken from sample DR22/01 from the Daleti Ultramafic.	42
Figure 3.18	SEM photomicrographs of a Ni-sulphide mineral (white spec, high mean atomic number) in the altered rim of a zoned spinel hosted by serpentine (black). In addition to the subhedral spinels (centre of image) there are many fine anhedral Fe-rich spinels which sometimes form schlieren. This image has been taken from sample AYR-016-01 from the northwestern flank of the Main Yubdo Intrusion.	43
Figure 3.19	An SEM back-scattered electron image photomicrographs of a subhedral Pt-Fe alloy (white colour, high mean atomic number) in a Cr-spinel hosted by serpentine. This image has been taken from sample AYR-016-01 from the northwestern edge of the Main Yubdo Intrusion.	45
Figure 3.20	An SEM back-scattered electron image photomicrographs of an anhedral Os-Ir alloy (white colour, high mean atomic number) hosted by serpentine. This image has been taken from sample KYR-019-01 located the northwestern flank of the Main Yubdo Intrusion.	46
Figure 3.21	An SEM back-scattered electron image photomicrographs of a subhedral Ir-Os alloy (white colour, high mean atomic number) within a Cr-spinel hosted by partially serpentinised olivine. This image has been taken from sample AYR-016-01 located on the far western flank of Main Yubdo Intrusion.	47
Figure 4.1	A photograph of a barren ridge above the Daleti Ultramafic. The ridge is almost devoid of vegetation when compared to the foreground. Furthermore, the houses to the right indicate the presence of fertile subsistence farmland.	49
Figure 4.2	A typical aerial photograph with the data block enlarged.	52
Figure 4.3	Principle components of a single-lens mapping camera (after Lillesand and Kiefer, 2000)	53
Figure 4.4	A section from an aerial photograph showing the boundary between a coarse dendritic (top left) and fine dendritic (bottom right) drainage patterns.	58
Figure 4.5	The six basic drainage patterns, after Lillesand and Keifer (2000)	59
Figure 4.6	Illustrations of drainage texture. A: coarse-textured and B: fine-textured, after Lillesand and Keifer (2000).	60
Figure 4.7	A section from an aerial photograph showing the boundary	60

	between areas with round-bottomed gullies (left) and v-shaped gullies (right).	
Figure 4.8	A section from an aerial photograph showing a ridge (center) and smaller hills around the outside.	62
Figure 4.9	A section from an aerial photograph showing the boundaries between bright and dark image tones. The darkest mottled texture is tree cover, however the dark tone of the soil can be observed between trees.	63
Figure 4.10	A section from an aerial photograph showing the boundary between cultivated land (bottom and top) and non-cultivated land (center). Subsistence farms in Ethiopia typically cultivate fields of no larger than 500m in width. These appear on aerial photographs as a "patchwork" texture.	64
Figure 4.11	A map of photmorphic regions for the Tulu Dimtu area. White lines indicate the course of the major rivers. Inset is a representative aerial photograph showing the main ultramafic formation.	68
Figure 4.12	A map of photmorphic regions for the Kingy area. White lines indicate the course of the major rivers. Inset is a representative aerial photograph showing the main ultramafic formation.	69
Figure 4.13	A map of photmorphic regions for the Daleti, Ankori, Tulu Kapi and Keley areas. White lines indicate the course of the major rivers. Inset is a representative aerial photograph showing the main ultramafic formation.	70
Figure 4.14	A map of photmorphic regions for the Yubdo, Andu and Sodu areas. White lines indicate the course of the major rivers. Inset is a representative aerial photograph showing the main ultramafic formation.	71
Figure 5.1	The geological map of the Tulu Dimtu area. Black lines indicate the course of the major rivers.	74
Figure 5.2	The geological map of the Kingy area. Black lines indicate the course of the major rivers.	76
Figure 5.3	The geological map of the Daleti, Ankori, Tulu Kapi and Keley areas. Black lines indicate the course of the major rivers.	78
Figure 5.4	The geological map of the Yubdo, Andu and Sodu areas. Black lines indicate the course of the major rivers.	80
Figure 6.1	The magnetometer sensor set up aligned to N and attached to a tree.	84
Figure 6.2	The survey point locations for the ground magnetic survey of the Main Yubdo Intrusion overlaid onto the geological map (see chapter 5).	85
Figure 6.3	The magnetic field strength at the base station over a 24 hour period (30^{th} to the 31^{st} of May 2002)	86
Figure 6.4	A 3D surface to illustrate the diurnally corrected magnetic field strength for the horizontal sensor orientation test.	89
Figure 6.5	A 3D surface to illustrate the diurnally corrected magnetic field strength for the vertical sensor orientation test.	90
Figure 6.6	Maps of the diurnally corrected magnetic field strength (Log10). The different colour schemes are used to highlight different aspects of the data,	92
Figure 6.7	Maps of the diurnally corrected magnetic field strength (Log10) with different orientations. The different colour schemes are used to highlight different aspects of the data.	93
Figure 6.8	The interpretation map of the magnetic field overlaid onto the geological map produced in chapter 5.	94
Figure 6.9	Maps of the diurnally corrected magnetic field strength (nT) over an area near to Yubdo School.	96
Figure 6.10	A map of the diurnally corrected magnetic field strength	101

	(Log10) displayed as a 3D surface.	
Figure 6.11	An interpretation map of the features of the magnetic field over the Main Yubdo Intrusion.	101
Figure 6.12	Schematic map of the model proposed to explain the nature of the magnetic field over the Main Yubdo Intrusion.	101
Figure 7.1	A schematic diagram of the stucture of the lateritic soils in the WES.	103
Figure 7.2	The interface between the pristine (top left) and weathered bedrock (bottom right) in the opencast workings near Yubdo. The left of the photograph shows a quartz stockwork which resists weathering to a greater degree than the surrounding serpentinite.	103
Figure 7.3	A photograph indicating the position of the saprolite layer (white arrow). Variations in the thickness of the laterite as seen in the quarry near the summit at Daleti. The light coloured rock at the base is the pristine serpentinite, the red material at the top is the laterite layer and between these is the yellow saprolite layer.	104
Figure 7.4	The extensive laterite layer in the workings at Yubdo. The laterite seen here is over 15m in thickness and the base of the horizon (the saprolite) is indicated by the arrow.	105
Figure 7.5	The distribution of soil samples in the Tulu Dimtu area.	109
Figure 7.6	Arithmetic and Log_{10} transformed histograms of Ni in the soils of the Tulu Dimtu area. The grey lines indicate the class-boundaries used in figure 7.12 .	114
Figure 7.7	Arithmetic and Log_{10} transformed histograms of Cu in the soils of the Tulu Dimtu area. The grey lines indicate the class-boundaries used in figure 7.12 .	115
Figure 7.8	Arithmetic and Log_{10} transformed histograms of Cr in the soils of the Tulu Dimtu area. The grey lines indicate the class-boundaries used in figure 7.12 .	116
Figure 7.9	Arithmetic and Log_{10} transformed histograms of Al in the soils of the Tulu Dimtu area. The grey lines indicate the class-boundaries used in figure 7.12 .	117
Figure 7.10	Arithmetic and Log_{10} transformed histograms of Pt in the soils of the Tulu Dimtu area. The grey lines indicate the class-boundaries used in figure c.	118
Figure 7.11	Arithmetic and Log_{10} transformed histograms of Pd in the soils of the Tulu Dimtu area. The grey lines indicate the class-boundaries used in figure 7.12.	119
Figure 7.12 A-F	Six geological maps of the Tulu Dimtu area with symbols representing Ni, Cu, Cr, Al, Pt and Pd values in soil samples overlaid.	123
Figure 7.13	The distribution of soil samples in the Kingy area.	124
Figure 7.14	Arithmetic and Log_{10} transformed histograms of Ni in the soils of the Kingy area. The grey lines indicate the class-boundaries used in figure 6.20.	129
Figure 7.15	Arithmetic and Log_{10} transformed histograms of Cu in the soils of the Kingy area. The grey lines indicate the class-boundaries used in figure 6.20.	130
Figure 7.16	Arithmetic and Log_{10} transformed histograms of Cr in the soils of the Kingy area. The grey lines indicate the class-boundaries used in figure 6.20.	131
Figure 7.17	Arithmetic and Log_{10} transformed histograms of Al in the soils of the Kingy area. The grey lines indicate the class-boundaries used in figure 6.20.	132
Figure 7.18	Arithmetic and Log_{10} transformed histograms of Pt in the soils of the Kingy area. The grey lines indicate the class-boundaries used in figure 6.20.	133
Figure 7.19	Arithmetic and Log_{10} transformed histograms of Pd in the	134

	soils of the Kingy area. The grey lines indicate the class-boundaries used in figure 6.20.	
Figure 7.20 A-F	Six geological maps of the Kingy area with symbols representing Ni, Cu, Cr, Al, Pt and Pd values in soil samples overlaid.	138
Figure 7.21	The distribution of soil samples in the Daleti, Ankori, Tulu Kapi and Keley areas.	139
Figure 7.22	Arithmetic and Log_{10} transformed histograms of Ni in the soils of the Daleti, Ankori, Tulu Kapi and Keley areas. The grey lines indicate the class-boundaries used in figure 6.28.	144
Figure 7.23	Arithmetic and Log_{10} transformed histograms of Cu in the soils of the Daleti, Ankori, Tulu Kapi and Keley areas. The grey lines indicate the class-boundaries used in figure 6.28.	145
Figure 7.24	Arithmetic and Log_{10} transformed histograms of Cr in the soils of the Daleti, Ankori, Tulu Kapi and Keley areas. The grey lines indicate the class-boundaries used in figure 6.28.	146
Figure 7.25	Arithmetic and Log_{10} transformed histograms of Al in the soils of the Daleti, Ankori, Tulu Kapi and Keley areas. The grey lines indicate the class-boundaries used in figure 6.28.	147
Figure 7.26	Arithmetic and Log_{10} transformed histograms of Pt in the soils of the Daleti, Ankori, Tulu Kapi and Keley areas. The grey lines indicate the class-boundaries used in figure 6.28.	148
Figure 7.27	Arithmetic and Log_{10} transformed histograms of Pd in the soils of the Daleti, Ankori, Tulu Kapi and Keley areas. The grey lines indicate the class-boundaries used in figure 6.28.	149
Figure 7.28 A-F	Six geological maps of the Daleti, Ankori, Tulu Kapi and Keley areas with symbols representing Ni, Cu, Cr, Al, Pt and Pd values in soil samples overlaid.	152
Figure 7.29	The distribution of soil samples in the Yubdo, Andu and Sodu areas.	153
Figure 7.30	Arithmetic and Log_{10} transformed histograms of Ni in the soils of the Yubdo, Andu and Sodu areas. The grey lines indicate the class-boundaries used in figure 6.34.	158
Figure 7.31	Arithmetic and Log_{10} transformed histograms of Cu in the soils of the Yubdo, Andu and Sodu areas. The grey lines indicate the class-boundaries used in figure 6.34.	159
Figure 7.32	Arithmetic and Log_{10} transformed histograms of Cr in the soils of the Yubdo, Andu and Sodu areas. The grey lines indicate the class-boundaries used in figure 6.34.	160
Figure 7.33	Arithmetic and Log_{10} transformed histograms of Al in the soils of the Yubdo, Andu and Sodu areas. The grey lines indicate the class-boundaries used in figure 6.34.	161
Figure 7.34	Arithmetic and Log_{10} transformed histograms of Pt in the soils of the Yubdo, Andu and Sodu areas. The grey lines indicate the class-boundaries used in figure 6.34.	162
Figure 7.35	Arithmetic and Log_{10} transformed histograms of Pd in the soils of the Yubdo, Andu and Sodu areas. The grey lines indicate the class-boundaries used in figure 6.34.	162
Figure 7.36 A-F	Six geological maps of the Yubdo, Andu and Sodu areas with symbols representing Ni, Cu, Cr, Al, Pt and Pd values in soil samples overlaid.	166
Figure 7.37	A graph comparing the distribution of Ni in each of the four areas studied. For histograms further illustrating the data see individual sections.	167
Figure 7.38	A graph comparing the distribution of Cu in each of the four areas studied. For histograms further illustrating the data see individual sections.	168
Figure 7.39	A graph comparing the distribution of Cr in each of the four areas studied. For histograms further illustrating the data see individual sections.	168

Figure 7.40	A graph comparing the distribution of Al in each of the four areas studied. For histograms further illustrating the data see individual sections.	169
Figure 7.41	A graph comparing the distribution of Pt in each of the four areas studied. For histograms further illustrating the data see individual sections.	169
Figure 7.42	A graph comparing the distribution of Pd in each of the four areas studied. For histograms further illustrating the data see individual sections.	169
Figure 8.1	A graph of the cumulative percent (by rank) of the Mg values of the dunite samples from the Tulu Dimtu area.	181
Figure 8.2	The distribution of rock samples within the Tulu Dimtu area.	184
Figure 8.3	Graphs of Ni, Cu, Cr and Al versus Pt and Pd in the fresher rocks of the Tulu Dimtu area. The key to symbols in the top right corner.	193
Figure 8.4 A-F	Six geological maps of the Tulu Dimtu area with symbols representing Ni, Cu, Cr, Al, Pt and Pd values in rock samples overlaid.	213
Figure 8.5	The distribution of rock samples within the Kingy area.	214
Figure 8.6	Graphs of Ni, Cu, Cr and Al versus Pt in the fresher rocks from the Kingy area. No Pd has been detected in the Kingy area.	222
Figure 8.7 A-F	Six geological maps of the Kingy area with symbols representing Ni, Cu, Cr, Al, Pt and Pd values in rock samples overlaid.	229
Figure 8.8	The distribution of rock samples within the Daleti area, with a map of the Daleti Ultramafic inset.	231
Figure 8.9	Graphs of Ni, Cu, Cr and Al versus Pt in the fresher dunites from the Daleti Ultramafic.	240
Figure 8.10 A-F	Six geological maps of the Daleti, Ankori, Tulu Kapi and Keley areas with symbols representing Ni, Cu, Cr, Al, Pt and Pd values in rock samples overlaid.	247
Figure 8.11	The distribution of rock samples within the Yubdo area.	248
Figure 8.12	Graphs of Ni, Cu, Cr and Al versus Pt in the fresher rocks from the Main Yubdo Ultramafic.	255
Figure 8.13 A-F	Six geological maps of the Yubdo, Andu and Sodu areas with symbols representing Ni, Cu, Cr, Al, Pt and Pd values in rock samples overlaid.	262
Figure 9.1	SEM backscattered electron image of a zoned spinel mineral from sample KYC-007-01.	273
Figure 9.2	The concept of an alteration rim around a 3-dimensional spinel.	274
Figure 9.3	Graphs showing the effect of alteration on the spinels from the WES.	276
Figure 9.4	The differences between magamtic trends and alteration trends on a graph of spinel Fe^{2+}# versus Cr# values.	288
Figure 9.5 A-G	Graphs and map presenting the spinel geochemistry of the Tulu Dimtu area.	289
Figure 9.6 A-G	Graphs and map presenting the spinel geochemistry of the Kingy area.	295
Figure 9.7 A-G	Graphs and map presenting the spinel geochemistry of the Daleti, Ankori, Tulu Kapi and Keley areas. A larger scale map of the Daleti Ultramafic is provided.	306
Figure 9.8 A-G	Graphs and map presenting the spinel geochemistry of the Yubdo, Andu and Sodu areas. A larger scale map of the Daleti Ultramafic is provided.	313
Figure 9.9	The Cr# and Fe^{2+}# values of the spinels of the five ultramafic complexes of the WES compared to Alaskan-type intrusions and ophiolites.	315

List of Tables

Figure	Caption	Page
Table 2.1	Pt/Pd ratios for dunites in Alaskan-type intrusions and dunite pods in ophiolite complexes.	27
Table 4.1	The details of the aerial photographs.	51
Table 4.2	Relief Displacements of Yubdo Village and Sodu Ridge.	51
Table 4.3	The mapping parameters used in the study.	56
Table 4.4	Gully cross-sections and their related textures.	61
Table 4.5	A table of the photomorphic regions of the WES.	67
Table 6.1	A table of magnetic susceptibility values in order of decreasing susceptibility (after Robinson and Coruh, 1988).	98
Table 7.1	A summary of the Pt values in the soil samples from Tulu Dimtu.	110
Table 7.2	A summary of the Pd values in the soil samples from Tulu Dimtu.	110
Table 7.3	A summary of the Au values in the soil samples from Tulu Dimtu.	111
Table 7.4	A summary of the Ni values in the soil samples from Tulu Dimtu.	111
Table 7.5	A summary of the Cu values in the soil samples from Tulu Dimtu.	112
Table 7.6	A summary of the Cr values in the soil samples from Tulu Dimtu.	112
Table 7.7	A summary of the Al values in the soil samples from Tulu Dimtu.	113
Table 7.8	A summary of the Pt values in the soil samples from Kingy.	125
Table 7.9	A summary of the Pd values in the soil samples from Kingy.	125
Table 7.10	A summary of the Au values in the soil samples from Kingy.	126
Table 7.11	A summary of the Ni values in the soil samples from Kingy.	126
Table 7.12	A summary of the Cu values in the soil samples from Kingy.	127
Table 7.13	A summary of the Cr values in the soil samples from Kingy.	127
Table 7.14	A summary of the Al values in the soil samples from Kingy.	128
Table 7.15	A summary of the Pt values in the soil samples from Daleti, Ankoiri, Tulu Kapi and Keley.	140
Table 7.16	A summary of the Pd values in the soil samples from Daleti, Ankoiri, Tulu Kapi and Keley.	140
Table 7.17	A summary of the Au values in the soil samples from Daleti, Ankoiri, Tulu Kapi and Keley.	141
Table 7.18	A summary of the Ni values in the soil samples from Daleti, Ankoiri, Tulu Kapi and Keley.	141
Table 7.19	A summary of the Cu values in the soil samples from Daleti, Ankoiri, Tulu Kapi and Keley.	142
Table 7.20	A summary of the Cr values in the soil samples from Daleti, Ankoiri, Tulu Kapi and Keley.	142
Table 7.21	A summary of the Al values in the soil samples from Daleti, Ankoiri, Tulu Kapi and Keley.	143
Table 7.22	A summary of the Pt values in the soil samples from Yubdo, Andu and Sodu.	154
Table 7.23	A summary of the Pd values in the soil samples from Yubdo, Andu and Sodu.	154
Table 7.24	A summary of the Au values in the soil samples from Yubdo, Andu and Sodu.	155
Table 7.25	A summary of the Ni values in the soil samples from Yubdo, Andu and Sodu.	155
Table 7.26	A summary of the Cu values in the soil samples from Yubdo, Andu and Sodu.	156
Table 7.27	A summary of the Cr values in the soil samples from Yubdo, Andu and Sodu.	156

Table 7.28	A summary of the Al values in the soil samples from Yubdo, Andu and Sodu.	157
Table 7.29	The maximum Pt and Pd values found in the soils above the ultramafic complexes of the WES.	171
Table 8.1	Summary statistics of 41 analyses of the standard sample SARM7b.	174
Table 8.2	The weight percent of minerals dissolved by aqua regia (Chruch et al., 1987).	176
Table 8.3	Percentages of various metals leached by aqua regia from olivine and spinel relative to total recovery calculated from an HF-HNO3-NClO4 digestion (Chruch et al., 1987).	176
Table 8.4	A table of 48 analyses of the OMAC laboratories in-house standard with a summary of the ranges of values obtained and a measurement of precision.	177
Table 8.5	Typical values of Mg for selected fresh ultramafic lithotypes.	179
Table 8.6	Table 6.2: The ranges of Mg values used to define the fresher rock samples.	180
Table 8.7	The Mg values for the dunite samples in the Tulu Dimtu area before classification into fresher and altered.	181
Table 8.8	The numbers of samples from the different ultramafic complexes of the WES.	183
Table 8.9	A summary of the numbers and types of samples used in the four geographic areas in this study.	183
Table 8.10	A summary of the rock samples from the Tulu Dimtu area.	185
Table 8.11	Mg, Ni, Cu, Cr, Al, Pt and Pd values for the fresher samples.	185
Table 8.12	Mg, Ni, Cu, Cr, Al, Pt and Pd values for the altered samples collected from the Tulu Dimtu area.	187
Table 8.13	A summary of Ni, Cu, Cr and Al values in the dunite samples of highest Pt and Pd grade of the fresher rocks.	192
Table 8.14	Partition co-efficients of Ni between olivine and melt or host rock type.	196
Table 8.15	Partition co-efficients of Cr between olivine and melt or host rock type.	197
Table 8.16	Partition co-efficients of Cr between spinel or magnetite and melt or host rock.	197
Table 8.17	The range of Ni values in analyses of olivine minerals.	203
Table 8.18	A summary of the rock samples from the Kingy area.	215
Table 8.19	Mg, Ni, Cu, Cr, Al, Pt and Pd values for the fresher samples collected from the Kingy area.	215
Table 8.20	Mg, Ni, Cu, Cr, Al, Pt and Pd values for the altered samples collected from the Kingy area.	217
Table 8.21	A summary of Ni, Cu, Cr and Al values in the dunite samples with the highest Pt and Pd grade from the fresher rocks of the Kingy area.	221
Table 8.22	A summary of the rock samples from the Daleti, Ankori, Tulu Kapi and Keley areas.	232
Table 8.23	Mg, Ni, Cu, Cr, Al, Pt and Pd values for the fresher samples collected from the Daleti, Ankori, Tulu Kapi and Keley areas.	232
Table 8.24	Mg, Ni, Cu, Cr, Al, Pt and Pd values for the altered samples collected from the Daleti, Ankori, Tulu Kapi and Keley areas.	234
Table 8.25	A summary of Ni, Cu, Cr and Al values in the dunites of highest Pt and Pd grade from the fresher rocks within the Daleti Ultramafic.	239
Table 8.26	A summary of the rock samples from the Yubdo, Andu and Sodu areas.	249
Table 8.27	Mg, Ni, Cu, Cr, Al, Pt and Pd values for the fresher samples collected from the Yubdo, Andu and Sodu areas.	249
Table 8.28	Mg, Ni, Cu, Cr, Al, Pt and Pd values for the altered samples collected from the Yubdo, Andu and Sodu areas.	251
Table 8.29	A summary of Ni, Cu, Cr and Al values in the fresher samples	254

	from the Main Yubdo Ultramafic.	
Table 8.30	Partition co-efficients of Cu between olivine and clinopyroxene and melt or host rock type.	257
Table 8.31	The maximum Pt and Pd values found in the fresher rocks of the ultramafic complexes of the WES.	262
Table 8.32	The maximum Pt and Pd values found in the altered rocks from the ultramafic complexes of the WES.	265
Table 9.1	The molecules used in the estimation of Fe valency with the minerals they represent.	270
Table 9.2	A worked example of the method used to calculate Fe^{2+} and Fe^{3+}.	271
Table 9.3	The numbers of analyses at various stages of manipulation of the data.	272
Table 9.4	The numbers of analyses in the various ultramafic formations of the WES.	272
Table 9.5	The results of analyses of the cores and the zones immediately surrounding the cores of zoned spinels in sample KYC-007-01.	275
Table 9.6	The geochemistry of the spinels analysed from the Tulu Dimtu area in wt %.	280
Table 9.7	A table of the minimum Cr# values for spinel analyses from dunite and olivine-clinopyroxenite samples.	284
Table 9.8	The geochemistry of the spinels analysed from the Kingy area in wt %.	291
Table 9.9	The geochemistry of the spinels analysed from the Daleti, Ankori, Tulu Kapi and Keley areas in wt %.	298
Table 9.10	The minimum Cr# values for spinel analyses from the samples of the Daleti Ultramafic.	303
Table 9.11	The geochemistry of the spinels analysed from the Yubdo, Sodu and Andu areas in wt %.	308
Table 9.12	A summary of the rocks which host acceptable spinel analyses for each geographic area.	314
Table 12.1	A comparison of Pb Fire Assay results from analyses performed on the same samples from OMAC and Genalysis	335
Table 12.2	A table detailing the repeat analyses performed by OMAC during the course of the sample analysis.	335
Table 12.3	A table of analysis of the standard sample SARM7b with a summary of the ranges of values obtained and a measurement of precision.	336
Table 12.4	A table of analysis of the OMAC laboratories in-house standard with a summary of the ranges of values obtained and a measurement of precision.	337

1. Introduction

1.1. Introduction

The Western Ethiopian Shield (WES) is 500 km west of the capital Addis Ababa (see figure 1.2). It is a Neoproterozoic ancient mining district (United Nations, 1971; Jelenc, 1966) and the alluvial and eluvial deposits around the Yubdo ultramafic complex have been mined for Pt-Fe alloys and Au since 1926 (Mogessie and Belete, 2000). Yubdo forms part of a line of ultramafic complexes located along a NNE-SSW trending structure. The ultramafic complexes from the WES are (from north to south) Tulu Dimtu, Kingy, Daleti, Ankori and Yubdo (see figure 1.2). None of these bodies are mined on a commercial scale but Pt-Fe alloys are known in the surrounding placers. Most of the WES is only accessible on foot. The rocks are covered by a thick laterite which is frequently over 15m in thickness and exposure is generally less than 5%.

Ethiopia is covered by extensive Quaternary and Tertiary flood basalts. In some areas, the older rocks can be observed as inliers between these sequences (Mohr, 1983). The WES is one of such inliers and has been correlated northwards to join the Arabian Nubian Shield and southwards to the Mozambique belt, all of which form part of the East African Orogen. Johnson et al. (2004) believe that the WES records a history of crustal formation and deformation of around 500Ma in duration, this may have begun with a rifting event starting at around 900Ma (Stern, 1994). The eastern and western flanks of the WES are orthogneissic and they surround a central zone of volcano-sediments and ultramafics (Johnson et al., 2004). These ultramafic bodies are the subject of this thesis (see figure 1.2).

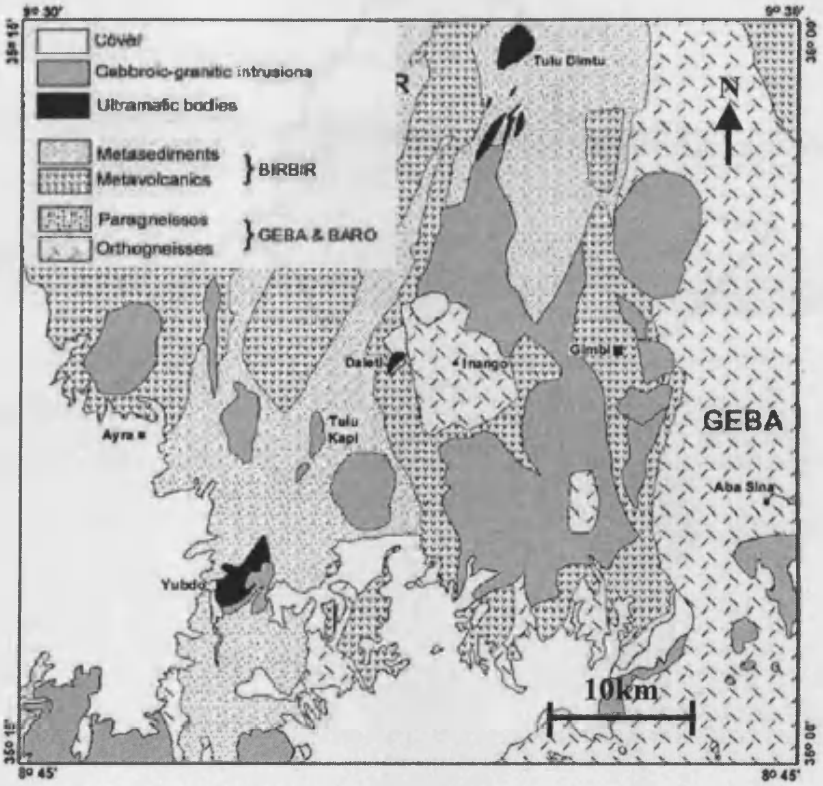

Figure 1.1: A geological map of the WES. (Johnson et al., 2004).

The southernmost ultramafic body (Yubdo) has been the subject of several publications (for a review see Mogessie et al., 1999). It is concentrically zoned with dunite at the core and clinopyroxenite on the outside (Kazmin and Demessie, 1971). The northernmost complex is also the subject of several petrological investigations (see Tadesse and Allen, 2005 and Sighinolfi et al., 1993). There are three additional, smaller, complexes which occur between Yubdo and Tulu Dimtu, these are Kingy, Daleti and Ankori which have been studied very little. All five bodies are highly altered and serpentinisation is greater than 50% in each case.

It is estimated that over 2700 kg of Pt has been mined from the laterites of the Yubdo area and an inferred resource of 20tons at a grade of $0.4g/m^2$ has been calculated (Mogessie and Belete, 2000). Although Pt-Fe nuggets are found in the rivers around the other five complexes, the origin of these grains is uncertain.

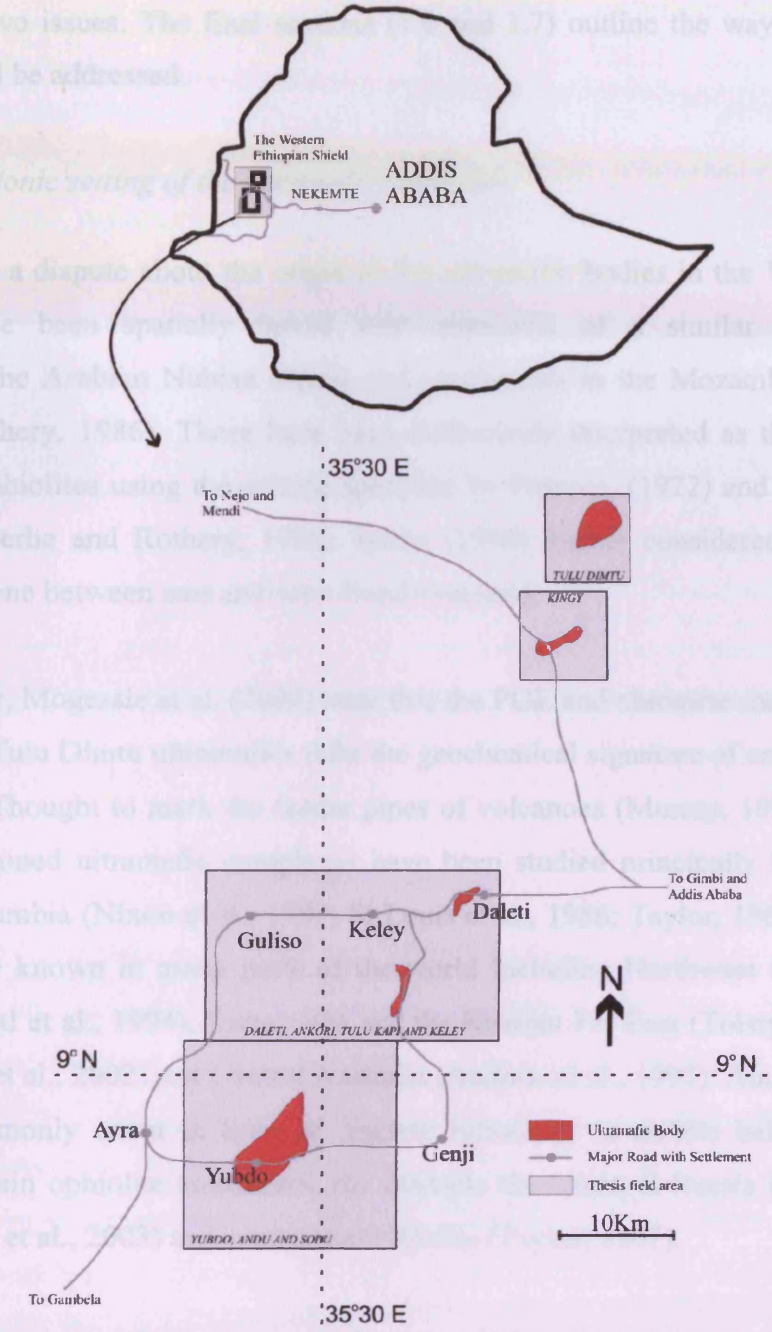

Figure 1.2: A map of the four field areas of this thesis, showing the largest ultramafic complexes and major roads and settlements. The map at the top of the figure is the outline of Ethiopia showing the location of the field area.

This thesis is intended to address two issues concerning the ultramafics in the WES. Firstly, there is a dispute over the tectonic setting of the complexes, many authors regard them to ophiolite complexes but others consider them to be Alaskan-type intrusions. Secondly, platinum group minerals (PGM) are extensively documented in the placers of the WES. However, little is known about the prospectivity of the primary mineralisation. The next two sections (1.2 and 1.3)

introduce the two issues. The final sections (1.6 and 1.7) outline the way in which these issues will be addressed.

1.2. The tectonic setting of the ultramafic complexes

There is a dispute about the origin of the ultramafic bodies in the WES. The complexes have been spatially linked with intrusions of a similar petrology northwards in the Arabian Nubian Shield and southwards in the Mozambique belt (Berhe and Rothery, 1986). These have been collectively interpreted as the mantle sequences of ophiolites using the criteria specified by Penrose, (1972) and structural observations (Berhe and Rothery, 1986). Berhe (1990) further considered these to mark a suture zone between east and west Gondwanaland.

However, Mogessie et al. (2000) state that the PGE and chromite chemistry of the Yubdo and Tulu Dimtu ultramafics infer the geochemical signature of an Alaskan-type intrusion. Thought to mark the feeder pipes of volcanoes (Murray, 1972), these concentrically zoned ultramafic complexes have been studied principally in Alaska and British Columbia (Nixon et al., 1997; St Louis et al., 1986; Taylor, 1967; Johan, 2002). They are known in many parts of the world including Northwest Columbia (Tistl, 1994, Tistl et al., 1994), Kamchatka and the Russian Far East (Tolstykh et al., 2000; Tolstykh et al., 2002) and Central Australia (Andrew et al., 1995). Alaskan-type complexes commonly occur in lines of discrete intrusions in mobile belt settings which also contain ophiolite complexes, for example the Urals, E Russia (Garuti et al., 1997; Garuti et al., 2003) and southeastern Alaska (Taylor, 1967).

Mogessie et al. (2000) suggested that an Alaskan-type intrusion origin for these bodies indicates that the Mozambique belt and Arabian Nubian Shield are not spatially linked and may only have an inter-fingering relationship.

This thesis includes an extensive study of the spinel geochemistry from the ultramafic samples throughout the WES (chapter 7). The results are compared with published spinel analyses from Alaskan-type intrusions and ophiolites worldwide.

1.3. The development of Pt and Pd

Research into Pt and Pd in the area has focused on studies of placer platinum group minerals (PGM) from the Yubdo area (see Belete et al., 2000 and Mogessie et al., 1999). Further mineralogical studies have characterized some PGM from serpentinised dunite within drill core (Mogessie et al., 1999). The only published geochemical work on the area is that of Mogessie et al. (1999) and Signolfi et al. (1993). Both studies discuss the likely effect of serpentinisation and comment only briefly on the mechanisms by which Pt and Pd may have become concentrated into the primary rocks before alteration.

An assessment of the geochemistry of altered ultramafic rocks with fresher rocks is included in this thesis (chapter 6). This may uncover some of the ore forming processes by which Pt and Pd may have been concentrated and hence develop future targets for exploration.

1.4. The mining history of the WES

Although it has been speculated that platinum grains from Yubdo were used to decorate objects in Egypt in the 7th century BC (Mogessie and Belete, 2000), the platinum deposit at Yubdo is generally regarded to have been discovered by a Russian missionary sometime in the early 20th century. In their account of the mining history of the area, Mogessie and Belete (2000) state that large scale extraction did not begin until 1926. Mining was conducted initially under a French company, which was then taken over by and Italian firm and by 1941 the mine was in the hands of the government. During the 1960's some mining and exploration was carried out by the Duval corporation. At the time of writing mining licences for the Yubdo and Sodu areas are held by Golden Prospect Mining (Ethiopia) Ltd, a wholly owned subsidiary of Golden Prospect Plc.

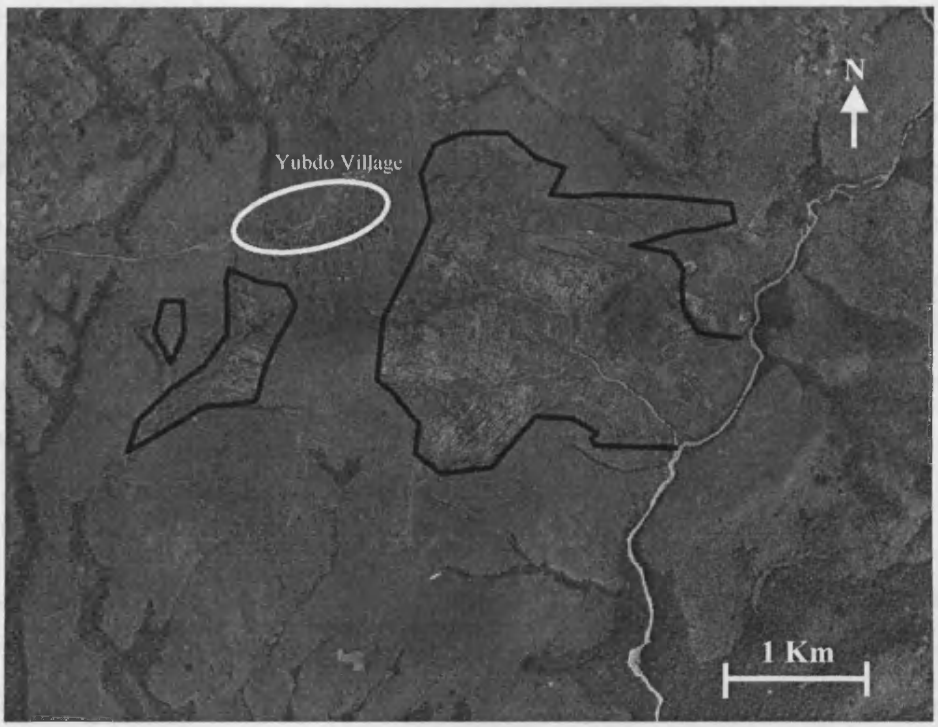

Figure 1.3: An aerial photograph of the opencast workings of the laterite in the Yubdo area (within the black lines) in 1957. The bright line is the course of the Birbir river.

The mining was conducted in two large open pits (see figure 1.3). In 2001, mining was conducted by pumping water into reservoirs high up in the soil profile. This water is then released and allowed to flow through the laterite where the soil particles are then taken into suspension. These waters then flow through a sluice system whereby selected fractions are panned to produce a concentrate. A study of the effectiveness of these systems was performed by Childs (2001). In the past these methods have been assisted by the use of monitors and also shaker tables (Mogessie and Belete, 2000).

Artisanal mining of both platinum group minerals and Au grains from stream sediments is common throughout the WES. It is not possible to determine when this practice started, the skill of panning has been past down through several generations of the local people. During the course of the fieldwork conducted for this project, Tan Range Exploration Corporation owned exploration licences for the area around Tulu Kapi and the eastern half of the Tulu Dimtu Main Intrusion.

1.5. The conduct of the study

This project was conducted in co-operation with and partially sponsored by Golden Prospect Mining Co Ltd (GPM). As a result these circumstances, there were certain constraints on the way in which the work could be performed. As detailed in chapters 7 and 8, many samples were collected and analysed for a suite of chemical elements. Although the author participated in the exploration programme which collected the samples, the geochemical analysis was conducted without his involvement.

Three bore-holes were sunk into the Yubdo Main Intrusion by the Duval corporation in 1969 (for a review see section 2.3.5). Studies of these cores were performed by Mogessie et al. (1999) and Belete et al. (2000). The rock retrieved by this method has been kept in archive by the Ethiopian Ministry of Mines and was available for study by members of the GPM team. Some geochemical analyses were performed on a few grab samples from within the core. A description of the core itself was not included within this study as this work had already been performed by other workers (see above). Furthermore, the manner in which samples had been taken from the drill-core meant that a scientific analysis of the geochemical variations was not possible.

1.6. Aims and methods used in the thesis

This thesis aims to use Ni, Cu, Cr, Al and Mg to investigate the differences in geochemistry between altered and fresher ultramafic rocks and hence suggest the mechanisms by which Pt and Pd have been concentrated. Furthermore, it aims to use spinel geochemistry investigate the tectonic origin of the ultramafic complexes of the WES with particular reference to Alaskan-type intrusions and ophiolites. The methods used for each theme are summarized as follows.

In chapter 8, the distribution of Ni, Cu, Cr, Al, Pt and Pd in the ultramafics is examined. The rocks are classified as fresher or altered (see section 8.3.1). The disitribution of these elements has lead to the development of ideas about potential magamtic and post-magmatic ore forming processes. These allow an assessment of

the prospectivity of the ultramafic bodies of the WES and the identification of possible exploration targets. To compliment this, a discussion of the possible factors affecting the distribution of Pt and Pd in the overburden of the WES is also included (see chapter 7).

To evaluate the tectonic origin of the ultramafic complexes, the geochemistry of spinels is studied (see chapter 7). The results of this analysis are compared with published spinel analyses from Alaskan-type intrusions and ophiolites. Furthermore, the relative influence of alteration and magmatic processes is evaluated using core and rim analyses and comparison with published work.

1.7. Layout of the thesis

In order to fulfill the above aims, chapter 2 describes the geological background to the area, introduces Alaskan-type intrusions and ophiolites, and discusses the key differences between them. Subsequently, chapter three describes the alteration to which the rocks have been exposed and the key minerals of interest to the thesis. Chapters 4 and 5 show the production of geological base-maps for the subsequent chapters using the analysis of terrain and geological observations. To support an understanding of the alteration processes in the Main Yubdo Intrusion, a magnetic survey was carried out, this is described in chapter 6. As a way of understanding the redistribution of the pathfinder elements in the overburden, chapter 7 describes the geochemistry of the soils. Chapter 8 describes an attempt to use rock geochemistry to ascertain the prospectivity of the complexes. Following this, the geochemistry of spinels is described in chapter 9 in order to investigate the tectonic origin of the complexes.

Each results chapter (4, 5, 6, 7, 8 and 9) considers each of the four geographic areas shown in figure 1.2 in turn. At the end of each results chapter the conclusions from all four areas is compared. Finally, in chapter 9 the conclusions for each method are summarized for each geographic area.

2. Literature Review

2.1. Introduction

Due to its position within the large Precambrian shield that extends from Egypt to Mozambique there have been several studies of the structural aspects of the WES. These are used in section 2.2 to set this thesis into context within East Africa. Studies of the ultramafic rocks in the area are less common, although there is an abundance of petrological studies which have been undertaken and these are reviewed in section 2.3. Two preliminary geochemical studies have been published and section 2.3 describes these along with a review of the research published on the famous Pt-Fe nuggets from Yubdo (see section 2.3.5)

An important theme of this thesis is the question of the tectonic origin of the ultramafic complexes. Section 2.4 introduces the structure, petrology, mineralogy and geochemistry of the Alaskan-type intrusions and ophiolite complexes and proposes several differences that may be used to distinguish the two.

2.2. Geological Setting

Most of Ethiopia is covered by Tertiary or Quaternary volcanic flood basalt sequences. The area of western Ethiopia examined in this thesis occurs within a window through this basalt plateau which allows the underlying Precambrian basement to be observed (United Nations, 1971). This 100 by 300 kilometer inlier is a N-S trending mobile belt hosting: metavolcano-sedimentary sequences, zones of gneiss and migmatite and the ultramafic complexes that are the subject of this study.

Using remote sensing, Berhe and Rothery (1986) linked the ultramafic complexes in western Ethiopia with those further north and south in East Africa and identified the position of five N-S trending sutures in this part of East Africa. In his discussion of the tectonic consequences, Berhe (1990) considers that these sutures with remnant ophiolites

represent the remnants of back arc basins, supra-subduction zones and sutures between two continental blocks. Berhe (1990) identified the Baraka – Yubdo - Sekerr suture (which includes the ultramafic complexes in this study) as being juxtaposed against a similar suture from Eastern Sudan that may continue southward into Tanzania. Satellite interpretation has shown that the structure continues northwards to Baraka in NE Sudan and Eritrea (Berhe and Rothery, 1986).

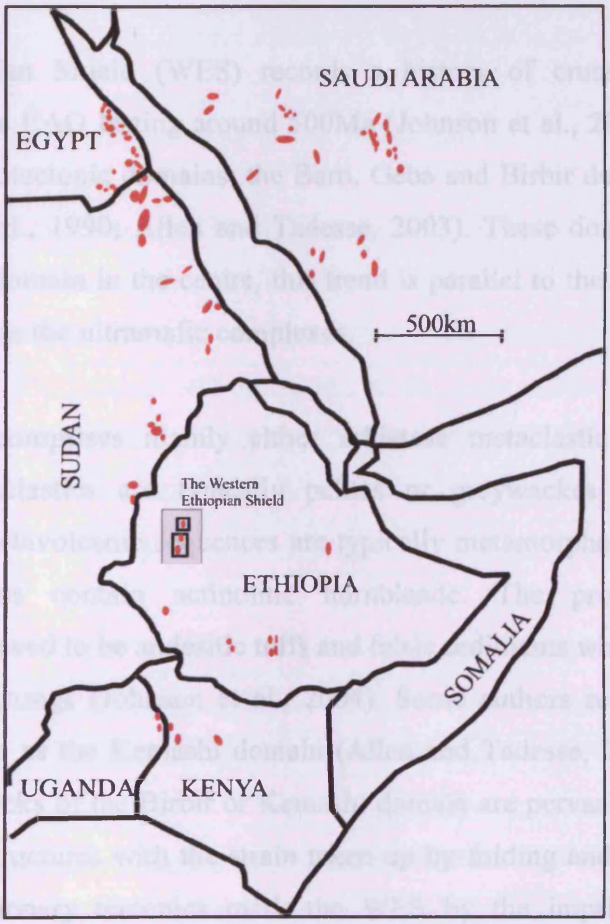

Figure 2.1: The "ophiolite belts" of northeast Africa (modified after Berhe, 1990).

The ultramafic complexes covered by this study are located within the the Western Ethiopian Shield (WES) which itself forms part of the greater East African Orogen (EAO). The deformational history of the EAO is divided into two phases: structures associated with collision and post accretionary structures (Abdelsalam and Stern, 1996). Of the collisional structures, two suture types are identified: arc-arc and arc-continental.

The Baraka – Yubdo – Sekerr suture is the result of the accretion of two arc terranes (Abdelsalam and Stern, 1996). The deformation within this suture is characterized by north trending sinistral transpression. Arc-arc sutures in the EAO typically have nappes containing ophiolitic material associated with them, and these were steepened by upright folding during the final stages of collision (Abdelsalam and Stern, 1996). Another aspect of the post accretionary deformation is the development of northwest trending strike slip faults and shear zones (Belete et al., 2000; Abelsalam and Stern, 1996).

The Western Ethiopian Shield (WES) records a history of crustal formation and deformation within the EAO lasting around 500Ma (Johnson et al., 2004). The shield is divided into three lithotectonic domains: the Baro, Geba and Birbir domains (Johnson et al., 2004; Ayalew et al., 1990; Allen and Tadesse, 2003). These domains strike NNE-SSW with the Birbir domain in the centre, this trend is parallel to the trend of the EAO. The Birbir domain hosts the ultramafic complexes.

The Birbir domain comprises mainly either schistose metaclastic or metavolcanic sequences. The metaclastics are typically pelites or greywackes with intercalated metavolcanics. The metavolcanic sequences are typically metamorphosed to greenschist facies and sometimes contain actinolitic hornblende. The protoliths for such metavolcanics are believed to be andesitic tuffs and felsic sediments which are commonly associated with arc settings (Johnson et al., 2004). Some authors refer to the domain hosting the ultramafics as the Kemashi domain (Allen and Tadesse, 2003; Tadesse and Allen, 2005). These rocks of the Birbir or Kemashi domain are pervasively deformed by NNE-SSW trending structures with the strain taken up by folding and westerly directed thrusting. Post accretionary tectonics mark the WES by the imprint of NNE-SSW transcurrent shearing and strike-slip faulting on top of the earlier N-S directed folds (Johnson et al., 2004). The shear zones related to this late stage of deformation appear to have been the conduits for hydrothermal fluids and further north in Baruda these deform the flanks of the mafic-ultramafic complexes (Braathen et al., 2001).

2.3. Previous Work on the Ultramafics of the WES

2.3.1. Introduction

Studies of the ultramafic rocks in the WES fall into two categories. Some authors consider the ultramafic complexes together and relate them to the other lithological and structural domains in the region. Other studies have focused on the individual bodies. In the following sections, the regional studies including the ultramafics are described and then an account of the work on individual ultramafic complexes is summarised.

2.3.2. Regional Studies of the Ultramafic bodies

The Yubdo complex is considered to be the southernmost ultramafic body in the WES. There are several more bodies north of Tulu Dimtu (these are not covered in this study). These additional bodies include: Jaja Kubsa (Alemu and Abebe 1998), Korka Meti (Alemu and Abebe, 1999; Tadesse and Allen, 2005) and Baruda (Braathen et al., 2001; Allen and Tadesse, 2003). The publications summarized in this section treat all complexes together and therefore some observations described may have originated from outside the coverage area of this study.

There is a general consensus that the ultramafic complexes studied here are elongate and occur in a zone associated with metavolcanics and metasediments (Johnson et al., 2004; Allen and Tadesse, 2003; Alemu and Abebe, 1998; Warden et al., 1982). The bodies are orientated parallel to the regional tectonic fabric (NNE-SSW). Allen and Tadesse (2003) report the presence of associated gabbros, diorites and plagiogranites. One publication states that the terrain associated with the ultramafic units is low-lying with some elevated areas where the rocks are less altered (Tadesse and Allen, 2005) but another reports that the ultramafics form prominent ridges almost devoid of vegetation (Alemu and Abebe, 1998).

Altered dunites and pyroxenites have been observed in all studies of petrology. Several publications report that the dunites are completely serpentinised, however, Alemu and

Abebe (1998) also report that fresh olivine is present at up to 20% in some samples. Furthermore, Tadesse and Allen (2005) describe metre-scale blocks of harzburgite, lherzolite and wehrlite within ultramafic schists. Warden et al. (1982) observed a relict cumulate texture in some samples from the WES. Tadesse and Allen (2005) also report only partial replacement towards the centre of the ultramafic masses. Alteration minerals such as talc and carbonate are found along thrust faults and shear-zones and also in rims around massive serpentinite blocks (Alemu and Abebe, 1998; Warden et al., 1982). Pyroxenite samples show variable alteration to chlorite, albite, epidote and sometimes actinolite (Johnson et al., 2004). Furthermore, pyroxene psedomorphs containing secondary hornblende suggests lower amphibolite facies metamorphism (Warden et al. 1982). In most publications, the strongest alteration is reported closest to fault or shear-zones. All descriptions of petrology report the presence of magnetite and chromite.

An account of the whole-rock geochemistry of the ultramafic rocks in the WES is provided by Warden et al. (1982) and is accompanied by a comprehensive study of alteration petrology. Chondrite normalized REE analyses show that the intrusive ultramafic rocks of the area have a very strong LREE enrichment and HREE depletion.

2.3.3. Tulu Dimtu and Kingy

This section covers Tulu Dimtu and Kingy together. This is because the publications summarized here do not distinguish between the two and they are jointly referred to as "Tulu Dimtu". Later in this thesis these two areas are described separately.

The Tulu Dimtu area was mapped at a scale of 1:50,000 by de Wit and Aguma (1977), they identified a large mass of partially serpentinised dunites surrounded by serpentinite schists. They also identified a zone of other more elongate bodies which extend southwards into the Kingy area. Many accounts comment on the fact that the largest ultramafic body in the area stands out as a conspicuous hill which is barren of vegetation. The rocks forming this large hill are referred to in this study as the Tulu Dimtu Main Intrusion.

The most comprehensive study of the petrology of the Tulu Dimtu area is that of de Wit and Aguma (1977), but further descriptions are given by Sighinolfi et al. (1993) and Alemu and Abebe (1998). The lithologies discovered in the Tulu Dimtu and Kingy areas include dunite, olivine-clinopyroxenite and hornblendite. Serpentinisation is never reported at less than 80% and it is often over 95% (de Wit and Aguma, 1977; Signolfi et al., 1993). The relict outlines of forsteritic olivine crystals with diameters of 0.2-0.5mm are observable and olivines can be observed now as chrysotile mesh and window structures. Fine grained magnetite occurs along silicate grain boundaries and Cr-spinel and chromite are also present. Furthermore, de Wit and Aguma (1977) describe original "magmatic" (sic, see chapter 3) galena and barite crystals within dunite. The olivine-clinopyroxenites include clinopyroxene crystals of up 0.5mm which all have tremolitic rims. There are believed to have been at least two phases of alteration which include one of serpentinisation and a separate silicification phase (de Wit and Aguma, 1977; Alemu and Abebe, 1998).

A study of the geochemistry of the rocks in the Tulu Dimtu complex was undertaken by Sighinolfi et al. (1993). The PGE analysed from serpentinised dunites were depleted with respect to chondrite, but Pt was found to be more enriched than the other elements. Furthermore, Sighinolfi et al. (1993) only found significant PGE values in serpentinised dunites and the silicified equivalents were almost barren. Although Ni is reported to increase with serpentinisation, the distribution in the altered lithotypes is similar to that of the less altered rocks suggesting that Ni remobilization is a local effect (Sighinolfi et al, 1993). A depletion in Cu values with serpentinisation led Sighinolfi et al. (1993) to suggest that serpentinisation had removed sulphides and chalcophile elements from the complex.

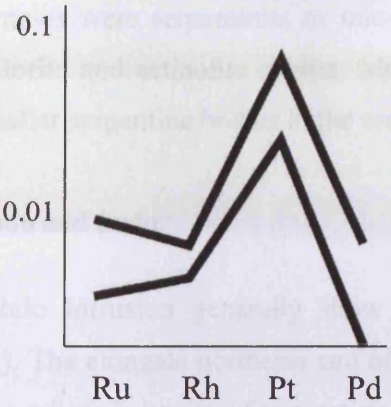

Figure 2.2: The average chondrite normalized Ru, Rh, Pt and Pd analyses for dunite from the Tulu Dimtu area (Sighinolfi, 1993).

2.3.4. Daleti, Ankori, Tulu Kapi and Keley

The ultramafics at Daleti (refered to in this study as the Daleti Ultramafic) occur in two parts, firstly a prominent ridge trending NE-SW and secondly a lower-lying area to the northeast (United Nations, 1971). The ridge is barren of vegetation. A report by the United Nations (1971) suggests that these two areas are offset by intersection faults and at least partially surrounded by diorites and gabbros. Athough the limited exposure only shows serpentinised dunite, a drill-hole has revealed an alternation of dunite and peridotite bands (Mogessie and Hoinkes, 1998). These bands are believed to be "concentric zoning" (United Nations, 1971).

The petrology of the ultramafic samples often reveals completely serpentinised rocks (United Nations, 1971; Mogessie and Hoinkes, 1998). However relict olivine grains can sometimes be observed with a mesh of chrysotile and antigorite. Fine grained magnetite and chromite is sometimes observed (Mogessie and Hoinkes, 1998). The faulted eastern contact of the intrusion is rich in hydrous alteration minerals such as talc, talc-serpentine, chlorite and chlorite-serpentine (United Nations, 1971). Birbirite can be found on the crest of the ridge (see chapter 3 for a definition of birbirite).

The United Nations report (1971) briefly mentions the Ankori Ultramafics near the road from Tulu Kapi to Genji. No fresh rocks were observed by the team of the United

Nations (1971) and most samples were serpentinite or talc-serpentine. The complex is reported to host lenses of chlorite and actinolite schists. Mogessie and Hoinkes (1998) also report the presence of smaller serpentine bodies in the area.

2.3.5. Yubdo, Andu and Sodu

The maps of the Main Yubdo Intrusion generally show a "pear" shaped intrusion (Kazmin and Demessie, 1971). The elongate northeast end of the intrusion forms a NNE-SSW trending prominent ridge which is barren of vegetation. The United Nations (1971) report that the eastern contact of the intrusion dips gently to the east and that further ultramafics to the north are caps of the same intrusion. The western contact is reported to be a steeply dipping thrust fault associated with shearing (United Nations, 1971). A system of NNE-SSW trending "en-echelon" shear-zones is said to cross-cut the centre of the complex. Furthermore, a set of WNW-ENE transcurrent faults are recorded that are frequently associated with both shearing and quartz-veins. The ultramafics are found to be zoned having dunite at the core, with peridotite then pyroxenite surrounding it (United Nations, 1971; Mogessie and Hoinkes, 1998). Some peridotites are found to be intercalated with dunite in the eastern and southern parts of the intrusion (Mogessie et al., 1999). Several cross-cutting diorite dykes are reported (United Nations, 1971). Most of the geological features recorded in the literature are also mentioned in a drilling report by the Duval Corporation (Howell, 1969). All the drill holes were sunk into the dunite zone and they only intersected dunite and peridotite layers. The drill core also intersected hairline magnetite veinlets which extend along fault zones and talc-chlorite dykelets.

There are two large studies of the petrology (United Nations, 1971 and Mogessie and Hoinkes, 1998) and these are supplemented by the work of Belete et al. (2000) and Mogessie et al. (1999). All studies report that the central dunites are serpentinised to a large degree and a relict cumulate texture can be observed (Mogessie and Hoinkes, 1998; Mogessie et al., 1999). The olivines have a forsterite content of 81-84% (Mogessie et al., 1999) and are typically rimmed by talc, carbonate and opaque minerals. Pyroxene is mainly diopside and is associated with chlorite. The United Nations report (1971)

commented that pyroxenes tend to be coarser than olivine minerals and are often found with tremolite and chlorite. Euhedral and subhedral chromites with altered rims can be observed in all the ultramafic host rocks. The United Nations (1971) report the occurrence of pyrite and arsenopyrite in the shear-zone on the northeastern contact of the intrusion.

Platinum-group minerals (PGM) have been found in both the rocks and placers around Yubdo. The two largest petrological studies report sperrylite ($PtAs_2$) in both dunite and pyroxenite (United Nations, 1971; Mogessie and Hoinkes, 1998). Furthermore, Augustithis (1965) discovered sperrylite in birbirite samples. The more systematic accounts of primary PGM in the area are of Pt-Fe nuggets in both chromite and serpentinite (Belete et al., 1999; Belete et al., 2002). These were discovered in the boreholes sunk by the Duval Corporation (Howell, 1969). The Pt-Fe alloys in the chromite appear to be rounded in shape and contain minor Ir (Mogessie et al., 1999). The Pt-Fe alloys (with minor Rh and Cu) found in the serpentinites are reported to be elongate and between 20μm and 30μm (Mogessie et al., 1999).

The placer Pt-Fe nuggets from Yubdo historically generated controversy over the formation of Pt-nuggets (Bowles, (1986); Hattori and Cabri, 1992). All nuggets reported from Yubdo are Pt-Fe (isoferroplatinum and tetraferroplatinum) in composition and Belete et al. (2000) analysed a wide variety of inclusions from these nuggets. The most abundant inclusions found were hollingworthite (RhAsS), genkinite ($(Pt,Pd)_4Pb_3$), irarsite (IrAsS), platarsite (PtAsS) and native Os.

2.4. Alaskan-type intrusions versus ophiolites

2.4.1. Introduction

Alaskan-type complexes and ophiolites represent different tectonic settings and have differing implications for mineralisation. Ophiolites are fragments of ancient oceanic lithosphere now emplaced on land at fossil subduction zones (eg Gass, 1990). The setting of Alaskan-type complexes is less well defined. There have been many attempts to

explain the characteristics of Alaskan-type intrusions (see Johan, 2002). The generally accepted model is that they originate as the feeder pipes of volcanoes in continental subduction zones (Murray, 1972).

Both comprise mafic and ultramafic sequences and considering the two genetic models, it may at first glance be hard to understand why the two may be confused. However the various modifications and complications of the models result in some overlap in structure, petrology, mineralogy and geochemistry. The ophiolite descriptions given here focus on the Troodos massif of Cyprus and the Semail nappe in eastern Arabia, as these provide the best exposed and studied complexes.

2.4.2. Scale of Alaskan-type intrusions and ophiolites

Complete ophiolite complexes typically consist of a basaltic unit predominantly composed of up to 0.5 to 1 km thickness of pillow lavas and sheeted dykes. This in turn is underlain by plutonic gabbro and ultramafic crustal units which in the Oman ophiolite make up a total of 3.6 km in thickness (Nicolas et al., 1996) and lie on top of mantle lherzolite or harzburgite which may also be several km thick. These sequences extend along strike for 450km (Lippard et al., 1986). Ophiolites are often truncated at the base by a thrust, below which is a metamorphic aureole that continues into lower grades of metamorphism away from the contact with the ophiolite (Gass, 1990).

In contrast, Alaskan-type intrusions are concentrically zoned with dunite in the centre grading outwards to clinopyroxenite and hornblendite, they are often associated with an outer gabbro zone. In many cases, one or more of these zones may be missing from the complex. The two largest Alaskan-type intrusions include Nizini Tagil ($70km^2$) and Tulameen ($80km^2$), but most range between $12km^2$ and $40km^2$ (Johan, 2002).

Both ophiolites and Alaskan-type intrusions are commonly highly fragmented. The Troodos and Oman complexes display the full lithological sequence and both are exposed over several hundreds of square kilometers. However, most ophiolites are much smaller,

are frequently highly deformed and occur in fault bounded blocks. The primary igneous textures of ophiolites are offset and juxtaposed against country rocks by thrust faulting related to their emplacement onto continental crust. Similarly, Alaskan-type complexes such as the Hickman and Polaris, British Columbia (Nixon et al., 1997) are highly disrupted by faulting and other types of deformation. There are further complications in that the proportions and sizes of primary igneous lithologies in Alaskan-type complexes may vary. The complete zonal structure of Alaskan-type intrusions is only seen in a few localities such as the Konder and Inagli intrusions of the Aldan shield, Eastern Siberia (Malitch, 1991) and Alto Condoto complex in NW Columbia (Tistl et al., 1994; Tistl, 1994). Konder and Inagli show central dunite cores comprising 60% of the total volume whereas in the Alto Condoto complex the dunite occupies around 20% of the intrusion. As with ophiolites, Alaskan-type complexes may either have one or more zones missing and/or the zonal structure could be disrupted by deformation. In some cases the central dunite core is missing, such as in the Duke Island western body (Taylor, 1967), Gnat Lakes and Menard Creek (Nixon, 1997). In others, there is no clinopyroxenite zone as in Duke Island East, Annette Island and Blashke Island (Taylor, 1967).

2.4.3. Structure of Alaskan-type intrusions and ophiolites

The large components of ophiolites (described above) cover much larger areas than those of Alaskan-type complexes. However, smaller features of fragmented ophiolites may resemble Alaskan-type intrusions (see figure 2.3). Lippard et al. (1986) and Robertson and Xenophontos (1993) describe how the ultramafic rocks of ophiolites within smaller features occur as three distinct lithological associations:

- The Mantle sequence: a residual suite of massive lherzolite or harzburgite frequently containing dunite pods.
- The Crustal layered sequence: a rhythmically layered series of dunite, wherlite and pyroxenite.
- The Late intrusive complexes: usually composed of wehrlite, peridotite or gabbro; these plutonic bodies intrude the crustal sequence.

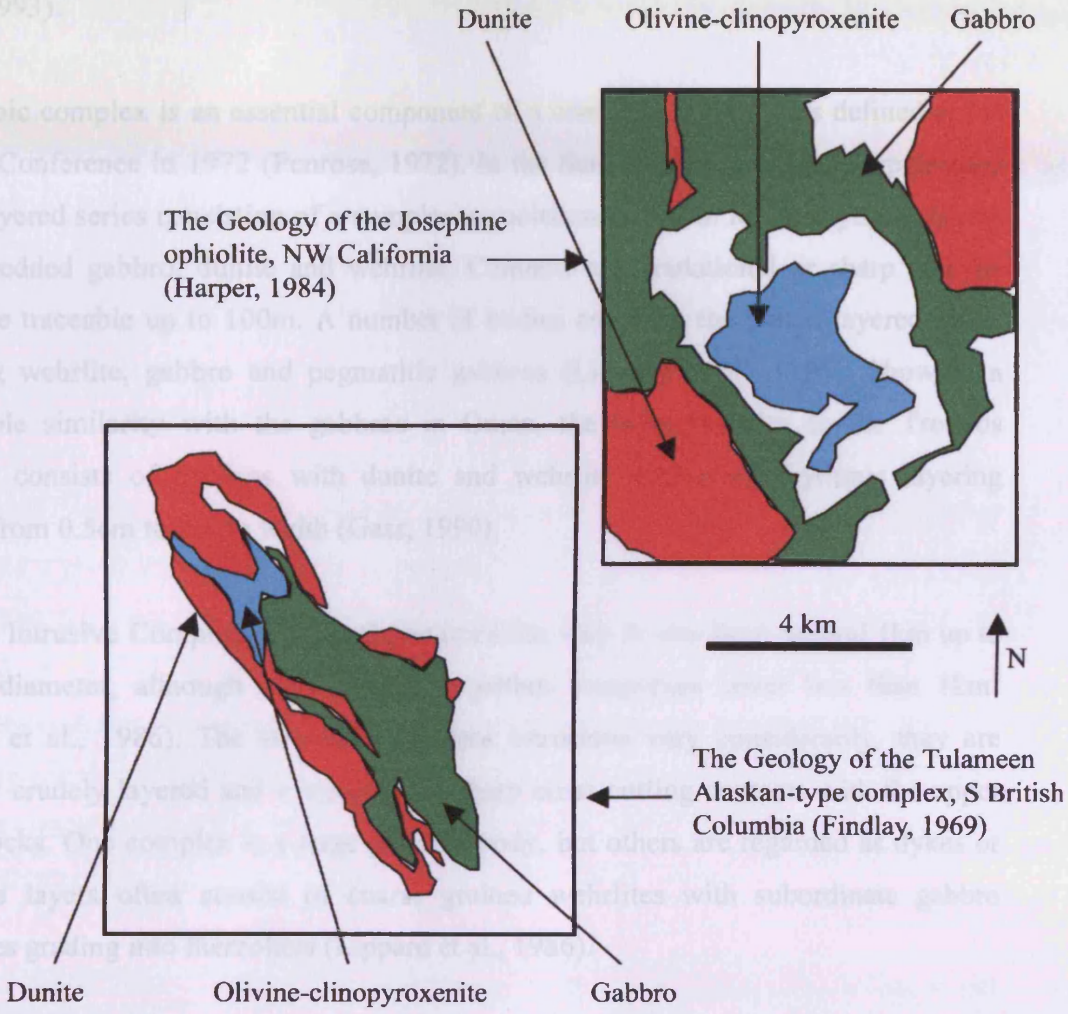

Figure 2.3: Schematic diagrams of the mafic and ultramafic units of the Josephiene Ophiolite and Tulameen Alaskan-type intrusion showing similar zoned outcrop patterns (modified from Findlay, 1969 and Harper, 1984).

Dunite bodies are common in the uppermost parts of the mantle sequence (Roberts and Neary, 1993; Gass, 1990). These bodies have relatively sharp interfingering contact relationships with the enclosing harzburgite (Gass, 1990). They are irregular with anastomosing offshoots. The more tectonised bodies, closer to the paleo Moho, are more elongate (Lippard et al., 1986). In the Oman ophiolite, dunites are generally under 100m in length but extremely tectonised and elongate bodies can be up to 14km in length Lippard et al., 1986). The dunites themselves envelop nodular, massive and schlieren

chromitite deposits, these display a gradational relationship with their host (Roberts and Neary, 1993).

A gabbroic complex is an essential component of a complete ophiolite as defined at the Penrose Conference in 1972 (Penrose, 1972). In the Semail ophiolite this is represented by the layered series consisting of a complex association of 0.5cm to 2m rhythmic layers of interbedded gabbro, dunite and wehrlite. Contacts are gradational or sharp and the layers are traceable up to 100m. A number of bodies cross-cut the Oman layered series including wehrlite, gabbro and pegmatitic gabbros (Lippard et al., 1986). Showing a remarkable similarity with the gabbros in Oman, the layered series in the Troodos ophiolite consists of gabbros with dunite and wehrlite displaying rhythmic layering ranging from 0.5cm to 2m in width (Gass, 1990).

The Late Intrusive Complexes in the Oman ophiolite vary in size from around 1km up to 5km in diameter, although some peridotite-gabbro complexes cover less than $1km^2$ (Lippard et al., 1986). The structures of these intrusions vary considerably, they are generally crudely layered and irregular with sharp cross-cutting contacts with the upper crustal rocks. One complex is a large plutonic body, but others are regarded as dykes or sills. The layers often consist of coarse grained wehrlites with subordinate gabbro sometimes grading into lherzolites (Lippard et al., 1986).

In contrast to the layering in ophiolites, Alaskan-type intrusions exhibit a pipe-like concentrically zoned structure with a dunite core (Taylor, 1967; Johan, 2002). The idealized sequence displays dunite surrounded successively by clinopyroxenite, hornblendite and monzonite-gabbro rims. The contacts at the rim of the dunite core of and Alaskan-type complex are typically gradational and it is common to find olivine-bearing clinopyroxenite rafts. However, dunite to clinopyroxenite contacts in ophiolites can be either sharp or gradational. The contact between Alaskan-type gabbro zones and the associated ultramafics is normally sharp (Johan, 2002; Taylor, 1967), however, the gabbros of ophiolites have either sharp or gradational contacts. Massive chromitite lenses and pods occur at the rims of some Alaskan-type intrusions (Nizini Tagil, Garuti et al.,

1997). In ophiolites, chromitites also form in dunite pods in the mantle sequence, however, they are more abundant towards the centre of each dunite body (Roberts and Neary, 1993).

Both ophiolites and Alaskan-type intrusions are often disrupted and deformed to the point at which they are indistinguishable on the basis of structure. Therefore, based on structure or proportions of lithotypes alone, it is difficult to distinguish between an Alaskan-type intrusion and a dismembered ophiolite.

2.4.4. Petrology and Mineralogy

The mantle sequences of the Semail and Troodos ophiolites consist of variably serpentinised peridotites (85%) with associated lherzolites and dunites (5 to 15%) (Gass, 1990; Lippard et al., 1986). The harzburgites are medium to coarse-grained and are composed of 75 to 85% olivine and 15 to 20% orthopyroxene. Within these, clinopyroxene forms an average <1% abundance and a maximum of 5% of the mode and chrome spinel forms 0.5 to 2%. Chromite is a ubiquitous and accessory phase. The dunites typically comprise >98% olivine and <2% chromite and are largely massive dunite with chromite segregations (Gass, 1990; Lippard et al., 1986).

The dominant lithology in the Layered Series is gabbro with dunites (including minor chromite) and wehrlite as the other main rock types (Gass, 1990). The primary minerals of the Semail and Troodos ophiolites are plagioclase, clinopyroxene, olivine, chrome spinel, orthopyroxene, hornblende and titanomagnetite (Lippard et al., 1986; Gass, 1990). Within each cyclic unit of the Semail Nappe the most common crystallization sequence shows that olivine and chromite form the earliest phases, followed by pyroxene and plagioclase as intercumulus phases, then titanomagnetite and hornblende as minor phases (Lippard et al., 1986). This means that the most common rock sequence is: dunite → wehrlite → olivine-gabbro → gabbro (Gass, 1990). Other ophiolites can display differing orders of crystallization including olivine → plagioclase → clinopyoxene (eg the Lizard ophiolite).

The Late Intrusive Complexes of the Semail are divided into two broad groups: gabbro-diorite-plagiogranite bodies and peridotite-gabbro complexes (Lippard et al., 1986; Browning and Smewing, 1981). The former composed mainly of layered gabbros, diorites and subordinate plagiogranite (Lippard et al. 1986). These gabbros are typically medium grained with plagioclase and interstitial clinopyroxene grading upwards into coarser diorites. The Mashin intrusion is a typical peridotite-gabbro complex in the Semail. Lippard et al. (1986) describes this as wehrlite grading upwards into coarse grained gabbros and diorites. The wehrlites are typically coarse grained poikilitically enclosed by clinopyroxenes and orthopyroxenes. Smaller peridotite-gabbro intrusions sometimes grade from wehrlite into lherzolite (Lippard et al., 1986).

Alaskan-type intrusions are composed of dunite, olivine-clinopyroxenite, clinopyroxenite, hornblendite and gabbro zones (Taylor, 1967). This compares with the more orthopyroxene-rich lherzolites and harzburgites which dominate ophiolite mantle sequences. Alaskan-type intrusions are noted for the absence of orthopyroxene. Considered on their own, the petrologies of the ophiolitic crustal sequence are similar to the zones of Alaskan-type intrusions. However, in Alaskan-type intrusions the contact between clinopyroxenites and gabbros is generally sharp whereas gabbro contacts in ophiolites may be either sharp or gradational. Additionally, plagioclase in Alaskan-type complexes is only observed in the peripheral hornblendite zone whereas it is ubiquitous in the typical ophiolite crustal sequence. Accessory chromite in Alaskan-type intrusions occurs exclusively and throughout the dunite zones (Johan, 2002). Alaskan-type intrusions show the crystalisation sequence olivine → clinopyroxene → plagioclase (Murray, 1972). The same crystallization sequence is observed in the Semail and Troodos ophiolites although some complexes show plagioclase crystalising before clinopyroxene. In both Alaskan-type intrusions and ophiolites, olivine generally crystallizes first.

2.4.5. Rare Earth Elements (REE)

Godard et al. (2000) showed that mantle sequence dunite pods from the Semail Nappe are highly depleted in REEs with respect to chondrite. The patterns show a smooth positive slope from La to Lu (Figure 2.4).

Light REEs from the Layered Series in the Semail Nappe are slightly enriched compared to chondrite (Lippard et al., 1986), however, analysis of the CY-4 drill core from the Troodos ophiolite shows considerable depletion in LREE. These wide ranging values converge for the heavier elements.

The Late Intrusive Complexes of the Semail Nappe display an enrichment of REE with respect to chondrite (figure 2.4). A slightly positive slope is observed with a pronounced negative Eu anomaly (Lippard et al., 1986).

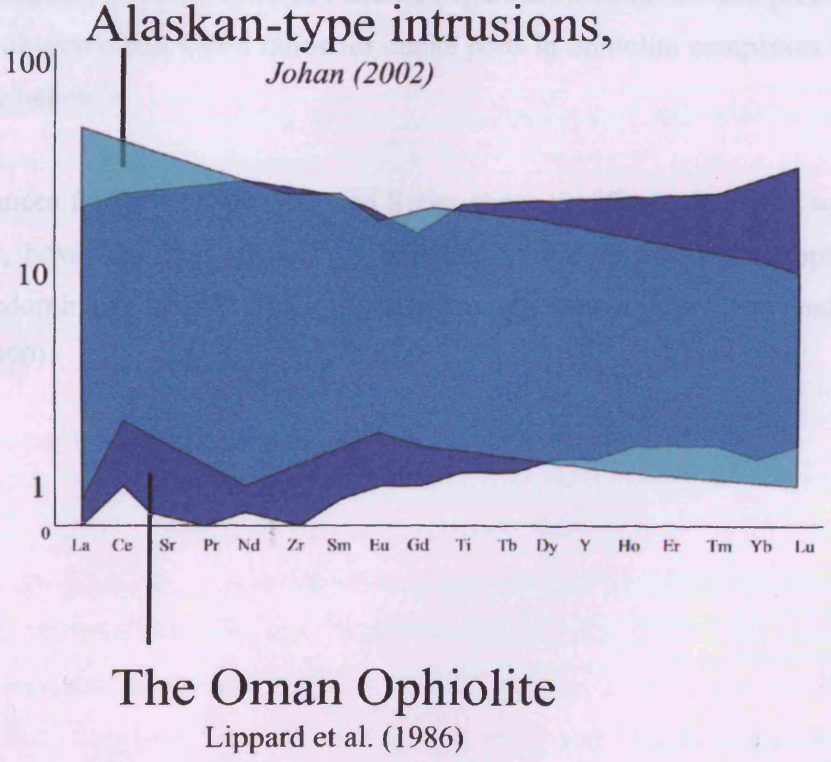

Figure 2.4: The typical REE geochemistry of Alaskan-type intrusions compared to Oman ophiolite (Johan, 2002; Lippard et al., 1986).

Alaskan-type intrusions are generally enriched in REE with respect to chondrites and the Late Intrusives complexes of the Semail Nappe are enriched to the same extent. These late Intrusive Complexes show a similar degree of enrichment, however, they have positive slopes. In general, the REE patterns from the Alaskan-type intrusions of Owendale and the Urals display gentle negative slopes with only slight Eu anomalies (Fershtater et al., 1997; Johan, 2002). This also contrasts with the mantle sequence dunites which display severe depletion and positive slopes. Commonly, the REE abundances in ophiolites show pronounced anomalies such as Ce, Eu and Gd - only broad anomalies are observed in Alaskan-type intrusions (figure 2.4).

2.4.6. Platinum-Group Elements

Platinum-group elements (PGE) in ophiolites are depleted in comparison with chondrite, they show a generally neutral slope with Os, Ir and Ru enrichment, however, some samples are slightly enriched in Rh, Pt and Pd (figure 2.5). Table 2.1 compares Pt and Pd values, it is observed that Pt/Pd ratios for dunite pods in ophiolite complexes worldwide are generally below 7.

PGE abundances for the Troodos Layered Series show significant depletion with respect to chondrite, however, they are slightly enriched in Rh, Pt and Pd. In ophiolites Pd typically predominates over Pt and a negative Ru anomaly is rarely observed (Prichard and Lord, 1990).

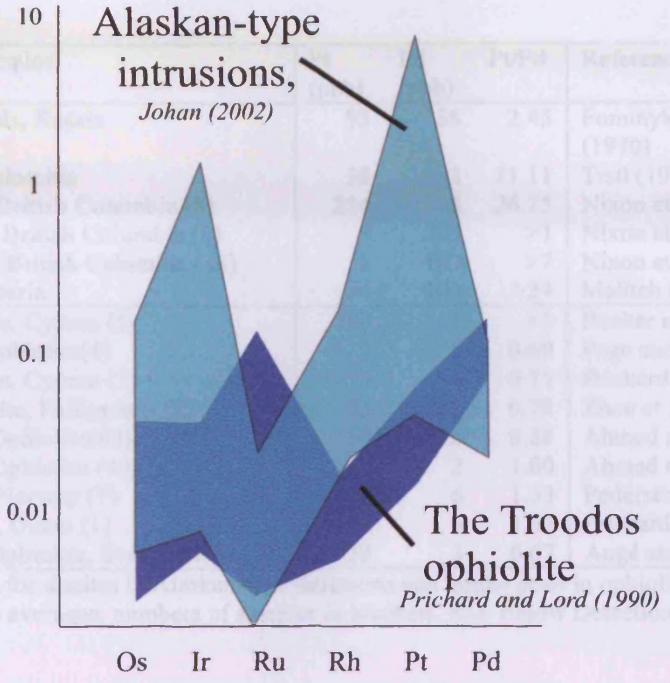

Figure 2.5: A comparison of the chrondrite normalized PGE abundances for Alaskan Type intrusions and the Troodos ophiolite. The Alaskan-type intrusions show strong negative Ru anomalies and a high Pt/Pd ratios when compared to ophiolites (After Johan, 2002 and Prichard and Lord, 1990).

Alaskan-type intrusions frequently display a negative Ru anomaly when displayed on a chrondrite normalised PGE diagram (Johan, 2002). The PGE patterns in the Troodos ophiolite rarely have negative Ru anomalies (Prichard and Lord, 1990). The elemental abundances of the mantle sequences of ophiolites are generally depleted in all the PGE whereas in Alaskan-type intrusions Ir and Pt are often enriched with respect to chondrite (Johan, 2002).

A significant difference between the dunites of ophiolites and Alaskan-type intrusions is in the Pt and Pd ratio. Table 2.1 shows Pt/Pt ratios for dunites from 7 ophiolite bodies and 6 Alaskan-type intrusions. The Pt/Pd ratios in ophiolites are normally less than Pt/Pd = 2 although the Pt/Pd ratio of the New Caledonia ophiolite is Pt/Pd = 6.67. The Pt/Pd ratio of Alaskan-type intrusions is normally significantly higher with values of Pt/Pd = 21-27 being recorded. The Pt/Pd ratio of the Nizhni Tagil and Wrede Creek Alaskan-type intrusions are, however, lower (Pt/Pd = 2.45 and >1).

	Complex and Location	Pt (ppb)	Pd (ppb)	Pt/Pd	Reference
Alaskan-type intrusions	Nizhni Tagil, Urals, Russia	93	38	2.45	Fominykh and Khvostova (1970)
	Alto Condoto, Colombia	38	2	21.11	Tistl (1994)
	Lunar Complex, British Columbia (8)	214	8	26.75	Nixon et al., 1997
	Wrede Complex, British Columbia (8)	7	BD	>1	Nixon et al., 1997
	Polaris Complex, British Columbia (18)	1	BD	>7	Nixon et al., 1997
	Chad, Eastern Siberia	24	BD	>24	Malitch (1996)
Ophiolites	Troodos Ophiolite, Cyprus (5)	BD	1	<1	Becker and Agiorgtis (1978)
	Newfoundland Ophiolite(4)	3	5	0.69	Page and Talkington (1984)
	Troodos Ophiolite, Cyprus (1)	3	4	0.71	Prichard and Lord (1990)
	Zambales Ophiolite, Philippines (2)	25	32	0.78	Zhou et al. (2000)
	Northern Oman Ophiolite(63)	14	16	0.88	Ahmed and Arai (2002)
	Northern Oman Ophiolite (40)	2	2	1.00	Ahmed and Arai (2002)
	Leka Ophioilite, Norway (7)	8	6	1.33	Pedersen et al. (1993)
	Semail Ophiolite, Oman (1)	10	6	1.67	Prichard et al. (1996)
	New Caledonia Ophiolite, South Pacific (8)	20	3	6.67	Augé and Maurizot (1995)

Table 2.1: Pt/Pd ratios for dunites in Alaskan-type intrusions and dunite pods in ophiolite complexes. Abundances are averages, numbers of samples in brackets. BD: Below Detection Limits

2.4.7. Fractionation of Nickel, Copper and Chromium

In the Layered Series in the Semail Nappe, the compatible elements Ni and Cr are most abundant in the early formed olivine- and pyroxene-rich lithologies. Their abundances decrease in the more mafic lithotypes (Lippard et al. 1986). The same is seen in ultramafics of Alaskan-type intrusions. Ni is concentrated and Cu depleted in the early dunites in the Urals. These abundances fall and rise respectively in the mafic lithotypes (Garuti et al., 1997). Similar patterns are observed in the Tulameen and Condoto complexes of British Columbia and Columbia (Findlay 1969; Tistl, 1994).

2.4.8. Summary

Alaskan-type intrusions are pipe-like concentrically zoned ultramafic-mafic intrusions (Taylor, 1967; Johan, 2002), in some cases this may be sufficient to distinguish them from the layering of ophiolites. However, due to the dynamic setting into which Alaskan-type complexes are intruded and ophiolites are obducted, both may be deformed so that the layering or zoning cannot always be observed.

In such geological situations, the following criteria are suggested to distinguish the type of mafic-ultramafic complex:

- In ophiolite sequences, gabbros can display both gradational and sharp contacts with ultramafic rocks, whereas, in Alaskan-type complexes such contacts are typically sharp.
- The mantle sequences of ophiolites are dominated by orthopyroxene-rich lithotypes. Conversely, Alaskan-type intrusions are noted for the absence of orthopyroxene.
- The ratio Pt/Pd for ophiolitic dunites is typically <7 whereas Alaskan-type dunites are generally >2 (Table 2.1)
- Alaskan-type intrusions frequently display negative Ru anomalies on chrondrite normalized PGE diagrams (see figure 2.5), whereas ophiolites rearely show negative Ru anomalies.
- Ophiolitic mafic and ultramafic rocks show neutral to positive gradients on REE abundance diagrams, whereas, similar mafic-ultramafics in Alaskan-type intrusions display negative gradients (figure 2.4)
- Ophiolite REE patterns can include pronounced positive or negative Ce, Eu and Gd anomalies. Whereas, all lithologies in Alaskan-type intrusions only display a slight rise in Sm, Eu and Gd abundances (figure 2.4).

3. Petrology and Mineralogy

3.1. Introduction

Samples of ultramafic rocks from the each of the four geographic areas of study within the WES were cut and mounted as either thin sections or polished blocks. These samples were then observed using transmitted light microscopy and scanning electron microscopy. The sulphide minerals were analysed using an energy dispersive X-ray analyzer attached to a Scanning Electron Microscope (SEM).

This chapter is divided into four sections. The first section describes the study of thin sections to define the rock-types and to document the degree of alteration present in the WES. The second section describes the texture of oxide minerals in order to support a study of their geochemistry. Another section describes typical sulphide minerals and lastly three PGM are described.

3.2. Methods

3.2.1. Scanning Electron Microscopy

Polished blocks were analysed using a Carl Zeiss SMT (Cambridge) S360 scanning electron microscope (SEM). The search for PGM and photographs of spinels and sulphides were performed using a 4-quadrant back-scattered electron detector. Photographs of PGM were taken using a Veeco FEI (Philips) XL30 environmental SEM.

3.2.2. Energy Dispersive X-Ray analyzer

Both quantitative and qualitative analyses were obtained using an Oxford Instruments INCA ENERGY (EDX) X-ray analyzer. Quantitative analyses were undertaken using an accelerating voltage of 20kV, a probe current of 1nA and a working distance of 25mm. During petrological studies, mineral identification was confirmed by qualitative analyses the SEM.

3.3. Petrology

3.3.1. Introduction

The petrology of the rocks from the WES was investigated using both transmitted light microscopy and electron microscopy. This section describes the typical petrology of the ultramafic rocks and is illustrated by photographs of thin sections taken under transmitted light. The degree of alteration is described and subsequently a definition and description of rock-types is described.

The petrology of each of the ultramafic complexes covered in this thesis has been documented by other workers (see chapter 2). Furthermore, many studies comment on the significant degree of alteration to which each complex has been subjected (eg Mogessie and Hoinkes, 1998). This section aims to describe the variation in alteration through the two key rock types: dunite and clinopyroxenite. Additionally, some rocks may be classified as olivine-clinopyroxenite, as this is composed of two minerals it is not described here because it is easier to describe the alteration of olivine and clinopyroxene separately. In order to demonstrate the degrees of alteration present, this study focuses only on the two mono-mineralic lithotypes. For both rock types, a number of thin sections are described from the least to most altered. In addition to this, a description of the little known lithotype known as birbirite is included. Birbirite is an alteration product and is widely distributed in the soils of the area. It is named after the Birbir river which flows around the Main Yubdo Intrusion.

3.3.2. Dunite

The following images illustrate the range of serpentinisation within the ultramafic rocks of the WES. The Mg values are quoted for reference with the geochemical assessment of alteration as described in chapter 8.

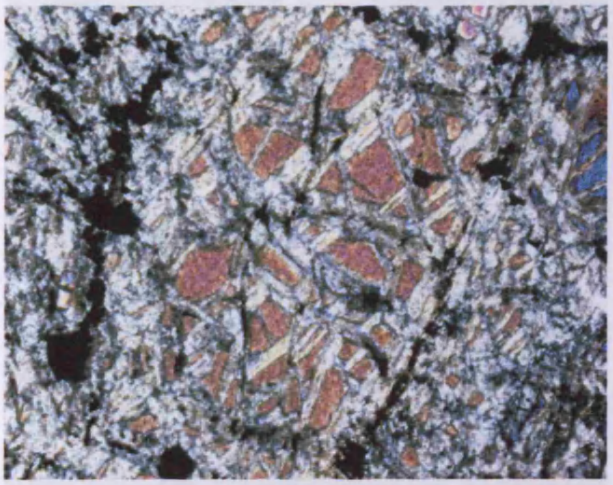

Figure 3.1: A photograph of a dunite sample under crossed polars. The lower edge of the image is 120μm in length.

This sample is composed of approximately 50% serpentine. The high birefringence marks relict olivine minerals. The olivine crystal in the centre of the image has been pulled-apart and partially replaced by serpentine. Fine anhedral Fe-rich spinels decorate the original edge of the olivine mineral.

This sample has 25.8% Mg

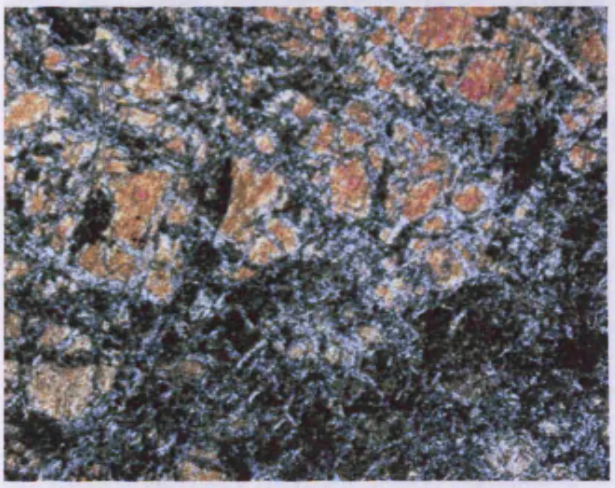

Figure 3.2: A photograph of a dunite sample under crossed polars. The lower edge of the image is 120μm in length.

This sample is composed of approximately 60% serpentine with a typical mesh texture. Some relict olivine minerals show high birefringence colours and slightly wavy extinction but are otherwise they are undeformed. The arrangement of the relict crystal edges indicates that the protolith had an adcumulate texture.

This sample has 22.0% Mg

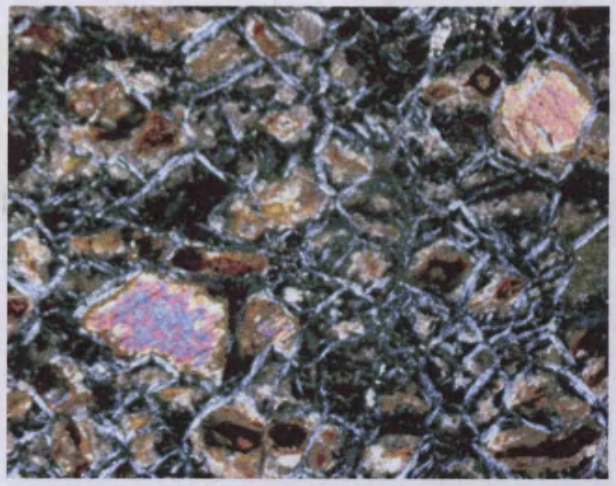

Figure 3.3: A photograph of a dunite sample under crossed polars. The lower edge of the image is 120μm in length.

This sample is composed of approximately 85% serpentine. Unaltered olivine grains have a high birefringence and they are surrounded a serpentine mesh.

This sample has 20.4 % Mg

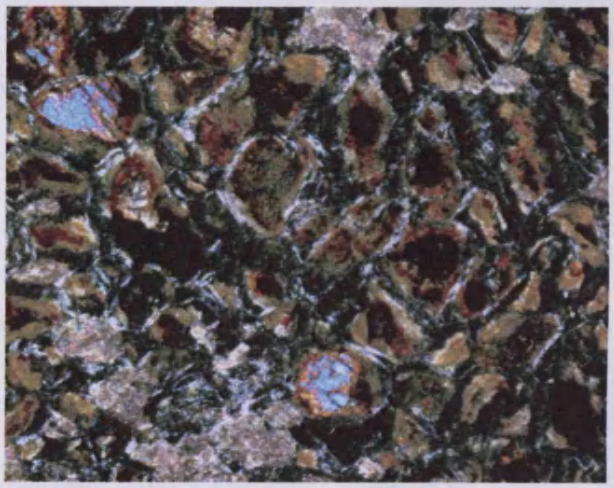

Figure 3.4: A photograph of a dunite sample under crossed polars. The lower edge of the image is 120μm in length.

This sample is composed of approximately 90% serpentine. Grains with a high birefringence indicates the presence of a few remaining fresh olivine minerals. This sample shows intense alteration along cracks and patchy alteration in places (not shown). Some minor pyroxene (<5%) is observed.

This sample has 16.4% Mg

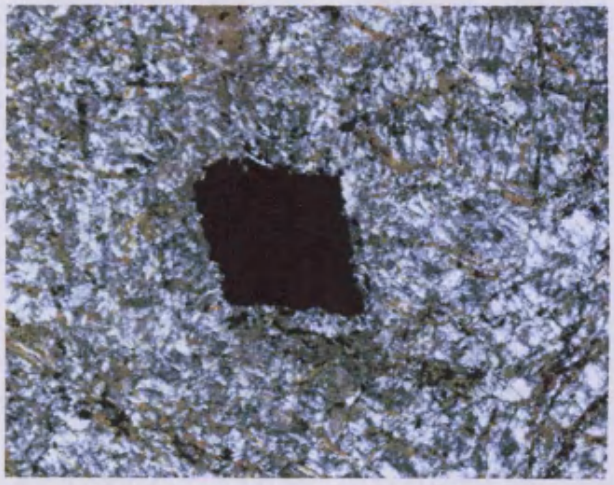

Figure 3.5: A photograph of a dunite sample under crossed polars. The lower edge of the image is 120μm in length.

This sample is completely serpentinised (not including the oxide minerals). This sample shows a relict olivine texture within the serpentine mesh which is decorated with fine anhedral spinels. Additionally, the sample contains subhedral spinels such as the one shown in the centre of the image.

This sample has 7.0% Mg

3.3.3. Clinopyroxenite

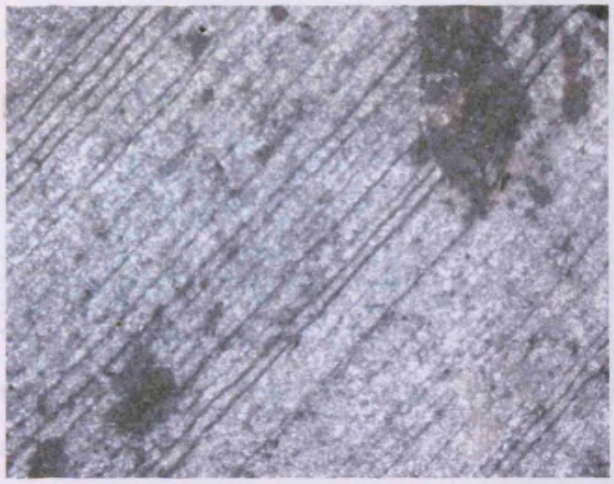

Figure 3.6: A photograph of a clinopyroxenite sample from Kingy area under crossed polars. The lower edge of the image is 120μm in length.

This sample is 100% replaced by fibrous amphibole. The clinopyroxene has a poikilitic texture enclosing minor olivine and can form up to 1cm in length.

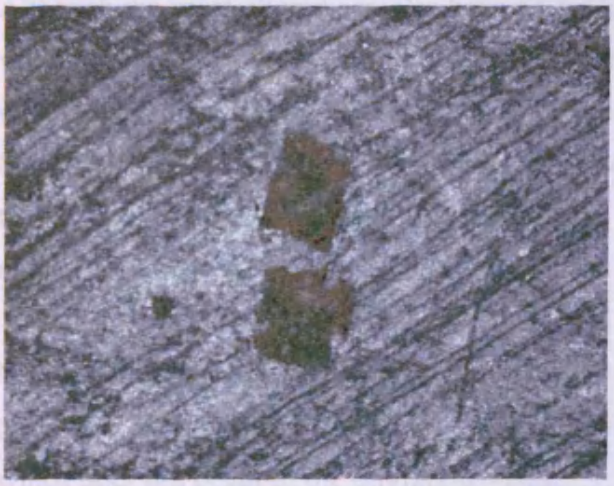

Figure 3.7: A photograph of a clinopyroxenite sample from the Kingy area under crossed polars. The lower edge of the image is 120μm in length.

This sample is 100% by fibrous amphibole minerals. The field of view is occupied by one large clinopyroxene and it is recognised by closely spaced which would be expected for orthopyroxene. The clinopyroxene minerals frequently occur in sizes over 1.5cm.

3.3.4. Birbirite

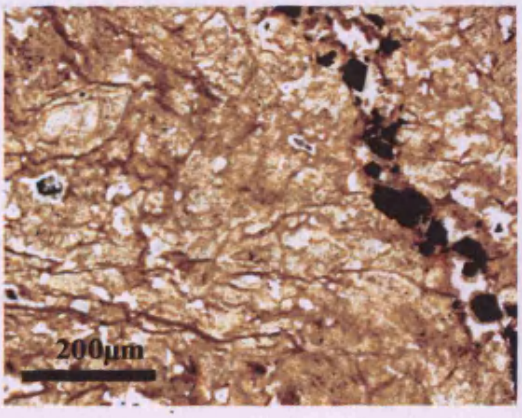

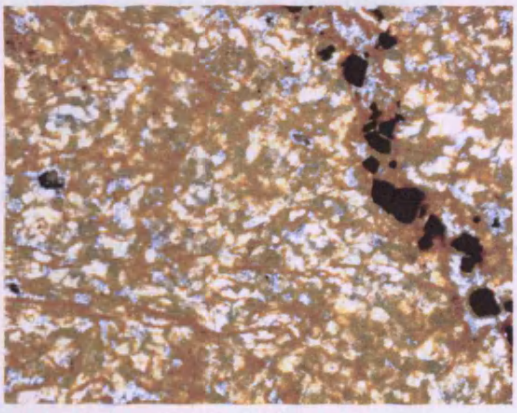

Figure 3.8: A photograph of a birbirite sample from the Tulu Dimtu Main Intrusion area. The lower edge of the image is 120μm in length. **Left: Plane polarized light. Right: Crossed polars**

This sample contains a fine silica network with highly altered spinels (hematite) sometimes disseminated and sometimes in veins (see figure 3.8).

3.3.5. Summary

The dunites show a gradual change in texture with serpentinisation (from 50% to 100%). The least altered samples (50%) show serpentine forming around fresh olivine grains and the edges of the original minerals are decorated with fine anhedral spinels. With further alteration serpentine becomes more abundant and the mesh texture more extensive. Although the most altered samples have no fresh olivine, a relict olivine texture remains visible within the serpentine mesh and fine spinels are visible. Regardless of the degree of alteration, euhedral to subhedral spinels can be observed in most samples in addition to the fine grained anhedral spinels found at the edges of the olivine grains. Furthermore throughout all samples, olivines show pull-apart textures and some show slightly wavy extinction.

No fresh clinopyroxene has been observed in this study of the WES. Some minor olivine (<10%) is observed. The clinopyroxene is recognized by a closely spaced relict cleavage which does not occur in the olivines or spinels. In one sample the clinopyroxene shows a poikilitic texture around olivine. The clinopyroxene has been replaced by fibrous amphibole and cleavage can continue as far as 1.5cm, indicating that the original crystals were large. Furthermore, no relict or fresh orthopyroxene has been identified.

3.3.6. Classification of Rock Types

This study uses the recommendations made by the IUGS subcommission on the Sytematics of Igneous Rocks (Streckeisen, 1976). The rock types used here are defined as follows:

- Dunite: greater than 90% olivine and less than 10% pyroxene
- Clinopyroxenite: greater than 90% clinopyroxene and less than 10% olivine.
- Olivine-olinopyroxenite: Greater than 60% clinopyroxene and less than 40% olivine.

Given the high degree of alteration observed in the WES (a minimum of 50%) minerals are often completely replaced. However, even in the most altered dunites (figure 3.5) and clinopyroxenites (figures 3.6 and 3.7) relict features of the key minerals can be observed. Therefore, in this study the identification of the primary magmatic minerals is made either using observations of fresh minerals (eg high birefringence for olivines) or by the identification of relict features. The following relict features have been used to identify olivine and clinopyroxene:

- Olivine: A relict olivine texture preserved within a serpentine mesh with or without fine anhedral spinels decorating the relict mineral edge.
- Clinopyroxene: A closely spaced cleavage which does not occur in spinels or olivines.

An ultramafic rock as classified here may not actually contain any of the igneous minerals specified by Streckeisen (1976). For example the term dunite as used in this thesis may refer to a rock entirely composed of serpentine, so long as pseudomorphed olivines can be recognized using a mesh texture. A further account of the degrees of alteration within each area is undertaken in chapter 6 which attempts to quantify the alteration using geochemical data.

In a situation where no relict features are observed the sample is classified as "unidentified".

3.4. Oxide Minerals

3.4.1. Introduction

Spinels often resist alteration and, therefore, a study of their morphology and geochemistry can help us understand the magmatic processes. The crustal cumulates and mantle tectonites of ophiolite complexes can host chromitite layers. Further down the crustal sequences of ophiolites, podiform chromitite bodies can form (eg Lippard et al., 1986). Disseminated spinels are common in many parts of ophiolite mantle sequences. Similarly, in Alaskan-type intrusions disseminated spinels are common but they can also form into schlieren and in some complexes podiform ore-bodies have been observed (Johan, 2002). In the WES, the only descriptions concerning spinels are those of Belete et al. (2000) who describe both magmatic and metamorphic forms.

In this section, photomicrographs of spinels and their host minerals were taken using the Cardiff S360 SEM (see section 3.2.1). This section presents an account of the typical textures of spinels from the WES in order to accompany a study of the geochemistry of the spinels described in chapter 7.

3.4.2. Tulu Dimtu

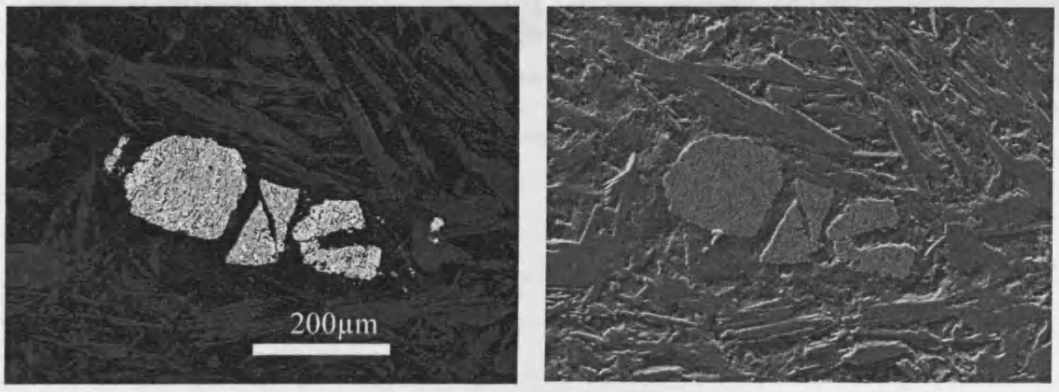

Figure 3.9: SEM photomicrographs of a disseminated spinel (white colour, high mean atomic number) in a clinopyroxenite sample (DTR-019-02). The spinel shows a pull apart tecture and is hosted by a gangue of fibrous amphibole. **Left: back-scattered electron image, Right: secondary electron image.**

3.4.3. Kingy

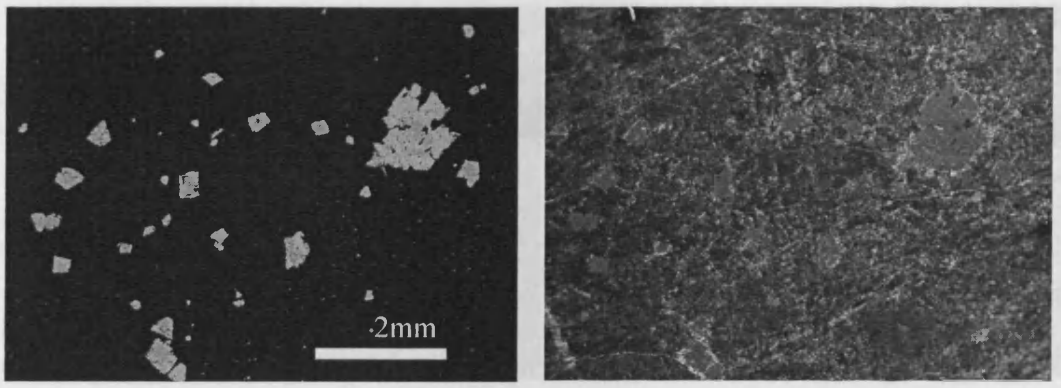

Figure 3.10: SEM photomicrographs of disseminated spinels (white colour, high mean atomic number) hosted by olivine in sample DTR-057-02. Some spinels are subhedral and zoned. **Left: back-scattered electron image, Right: secondary electron image.**

3.4.4. Daleti, Ankori, Tulu Kapi and Keley

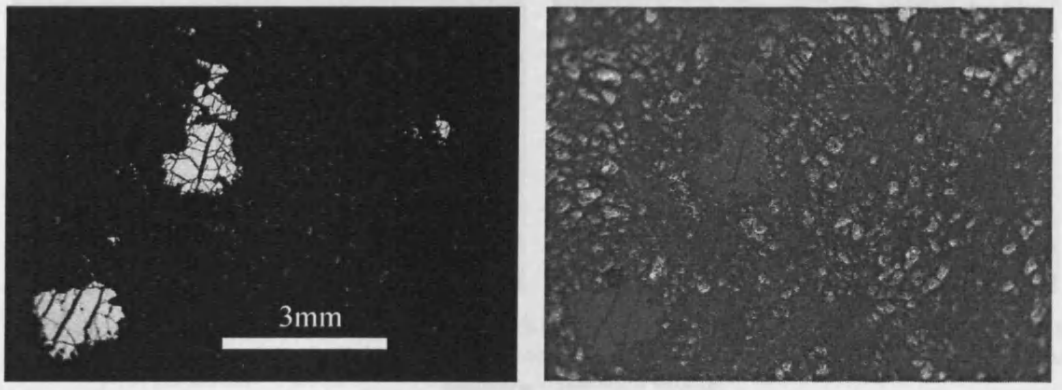

Figure 3.11: SEM photomicrographs of disseminated spinels (white colour, high mean atomic number) hosted by partially serpentinised olvines from sample D19. Many spinels show pull-apart textures. **Left: back-scattered electron image, Right: secondary electron image.**

3.4.5. Yubdo, Andu and Sodu

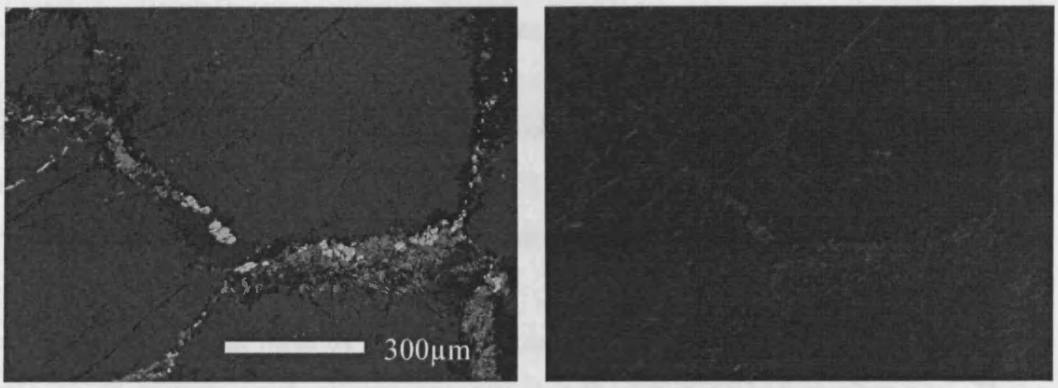

Figure 3.12: SEM photomicrographs of anhedral spinels (white colour, high mean atomic number) from sample Y28. The spinels occur in serpentine filled cracks between fresh clinopyroxenes minerals (large grey coloured minerals. **Left: back-scattered electron image, Right: secondary electron image.**

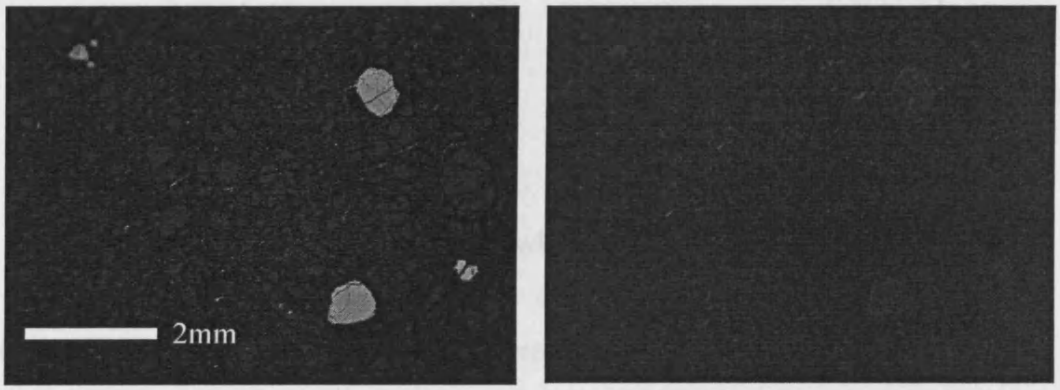

Figure 3.13: SEM photomicrographs of disseminated spinels (white colour, high mean atomic number) partially serpentinised olivines from sample Y30. **Left: back-scattered electron image, Right: secondary electron image.**

3.4.6. Summary

In all areas, two distinct groups of spinels are found, fine anhedral minerals and coarser subhedral to euhedral ones. In some samples anhedral spinels up to 100µm across occur (see figures 3.1 and 3.12). These form at the edges of silicate phases in association with serpentine. In contrast, it is common to find more regular disseminated spinels which are hosted by olivine, serpentine or fibrous amphibole. These minerals commonly show pull-apart textures and are often well over 500µm in length.

3.4.7. Discussion

The observation that there are two types of spinel textures is common in ultramafic rocks (Sack and Giorso, 1995). The serpentinisation of olivine minerals releases Fe from the crystal lattice to form Fe-oxides. The irregular shapes, formation at the edges of olivines and association with serpentine support this hypothesis. Furthermore, preliminary analysis of the geochemistry of these minerals show a high Fe content.

The euhdral to subhedral form of the second spinel group and their association with host minerals which include fresh olivine suggests that they formed before alteration. These may be cumulus spinels and therefore their geochemistry may reflect magmatic processes (see chapter 7).

3.5. Sulphide Minerals

3.5.1. Introduction

PGE are known to form a close association with sulphide minerals and many models have been developed whereby the behaviour of sulphur is used to help explain the development of PGE deposits. In magmas where sulphur is present, geochemical models suggest that PGE are likely to be taken into solution within sulphide melts (Naldrett and Duke, 1980). Furthermore, Pt and Pd are most likely to partiton into Cu-rich sulphides (Barnes et al., 1997). Such geochemical models are complimented by mineralogical studies. Prichard et al. (2004) have observed the expression of such geochemical models in sulphide blebs from a mafic dyke in Uruguay. After the crystallization of the magma, it is believed that the same hydrothermal fluids which remobilize sulphur also remobilize PGE (Wood, 2002)

This section provides a description of sulphide minerals from the WES and the subsequent discussion may provide a further insight into the processes which influence the PGE distribution.

3.5.2. Tulu Dimtu

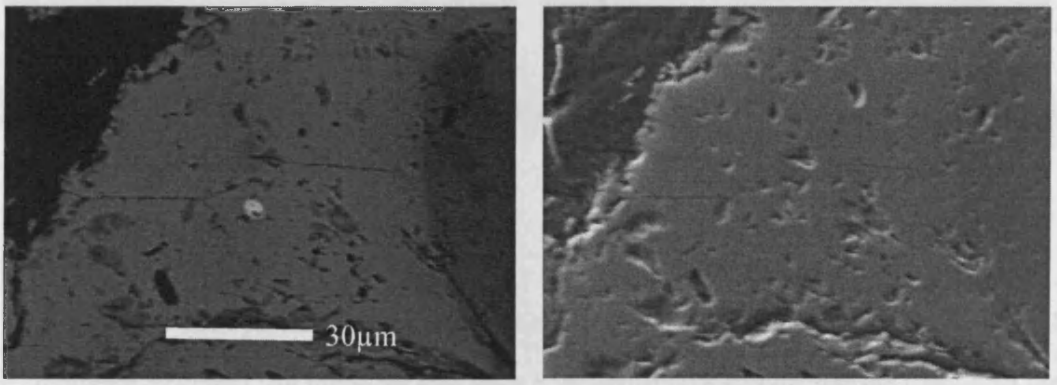

Figure 3.14: SEM photomicrographs of an altered bornite (white colour, high mean atomic number in the centre of image) in the altered rim of a Cr-spinel (grey colour), hosted by serpentine (black). This image has been taken from sample TDR19/01 which is located on the southern flank of the Tulu Dimtu Main Intrusion. **Left: back-scattered electron image, Right: secondary electron image.**

Cu	S	Fe	O	Total
59.41	24.47	12.24	2.64	98.76

This analysis can be quoted as $Cu_{4.88}Fe_{1.14}S_{3.98}$ – ignoring oxygen - which is close to bornite (Cu_5FeS_4). The oxygen indicates that the mineral has been altered. As bornite is an alteration product of chalcopyrite, this mineral infers that at least two phases of alteration have occurred.

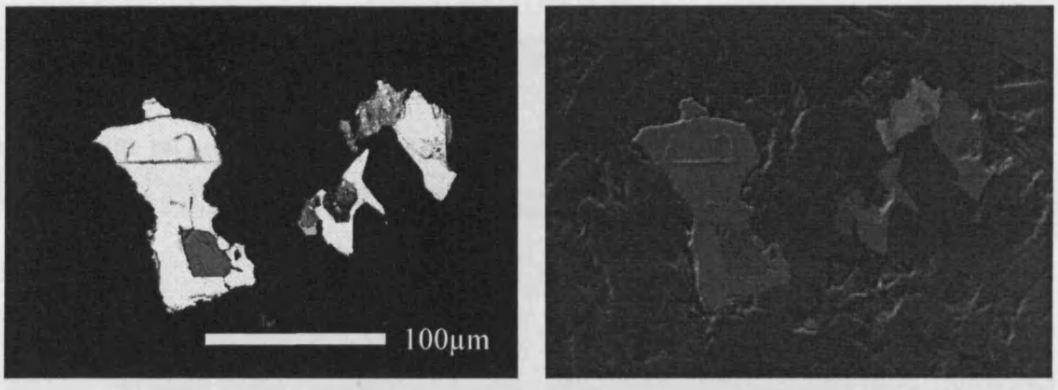

Figure 3.15: SEM photomicrographs of an anhedral glaucodot split into three parts (white colour, high mean atomic number) hosted by serpentine. The sulphide mineral on the left hosts a Ni- As-bearing magnetite inclusion. This image has been taken from sample DTR-019-02 from the Tulu Dimtu Lensoid Ultramafics. **Left: back-scattered electron image, Right: secondary electron image.**

As	S	Co	Ni	Fe	O	Total
44.88	17.77	15.77	13.74	4.44	3.7	100.3

If the oxygen is ignored then this analysis may be quoted as $(Co,Ni,Fe)_{1.01}As_{1.04}S_{0.96}$ which is close to glaucodot and is represented by the formula (Co,Fe)AsS. This assumes that the Ni has substituted for Co. The oxygen could indicate that the mineral has been altered.

3.5.3. Kingy

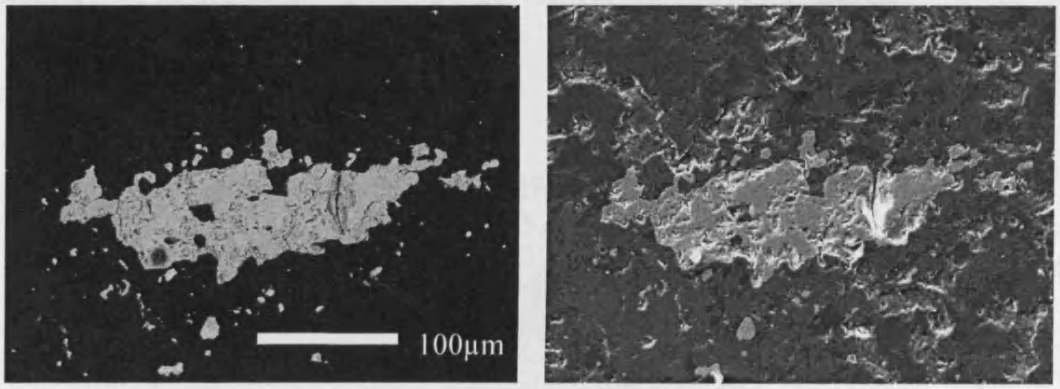

Figure 3.16: SEM photomicrographs of an anhedral chalcopyrite mineral (white colour, high mean atomic number) hosted by quartz in an extremely altered olivine-clinopyroxenite sample. This image has been taken from sample KTR-049-02 from the Kingy Ridge Ultramafic. **Left: back-scattered electron image, Right: secondary electron image.**

S	Cu	Fe	Total
34.3	32.69	29.9	96.89

This mineral can be quoted as $Cu_{0.97}Fe_{1.01}S_{2.02}$ which is close to chalcopyrite ($CuFeS_2$).

3.5.4. Daleti, Ankori, Tulu Kapi and Keley

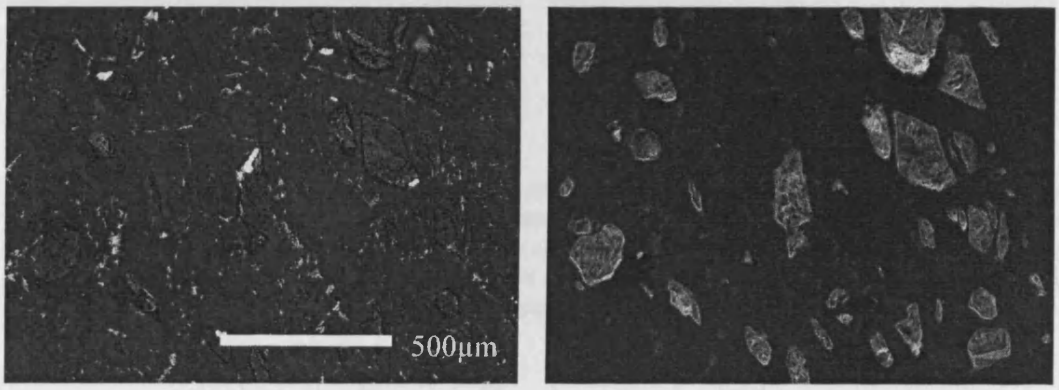

Figure 3.17: SEM photomicrographs of several anhedral barite crystals (white specs, high mean atomic number) on the edge of larger partially serpentinised olivine minerals. There are many anhedral Fe-rich spinels. This image has been taken from sample DR22/01 from the Daleti Ultramafic. **Left: back-scattered electron image, Right: secondary electron image.**

Ba	S	Fe	Si	Al	Mg	O	Total
55.16	12.19	0.66	0.29	0.25	0.18	24.21	92.94

This analysis can be quoted as $Ba_{1.03}S_{0.98}O_{3.89}$ which is close to barite ($BaSO_4$)

3.5.5. Yubdo, Andu and Sodu

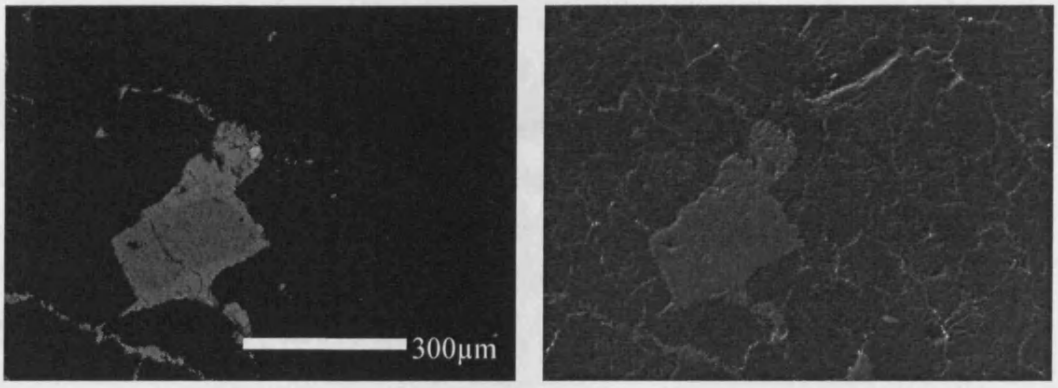

Figure 3.18: SEM photomicrographs of a Ni-sulphide mineral (white spec, high mean atomic number) in the altered rim of a zoned spinel hosted by serpentine (black). In addition to the subhedral spinels (centre of image) there are many fine anhedral Fe-rich spinels which sometimes form schlieren. This image has been taken from sample AYR-016-01 from the northwestern flank of the Main Yubdo Intrusion. **Left: back-scattered electron image, Right: secondary electron image.**

S	Ni	Fe	Co	Total
33.19	25.96	22.8	18.93	100.88

This analysis could be quoted as $Fe_{1.30}(Ni,Co)_{2.42}S_{3.28}$. The most similar mineral found is violarite ($FeNi_2S_4$), unfortunately the fit for this mineral is poor and attempts to fit the analysis to the following minerals less successful: bravoite, $(Fe,Ni,Co)S_2$; pentlandite, $(Fe,Ni)_9S_6$; siegenite, $(Co,Ni)_3S_4$.

3.5.6. Summary

Most sulphides are hosted by serpentine but some by quartz or altered spinel. Those sulphides sufficiently large to be resolved by the SEM, they appear to be anhedral in shape.

It is observed that Ni-barren, Cu-sulphides occur in both the southern flank of the Tulu Dimtu Main Intrusion and the Kingy Ridge Ultramafic. However, in the Tulu Dimtu Lensoid Ultramafics, several Ni-sulpharsenides have been discovered. In the Main Yubdo Intrusion only Cu barren, Ni-sulphide minerals are observed.

3.5.7. Discussion

Most sulphides described here are hosted by minerals such as serpentine and quartz which are often associated with the action of medium and low temperature fluids. A highly irregular shape is observed for the base-metal sulphides in most cases and this is unlike the euhedral or rounded shapes expected if these minerals crystallised from a magma. Furthermore, the presence of magnetite inclusions within the sulphides from the Tulu Dimtu Lensoid Ultramafics suggests that they formed after the magma cooled and possibly after at least one phase of alteration.

Given the affinity of these sulphides with high temperature fluids (as discussed above), the division between the Cu-bearing sulphides (Tulu Dimtu Main Intrusion and Kingy Ridge Ultramafic) and the Ni bearing-sulphides (Tulu Dimtu Lensoid Ultramafics and the Main Yubdo Intrusion) could have two interpretations. Firstly, the Cu and Ni could have formed in the same magmatic site and then been remobilized different degrees by alteration – maybe one Ni-rich phase and another Cu-rich. Alternatively, the Ni and Cu could have been driven apart at a magmatic stage (as proposed by Barnes et al., 1997 and Prichard et al., 2004).

Two sulphide minerals are observed in the altered rims of spinels, one Cu-rich and the other Ni-rich (figures 3.9 and 3.19 respectively). Although their presence in the alteration rim of a spinel suggests that alteration fluids have affected their host, there is no direct evidence for large amounts of fluid transport through the spinel itself. Furthermore, as spinels resist alteration to a greater degree than silicate phases, it is possible that little transport of fluid has been made into the mineral. Even if the sulphide phases have recrystallised in situ, these two minerals may infer the possibility that Ni and Cu formed at different sites during magmatic processes.

The low number of sulphide minerals studied here means that this study does not provide a comprehensive account of the behaviour of S, Cu and Ni in the WES. However it is one of the first accounts of sulphide minerals in these igneous complexes in the WES.

3.6. Platinum Group Minerals

3.6.1. Introduction

A search for PGM was performed in the 10 rock samples with the highest Pt and Pd values which included two samples from the Tulu Dimtu Main Intrusion (see chapter 6). Three PGM were discovered in rock samples from the Main Yubdo Intrusion and none from the Tulu Dimtu Main Intrusion. In the following section the geochemistry and association of each PGM is described.

3.6.2. Sample AYR-016-01

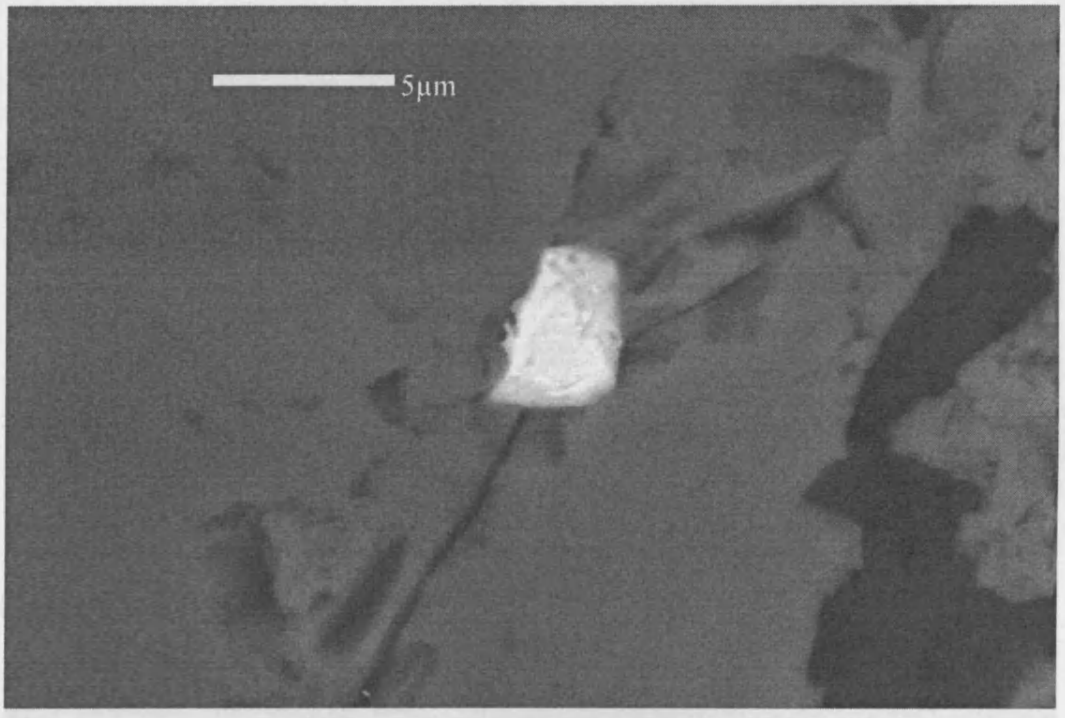

Figure 3.19: An SEM back-scattered electron image photomicrographs of a subhedral Pt-Fe alloy (white colour, high mean atomic number) in a Cr-spinel hosted by serpentine. This image has been taken from sample AYR-016-01 from the northwestern edge of the Main Yubdo Intrusion.

Pt	Fe	Cr	O	Total
92.29	11.86	1.12	2.27	107.55

It is possible that all Cr and Fe in this analysis originated from chromite and hematite as a result of fluorescence. If chromite and hematite are removed (resulting in a total of 99.87), then the analysis can be quoted as $Pt_{3.10}Fe_{0.89}$ which is close to Pt_3Fe. Although both Cr and Fe are common in the host rock, the poor total raises suspicion about the quality of original analysis.

3.6.3. Sample KYR-019-02

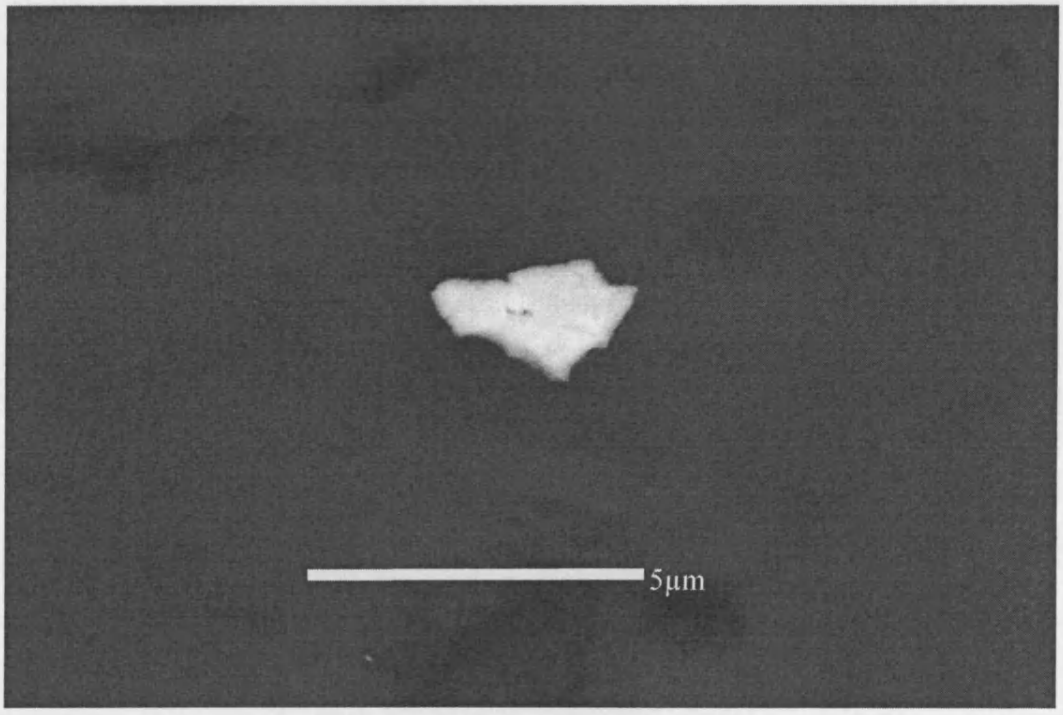

Figure 3.20: An SEM back-scattered electron image photomicrographs of an anhedral Os-Ir alloy (white colour, high mean atomic number) hosted by serpentine. This image has been taken from sample KYR-019-01 located the northwestern flank of the Main Yubdo Intrusion.

Qualitative analysis shows that this mineral contains major Os and Ir, lesser amounts of Ru, Fe and O, and traces of Si and Mg.

3.6.4. Sample Y30

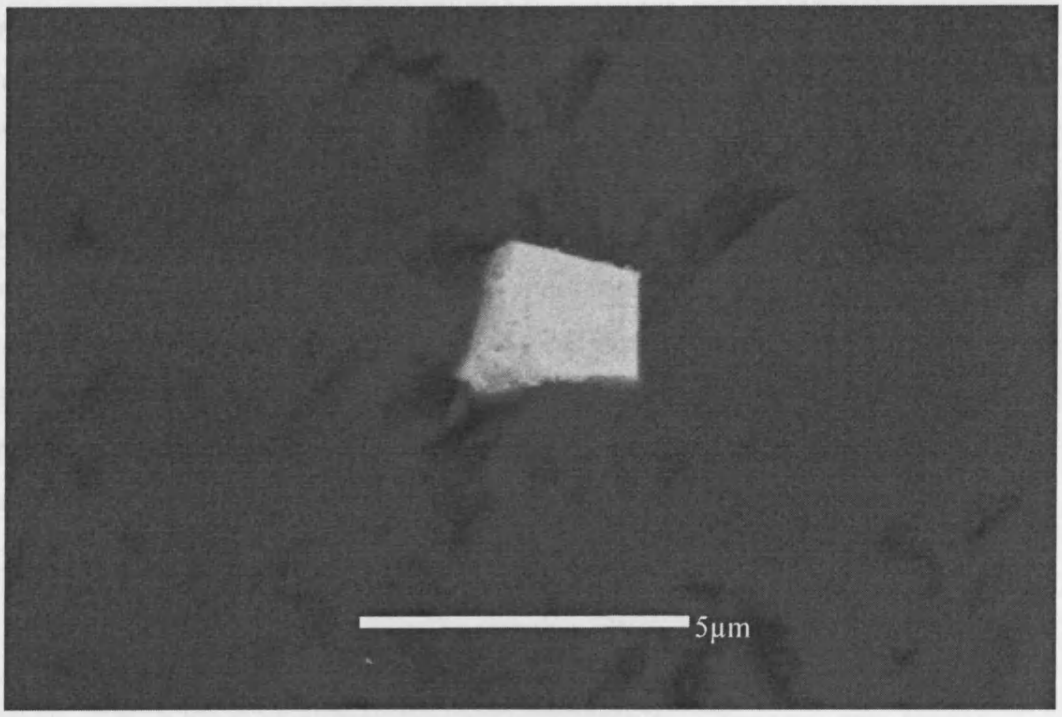

Figure 3.21: An SEM back-scattered electron image photomicrographs of a subhedral Ir-Os alloy (white colour, high mean atomic number) within a Cr-spinel hosted by partially serpentinised olivine. This image has been taken from sample AYR-016-01 located on the far western flank of Main Yubdo Intrusion.

Ir	Os	Zr	Ru	Fe	Rh	Cr	S	O	Total
79.11	9.25	6.33	2.76	2.18	2.55	1.71	0.45	1.14	105.48

It is possible that all Cr and Fe in this analysis originated from chromite and hematite as a result of fluorescence. If chromite and hematite are removed (resulting in a total of 101.50), then the analysis can be quoted as $Ir_{0.67}Os_{0.08}Ru_{0.04}Rh_{0.04}Zr_{0.11}Fe_{0.03}S_{0.02}$. Although both Cr and Fe are common in the host rock, the poor total raises suspicion about the quality of original analysis.

3.6.5. Discussion

The only other account of PGM in the rocks from the Yubdo area is a description of Pt-Fe alloys (Mogessie et al., 1999). These contain minor Ir and are hosted by either chromite or serpentine. The Zr found in the Ir-Os alloy from sample Y30 is unusual for a platinum group mineral. The Pt-Fe alloy described here (sample AYR-016-01) has a similar chemistry and shape to those found by Mogessie et al. (1999) however it is considerably smaller. The Pt-Fe alloys which are hosted by serpentine are typically 20-30μm in diameter.

There are many studies of placer PGM from the rivers and laterites around Yubdo (as reviewed in chaper 2). Most of the placer PGM described are Pt-Fe nuggets and a recent study documents 3 grains which contain Os-Ir inclusions (Belete et al., 2000). It is possible that the Os and Ir bearing PGM described here could be magmatic or postmagmatic minerals around which further PGE-bearing phases will nucleate. This preliminary study is one of the few accounts of PGM in the WES and may prompt further work to understand the genesis of placer Pt-Fe alloys.

4. Terrain Mapping

4.1. Introduction

This chapter details the use of terrain mapping from aerial photographs to identify the characteristic terrain for the larger ultramafic complexes in the WES (Yubdo and Tulu Dimtu) and to map these features elsewhere in the WES. In this area terrain mapping is more appropriate than normal geological mapping as there is little exposure (<5% in some areas), the rocks are very weathered and access is often difficult. Preliminary studies around the Yubdo and Daleti areas have indicated that the ultramafic complexes form high ridges on which vegetation is sparse and no cultivation is being undertaken. By contrast, the surrounding terrain is densely vegetated and subsistence farming is common.

Figure 4.1: A photograph of a barren ridge above the Daleti Ultramafic. The ridge is almost devoid of vegetation when compared to the foreground. Furthermore, the houses to the right indicate the presence of fertile subsistence farmland.

The lack of vegetation and agriculture may result from high Ni or low Ca values in the soil, which is characteristic of lateritic soils above ultramafic rocks. As detailed in chapter 2, the ultramafics of the WES are commonly surrounded by volcano-sedimentary sequences. These units are less resistant to weathering and therefore the harder ultramafic complexes are likely to stand out from the softer sedimentary sequences and therefore form ridges. Hence it is thought likely that the "barren-ridge" terrain will be characteristic of the ultramafic complexes.

A set of aerial photographs were procured from the Ministry of Mines (Addis Ababa). In section 4.2, the method of acquisition of these images and their compilation into map form is described. Subsequently, a description of the use of terrain elements to describe the terrain in the WES is provided (see section 4.3). The results are recorded as a set of maps containing photomorphic regions covering four geographic areas (as described in chapter 5), the boundaries of which were confirmed by field observations (see section 4.4).

4.2. Aerial Photography

4.2.1. Introduction

When aerial photographs are used for mapping, the user must consider the method by which the photograph was acquired, as the equipment used will create distortions of the scene being recorded. Before maps are created, these distortions must be corrected. This section describes the acquisition and processing of the aerial photographs from the WES. Finally an account of the specifications of the aerial photographs is provided.

4.2.2. The Aerial Photographs of the WES

The aerial photographs (from the Ministry of Mines, Addis Ababa) used in this study can be divided into two groups: those acquired during 1957/58 and those taken in 1980. The images taken in 1957/58 covered the Yubdo and Daleti areas however the 1980 set covered Tulu Dimtu and Daleti.

	1957/58	1980
Camera Type	Single Lens Frame	Single Lens Frame
Camera Focal Length	53.046mm	53.66
Film Format	230mm	233mm
Dates of acquisition	19-Dec-1957 20-Dec-1957 1-Jan-1958	15-Jan-1980 18-Jan-1980 22-Jan-1980 24-Jan-1980 31-Jan-1980
Time of acquisition	Between 9:45AM and 11:49AM	*
Lens Serial Number	XF6751	UAGII 3119
Orientation of Flight	North - South	East - West
Average Scale	1:55715	1:53063
Mean distance between Aerial photographs (m)	5,233	4,667
Average distance to Terrain (m)	9,370	*
Apparent Stereoscopic Viewing Distance (cm)	24	*
Stereoscopic Vertical Exaggeration	1.97	*
Digital resolution	10m	10m

Table 4.1: The details of the aerial photographs. *: Data obscured during development.

To demonstrate the degree of distortion present in the images, figures for the relief displacement of two prominent features have been calculated. This is done using an equation based on the distance from the feature to the centre of the image image and the altitude (see table 4.2). Sodu ridge is the highest point in the image and is close to the edge and therefore is likely to have the largest relief displacement. However, this figure is only 3mm which equates to around 150m on the ground. These figures show that relief displacements are negligible for these images.

Feature	Distance from photograph centre to top of feature (m)	Altitude of feature (m)	Relief Displacement (m)
Yubdo Village	0.02	1670	0.00059
Sodu Ridge	0.102	1668	0.00300

Table 4.2: Relief Displacements of Yubdo Village and Sodu Ridge.

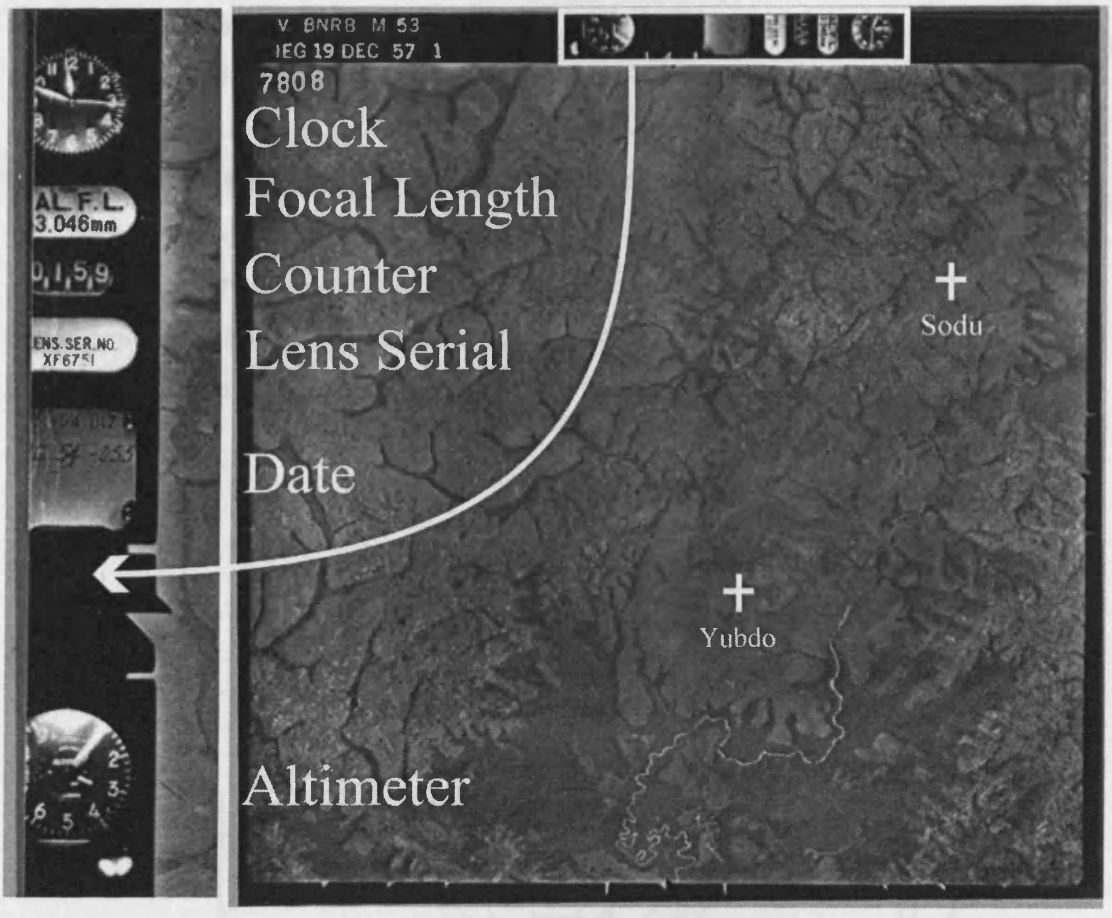

Figure 4.2: A typical aerial photograph with the data block enlarged.

4.2.3. The Acquisition of Aerial Photographs

This section covers the physics of the acquisition of aerial photography. Typical cameras used in aerial photography are described, followed by an account of the properties of photographic film. The characteristics of photographic films and cameras cause several distortions and displacements which are described at the end of this section.

There are several types of camera used on aircraft; panoramic, multilens, strip (for a review see Wolf, 1983). However in this study, airphotos were aquired using a single lens frame mapping camera. Single lens frame cameras are the simplest type of aerial camera. The setup of the camera is based around the focal length, which is selected according to the intended application for the resulting images. The focal length of a camera is of

importance as it determines the angular field of view of the photographs. As the camera is always set up with the image distance as the focal length of the lens, the shorter the focal length the wider the field of view (Wolf, 1983; Paine, 1981). Figure 4.3 shows the three main sections of the single lens frame mapping camera: magazine, body and lens cone assembly (Lillesand and Kiefer, 2000). The "data block" is shown on figures 4.3 and 4.2. In this feature several measurements are displayed so that the photograph includes a number of key readings including: altitude, time of day, focal length, exposure number, lens serial number and date.

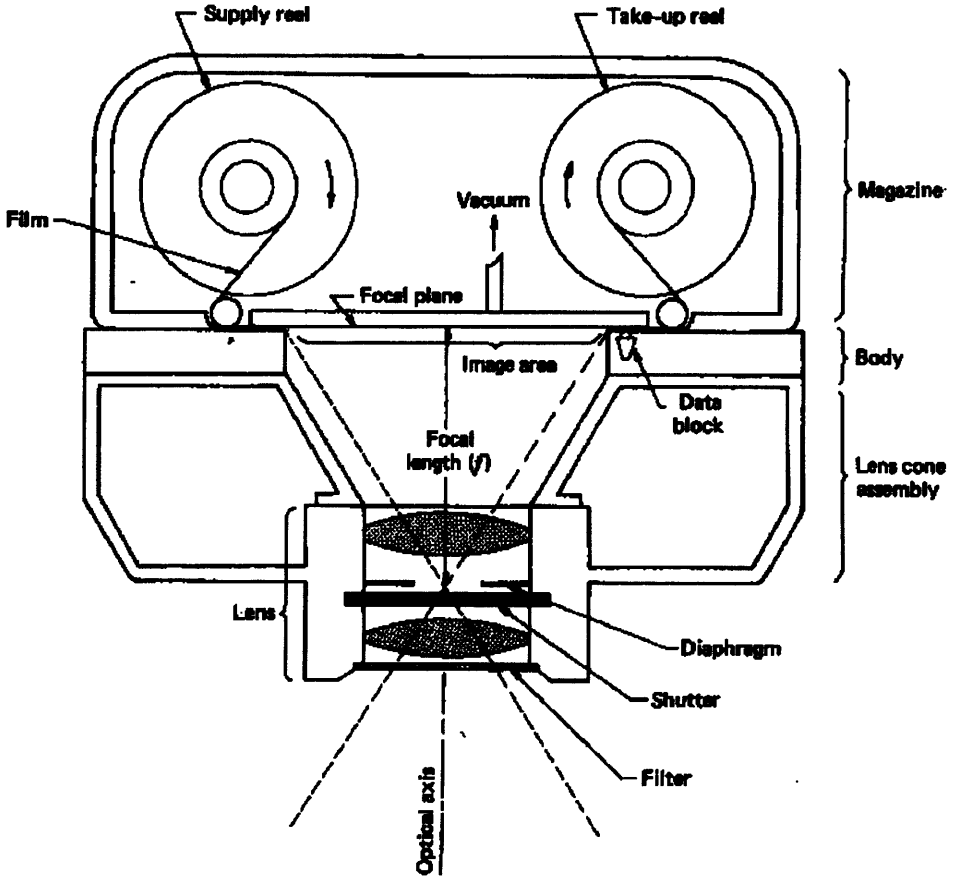

Figure 4.3: Principle components of a single-lens mapping camera (Lillesand and Kiefer, 2000)

Within the camera, light rays traveling from the scene are focused through a lens onto a film creating an invisible "latent" image. As a result the image acquired in the camera is negative (black and white exchanged) and reversed both left for right and top for bottom through the camera lens. Printing then produces a visible image on print paper and the

image is positive with axes corrected. Although many types of film are available such as colour and infra-red, the film used in this study is panchromatic. Such films are not the same as a "black and white" films. Panchromatic films produce an image based on the total light intensity, so a bright scene at any wavelength appears as white on the image (Lillesand and Kiefer, 2000).

A vertical aerial photograph is not a map. It is the product of a perspective projection and as such there are displacements and distortions which affect the image which are as follows:

- **Exposure fall-off.** The image appears brighter in the centre than at the edges of the scene. This is because the light collected from the further points has traveled further through the dust in the air and the scene is viewed from a more oblique angle. This is more obvious when using wide angle lenses.
- **Vignetting.** These are shadowing effects as a result of lens imperfections and parts of the camera.
- **Relief displacement.** This has the strongest effect in mountainous or urban scenes. The top of a vertical object is observed as being further away from the centre of the image than the bottom of the object (Wolf, 1983).
- **Tilt displacement.** An aerial photograph is never truly vertical and as such, relief displacement (see above) is exaggerated in particular directions.
- **Lens distortion.** This is the effect of imperfections in the grinding and production of the lens causing the image to be blurred or distorted mainly on the outside of the image and depends on the f-stop used in the aperture.

Some of these problems, such as exposure fall-off, vignetting and lens distortion are normally corrected through calibration. A scene of known and uniform brightness is imaged and the systematic variations in image tone recorded on the film are used to

create a filter, or recalibrate parts of the camera apparatus (Lillesand and Kiefer, 2000). However, the problems associated with relief and tilt displacement need to be addressed by image processing.

4.2.4. Image Processing

An aerial photograph does not exactly match the scene it represents due to a number of factors (see section 4.2.3). The process of orthocorrection reduces the impact of relief and tilt displacement. Furthermore the images must be associated with a map projection to allow other spatial data to be compared with it, a process known as georeferencing. The aerial photography used in this study was orthocorrected and georeferenced simultaneously, using PCI Geomatica Orthoengine (version 8.3).

Geomatica is a suite of programs used to create Geographic Information System (GIS) databases. Within this software package, Orthoengine is an image processing tool which can be used to allow aerial photographs to be used with GIS applications. In this study it is used to correct geometric distortions and to georeference the aerial photographs. The method used to correct the photographs is called polynomial correction. The aerial photograph is scanned at a resolution of 600dpi and saved in TIFF file format. The user defines 5 to 10 points on the image and these are known as Ground Control Points (GCPs). Each point is then located on a map and each GCP is assigned to a location based on the grid system used on the map. Each image has a number of defined points with a grid reference assigned, the program uses an iteration technique to determine a polynomial function (unique to each image) which describes the translation and rotation necessary to distort those image points to fit the grid defined by the grid references. It then uses this polynomial to distort the entire image to fit the grid. This process is completed for all images. These corrected images were then combined as a mosaic and saved as one image.

The cartographic system chosen for this study is the Universal Transverse Mercator which matches the Ethiopian national grid. It was chosen to allow an easy comparison between this study and other work in the area and provides a smaller degree of distortion

than latitude and longitude grids. The aerial photographs of this study were georeferenced to the following grid:

Grid	UTM Zone 36
Projection	Transverse Mercator
Spheroid	Clarke 1880 (modified)
Unit of measurement	Metre
Meridian of origin	33°E
Latitude at origin	Equator
Datum	Adindan (30th Arc)

Table 4.3: The mapping parameters used in the study.

4.3. Terrain Analysis

4.3.1. Introduction

In this study, the technique of Terrain Analysis is used to evaluate the landforms in the WES with the aim of producing a map of photomorphic regions which the reflect the underlying geology and the soil geochemistry. The term "Terrain Analysis" has been used to describe a variety of activities which evaluate landforms (for example see Wilson and Gallant, 2000 or Townshend, 1981). The method used here is the form of Terrain Analysis which is reviewed by Lillesand and Kiefer (2000). For a more detailed account of the method see Way (1973).

The aerial photographs described in section 4.2 were viewed using a mirror stereoscope (see section 4.3.2) and the landforms in each stereo-pair were analysed using five "terrain elements" which are explained in section 4.3.3. These landform properties were then used to delineate "photomorphic regions" (see section 4.3.9) and the boundaries of such regions were then tested by field work (see section 4.3.10).

4.3.2. Stereoscopy

A stereoscope was used to aid in the analysis of the landforms which have been photographed. This enables an operator to view two images simultaneously and thereby observe the landforms in 3-dimensions. The two photographs are referred to as a stereo-pair. The aerial photographs used here have an overlap at least 50% with of the

4.3.4. Terrain Elements: Drainage pattern

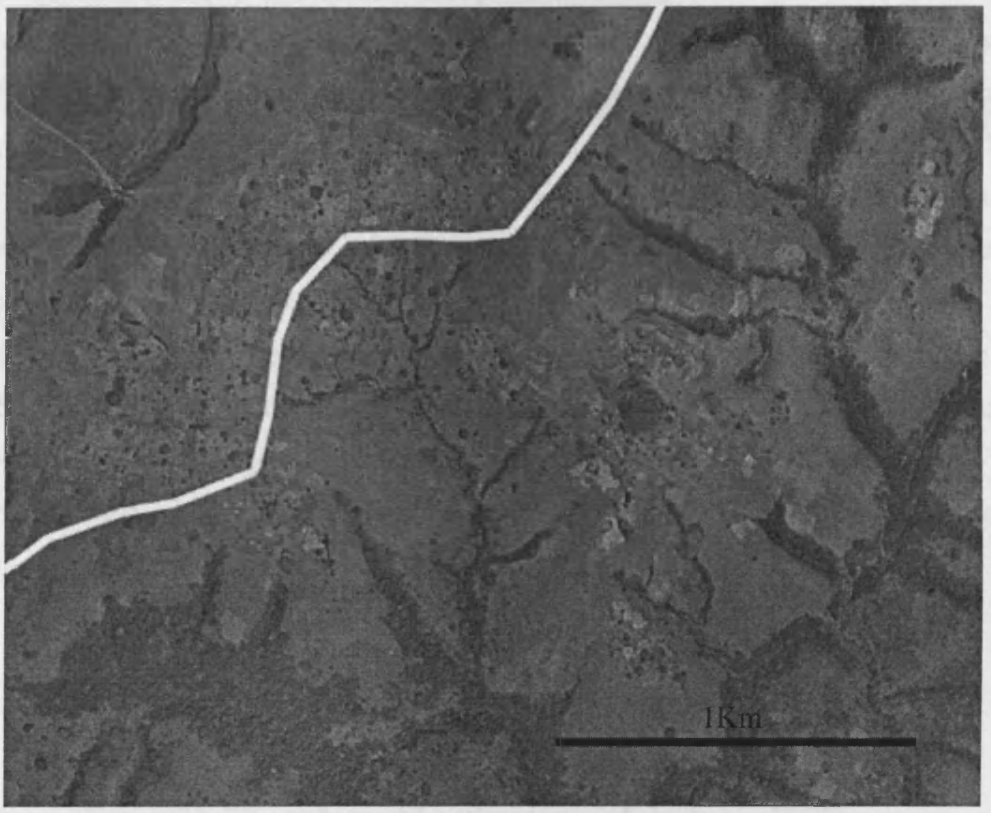

Figure 4.4: A section from an aerial photograph showing the boundary between a coarse dendritic (top left) and fine dendritic (bottom right) drainage patterns. This image is uncorrected and therefore the scale is approximate.

The drainage pattern of an area is the pattern made by the network of waterways. Drainage patterns are classified according both pattern and texture. The pattern is determined according to the direction and shape of the waterways (see figure 4.5). The texture is the density of waterways in an area, ranging from fine to coarse (see figure 4.6). In this study drainage pattern textures are classified as follows:

- **Coarse.** Less than or equal to 3 waterway intersections per km^2
- **Medium.** Between 3 and 6 waterway intersections per km^2
- **Fine.** Greater than 6 waterway intersections per km^2

There are many factors which affect the drainage pattern. Some factors are equal over areas the size of the WES, these include: rainfall, temperature and evaporation rate. However over a few kilometers, the relative proportions of overland flow to groundwater flow determine the texture of drainage pattern. In a situation where rain falls onto ground which is entirely impermeable, all runoff must be overland, and therefore due to the large flux of water over the surface, many waterways will be formed. Where most runoff passes through the groundwater, few waterways will form and the drainage texture will be coarser. Thus drainage pattern directly reflects underlying rock and soil type Furthermore, the strike of geological layering will affect the direction in which water runs off the land surface and therefore drainage pattern can reflect the underlying structure. For example trellis drainage patterns typically form over inclined sedimentary beds whereas dendritic may form over homogenous igneous bodies. For further discussion of the interpretation of drainage patterns see Way (1973).

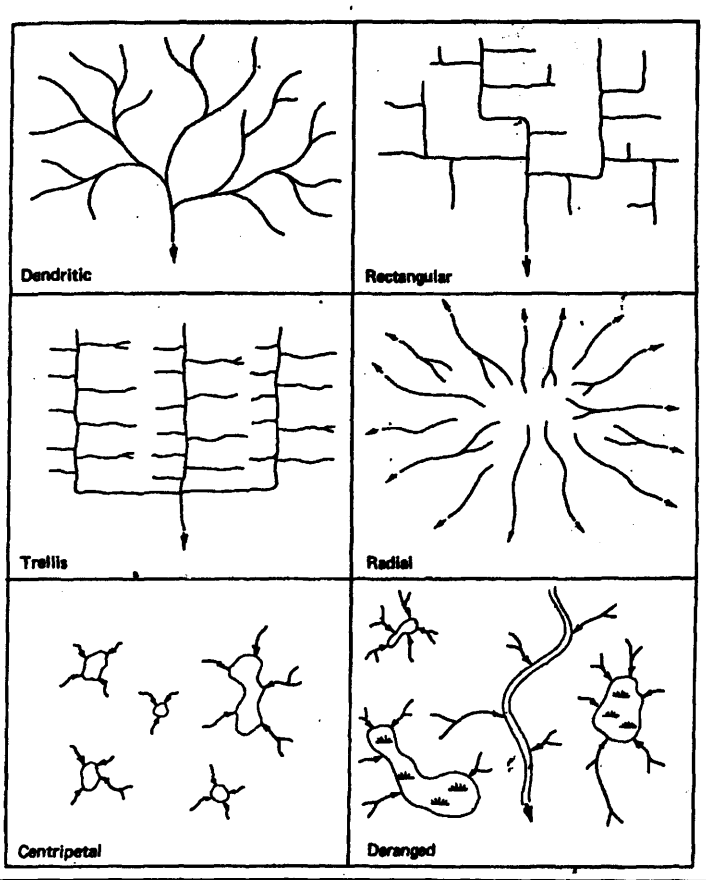

Figure 4.5: The six basic drainage patterns, after Lillesand and Keifer (2000)

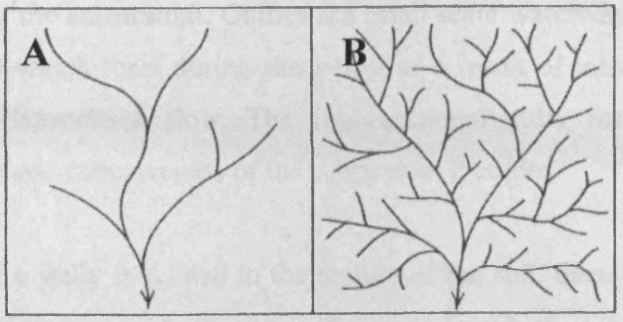

Figure 4.6: Illustrations of drainage texture. A: coarse-textured and B: fine-textured, after Lillesand and Keifer (2000).

4.3.5. Terrain Elements: Erosion

Figure 4.7: A section from an aerial photograph showing the boundary between areas with round-bottomed gullies (left) and v-shaped gullies (right). This image is uncorrected and therefore the scale is approximate.

The form of gullies in an area is assessed in order to determine the way in which erosion has been controlled by the substratum. Gullies are small scale waterways (sometimes as small as 1m in width) which form during sheet flow as a result of intense precipitation which changes into channelised flow. The cross-sectional gully form is controlled partially by the texture and cohesiveness of the substratum it erodes.

Although the shape of a gully is related to the texture of the soil, these textures may be controlled by the underlying bedrock. Since the way in which a rock weathers is controlled in part by its hardness, the underlying lithotype may exert some control over the texture of the overlying soils and thereby the gully shape. Table 4.4 shows the three cross-sectional forms and the substratum textures associated with them.

Name	Cross-section	Related textures (Way, 1973; Lillesand and Kiefer, 2000)
Round bottomed		Cohesive clays and silty clays. Usually found in lake beds, marine terraces and clay-shale areas.
Flat bottomed		Moderately cohesive silt. Often loess and alluvial silt deposits.
V-Shaped		Noncohesive granular materials. Sand and Gravel. Often terraces and outwash plains.

Table 4.4: Gully cross-sections and their related textures.

4.3.6. Terrain Elements: Topography

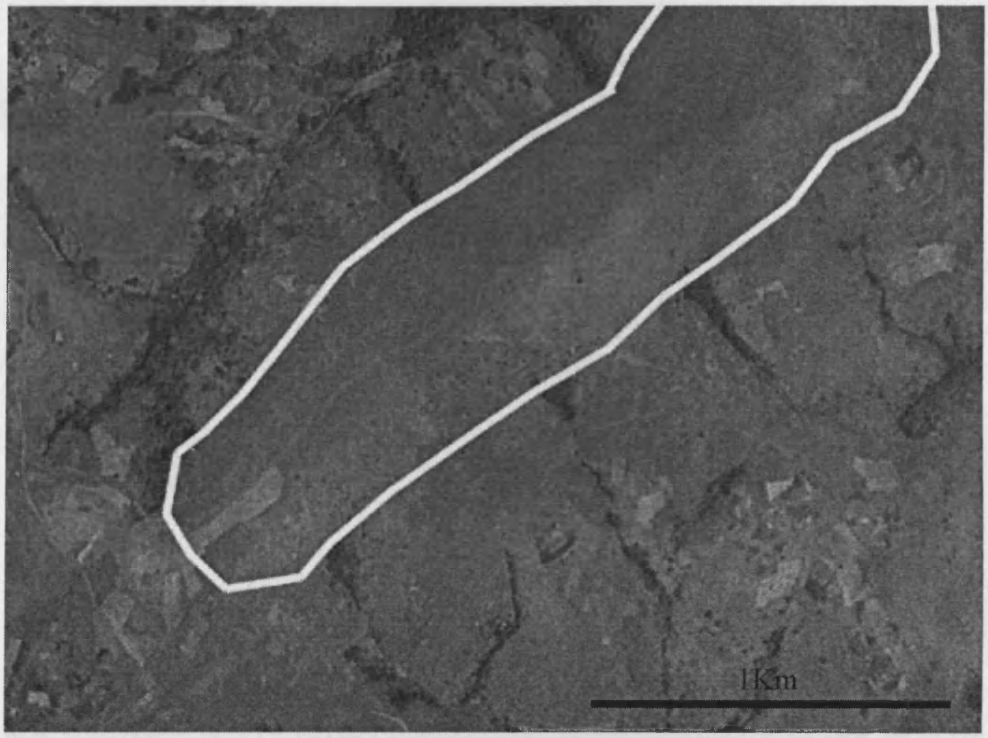

Figure 4.8: A section from an aerial photograph showing a ridge (center) and smaller hills around the outside. This image is uncorrected and therefore the scale is approximate.

There are numerous ways in which topography can be characterized (see Way, 1973) and modern landform analysis uses slope measurements from digital terrain models (Wilson and Gallant, 2000). In this study, the assessment of topography is used to record only whether or not the terrain forms a ridge (as shown in figure 4.1). Hard lithotypes are eroded less than softer rocks and hence hard formations form ridges.

4.3.7. Terrain Elements: Relative image tone and texture

Figure 4.9: A section from an aerial photograph showing the boundaries between bright and dark image tones. The darkest mottled texture is tree cover, however the dark tone of the soil can be observed between trees. This image is uncorrected and therefore the scale is approximate.

The brightness of a land-form (tone) can vary widely (see figure 4.9). Within areas of bare soil or thin vegetation, changes in image tone reflect the moisture content of that soil, this can vary according the texture of that soil and the parent rock material. Within areas of bare soil, the tone may vary and create a tonal texture. This texture can be a useful indicator of soil conditions and soil textures themselves. Within areas of apparently homogenous tone, very fine changes in tone may occur, showing the differences in moisture content.

The images used in this study are panchromatic, which means that they record the total light exposure of all colour bands (including some near-infrared). Due to the exposure fall-off (see section 4.2.3) it is only possible to determine differences in relative image tone. Absolute values for image tone cannot be determined using these images.

4.3.8. Terrain Elements: Land use

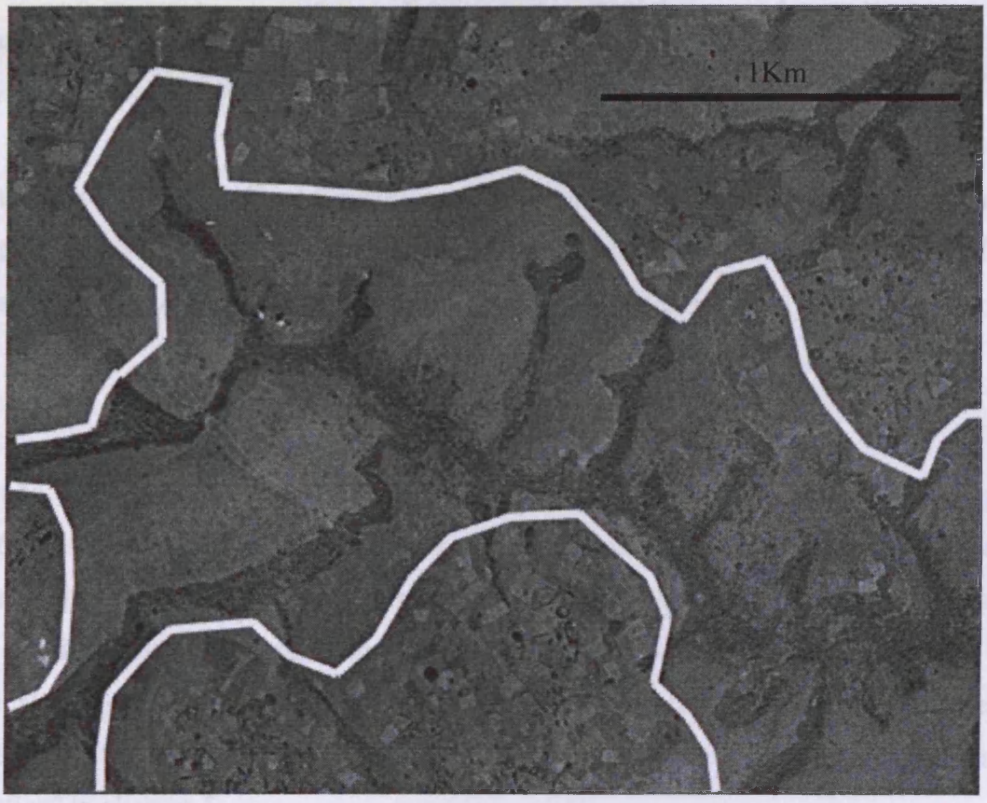

Figure 4.10: A section from an aerial photograph showing the boundary between cultivated land (bottom and top) and non-cultivated land (center). Subsistence farms in Ethiopia typically cultivate fields of no larger than 500m in width. These appear on aerial photographs as a "patchwork" texture. This image is uncorrected and therefore the scale is approximate.

This categorory is an assessment of land use either as vegetation, cultivation or neither. The type and origin of vegetation can indicate important changes in soil geochemistry which are closely related to the parent rock type. Areas of dense cultivation tend to follow water-courses and can also indicate a fertile soil and areas of dense vegetation may indicate other properties such as a high moisture content.

4.3.9. Photomorphic Regions

In order to combine and illustrate the information recorded from the analysis of the air photo stereopairs, a number of photomorphic regions are delineated. A photomorphic

region is defined as a discrete geographic unit within which at least one terrain element is uniform (Lillesand and Kiefer, 2000). In some cases more than one terrain element may be uniform within the photomorphic region. The concept of photomorphic regions is used in many remote sensing mapping applications, not only geological investigations (Lillesand and Kiefer, 2000).

Using the ArcView 3.2 software package, the photomorphic regions were overlain onto the orthocorrected and georeferenced aerial photographs (see section 4.2.4). The information has been presented as a set of four maps (see section 4.4).

4.3.10. Ground Truth

In order to validate the relationship between the land-forms and the underlying geology, each of the suspected ultramafic complexes was studied in the field and samples were collected. The petrology and geochemistry of these samples was investigated and the results are discussed in the subsequent chapters. Chapter 5 describes the full results of geological mapping in the WES. In some areas, there are landforms which have been mapped as ultramafic but no exposure has been found, these are defined as "suspected ultramafics" in chapter 5.

4.4. The Terrain in the WES

4.4.1. The photomorphic regions

A total of 25 photomorphic regions have been defined in this study but not all occur in any one of the four geographic maps. A description of the terrain for each region is contained in table 4.5. The ground truth study established that four formations can be effectively mapped by using terrain analysis, these are Basement, Graphitic Schist, Basalt and Ultramafic. In addition to this, the ground truth investigation discovered that the geological terrain information in some areas is obscured by the practice of burning savanna grass.

Photomorphic region	Drainage Pattern	Erosion	Topography	Relative Image Tone and Texture	Land use
Basalt A	coarse dendritic	flat bottomed	plateau rolling hills	bright polygonal texture.	Highly cultivated. Vegetation along roads and bottoms of valleys.
Basalt B	coarse dendritic	v-shaped	non-orientated hills and ridges	heterogenous	Sparse vegetation everywhere (individual trees) small fields everywhere.
Basalt C	medium to fine dendritic	v-shaped and flat in places	non-orientated hills and ridges	dark in most places	Dense vegetation covering most parts. Small patches of cultivation.
Basalt D	medium to fine dendritic	v-shaped	non-orientated hills and ridges	mainly heterogenous. One patch of dark tone	Cultivation in many places. Dense veg at the bottom of gullies.
Ultramafic A	very fine parallel	v-shaped	single big hill	mostly very dark some light swathes	No cultivation very little vegetation
Ultramafic B	coarse dendritic	v-shaped	large distinct hills	medium to light (dep on exp. cond.)	V. sparse veg, v. little cultivation although some.
Ultramafic C	fine dendritic	v-shaped	incline	dark tone	No cultivation, sparse vegetation in most places.
Ultramafic D	medium trellis	rounded	ridges, one elongate	light homogenous	Vegetation strictly at bottoms of valleys. No cultivation.
Basement A	fine trellis	v-shaped	steep sided, ridges NNE-SSW.	homogenous light tone on valley sides	Only ridge tops cultivated. Natural vegetation at bottom of valleys only.
Basement B	fine dendritic	v shaped	small hills and ridges	medium to dark tone. homogenous	Some vegetation out of gullies, very little cultivation.
Basement C	v fine dendritic	v-shaped	non-orientated ridges	generally dark tone	Vegetation in most areas. Very little cultivation
Basement D	medium to fine dendritic	rounded	non-orientated hills and ridges	mainly dark tone	Mostly covered by dense veg. Cultivation at the top of the ridges/hills.
Basement E	fine dendritic		non-oriented hills	dark	Dense vegetation and no cultivation.
Basement F	medium dendritic	rounded	non-orientated hills	heterogenous	Generally barren but some areas of cultivation

Basement G	medium to fine dendritic		non-orientated hills and ridges	heterogenous	Veg in bottom of gullies. Cultivation in most places
Basement H	fine dendritic	v-shaped	non-oreintated hills and ridges	heterogenous	Cultivated in most places some vegetataion out of gullies
Basement I	v fine dendritic	v-shaped	large ridge, high elevation	heterogenous	Veg in bottom of gullies. Cultivation in most places
Basement J	medium trellis	rounded	ridge	bright near the top of the ridge. Darker tone generally towards the bottoms of slopes	Cultivtaion at the top of the ridge. Spare cult in most places.
Basement K	fine parralell on the west, fine dendritic on the east	v-shaped	large ridge, high elevation	medium tone	No cultivation very little vegetation.
Basement L	N/A ?coarse?	rounded	ridge	light tone	Cultivated in most places.
Basement M	medium to fine dendritic	v-shaped	variably oriented large ridges	generally light tone	Cultivation widespread but sparse. Little dense vegetation.
Basement N	v coarse dendritic	rounded	low gradient rounded hills	homogenous medium tone	Completely uncultivated, some large patches of dense vegetation.
Basement O	medium radial	v-shaped	large hill	medium tone	No cultivation very little vegetation.
Graphitic Schist	trellis	v-shaped	small distinctive ridges	mostly dark altough some lighter	Dense vegetation no cultivation.
Burnt Grass	fine dendritic	v-shaped	variable	very dark	no cultivation or vegetation

Table 4.5: A table of the photomorphic regions of the WES.

4.4.2. Tulu Dimtu

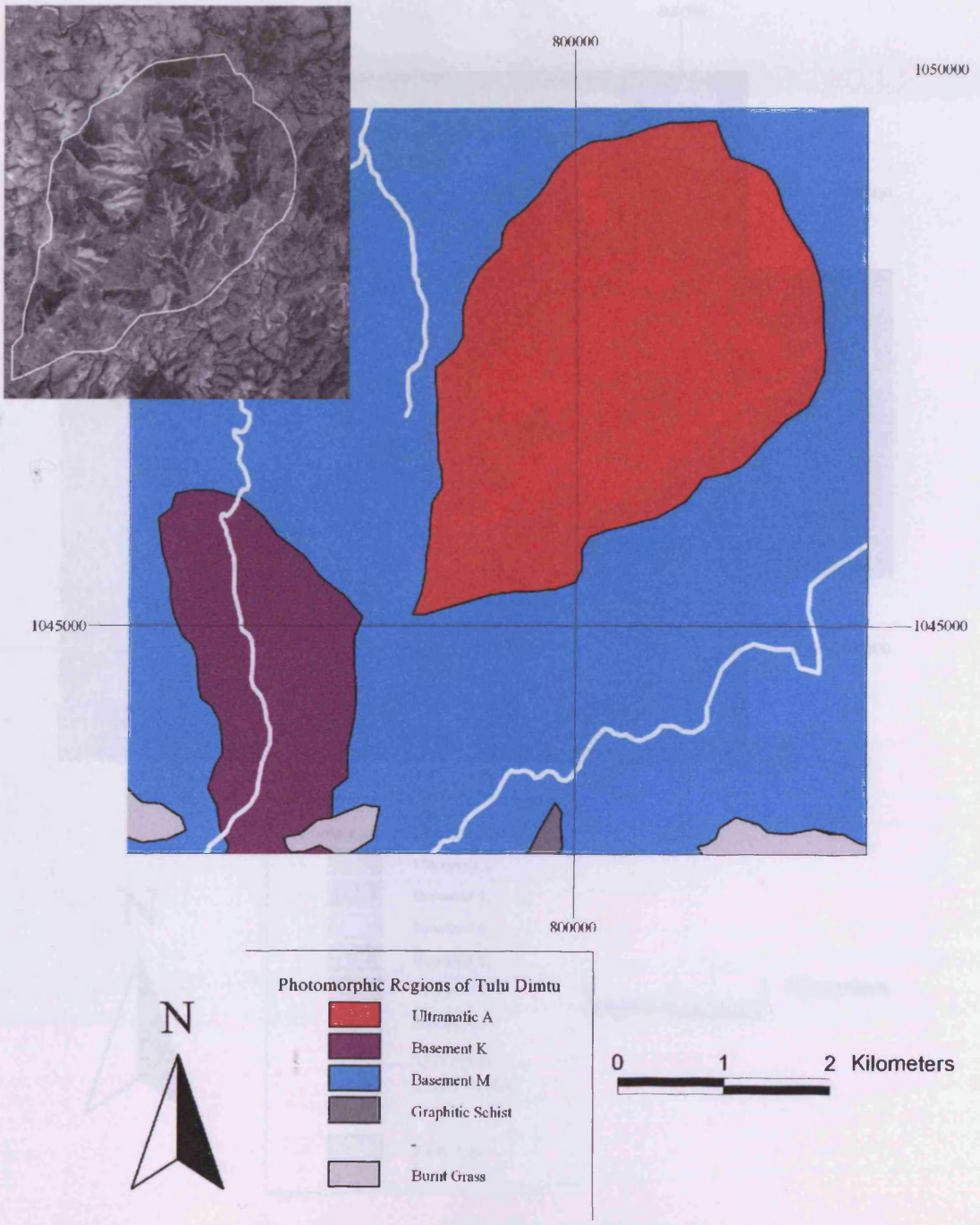

Figure 4.11: A map of photomorphic regions for the Tulu Dimtu area. White lines indicate the course of the major rivers. Inset is a representative aerial photograph showing the main ultramafic formation.

4.4.3. Kingy

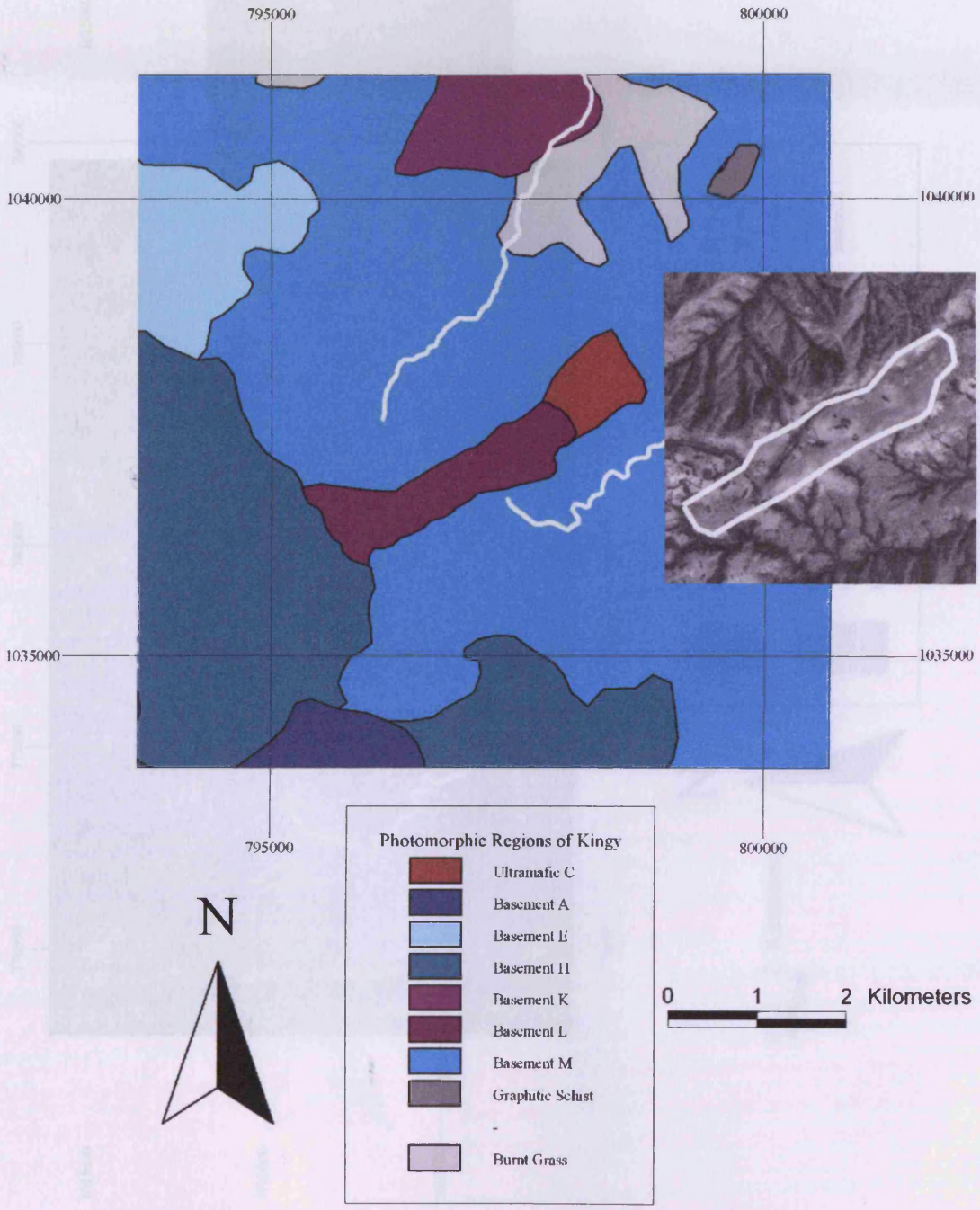

Figure 4.12: A map of photmorphic regions for the Kingy area. White lines indicate the course of the major rivers. Inset is a representative aerial photograph showing the main ultramafic formation.

4.4.4. Daleti, Ankori, Tulu Kapi and Keley

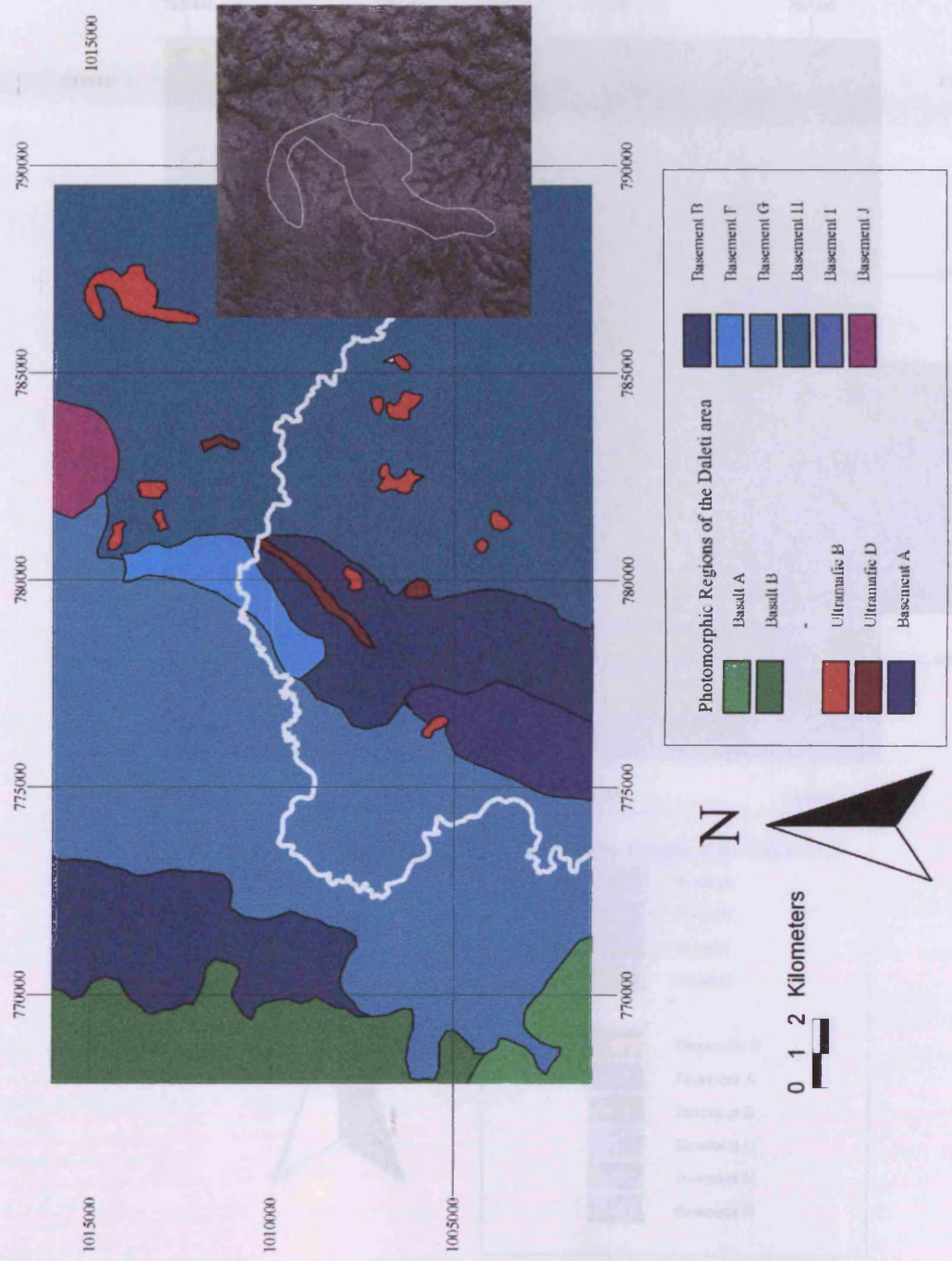

Figure 4.13: A map of photmorphic regions for the Daleti, Ankori, Tulu Kapi and Keley areas. White lines indicate the course of the Birbir river. Inset is a representative aerial photograph showing the main ultramafic formation.

4.4.5. Yubdo, Sodu and Andu

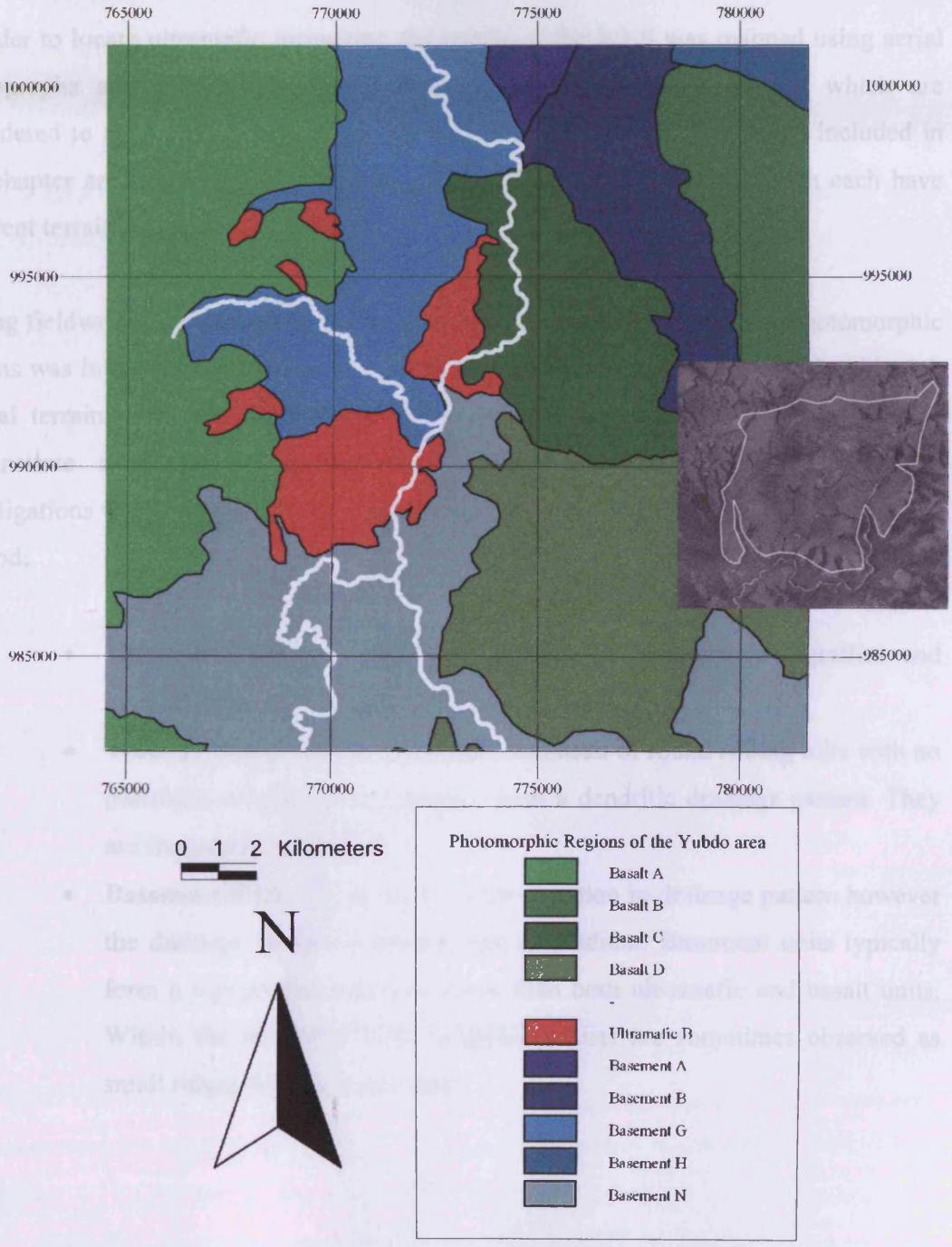

Figure 4.14: A map of photmorphic regions for the Yubdo, Andu and Sodu areas. White lines indicate the course of the major rivers. Inset is a representative aerial photograph showing the main ultramafic formation.

4.4.6. Summary

In order to locate ultramafic intrusions, the terrain of the WES was mapped using aerial photographs and the results plotted as maps of photomorphic regions which are considered to reflect the geology (see sections 4.2 and 4.3). The four maps included in this chapter are composed of a selection of 25 photomorphic regions which each have different terrain features.

During fieldwork, the changes in the geology over the boundaries between photomorphic regions was investigated. The results of such fieldwork is covered in chapter 5. Although several terrain units are identified as basement, in this study, it was not possible to demonstrate a change in geology over these boundaries. However, geological investigations have suggested that three major formations can be mapped using this method:

- **Ultramafic units.** These are identified as areas of sparse vegetation and no cultivation and almost always form ridges.
- **Tertiary Basalt units**. These form a plateau of round rolling hills with no particular orientation and always form a dendritic drainage pattern. They are frequently cultivated.
- **Basement units.** These have a wide variation in drainage pattern however the drainage texture is always fine or medium. Basement units typically form a topography which is lower than both ultramafic and basalt units. Within the basement units, graphitic schists are sometimes observed as small ridges with no cultivation.

5. Geological Mapping

5.1. Introduction

Small scale maps of the WES have been published by various authors. Additionally, large scale maps of the Main Yubdo Intrusion and the Tulu Dimtu Main Intrusion have been produced (Kazmin and Demessie, 1971; de Wit and Aguma, 1977). Of these maps, it is only those of the Main Yubdo Intrusion that provides details of the internal structure of the ultramafic complexes. It is for this reason that new maps have been produced during this study for Tulu Dimtu, Kingy and Daleti and the Kazmin and Demessie (1971) map of the Yubdo area has been modified in light of the observations made during this study.

These new maps have been created for use as a base for the presentation of geochemical data (see chapter 6) They are the result of a combination of field observations and terrain mapping. The lithologies identified here are those defined in chapter 3. Although the ultramafic formations are given names based on their fresh protoliths many of the rocks they represent may be completely replaced by metamorphic minerals (see chapters 2 and 3). Furthermore, the poor exposure and high degree of weathering makes the collection of structural measurements difficult. Although some geological structures (such as shear tension indicators) are visible in the basement, such information is not clear in the ultramafic units.

5.2. Method

The geological maps were compiled using several methods which were combined using a GIS database (ArcView 3.2). Fieldwork was carried out in four trips between September 2001 and June 2002. As a result, lithological descriptions of samples and field observations were combined with the terrain mapping information as described in chapter 4. Therefore on the maps, the basalt and basement units were mapped mainly using the terrain but verified geologically at the locations indicated on each map. The next four sections show the geological map of each of the geographic areas followed by a description of the geology.

5.3. *Geological Maps of the WES*

5.3.1. Tulu Dimtu

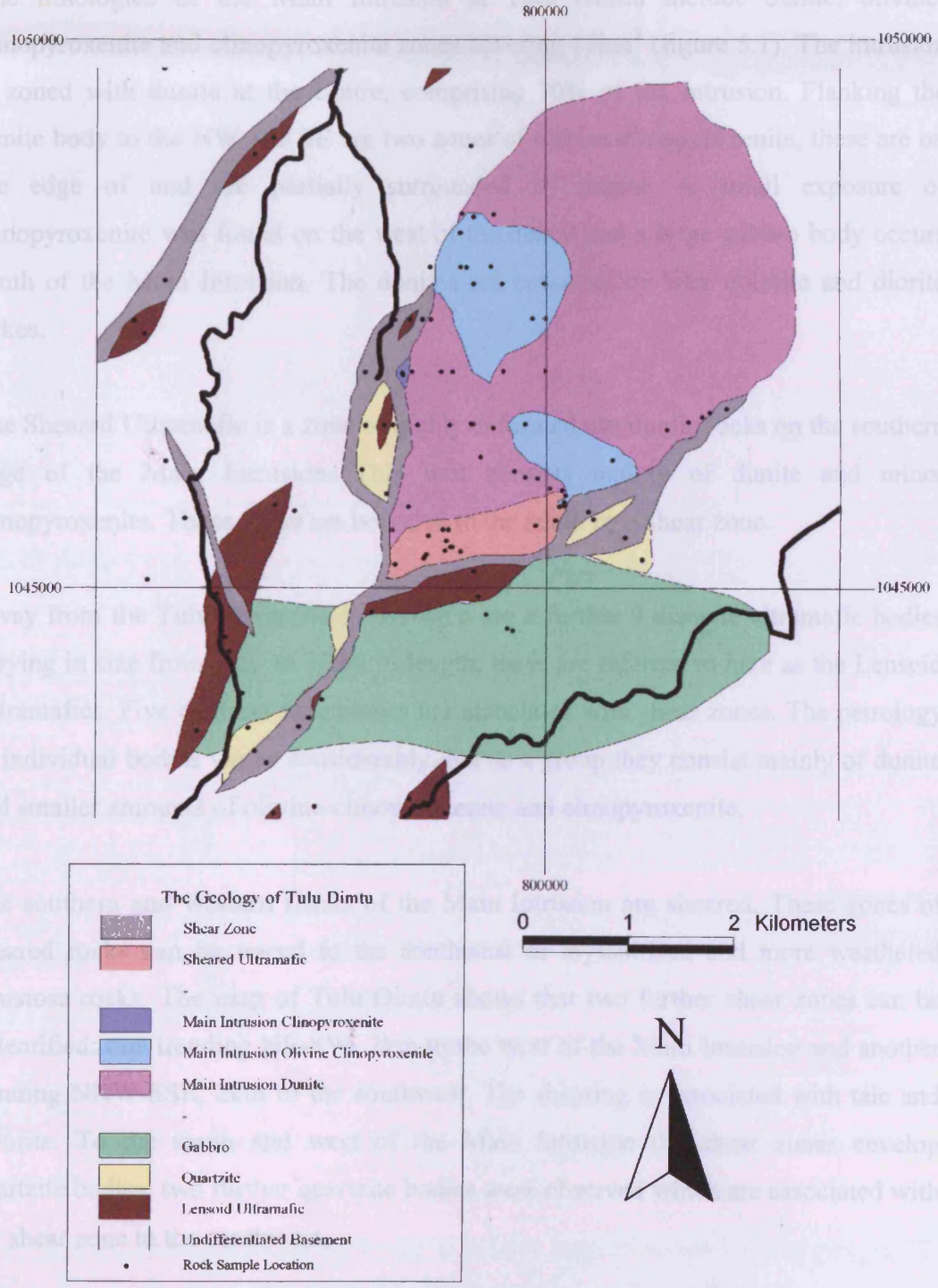

Figure 5.1: The geological map of the Tulu Dimtu area. Black lines indicate the course of the major rivers.

There are three groups of ultramafic rocks in the Tulu Dimtu area: The Main Intrusion, Sheared Ultramafic and the Lensoid Ultramafics.

The lithologies of the Main Intrusion at Tulu Dimtu include dunite, olivine-clinopyroxenite and clinopyroxenite zones covering 17km^2 (figure 5.1). The intrusion is zoned with dunite at the centre, comprising 70% of the intrusion. Flanking the dunite body to the NW and SE are two zones of olivine-clinopyroxenite, these are on the edge of and are partially surrounded by dunite. A small exposure of clinopyroxenite was found on the west of the dunite and a large gabbro body occurs south of the Main Intrusion. The dunites are cross-cut by later dolerite and diorite dykes.

The Sheared Ultramafic is a zone of highly deformed ultramafic rocks on the southern edge of the Main Intrusion. This unit consists mainly of dunite and minor clinopyroxenite. These rocks are bounded to the south by a shear zone.

Away from the Tulu Dimtu Main Intrusion are a further 9 discrete ultramafic bodies varying in size from 3km to 700m in length, these are referred to here as the Lensoid Ultramafics. Five of these nine bodies are associated with shear zones. The petrology of individual bodies varies considerably, but as a group they consist mainly of dunite and smaller amounts of olivine-clinopyroxenite and clinopyroxenite.

The southern and western flanks of the Main Intrusion are sheared. These zones of sheared rocks can be traced to the southwest as mylonitised and more weathered schistose rocks. The map of Tulu Dimtu shows that two further shear zones can be indentified: one trending NE-SW, 2km to the west of the Main Intrusion and another trending NNW-SSE, 2km to the southwest. The shearing is associated with talc and chlorite. To the south and west of the Main Intrusion the shear zones envelop quartzite bodies, two further quartzite bodies were observed which are associated with the shear zone to the southwest.

5.3.2. Kingy

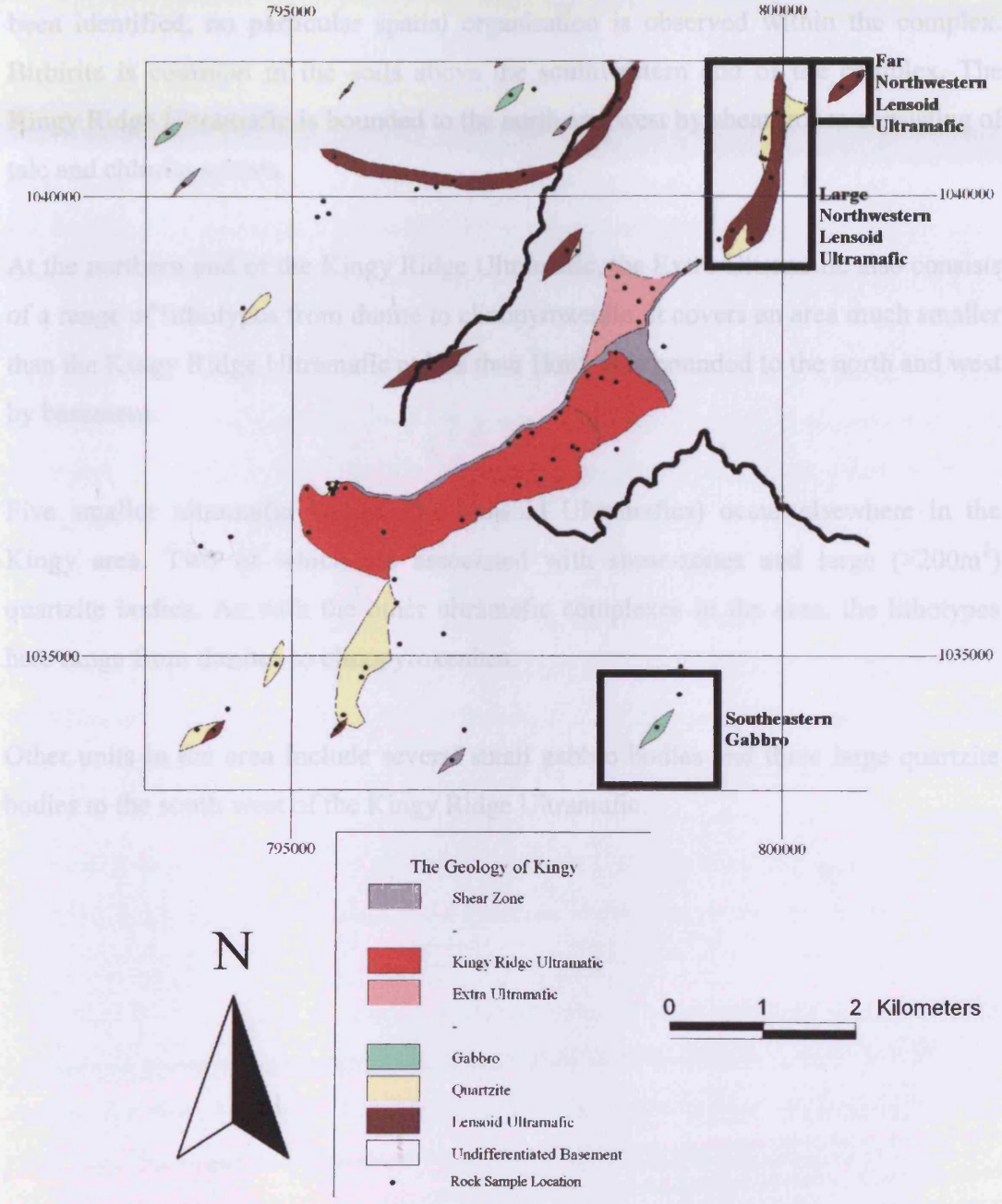

Figure 5.2: The geological map of the Kingy area. Black lines indicate the course of the major rivers.

The ultramafic complexes of the Kingy area have been allocated to three groups: The Kingy Ridge Ultramafic, the Extra Ultramafic and the Lensoid Ultramafics.

The Kingy Ridge Ultramafic is an NE-SW trending elongate body composed mainly of dunite and olivine-clinopyroxenite with a small amount of clinopyroxenite. These ultramafic lithologies cover a total area of 6km^2 and although three lithotypes have been identified, no particular spatial organisation is observed within the complex. Birbirite is common in the soils above the southwestern end of the complex. The Kingy Ridge Ultramafic is bounded to the north and west by shear-zones consisting of talc and chlorite schists.

At the northern end of the Kingy Ridge Ultramafic, the Extra Ultramafic also consists of a range of lithotypes from dunite to clinopyroxenite. It covers an area much smaller than the Kingy Ridge Ultramafic at less than 1km^2. It is bounded to the north and west by basement.

Five smaller ultramafic bodies (the Lensoid Ultramafics) occur elsewhere in the Kingy area. Two of which are associated with shear-zones and large (>200m^2) quartzite bodies. As with the other ultramafic complexes in the area, the lithotypes here range from dunites to clinopyroxenites.

Other units in the area include several small gabbro bodies and three large quartzite bodies to the south west of the Kingy Ridge Ultramafic.

of the Ankori Ultramafic have been located using terrain mapping (see chapter 4). However, no exposure could be found at these locations and therefore they are named "suspected ultramafics".

The largest complex is the Daleti Ultramafic which covers an area of around $5km^2$. The complex is a large dunite body with several pods of a mafic monomineralic rock around 6m in length and 2m in width and consisting mainly of spinel ($MgAl_2O_4$). To the northwest, the complex is bounded by a shear-zone consisting of talc-schists and a small gabbro body occurs close to the southern contact with the basement.

The Ankori Ultramafic is an elongate body of around 5km in length and up to 800m in width. It is composed mainly of dunite, but some minor clinopyroxene was observed near the northern tip. The complex is associated with some small quartzite bodies and is mostly surrounded by basement.

The five Lensoid Ultramafics occur throughout the area covered in this section. Only one locality has been found for each complex and as a result structural control on their association is very poor. Two of these bodies, in the Keley area, are closely associated with extensive shear-zones. Furthermore, a troctolite body has been located at Gudeya Guji associated with an elongate zone of talc and chlorite-schists. One Lensoid Ultramafic was located in the southern basement and a further ultramafic body was located close to a Tertiary Basalt and a quartzite in the northwest of the area.

Shear-zones are common within the basement units and they are often associated with ultramafics and quartzite bodies. The shear-zones at Gudeya Guji form in a distinctive straight NE-SW trending ridge in line with several smaller shear-zones to the southwest. Some gabbro units have been observed within the basement.

5.3.3. Daleti, Ankori, Tulu Kapi and Keley

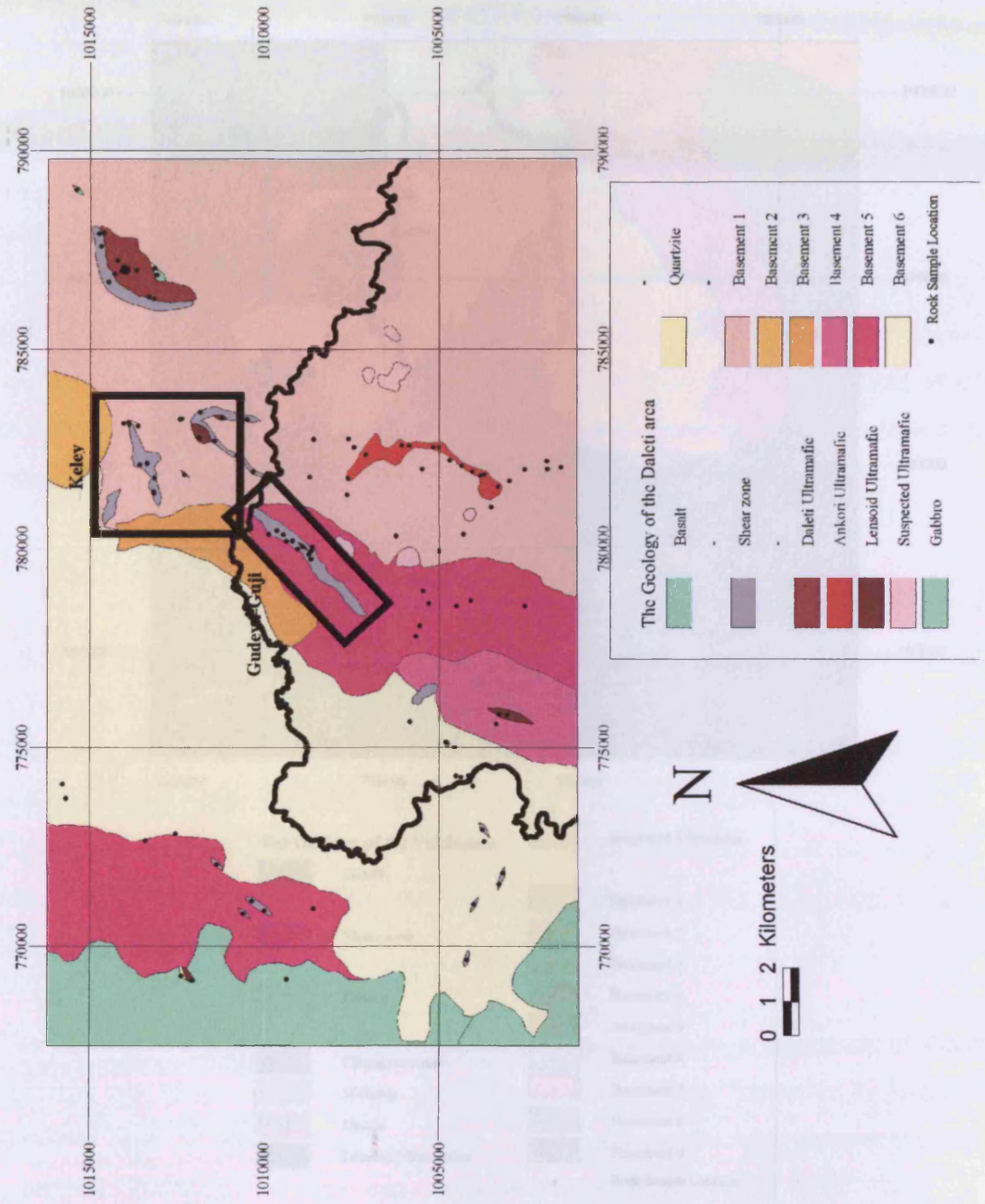

Figure 5.3: The geological map of the Daleti, Ankori, Tulu Kapi and Keley areas. Black lines indicate the course of the major rivers.

There are two large ultramafic complexes in this area, the Daleti Ultramafic and the Ankori Ultramafic. Additionally, there are five smaller complexes described here as the Lensoid Ultramafics. Several more possible ultramafic bodies to the east and west

5.3.4. Yubdo, Sodu and Andu

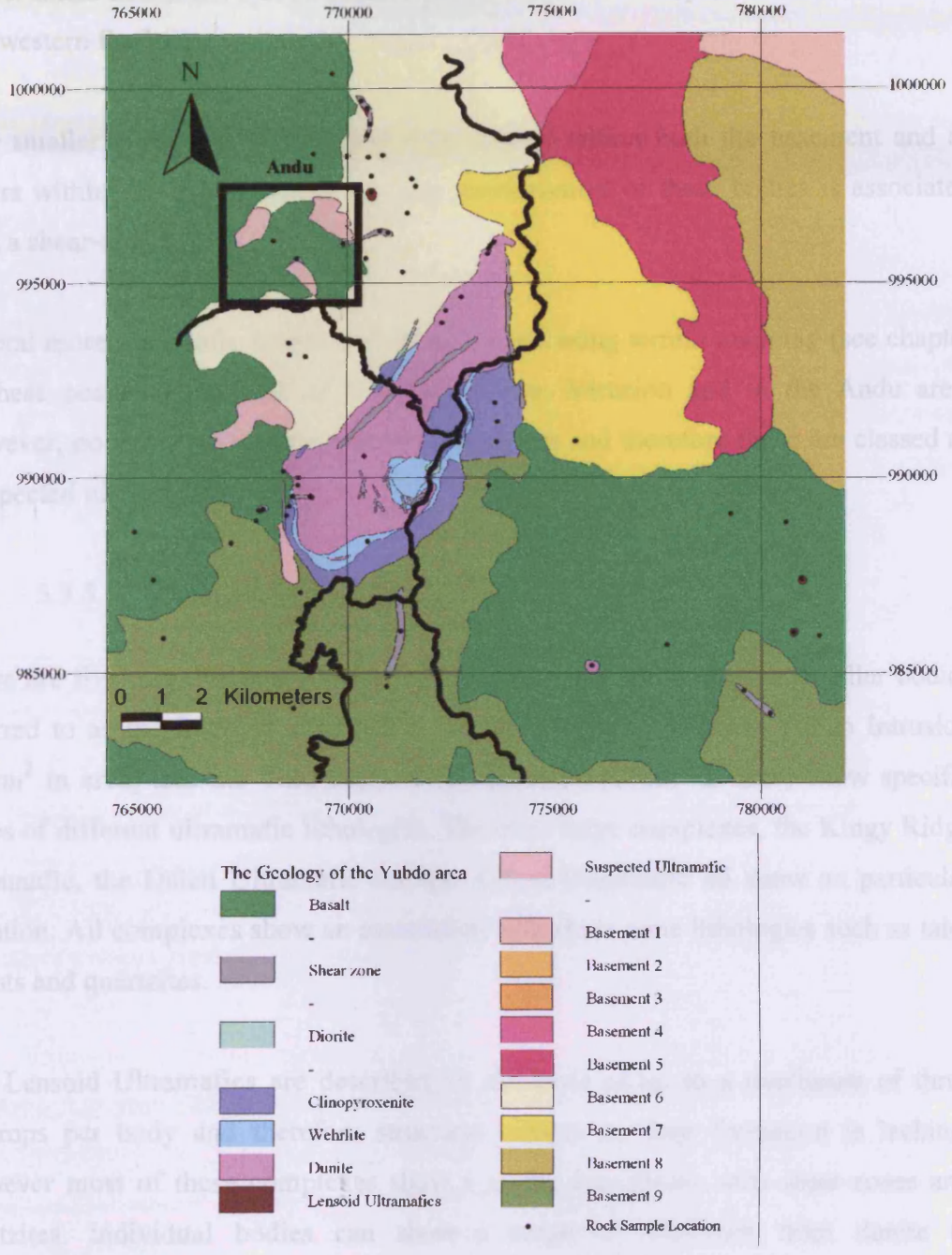

Figure 5.4: The geological map of the Yubdo, Andu and Sodu areas. Black lines indicate the course of the major rivers.

The Main Yubdo Intrusion covers an area of around 30km^2 and consists of three concentric zones with dunite in the core continuing outwards to olivine-clinopyroxenite and then clinopyroxenite. The clinopyroxenite zone is widest on the

eastern flank and only a few thin remnants are observed on the northwestern edge. Diorite dykes have been located in both the eastern and northwestern clinopyroxenite zones. Shear-zones have been observed both within the complex and on the eastern and western flanks.

Five smaller ultramafic bodies have been located within both the basement and as inliers within the Basalt formations. The northernmost of these bodies is associated with a shear-zone.

Several more ultramafic bodies have been located using terrain mapping (see chapter 4) these occur to the west of the Main Yubdo Intrusion and in the Andu area. However, no exposure was found over these bodes and therefore these are classed as "suspected ultramafics".

5.3.5. Summary

There are five large ultramafic complexes in the WES and numerous smaller bodies referred to as the Lensoid Ultramafics. The two largest, the Main Yubdo Intrusion (30km^2 in area) and the Tulu Dimtu Main Intrusion (17km^2 in area) show specific zones of different ultramafic lithologies. The other large complexes, the Kingy Ridge Ultramafic, the Daleti Ultramafic and the Ankori Ultramafic all show no particular zonation. All complexes show an association with shear-zone lithologies such as talc-schists and quartzites.

The Lensoid Ultramafics are described on the basis of up to a maximum of three outcrops per body and therefore structural control on their formation is lacking. However most of these complexes show a strong association with shear-zones and quartzites. Individual bodies can show a range of lithotypes from dunite to clinopyroxenite.

6. Ground Magnetics

6.1. Introduction

During the period from 25/5/2002 to 7/6/2002 a ground magnetic survey was conducted over the Main Yubdo Intrusion. This chapter examines the features of the magnetic field in the area and proposes a model to explain them.

The magnetic survey was conducted using two proton precession magnetometers. To allow for a high sensitivity, fluctuations in the magnetic field were eliminated by using one magnetometer as a base station. The results are displayed as 3 dimensional maps of the magnetic field in the 3rd dimension. Different colours are used to highlight high and low anomalies in the data.

In general a magnetic survey records the distribution of magnetic minerals including magnetite. Such variations may distinguish between different igneous lithologies such as pyroxenite and dunite or different degrees of alteration. In the Yubdo area there is field evidence for secondary alteration episodes such as shearing and silicification. Belete et al. (2000) suggest that hydrothermal processes are an important part of the PGE concentration mechanism. It is possible that alteration occurs either along zones of weakness related to shearing or it may be related to zoning of the igneous lithologies due to magmatic processes.

The aim of the survey described here was to understand the geometry of the alteration and therefore was carried out almost entirely within the dunitic core of the Main Yubdo Intrusion. The following sections describe the collection and description of the data and the results are displayed in several pull-out pages.

6.2. Methods

6.2.1. Data collection

Two Geometrics G856AX portable proton precession magnetometers were used, one set as the base station and one used to measure the magnetic field strength at the survey points. To allow for the greatest possible radiometric resolution, the base station was used to correct for diurnal fluctuations (see section 6.2.2). The base station was also run overnight in order to detect disturbances in the magnetic field caused by magnetic storms.

The base station magnetometer was powered using a car battery. The sensor was aligned to north and attached to a strong tree to prevent movement (figure 6.1). The strength of the magnetic field was recorded every 60 seconds and stored within a memory on the magnetometer. Each field strength reading was recorded against the day and time so that temporal fluctuations in the earth's magnetic field could be reconstructed. The sensor of the base station remained in the same place throughout the duration of the survey. The location of the base station was located at grid reference (769657,990747). The sensor was mounted 2.5m above the ground and the magnetometer was tuned to 34,400nT and the sensor coil mounted vertically. The coil orientation was decided by a test at the beginning of the survey (the results are described in section 6.3.1). Before and after the ground survey was carried out the base-station data was analysed with the aid of the Magmap program to detect the signs of any magnetic storms.

Figure 6.1: The magnetometer sensor set up aligned to N and attached to a tree.

The survey was carried out using a second G856AX magnetometer mounted on a harness. The sensor was mounted on a staff 2.5m high and oriented vertically. At each survey location, the sensor was aligned to north. For each reading stored in the magnetometer, a number of other items of data were also stored, including day, time, line number and mark number.

The two types of survey that were carried out were: wide and close grid spacing. During the wide grid spacing survey, the location of each survey point was determined using a handheld GPS receiver and stored as a waypoint. The GPS location data was combined with the magnetic field strength data using a spreadsheet. During a close grid spacing survey (<10m between survey points), the spacing between subsequent points was too small to be accurately determined using a handheld GPS, therefore the location of each point was surveyed using canvas based measuring tape. The location of the origin was determined using a GPS, the x-axis co-ordinate was recorded within the magnetometer as the line number. The Y co-ordinate was determined using pacing.

During the wide spacing survey the aim was to cover the largest possible area with 100m between each point. In open ground, a 100m spacing was achieved. However, figure 6.2 shows that large areas have no coverage at all. This is because areas of human influence should not be covered due to false readings from metal objects. Furthermore, there are two large open-cast pits which cannot be entered as they are unsafe and in places dense vegetation makes access unavailable. The location of the tight grid spacing survey is shown on figure 6.2.

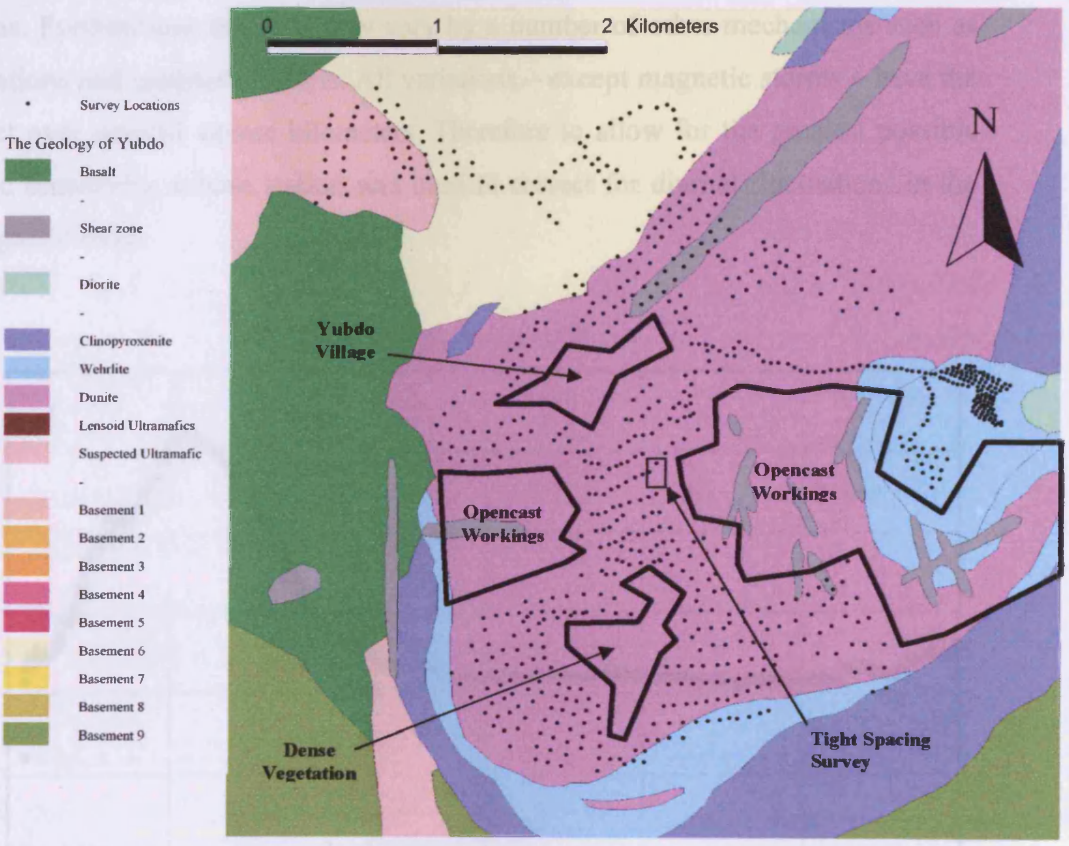

Figure 6.2: The survey point locations for the ground magnetic survey of the Main Yubdo Intrusion overlaid onto the geological map (see chapter 5).

During the coil orientation test a 4m grid spacing survey was carried out twice using two different methods: 1st with both sensors oriented vertically and 2nd with both sensor coils fixed horizontally. In both cases the origin of the grid was at grid reference (769950,990211) and the X-axis was oriented on a bearing of 196°. The aim of this test

was to assess which sensor orientation was the most radiometrically sensitive at the survey site.

6.2.2. Diurnal correction

The magnetic field at a location depends on a number of factors including the underlying geology. Diurnal variation is where the magnetic field varies with time over a 24 hour period, as illustrated in figure 6.3. At Yubdo this variation is frequently over 150gammas. Furthermore the field may vary by a number of other mechanisms such as micropulsations and magnetic storms. All variations – except magnetic storms – have the same effect over several square kilometers. Therefore to allow for the greatest possible radiometric sensitivity, a base station was used to correct for diurnal fluctuations in the Earths magnetic field.

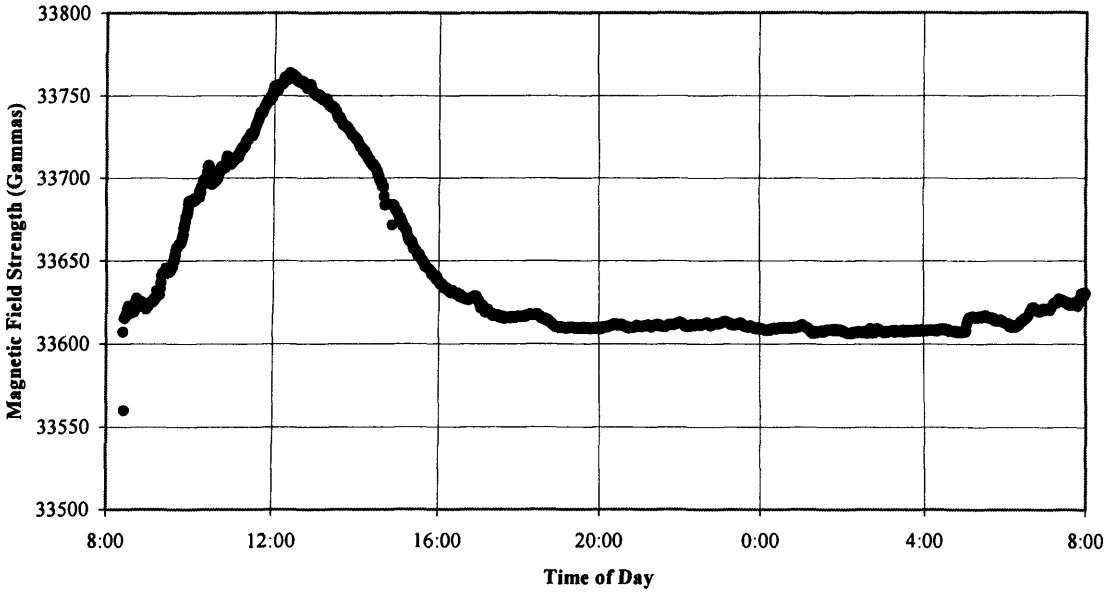

Figure 6.3: The magnetic field strength at the base station over a 24 hour period (30th to the 31st of May 2002)

Magnetic storms disrupt the magnetic field on a scale of several hundreds of metres and therefore a base station cannot cancel out this effect. No magnetic storms were detected during the period of this investigation.

As described in section 6.2.1, the base station automatically recorded the magnetic field every 60 seconds. The nearest base-station reading is subtracted from each reading taken with the portable magnetometer. Ideally, the readings at the portable magnetometer and the base station will have been taken at exactly the same time, but in reality this is unlikely to have been the case. Where no reading at the base station has been taken at the same time as the portable magnetometer, the MagMap software uses a linear time interpolation procedure to calculate an appropriate value.

6.2.3. Data presentation

The results of the survey at Yubdo are displayed as a three dimensional surface where the height of the surface is determined by the difference in the magnetic field strength at that point. The values for the locations between survey points have been interpolated using a kriging function. The magnetic field strength is diurnally corrected (see section 6.2.2) and displayed as a Log_{10} scale. Both negative and positive values for the corrected field strength occur in the dataset. These were processed separately so that the negative values remain negative on the Log_{10} scale. There are, in effect, two logarithmic scales used simultaneously: negative and positive.

The 3D maps are plotted with three different colour scales in order to emphasize key features. Figure 6.6 shows that map A uses the simplest set of colours, grading from blue at the lowest to red at the highest. Map B is the same as A except that a blue stripe is added at 0 and everything immediately lower than 0 is yellow grading to blue and everything immediately above 0 is green grading to red. Map C is the same as B except the blue stripe is just above $Log_{10} = 3$.

In order to demonstrate the variation in the field strength, Figure 6.7 shows the same area in 4 different orientations in 3D maps where the height represents the Log_{10} magnetic field strength with the same colour schemes as figure 6.6.

6.2.4. Limitations and accuracy

Two inaccuracies are involved with the method used for the collection of the data in this study and these must be considered during interpretation. One limitation is the accuracy of the handheld GPS. Although the location of each survey point is quoted to 12 figures – implying an accuracy of 1m – the location is only accurate to 10m. This does not have a direct effect on the nature of the conclusions, however any detailed work targeted by this survey should consider this inaccuracy.

The use of an interpolation function to calculate expected total field values away from survey points is necessary for the estimation of the shape of the magnetic field and the easy analysis of results. However it is possible that these estimated values are entirely incorrect. The varied results contained in this survey indicate that it is not only possible but quite likely that some estimated values are incorrect, however the use of this interpolation function is necessary for ease of analysis. The images of 3D surfaces (figures 6.6 and 6.7) show interpolated values for some areas over 1km away from the survey points. Interpolated values at large distances away from survey points are meaningless and are marked as white on figure 6.11.

The nature of the ground has meant that there were some areas where it was not possible to collect magnetic field data. As figure 6.2 shows, the size and shape of the survey means that there is barely 1km square of unbroken survey area. The areas shown in white in figure 6.11 are those areas where it is not possible to make interpretations due to lack of data. All areas delineated in figures 6.8 and 6.11 are only marked in areas where there is sufficient data to distinguish between two different patterns.

Given the use of a base station to correct for temporal changes and the use of proton precession magnetometers, the radiometric accuracy of the survey is considered to be 1 gamma which is a greater degree of accuracy than required for a geological investigation of this type.

The three colour schemes applied to the same data show two different groups of anomaly in the magnetic field of the Main Yubdo Intrusion (see figures 6.6 and 6.7). Map A in figure 6.6 shows that there are two large zones of negative anomalies in northern and southern parts of the survey area. However, the colour scheme used on map C shows that in addition to the wide anomalies (covering >200m in width), there are many smaller anomalies with widths of less than 100m. The wide anomalies cover two discrete zones in the north and south whereas the shorter anomalies occur over the whole area. The farthest northern and southern parts of the survey have a magnetic field which is relatively uniform and neither of the anomalies described above are observed.

- **Area 2 (red dots)**: Covering a total of ≈ 2.5km^2, the magnetic field strength in this area ranges from 3.2 to 3.5 Log_{10} units. It covers two large tracts in the north and south of the area shown in figure 6.8.
- **Area 3 (pink dots)**: This isolated area located at the centre of the the Main Yubdo Intrusion is characterized by an uneven magnetic field strength of around 3 Log_{10} units with small negative anomalies which can fall to 2.3 Log_{10} units.
- **Area 4 (yellow dots)**: This zone in the southern part of the survey area is entirely surrounded by area 2. The field strength is 2.5 Log_{10} units.
- **Area 5 (orange dots)**: Numerous small parts of the survey are covered by this form of non-uniform magnetic field ranging from 2.5 to 3.5 Log_{10} units.

UNIVERSITY PRIFYSGOL

Figure 6.9 shows the results of the tight grid spacing survey at Yubdo. Two distinct negative magnetic anomalies are observed. Both anomalies have a linear sinuous shape. The depth of the anomaly is approximately 2000 gammas. The shoulders of the anomaly are symmetrical. The very deep anomaly in the NW of the survey, corresponds to a small hut with a tin roof. Slight N-S trending offsets in the northernmost anomaly have been caused by slight inaccuracy in the pacing method of measuring the Y-coordinate.

6.4. Discussion

It is expected that the nature of the magnetic field can be explained by a heterogeneous distribution of magnetic minerals throughout the intrusion. These magnetic minerals are largely magnetite but possibly also maghemite, ulvöspinel and titanomagnetite. There are a number of models which could be used to explain all of or some of the features of the field, they are listed below.

- **Quartz Veining**: Siliceous veining can dilute the abundance of magnetite in parts of the ultramafic body. Variations in the density of veining will cause differences in patterns of magnetic field strength.
- **Serpentine Distribution**: During the alteration of olivine to serpentine Fe is released to form magnetite. Therefore different stages of alteration of the igneous rocks to serpentinite will produce different quantities of magnetite.
- **Chromitite Lenses**: Magnetite is less abundant in some areas due to the presence of fresh chromitite lenses. However, where chromite is altered to ferrichromite a greater magnetic susceptibility can occur.
- **Juxtaposition of magnetite bearing units**: Fault action causes preferential concentration of magnetite formed due to the alteration and focused along fault planes.

The magnetic field surveyed above the Main Yubdo Intrusion shows generally high values with 2 zones of large negative anomalies and numerous smaller negative

anomalies. The generally high values observed here are likely to be ultramafic rocks as they have some of the highest magnetic susceptibilities known (see table 6.1). Therefore the origin of the negative anomalies could be explained by the presence of some less magnetically susceptible units. It is unlikely that the presence of magnetite or chromite could have caused such a decrease in magnetic field strength as alteration would have created a high magnetic susceptibility. As seen in table 6.1 both quartzite and serpentinite have significantly lower magnetic susceptibilities than olivine or pyroxene-bearing rocks. However, the presence of Fe-rich spinels at the rims of olivine minerals in the Main Yubdo Intrusion (see chapter 3) suggests a role for serpentinisation in the formation of ferrichromite. Hence, it is likely that this ferrichromite would increase the magnetic field strength as a result of sepentinisation.

Rock	Average Magnetic Susceptibility ($x10^6$ emu)
Andesite	13,500
Peridotite	13,000
Pyroxenite	10,500
Diorite	7,000
Basalt	6,000
Gabbro	6,000
Serpentinite*	1,000
Quartzite	350
Amphibolite	60
Sandstone	30

Table 6.1: A table of magnetic susceptibility values in order of decreasing susceptibility (after Robinson and Coruh, 1988). *: This value is for pure serpentinite with very little magnetite.

Of the possible explanations covered above, the most likely cause of the variation in magnetic field strength over the Main Yubdo Intrusion is different degrees of quartz veining through the ultramafic lithotypes. Quartz veins can frequently be observed in the rocks of the Main Yubdo Intrusion and the remnants of such veins can also be seen in the laterites exposed in the quarry faces. Furthermore, Kazmin and Demessie (1971) have mapped a shear-zone which intersects with a zone of very low magnetic field strength observed here (see figure 6.8). It is feasible that the one of the major conduits of silica-rich fluids could have been a shear-zone. Smaller siliceous fluids could well have permeated through the rest of the complex to precipitate silica and create the lower magnetic anomalies. The value quoted for the magnetitic susceptibility of serpentinite in

table 6.1 is that of pure serpentinite with very little magnetite. When olivine is serpentinised, magnetite is formed as a result and hence a serpentinised dunite (as is observed at Yubdo, see chapter 3) will have a magnetitic susceptibility comparable to peridotite.

The negative anomalies mapped in the tight grid spacing survey may also be caused by siliceous veining. In the wide spacing survey, such anomalies appear to be circular due to the kriging interpolation function. However the tight spacing survey may have uncovered the geometry of these smaller veins. E-W trending quartz-veins can be observed in a quarry cutting 300m east of the tight spacing survey.

There are two zones in the farthest north and south (classified as area 2, see figure 6.8) where the magnetic field is relatively uniform and strong negative anomalies are not seen. The northernmost of these zones is over the area mapped as basement by terrain mapping and Kazmin and Demessie (1971). A possible explanation for this is that either the ultramafics or the basalts extend further than expected from geological mapping. Alternatively, this magnetic field could have been caused by ultramafic rocks which have not been silicified.

6.5. Conclusions

The results of the wide grid spacing survey are summarized by figure magintmap. Figure magmodel is a schematic diagram to illustrate the model suggested here to explain the anomalies observed in the total field during the magnetic survey. The features of this model are as follows:

- **High Frequency Siliceous Veining**: These are thin (around 10m wide) elongate zones of silicification. There are likely to be large slivers of ultramafics surrounded by quartz veining within the zone. The frequency of veins within the zone is likely to be greater than anywhere else in the survey. This results in some very low magnetic field readings directly over

veins and some higher readings – even within the zone – over slivers of trapped ultramafic. This vein morphology could be the result of hydrothermal fluids passing through a zone of structural weakness perhaps associated with shear deformation.

- **Low Frequency Siliceous Veining**: This zone generally has a greater proportion of ultramafic than the high frequency zone described above, but the veining is thinner and distributed more pervasively throughout the host rock. The result is a generally low and variable magnetic field (see section 6.3.2).
- **Non-silicified Ultramafic rocks**: These rocks contain very little variation in composition and must be either ultramafic rock or basalt. The two zones (figure 6.11) may be different rock types but both must be generally homogenous and of a high magnetic susceptibility. This results in a high magnetic field strength which varies very little.
- **Unidentified Anomalous rock**: This small zone to the south, is completely covered by a non-silicified ultramafic rock but shows anomalously low total field readings. This may be related to silicification, but the size and restricted shape does not support this idea.

The explanation of the anomaly patterns described above is supported by the results of the of the close spaced grid survey (figure 6.9). The characteristics of the anomalies observed can be explained by the presence of a steeply dipping planar feature having a lower magnetic susceptibility than its surroundings. This fits well with the idea of a quartz vein. The location of this anomaly is in the Low frequency Siliceous Veining zone identified in the wide spaced survey.

7. Soil Geochemical Data

7.1. Introduction

The Precambrian volcano-sediments and ultramafics of the WES are overlain by a thick and extensive laterite. As part of the exploration program in the WES, a total of 930 soil samples were collected from the four areas of study in this thesis. The samples were analysed for major and trace elements by OMAC laboratories with the aim of gaining an understanding of the economic value of the prospects being studied.

This chapter contains several sections within which the soils of the WES are described and observations of several key elements are made. After the sampling strategy and methods used to analyze the samples has been considered, a number of interpretation techniques have been applied to the data. As exploration data frequently displays gaussian distributions it was considered valuable to examine the dataset by using univariate statistical methods (Sinclair, 1983; Moon, 1995). This has allowed an understanding of the populations and modes present within the dataset, which in turn can be of use in evaluating PGE prospects. To compliment the statistical methods used, maps of the elemental distribution of Ni, Cu, Cr, Al, Pt and Pd are included and these are used to evaluate the use of overburden geochemistry to exploration within the WES.

Observations are made within this chapter which indicate a control on the geochemistry of the laterites in question not only by the underlying bedrock but also by hydromorphic dispersion.

7.2. The overburden of the WES

As a result of the important PGE placer deposits they contain, accounts of the structure and morphology of the lateritic soils in the WES occur in several publications the most recent of which is an MSc thesis (Childs, 2001). Other important documents include Augustithis (1965), Molly (1959) and Jelenc (1966), who all give extensive accounts of the nature of these bodies.

7.3. Sampling strategy

Soils samples were taken in traverses across open ground and in areas where access was not possible, the samples were taken parallel to roads but away from areas of human influence. They were taken within the bounds of the licence areas stated by the Ethiopian government. Furthermore, under the terms of their agreement with the government, GPM were required to take over 900 samples covering the whole licence area. The spatial constraints on sampling areas are described at the start of each section.

For the best geological use, the soil samples collected should be as close to the weathered bedrock as possible. However, given the depth of the laterite (often greater than 15m) it was impractical to collect samples close to the bedrock. In this study, the samples were taken from a depth of 10-20cm below the surface, within the laterite horizon (see section 7.2). In the poor agricultural conditions of Western Ethiopia, this was considered to be low enough not be influenced by humic acids from plant roots or human influence.

Noting the soil profile described in section 7.2, this sampling depth was considered to be appropriate for comparison with other samples from the same dataset for a number of reasons. Studies of the soil horizons in the Yubdo area (Childs, 2001) found no significant barriers or weathered horizons within the soil profile and similarly no such horizons were found in the road cutting at Daleti or Kingy. The laterite horizon (Chirecha) is a homogenous mass of friable soils and therefore the material at the top of the layer is considered to be comparable in geochemistry to that of the bottom.

Given the arguments made above and the absence of slump and mass wasting features around the laterites in the WES (United Nations, 1971) this thesis suggests that these soil samples are likely to reflect the in-situ geochemistry and therefore are suitable for exploration activities. However given that the studies of soil profiles can only be performed in the road cuttings or open cast workings, it was always intended that anomalous values would be followed up by a pitting program. Such a system of sampling from high in the lateritic profile and validation with samples from lower in

the stratigraphy has been recommended through work in Australia (Smith et al., 2000). Furthermore, some degree of hydromorphic remobilization (as described by Smith et al., 2000) of metals is to be expected and therefore, this needs to be considered when interpreting the data. The factors affecting the geochemistry of the soils studied are described further in section 7.5).

7.4. Method of Analysis

A total of 981 soil samples were analysed by OMAC Laboratories (Co Galway, Ireland) by two different procedures: one for Pt and Pd and another for 47 additional elements. Considerably more detail about this method is given in the analytic methods section of chapter 8. For Pt and Pd analyses, each sample was ground to 100μm and split to 30g. Subsequently, the powders were analysed using a 30g lead fire assay with an inductively coupled plasma finish, resulting in detection limits of 2ppb for both Pt, Pd and Au. For other elements, the samples were also ground to 100μm but they were subjected to an Aqua Regia digestion with Inductively Coupled Plasma – Optical Emission Spectroscopy finish. It is necessary to point out that an aqua regia digestion will not be total, some of the more refractory minerals will not have been digested (see chapter 8).

7.5. Soil Forming processes and geochemical dispersion

7.5.1. Ni, Cu, Cr and Al

A high degree of Ni concentration in laterites is common over ultramafic units (Schellmann, 1989). The increase in Ni values is caused by a removal of Si and Mg which are both highly mobile in soils. The Ni concentration can be further facilitated by remobilisation to form gossans. Studies of the behaviour of Ni and Cu in the surficial environment are summarized by Smith et al. (2000). Ni and Cu (amongst other elements) are frequently used to determine the location of primary ore deposits covered by laterites in Australia by identifying dispersion haloes. Ni and Cu can be taken into solution by meteoric water, which then forms part of the aquifer system within the laterite body. The elements are then dispersed through the laterite in the direction of groundwater flow, in the same way as As groundwater contamination (Nickson et al., 2000).

When partitioned into spinel minerals, Cr is known to be highly immobile. Unlike sulphide minerals, Cr-spinels in the WES remain intact throughout severe alteration (chapter 3) and weathering. Aluminium is also known to be immobile in soils. The immobility of Al means that small amounts of it will be concentrated by volume loss during soil formation (Schellmann, 1989). It can be expected that immobile elements will become concentrated in soils compared with the underlying rocks. This is owing to the mobile components of the rock being removed and hence a soil will have originated from a rock volume larger than that of the soil.

7.5.2. Pt and Pd

The fluids involved with the remobilisation of Pt and Pd in soils could be regarded as the lower temperature equivalents (≈85°C according to Tarkian et al. 1996) of those fluids involved in the high-temperature alteration (see chapter 8). In addition to the Cl-complexes thought to occur at high temperatures, it is possible that hydroxide, thiosulphate and organic complexes may be the dominant forms of dissolved Pt and Pd. Such situations may form from natural humic and fulvic acids (Bowles et al., 1995). For example, Wood (1990) reacted with aqueous solutions of K_2PtCl_4 to discover that such acids can hold over 140ppm Pt in solution.

In addition to the Cl-rich fluid and hydrothermal fluid models, many studies have shown that PGE can be oxidised in the surficial environment (see papers in Bowles and Gize, 2005). For example, studies of the mineralogy of the Massive Sulphide Zone of the Great Dyke of Zimbabwe have shown that with progressive alteration, the PGM become oxidised with concomitant destruction of the sulphide minerals present in the fresher rock (Oberthür et al., 2003). Oberthür et al. (2003) also remark that – as in hydrothermal fluids – Pd is more mobile than Pt and is dispersed in the surficial environment. The preferential mobility of Pd over Pt is also observed by many other authors including Wood and Vlassopoulos (1990) and Bowles et al. (1994).

Class Upper Limit (ppm)	Frequency	Cumulative Frequency	Cumulative Frequency (%)		
58	1	261	100.0	Mean	6.5
55.1	0	260	99.6	Standard Deviation	8.3
52.2	0	260	99.6		
49.3	0	260	99.6	Minimum	0
46.4	0	260	99.6	Lower Quartile	0
43.5	0	260	99.6		
40.6	3	260	99.6	Median	4
37.7	0	257	98.5	Upper Quartile	9
34.8	1	257	98.5		
31.9	0	256	98.1	Maximum	58
29	1	256	98.1	Mode	0
26.1	6	255	97.7	Number of samples	261
23.2	9	249	95.4		
20.3	8	240	92.0		
17.4	11	232	88.9		
14.5	10	221	84.7		
11.6	19	211	80.8		
8.7	28	192	73.6		
5.8	63	164	62.8		
2.9	20	101	38.7		
0	81	81	31.0		

Table 7.1: A summary of the Pt values in the soil samples from Tulu Dimtu.

Class Upper Limit (ppm)	Frequency	Cumulative Frequency	Cumulative Frequency (%)		
31	1	261	100.0	Mean	3.0
29	0	260	99.6	Standard Deviation	3.9
28	0	260	99.6		
26	0	260	99.6	Minimum	0
25	1	260	99.6	Lower Quartile	0
23	0	259	99.2		
22	0	259	99.2	Median	2
20	0	259	99.2	Upper Quartile	4
19	0	259	99.2		
17	2	259	99.2	Maximum	31
16	2	257	98.5	Mode	0
14	4	255	97.7	Number of samples	261
12	2	251	96.2		
11	1	249	95.4		
9	2	248	95.0		
8	13	246	94.3		
6	33	233	89.3		
5	38	200	76.6		
3	53	162	62.1		
2	0	109	41.8		
0	109	109	41.8		

Table 7.2: A summary of the Pd values in the soil samples from Tulu Dimtu.

Class Upper Limitc	Frequency	Cumulative Frequency	Cumulative Frequency (%)		
4869	1	261	100.0	Mean	24
4626	0	260	99.6	Standard Deviation	301
4382	0	260	99.6		
4139	0	260	99.6	Minimum	0
3895	0	260	99.6	Lower Quartile	0
3652	0	260	99.6		
3408	0	260	99.6	Median	2
3165	0	260	99.6	Upper Quartile	5
2921	0	260	99.6		
2678	0	260	99.6	Maximum	4869
2435	0	260	99.6	Mode	0
2191	0	260	99.6	Number of samples	261
1948	0	260	99.6		
1704	0	260	99.6		
1461	0	260	99.6		
1217	0	260	99.6		
974	0	260	99.6		
730	0	260	99.6		
487	0	260	99.6		
243	164	260	99.6		
0	96	96	36.8		

Table 7.3: A summary of the Au values in the soil samples from Tulu Dimtu.

Class Upper Limit (ppm)	Frequency	Cumulative Frequency	Cumulative Frequency (%)		
10648	1	261	100.0	Mean	2406
10116	1	260	99.6	Standard Deviation	3001
9584	1	259	99.2		
9053	5	258	98.9	Minimum	12
8521	3	253	96.9	Lower Quartile	130
7989	6	250	95.8		
7457	9	244	93.5	Median	336
6925	12	235	90.0	Upper Quartile	5288
6394	18	223	85.4		
5862	9	205	78.5	Maximum	10648
5330	12	196	75.1	Mode	103
4798	6	184	70.5	Number of samples	261
4266	6	178	68.2		
3735	4	172	65.9		
3203	1	168	64.4		
2671	2	167	64.0		
2139	3	165	63.2		
1607	3	162	62.1		
1076	7	159	60.9		
544	152	152	58.2		
0	0	0	0.0		

Table 7.4: A summary of the Ni values in the soil samples from Tulu Dimtu.

Class Upper Limit (ppm)	Frequency	Cumulative Frequency	Cumulative Frequency (%)		
146	4	261	100.0	Mean	54
139	3	257	98.5	Standard Deviation	42
132	7	254	97.3		
125	4	247	94.6	Minimum	3
117	16	243	93.1	Lower Quartile	10
110	5	227	87.0		
103	16	222	85.1	Median	50
96	10	206	78.9	Upper Quartile	88
89	12	196	75.1		
82	12	184	70.5	Maximum	146
75	11	172	65.9	Mode	6
67	12	161	61.7	Number of samples	261
60	12	149	57.1		
53	18	137	52.5		
46	12	119	45.6		
39	5	107	41.0		
32	12	102	39.1		
24	9	90	34.5		
17	13	81	31.0		
10	68	68	26.1		
0	0	0	0.0		

Table 7.5: A summary of the Cu values in the soil samples from Tulu Dimtu.

Class Upper Limit (ppm)	Frequency	Cumulative Frequency	Cumulative Frequency (%)		
3098	2	261	100.0	Mean	428
2944	1	259	99.2	Standard Deviation	438
2790	0	258	98.9		
2636	0	258	98.9	Minimum	18
2482	0	258	98.9	Lower Quartile	158
2328	0	258	98.9		
2174	0	258	98.9	Median	304
2020	0	258	98.9	Upper Quartile	575
1866	3	258	98.9		
1712	3	255	97.7	Maximum	3098
1558	0	252	96.6	Mode	218
1404	2	252	96.6	Number of samples	261
1250	4	250	95.8		
1096	4	246	94.3		
942	13	242	92.7		
788	20	229	87.7		
634	28	209	80.1		
480	46	181	69.3		
326	61	135	51.7		
172	74	74	28.4		
0	0	0	0.0		

Table 7.6: A summary of the Cr values in the soil samples from Tulu Dimtu.

Class Upper Limit (%)	Frequency	Cumulative Frequency	Cumulative Frequency (%)		
7.3	1	261	100.0	Mean	3.62
7.0	7	260	99.6	Standard Deviation	1.91
6.6	8	253	96.9		
6.3	6	245	93.9	Minimum	0.4
5.9	20	239	91.6	Lower Quartile	1.4
5.6	15	219	83.9		
5.2	26	204	78.2	Median	4.0
4.9	17	178	68.2	Upper Quartile	5.1
4.5	26	161	61.7		
4.2	19	135	51.7	Maximum	7.3
3.9	7	116	44.4	Mode	1
3.5	16	109	41.8	Number of samples	261
3.2	4	93	35.6		
2.8	8	89	34.1		
2.5	6	81	31.0		
2.1	4	75	28.7		
1.8	4	71	27.2		
1.4	23	67	25.7		
1.1	30	44	16.9		
0.7	14	14	5.4		
0.0	0	0	0.0		

Table 7.7: A summary of the Al values in the soil samples from Tulu Dimtu.

The following sections describe the distribution of Ni, Cu, Cr and Al in the soils covering the Tulu Dimtu area. It is important to remember that it is unlikely that complete digestion has been acheieved during the aqua regia leach of these samples. Each section describes one element and its distribution in the soils in turn. These sections are accompanied by two fold-out pages (page 123) of maps showing the distribution of all elements which the reader should refer to as each section is read.

7.6.3. Nickel

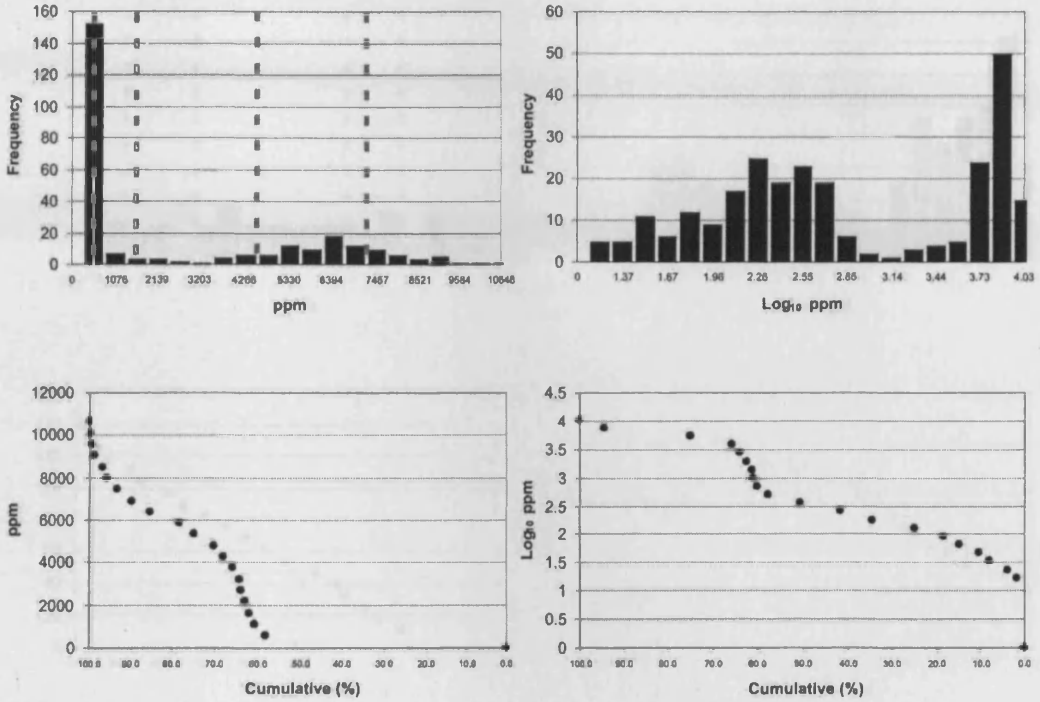

Figure 7.6: Arithmetic and Log_{10} transformed histograms of Ni in the soils of the Tulu Dimtu area. The grey lines indicate the class-boundaries used in figure 7.12A.

Nickel is enriched only over the Tulu Dimtu Main Intrusion and Sheared Ultramafic (see figure 7.12A). Two regions of high values are observed in the soils overlying the Main Intrusion. These are firstly on the flanks of the intrusion and additionally forming a N-S trending feature 1km east of the western flank; here values rise to over 8000ppm (figure 7.12A). The highest value of Ni in the Tulu Dimtu area is found in the soils above the southwestern flank of the intrusion.

There are two populations of Ni values in the Tulu Dimtu area. Figure 7.6 shows that above 3000ppm (found over the Tulu Dimtu Main Intrusion and Sheared Ultramafic), the Ni values have an approximately normal distribution. However, the samples with Ni values of lower than 3000ppm (generally found over the basement units have an approximnately log normal distribution.

7.6.4. Copper

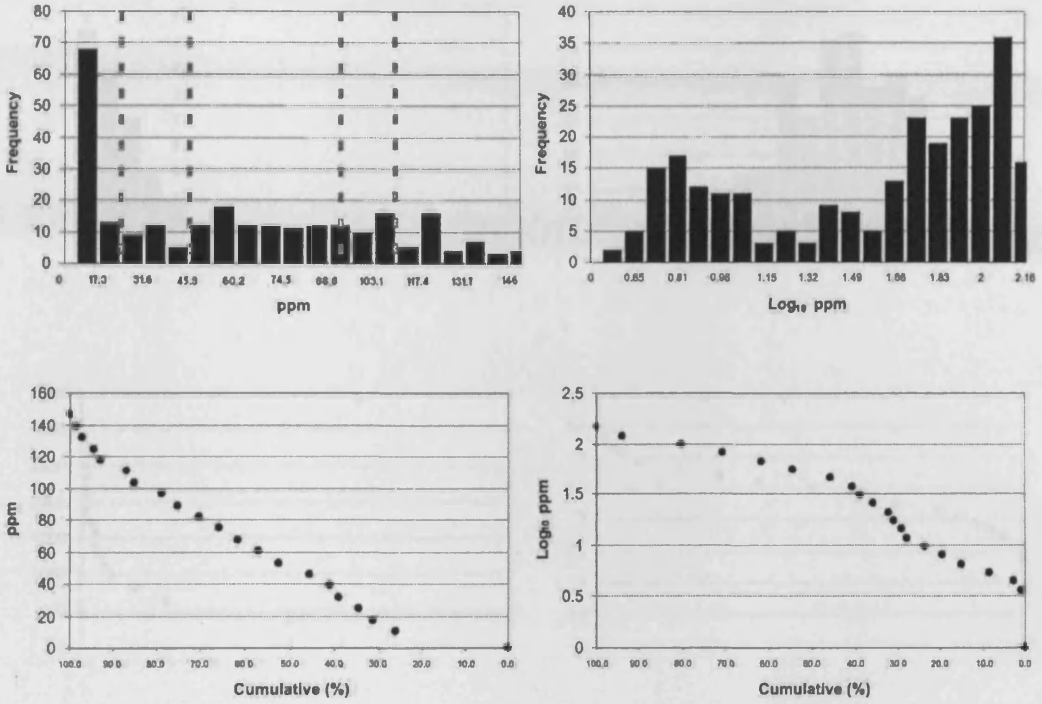

Figure 7.7: Arithmetic and Log_{10} transformed histograms of Cu the soils of the Tulu Dimtu area. The grey lines indicate the class-boundaries used in figure 7.12B.

Within the Tulu Dimtu Main Intrusion, only one soil sample – located on the western flank - contains a Cu value which is above 70ppm. All remaining samples from soils above the Tulu Dimtu Main Intrusion have Cu values below 50ppm. However, over the rest of the area, Cu rises to above 90ppm in soils overlying many different rock formations. Although some values of less than 500ppm are found in soils over the basement units.

There are two populations of Cu values in the Tulu Dimtu area. Above 25ppm there is an approximately even distribution of Cu values (not normally distributed, see figure 7.7). However, an additional population of Cu values below 25ppm show a roughly Log normal distribution.

When displayed on an arithmetic scale (see figure 7.10 and 7.11) the Pt and Pd distributions appear to be Log normal. However a logarithmic scale reveals that the Pt and Pd values in the soils of the Tulu Dimtu area show an erratic distribution.

7.6.9. Discussion

7.6.10. Ni, Cu, Cr, and Al distribution in soils

It is observed that the distribution of Ni over the Tulu Dimtu area is the opposite of the Cu distribution. The highest values of Ni and lowest values of Cu occur only over the ultramafic lithologies as defined by geological mapping (chapter 5) and by the interpretation of aerial photography (chapter 4). Additionally, a zone of high Cr values is seen in the soils over the western and southern flanks of the Main Intrusion. Al also shows anomalously high values over the same areas, in addition to the high values seen over the basement.

There are two possible explanations for the marked change in Ni and Cu values across the boundary between the Main Intrusion and the basement. Firstly, the change could be reflecting the change in rock-type below and secondly, the Cu may have been remobilized from the soils above the ultramafic rocks and redeposited at the base of the slope.

If the high increase in Cu values at the contact of the Tulu Dimtu Main Intrusion with the basement were solely due to hydromorphic dispersion then those high values would only be expected at the base of the slope. However, analysis of the aerial photographs (chapter 4) shows that high Cu values are also found in soils above the basement many of which are located at ridge summits. However, given the porous nature of the laterite and frequent rains in the area it is likely that hydromorphic dispersion will have had some effect on the Cu distribution, in combination with the effect from the relict rocks. This combined effect is discussed further in section 7.10.

The poor exposure means that the western boundary of the Tulu Dimtu Main Intrusion has been defined principally by the change in vegetation (chapter 4). The change in Ni and Cu concentrations across the same boundary supports the validity of

this method of geological mapping and suggests that some form of biogeochemical change has occurred. A high degree of Ni concentration in laterites is common over ultramafic units (Schellmann, 1989).

When partitioned into spinel minerals, Cr is known to be highly immobile. Unlike sulphide minerals, in the WES, Cr-spinels often remain intact throughout severe alteration (chapter 3) and also weathering. Therefore the locations of high Cr values in soils can be considered as being in-situ – given that soil transport is likely to have been minimal. Given that the high Cr values in soils show the same patterns and locations as those seen in altered and fresher rocks (see chapter 8), the distances by which these soils have moved are considered to be low ($\approx$<10m).

Aluminium is also known to be immobile in soils and therefore it is to be expected that Al may be present in the soils above the basement, given the high proportion of alumino-silicates in the underlying rocks. The zone of high Al at the flanks of the Main Intrusion is less easy to explain. The immobility of Al means that small amounts of it will be concentrated by volume loss during soil formation. The fresher ultramafics of Tulu Dimtu contain 1% Al at most and these values could potentially be increased to 4% if the volume loss effect of hydrothermal alteration acting at the flanks of the intrusion is also taken into account (see chapter 8).

7.6.11. Genesis of Pt and Pd in soils

In the Tulu Dimtu area, Pt is enriched over the soils of the Main Intrusion but not over the Lensoid Ultramafics. Also, a greater proportion of soil samples compared to rock samples are enriched in Pt to greater than 20ppb (see figures 7.12E and 7.12F). Theoretically, it is known that the high Eh, acid and chloride-rich conditions in lateritic soil covers can mobilise the PGE (see section 7.5.2). The predominance of Pt over Pd in the soils above the Tulu Dimtu Main Intrusion may be attributed to prefential leaching of Pd during the soil-formation. The Pt acts as a less mobile element and is retained within the soil. The increased proportion of Pt-bearing soil samples compared to rock samples over the Main Intrusion may be attributed to either the loss in volume from rock to soil or to the reconcentration of Pt within the lateritic conditions (as proposed by Bowles, 1995; see section 7.5.2). It is not possible to

assess the behaviour of Pt and Pd in the soils overlying the Lensoid Ultramafics because the rock samples are located far from the soil samples.

7.6.12. Conclusion

The distribution of Ni and Cu in the Tulu Dimtu area is likely to have been partially influenced by the geochemistry of the underlying rocks. However, it is likely that hydromorphic dispersion will have had an additional influence. Cr and Al have both acted as immobile elements and may reflect the same patterns seen in primary rocks (see chapter 8).

Redistribution of Pt and Pd is observed in the soils above the Tulu Dimtu Main Intrusion (see chapter 8). It is likely that Pt acted as a less mobile element and Pd was taken into solution. Consequently, Pd will have been leached out and some Pt may remain. The increase in Pt values from rock to soil may be accounted for by either by the volume change from rock to soil or by the reconcentration of Pt within the lateritic conditions as first suggested by Ottemann and Augustithis (1967).

7.7.2. Summary of Analytical Results

Class Upper Limit (ppb)	Frequency	Cumulative Frequency	Cumulative Frequency (%)		
69	1	201	100.0		
66	0	200	99.5	Mean	4.4
62	0	200	99.5	Standard	7.1
59	0	200	99.5	Deviation	
55	0	200	99.5	Minimum	0
52	0	200	99.5	Lower	0
48	0	200	99.5	Quartile	
45	0	200	99.5	Median	3
41	0	200	99.5	Upper	5
38	0	200	99.5	Quartile	
35	1	200	99.5	Maximum	69
31	1	199	99.0	Mode	0
28	0	198	98.5	Number of	201
24	1	198	98.5	samples	
21	3	197	98.0		
17	11	194	96.5		
14	5	183	91.0		
10	17	178	88.6		
7	39	161	80.1		
3	43	122	60.7		
0	79	79	39.3		

Table 7.8: A summary of the Pt values in the soil samples from the Kingy area.

Class Upper Limit (ppb)	Frequency	Cumulative Frequency	Cumulative Frequency (%)		
71	1	201	100.0		
67	0	200	99.5		
64	0	200	99.5	Mean	5.1
60	0	200	99.5	Standard	7.1
57	0	200	99.5	Deviation	
53	0	200	99.5	Minimum	0
50	0	200	99.5	Lower	0
46	0	200	99.5	Quartile	
43	0	200	99.5	Median	4
39	0	200	99.5	Upper	7
36	1	200	99.5	Quartile	
32	1	199	99.0	Maximum	71
28	1	198	98.5	Mode	0
25	0	197	98.0	Number of	201
21	1	197	98.0	samples	
18	6	196	97.5		
14	11	190	94.5		
11	25	179	89.1		
7	59	154	76.6		
4	32	95	47.3		
0	63	63	31.3		

Table 7.9: A summary of the Pd values in the soil samples from the Kingy area.

Class Upper Limit (ppb)	Frequency	Cumulative Frequency	Cumulative Frequency (%)		
304	1	201	100.0		
289	0	200	99.5		
274	0	200	99.5	Mean	10
258	0	200	99.5	Standard	26
243	0	200	99.5	Deviation	
228	0	200	99.5	Minimum	0
213	0	200	99.5	Lower	2
198	0	200	99.5	Quartile	
182	0	200	99.5	Median	4
167	0	200	99.5	Upper	9
152	0	200	99.5	Quartile	
137	1	200	99.5	Maximum	304
122	1	199	99.0	Mode	2
106	0	198	98.5	Number of	201
91	0	198	98.5	samples	
76	2	198	98.5		
61	1	196	97.5		
46	3	195	97.0		
30	18	192	95.5		
15	148	174	86.6		
0	26	26	12.9		

Table 7.10: A summary of the Au values in the soil samples from the Kingy area.

Class Upper Limit (ppm)	Frequency	Cumulative Frequency	Cumulative Frequency (%)		
6976	1	201	100.0		
6627	1	200	99.5		
6279	0	199	99.0	Mean	460.9
5930	0	199	99.0	Standard	999.8
5581	0	199	99.0	Deviation	
5232	0	199	99.0	Minimum	1
4884	0	199	99.0	Lower	29
4535	2	199	99.0	Quartile	
4186	1	197	98.0	Median	86
3837	0	196	97.5	Upper	345
3489	2	196	97.5	Quartile	
3140	2	194	96.5	Maximum	6976
2791	3	192	95.5	Mode	29
2442	2	189	94.0	Number of	201
2094	2	187	93.0	samples	
1745	4	185	92.0		
1396	5	181	90.0		
1047	5	176	87.6		
699	20	171	85.1		
350	151	151	75.1		
0	0	0	0.0		

Table 7.11: A summary of the Ni values in the soil samples from the Kingy area.

Class Upper Limit (ppm)	Frequency	Cumulative Frequency	Cumulative Frequency (%)		
188	2	201	100.0		
179	2	199	99.0		
170	4	197	98.0	Mean	80.0
160	2	193	96.0	Standard	41.3
151	2	191	95.0	Deviation	
142	5	189	94.0	Minimum	4
133	11	184	91.5	Lower	49
124	15	173	86.1	Quartile	
114	13	158	78.6	Median	80
105	19	145	72.1	Upper	108
96	16	126	62.7	Quartile	
87	13	110	54.7	Maximum	188
78	18	97	48.3	Mode	90
68	18	79	39.3	Number of	201
59	7	61	30.3	samples	
50	17	54	26.9		
41	8	37	18.4		
32	6	29	14.4		
22	12	23	11.4		
13	11	11	5.5		
0	0	0	0.0		

Table 7.12: A summary of the Cu values in the soil samples from the Kingy area.

Class Upper Limit (ppm)	Frequency	Cumulative Frequency	Cumulative Frequency (%)		
3861	1	201	100.0		
3668	0	200	99.5		
3475	0	200	99.5	Mean	481
3282	0	200	99.5	Standard	601
3089	0	200	99.5	Deviation	
2896	0	200	99.5	Minimum	0
2703	1	200	99.5	Lower	83
2510	3	199	99.0	Quartile	
2317	2	196	97.5	Median	258
2124	1	194	96.5	Upper	635
1931	3	193	96.0	Quartile	
1737	2	190	94.5	Maximum	3861
1544	4	188	93.5	Mode	55
1351	7	184	91.5	Number of	201
1158	9	177	88.1	samples	
965	8	168	83.6		
772	13	160	79.6		
579	19	147	73.1		
386	43	128	63.7		
193	84	85	42.3		
0	1	1	0.5		

Table 7.13: A summary of the Cr values in the soil samples from the Kingy area.

Class Upper Limit (%)	Frequency	Cumulative Frequency	Cumulative Frequency (%)		
8.4	1	201	100.0		
8.0	3	200	99.5		
7.6	4	197	98.0	Mean	4.2
7.2	4	193	96.0	Standard Deviation	1.6
6.9	4	189	94.0		
6.5	11	185	92.0	Minimum	0.7
6.1	11	174	86.6	Lower Quartile	3.1
5.7	10	163	81.1		
5.3	13	153	76.1	Median	4.1
4.9	19	140	69.7	Upper Quartile	5.2
4.6	17	121	60.2		
4.2	25	104	51.7	Maximum	8.4
3.8	19	79	39.3	Mode	3.6
3.4	12	60	29.9	Number of samples	201
3.0	10	48	23.9		
2.6	12	38	18.9		
2.2	13	26	12.9		
1.9	8	13	6.5		
1.5	3	5	2.5		
1.1	2	2	1.0		
0.0	0	0	0.0		

Table 7.14: A summary of the Al values in the soil samples from the Kingy area.

The following sections cover the distribution of Ni, Cu, Cr and Al in the Kingy area. It is important to remember that it is unlikely that complete digestion has been acheieved during the aqua regia leach of these samples. Each section covers one element and describes its distribution in turn.

Ultramafic but does not rise above 9ppb over the northeastern basement (figure 7.20E). Additionally, high Pt and Pd values are more common in soils than rocks.

The highest grades of both Pt and Pd in the whole Kingy area are in a soil sample above the isolated gabbro in the southeastern corner of the area. However, the soils elsewhere in the Kingy area, show Pt and Pd anomalies in very different areas (see figure 7.20E and 7.20F).

On the arithmetic scale (figure 7.18 and 7.19) both Pt and Pd seem to have approximately log normal distributions. However on a log scale, only Pd shows a roughly log normal distribution and Pt seems much more uneven.

7.7.9. Discussion

7.7.10. Trace Element distribution in soils

Except for the isolated gabbro (see chapter 5) all high Cr and Ni values in soils of the Kingy area only occur over the ultramafic units. However, high Cu and Al values are observed over all formations. The high Cr, Cu and Ni values observed above the ultramafic units are to be expected and these reflect the geochemistry of the underlying rocks. Additionally the elevated Al content of the soils is to be expected as this immobile element will be concentrated even from the low amounts seen in the rocks from the Kingy Ridge Ultramafic.

7.7.11. Genesis of Pt and Pd in soils

The distribution of Pt and Pd values in the soils from the Kingy area show a distinct geographical split between the two elements (see figures 7.20E and 7.20F). Pd is concentrated mainly in the soils over the basement of the northwest and the Pt is concentrated over the Kingy Ridge area – although a few anomalous Pd values also occur.

As discussed in section 7.5.2, Pt and Pd are likely to be concentrated in the soils above PGE-bearing ultramafic complexes and some Pd may also be lost between the rocks and soils. It appears that Pt is more extensively mineralised in soils than in

the rocks over the Kingy Ridge Ultramafic. It is possible that due to the large volume of rock from which a thick laterite is formed (several times greater than the thickness of the laterite itself) small amounts of the immobile Pt may have become concentrated. At the same time as the immobile Pt particles are concentrated, the mobile Pd is leached out. In the soils above the Kingy Ridge Ultramafic, the relative distributions of Pt and Pd in soils versus rock support the hypothesis that Pd is more mobile than Pt in lateritic soils.

Given the mobility differences described above, it is hard to understand the origins of the Pd concentration observed over the basement in the northwest where the laterites are known to be of a similar thickness to those from the Kingy Ridge areas. If Pd is mobile in the fluids of lateritic covers from the Kingy Ridge why is it retained in the soils seen here? It is possible that there are some different aqueous conditions occurring in these laterites due to a different protolith (metavolcanic and meta sedments as opposed to ultramafic) whereby Pd becomes immobile. However, there is also a difference in vegetation type seen from aerial photography (chapter 4) between this area and the Kingy Ridge Ultramafic and it is conceivable that biochemical factors may have caused Pd to complex with humic or fulvic acid as a locked molecule.

The primary source of the Pd in the soils from the northwest of the Kingy area could be attributed to some Pd-bearing (9 or 10ppb) Shear Zones and gabbros (see figure 7.20F). However, the Pd distribution in the soils covers a wider area than the known extent of these exposures and therefore hints towards a larger system of Pd-bearing rocks not yet exposed.

The highest Pt and Pd values in soils occur above the isolated gabbro exposure in the southeast. Lack of further geological information about this area precludes precludes a definite conclusion however the presence of a high Cu value in soil hints towards either magmatic or hydrothermal origin. This area merits further investigation.

7.7.12. Conclusions

The distribution of Ni and Cr over the ultramafic complexes in the Kingy area suggests that their distribution is connected to the underlying lithotypes. However Cu and Al show no particular pattern with lithotype.

The extent of Pt mineralisation in the soils overlying the Kingy Ridge Ultramafic is wider than seen in the fresher rocks, which may be attributed to either volume loss from rock to soil or by in-situ remobilisation of Pt and Pd. The most striking feature of the Pt and Pd distribution in soils from the Kingy area is the division between northwest and southeast, the origin of this pattern cannot be ascertained here.

7.8.2. Summary of Analytical Results

Class Upper Limit (ppb)	Frequency	Cumulative Frequency	Cumulative Frequency (%)		
34	2	240	100.0		
32	0	238	99.2		
31	0	238	99.2	Mean	1.8
29	0	238	99.2	Standard	4.5
27	0	238	99.2	Deviation	
26	0	238	99.2	Minimum	0
24	0	238	99.2	Lower	0
22	1	238	99.2	Quartile	
20	0	237	98.8	Median	0
19	1	237	98.8	Upper	2
17	1	236	98.3	Quartile	
15	3	235	97.9	Maximum	34
14	2	232	96.7	Mode	0
12	1	230	95.8	Number of	240
10	5	229	95.4	samples	
9	2	224	93.3		
7	3	222	92.5		
5	15	219	91.3		
3	35	204	85.0		
2	0	169	70.4		
0	169	169	70.4		

Table 7.15: A summary of the Pt values in the soil samples from the Daleti, Ankori, and Tulu Kapi areas.

Class Upper Limit (ppb)	Frequency	Cumulative Frequency	Cumulative Frequency (%)		
48	1	240	100.0		
46	1	239	99.6	Mean	2.0
43	0	238	99.2	Standard	5.6
41	0	238	99.2	Deviation	
38	0	238	99.2	Minimum	0
36	0	238	99.2	Lower	0
34	0	238	99.2	Quartile	
31	0	238	99.2	Median	0
29	1	238	99.2	Upper	3
26	0	237	98.8	Quartile	
24	0	237	98.8	Maximum	48
22	1	237	98.8	Mode	0
19	3	236	98.3	Number of	240
17	0	233	97.1	samples	
14	2	233	97.1		
12	3	231	96.3		
10	5	228	95.0		
7	14	223	92.9		
5	30	209	87.1		
2	11	179	74.6		
0	168	168	70.0		

Table 7.16: A summary of the Pd values in the soil samples from the Daleti, Ankori, and Tulu Kapi areas.

Class Upper Limit (ppb)	Frequency	Cumulative Frequency	Cumulative Frequency (%)		
17639	1	240	100.0		
16757	0	239	99.6	Mean	99
15875	0	239	99.6	Standard Deviation	1145
14993	0	239	99.6		
14111	0	239	99.6	Minimum	0
13229	0	239	99.6	Lower Quartile	2
12347	0	239	99.6		
11465	0	239	99.6	Median	4
10583	0	239	99.6	Upper Quartile	10.25
9701	0	239	99.6		
8820	0	239	99.6	Maximum	17639
7938	0	239	99.6	Mode	2
7056	0	239	99.6	Number of samples	240
6174	0	239	99.6		
5292	0	239	99.6		
4410	0	239	99.6		
3528	0	239	99.6		
2646	1	239	99.6		
1764	1	238	99.2		
882	202	237	98.8		
0	35	35	14.6		

Table 7.17: A summary of the Au values in the soil samples from the Daleti, Ankori, and Tulu Kapi areas.

Class Upper Limit (ppm)	Frequency	Cumulative Frequency	Cumulative Frequency (%)		
19266	1	240	100.0		
18303	0	239	99.6		
17340	1	239	99.6	Mean	459
16378	1	238	99.2	Standard Deviation	2161
15415	0	237	98.8		
14452	0	237	98.8	Minimum	10
13489	0	237	98.8	Lower Quartile	29
12526	0	237	98.8		
11564	0	237	98.8	Median	38
10601	0	237	98.8	Upper Quartile	57
9638	1	237	98.8		
8675	2	236	98.3	Maximum	19266
7712	0	234	97.5	Mode	41
6750	1	234	97.5	Number of samples	240
5787	0	233	97.1		
4824	0	233	97.1		
3861	1	233	97.1		
2898	0	232	96.7		
1936	6	232	96.7		
973	226	226	94.2		
0	0	0	0.0		

Table 7.18: A summary of the Ni values in the soil samples from the Daleti, Ankori, and Tulu Kapi areas.

Class Upper Limit (ppm)	Frequency	Cumulative Frequency	Cumulative Frequency (%)		
366	1	240	100.0		
348	0	239	99.6		
330	0	239	99.6	Mean	50.4
311	0	239	99.6	Standard	35.6
293	0	239	99.6	Deviation	
275	0	239	99.6	Minimum	2
257	0	239	99.6	Lower	32
239	0	239	99.6	Quartile	
220	0	239	99.6	Median	42
202	0	239	99.6	Upper	60
184	1	239	99.6	Quartile	
166	1	238	99.2	Maximum	366
148	4	237	98.8	Mode	39
129	5	233	97.1	Number of	240
111	10	228	95.0	samples	
93	17	218	90.8		
75	23	201	83.8		
57	82	178	74.2		
38	70	96	40.0		
20	26	26	10.8		
0	0	0	0.0		

Table 7.19: A summary of the Cu values in the soil samples from the Daleti, Ankori, and Tulu Kapi areas.

Class Upper Limit (ppm)	Frequency	Cumulative Frequency	Cumulative Frequency (%)		
3056	1	240	100.0		
2904	1	239	99.6		
2752	1	238	99.2	Mean	243
2599	0	237	98.8	Standard	432
2447	0	237	98.8	Deviation	
2295	1	237	98.8	Minimum	12
2143	0	236	98.3	Lower	76
1991	0	236	98.3	Quartile	
1838	1	236	98.3	Median	104
1686	1	235	97.9	Upper	154
1534	3	234	97.5	Quartile	
1382	3	231	96.3	Maximum	3056
1230	0	228	95.0	Mode	103
1077	1	228	95.0	Number of	240
925	2	227	94.6	samples	
773	8	225	93.8		
621	8	217	90.4		
469	6	209	87.1		
316	20	203	84.6		
164	183	183	76.3		
0	0	0	0.0		

Table 7.20: A summary of the Cr values in the soil samples from the Daleti, Ankori, and Tulu Kapi areas.

Class Upper Limit (%)	Frequency	Cumulative Frequency	Cumulative Frequency (%)		
7.4	1	240	100.0		
7.0	1	239	99.6		
6.7	2	238	99.2	Mean	3.82
6.3	5	236	98.3	Standard Deviation	1.24
6.0	10	231	96.3		
5.6	17	221	92.1	Minimum	0.2
5.2	15	204	85.0	Lower Quartile	3.0
4.9	21	189	78.8		
4.5	19	168	70.0	Median	3.7
4.2	27	149	62.1	Upper Quartile	4.7
3.8	32	122	50.8		
3.4	28	90	37.5	Maximum	7.4
3.1	15	62	25.8	Mode	3.6
2.7	23	47	19.6	Number of samples	240
2.4	12	24	10.0		
2.0	2	12	5.0		
1.6	3	10	4.2		
1.3	4	7	2.9		
0.9	1	3	1.3		
0.6	2	2	0.8		
0.0	0	0	0.0		

Table 7.21: A summary of the Al values in the soil samples from the Daleti, Ankori, and Tulu Kapi areas.

The following sections cover the distribution of Ni, Cu, Cr and Al in the Daleti, Ankori, Tulu Kapi and Keley areas. It is important to remember that it is unlikely that complete digestion has been acheieved during the aqua regia leach of these samples. Each section covers one element and describes its distribution in the soils.

7.8.3. Nickel

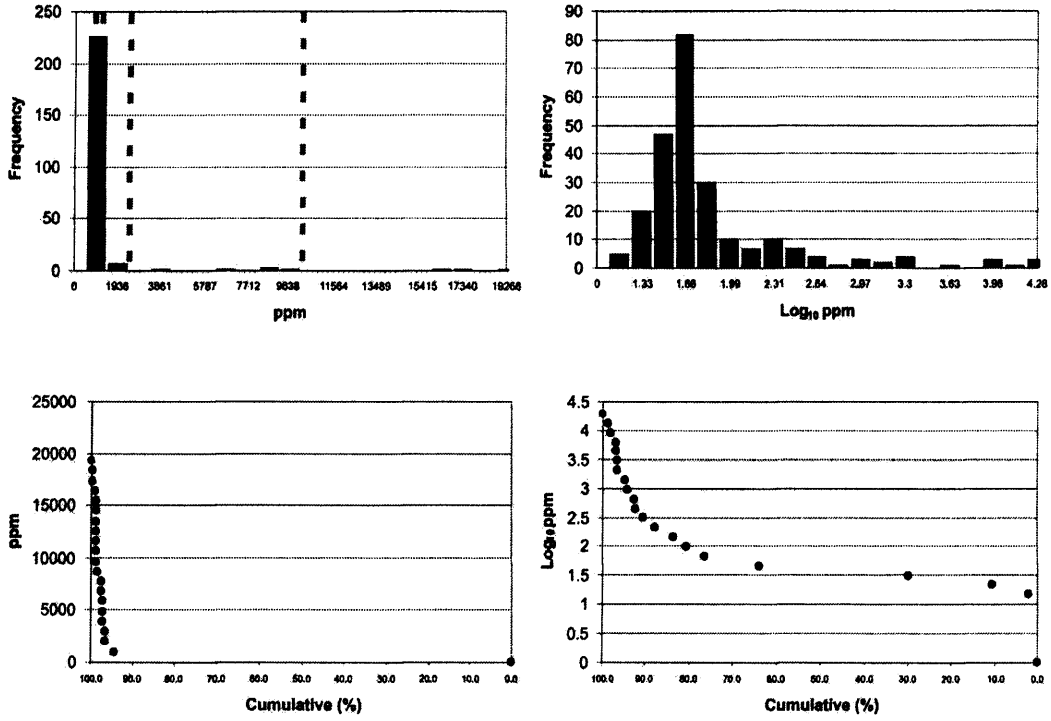

Figure 7.22: Arithmetic and Log_{10} transformed histograms of Ni the soils of the Daleti, Ankori, Tulu Kapi and Keley areas. The grey lines indicate the class-boundaries used in figure 7.28A.

High values of Ni in soil (over 1120ppm) are only seen in two areas, over the Daleti Ultramafic and the Ankori Ultramafic. The highest value of Ni in soil (19,266ppm) is seen over the Daleti Ultramafic. As with the fresher rocks, a high degree of local variation (within 250m) in Ni values is seen in soils (see figure 7.28A).

The Ni values in the soils of the Daleti, Ankori, Tulu Kapi and Keley areas show a positively skewed log normal distribution with a mode at around 41ppm.

7.8.9. Discussion

7.8.10. Trace element distribution in soils

With one exception, the highest Ni values in soil occur over the ultramafic bodies whereas the highest Cu values occur over the basement. The exception occurs at Keley where the highest Cu value in soil occurs over a dunite body. The high Cu value at Keley can be explained as it reflects the high Cu value found in rock (see chapter 8). It is common to find Ni-rich lateritic bodies over ultramafic complexes (Schellmann, 1989; Schellmann, 1971). It is notable that, high Cu values occur in soils at ridge summits and hence it appears that the element acts as an immobile element in the soils above the basement but also in the ultramafics where it exists in the underlying rocks. The Cu values found in the soils above the basement may have originated from Cu-bearing veins which have scavenged the element from the ultramafic intrusions. The clear-boundaries between Ni and Cu distribution co-incide with the contacts mapped in this study and therefore these elements validate the mapping technique.

7.8.11. Genesis of Pt and Pd in soils

Soil samples at only two locations studied in this section contain Pt or Pd values of above 20ppb, one at the southwestern basement and one above the Ankori complex. The soils above the Daleti Ultramafic are entirely barren of both elements. As expected, both of the soil anomalies lie close to high Pt and Pd values in rock (see figures 7.28E, 8.10E, 7.28F and 8.10F). These soils probably represent the weathered equivalent of the PGE-bearing rocks.

There is an absence of PGE-bearing soils over many other Pt and Pd bearing complexes. Furthermore, the highest value PGE-bearing soils from the Ankori complex does not co-coincide with the locations of highest Pt and Pd values in rock. This difference in location of the rock and soil anomalies in the Ankori Ultramafic may be due to soil transport. However the lack of Pt and Pd over the other complexes cannot be explained here.

7.8.12. Conclusions

Both Ni and Cr show high values solely over the ultramafic intrusions whereas Al and Cu show high values over many formations, including the basement. Some notably high (>19,000ppm) Ni values occur in the laterites covering the Daleti Ultramafic. Significant Pt and Pt values are only found in two places, the Ankori complex and the soils around a system of shear zones to the southwest of Gudeya Guji (see figures 7.28E and 7.28F).

7.9.2. Summary of Analytical Results

Class Upper Limit (ppb)	Frequency	Cumulative Frequency	Cumulative Frequency (%)		
232	1	227	100.0		
220	0	226	99.6		
209	0	226	99.6	Mean	4.7
197	1	226	99.6	Standard	25.0
186	0	225	99.1	Deviation	
174	0	225	99.1	Minimum	0
162	1	225	99.1	Lower	0
151	0	224	98.7	Quartile	
139	0	224	98.7	Median	0
128	1	224	98.7	Upper	0
116	0	223	98.2	Quartile	
104	1	223	98.2	Maximum	232
93	0	222	97.8	Mode	0
81	0	222	97.8	Number of	227
70	0	222	97.8	samples	
58	1	222	97.8		
46	1	221	97.4		
35	0	220	96.9		
23	3	220	96.9		
12	32	217	95.6		
0	185	185	81.5		

Table 7.22: A summary of the Pt values in the soil samples from the Yubdo, Andu and Sodu areas.

Class Upper Limit (ppb)	Frequency	Cumulative Frequency	Cumulative Frequency (%)		
31	1	227	100.0		
29	0	226	99.6		
28	0	226	99.6		
26	0	226	99.6	Mean	1.2
25	0	226	99.6	Standard	3.7
23	1	226	99.6	Deviation	
22	0	225	99.1	Minimum	0
20	2	225	99.1	Lower	0
19	0	223	98.2	Quartile	
17	1	223	98.2	Median	0
16	1	222	97.8	Upper	0
14	0	221	97.4	Quartile	
12	1	221	97.4	Maximum	31
11	0	220	96.9	Mode	0
9	2	220	96.9	Number of	227
8	2	218	96.0	samples	
6	3	216	95.2		
5	3	213	93.8		
3	39	210	92.5		
2	0	171	75.3		
0	171	171	75.3		

Table 7.23: A summary of the Pd values in the soil samples from the Yubdo, Andu and Sodu areas.

Class Upper Limit (ppb)	Frequency	Cumulative Frequency	Cumulative Frequency (%)		
102	1	227	100.0		
97	0	226	99.6		
92	0	226	99.6	Mean	4.2
87	0	226	99.6	Standard	11.4
82	1	226	99.6	Deviation	
77	0	225	99.1	Minimum	0
71	0	225	99.1	Lower	0
66	2	225	99.1	Quartile	
61	0	223	98.2	Median	2
56	0	223	98.2	Upper	3
51	0	223	98.2	Quartile	
46	0	223	98.2	Maximum	102
41	2	223	98.2	Mode	0
36	2	221	97.4	Number of	227
31	1	219	96.5	samples	
26	0	218	96.0		
20	3	218	96.0		
15	5	215	94.7		
10	15	210	92.5		
5	89	195	85.9		
0	106	106	46.7		

Table 7.24: A summary of the Au values in the soil samples from the Yubdo, Andu and Sodu areas.

Class Upper Limit (ppm)	Frequency	Cumulative Frequency	Cumulative Frequency (%)		
10454	1	227	100.0		
9932	0	226	99.6	Mean	504
9410	0	226	99.6	Standard	1168
8888	0	226	99.6	Deviation	
8366	0	226	99.6	Minimum	14
7844	0	226	99.6	Lower	52
7322	0	226	99.6	Quartile	
6800	0	226	99.6	Median	70
6278	1	226	99.6	Upper	416
5756	1	225	99.1	Quartile	
5234	2	224	98.7	Maximum	10,454
4712	0	222	97.8	Mode	72
4190	1	222	97.8	Number of	227
3668	2	221	97.4	samples	
3146	6	219	96.5		
2624	1	213	93.8		
2102	2	212	93.4		
1580	12	210	92.5		
1058	20	198	87.2		
536	178	178	78.4		
0	0	0	0.0		

Table 7.25: A summary of the Ni values in the soil samples from the Yubdo, Andu and Sodu areas.

Class Upper Limit (ppm)	Frequency	Cumulative Frequency	Cumulative Frequency (%)		
409	2	227	100.0		
389	0	225	99.1		
369	0	225	99.1	Mean	61
349	0	225	99.1	Standard	48
329	0	225	99.1	Deviation	
309	1	225	99.1	Minimum	8
289	0	224	98.7	Lower	40
269	0	224	98.7	Quartile	
249	1	224	98.7	Median	48
229	2	223	98.2	Upper	64
209	0	221	97.4	Quartile	
188	0	221	97.4	Maximum	409
168	2	221	97.4	Mode	40
148	3	219	96.5	Number of	227
128	6	216	95.2	samples	
108	9	210	92.5		
88	21	201	88.5		
68	66	180	79.3		
48	102	114	50.2		
28	12	12	5.3		
0	0	0	0.0		

Table 7.26: A summary of the Cu values in the soil samples from the Yubdo, Andu and Sodu areas.

Class Upper Limit (ppm)	Frequency	Cumulative Frequency	Cumulative Frequency (%)		
6504	1	227	100.0		
6180	0	226	99.6		
5855	0	226	99.6	Mean	649.7
5531	0	226	99.6	Standard	942.1
5206	0	226	99.6	Deviation	
4882	0	226	99.6	Minimum	16
4558	1	226	99.6	Lower	122.5
4233	1	225	99.1	Quartile	
3909	0	224	98.7	Median	187
3584	2	224	98.7	Upper	869
3260	4	222	97.8	Quartile	
2936	2	218	96.0	Maximum	6504
2611	3	216	95.2	Mode	238
2287	12	213	93.8	Number of	227
1962	8	201	88.5	samples	
1638	9	193	85.0		
1314	12	184	81.1		
989	6	172	75.8		
665	12	166	73.1		
340	154	154	67.8		
0	0	0	0.0		

Table 7.27: A summary of the Cr values in the soil samples from the Yubdo, Andu and Sodu areas.

Class Upper Limit (%)	Frequency	Cumulative Frequency	Cumulative Frequency (%)		
8.7	3	227	100.0		
8.3	3	224	98.7		
7.9	4	221	97.4	Mean	5.39
7.5	15	217	95.6	Standard	1.60
7.1	17	202	89.0	Deviation	
6.8	35	185	81.5	Minimum	0.9
6.4	18	150	66.1	Lower	4.2
6.0	28	132	58.1	Quartile	
5.6	18	104	45.8	Median	5.7
5.2	10	86	37.9	Upper	6.6
4.8	10	76	33.5	Quartile	
4.4	14	66	29.1	Maximum	8.7
4.0	8	52	22.9	Mode	6.6
3.6	15	44	19.4	Number of	227
3.2	9	29	12.8	samples	
2.9	12	20	8.8		
2.5	5	8	3.5		
2.1	0	3	1.3		
1.7	1	3	1.3		
1.3	2	2	0.9		
0.0	0	0	0.0		

Table 7.28: A summary of the Al values in the soil samples from the Yubdo, Andu and Sodu areas.

The spatial and statistical distribution of each element is considered in turn in the next sections. It is important to remember that it is unlikely that complete digestion has been acheieved during the aqua regia leach of these samples. The maps which accompany the section are included at the rear.

Within the Main Yubdo Ultramafic, Pd is enriched (up to 31ppb) in soils over the southeastern clinopyroxenite zone and Pt enriched (up to 232ppb) above the northern tip of the dunite and talc-schist zones. In addition to this, a sample from above an associated diorite dyke (north of Yubdo) has returned assay results of 13ppb for Pt and 8ppb for Pd. Many samples of soil overlying the Main Yubdo Intrusion return analyses of Pt and Pd below detection limits (see figures 7.36E and 7.36F). One kilometre south of the Main Yubdo Ultramafic, a soil sample above a shear zone gave 5ppb for Pt and 19ppb for Pd. Similarly, a soil sample above a talc-schist in the southeast of the study area returned Pt values of 5ppb and Pd a value of 19ppb.

A significant Pt value occurs in a hard-pan and other soil samples contain Pt and Pd anomalies in soil occur in different locations. At the northern tip of the Yubdo main complex Pd is low and Pt is elevated above 100ppb in several places. This contrasts with the soils above the eastern clinopyroxenite zone where both Pt and Pd both rise to similar values.

Additionally, the soils in the southeast of the study area are enriched in Pd and Pt around a talc-schist. And Pd returned higher values than Pt in both cases

Neither Pt nor Pd show normal distributions on arithmetic or logarithmic scales.

7.9.9. Discussion

7.9.10. Ni and Cr values in soils above the Main Yubdo Ultramafic

The highest Cr value occurs in a hard-pan found above the western clinopyroxenite zone of Main Yubdo Ultramafic. Furthermore, high Cr contents are restricted to the soils above the Main Yubdo Ultramafic. The highest Ni values in soil occur either over the northern tip of the complex or in the centre of the intrusion.

Elevation in the Cr content of the hard-pan found above the clinopyroxenite zone from the Main Yubdo Ultramafic supports the evidence for high Cr-spinel concentration at the flanks of the intrusion. The high value could be attributed to the extreme volume change from rock to soil and further during the compaction into a

hard-pan lithotype. The presence of Cr in the soils overlying the flanks of the intrusion together with the known resistance of spinels to weathering indicates that the most primitive rocks occur at the flanks of the intrusion. However, surprisingly high Cr values occur in soils at the centre of the intrusion. The concentration of Cr in these samples may possibly be accounted for by a higher degree of concentration due to deeper weathering over the top of the Yubdo hill. Similarly, the variations in Ni content in the soils over the Yubdo Main Intrusion may be understood in terms of the relative degrees of weathering.

7.9.11. Genesis of Pt and Pd in soils

A hard pan of the western flank of the intrusion contains the highest Pt value in this study of the WES at 143ppb and a corresponding Pd value of 3ppb. Furthermore, the maximum Pt value in the soils collected here is over 100ppb higher than that seen in rock. Additionally, it is observed here that in the soils above the Main Yubdo Ultramafic that Pt is only enriched in soils above the northern tip and Pd is only enriched over the eastern clinopyroxenite zone.

As described in section 7.5.2 the increase in Pt grade between the rocks and soils from the Main Yubdo Ultramafic could be explained either by the element being immobile within the soil, or alternatively the element might have been reconcentrated into the soils. The hard-pan sample perhaps represents an extreme case of volume loss from rock to soil as it shows an increased Pt value from the equivalent rocks nearby (see figure 8.13E). This sample may also be the product of a longer time-period of the action of aqueous fluids in laterites. Furthermore, the hardpan may also have been cemented by circulating Si-rich fluids which could have redeposited the Pt. The difference in locations of Pt and Pd highs indicates that Pd has become immobile in the soils over the eastern clinopyroxenite zone. This may possibly be due to Pd being complexed with a different organic compound to Pt. The data presented here cannot be used to determine the aqueous conditions of these laterites and therefore we cannot determine the solution to this anomalous distribution.

7.9.12. Conclusions

Although high Ni and Cr values only occur in the soils over the Main Yubdo Ultramafic, high Cu values are only found in the basement and high Al values are found throughout the area. This indicates a relationship between the underlying lithotype and the the geochemistry of the soils. However, it is likely that both Ni and Cr will have become concentrated partially by volume loss from rock to soil.

Similarly, the immobile nature of Pt is likely to have increased the content in soils when compared to rock samples. The difference in location of the highest Pt and Pd concentrations is distinct in the soils of the Main Yubdo Intrusion, and from this study it is not possible to determine the mechanism which causes this feature.

7.10. Discussion of the distribution of Ni, Cu, Cr, Al, Pt and Pd in the soils of the WES

Some notable differences in the distribution of the elements in question can be seen between the four areas studied, as described with the following figures. For ease of comparison between the four areas studied, graphs using cumulative % are used. Histograms showing the same data can be found in the respective sections earlier in this chapter.

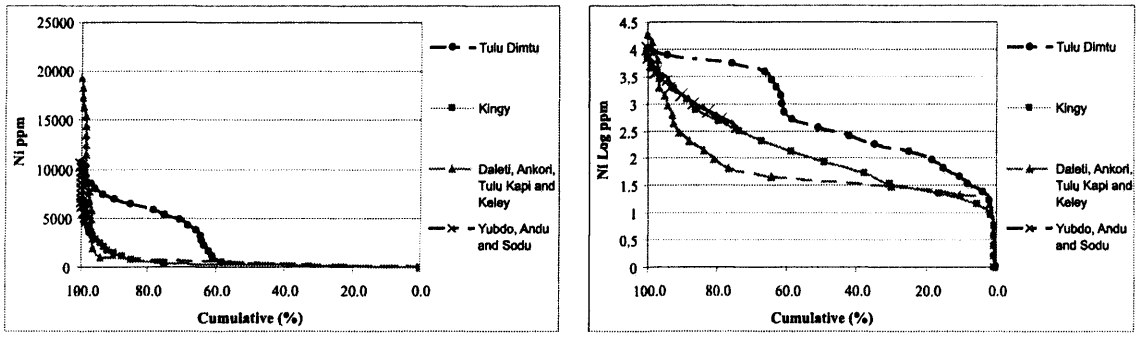

Figure 7.37: A graph comparing the distribution of Ni in each of the four areas studied. For histograms further illustrating the data see individual sections.

There are several differences in the distribution of Ni in the four areas studied in this chapter. Tulu Dimtu is the only area where an arithmetic normal distribution occurs however there is an additional population which is log normal. In the remaining three areas, all Ni disitributions are log normal. The only unimodal distribution occurs in the area containing the Daleti, Ankori, Tulu Kapi and Keley complexes.

Such distributions are difficult to understand in terms of the number of ultramafic complexes within the area, given that the only area with one population is the area with four discrete complexes (Daleti, Ankori, Tulu Kapi and Keley). It is possible that one population in each area could be created by hydromorphic dispersion in additional to the original population which reflects the bedrock values.

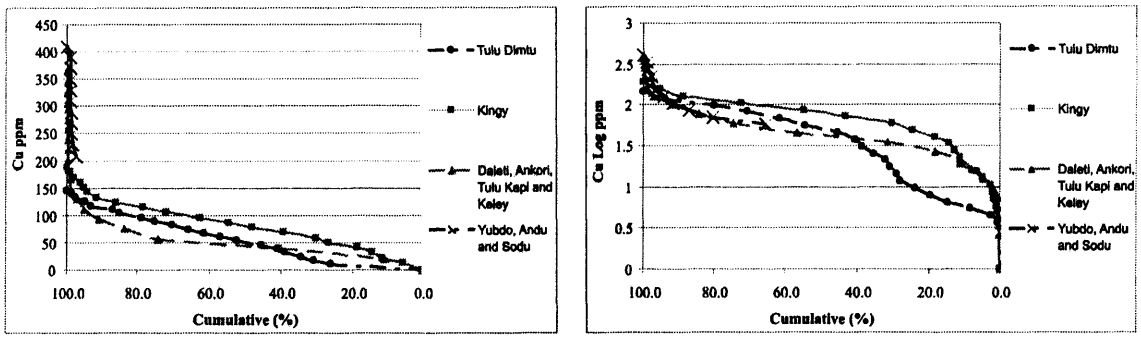

Figure 7.38: A graph comparing the distribution of Cu in each of the four areas studied. For histograms further illustrating the data see individual sections.

The Cu distribution in each area of the WES is log normal, however the distributution of the Tulu Dimtu area has two modes (see figure 7.7).

As discussed in section 7.6.4, it is possible that the Cu distribution in the Tulu Dimtu area may be influenced partially by the underlying bedrock and partially by hydromorphic dispersion. In a situation where the Cu was remobilized by groundwater, a lower value population could occur due to dilution. These lower values (<25ppm) would represent the remobilized values, and the higher population would be related to the original composition of the protolith.

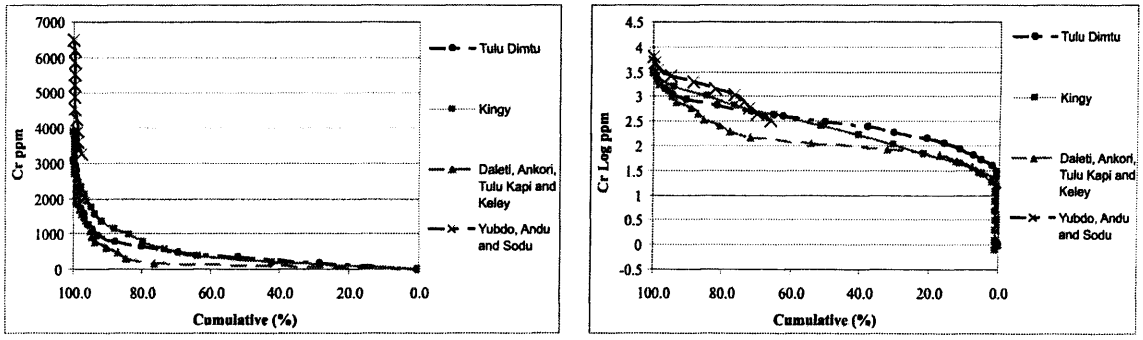

Figure 7.39: A graph comparing the distribution of Cr in each of the four areas studied. For histograms further illustrating the data see individual sections.

All Cr populations in the WES are log normal and unimodal, except the Yubdo area where two populations occur (see figure 7.32).

Unlike Ni and Cu, this additional population is difficult to explain in terms of hydromorphic dispersion as Cr typically remains intact within Cr-spinels (see chapter 3). It is possible that such an observation could be the result of two magmatic phases

of Cr-spinel precipitation. Such an interpretation would need to be supported by petrological investigation.

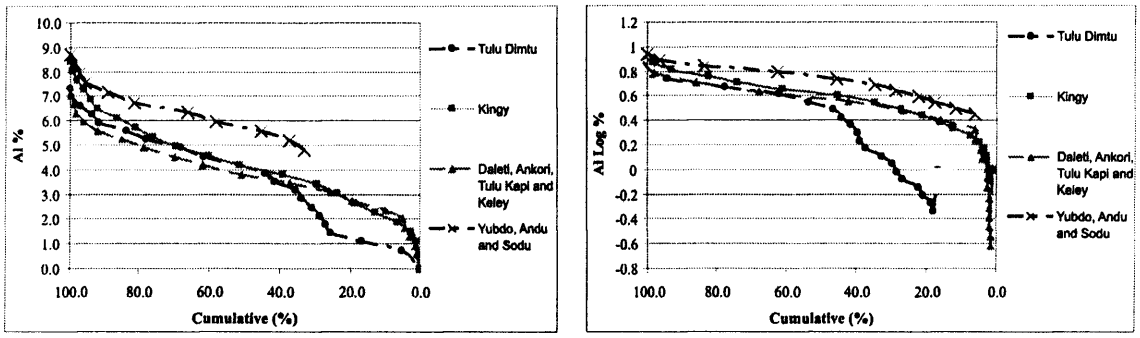

Figure 7.40: A graph comparing the distribution of Al in each of the four areas studied. For histograms further illustrating the data see individual sections.

Unlike Ni, Cu and Cr the Al values in the soils of the WES are the only ones which are normally distributed. However, in the Tulu Dimtu area, the distribution is sufficiently erratic that it cannot be regarded as being normally distributed.

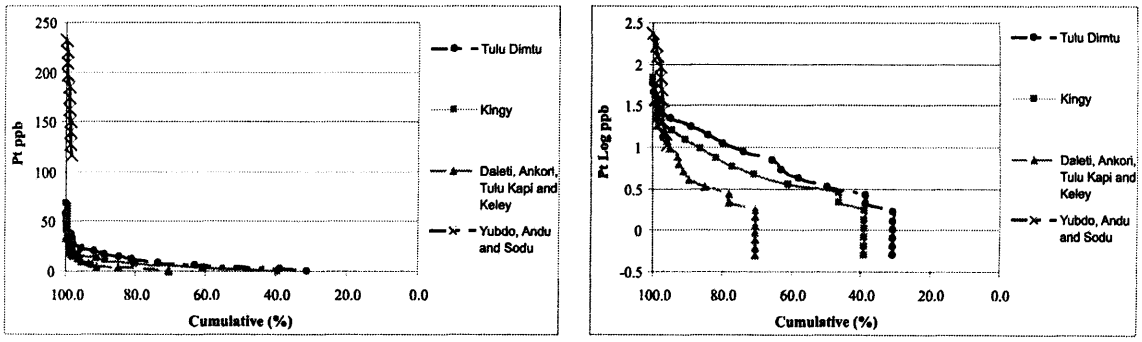

Figure 7.41: A graph comparing the distribution of Pt in each of the four areas studied. For histograms further illustrating the data see individual sections.

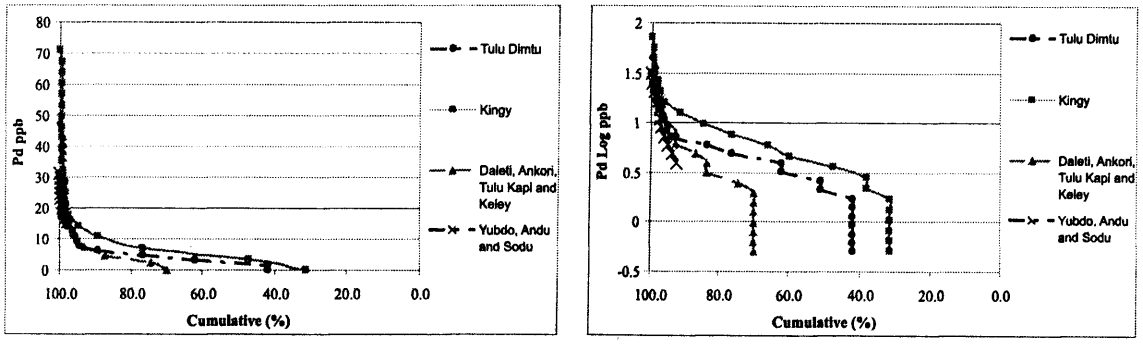

Figure 7.42: A graph comparing the distribution of Pd in each of the four areas studied. For histograms further illustrating the data see individual sections.

The distribution of both Pt and Pd in the WES is generally erratic. However, in all areas but Yubdo, this erratic nature is tends slightly towards a log normal distribution.

The erratic nature of of Pt and Pd distributions is well known given their tendency to form nuggets. However the slightly log normal patterns observed suggest that there is a more statistically uniform mechanism operating. This mechanism may be the underlying magmatic dissolution process, however given the severe degree of the alteration and weathering it is unlikely. However, the log normal patterns may reflect the dissolution of the elements the fluids within the laterite (see section 7.5.2).

7.11. Summary of the Soil development in the WES

7.11.1. Ni, Cu, Cr and Al

Distinct changes in the proportions of Ni and Cu are seen in the soils over the different lithologies of the WES. Ni is typically higher over the ultramafic units than the basement, whereas Cu tends to show higher values over the basement units, in particular the shear-zone related lithologies. Although such trends indicate a relationship between Ni and Cu distribution with lithotype, univariate statistical methods show that at Tulu Dimtu a second population exists. Such lower value populations may be the result of the hydromorphic dispersion of Ni and Cu. Although Al shows no particular relationship with the underlying lithotype, Cr is present in the highest values in soils over ultramafic units. Given the resistance of Cr-spinels to alteration and weathering (chapter 3) it is unlikely that it has undergone remobilization within the soil.

These geochemical differences are important to this study as in some places they are considered to validate the mapping technique. Large scale changes in the value of Ni (at values >1000ppm) and Cu (at values >25ppm) are likely to have been controlled by the underlying lithotype. However Ni and Cu values below those stated are likely to have been influenced strongly by hydromorphic dispersion. For example clear changes in Ni and Cu value can be seen at the contact between the Tulu Dimtu Main Intrusion and the basement (see figures 7.12A and 7.12B). This contact was

mapped using a change in vegetation seen from aerial photography (chapter 4). However, additional populations can be seen in figures 7.6 and 7.7 which are likely to have been the result of hydromorphic dispersion.

7.11.2. Pt and Pd

Area	Formation	Soil samples	
		Pt (ppb)	Pd (ppb)
Yubdo	Main Yubdo Ultramafic	232	31
Tulu Dimtu	Tulu Dimtu Main Intrusion	58	31
Daleti	Ankori	34	48
Kingy	Kingy Ridge Ultramafic	29	29
Daleti	Daleti Ultramafic	< 2	< 2
Daleti	Keley	< 2	< 2

Table 7.29: The maximum Pt and Pd values found in the soils above the ultramafic complexes of the WES.

A full understanding of the mechanisms controlling the development of Pt and Pd in the soils above the ultramafic bodies in the WES is difficult. However, this chapter gives an account of the salient features of the distribution and proposes some mechanisms which may have caused them

The distribution of the elements is nuggety, but some evidence is present for remobilization within the laterites. Figures 7.41 and 7.42 show an erratic distribution of values which may have formed through the presence of nuggets. However there is a division in the distribution of Pt and Pd in the soils above the Kingy area (figures 7.20E and 7.20F). The soils above the basement in the northwest havce greater amounts of Pd and the soils above the Kingy Ridge Ultramafic contain much more Pt. There is a similar division between Pt and Pd in the soils above the Yubdo Main Intrusion. These differences in distribution could possibly be explained by a difference in lateritic conditions as a result of the different basement lithotype. However, it is not possible to determine these conditions in this study. An alternative hypothesis is that Pd has become immobile instead of Pt in certain areas perhaps by being complexed with a different type of vegetation (see chapter 4).

8. Rock Geochemical Data

8.1. Introduction

Samples of rocks were collected from the 4 complexes: Tulu Dimtu, Kingy, Daleti and Yubdo. With the aim of assessing the prospectivity of each of the ultramafic complexes, these samples were analysed for major and trace elements including Pt, Pd and Au by the OMAC laboratories as part of an exploration program for Golden Prospect Mining Co Ltd (GPM). In order to identify targets for detailed exploration, this chapter examines this dataset describing the distribution of key elements that characterise: each rock type, fresher and altered rocks, pathfinders for PGE and the Pt and Pd distribution itself.

The dataset used in this chapter is the result of samples collected during the 2001-2002 field season by the author and several GPM geologists. The grids and traverses used are typical of those used in geological exploration, where geochemical anomalies are sought. Samples were collected in order to both characterise known ultramafics and also to discover unknown deposits.

These complexes are examined using two types of sample: fresher rocks which are used to interpret magmatic ore formation processes and altered rocks, which display magmatic features that have been overprinted by the effects of alteration.

The elements analysed include Au, Pd, Pt, Ag, Al, As, B, Ba, Be, Bi, Ca, Cd, Ce, Co, Cr, Cu, Fe, Ga, Ge, Hg, In, K, La, Li, Mg, Mn, Mo, Na, Nb, Ni, P, Pb, Rb, S, Sb, Sc, Se, Sn, Sr, Ta, Te, Th, Ti, Tl, U, V, W, Y, Zn and Zr. This chapter focuses on Ni, Cu, Cr, Al, Pt and Pd. Each of these elements - except Al - are chosen as they characterize, and are affected by, the processes which concentrate Pt and Pd. Pt and Pd are considered to be concentrated in magmas with sulphur as immiscible sulphide liquids in a silicate magma (Naldrett et al., 1979). After sulphide segregation of a magma, Pt and Pd crystallise with Ni- and Cu-rich sulphides in ultramafic or mafic complexes (Barnes et al., 1997). Sulphur

saturation in a magma is often associated with chromite crystallisation as removal of Fe and Cr from a magma will cause sulphides to segregate (Naldrett and von Gruenewaldt, 1989). Alaskan-type complexes such as those studied here, are traditionally S-poor (Nixon et al., 1997). Ophiolite complexes such as the Shetland ophiolite complex do contain small percentages (1-2%) of sulphides which are Pt and Pd enriched in the ultramafic parts of the complex (Prichard et al., 1996). Thus if base-metal sulphides are Pt and Pd collectors in these complexes in the WES then Ni, Cu and Cr should be path-finders for Pt and Pd. Hence their distribution is studied here to attempt to understand their inter-relationships during magmatic and secondary alteration processes.

The Al content of a magma should increase with fractionation, therefore if PGE content is controlled by the evolution of a magma then Al should correlate with Pt and Pd. Furthermore, the surrounding basement rocks should have a greater proportion of alumino-silicate minerals and therefore Al will help to validate the mapping technique.

Graphs of base metals and other elements against Pt and Pd show no clear trends or correlations and it was therefore decided that a different method of interpretation was required. The results were compiled to produce element concentrations on maps showing the geology. The geological sketch maps were produced using a combination of published maps (at Yubdo) and field observations made in this study (chapters 4 and 5). The GIS application ArcView 3.2 was used display these maps.

This chapter is divided into four sections covering each of the four geographic areas. At the end of each section there is a "pull-out" page which contain the maps which are referred to throughout the chapter.

8.2. Analytical Techniques

8.2.1. Introduction

A total of 481 rock samples were analysed by OMAC Laboratories (Co Galway, Ireland) by two different procedures: one for Pt, Pd, Au and another for 47 additional

elements. After crushing, each sample was ground to 100μm, split to 30g and then prepared and analysed by the two different methods. For Pt and Pd analyses, the powders were analysed using a 30g Pb fire assay with an inductively coupled plasma analysis, resulting in detection limits of 2ppb for both Pt and Pd. For other elements, the samples were subjected to an Aqua Regia digestion with Inductively Coupled Plasma – Optical Emission Spectroscopy finish.

The next sections describe the methods and validation for each stage for each of of each analytical process.

8.2.2. Pb Fire Assay

	Au (ppb)	Pd (ppb)	Pt (ppb)
min	212	1381	3624
max	986.00	1636.88	3883.36
range	774.00	255.53	259.37
Recomended Value Standard SARM-7b	310	1530	3740
Precision (range as % of recomended value)	249.68	16.70	6.94

Table 8.1: Summary statistics of 41 analyses of the standard sample SARM7b.

The standard sample SARM 7b was analysed for Pt, Pd and Au a total of 41 times through 9 batches of samples processed by OMAC laboratories. The full listing of results is included in table 12.3 in section 12.2 and a summary of the ranges of values obtained is included in table 8.1. For all three elements the range encompassed the recommended value for the standard, which can be regarded as a reasonable accuracy. Given the relative inhomogeneity of Pt, and Pd standards, both Pt and Pd varied only slightly from the recommended values (16.7% and 7.0%) in each case. The variation in measured Au values was significantly larger (see table 8.1). This indicates an acceptable degree of accuracy and precision for both Pt and Pd and a slightly lesser degree for Au analyses.

The analysis of blank samples returned values which were at or below detection limits in each case.

In order to assess the accuracy of the Pb fire assay method performed at the OMAC laboratories, four samples were analysed at a different laboratory (Genalysis). Table 12.1 (section 12.1) shows that the biggest difference in Pt values between the two laboratories was 64.7% which corresponds to a difference of 36ppb versus 102ppb. The biggest difference between the analyses of Pd was 5ppb versus below detection limts and other results are comparable. The accuracy of the analyses performed at the OMAC laboratories have been accepted for this investigation.

To test the precision of the analyses, repeat analyses were also carried by the OMAC laboratories. Within each batch, repeats were performed in every sample which produced anomalous results. If no significantly anomalous results are produced from a batch then every 10^{th} sample was repeated. In some batches, repeats were carried out at a greater frequency, in order to assure confidence in the procedure. In a some cases, two repeat analyses were performed on the same sample, this was done in situations where either the first repeat showed an unacceptable variance or where particularly unusual results were obtained at first.

Repeat analyses were performed for 48 rock samples from the WES, for three samples two repeat analyses were performed (see table 12.2 in section 12.1). For all three precious metals, there was no measurable variation in the results between each repeat for slightly less than half the samples. High repeatability was only present in analyses of low values (<5ppb). The least precise analysis is of Au, where the greatest variation between repeats is between 22ppb and below detection limits. For Pd the highest variation is between 2ppb and 33ppb (93.9% difference). The greatest degree of precision is found for Pt where the highest variance is between 7ppb and 16ppb (56.3%). Although poor repeatability occurs in some individual samples, there is an acceptable variation between analyses in most cases. It is therefore considered that this dataset is sufficiently accurate for this investigation; however, a degree of natural variation is to be expected due to nugget effect.

8.2.3. Aqua Regia Digestion

Aqua regia constitutes a 3:1 ratio of $HCl:HNO_3$. The effectiveness of this technique is due to the complexing power of the chloride ion acting in the presence of Cl_2 and NOCl as catalysts. An aqua regia leach is frequently used in exploration applications to selectively dissolve certain minerals of interest to the geologist (Snäll and Liljefors, 2000; Chao, 1984). When a sample is subjected to an aqua regia leach some minerals are taken into solution and other, more resistant minerals, remain undissolved. When interpreting the results of a partial leach, it is nessecary to consider which minerals have been taken into solution. Furthermore, when a mineral is dissolved, some elements are taken into solution easier than others (Church et al., 1987).

Mineral	Minerals dissolved (wt %) lower limit	upper limit
olivine	70	80
pyroxenes	30	40
amphiboles	20	40
quartz	10	10
plagioclaise	10	60
spinel	10	100
disulphides	50	100
monosulphides	40	100
bisulphides	40	100
arsenides	80	80

Table 8.2: The weight percent of minerals dissolved by aqua regia (Chruch et al., 1987).

Mineral	Metal	Leachability (%)
Olivine	Cr	60
	Cu	35
	Ni	98
	Al	30
	Mg	99
Spinel	Cr	2
	Cu	70
	Ni	75
	Al	20
	Mg	60

Table 8.3: Percentages of various metals leached by aqua regia from olivine and spinel relative to total recovery calculated from an HF-HNO3-NClO4 digestion (Chruch et al., 1987).

Although a quantitative dataset of the leachability of all minerals and metals by aqua regia is not available, a study of the leachability of some minerals was performed by Church et al. (1987). The most reliably dissolved minerals were sulphides, where complete digestion was possible. Additionally, table 8.2 shows that 70 to 80 wt% of the olivine minerals were dissolved. Furthermore, Church et al. (1987) (see table 8.3) showed that of the minerals tested almost all Mg and Ni could be extracted from olivine. Similarly, a large amount of Ni and Cu could leached from spinel minerals almost no Cr could be extracted.

The study by Church et al. (2000) showed that an Aqua Regia leach will attack the secondary minerals as well as the sulphides. Mafic chain silicates and the phyllosilicates (such as the serpentine minerals) are attacked and leached. With such silicates the study concluded that the method will leach many of elements attached to octahedrally coordinated lattice sites (including Mg and in some cases Al). However it will not attack the tetrahedrally coordinated sites, occupied by ions such as Si and Al (Klein and Hurlbut, 1993). Further to the studies performed by Church et al. (2000), information provided by the OMAC laboratories states that the dissolution is partial for a number of elements including Al and Cr.

8.2.4. Inductively Coupled Plasma – Optical Emmission Spectroscopy

	Mg (%)	Ni (ppm)	Cu (ppm)	Cr (ppm)	Al (%)
Min	2.80	657.83	2556.53	112.38	0.99
Max	3.01	685.98	2707.82	132.05	1.60
Range	0.21	28.15	151.29	19.67	0.62
Assigned Value	2.90	683	2650	N/A	N/A
Precision (variation as % of assigned value)	7.26	4.12	5.71	N/A	N/A

Table 8.4: A table of 48 analyses of the OMAC laboratories in-house standard with a summary of the ranges of values obtained and a measurement of precision.

An in house standard was used by the OMAC laboratories to assess accuracy and precision during elemental analysis using aqua regia, ICP-OES. A total of 48 analyses were performed throught the 9 batches processed at the laboratory. The full dataset is

included in section 12.2 (table 12.4) and a summary of the range of values is included in table 8.4. The elements Mg, Ni and Cu show a variation of around 7.26, 4.12 and 5.71% respectively. Although no assigned values are available for the analysis of Cr and Al, it is possible to see that the precision for these elements is significantly poorer. These results are as expected given that Ni and Cu will be easily leached by aqua regia and Mg can be leached from its silicate octahedral lattice sites (see section 8.2.3).

All blanks analysed showed results which were at or below detection limits.

8.3. Methods

8.3.1. Definition of a fresher sample

The rock samples from the WES lie along a spectrum of alteration from "nearly-soil" to completely fresh (see chapter 3), therefore for comparison it was necessary to divide them on that basis. This was done principally by a combination of methods including the identification of weathering and alteration minerals in hand specimen and using transmitted light microscopy.

However, the samples analysed petrologically were one half of the same sample sent for analysis. Therefore, it was necessary to make a geochemical determination of the degree of weathering and alteration on the half of the sample which was sent for analysis. As this analysis could be compared with the half analysed petrologically. This geochemical analysis was intended to support the petrological determination which is the main method for determining the degree of alteration.

The geochemical assesement of alteration was performed using the Mg value. Although Church et al. (1987) suggest that Mg ions can be leached from olivine minerals (see section 8.2.3) in practice it is known that often silicate minerals are not dissolved. As no data is available on the degree of dissolution in the samples from the WES it must be considered that the Mg values in this dataset could originate from either olivine or serpentine. Hence this method is intended simply to support petrological determination.

Ultramafic rocks are characteristically Mg-rich. Dunites and pyroxenites have a range of Mg values which are shown in table 8.6. The ranges of Mg-values for fresher ultramafic rocks can be calculated using published Mg values of fresher olivine and clinopyroxene combined with the mineral proportions of dunite, olivine-clinopyroxenite and pyroxenite as set out by Streckeisen (1976). Examples of Mg values for fresher ultramafic minerals are shown by the analyses shown in table 8.5.

Mineral	Min MgO (%)	Max MgO (%)	Min Mg (%)	Max Mg (%)	Number of samples	Reference
olivine	47.46	47.58	28.6	28.7	2	Révillon (2000)
olivine	46.46	46.46	28.0	28.0	1	Morishita (2001)
olivine	35.97	45.68	21.7	27.5	10	Neumann(2000)
olivine	38.24	44.13	23.1	26.6	12	Mattioli (2003)
olivine	30.4	41.8	18.3	25.2	2	Fodor (2001)
olivine	34.44	39.18	20.8	23.6	2	Upton (2000)
olivine	37.26	38.03	22.5	22.9	3	Renzulli (2001)
olivine	37.47	37.47	22.6	22.6	1	Leonard (2002)
olivine	36.58	37.1	22.1	22.4	2	Müller (2001)
olivine	33.41	36.49	20.1	22.0	6	Gibson (2000)
clinopyroxene	14.42	27.84	8.7	16.8	6	Spandler (2003)
clinopyroxene	14.6	17.6	8.8	10.6	4	Cole (2001)
clinopyroxene	9.27	16.96	5.6	10.2	25	Neumann (2000)
clinopyroxene	16.02	16.02	9.7	9.7	1	Leonard (2002)
clinopyroxene	15.71	15.86	9.5	9.6	2	Morishita (2001)
clinopyroxene	14.28	15.72	8.6	9.5	9	Mattioli (2003)
clinopyroxene	13.4	15.7	8.1	9.5	7	Fodor (2001)
clinopyroxene	14.54	15.53	8.8	9.4	2	Müller (2001)
clinopyroxene	13.1	13.86	7.9	8.4	2	Turner (2003)

Table 8.5: Typical values of Mg for selected fresher ultramafic lithotypes. This data was compiled using the GEOROC database (2005).

The minimum and maximum Mg values for olivine and clinopyroxene were determined from table 8.5 and combined with the proportions of minerals for each lithotype according to Streckeisen (1976). As such, the likely maximum and minimum Mg values for ideal ultramafic rocks can be calculated, as shown in table 8.6.

Rock	Min or Max	olivine value	clinopyroxene value	olivine proportion	clinopyroxene proportion	boundary
Dunite	MIN	20.1	7.9	90%	10%	18.88
Dunite	MAX	28.7	16.8	100%	0%	28.7
Olivine - Clinopyroxenite	MIN	20.1	7.9	60%	40%	15.22

Olivine - Clinopyroxenite	MAX	28.7	16.8	10%	90%	17.99
Clinopyroxenite	MIN	20.1	7.9	10%	90%	9.12
Clinopyroxenite	MAX	28.7	16.8	0%	100%	16.8

Table 8.6: The ranges of Mg values used to define the fresher rock samples. The proportions of olivine and clinopyroxene are defined by Streckeisen (1976). These values represent the range of Mg values which are likely to occur in a hypothetical fresher dunite, olivine-clinopyroxenite or clinopyroxenite.

This method of selection of fresher samples is validated by virtue of a break seen in the unclassified samples at around the boundaries calculated (see table 8.7). This break is seen in all four areas. For example, the analyses of the dunite samples from the Tulu Dimtu area show a range of Mg values from 24.8% to 1.1%. In table 8.7 these are ordered with the highest Mg values at the top and the break can be seen below 18.8% where the next value is 17.0%. This is a difference of 1.8%; the differences further up the table are all lower than 1%. A break at approximately the same level is seen in all four geographic areas (particularly at Daleti, see 8.15.2) and also with pyroxenite samples, however the lower numbers of these lithologies mean that this arguement is illustrated more effectively with dunite samples.

Sample	Mg (%)	Al (%)	Cr (ppm)	Cu (ppm)	Ni (ppm)	Petrological description
DTR-035-02	25.8	0.0	16	3	2327	Figure 3.1
TD12	24.8	0.0	102	16	1456	
ATR-051-02	24.4	0.0	19	4	3380	
DTR-005-02	23.6	0.0	40	3	2691	
TDR 20/01	23.2	0.0	97	0	2617	
DTR-009-02	22.8	0.0	13	2	2945	
ATR-053-02	22.8	0.1	131	6	2037	
ATR-057-02	22.7	0.0	55	3	2574	
KTR-035-02	22.4	0.1	61	9	2182	
DTR-026-02	22.4	0.2	72	5	2340	
DTR-001-02	22.3	0.1	18	5	2942	
TDR 12/01	22.1	0.0	46	0	2856	
TDR 24/01	22.0	0.0	42	0	2312	
TD11	22.0	0.1	366	2	1846	
DTR-007-02	22.0	0.4	33	3	2091	Figure 3.2
DTR-004-02	21.9	0.1	61	4	2686	
TD3	21.8	0.0	70	0	3575	
TD10	21.5	0.1	634	4	1909	
TDR 08/01	21.0	1.0	25	0	4543	
TDR 07/01	21.0	0.0	76	0	5860	
ATR-044-02	20.6	0.1	304	4	3880	
TDR 05/01	20.5	0.1	651	0	2155	
TTR-018A-02	20.4	0.1	119	3	2824	Figure 3.3
KTR-002B-02	20.4	0.1	379	3	3285	

TD14	20.3	0.0	64	0	3062	
TD4	19.9	0.1	292	0	1802	
TDR 19/01	19.5	0.1	436	16	2872	
ATR-056-02	19.5	0.1	196	4	2154	
DTR-034-02	19.4	0.0	27	0	3469	
TD9	18.8	0.5	2728	8	2992	
			NATURAL BREAK			
TDR 06/01	17.0	0.0	187	0	7695	
TDR 11/01	16.4	0.1	223	2	2894	Figure 3.4
TDR 22/01	16.1	0.0	91	3	1962	
TDR 09/01	16.0	0.3	383	0	2129	
DTR-050-0	9.4	0.1	139	2	2190	
TDR 25/01	7.0	0.1	48	0	586	Figure 3.5
TD17	4.6	3.7	705	22	527	
KTR-004-0	4.2	5.5	1517	95	887	
TD13	4.1	2.5	43	70	113	
TDR 10/01	3.2	3.3	88	3	1447	
TDR 27/01	2.6	3.1	1022	12	453	
DTR-029-0	1.2	2.2	64	89	75	
ATR-045-0	1.1	0.8	20	25	154	
ATR-034-0	1.1	0.9	118	180	107	
DTR-040-0	0.5	0.1	32	6	72	
DTR-039-0	0.5	2.4	21	8	87	
TDR 26/01	0.3	1.0	28	169	30	
TDR 01/01	0.0	0.0	11	3	5	
DTR-033-0	0.0	0.1	42	9	55	

Table 8.7: The Mg values for the dunite samples in the Tulu Dimtu area before classification into fresher and altered. Ordered with the highest Mg value at the top and lowest at the bottom. For validation of the method, selected samples are referred to the petrological descriptions contained in chapter 3.

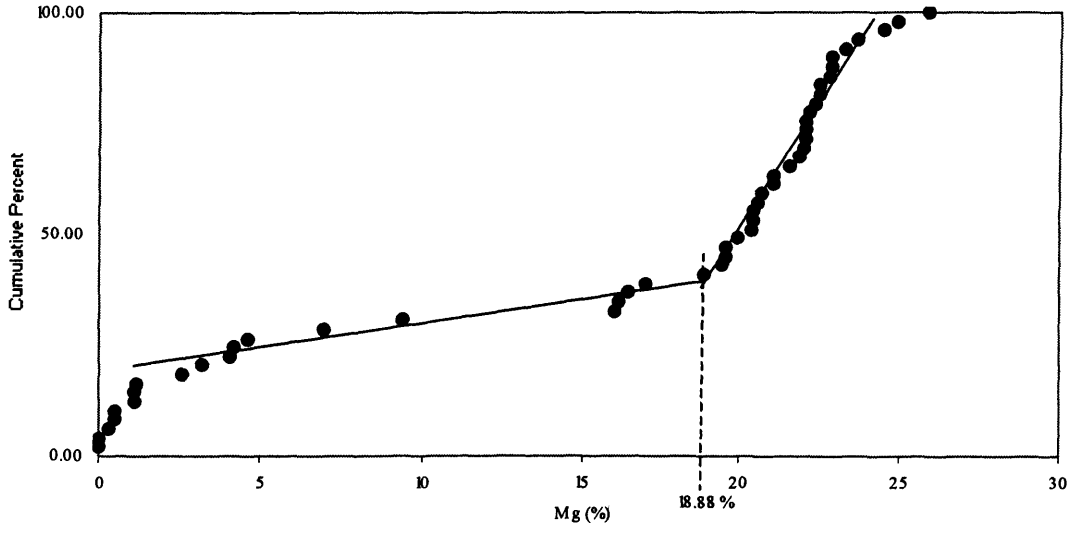

Figure 8.1: A graph of the cumulative percent (by rank) of the Mg values of the dunite samples from the Tulu Dimtu area. The value of 18.88% is marked onto the graph as it is the lowest possible Mg value for an ideal fresher dunite (see figure 8.6).

Figure 8.1 shows a clear difference between two populations of Mg values in the dunite samples from Tulu Dimtu. One population has values which are greater than 18.88% and another population has values which are less 18.88%. The two populations can be summarised with two linear lines of best fit which intercept very close to 18.88% (as calculated above). This suggests that there are two distinct groups of dunite samples from Tulu Dimtu separated at 18.88% which was calculated as the minimum Mg value for a fresh dunite.

Furthermore, figure 8.1 shows that although there is a break just below 18.8%, there are four samples which have Mg values between 16.0% and 17.0%. Below these values there is another, larger, break which may infer that the break should be below 16.0%. However, these values are still significantly lower than the ideal Mg values calculated in table 8.6. Furthermore, these values could be explained as being due to serpentinisation with very little silicification. Although alteration generally decreases the Mg content of a rock, the alteration of olivine to serpentine can retain high Mg values. For example Lecuyer et al. (1994) analysed serpentine minerals which have Mg compositions as high as 22.6%. However the action of sepentinisation also introduces some OH^- which would reduce the Mg value in some cases.

Given the fact that serpentine can contain Mg at up to 22.6% (Lecuyer et al., 1994). With the classification system described above, a 100% serpentinised dunite could be classed as "fresher". It is therefore this method using Mg is intended simply to support petrological analysis (see chapter 3). The samples classified as "fresher" in this manner are only expected simply to be more likely to retain magmatic features than the samples regarded as being altered.

8.3.2. The samples

Samples were taken from both the ultramafic complexes of the WES and also the surrounding basement. Of the ultramafic complexes, the following numbers of samples were taken:

Ultramafic Complex	Number of Samples
Tulu Dimtu Main Intrusion	59
Kingy Ridge Ultramafic (including the extra ultramafic)	30
Daleti Intrusion	21
Ankori Complex	13
Main Yubdo Intrusion	34
Lensoid Ultramafics (from all four geographic areas)	*68*

Table 8.8: The numbers of samples from the ultramafic complexes of the WES. A summary of entire dataset is provided in table 8.9.

When considering the ultramafic complexes, the greatest number of samples were taken from the Lensoid Ultramafics from over the entire study area. Of the main complexes, the greatest samples were taken from the Tulu Dimtu Main Intrusion, followed by the Main Yubdo Intrusion

After classification as fresher and altered rocks (see section 8.3.1), the following numbers of samples were used for the analysis of geochemical processes in the WES.

Area	Total	Altered ultramafic rocks	Fresher ultramafic rocks	Non-ultramafic rocks	Birbirite samples
Tulu Dimtu	116	35	31	47	3
Kingy	110	33	6	67	4
Daleti, Ankori, Keley and Tulu Kapi	155	14	13	115	13
Yubdo, Andu and Sodu	100	18	6	68	8
TOTAL	481	100	56	297	28

Table 8.9: A summary of the numbers and types of samples used in the four geographic areas in this study. A further breakdown of these is provided in each respective section.

8.4. Tulu Dimtu: Selected Major and Trace Elements

8.4.1. Introduction

There are 115 rock samples from the Tulu Dimtu area. Using the classification method shown in section 8.3.1, thirty-one are samples are fresher ultramafics, 43 are altered ultramafics and 6 are from the surrounding basement. The numbers and types of

Lensoid Ultramafics	25	14	2	7	1
Basement	6	0	0	6	0
TOTAL	**115**	**34**	**31**	**47**	**3**

Table 8.10: A summary of the samples from the Tulu Dimtu area. The classification of fresher and altered rocks is covered in section 8.3.1 and the classification of ultramafic lithotypes including birbirite is covered in chapter 3.

8.4.2. Data

Formation	Description	Mg (%)	Ni (ppm)	Cu (ppm)	Cr (ppm)	Al (%)	Pt (ppb)	Pd (ppb)	Pt/Pd	Au (ppb)	Sample
Tulu Dimtu Main Intrusion	Dun	24.4	3380	4	19	<0.1	3	<2	-	3	ATR-051-02
	Dun	22.8	2037	6	131	0.1	8	3	2.7	2	ATR-053-02
	Dun	22.8	2945	2	13	<0.1	5	4	1.3	2	DTR-009-02
	Dun	22.7	2574	3	55	<0.1	4	5	0.8	35	ATR-057-02
	Dun	19.5	2154	4	196	0.1	5	7	0.7	<2	ATR-056-02
	Dun	19.4	3469	<2	27	<0.1	<2	<2	-	70	DTR-034-02
	Dun	18.8	2992	8	2728	0.5	27	37	0.7	<2	TD9
	Dun	25.8	2327	3	16	<0.1	4	<2	-	<2	DTR-035-02
	Dun	24.8	1456	16	102	<0.1	<2	<2	-	<2	TD12
	Dun	23.6	2691	3	40	<0.1	3	<2	-	<2	DTR-005-02
	Dun	23.2	2617	<2	97	<0.1	4	<2	-	2	TDR 20/01
	Dun	22.4	2340	5	72	0.2	7	<2	-	<2	DTR-026-02
	Dun	22.4	2182	9	61	0.1	9	<2	-	<2	KTR-035-02
	Dun	22.3	2942	5	18	0.1	5	5	1.0	<2	DTR-001-02
	Dun	22.1	2856	<2	46	<0.1	4	<2	-	2	TDR 12/01
	Dun	22.0	2091	3	33	0.4	5	<2	-	<2	DTR-007-02
	Dun	22.0	1846	2	366	0.1	2	2	1.0	<2	TD11
	Dun	22.0	2312	<2	42	<0.1	4	<2	-	<2	TDR 24/01
	Dun	21.9	2686	4	61	0.1	6	<2	-	<2	DTR-004-02
	Dun	21.8	3575	<2	70	<0.1	<2	<2	-	<2	TD3
	Dun	21.5	1909	4	634	0.1	40	2	20.0	<2	TD10
	Dun	21.0	5860	<2	76	<0.1	<2	<2	-	<2	TDR 07/01
	Dun	21.0	4543	<2	25	1.0	4	<2	-	<2	TDR 08/01
	Dun	20.6	3880	4	304	0.1	8	5	1.6	<2	ATR-044-02
	Dun	20.4	3285	3	379	0.1	7	<2	-	<2	KTR-002B-02
	Dun	20.3	3062	<2	64	<0.1	<2	<2	-	<2	TD14
	Dun	19.9	1802	<2	292	0.1	4	<2	-	<2	TD4
	Dun	19.5	2872	16	436	0.1	30	37	0.8	2	TDR 19/01
Sheared Ultramafic	Dun	20.5	2155	<2	651	0.1	7	8	0.9	2	TDR 05/01
Lensoid Ultramafics	Cpxite	7.3	1644	9	294	0.1	3	<2	-	4	DTR-016-02
	Dun	20.4	2824	3	119	0.1	9	<2	-	0	TTR-018A-02

Table 8.11: Mg, Ni, Cu, Cr, Al, Pt and Pd values for the fresher samples (as defined in section 8.3.1) collected from the Tulu Dimtu area. Dun: Dunite. Cpxite: Clinopyroxenite.

Formation	Description	Mg (%)	Ni (ppm)	Cu (ppm)	Cr (ppm)	Al (%)	Pt (ppb)	Pd (ppb)	Pt/Pd	Au (ppb)	Sample
Tulu Dimtu Main Intrusion	Dun	9.4	2190	2	139	0.1	6	<2	-	5	DTR-050-0
	Dun	16.1	1962	3	91	<0.1	5	<2	-	27	TDR 22/01
	Dun	7.0	586	<2	48	0.1	24	<2	-	<2	TDR 25/01
	Dun	1.1	154	25	20	0.8	<2	<2	-	2	ATR-045-0
	Dun	<0.1	55	9	42	0.1	<2	<2	-	<2	DTR-033-0
	Ol-cpxite	1.9	150	112	216	2.0	2	2	1.0	2	ATR-047-0
	Ol-cpxite	9.4	705	4	220	0.1	24	<2	-	<2	ATR-052-0
	Ol-cpxite	4.8	816	18	502	1.9	5	<2	-	<2	TD7
	Ol-cpxite	2.2	350	116	60	2.5	4	15	0.3	<2	TD8
	Cpxite	0.6	37	51	12	1.0	<2	<2	-	<2	ATR-046-0
	Cpxite	0.7	139	41	474	0.5	3	<2	-	<2	DTR-032-0
Sheared Ultramafic	Dun	4.1	113	70	43	2.5	<2	<2	-	<2	TD13
	Dun	4.6	527	22	705	3.7	4	4	1.0	<2	TD17
	Dun	17.0	7695	<2	187	<0.1	5	<2	-	4	TDR 06/01
	Dun	16.0	2129	<2	383	0.3	6	<2	-	<2	TDR 09/01

	Dun	3.2	1447	3	88	3.3	6	13	0.5	2	TDR 10/01
	Dun	16.4	2894	2	223	0.1	6	<2	-	<2	TDR 11/01
	Cpxite	1.9	232	14	17	6.3	<2	<2	-	2	KTR-034-0
	Cpxite	1.3	300	5	5	2.5	<2	<2	-	2	TD15
	Cpxite	0.8	100	4	34	3.6	<2	<2	-	<2	TD16
Lensoid Ultramafics	Dun	1.1	107	180	118	0.9	3	2	1.5	3	ATR-034-0
	Dun	4.2	887	95	1517	5.5	4	4	1.0	2	KTR-004-0
	Dun	2.6	453	12	1022	3.1	6	6	1.0	8	TDR 27/01
	Dun	<0.1	5	3	11	<0.1	<2	<2	-	3	TDR 01/01
	Dun	0.3	30	169	28	1.0	3	3	1.0	<2	TDR 26/01
	Dun	1.2	75	89	64	2.2	<2	2	0.0	4	DTR-029-0
	Dun	0.5	87	8	21	2.4	<2	<2	-	8	DTR-039-0
	Dun	0.5	72	6	32	0.1	<2	<2	-	<2	DTR-040-0
	Ol-cpxite	3.1	467	75	708	3.4	14	3	4.7	6	DTR-014-0
	Ol-cpxite	1.8	80	47	143	2.5	<2	3	0.0	3	DTR-041-0
	Ol-cpxite	1.6	31	104	33	2.0	2	10	0.2	4	KTR-006-0
	Ol-cpxite	0.7	138	4	6	2.5	<2	<2	-	<2	TTR-020-0
	Cpxite	1.6	210	34	428	1.6	21	<2	-	<2	ATR-036-0
	Cpxite	0.4	109	39	210	0.2	3	<2	-	2	DTR-015-0
Other	Basa	0.6	122	30	309	0.2	5	<2	-	<2	DTR-017-0
	Basa	1.1	215	155	2095	0.9	19	26	0.7	3	TTR-007A-
	Basa	<0.1	7	6	29	0.1	<2	<2	-	<2	TTR-010-0
	Birb	0.1	1364	12	387	0.1	3	<2	-	<2	ATR-050-0
	Birb	1.9	1437	5	280	0.2	4	<2	-	<2	KTR-002-0
	Birb	0.2	38	2	29	0.1	<2	<2	-	2	TD23
	ChSchi	0.2	16	55	17	1.8	2	3	0.7	<2	TDR 18/01
	ChSchi	19.0	6899	22	459	0.4	9	41	0.2	13	TTR-057-0
	Dior	1.2	13	60	3	1.9	<2	<2	-	3	ATR-035-0
	Dior	2.6	637	58	236	1.8	4	5	0.8	<2	TD5
	Dole	0.6	13	53	14	1.3	<2	<2	-	2	KTR-010-0
	Dole	24.7	2195	<2	26	<0.1	4	12	0.3	<2	TTR-025-0
	Fels	1.2	16	28	8	1.6	<2	6	0.0	<2	ATR-043-0
	Fels	1.3	37	110	65	1.7	<2	10	0.0	2	DTR-042-0
	Gabb	1.1	27	43	32	4.5	<2	<2	-	<2	DTR-025-0
	Gabb	0.9	29	105	23	1.5	4	4	1.0	2	TTR-050-0
	Gabb	2.5	356	41	486	2.4	8	5	1.6	<2	TTR-052-0
	GranDi	0.1	19	19	44	0.3	4	15	0.3	4	DTR-012-0
	GranDi	1.5	173	16	23	1.2	<2	<2	-	<2	DTR-038-0
	HardP	19.6	2056	6	53	<0.1	4	<2	-	8	TTR-030-0
	MetaBas	18.9	4141	4	67	<0.1	7	<2	-	<2	TTR-027-0
	MetaBas	23.2	2527	2	7	<0.1	4	<2	-	2	TTR-028-0
	Mylo	3.5	530	32	924	3.5	7	<2	-	<2	ATR-048-0
	Mylo	0.2	14	6	22	0.2	<2	<2	-	<2	DTR-030-0
	Mylo	2.0	160	148	193	2.0	7	4	1.8	<2	KTR-011-0
	Mylo	20.3	5079	5	150	0.1	25	38	0.7	<2	TTR-018-0
	Quar	0.2	36	15	22	0.1	<2	<2	-	<2	DTR-011-0
	Quar	1.5	312	12	141	0.5	<2	<2	-	<2	KTR-003-0
	Quar	0.1	25	9	22	0.2	<2	<2	-	<2	KTR-005-0
	Quar	0.2	32	3	19	0.1	<2	2	0.0	<2	TDR 13/01
	Quar	0.1	18	3	25	0.1	<2	<2	-	<2	TDR 14/01
	Quar	0.1	15	<2	17	<0.1	<2	<2	-	3	TDR 15/01
	Quar	0.1	15	41	29	0.2	31	37	0.8	3	TDR 17/01
	Schi	15.3	11044	2	842	0.1	<2	<2	-	<2	TD1
	Schi	7.8	1975	<2	1127	0.1	36	<2	-	<2	TD2
	Schi	0.2	15	3	33	1.1	<2	<2	-	<2	TDR 16/01
	Schi	0.2	29	14	43	0.3	<2	<2	-	<2	TTR-014-0
	Sed	0.1	16	36	22	0.2	<2	4	0.0	<2	DTR-031-0
	TaSchi	1.7	396	10	215	0.2	3	3	1.0	<2	DTR-010-0
	TaSchi	10.6	954	4	580	6.0	15	16	0.9	2	DTR-027-0
	TaSchi	4.4	573	71	983	4.3	7	4	1.8	19	TTR-051-0
	TCSchi	1.6	205	59	228	1.5	<2	4	0.0	8	TD18
	Unid	1.0	687	4	23	0.1	<2	<2	-	2	ATR-054-0
	Unid	0.2	29	22	19	1.5	<2	<2	-	<2	DTR-024-0
	Unid	4.9	1262	68	287	2.5	<2	<2	-	<2	TDR 21/01
	VQuar	21.1	2595	<2	169	<0.1	5	<2	-	<2	TD6
	VQuar	<0.1	3	<2	5	<0.1	7	9	0.8	<2	TDR 02/01
	VQuar	<0.1	13	<2	7	0.1	<2	<2	-	<2	TDR 03/01
	VQuar	<0.1	20	8	12	0.1	<2	<2	-	<2	TDR 04/01
	VQuar	12.1	2656	4	465	0.1	16	<2	-	<2	TDR 23/01

Table 8.12: Mg, Ni, Cu, Cr, Al, Pt and Pd values for the altered samples collected from the Tulu Dimtu area. Anor: Anorthosite. Basa: Basalt. Birb: Birbirite. ChSchi: Chlorite-Schist. ChSchi: Chlorite-Schist. Cpxite: Clinopyroxenite. Dior: Diorite. Dole: Dolerite. Dun: Dunite. Fels: Felsite. Gabb: Gabbro. GranDi: Granodiorite. HardP: Hard pan. MetaBas: Metabasalt. MetaSed: Metasediment. Mylo: Mylonite. Ol-cpxite: Olivine-clinopyroxenite. Quar: Quartzite. Schi: Schist. Sed: Sediment. TaSchi: Talc-Schist. TCSchi: Talc-Chlorite-Schist. Troc: Troctolite. Unid: Unidentified. VQuar: Vein Quartz.

The following sections describe the distribution of Ni, Cu, Cr and Al in the Tulu Dimtu area. Each section describes one element and its distribution in fresher ultramafics and then altered rocks (as defined in section 8.3.1). These sections are accompanied by a fold-out page (page 213) of maps showing the distribution of all elements which the reader should refer to as each section is read.

8.4.3. Nickel

The fresher rocks on the flanks of the Tulu Dimtu Main Intrusion are enriched in Ni to a much greater degree than those in the centre. In fresher rocks nickel rises above 3000ppm (and up to 5860ppm) only within 500m of the contact of the Main Intrusion with the surrounding basement. Figure 8.4A shows that throughout the centre of the intrusion and in two places near the flanks, Ni is below 3000ppm but not lower than 1456ppm. The two fresher samples from the Lensoid Ultramafics contain significant Ni (2824ppm and 1644ppm), the remaining samples from Lensoid Ultramafics show negligible amounts (31 to 467ppm). The highest Ni content in fresher rocks (5860ppm) is found within 150m of the southern flank of the Sheared Ultramafic.

In samples classified as altered, Ni is enriched almost exclusively in the Main Intrusion and the Sheared Ultramafic (figure 8.4A). Although most samples outside of the Main Intrusion and Sheared Ultramafic do not host significant Ni, three samples do contain significant amounts. These come from two Shear Zones (containing 11,044ppm and 6899ppm) and one Lensoid Ultramafic (5079ppm). Indeed, the highest Ni content in the samples of the Tulu Dimtu area (11044ppm) is contained in a schistose rock from a shear-zone bounding the southeast flank of the Main Intrusion.

At one location in the northwestern Lensoid Ultramafic both altered and fresher rocks show Ni enrichment. A fresher dunite has 2824ppm Ni and this value rises to 5079ppm in a mylonitised rock.

8.4.4. Copper

In fresher rocks Cu reaches a maximum of 16ppm in two samples of the Sheared Ultramafic. Everywhere else - including the Lensoid Ultramafics - Cu never rises above 5ppm in fresher rocks.

Cu values of greater than 70ppm in altered rock are almost entirely situated over the basement and units other than the Main Intrusion and Sheared Ultramafic (figure 8.4A). Within the Main Intrusion, the highest values of Cu occur close to the western and southern flanks. The highest Cu analysis within the altered samples of the Main Intrusion (116ppm) occurs close to the samples with the highest values in the fresher rocks. Analyses of Cu in samples from the Lensoid Ultramafics and Shear Zones frequently rise above 70ppm, however some samples show negligible amounts (<5ppm).

8.4.5. Chromium

The highest Cr value in the Tulu Dimtu area (2728ppm) occurs in a fresher dunite on the southern flank of the Main Intrusion, close to the Sheared Ultramafic. Of the other fresher rocks, all other Cr values above 100ppm in the Main Intrusion are found in a zone close to the western flank of the formation. None of the three fresher ultramafics of the Lensoid Ultramafics show Cr values which rise above 500ppm, however all are higher than 100ppm.

In altered rocks, the dunites and olivine-clinopyroxenites at the centre of the intrusion are depleted in Cr. As seen in the fresher rocks, some higher Cr values (<100ppm) are found towards the outside of the formation. A schistose rock in a shear-zone bounding the southeastern parts of the Main Intrusion has a Cr value of 1127ppm.

Outside the Main Intrusion high Cr values (<900ppm) can be found in Lensoid Ultramafics and Shear Zones.

8.4.6. Aluminium

In all of the fresher rocks (except two) of the Tulu Dimtu area, Al is below detection limits. Two dunites from the Sheared Ultramafic returned values of 1% for Al.

The altered dunites in the centre of the Main Intrusion are almost entirely depleted in Al. The flanks of the Main Intrusion and Sheared Ultramafic are slightly elevated in Al. A high Al value (4.5%) occurs in a gabbro on the western flank of the intrusion and a zone of slightly elevated Al values occurs on the southern flank of the formation. Several pyroxenites and dunites in the Sheared Ultramafic show Al elevated above 2%. Several high values of Al (>4%) occur in the Shear Zones and Lensoid Ultramafics.

8.4.7. Summary of the Ni, Cu, Cr and Al values in the Main Intrusion and Sheared Ultramafic

Of the fresher rocks of the Main Intrusion (including the Sheared Ultramafic) the highest Ni values in the complex are close to the edge. As such, the highest Ni (5860ppm) is found within 150m of the southern flank of the Sheared Ultramafic. Similarly, the highest Cr values are found close to the flanks. Although these high Cr values are found in five samples within the Main Intrusion, only two fresher samples contain both high Ni and high Cr. At the southern edge and near the junction between the Main Intrusion, the Sheared Ultramafic and the southern shear-zone, both Cr and Cu rise to their highest values in two separate fresher dunites. Figure 8.3 shows the relative proportions of Cu and Cr in these samples (TDR 19/01 and TD9).

As seen in the fresher rocks, the altered samples also show the largest values of Cr at the flanks of the Main Intrusion. Additionally, Cu and Al show their highest values in the same samples located near the southern flank. As with Cu, Cr and Al the altered ultramafics show the highest values of Ni close to the flanks of the Main Intrusion,

similar to those values seen in the fresher rocks. However, unlike the other elements, Ni is enriched in two samples in the centre of the intrusion (4141 and 2527ppm).

8.4.8. Summary of the Ni, Cu, Cr and Al values in the Lensoid Ultramafics

When compared to the Main Intrusion the three fresher samples of the Lensoid Ultramafics (two dunites and one pyroxenite) display elevated Cr and intermediate Ni values.

The altered ultramafics show similar patterns to those seen in the Shear Zones (see section 8.4.9). One altered dunite sample is enriched in Ni but two different dunites are enriched in Cu. Elsewhere in the Lensoid Ultramafics, one altered olivine-clinopyroxenite is enriched in both Cr and Al (700ppm and 3% respectively).

8.4.9. Summary of the Ni, Cu, Cr and Al values in the Shear Zones

Two samples within Shear Zones (a mylonite and a talc-schist) have high values of both Cr and Al. High Ni and Cu values occur in different samples, two schistose rocks show high Ni values and a mylonite shows Cu enriched above 130ppm.

8.5. Tulu Dimtu: Pt and Pd Distribution

8.5.1. Rock

The highest Pt and Pd grades of fresher rocks in the Tulu Dimtu area occur at the south of the Main Intrusion. Pt is present from below detection to 40ppb and Pd from below detection to 37ppb in the three samples. These samples are located at the junction between the Tulu Dimtu Main Intrusion, the Sheared Ultramafic and the southern shear zone. Elsewhere, neither Pt nor Pd rise above 9ppb and drop to below detection limits (<2ppb).

Within the Tulu Dimtu Main Intrusion, the three highest Pt analyses (36ppb, 24ppb and 24ppb) in the altered rocks occur at the edge of the complex and these all coincide with Pd below detection limits (<2ppb). All other altered ultramafics show Pt assays between 7ppb and 3ppb. The maximum Pd value within the altered rocks of the Main Intrusion is 15ppb found near the southern flank. A dolerite dyke cross-cutting the intrusion near the western flank has a Pt at a value of 4ppb and a Pd value of 12ppb. The two Pt- and Pd-bearing samples from the Lensoid Ultramafic units are an altered ultramafic with a Pt value of 21ppb and a Pd value below detection and a mylonitised sample with a Pt value of 25ppb and a Pd value of 38ppb. These are found in two separate ultramafic units to the northwest of the Main Intrusion (figure 8.4E and 8.4F).

Other Pt- and Pd-bearing samples include a chlorite schist in a zone cross-cutting the gabbro and this shows results of 9ppb Pt and 41ppb Pd. A talc schist occurs close to the sheared western contact of the Tulu Dimtu Main Intrusion and this has returned results of 15ppb and 16ppb for Pt and Pd respectively. A fine-grained volcanic sample close to the isolated shear zone west of the Main Intrusion has Pt and Pd concentrations of 26ppb and 19ppb respectively.

8.5.2. Summary of Pt and Pd distribution in the Main Intrusion and Sheared Ultramafic

The highest Pt and Pd grades of the Tulu Dimtu area occur in a fresher rock on the southern flank of the intrusion. This occurs with two other fresher samples which are also relatively high in both Pt and Pd (see table 8.13). These samples occur at the junction between the Main Intrusion, Sheared Ultramafic and Shear Zones.

Within the altered rocks of the Main Intrusion all Pt grades above 20ppb also occur in the flanks of the intrusion – which may suggest a zonation in Pt values. As seen with Pt, all Pd values in altered rocks are 15ppb or below and occur within 400m of the flanks of the intrusion. However - unlike the fresher rocks – Pt reaches the highest values in different altered samples from those of Pd (figure 8.4E).

The comparison between PGE and Ni, Cu, Cr and Al in the highest samples is summarised as follows:

Sample	Pt	Pd	Ni	Cu	Cr	Al
TDR 19/01	37	30	2872	16	436	0.1
TD9	37	27	2992	8	2728	0.5
TD10	2	40	1909	4	634	0.1
TD12*	< 2	< 2	1456	16	102	< 0.1

Table 8.13: A summary of Ni, Cu, Cr and Al values in the dunite samples of highest Pt and Pd grade of the fresher rocks. A graphical representation of this data is provided in figure 8.3. *: Sample TD12 is included regardless of low Pt and Pd values as it contains a high Cu value and is located close to the Pt- and Pd-bearing samples.

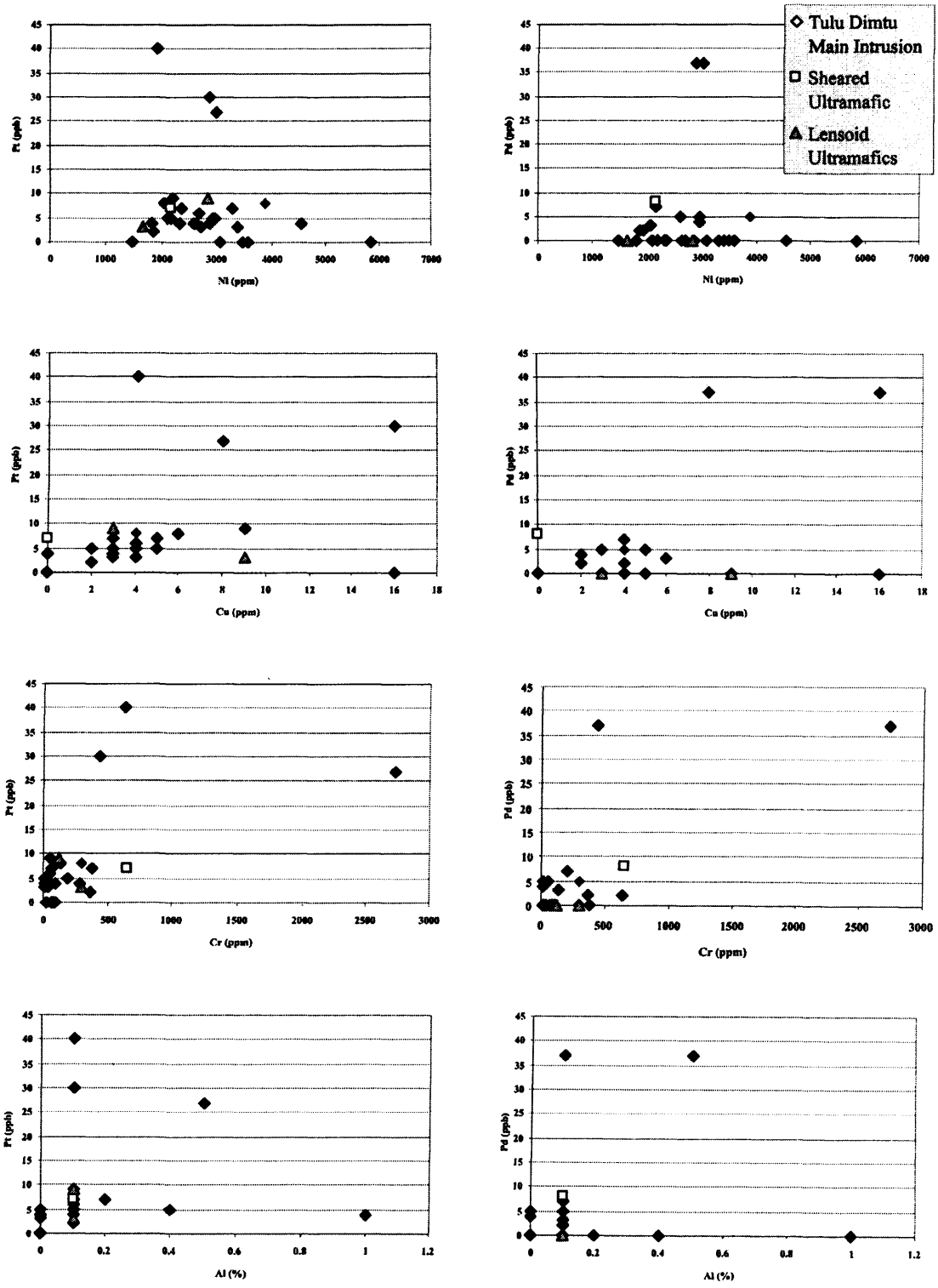

Figure 8.3: Graphs of Ni, Cu, Cr and Al versus Pt and Pd in the fresher rocks of the Tulu Dimtu area. The key to symbols in the top right corner.

8.5.3. Summary of Pt and Pd distribution in the Lensoid Ultramafics

The highest Pt and Pd values in fresher rocks are 9 and 8ppb respectively. Whereas the highest Pt and Pd values in altered Lensoid Ultramafics are 25 and 38ppb. There are three altered samples from the Lensoid Ultramafics which contain Pt or Pd. An altered pyroxenite and an olivine-clinopyroxenite sample are more enriched in Pt rather than Pd and one mylonite sample contains both Pt and Pd.

8.5.4. Summary of Pt and Pd distribution in the Shear Zones

Two samples within the Shear Zones are Pt- and Pd-bearing. These are a talc-schist close to the western contact of the Main Intrusion and a chlorite-schist in the southwestern corner of the area. In the chlorite-schist Pd predominates over Pt, but in the talc-schist Pt shows similar values to Pd.

8.5.5. Summary of Pt and Pd distribution in the basement

Two basement rocks are Pt- or Pd-bearing. These are a quartzite (with a Pt value of 31ppb and Pd value of 37ppb) and a fine-grained volcanic rock (with a Pt value of 19ppb and Pd value of 26ppb).

8.5.6. Comparison of the geochemistry of the soil versus rock samples

Ni and Cu anomalies in soil occur in different places from those of the rocks (when compared to chapter 8). As with the rock samples (see chapter 8), the highest Cr values in soil are found above the western and southern flanks of the Main Intrusion and the lowest values are in the centre of the intrusion.

There are a greater number of soil samples enriched to above 20ppb Pt compared to the number of rock samples. In fresher and altered rocks 7% of the samples (3/42) contain more than 20ppb Pt whereas in soils 33% (23/70) contain more than 20ppb. Pd anomalies (13 and 15ppb) only occur in the centre of the intrusion.

8.6. Review of processes concentrating Pt and Pd

8.6.1. Introduction

There are several mechanisms cited to explain the distribution of PGE within mafic and ultramafic complexes. Much research has been directed towards the role of sulphur in magmas but alternatively some authors advocate a role for hydrothermal fluids. Furthermore, some models have been developed whereby PGE are concentrated without sulphur or hydrothermal fluids.

The proponents of the role of sulphur argue that PGE-rich droplets of liquid sulphide segregate out of a silicate magma and then concentrate the PGE into a horizon (for a review see Naldrett, 1998). Alternatively, the study of polyphase silicate inclusions within Pt-Fe alloys from sulphur-poor complexes suggests that the magma involved in the precipitation of PGM is highly water-rich (Johan, 2002). Studies of fO_2 and fluid inclusions can also be used to support the role of high temperature fluids in concentrating PGE. Some recent work has begun to reveal an additional view on PGE concentration. Macambria and Filho (2005) cite a correlation between Al and PGE to suggest that neither sulphur nor high temperature fluids are required to create a PGE "reef".

In order to aid the subsequent discussion this section reviews the igneous processes believed to have a role in the concentration of Ni, Cu, Cr, Al and PGE. This is followed by an account of the study of PGE solubility in medium to low temperature fluids.

8.6.2. The fractionation of Ni

The partitioning behaviour of Ni can vary with magmatic conditions of formation such as fO_2 and fS_2 (Kinzler et al., 1990; Gaetani and Grove, 1997). Table 8.14 shows the range of partition co-effcient (D_{Ni}) values determined from in-situ measurements of natural examples and from experimental systems. The lowest partition cocoefficient of Ni

8.6.4. Sulphide immiscibility and solubility

As the primitive magma rises through the Earth's crust, a small amount of precipitation of silicate or oxide minerals occurs and then sulphur may become saturated in the magma. At this point S comes out of solution in the silicate melt and a situation occurs where both silicate and sulphide melts exist together as immiscible liquids – an event called sulphide segregation. Ni, Cu, Pt and Pd are known to be concentrated into the sulphide melt within a magma by sulphide segregation (Naldrett and von Gruenewaldt, 1989) which may be triggered by several different changes in conditions.

Sulphur saturation in a magma can be achieved in a situation where sulphur becomes insoluble. The most common explanation for this is through the precipitation of silicate minerals, or a fall in temperature, or an increase in fO_2 or by a decrease in the amount of Fe^{2+} in the magma. However, there are several other factors which affect sulphide solubility (for a review see Robb, 2005) including the injection of a new magma (see section 8.6.7).

8.6.5. Sulphide fractionation

As an immiscible mixture of silicate and sulphide liquids rise through the crust crystallisation occurs in each melt. The sulphides fractionate to produce a Ni-bearing monosulphide solid solution (MSS) which is precipitated leaving a Cu-rich residual sulphide liquid (Fleet and Pan, 1994; Barnes et al., 1997). Partition coefficients confirmed by geological studies have demonstrated that during sulphide fractionation, Pt and Pd are compatible with the Cu-rich residual sulphide liquid (Barnes et al. 1997; Fleet et al., 1993). The residual sulphide liquid may then crystallise as a Pt-, Pd- and Cu-rich Intermediate Solid Solution (ISS). Alternatively, the Cu-rich liquids could be driven away from the MSS, through filter-pressing (see section 8.6.6). The products of sulphide fractionation are seen in-situ in the sulphide blebs described by Prichard et al. (2004).

It has been argued that the concentration of PGE by the action of sulphides is only valid in magmas of large bulk-S content such as the Bushveld or Sudury Intrusive complexes. Furthermore, a sulphur solubility assessment has suggested that the Bushveld complex does not contain sufficient sulphur to explain the amount of PGE present (see Cawthorn, 2005). These arguments suggest that alternative models (not involving sulphur) should also be explored. However, Peregoedova and Ohnenstetter (2002) argue that a high fS_2 can be obtained in low-S magmas through fractionation of the silicate melt and immiscibility of the sulphides. Furthermore, Tolskykh et al. (2000) have shown that in Alaskan-type intrusions – which are commonly low-S - it is common to find cooperite (PtS) rimming Pt-Fe alloys. This presence of cooperite suggests that the fS_2 of the magma must have risen high enough to allow the sulphuration of Pt (Peregoedova and Ohnenstetter, 2002).

8.6.6. Filter-pressing

After and during sulphide fractionation, the Cu-rich residual sulphide liquid can migrate away from the MSS crystals and precipitate. This is proposed by the "filter-pressing" model of Andersen et al. (1998) to explain the zonation of Au and PGE in the Skaergaard Intrusion (East Greenland). As sulphide fractionation occurs, cumulus silicate crystals precipitate, and the residual sulphide liquid will be interstitial. As further accumulation of cumulus material occurs, the volume of interstitial space will drop and the residual sulphide material will be entrained along with the other interstitial fluids and migrate towards the more evolved portions of the system. The MSS, however, will have already crystallised will therefore be trapped within the cumulate pile thereby allowing ISS to crystallise away from MSS.

In a situation where bulk sulphur content is very low, it may be hard to understand how a residual sulphide liquid can migrate. However, the validity of this model is dependant on the potential for the residual sulphide liquid to be entrained in the bulk interstitial liquids. Smaller amounts of liquid are more likely to become entrained than larger amounts and hence the model becomes more feasible with smaller amounts of

fluid. Additionally, when the residual sulphide liquid is moving away from the MSS, a "tail" will form behind the bulk of the entrained liquid. The more entrained the liquid, the larger the tail and, therefore, the less likely that ISS will be split apart from MSS. So the smaller the proportion of residual sulphide liquid, the greater the potential for filter-pressing to occur and the more likely Cu-rich sulphides (ISS) will be split apart from Ni-rich sulphides (MSS).

It may be argued that the residual sulphide liquid is unlikely to travel distances larger than 1cm. However the evolved Cu-rich liquid can behave in a number of ways. Prichard et al. (2004) describe a situation in a mafic dyke whereby both MSS and ISS crystallise together as sulphide blebs less than 1cm in diameter. In contrast, Naldrett et al. (1992) describe how the ores of the "Copper" and "Deep Copper" zones of the Strathcona mine are the end product of fractionation of the Main Zone Sulphides over 200m away. Furthermore, Andersen et al. (1998) document the effect of filter pressing in separating Au and PGE reefs over several 100s of metres in the relatively sulphur-poor Skaergaard complex. And as such, it is expected that under the appropriate conditions, the evolved residual sulphide liquid can travel up to 200m away from the location of the MSS.

8.6.7. Magma mixing

Magma mixing may result in the precipitation of large amounts of chromite which may be accompanied by sulphide immiscibility The mechanism of chromitite formation is dealt with first. Chromite saturation can be reached in a situation where a slightly evolved melt (precipitating olivine) is mixed with a primitive melt (Naldrett et al., 1990; Naldrett and von Gruenewaldt, 1989). The precipitation of chromite by the mixing of two magmas was proposed by Irvine (1977) to explain the formation of massive chromitites in the Muskox intrusion in NW Canada. His model is consistent with observations of chromitites from the Bushveld and Stillwater complexes where chromitites form at the base of well-defined cyclic units (Naldrett et al., 1990). Naldrett et al. (1990) suggest that if a magma on the olivine-chromite cotectic (point A) is mixed with a magma in the orthopyroxene field (point D) the resulting melt (AD) may fall within the chromite field

and as cooling occurs, chromite will be precipitated followed by olivine. This will then be followed by the typical fractionation sequence. This only occurs in a situation where the fresher magma intrudes the evolved melt well before plagioclase is precipitated.

Where an advanced differentiate (precipitating plagioclase) mixes with a primitive melt, sulphides may become immiscible with the silicate melt (Naldrett and von Gruenewaldt, 1989). Subsequently, suitable conditions for the crystallisation of these sulphides may then allow Ni, Cu and the PGE to become concentrated. In order for chromite to be precipitated only a slightly evolved melt is required, but for chromites to be precipitated and sulphides to become immiscible the influx of a more advanced melt is necessary. This raises the possibility within this model of the existence of sulphide-barren and sulphide-poor chromitites.

8.6.8. Hydrothermal remobilisation

When associated with primary sulphides of a small grain size, Ni and Cu are both known to be highly soluble in hydrothermal fluids. This behaviour is indicated from precipitates of hydrothermal fluids (Marshall and Gilligan, 1987; Keays, 1987; Canals et al., 1992). Furthermore, the presence of Cu in hydrothermal fluid inclusions has been noted by Vanko et al. (2001) and Baker et al., (2004) – for a synopsis of previous studies see Kesler (2005). Fluids in such systems are regarded to be of nearly neutral pH, with temperatures from 200-300°C and salinities of less than 3wt% NaCl (Kesler, 2005) all of which are obtainable in a mobile belt such as the WES. Therefore the presence of Ni and Cu in highly sheared rocks (at values much higher than in fresher rocks) may be the result of shear-zone hosted high-temperature fluids.

In comparison to sulphide-associated elements, Cr-bearing spinels are highly resistant to hydrothermal alteration. It is therefore likely that a fresher rock with high Cr will retain a high Cr value in the subsequent altered rock. Aluminium is also immobile in hydrothermal fluids and, therefore, if present it may indicate the presence of aluminosilicates in the protolith.

The evidence for the stability of Pd- and Pt-chloride complexes in fluids at equilibrium with typical alteration minerals at temperatures up to 300°C is well established (Wood, 2002; Wood 1987; Gammons et al., 1992). At higher temperatures, it is expected that the solubility of these elements in alteration fluids will increase and lower salinities and pH will be required. Solutions in equilibrium with clay minerals and/or hematite are thought to take more Pt and Pd into solution than those fluids which precipitate pyrite, pyrrhotite and other alteration minerals (Tarkian et al., 1996). The solubility of Pt- and Pd-bisulphide complexes is not well understood, but may be capable of transporting far more of the elements under less extreme conditions. Additionally, the case for preferential dissolution and transport of Pd over Pt has been made clearly by experimental studies of several conditions (see numerous references in Wood, 2002).

8.7. Tulu Dimtu: Discussion

Here the processes likely to have affected the distribution of Ni, Cu, Cr Al, Pt and Pd in the Tulu Dimtu area are discussed. The processes involved with the distribution of Ni, Cu, Cr and Al in fresher ultramafics are considered from 8.7.1 to 8.7.3, followed by those processes which affect altered rocks in 8.7.4 and 8.7.5. The mechanisms which distribute Pt and Pd are considered from section 8.7.6 to section 8.7.7.

8.7.1. Zonation of nickel and chromium in fresher rocks

The highest Ni value in the fresher rocks (5960ppm) occurs within 150m of the southern flank of the Sheared Ultramafic. Ni values then drop steadily towards the centre of the Tulu Dimtu Main Intrusion and as such, all Ni values above 3000ppm occur within 500m of the edges (figure 8.4A). Similarly, the highest Cr value (2728ppm) occurs at the edge of the Main Intrusion and all Cr values above 100ppm occur within 700m of the flanks of the complex (figure 8.4C). Although both elements show a gradual variation in values with distance away from the edge of the intrusion there are only two samples which contain both elevated Cr and elevated Ni. Additionally, the highest Cr values occur in a different location to the highest Ni values.

into olivine, it would be expected that the higher Cr values would form uniform zones. However, in the Tulu Dimtu Main Intrusion (figure 8.4C) several isolated samples with high Cr values occur – an observation which is consistent with the concentration of Cr within discrete spinel minerals. In most spinel-bearing complexes, Cr-spinels precipitate with olivine early during fractional crystallization and/or relate to an increase in fO_2 (Barnes and Roeder, 2001). The refractory nature of the spinels mean that they will not go into solution easily in aqua regia. It is likely that the Cr values found in the analyses presented here represent Cr partitioned mainly into olivine and to a small degree into spinel. With this in mind, a rock with a high Cr value remains a relatively primitive rock.

It is proposed here that as a partial melt rose through the Earth's crust, olivine precipitated and took Cr and some Ni into its crystal structure. As silicates continued to crystallise from the melt a point came whereby the dissolved sulphides became immiscible (Naldrett and von Gruenewaldt, 1989). When this occurred, Ni was scavenged from the silicate melt into the immiscible sulphide liquid. Subsequently sulphur saturation of the magma occurred and Ni-bearing (and possibly Cu-bearing) sulphides crystallised. After these immiscible sulphides had precipitated, Ni continued to be partitioned to a lesser degree into the olivine and oxides in the more evolved rocks. Simultaneously as olivine crystallised, discrete spinel minerals precipitated into which Cr partitioned. It can be suggested that the rocks of the western and southern flanks of the Tulu Dimtu Main Intrusion are the most primitive and that progressive fractionation was directed towards the centre of the intrusion.

It could be argued that the action of sulphur in concentrating Ni is not relevent due to the low sulphur content. Only one fresher ultramafic rock returned S values above detection limits (0.02% found in DTR-007-02). However, Peregoedova and Ohnenstetter (2002) argue that a high fS_2 can be obtained in low-S magmas through fractionation of the silicate melt and immiscibility of the sulphides (8.6.5).

It is not possible to rule out the effects of re-mobilisation of Ni by late or post magmatic hydrothermal fluids. It is likely that hydrothermal fluids have remobilised Ni in

these rocks to some degree. However, as shown in section 8.3.1 the rocks classed as "fresher" in this study all retain Mg values which are as high as can be expected for a typical fresher dunite or clinopyroxenite. Therefore, these samples cannot have been subjected to pervasive alteration, however it is still possible that some limited action of hot fluids may have affected the Ni values (in the order of 100's of ppm) without a significant difference in Mg values. Narrow veinlets containing Ni-bearing phases may cross-cut an otherwise fresher sample and this is documented in chapter 3. However, unlike Ni, Cr is not known to be remobilised by hydrothermal fluids – even from olivine - and shows similar zoning to Ni and this therefore, supports the fractionation hypothesis.

8.7.2. Locations of highest copper and chromium values in fresher rocks

The highest values of Cu in the fresher rocks (16ppb in two samples) occur 200m from the southern flank of the intrusion. The highest Cr values occur in a different sample located close by (<100m). The highest values of Cu and Cr do not occur with the highest Ni values – which are located over 1km away.

Although crystal fractionation and the immiscibility of sulphides can explain the Ni values and some of the Cr values, this model (section 8.7.1) cannot explain why the highest Cu values are located in a different location from Ni. Furthermore, it cannot explain why the highest Cr values occur close to the highest Cu but not Ni. In a situation where sulphide minerals crystallise at the same time Cr partitions into olivine, the highest Ni and Cu values would initially occur close to the highest Cr values. Subsequently, the Cu may be moved away from the highest Ni and Cr by either filter-pressing or high temperature fluids (see below). Here, the close proximity of the highest Cu and Cr values and their dislocation from the highest Ni values suggests that a different or more complex model is required. In this section two possible explanations are discussed, firstly a combination of filter-pressing and magma-mixing and secondly the remobilisation of Cu.

During filter-pressing, the Ni-rich MSS precipitates and then the Cu-rich residual sulphide liquid migrates away from the MSS by the compaction of the cumulus olivines.

8.7.3. Trace element distribution in fresher rocks of the Lensoid Ultramafics

Ni values in the limited number of fresher samples from the Lensoid Ultramafics are above 1000ppm but lower than 3000ppm and Cr values are higher than 100ppm. These values are similar to those seen close to the edge of the Tulu Dimtu Main Intrusion. The Ni values are low enough for this element to be taken into the crystal structure of olivine without the involving other phases. The Cr values are comparable to those seen on the western flank of the Tulu Dimtu Main Intrusion. By comparison with the Tulu Dimtu Main Intrusion, it is inferred that these rocks crystallised before sulphide saturation. It is plausible that these smaller ultramafic bodies could be considered as slivers of "sheared-off" material from the flanks of a larger intrusion. Although with only three samples of fresher rocks from the Lensoid Ultramafics these interpretations are preliminary.

8.7.4. Trace element distribution in Shear Zones

The highest value of Ni in the rocks of Tulu Dimtu (11,044ppm) occurs in a sheared rock at the southeastern flank of the Tulu Dimtu Main Intrusion , this is almost twice the highest value seen in fresher rocks (5860ppm). Additionally, a mylonite sample shows Cu values of 148ppm which is much higher than the amount of Cu in fresher rocks which is 16ppm. Two samples within Shear Zones (a mylonite and a talc-schist) show high Cr and Al at over 900ppm and 4% respectively.

The necessary aqueous conditions for the remobilisation of Ni and Cu are obtainable in a mobile belt such as the WES (section 8.6.8). Therefore the presence of Ni and Cu in highly sheared rocks - at values much higher than in fresher rocks - may be the result of the redeposition by hot aqueous fluids transported along Shear Zones.

This leaves the question of how both Al and Cr are concentrated into the samples since Al is to be expected in a felsic protolith and Cr is expected in primitive ultramafics. Given that some altered rocks may more resemble soils it is possible that the Al has been

concentrated by soil-forming processes occurring above a Cr bearing ultramafic protolith or alternatively that two different protoliths have been juxtaposed in the shear-zone.

8.7.5. Zonation of trace elements in altered rocks

The altered rocks of the Tulu Dimtu Main Intrusion show a zonation in Ni and Cr similar to that seen in the zones of the fresher rocks (>3000ppm and >100ppm respectively). Patterns seen in altered rocks but not seen in the fresher samples are that Cu and Al also have high values at the edge of the intrusion (>30ppm and 0.7% respectively). Individual samples from the Lensoid Ultramafics also show elevated values for all four elements in question. Chapter 3 shows that the principle mineral in these samples is serpentine and as a phyllosilicates is likely to be affectively digested by aqua regia along with the sulphides (see section 8.2.3).

The altered samples studied here represent a magmatic signature overprinted by alteration. It has been seen (chapter 2) that the WES has been subjected to considerable deformation and the movement of hydrothermal fluids. This deformation has been observed at Tulu Dimtu by De Wit and Chewaka (1977) who described alteration in Shear Zones flanking the intrusion resulting in a talc-carbonate and serpentine-talc assemblage. It is therefore likely that the same hydrous fluids could have penetrated the flanks of the Tulu Dimtu intrusion to remobilise and precipitate both Ni and Cu. Hence the elevated Ni and Cu values could be the result of either or both hydrothermal remobilisation or magmatic concentration. Cr is unlikely to have been remobilised from its primary position and, therefore, the zonation in high Cr values at the flanks of the intrusion supports similar zones seen in fresher rocks. The values of Cr in an altered rock may be elevated slightly from the equivalent in the protolith, due to changes in volume between fresher and altered rocks (Giggenbach, 1984). Slightly elevated Al values at the flanks of the intrusion may be attributed to the concentration of the element – seen in trace amounts in fresher rocks - during soil-forming. However, the original source of the Al is unknown. For this study, an "altered" rock may be partially affected by soil-forming processes at the start of the transformation from rock to soil.

As with the Tulu Dimtu Main Intrusion, hydrothermal fluids can be invoked to explain the distribution Ni and Cu in the Lensoid Ultramafics. If the Lensoid Ultramafics are considered as deformed slivers of the Tulu Dimtu Main Intrusion (as suggested in section 8.7.3) it is to be expected that they have been subjected to similar and possibly more intense alteration systems due to the deformation required to dismember them from the Tulu Dimtu Main Intrusion. Both Ni and Cu are observed in concentrations much higher than those seen in the fresher samples of the Lensoid Ultramafics and also higher than the altered samples of the Main Intrusion. It is to be expected that the deformation required to dismember the lensoid bodies from the Main Intrusion is greater than that seen at the flanks of the Main Intrusion itself. It is possible that the subsequent alteration will have been more intense and the potential for concentration of Ni and Cu greater as a result. However, hydrothermal fluids may also act to disperse the elements which are soluble within them.

8.7.6. Genesis of Pt and Pd in fresher rocks

Three fresher dunites from the Tulu Dimtu Main Intrusion contain significant Pt and/or Pd values (TD10, TD9 and TDR 19/01). Each of these three samples contains significant amounts of either Ni, Cu and/or Cr and the variations of these elements are summarised in table 8.13 and figure 8.3. The three Pt- and Pd-bearing samples are located close to another fresher dunite (TD12) which is barren of both elements but contains the highest Cu value.

A model to explain the origin of the high Cr value found in sample TD9 by the mixing of a fresher primitive magma is outlined in section 8.7.2 and this can also explain the high Ni value as it will concentrate strongly into the early crystallised olivines. Naldrett and von Gruenewaldt (1989) have determined that magma mixing may account for sulphide segregation where an advanced differentiate (precipitating plagioclase) mixes with a primitive melt (see section 8.6.7). However plagioclase is not observed in the ultramafics from the Tulu Dimtu Main Intrusion and therefore this is seen as unlikely.

The model used to explain the dislocation of Cr and Cu anomalies from Ni (see section 8.7.2) can be used to explain the Pt and Pd distribution. In this model the Pt and Pd was filter pressed into the fresher cumulate pile along with the Cu-rich residual sulphide liquid.

As with Cu, the locations of the highest Pt and Pd values can be explained on the basis of either magmatic processes (filter-pressing) or alteration. The Pt and Pd of sample TDR 19/01 (see table 8.13) could be explained as being partitioned into a Cu-bearing residual sulphide liquid which was subsequently filter-pressed through the pile of cumulate olivines so that it is separated from the crystallised Ni-rich MSS (as described in section 8.6.6). A similar explanation may be given for the Pt- and Pd-barren sample TD12, however in this case the ISS crystals precipitated from the sulphide liquid after the precious metals had already partitioned out of this melt.

Alternatively, both Pt and Pd in each sample could have been remobilised along with Cu. The origin of high Pd in sample TD10 is hard to explain by magmatic processes as Pt should behave similarly in a magma. The absence of Pt indicates that a Pd mineral was present in this sample. The Cu value is too low to conceive the presence of residual sulphides and the Ni value is low enough to be partitioned into olivine alone. It is possible that the anomalous Pd value may have been transported in by aqueous fluids, as this is seen frequently in other deposits (section 8.6.8). The reason for the dislocation of Pt and Pd from the areas of the highest Ni can only be determined through the analysis of the morphology of the PGM.

8.7.7. Genesis of Pt and Pd in altered rocks

Pt- and Pd-bearing altered rocks occur at different locations in the Main Intrusion (figures 8.4E and 8.4F). The dislocation of Pt and Pd anomalies at the flanks of the Tulu Dimtu Main Intrusion could be explained by the preferential transport of Pd away from the sites of magmatic concentration (see section 8.6.8). The preferential remobilisation of Pd over Pt has been documented by many other authors (for example Oberthür et al.,

2003; Prichard et al., 1996). The sites of magmatic PGE concentration are likely to occur at the flanks of the intrusion which is also where hydrothermal fluids are likely to act. So the two modes of transport are likely to have been superimposed.

There are seven Pt- and Pd-bearing rocks outside of the Tulu Dimtu Main Intrusion and these are from the Shear Zones, Lensoid Ultramafics and basement units (see section 8.5.2). Five of these samples contain higher Pd values than Pt. Of particular note is a chlorite schist which returned values of 9ppb for Pt and 41ppb for Pd. This further suggests that Pd has been preferentially reconcentrated by hydrothermal fluids in the area. The higher Pd values than Pt in the Lensoid Ultramafics may indicate the redeposition of Pd in these complexes as the chlorite schist is likely to contain precipitates from the alteration fluids.

8.8. Tulu Dimtu: Conclusions

Throughout the Tulu Dimtu area, distinguishing the effects of hydrothermal alteration from magmatic processes is difficult. The geochemical analyses discussed in this chapter suggest that both hydrothermal and magmatic processes are likely influence Pt and Pd grade at the flanks of the intrusion. Consequently, it is recommended that any further exploration activities are focussed in these areas.

Some preliminary ideas have been proposed to explain the development of Pt and Pd in the fresher rocks of the Tulu Dimtu Main Intrusion. A large variation Cr values between the centre and the edges of the intrusion indicate that the most primitve rocks occur at the edge of the complex. Further variations in Cr value may indicate the presence of a second melt influx. A series of processes may then have occurred to concetrate Pt and Pd from the magma. High Ni values and significant vairaitions in Cu values indicate that sulphide immiscibility and fractionation may have occurred, in such a situation the Pt and Pd would be associated with the Cu-rich residual sulphide.

Although sulphide fractionation may explain the dislocation of Cu and Ni values, it is also possible that the Cu – along with Pt and Pd - could have become remobilised by hot aqueous fluids and then redeposited close to magmatic Cr-spinels. Analysis of PGM and sulphide mineralogy is required to test the filter-pressing and hydrothermal models. Furthermore, there is no direct evidence for the influx of a fresher batch of melt, it is nessecary for this to be validated using spinel geochemistry (see chapter 9).

A limited number of fresher ultramafic samples from the Lensoid Ultramafics have been described, these indicate that the samples formed after chromite precipitation but before sulphur saturation. These complexes may be slivers from the edges of larger intrusions, such as the Tulu Dimtu Main Intrusion.

From the presence of Ni and Cu in shear-zone related lithotypes it can be inferred that either during or after the deformation of the Lensoid Ultramafics hydrothermal fluids have been directed along Shear Zones. Furthermore, these fluids may have permeated and circulated around the flanks of the Tulu Dimtu Main Intrusion thereby remobilising and re-precipitating Ni and Cu. Both Pt and Pd are also likely to have been taken into solution, but Pd to a much greater extent. Hence, the locations of Pt and Pd anomalies have become separated (figure 8.4E and 8.4F).

Unid	0.1	972	11	347	0.2	4	<2	-	<2	KTR-050-02
VQuar	0.1	10	<2	8	0.1	<2	<2	-	<2	DTR-059-02
VQuar	0.1	34	8	10	0.1	<2	<2	-	2	KTR-064-02
VQuar	0.1	11	7	11	0.1	<2	<2	-	5	TD20
VQuar	<0.1	4	4	10	0.1	<2	<2	-	1262	TD21
VQuar	0.1	11	<2	28	0.1	<2	<2	-	<2	TDR 28/01
VQuar	<0.1	2	7	11	0.1	<2	<2	-	3	TDR 30/01

Table 8.20: Mg, Ni, Cu, Cr, Al, Pt and Pd values for the altered samples collected from the Kingy area. Anor: Anorthosite. Basa: Basalt. Birb: Birbirite. ChSchi: Chlorite-Schist. ChSchi: Chlorite-Schist. Cpxite: Clinopyroxenite. Dior: Diorite. Dole: Dolerite. Dun: Dunite. Fels: Felsite. Gabb: Gabbro. GranDi: Granodiorite. HardP: Hard pan. MetaBas: Metabasalt. MetaSed: Metasediment. Mylo: Mylonite. Ol-cpxite: Olivine-clinopyroxenite. Quar: Quartzite. Schi: Schist. Sed: Sediment. TaSchi: Talc-Schist. TCSchi: Talc-Chlorite-Schist. Troc: Troctolite. Unid: Unidentified. VQuar: Vein Quartz.

The following sections cover the distribution of Ni, Cu, Cr and Al in the Kingy area. Each section covers one element and describes its distribution in fresher ultramafics and altered rocks. These sections are accompanied by a fold-out page (page 229) of maps showing the distribution of all elements which the reader should refer to as each section is read.

8.10.3. Nickel

The highest Ni value in the fresher ultramafic samples is 4646ppm in a dunite located within the large Lensoid Ultramafic in north-eastern side of the Kingy area. Another sample in the same body shows Ni at 2131ppm all other Ni values are below 2000ppm but not lower than 485ppm.

The altered rocks from the Kingy Ridge Ultramafic show that the highest Ni abundances (1718ppm) occur in the centre and decrease to below detection limits towards the southwest and northeast (figure 8.7A). Elsewhere, the Ni contents in the altered ultramafics rise to a maximum of 963ppm in the Extra Ultramafic but 5 samples fall to as low as 8ppm in a Lensoid Ultramafic body. Within the basement units and quartzites, Ni remains below 100ppm and frequently falls below detection limits.

8.10.4. Copper

All Cu values in the samples of fresher ultramafics from the Kingy ridge are lower than or equal to 13ppm. The highest value of Cu (13ppm) occurs in a pyroxenite from the Extra Ultramafic all other Cu values are lower than 5ppm.

In altered rocks, the highest Cu value in the area (263ppm) occurs in an isolated gabbro body to the south-east of the study area (figure 8.7B). Of the ultramafic complexes, the highest Cu occurrences (up to 216ppm) lie in the altered dunites from the Kingy Ridge Ultramafic but some samples of the same rock formation contain Cu values below detection limits. The highest value occurs in a dunite on the farthest western point of the complex, Similarly, within the Extra Ultramafic the highest value (183ppm) occurs close to the bounding shear-zone.

8.10.5. Chromium

The highest Cr value in fresher rocks (833ppm) occurs in a pyroxenite from the Extra Ultramafic. All other Cr values in fresher rocks lie below 200ppm, the lowest of which is 59ppm in a dunite of the large northwestern Lensoid Ultramafic.

High Cr values (>200ppm) in altered rocks only occur in the ultramafic complexes and related shear-zones. The highest Cr values in altered rocks (up to 1993ppm in an olivine-clinopyroxenite occur close to the centre of the Kingy Ridge Ultramafic (figure 8.7C). The values drop to below 200ppm on the southwestern end of Kingy Ridge Ultramafic forming a crude zonation from northwest to southeast, where the lowest value is 6ppm in a dunite. Samples from the Lensoid Ultramafics contain intermediate Cr values, from 200ppm to 1000ppm.

8.10.6. Aluminium

The fresher rocks at Kingy contain up to 0.4% Al, this figure is obtained from an olivine-clinopyroxenite from the Extra Ultramafic. All other fresher ultramafics contain less than 0.2% Al.

The four largest Al values (>7%) in the altered rocks occur in samples from the Kingy Ridge Ultramafic. The highest Al value (14.6%) occurs in an altered dunite within the south western part of the Kingy Ridge Ultramafic. Al is enriched (over 5%) in some rocks from the Kingy Ridge Ultramafic and the Extra Ultramafic (figure 8.7D). Values of Al can drop below detection limits in rocks from both the Basement and the Kingy Ridge Ultramafic. The altered Lensoid Ultramafics display Al contents between 0.6% and 5% (see figure 8.7D).

8.10.7. Summary of Ni, Cu, Cr and Al distribution in the Kingy Ridge Ultramafic and Extra Ultramafic

No fresher samples are available from the Kingy Ridge Ultramafic but a sample from the Extra Ultramafic contains the highest values of Cu, Cr and Al of the fresher samples (see figure 8.6). This sample is located on the northernmost corner of the Extra Ultramafic complex.

Some spatial trends in Ni and Cr are observed in the altered dunites from the Kingy Ridge Ultramafic. The highest values of Ni and Cr occur in the central and northeastern end of the intrusion. These values drop to low values towards the southwestern end of the ridge. Unlike Ni and Cr, both Cu and Al are distributed unevenly in the Kingy Ridge Ultramafic. The four highest Al values come from samples located in the Kingy Ridge Ultramafic. A different sample contains the largest Cu value in the complex.

8.10.8. Summary of Ni, Cu, Cr and Al distribution in the Lensoid Ultramafics

The two highest Ni values in the Kingy area (4646ppm and 2131ppm) occur in the fresher rocks from the large northwestern Lensoid Ultramafic. Ni values in the altered Lensoid Ultramafics are much lower. Cu values are high, sometimes over 120ppm. Cr and Al values are intermediate compared to the Kingy Ridge Ultramafic.

8.10.9. Summary of Ni, Cu, Cr and Al distribution in the Isolated Gabbro

The highest Cu values (263ppm) occur in an altered gabbro sample in the southeastern quadrant of the Kingy area.

8.11. Kingy: Pt and Pd distribution

Aall Pt and Pd values from the fresher rocks of the Kingy area are almost below detection. Two fresher rocks resulted in assays of Pt at 3ppb each. One was an olivine-clinopyroxenite from a Lensoid Ultramafic (KTR-052-02) and the other was a pyroxenite from the small northeastern Lensoid Ultramafic (ATR-132-02). No Pd was found above detection limits in the fresher rocks from the Kingy area.

In altered rocks, assays for Pt and Pd in the samples from the Kingy area are dominated by Pd where 14 of 104 samples have >8ppb Pd and only 3 samples returned a Pt assay of >8ppb (see figures 8.7E and 8.7F). The highest Pd grade (28ppb) occurs in an altered dunite from the Extra Ultramafic and the highest Pt grade (18ppb) occurs in a clinopyroxenite from the Lensoid Ultramafics (figure 8.7E). In the Kingy Ridge Ultramafic the highest Pt value is 7ppb and occurs twice in two dunite samples. An olivine-clinopyroxenite showed the largest Pd assay of 13ppb. The three highest Pd assays occur at the periphery of the complex. The highest Pt and Pd values in the altered samples of the Lensoid Ultramafics occur in an olivine-clinopyroxenite which assays at 6ppb for Pd and 8ppb for Pt. In all ultramafic complexes of the area, both Pt and Pd can be below detection limits.

Of the lithologies associated with Shear Zones, the highest Pt and Pd values occur in the same mylonite sample showing Pt values of 18ppb and Pd values of 19ppb. The next highest Pt value is 9ppb in a talc-schist and the second highest Pd assay is 10ppb and occurs 3 times in two mylonitised samples and one talc-schist. Of the basement units, two dolerite dykes, one diorite and a basalt returned analyses of <10ppb for Pt and <15ppb for Pd and ranging to below detection for both elements. The highest Pt value in the basement (10ppb) occurs in the dolerite and highest Pd values (15ppb) occurring in the basalt and diorite samples.

A comparison between PGE and Ni, Cu, Cr and Al in the highest samples is summarised as follows:

Sample	Description	Pt (ppb)	Pd (ppb)	Ni ppm	Cu ppm	Cr ppm	Al %
KTR-052-02	Olivine-clinopyroxenite	3	< 2	1615	13	833	0.4
ATR-132-02	Pyroxenite	3	< 2	548	2	107	0.1

Table 8.21: A summary of Ni, Cu, Cr and Al values in the dunite samples with the highest Pt and Pd grade from the fresher rocks. A graphical representation of this data is provided in figure 8.6.

8.11.1. Comparison of the geochemistry of the soil versus rock samples

Other than the isolated gabbro body, the largest Pd value in soil occurs above the Extra Ultramafic. Additionally, high Pt and Pd values are more common in soils than rocks. 7% (7 of 104) rock samples returned assays at >12ppb for either Pt or Pd whereas 18% (36 of 202) soil samples assayed above that figure.

8.12. Kingy: Discussion

The processes that involve the distribution of Ni, Cu, Cr and Al in fresher ultramafics are considered in 8.12.1 and 8.12.2, followed by those processes which affect altered rocks in 8.12.3 and 8.12.5. The mechanisms which distribute Pt and Pd are considered from section 8.12.6 to section 8.12.7.

8.12.1. The locations of the highest Ni and Cu values in fresher rocks

The difference in location of the highest Cu values and the highest Ni could be explained by the process of filter-pressing (see section 8.6.6). This is where an immiscible sulphide liquid fractionates then the Cu-rich liquids migrate through interstitial space to become located with more evolved rocks. Alternatively, hot aqueous fluids could have remobilised the Cu and reconcentrated it away from the site of magmatic concentration. The study of mineral morphology is required in order to understand the degree of influence of high temperature fluids on Cu mineralisation.

Although it appears that the Cu and Ni highs occur in two separate complexes, the ultramafic complexes of the Kingy area could have become dismembered from one conformable unit. Johnson et al. (2004) discuss the tectonic evolution of the WES and transcurrent movement along a NE-SW striking faults (D_3). A reconstruction of this deformation may bring the highest Ni and Cu values to within 500m of each other.

8.12.2. Locations of highest Cu and Cr values in fresher rocks

Sample KTR-052-02 from the Extra Ultramafic, contains the highest Cu and Cr values of the fresher rocks from the Kingy area (13ppb and 833ppb respectively). As discussed for a similar situation in the Tulu Dimtu Main Intrusion (see section 8.7.2), if the Cu-rich residual sulphide is filter-pressed away from the MSS then it will be forced into the more evolved cumulate pile, with less Cr. However, if a new primitive magma is mixed with a slightly evolved melt then chromite will precipitate and consequently, the residual sulphide could be filter-pressed against primitive chromite grains. Unlike the same observations made at the Tulu Dimtu Main Intrusion, the Cu analyses made here are sufficiently low that it is difficult conlude that sulphide segregation has occurred.

An alternate explanation for the location of the highest Cu values is that both Ni and Cu were located in the same location by sulphides and subsequently, later hydrothermal fluids have brought Cu into contact areas of high Cr. This assumes the preferential remobilisation of Cu over Ni. Furthermore, the small amount of Cu may have been deposited in it's position by hydrothermal fluids themselves.

8.12.3. Zonation of Ni and Cr in altered rocks from the Kingy Ridge Ultramafic

In the Kingy Ridge Ultramafic the Ni and Cr values in altered rocks drop steadily towards the southwestern end of the intrusion (see figure 8.6A and 8.6C). It is likely that the Cr has been partitioned into the spinels which have been observed in these rocks (see chapter 3). However, given the refractory nature of spinels, it is likely that the Cr analysed here was partitioned into the olivine lattice. Hence it is likely that the highest Cr values in altered rocks mark the most primitive part of the complex with apparent fractionation directed towards the south-western end of the intrusion. As Ni is compatible in olivine (see section 8.6.2) the trend seen in its concentration could also be attributed to fractionation. However due to the mobility of the element under hydrothermal conditions (see section 8.6.8), the role of alteration on the control of this distribution cannot be eliminated.

8.12.4. Uneven Cu and Al distribution in the altered rocks from the Kingy Ridge Ultramafic

The distribution of Cu and Al shows no distinct spatial pattern (see figures 8.6B and 8.6D). As Cu is known to be easily taken into solution in hydrothermal fluids of various conditions (see section 8.6.8) it is expected that the Cu has been remobilised and precipitated in association with hydrous phases throughout the complex. As Ni is soluble in similar fluids, it would be expected that it would show a similar distribution to Cu – however this is not the case. There are two possible explanations for this. Firstly, the two elements may have been remobilised by different alteration episodes under slightly different conditions or acting on different areas. Or secondly, that Ni has not been remobilised which would mean that the distribution observed (section 8.12.3) is magmatic in origin as suggested by its similarity to the Cr distribution.

Slightly elevated Al values in places throughout the intrusion may be attributed to the concentration of the element – seen in low amounts in fresher rocks - during soil forming. A study of the degree of alteration is out of the scope of this study and therefore an "altered" rock – as classified here - may be partially affected by soil forming processes.

8.12.5. Trace element distribution in the altered rocks from the Lensoid Ultramafics

Nickel values in the altered Lensoid Ultramafics are typically low and Cu values are high. Cr and Al values are intermediate when compared to the Kingy Ridge Ultramafic. The elevation of Cu values above those found in fresher rocks (<13ppm) could be attributed to alteration as hydrothermal fluids can take large amounts of Cu into solution (see section 8.6.8). The Ni values are low enough that the element could be completely contained within the olivine crystal structure, without the presence of sulphide or alteration phases although the effect of both cannot be ruled out. The low mobility of Cr-spinels means that the intermediate Cr values indicate that the fresher protoliths could have been primitive or slightly evolved – as Cr value could be increased

slightly due to volume loss from fresher rocks (see section 8.6.8). The relatively minor degree of fractionation show by the Cr values in these rocks means that they could represent slivers of rock "shaved" off from the flanks of a larger complex such as the Tulu Dimtu Main Intrusion.

8.12.6. Genesis of Pt and Pd in fresher rocks

Almost no Pt or Pd has been detected in the fresher rocks of the Kingy area. Two fresher samples are Pt-bearing (3ppb each) and no Pd has been detected in the Kingy area.

Section 8.7.2 discusses the origin of the high Cu and Cr values in sample KTR-052-02 and it is possible that sulphide segregation and fractionation has occurred - yet the Pt value is very low. If the conditions have been set for the concentration of the PGE in the magma and it remains that very little has been found then it is possible that the magma was not Pt enriched before sulphide segregation. However, the Cu value in such samples is very low and it is therefore considered difficult to demonstrate that sulphide segregaton has occurred.

An alternative hypothesis for concentration of the Cu in the Extra Ultramafic is that the magmatic Cu has been remobilised by hydrothermal fluids and redeposited near to Cr-bearing spinels (see section 8.12.2). It is, therefore, also possible that the Pt values seen are either magmatic in origin or have been redeposited by hydrothermal fluids. The determination of the origin of the Pt values seen here can only be ascertained by the analysis of PGM and associated minerals. Unfortunately, given the low values of Pt at Kingy (3ppb) it is highly unlikely that any PGM can be found.

8.12.7. Genesis of Pt and Pd in altered rocks

Pd is more common and reaches higher values than Pt in the Kingy area. Figures 8.6E and 8.6F clearly show predominance of Pd over Pt in altered rocks. This is in stark contrast to fresher rocks where Pt and Pd were barely detected. Pd is more mobile than Pt

in hydrothermal systems. The preferential mobility of Pd over Pt in chloride-rich high-temperature fluids is discussed in section 8.7.7. The increase in Pd values and the movement of Pd away from the locations of magmatic Pt concentration could be attributed to hydrothermal fluids. From the data currently available, the distribution of Pt and Pd in the altered rocks from the Kingy area can only be explained by the preferential movement of Pd by high-temperature fluids. However, it is difficult to imagine a situation where such a low and spatially restricted Pt content in the fresher rocks from a complex (3ppb) could give rise to the extent of Pd mineralisation seen in the altered lithologies. Therefore it is reasonable to believe that further and richer magmatic sources of Pt and Pd exist which have not been uncovered by this study. Further sampling around the Extra Ultramafic or investigation of the area around the isolated gabbro may give an insight into this distribution.

8.13. Kingy: Conclusions

As Pt and Pd has barely been detected in the fresher rocks of the Kingy area it is not possible to recommend a strategy to discover or evaluate a "magmatic" ore deposit. However, there is much evidence for the remobilisation of Pd along shear-zones in the area and an improved understanding of the structure and fluids involved with these features may point to a richer source material.

There is little evidence in the Kingy area to construct a magmatic model of the events. However, a fractionation trend in Cr values can be observed in altered rocks and soil samples (see chapter 7) of the Kingy Ridge Ultramafic (see figure 8.6C).

The erratic distribution of Cu-values in altered rocks indicates that the element has been remobilised. Unlike Cu, the distribution of Ni mirrors the fractionation trend seen in Cr, this suggests that Ni has been remobilised by a different alteration episode or has not been remobilised at all. The intermediate Cr values from the altered Lensoid Ultramafics raise the possibility that they may represent slivers of rock "shaved" off a

larger complex. Detailed study of the structure and geochemistry of these bodies is required to test this hypothesis.

Pd dominates Pt in the altered rocks and is distributed over a much wider extent than the Pt in fresher rocks. This suggests firstly that the PGE distribution in the altered rocks is controlled largely by hydrothermal fluids. Additionally, it is inferred that further sites of magmatic Pt and Pd exist which have not been discovered here.

8.15. Daleti, Ankori, Tulu Kapi and Keley: Selected Major and Trace Elements

8.15.1. Introduction

There are 155 samples from the area around Daleti, Ankori, Tulu Kapi and Keley. According to the classification method outlined in section 8.3.1 only 13 samples are considered to be fresher ultramafics and a further 14 are altered ultramafics. The remaining 128 are basement lithologies. The fresher ultramafics are all dunites from the quarry and road-cuttings at Daleti. The altered ultramafic rocks are from the Ankori Ultramafic, Daleti Ultramafic and Lensoid Ultramafics. Samples were taken along roads and tracks where exposure was found (see figure 8.8).

Dole	2.2	34	22	20	2.6	<2	<2	-	2	DYR-006-01
Dole	<0.1	17	49	21	0.1	<2	7	0.0	5	DYR-010-01
Dole	0.1	50	71	187	1.6	2	5	0.4	4	KYC-009-01
Dole	<0.1	150	88	119	0.6	<2	<2	-	3	KYR-004-01
Dole	0.9	12	89	6	1.8	3	8	0.4	4	KYR-014-01
Dole	0.7	19	39	29	0.9	<2	<2	-	2	TYR-028-01
Dole	0.4	20	24	18	1.1	4	9	0.4	<2	TYR-033-01
Dole	0.4	16	86	14	1.8	<2	<2	-	<2	TYR-034-01
Fels	0.5	16	15	25	1.1	<2	3	0.0	6	AYR-004-01
Fels	0.1	14	8	13	1.2	<2	<2	-	<2	AYR-008-01
Fels	0.2	2	4	4	1.6	<2	<2	-	<2	DYR-034-01
Fels	0.1	2	3	4	0.6	<2	<2	-	2	DYR-035-01
Fels	<0.1	<2	4	2	0.2	<2	<2	-	2	DYR-037-01
Fels	<0.1	8	16	14	0.1	<2	<2	-	<2	DYR-038-01
Fels	0.2	104	21	317	0.2	4	5	0.8	2	KYR-009-01
Gabb	0.1	187	65	335	1.1	4	3	1.3	<2	AYR-022-01
Gabb	3.9	1061	10	1650	5.3	11	13	0.8	2	AYR-023-01
Gabb	<0.1	12	68	301	23.3	2	<2	-	<2	AYR-025-01
Gabb	1.2	21	81	71	1.8	<2	<2	-	3	AYR-026-01
Gabb	1.3	17	14	29	1.9	<2	<2	-	3	AYR-037-01
Gabb	1.9	24	17	23	2.4	<2	<2	-	<2	D4
Gabb	<0.1	18	7	14	0.1	<2	<2	-	<2	DR 06/01
Gabb	0.2	19	40	30	1.1	<2	<2	-	<2	DYR-001-01
Gabb	1.2	41	19	68	1.8	<2	<2	-	8	DYR-004-01
Gabb	7.9	656	4	854	0.2	5	<2	-	<2	KYC-008-01
Gabb	0.1	2	7	9	0.4	<2	<2	-	2	KYR-011-01
Gabb	0.2	2158	66	2510	0.6	3	<2	-	4	KYR-025-01
Gabb	1.3	13	37	37	1.8	<2	<2	-	3	TYR-002-01
Gabb	3.1	104	5	279	0.4	19	3	6.3	2	TYR-006-01
Gabb	0.6	6	22	10	1.2	<2	<2	-	2	TYR-027-01
Gran	0.2	2	4	3	0.6	<2	<2	-	<2	AYR-042-01
Gran	0.5	8	8	12	1.0	<2	<2	-	<2	KYR-026-01
Gran	<0.1	5	3	5	0.3	<2	<2	-	<2	TYC-003-01
Gran	0.2	2	4	<2	0.8	<2	<2	-	<2	TYR-030-01
GranDi	0.5	24	14	22	0.9	<2	<2	-	<2	AYR-046-01
GranDi	0.4	1	7	4	1.0	<2	<2	-	<2	DYR-018-01
GranDi	0.7	11	25	12	1.7	<2	<2	-	3	DYR-040-01
GranDi	0.1	2	16	4	1.1	<2	<2	-	<2	KYR-015-01
GranDi	<0.1	2	2	2	0.3	<2	<2	-	<2	TYR-005-01
HardP	0.5	23	259	33	1.5	<2	3	0.0	5	TYR-032-01
MetaSed	0.1	12	2	14	0.2	<2	<2	-	<2	TYR-003-01
Mylo	<0.1	8	14	8	0.4	<2	<2	-	24	AYR-041-01
Mylo	<0.1	26	7	16	0.3	<2	<2	-	<2	DYC-002-01
Mylo	0.5	14	9	9	1.1	<2	<2	-	<2	DYC-005-01
Mylo	<0.1	3	24	5	0.1	<2	<2	-	214	DYR-003-01
Mylo	3.4	186	19	401	6.8	<2	<2	-	<2	DYR-030-01
Mylo	1.4	95	14	81	2.0	<2	<2	-	3	DYR-041-01
Mylo	0.1	105	70	16	0.3	<2	<2	-	3	KYR-006-01
Mylo	0.1	5	4	21	0.7	<2	<2	-	<2	TYR-029-01
Quar	<0.1	29	70	33	0.4	10	13	0.8	4	ANR 06/01
Quar	0.2	48	5	8	0.3	<2	<2	-	28	DR 04/01
Quar	0.1	759	5	273	<0.1	5	<2	-	<2	DR 14/01
Quar	<0.1	21	7	14	<0.1	<2	<2	-	2	DR 15/01
Quar	<0.1	24	143	39	0.1	2	9	0.2	12	DR 16/01
Quar	<0.1	17	101	15	0.2	2	<2	-	132	DR 17/01
Quar	0.1	26	19	16	0.1	4	33	0.1	11	DR 18/01
Quar	<0.1	5	20	18	0.2	<2	8	0.0	15	DR 20/01
Quar	<0.1	2	3	3	<0.1	<2	<2	-	3	DYR-032-01
Quar	<0.1	5	7	26	0.1	<2	<2	-	<2	KYR-010-01
Schi	<0.1	45	77	95	0.4	<2	<2	-	<2	A3
Schi	2.4	63	46	38	1.6	<2	<2	-	20	AYR-005-01
Schi	10.6	373	5	162	9.3	<2	<2	-	2	AYR-044-01
Schi	11.0	349	17	265	6.6	<2	<2	-	<2	D1
Schi	<0.1	7	<2	9	0.1	<2	<2	-	<2	DYC-003-01
Schi	<0.1	4	24	14	0.2	3	8	0.4	2	DYC-007-01
Schi	0.3	6	29	18	1.3	<2	<2	-	2	DYR-031-01
Schi	<0.1	15	88	14	0.2	2	<2	-	2	DYR-039-01
Schi	0.1	54	4	43	0.4	<2	<2	-	2	KYR-008-01
Schi	<0.1	1	<2	22	0.2	<2	<2	-	<2	TYR-001-01
Schi	0.7	15	19	27	1.9	<2	<2	-	<2	TYR-016-01

Schi	8.6	489	19	1123	6.7	<2	<2	-	45	TYR-018-01
Sed	<0.1	8	21	47	2.1	4	3	1.3	3	AYC-007-01
Sed	<0.1	15	7	19	2.1	<2	<2	-	2	AYC-008-01
Sed	<0.1	7	90	32	0.5	6	7	0.9	4	AYC-009-01
Sed	0.3	7	179	35	0.8	4	5	0.8	24	AYC-011-01
Sed	0.1	2	45	20	0.4	3	5	0.6	5	AYR-009-01
Sed	<0.1	104	140	340	1.4	<2	<2	-	3	KYR-024-01
TaSchi	0.4	64	32	531	0.1	3	<2	-	2	AYR-007-01
TaSchi	0.1	20	22	32	1.8	<2	3	0.0	2	AYR-021-01
TaSchi	3.2	422	2	987	2.8	4	6	0.7	<2	AYR-024-01
TaSchi	0.3	8	20	12	1.0	<2	<2	-	<2	AYR-038-01
TaSchi	0.6	129	19	647	0.2	<2	<2	-	<2	D2
TaSchi	9.7	159	7	49	9.3	<2	<2	-	<2	D21
TaSchi	0.3	110	<2	158	0.3	<2	<2	-	<2	D7
TaSchi	0.8	223	<2	563	0.2	<2	<2	-	<2	D9
TaSchi	0.2	238	184	205	4.8	<2	<2	-	109	DYR-002-01
TaSchi	0.1	24	10	14	0.4	<2	<2	-	<2	DYR-009-01
TaSchi	<0.1	39	9	59	0.3	<2	<2	-	2	KYR-003-01
TaSchi	0.1	21	69	21	0.9	<2	<2	-	10	TYR-017-01
TCSchi	0.7	355	8	492	0.2	5	<2	-	<2	DR 11/01
TCSchi	9.4	941	11	138	11.7	2	7	0.3	4.51	DR 19/01
Unid	<0.1	348	9	87	0.2	<2	<2	-	25	AYC-020-01
Unid	<0.1	17	159	24	0.4	6	9	0.7	13	DYC-008-01
Unid	0.9	149	35	634	0.4	<2	<2	-	4	AFYC-004-01
VQuar	<0.1	1406	3	742	0.2	<2	<2	-	<2	ANR 04/01
VQuar	<0.1	2	<2	4	0.1	<2	<2	-	<2	AYC-018-01
VQuar	8.6	47	5	17	5.7	<2	<2	-	<2	AYR-006-01
VQuar	0.2	1413	19	388	0.2	4	<2	-	2	DR 13/01
VQuar	<0.1	2	<2	8	0.1	<2	<2	-	<2	DYC-006-01
VQuar	<0.1	2	3	6	0.1	<2	<2	-	<2	DYR-007-01
VQuar	<0.1	1	2	3	0.1	2	<2	-	2	DYR-008-01
VQuar	1.2	28	15	15	1.6	<2	<2	-	2	DYR-033-01
VQuar	<0.1	13	12	10	0.1	<2	<2	-	<2	KYR-001-01
VQuar	<0.1	19	37	8	0.1	<2	<2	-	3	KYR-002-01
VQuar	<0.1	66	50	9	0.1	<2	<2	-	9	KYR-007-01
VQuar	<0.1	9	3	52	0.1	<2	<2	-	<2	KYR-012-01
VQuar	<0.1	3	<2	7	<0.1	<2	<2	-	72	KYR-013-01
VQuar	0.1	25	2	102	0.1	<2	<2	-	<2	KYR-023-01
VQuar	<0.1	3	<2	11	<0.1	<2	<2	-	<2	KYR-033-01
VQuar	<0.1	11	28	16	0.3	<2	<2	-	<2	TK1

Table 8.24: Mg, Ni, Cu, Cr, Al, Pt and Pd values for the altered samples collected from the Daleti, Ankori, Tulu Kapi and Keley areas. Anor: Anorthosite. Basa: Basalt. Birb: Birbirite. ChSchi: Chlorite-Schist. ChSchi: Chlorite-Schist. Cpxite: Clinopyroxenite. Dior: Diorite. Dole: Dolerite. Dun: Dunite. Fels: Felsite. Gabb: Gabbro. GranDi: Granodiorite. HardP: Hard pan. MetaBas: Metabasalt. MetaSed: Metasediment. Mylo: Mylonite. Ol-cpxite: Olivine-clinopyroxenite. Quar: Quartzite. Schi: Schist. Sed: Sediment. Spin: spinel-like rocks (see chapter 3) TaSchi: Talc-Schist. TCSchi: Talc-Chlorite-Schist. Troc: Troctolite. Unid: Unidentified. VQuar: Vein Quartz.

The following sections cover the distribution of Ni, Cu, Cr and Al in the Daleti, Ankori, Tulu Kapi and Keley areas. Each section covers one element and describes its distribution in fresher ultramafics and then altered rocks. These sections are accompanied by a fold-out page (on page 247) of maps showing the distribution of all elements which the reader should refer to as each section is read.

8.15.3. Nickel

The fresher dunites from the Daleti Ultramafic show the highest Ni value in the WES at 24,035ppm from the northern tip of the complex. At the centre of the Daleti Ultramafic local variations are large, of 8 samples of fresher dunite located within 250m of each other Ni content varies from 1,876ppm to above 22,952ppm.

All Ni analyses above 2,100ppm in altered rock are located in samples from the ultramafic bodies. The altered rocks from the Ankori Ultramafic and the Lensoid Ultramafics have less Ni than the samples from the Daleti Ultramafic, with maximas of 1,248ppm and 138ppm respectively (figure 8.10A). The 5 samples of ultramafic rocks from the Ankori complex show no distinct pattern in Ni content and the lowest Ni value is 95ppm in an olivine-clinopyroxenite. Ni values in the dunites of the Lensoid Ultramafics vary from 1ppm to 111ppm and no particular spatial pattern can be observed. Shear-zone related rocks show no more than 941ppm of Ni, this value occurring in a talc-chlorite-schist near Keley.

8.15.4. Copper

Only two fresher rocks returned positive results slightly above detection for Cu. These are located at the northernmost tip of the Daleti Ultramafic (3ppm) and on the western flank of the intrusion (2ppm)

Within the altered ultramafics only 2 of 31 samples contain Cu above 65ppm, these are a dunite (298ppm) and a troctolite (101ppm) from the Lensoid Ultramafics. The highest Cu value from the Daleti, Ankori, Tulu Kapi and Keley areas (298ppm) occurs in a dunite from the Lensoid Ultramafics near Keley. The maximum Cu value in the Daleti Ultramafic is 65ppm – from spinel-like rocks (see chapter 3) in the centre of the formation, some dunites have Cu values below detection limits. In the Ankori Ultramafic the maximum is 46ppm from a dunite and some values fall below detection limits. No spatial trends in Cu content can be observed within any of the ultramafic complexes. Two of 15 shear-zone related samples display high Cu values the highest of which is a talc-

schist 3km south of the Keley complex (184ppm), the next highest is a schistose-rock from Gudeya Guji (88ppm). Some shear-zone related rocks returned Cu analyses which are below detection limits.

8.15.5. Chromium

The three highest Cr values (above 500ppm) in fresher rocks occur in dunites of the centre of the Daleti Ultramafic. The maximum Cr value in the fresher rocks from Daleti is 804ppm. Most of the Cr values below 100ppm occur close to the edge of the intrusion near to the contact with the shear zones, however the lowest Cr value (24ppm) occurs in a dunite in the centre within 200m of the highest Cr value.

Chromium values above 300ppm in rock are restricted to the ultramafic complexes and related shear zones. Of all the Daleti, Ankori, Tulu Kapi and Keley areas the highest Cr value (2510ppm) occurs in a gabbro from the basement north of the Ankori complex. The lowest Cr values occur in an altered pyroxenite also in the centre of the intrusion. In the Ankori complex the highest Cr composition is 1063ppm in the southern end of the intrusion and the lowest values are 45ppm in a dunite from the centre of the intrusion. The highest Cr composition in the Lensoid Ultramafics (322ppm) is found in a dunite of the body farthest to the southwest. In addition to this the talc-schists and gabbros from the basement in the south-western part of the study area contain Cr (<1650ppm in gabbro).

8.15.6. Aluminium

Three fresher dunites from the Daleti Ultramafic contain 0.2% of Al and for 10 of 13 samples Al was not detected. All three of these rocks occur close to the centre of the complex.

With the exception of the spinel-like rocks (see chapter 3) of the Daleti Ultramafic all Al analyses above 4.1% are found in the basement or shear-zone related rocks. The highest Al content of the study area (23.3.%) is found in a gabbro from the